ECBC-SP-009

CB Defense Research Proceedings

Home | Introduction | Table of Contents | Download

Author Index

2001 Scientific Conference on Chemical & Biological Defense Research

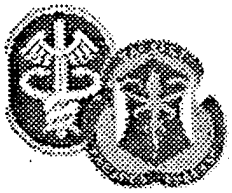

6–8 March 2001
Marriott's Hunt Valley Inn
Hunt Valley, Maryland

Approved for public release;
distribution is unlimited.

20030131 153

REPORT DOCUMENTATION PAGE

Form Approved
OMB No. 0704-0188

Public reporting burden for this collection of information is estimated to average 1 hour per response, including the time for reviewing instructions, searching existing data sources, gathering and maintaining the data needed, and completing and reviewing the collection of information. Send comments regarding this burden estimate or any other aspect of this collection of information, including suggestions for reducing this burden, to Washington Headquarters Services, Directorate for Information Operations and Reports, 1215 Jefferson Davis Highway, Suite 1204, Arlington, VA 22202-4302, and to the Office of Management and Budget, Paperwork Reduction Project (0704-0188), Washington, DC 20503.

1. AGENCY USE ONLY *(Leave blank)*	2. REPORT DATE	3. REPORT TYPE AND DATES COVERED
	January 2002	Final; 2001 March

4. TITLE AND SUBTITLE
Proceedings of the 2001 ECBC Scientific Conference on Chemical and Biological Defense Research, 6-8 March 2001

5. FUNDING NUMBERS
C-DAAM01-97-D-0007

6. AUTHOR(S)
Berg, Dorothy A. (Compiler)

7. PERFORMING ORGANIZATION NAME(S) AND ADDRESS(ES)
DIR, ECBC, ATTN: AMSSB-RRT, APG, MD 21010-5424

8. PERFORMING ORGANIZATION REPORT NUMBER
ECBC-SP-009

9. SPONSORING / MONITORING AGENCY NAME(S) AND ADDRESS(ES)

10. SPONSORING / MONITORING AGENCY REPORT NUMBER

11. SUPPLEMENTARY NOTES

12a. DISTRIBUTION / AVAILABILITY STATEMENT
Approved for public release; distribution is unlimited.

12b. DISTRIBUTION CODE

13. ABSTRACT *(Maximum 200 words)*
This report contains 65 papers presented at the 2001 Scientific Conference on Chemical and Biological Defense Research under the headings of Medical Protection/Training & Education, Standoff Detection, Collective Protection, Individual Protection, Modeling & Simulation, Point Detection/Diatgostics, Therapeutics/Forensics, Aerosol Science/Environmental, Low Dose, Decontamination, New Technologies and Emerging Threats. In addition, papers are included for posters presented at the meeting under the topic areas listed above, as well as for Vaccines and Therapeutics, and Toxicology.

14. SUBJECT TERMS

Protection	Modeling & Simulation	Environmental	New Technologies
Therapeutics/Forensics	Diagnostics	Low Dose	Emerging Threats
Detection	Aerosol Science	Decontamination	Toxicology

15. NUMBER OF PAGES

16. PRICE CODE

17. SECURITY CLASSIFICATION OF REPORT	18. SECURITY CLASSIFICATION OF THIS PAGE	19. SECURITY CLASSIFICATION OF ABSTRACT	20. LIMITATION OF ABSTRACT
UNCLASSIFIED	UNCLASSIFIED	UNCLASSIFIED	UL

CB Defense Research Proceedings

Home | Introduction | Table of Contents | Download | Author Index

2001 SCIENTIFIC CONFERENCE ON CHEMICAL & BIOLOGICAL DEFENSE RESEARCH

6–8 March 2001
MARRIOTT'S HUNT VALLEY INN
HUNT VALLEY, MARYLAND

Introduction

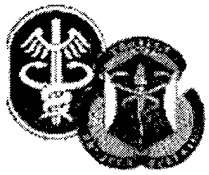

Home | Introduction | Table of Contents | Download | Author Index

PREFACE

All of the manuscripts contained on this CDROM are in Adobe Acrobat Reader format (.PDF). You may download some of the most common versions of this software directly from this CDROM by clicking here.

The 2001 Scientific Conference on Chemical and Biological Defense Research was jointly sponsored by the **U.S. Army Medical Research and Materiel Command and the U.S. Army Soldier and Biological Chemical Command.** The Conference was held at the Hunt Valley Inn, Hunt Valley, Maryland, 6-8 March 2001. The topics addressed covered medical and nonmedical research efforts. This proceedings contains 65 unclassified papers presented at the Conference. Science and Technology Corporation provided administrative and logistical support services.

MG John S. Parker, Commander, U.S. Army Medical Research and Materiel Command, opened the Conference Tuesday afternoon, 6 March. A panel discussion followed.

Panel Members

- **Dr. Carol D. Linden**
  U.S. Army Medical Research and Materiel Command
- **Mr. James H. Zarzycki**
  U.S. Army Edgewood Chemical Biological Center
- **COL James A. Romano**
  U.S. Army Medical Research Institute of Chemical Defense
- **Dr. Raymond A. Mackay**
  U.S. Army Edgewood Chemical Biological

Panel Moderator

- ***Dr. I. Gary Resnick***

Defense Threat Reduction Agency

Keynote Speaker

The **Keynote Speaker** was **Dr. Anna Johnson-Winegar,** Deputy Assistant to the Secretary of Defense for Chemical and Biological Defense Matters.

Session Chairs

Prevention and Preparation

- COL Theodore Cieslak
  U.S. Army Medical Research Institute of Infectious Diseases
- Dr. Richard R. Smardzewski
  U.S. Edgewood Chemical Biological Center

Response

- COL Gennady Platoff
  U.S. Army Medical Research Institute of Chemical Defense
- Dr. James A. Baker
  U.S. Army Edgewood Chemical Biological Center

Aftermath/Emerging Technologies for the Future

- LTC William Pratt
  U.S. Army Medical Research Institute of Infectious Diseases
- Dr. James J. Valdes
  U.S. Army Edgewood Chemical Biological Center

Moderators

- COL Theodore Cieslak
  U.S. Army Medical Research Institute of Infectious Diseases
- COL Jonathan Newmark
  U.S. Army Medical Research Institute of Chemical Defense
- Mr. William R. Loerop
  U.S. Edgewood Chemical Biological Center
- Dr. David E. Tevault
  U.S. Edgewood Chemical Biological Center
- Mr. Wade D. Kuhlmann

U.S. Edgewood Chemical Biological Center

- Dr. John R. White
  U.S. Edgewood Chemical Biological Center
- Dr. Stephen Lee
  U.S. Army Research Office
- LTC Brian J. Lukey
  U.S. Army Medical Research Institute of Chemical Defense
- Dr. Shawn R. Feaster
  Walter Reed Army Institute for Research
- Dr. William J. Smith
  U.S. Army Medical Research Institute of Chemical Defense
- Dr. Harry Salem
  U.S. Edgewood Chemical Biological Center
- Dr. Louise Pitt
  U.S. Army Medical Research Institute of Infectious Diseases
- Dr. Sandra Thomson
  U.S. Army Edgewood Chemical Biological Center
- COL James A. Romano
  U.S. Army Medical Research Institute of Chemical Defense
- Dr. Joseph J. DeFrank
  U.S. Army Edgewood Chemical Biological Center
- Dr. Richard K. Gordon
  U.S. Army Medical Research Institute of Chemical Defense
- CPT John Lee
  U.S. Army Medical Research Institute of Infectious Diseases
- Dr. Akbar Khan
  U.S. Army Edgewood Chemical Biological Center
- Dr. Luther Lindler
  Walter Reed Army Institute of Research
- Dr. Edward Stuebing
  U.S. Army Edgewood Chemical Biological Center

Conference Administrator:

Ms. Dorothy Berg
ATTN: AMSSB-RRT
U.S. Army Edgewood Chemical Biological Center
Aberdeen Proving Ground, MD 21010-5424

Conference Administrative Support:

Science and Technology Corp.
Meetings Services International
10 Basil Sawyer Drive
Hampton, VA 23666-1393
Phone: 757-766-5831
Fax: 757-865-8721

Coordinators:

Ms. Diana McQuestion
E-mail: mcquestion@stcnet.com
Ms. Judy Cole

Table of Contents

Home | Introduction | Table of Contents | Download | Author Index

Panel Presentations

Prevention & Preparation
- -Medical Protection/Training & Education-
- -Standoff Detection-
- -Collective Protection-
- -Individual Protection-
- -Modeling & Simulation-

Response
- -Point Detection/Diagnostics-
- -Therapeutics/Forensics-
- -Aerosol Science/Environmental-

Aftermath/Emerging Technologies For The Future
- -Low Dose-
- -Decontamination-
- -New Technologies-
- -Emerging Threats-

Poster Presentations
- -Individual Protection-
- -Modeling & Simulation-
- -Vaccines And Therapeutics-
- -Medical Diagnostics-
- -Environmental-
- -Point Detection-
- -Forensics-
- -Aerosol Sciences-
- -Decontamination-
- -Emerging Threats-
- -New Technologies-
- -Toxicology-
- -Low Dose-

Panel Presentations

Medical Chemical and Biological Defense Research

Dr. Carol Linden, Research Area Director, Medical Chemical & Biological Defense Research Program, U.S. Army Medical Research & Materiel Command

Research for the Warfighter
COL James A. Romano, Commander, U.S. Army Medical Research Institute of Chemical Defense

Joint Science and Technology Panel for Chemical/Biological Defense
Dr. Raymond A. Mackay, Acting Director, Research & Technology, U.S. Army Edgewood Chemical Biological Center

Prevention & Preparation

-Medical Protection/Training & Education-

Bioscavengers as a Pretreatment for Nerve Agent Exposure
David Lenz, USAMRICD

Neuroprotection for Nerve Agent-Induced Brain Damage
COL Jonathan Newmark, Gerald P.H. Ballough and Margaret G. Filbert, USAMRICD

-Standoff Detection-

Trace Chemical Vapor Detection by Photothermal Interferometry
Paul M. Pellegrino, *Nicholas F. Fell, Jr., Scott D. Sarama* and *James B. Gillespie,* U.S. Army Research Laboratory

Passive Standoff Detection Team at SBCCOM Results from the Owl Field Test, Nevada Test Site 31 July Through 11 August 2000
James O. Jensen, Agustin I. Ifarraguerri, Alan Samuels, and William R. Loerop, U. S. Army SBCCOM; Richard Matta, Aerospace C2, Intelligence, Surveillance and Reconnaissance Center; Avishai Ben-David, Science and Technology Corp.; James W. Yang, Geocenters Inc.; Christopher Gittens and William Marinelli, Physical Science Inc.; Thomas Gruber and Dustin Grim, Mesh Inc.

-Collective Protection-

Development of a CB Resistant Durable, Flexible Hydration System
Peyton W. Hall, *Frank T. Zeller, John W. Bulluck,* and *Michael L. Dingus,* Texas Research Institute

-Individual Protection-

Evaluation of Personal Chemical Vapor Protection for Patrol and Tactical Law Enforcement
Paul D. Fedele, *William L. Lake, Victor J. Arca* and *Stephen M. Marshall,* U.S. Army SBCCOM

Development of Self-Decontaminating Textiles with Microporous Membranes
John Walker, ***Heidi L. Schreuder-Gibson***, *Walter Yeomans,* and *Francis Hoskin,* U.S. Army

SBCCOM; *Tu-chen Cheng,* U.S. Army ECBC; *Ray Yin,* ARL; and *Craig Hill,* Emory University

-Modeling & Simulation-

Structure and Reactivity of the Phosphotriesterase Active Site
Morris Krauss, Center for Advanced Research in Biotechnology

Response

-Point Detection/Diagnostics-

Critique of Test Methodologies for Biological Agent Detection and Identification Systems for Military and First Responders
David Trudil, New Horizons Diagnostics

Detection of Biological Aerosols by MALDI On-line Aerosol TOF MS
Ben L. M. van Baar, *Charles E. Kientz* and *Ruud W. Busker,* TNO, Prins Maurits Laboratory, The Netherlands; *Michael A. Stowers, Arjan L. van Wuijckhuijse, Brian Scarlett* and *Jan C. M. Marijnissen,* Delft University of Technology, The Netherlands

-Therapeutics/Forensics-

Development of Medical Countermeasures to Sulfur Mustard Vesication
William J. Smith and *Michael C. Babin*, USAMRICD; *Robyn C. Kiser* and *Robert P. Casillas,* Battelle

Midazolam: An Improved Anticonvulsant Treatment for Nerve Agent-Induced Seizures
John H. McDonough, USAMRICD

Control of Nerve Agent-Induced Seizures is Critical for Neuroprotection and Survival
Tsung-Ming Shih, *S. Duniho,* and *John H. McDonough*, USAMRICD

-Aerosol Science/Environmental-

Utility of Respiratory Vaccination with Recombinant Subunit Vaccines for Protection Against Pneumonic Plague
Douglas Reed and *Jennifer Smoll*, USAMRIID

Determination of Thiodiglycol in Groundwater Using Solid Phase Extraction Followed by Gas Chromatography with Mass Spectrometric Detection in the Selected Ion Mode
Bruce A. Tomkins and *Gary A. Sega*, Oak Ridge National Laboratory

Aftermath/Emerging Technologies For The Future

-Low Dose-

Interaction of Exposure Concentration and Duration in Determining Acute Toxic Effects of Sarin Vapor in Rats
Robert J. Mioduszewski, *James A. Manthei, Ruth A. Way, David C. Burnett, Bernardita P. Gaviola, William T. Muse, Sandra A. Thomson, Douglas R. Sommerville* and *Ronald B. Crosier*, U.S. Army ECBC

Analysis of Rat Blood Samples for Agent Biomarkers After GB Inhalation Exposure
E. Michael Jakubowski and *L.S. Heykamp*, EAI Corporation; *R.J. Mioduszewski, J. Manthei, D.C. Burnett, R. Way, B. Gaviola, W. Muse, J. Anthony, C. Crouse, H.D. Durst* and *S.A. Thomson,* U.S. Army ECBC

-Decontamination-

Novel Photocatalysts and Processes for the Destruction of Chemical Warfare Agents (CWA)
Panagiotis G. Smirniotis, Department of Chemical Engineering, University of Cincinnati

Decontamination and Detoxification with Sponges
Richard K. Gordon, *Shawn R. Feaster, Alper T. Gunduz* and *Bhupendra P. Doctor,* WRAIR; *David E. Lenz, Donald M. Maxwell, Rudy C. Macalalag, Edward D. Clarkson* and *John P. Skvorak,* USAMRICD; *Michelle C. Ross,* Defense Threat Reduction Agency/CB

-New Technologies-

Concepts for Injectable Nanoparticles for *In Vivo* Removal of Overdose Toxins from Blood
Richard Partch, Dinesh Shah and Chuck Martin, University of Florida

The Army's University Affiliated Research Center Chemical/Biological Countermeasures
Steven Kornguth, and *Walter Zielinski*, University of Texas at Austin; *James Valdes*, SBCCOM; and *Gordon Boezer*, Institute for Defense Analyses

-Emerging Threats-

Development of a Genome Fingerprint Database to Identify Genetically Engineered Microbes
Luther E. Lindler and Xiaozhe Huang, Walter Reed Army Institute of Research

POSTER PRESENTATIONS

-Individual Protection-

Assessment of the Thermal Load Attributable to Protective Masks
David M. Caretti, U.S. Army ECBC

Immobilized Filters for Air Filtration
John J. Mahle, U.S. Army ECBC; *Saeed Zaiee,* University of Delaware

-Modeling & Simulation-

Four Portraits of the Plague Organism
Millard M. Mershon, SAIC

-Vaccines And Therapeutics-

Protection Against Chemical Agent Induced, Seizure-Related Neuronal Cell Death
Margaret G. Filbert, USAMRICD; and *Gerald P.H. Ballough*, La Salle University

-Medical Diagnostics-

Selective, Specific, and Versatile Personal Biosensors to Organophosphate Chemical Toxins Composed of Polyurethane Imobilized Enzymes
Richard K. Gordon, *Alper T. Gunduz, Shawn R. Feaster* and *Bhupendra P. Doctor,* WRAIR; and *Tracy Cronin*, CBRNCTSWG

Studies in the Formation of Ethyl Methylphosphonofluoridate from Rat and Human Serum Exposed to VX and in the Presence of Fluoride Ion
E. Michael Jakubowski and *L. S. Heykamp,* EAI Corporation; *H. D. Durst* and *S. A. Thomson*, U.S. Army ECBC

-Environmental-

Treatment of M1 and M8 Hydrolysates with HD/Tetrytol Adapted Immobilized Cell Bioreactors
Joseph J. DeFrank, *Mark A. Guelta,* and *Mark V. Haley,* U.S. Army ECBC; and *F. Stephen Lupton*, Honeywell

-Point Detection-

High Sensitivity Detection of Bacterial Endospores via Tb Photoluminescence Enhancement
Nicholas F. Fell, Jr., *Paul M. Pellegrino* and *James B. Gillespie,* U.S. Army Research Laboratory

BioHAZ: Biological Detection for the Emergency Responders
David L. Gray and *Randall Bright,* EAI Corporation; *Peter J. Stopa* and *Philip A. Coon,* U.S. Army ECBC; *David Trudil*, New Horizons Diagnostics

Quantification of Lewisite in Air by Liquid Chromatography Mass Spectrometry (LC/MS)
Wesley Ercanbrack, *Sherry Sheffield, Steve Freudenberger,* and *Aaron Jenkins*, Science and Technology Corp./Mellor Engineering Corp.

Real-Time Biodetection of Individual Pathogenic Microorganisms with a Rugged, Sub-Briefcase-Sized System
Paul E. Johnson, Michael Lund, Amanda Votaw, Jerome Swanson, Julie Kellogg and Dehua Zhao, University of Wyoming; Richard Shorthill and William Asprey, SoftRay, Inc.

Gas Chromatographic Analysis of the Stereoisomers of the Chemical Warfare Agent GF
Jan E. Kolakowski, *Steven P. Harvey* and *Louis P. Reiff*, U.S. Army Edgewood Chemical Biological Center

Activity of Pera Safe™ Against *Bacillus Anthracis* Spores
Michal Bartoszcze, *Krzysztof Chomiczewski* and *Lidia Mizak,* Military Institute of Hygiene and Epidemiology

A Biological Warfare Detection Device (BIOWARD I)
K. Gerritse, B. van der Gaag, E. Stigter, S. van Hövell tot Westerflier, H. Harteveld and ***R.W. Busker,*** TNO, The Netherlands

-Forensics-

The Interference of Stress on Physostigmine Pretreatment Against Soman Intoxication in Guinea Pigs
Ingrid H.C.H.M. Philippens, Marloes J.A. Joosen, Bas Groen, Raymond A. P. Vanwersch, Ruud W. Busker and ***Maarten S. Nieuwenhuizen***, TNO Prins Maurits Laboratory, The Netherlands

-Aerosol Sciences-

Factors Influencing the Transport of Biological Aerosol Through the Atmosphere: And Their Injection Into It
C. H. Wick, U.S. Army ECBC; and ***John Latham***

-Decontamination-

Performance of the ACWA Pilot Scale Immobilized Cell Bioreactor in Degradation of HD and Tetrytol Payloads of the M60 Chemical Round
Mark A. Guelta, *Nancy A. Chester, Carl W. Curnas* and *Mark V. Haley,* U.S. Army ECBC; *Stephen Lupton* and *Mark Koch*, Honeywell International

Furthering the Enzymatic Destruction of Nerve Agents
Ilya Elashvili and *Joseph J. DeFrank*, U.S. Army ECBC

Molybdate/Peroxide Oxidation of Mustard in Microemulsions
Lawrence R. Procell, *George W. Wagner* and *Yu-Chu Yang,* U.S. Army ECBC; *Clifford A. Bunton*, University of California

Interaction of Candidate Cleaning Solutions for Sensitive Equipment Decontamination with Polymeric Materials
Brian S. Ince and *Wendel J. Shuely*, U.S. Army SBCCOM

Assessment of Environmentally Benign Decontaminant Towards Anthrax Spores
Vipin K. Rastogi, Geo-Centers, Inc.; *Tu-chen Cheng, Phillip Bartram, George Wagner* and *Abe Turetsky*, U.S. Army ECBC

Microarray Bactericidal Testing of Natural Products Against *Yersinia intermedia* and *Bacillus anthracis*
Ilona J. Fry, Geo-Centers, Inc.; *Fred K. Lee, Abraham L. Turetsky*, and *Joseph J. DeFrank*,

U.S. Army ECBC

Methylphosphonofluoridic Acid – A Thermal Degradation Product of Some Nerve Agents
Michael D. Crenshaw, Battelle Memorial Institute

Synthesis and Characterization of a New Genre of CS-Compounds
Shekar Munavalli, Geo-Centers, Inc.; *D. K. Rohrbaugh* and *G. W. Wagner*, U.S. Army ECBC; *F. R. Longo*, Sci-Tech Services, Inc.; *B. Black*, Geo-Centers, Inc.; and *H. D. Durst*, U.S. Army ECBC

Batch and High Cell Density Fed-Batch Culture Productions of an Organophosphorus Hydrolase
Michael H. Kim and *Vipin K. Rastogi*, Geo-Centers, Inc.; *Tu-chen Cheng* and *Joseph J. DeFrank*, U.S. Army ECBC

Microwave Induced Reaction of H-Dimethylphosphonate with Styrene Oxide
Shekar Munavalli and *F. R. Longo*, Geo-Centers, Inc.; *D. K. Rohrbaugh, G. W. Wagner* and *H. D. Durst*, U.S. Army ECBC

Dehalogenase: The Follow-up Enzyme After Mustard Oxidation
Ilya Elashvili and *Joseph J. DeFrank*, U.S. Army ECBC

Room Temperature Mineralization of Chemical Warfare Agents using Hydrogen Peroxide – Pd/C
Lawrence R. Procell, *George W. Wagner* and *Yu-Chu Yang,* U.S. Army ECBC

Decon Green
George W. Wagner, *Philip W. Bartman, Lawrence R. Procell, Vikki D. Henderson* and *Yu-Chu Yang,* U.S. Army SBCCOM

-Emerging Threats-

Ab Initio Studies on Hexavalent Phosphorous Compounds
Ashley L. Wilson, Aberdeen High School; and *William White,* U.S. Army ECBC

-New Technologies-

Next-Generation Recombinant Antibodies and Antigens for the Detection of Biological Threat Agents and Simulants
Kevin O'Connell, Roy G. Thompson, Akbar S. Khan and James J. Valdes, U.S. Army ECBC

Self-Disinfection and Decontaminating Interior Surfaces Based on Photocatalytic Titania/Easy-Release Coatings
Robert Baier, State University of New York at Buffalo; Christopher Izzo, Harmac Industries; and Paul Nicotera, Rensselaer Polytechnic Institute

Distributed Software Decision Support Systems for Heterogenous Coordination in Chemical and Biological Response
K. Suzanne Barber, Matthew MacMahon, Ryan McKay and Cheryl Martin, University of Texas at Austin

An Effective CB Material From Combined Components of Triosyn® Resin and Surface Enhanced Carbon

Lucy Di Ionno, *Jean-Pierre St-Louis, Stéphane Bourget* and *Pierre Jean Messier,* Triosyn Corp.

Broad Bandwidth Lidar for Standoff Bioaerosol Size Distribution
James Gillespie*, David L. Ligon, Paul M. Pellegrino* and *Nicholas F. Fell, Jr.,* U.S. Army Research Laboratory

Cooperative Relational Database Initiative for Threat Reduction
Michelle Sheahan and *Luther Lindler*, Walter Reed Army Institute of Research

-Toxicology-

Chemical Characterization of the Pyrotechnically Disseminated XM30 Main Gun Signature Simulator
J. Steven Anthony, *Mark V. Haley* and *Sandra A. Thomson,* U.S. Army ECBC; and *Charles L. Crouse*, Geo-Centers, Inc.

Generation, Sampling and Analysis of GB (Sarin) Vapor for Inhalation Toxicology Studies
William Muse*, Steven Anthony, Leonard Buettner, Charles Crouse, Lee Crouse, Robert Mioduszewski* and *Sandra Thomson*, U.S. Army SBCCOM

Toxicity and Treatment of Russian V-Agent (VR) Intoxication in Guinea Pigs
Irwin Koplovitz, Michael Shutz, Susan Schulz and Roy Railer, USAMRICD

-Low Dose-

The Potential Neurotoxic Effects of Low-Dose Sarin Exposure in a Guinea Pig Model
Melinda R. Roberson*, Michelle B. Schmidt, SSG Mary D. Gonzales* and *John H. McDonough, Jr.,* USAMRICD

Medical Chemical and Biological Defense Research

Presented to the

Scientific Conference on Chemical and Biological Defense Research

6 March 2001

Carol D. Linden, Ph.D.

Research Area Director

Medical Chemical & Biological Defense Research Program

(301) 619-7439/ DSN 343-7439

carol.linden@det.amedd.army.mil

Medical Chemical/Biological Defense Rationale for Investment

- *...the threat or use of NBC weapons is "a likely condition of future warfare."* **Quadrennial Defense Review (May 1997)**
- **Direct payoff of chemical/biological defense R&D:** Reduction, even elimination, of casualties which would otherwise follow a CW/BW attack.
- **Indirect payoffs:** Effective products against CW/BW deter employment and proliferation of CW/BW capabilities.
- **Efforts address Joint Service/CINC requirements**

Medical Chemical and Biological Defense Research Program Mission

- Provide medical solutions for military requirements to protect and sustain the force in a Chemical and/or Biological Warfare environment

MCBDRP Vision

- **To Preserve Total Warfighter Effectiveness on a CW/BW Battlefield**
  - Prevent casualties
  - Provide effective treatment of casualties for rapid return to duty
  - Provide rapid, far-forward diagnosis of CW/BW disease

Protecting Warfighters Through Integration and Teamwork

Intelligence
- Agent
- Delivery System
- Organization
- Time

Education & Training
- Military and Civilian Health Care Providers
- Electronic Communication
- Distance Learning

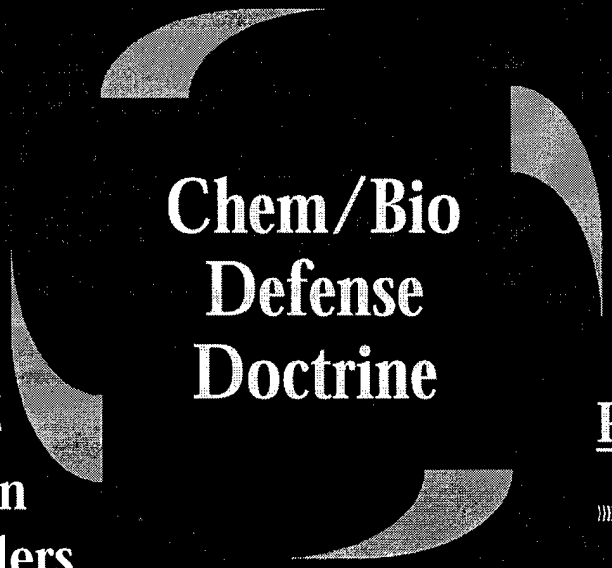

Medical Countermeasures
- Vaccines & Prophylaxes
- Diagnostics
- Therapeutics

Physical Countermeasures
- Detection
- Physical Protection
- Decontamination

Product Development Overview

Acquisition of Products for Future Warfighters
Soldier, Biological and Chemical Command
JPO-BD/JVAP
Other Commodity Area Managers

Medical Products for Chemical Agents

Medical Products for Biological Agents

USAMMDA

6.4 - 6.5 Advanced Development

JPO-JVAP

6.3 Concept Exploration

6.2 Applied Research

6.1 Basic Research

The "Tech Base" Products

- Basic Research Discoveries (Scientific Knowledge)
- Model Development for Agents of DoD Interest
- Vaccine/pretreatment Candidates
- Therapeutic Candidates
- Diagnostic Tests and Reagents
- Information
- Education
- Expertise & Consultation
- Technology Watch

Tech Base

Our Readiness Posture For Meeting Future Threats And Avoiding Technological Surprise

Medical Biological Defense

- Technical Approach:
  - Identify mechanisms involved in disease process.
  - Develop and evaluate products (vaccines or drugs) to prevent or counter effects of biological toxins, bacteria, and viruses.
  - Develop methods to measure effectiveness of medical countermeasures in animal models which are predictive of human response.
  - Develop diagnostic systems and reagents.

Medical Biological Defense Organizational Taxonomy

MEDICAL BIOLOGICAL DEFENSE

Medical Countermeasures (MC) against BW Agents

DTO Efforts

- CB.24 MC for Encephalitis Viruses
- CB.25 Multiagent Vaccines for Biological Threat Agents
- CB.26 Common Diagnostic Systems
- CB.31 MC for Brucellae
- CB.32 Needleless Delivery Methods for Recombinant Protein Vaccines
- CB.33 Recombinant Protective Antigen (rPA) Vaccine Candidate
- CB.34 Recombinant Plague Vaccine Candidate

TASK AREAS

- Vaccines
- Therapeutics
- Diagnostics

Medical Biological Defense Transitions

- FY99/00
  - Multivalent (A,B,C,E,F) Recombinant Botulinum Vaccine - MS I
  - Plague (F1-V) Antigen Vaccine - MS 0
  - Recombinant VEE Vaccine - MS 0
- FY01
  - Next Generation Anthrax Vaccine - MS I
  - Plague (F1-V) Antigen Vaccine - MS I
  - Common Diagnostics - MS 0
  - Multiagent Vaccine - MS 0
  - Brucella Vaccine - MS 0
  - Marburg (Filovirus) Vaccine - MS 0

Medical Biological Defense Products in Development (Projected Fielding)

- Q-Fever Vaccine – 2004 ?
- Smallpox Vaccine (Cell Culture Derived) - 2005
- Recombinant Plague Vaccine - 2006
- Venezuelan Equine Encephalitis Vaccine - 2008
- Tularemia Vaccine - 2008
- Recombinant Botulinum Vaccine - 2009
- Brucella Vaccine - 2010

Emerging Medical BD Products

- VEE/EEE/WEE Combined Vaccine
- Staphylococcal Enterotoxins Vaccine
- Ricin Vaccine
- Common Diagnostic System for BD Threats and ID Diseases
- Next Generation Anthrax Vaccine

Medical Biological Defense Investment in the Future

- Countermeasures for Genetically Engineered Microbes
  - Genomic sequencing of BW threat agents to identify and understand virulence factors, toxins and drug resistance genes
- Immunomodulators and Therapies
  - Alternatives to agent-specific vaccines or therapies
- Multiagent Vaccines
  - Alternative to one vaccine for one BW threat agent

Strategic Challenges
Medical Chemical and Biological Defense RDT&E

- Acquisition Model
- FDA Regulations
- Multiplicity of Threats

Strategic Challenges

- **Acquisition Model - Linear**
  - Old DoD 5000
  - New DoD 5000
  - Technology Readiness Levels
  - Risk Reduction
- **Biologicals/Pharmaceuticals – Recursive**
  - Iterative testing of numerous candidates
  - Kill products early
  - Finite lifetime

Integration of DoD Milestones and FDA Licensure Process

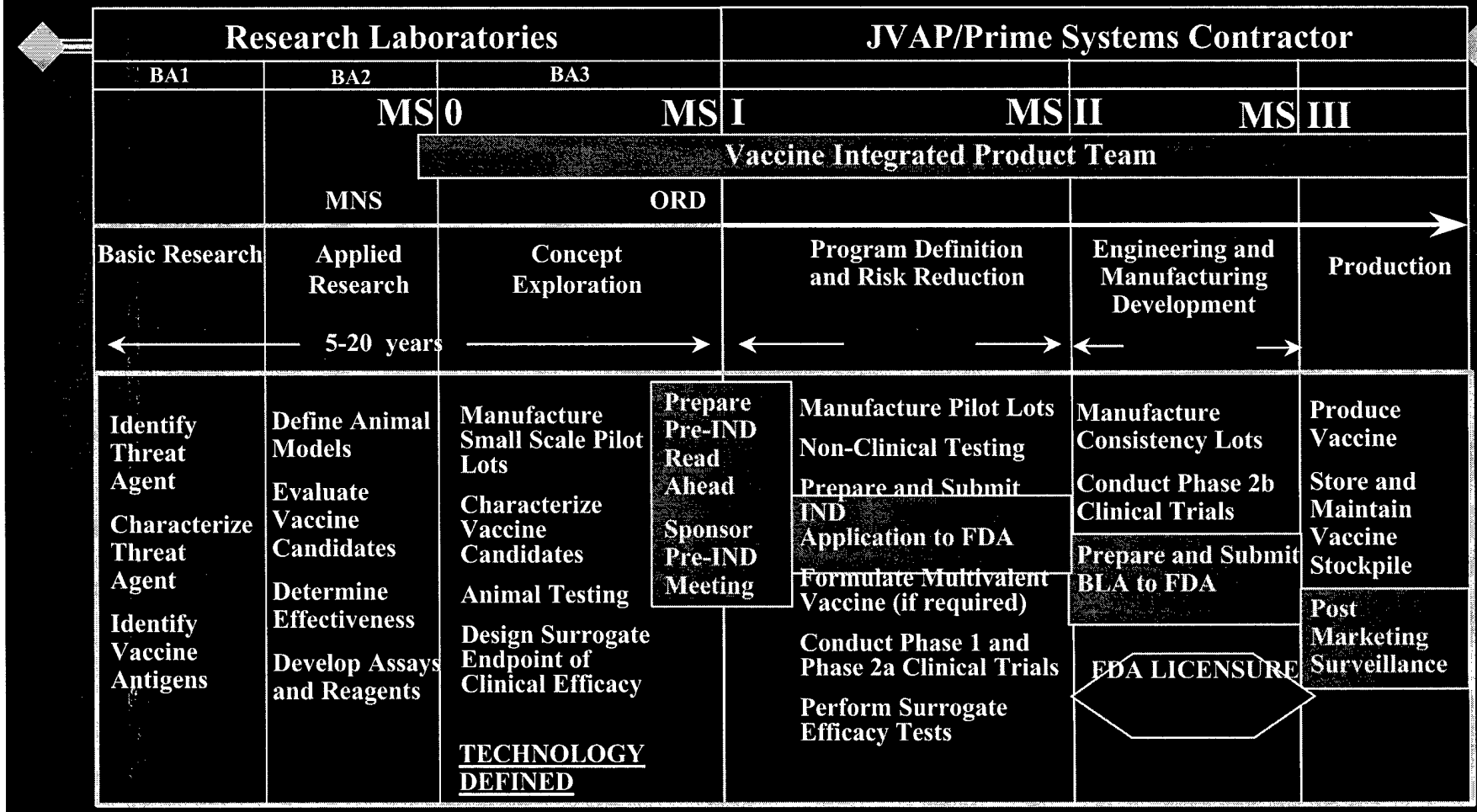

Defense Acquisition Management Framework

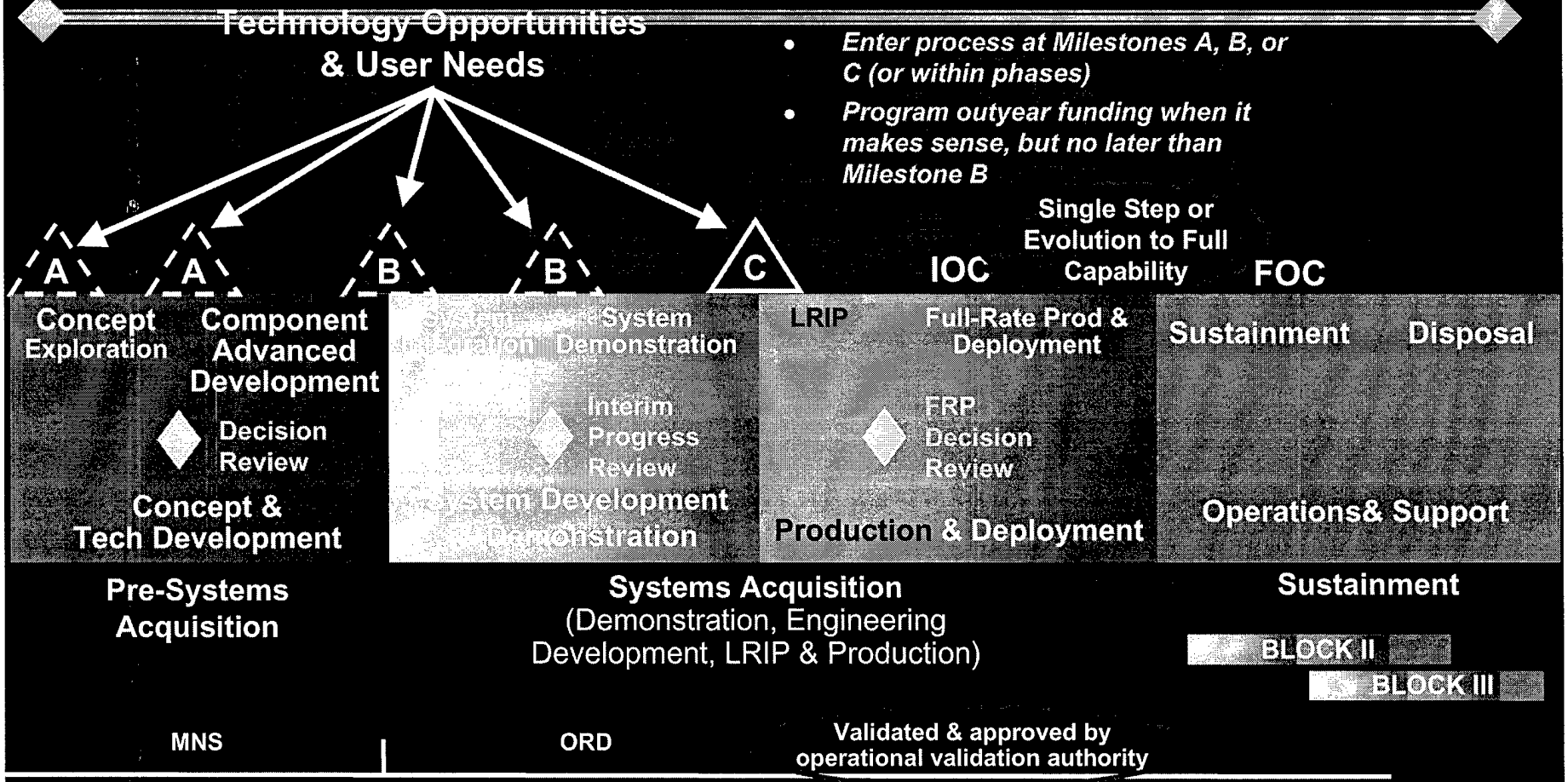

Strategic Challenges

- **FDA Regulatory Requirements**
  - Products must be safe
    - Demonstrate in animals
    - Demonstrate in humans
  - Products must be effective
    - Demonstrate in animals
    - Demonstrate in human clinical studies and field trials
- **Medical Chem/Bio Products – we can:**
  - Demonstrate safety in animals and humans
  - Demonstrate efficacy in animals
  - Estimate efficacy in humans

Strategic Challenges

- Proposed new FDA Rule
  - Allows consideration of animal efficacy studies in support of licensure request
  - Additional requirements
    - Understand mechanisms of action of the disease-causing agent
    - Understand basis of action of the vaccine or drug
    - Demonstrate efficacy in two relevant animal models
    - Identify surrogate markers of efficacy

Strategic Challenges

- **Multiplicity of Threats**
  - Chemical Warfare Agents
    - Nerve agents
    - Mustards
    - Blood/Choking agents
  - Biological Warfare Agents
    - Viruses
    - Bacteria
    - Toxins
  - Emerging Threats

Summary

- Medical chemical and biological defense research presents unique challenges
  - Chemical threat agents
  - Biological threat agents
  - Medical regulatory compliance and DoD acquisition
- We need cutting edge technologies to develop medical countermeasures for the warfighter
  - Biotechnology
  - Informatics
  - Genomics and Proteomics
- Partnerships with the science community & industry are essential
  - CRADAs
  - Contracts

USAMRICD

"Research for the Warfighter"

United States Army Medical Research
Institute of Chemical Defense

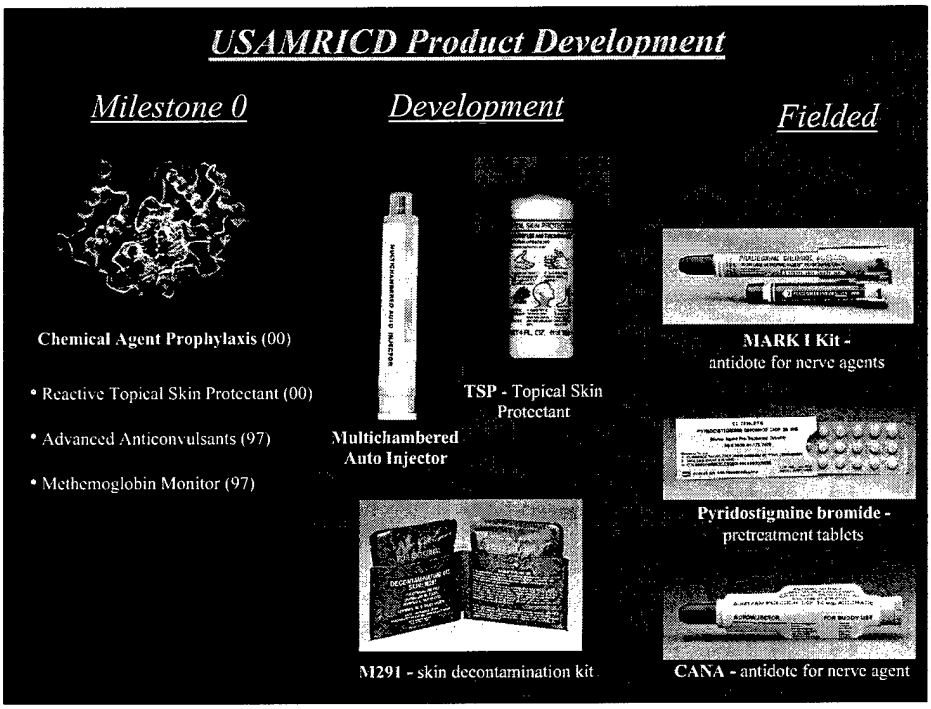

Therefore, based on what we've already fielded and what will be available in the future, we define four research priorities:

(a) Simplify the approach to nerve agent medical protection by scavenging enzymes

(b) Develop a specific countermeasure to HD

(c) Develop and advanced or active TSP

(d) In the short term, build a better mousetrap to anticonvulsants.

Let us look at each of these strategies in turn>

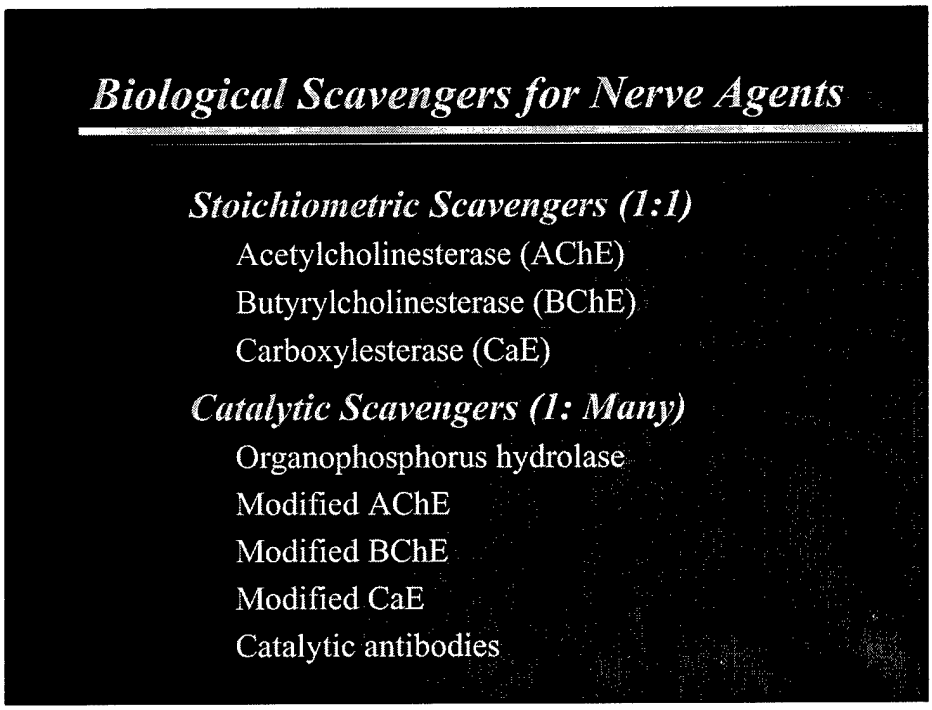

Studies with equine or human BuChE or fetal bovine scrum AChE showed that none of these scavengers exhibited behavioral side effects when given alone to rats or monkeys. Futhermore, each was capable of providing protection against 2 to 16 LD50s of GD, GB or VX depending on the scavenger and the test species.

Candidate bioscavenger proteins, in general, function either by stoichiometricly binding and sequestering the anticholinesterase or by catalytically cleaving the OP substrate into biologically inert products. Enzymes such as cholinesterases (ChEs) and carboxylesterases (CaEs), as well as antibodies specific for nerve agent haptens are stoichiometric. Each of these stoichiometric scavengers has the capacity to bind one or two molecules of nerve agent per molecule of protein scavenger. While this approach has been proven to be effective in laboratory animals, it has the disadvantage that the extent of protection is directly proportinal to the concentration of unexposed, active scavenger in the bloodstream at the time of nerve agent exposure.

Candidate enzymes with *bona fide* catalytic activity against nerve agents include the human organophosphorus acid anhydride hydrolases (OPAHs), such as paraoxonase (hu-Pon). Additionally, the ability to generate catalytic antibodies in response to appropriate transition state analogs (16, 17) suggests that nerve agent-specific antibodies that catalyze hyrolysis of their ligands could be effective bioscavengers. Finally, the ability to engineer site-specific amino acod mutations into naturally occurring scavenger enzymes can allow investigators to alter the binding and/or catalytic activities of these anzymes. In general, the use of scavengers with catalytic activity would be advantageous because small amounts of enzyme, meaning lower concentrations in circulation, would be sufficient to detoxify both large amounts of nerve agent.

Defense Technology Objective (DTO)

Chemical Agent Prophylaxes

Develop countermeasures that provide protection against CW agents without operationally significant side effects.

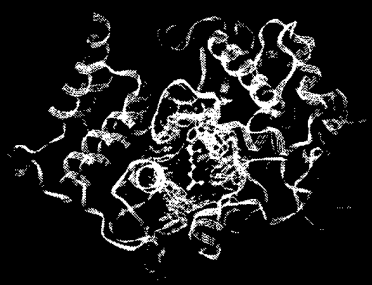

Accomplishments:

- AChE and BuChE
- Organophosphorus anhydride hydrolase
- Human BuChE
- Human carboxylesterase
- Met Milestone 0 (Feb 00)

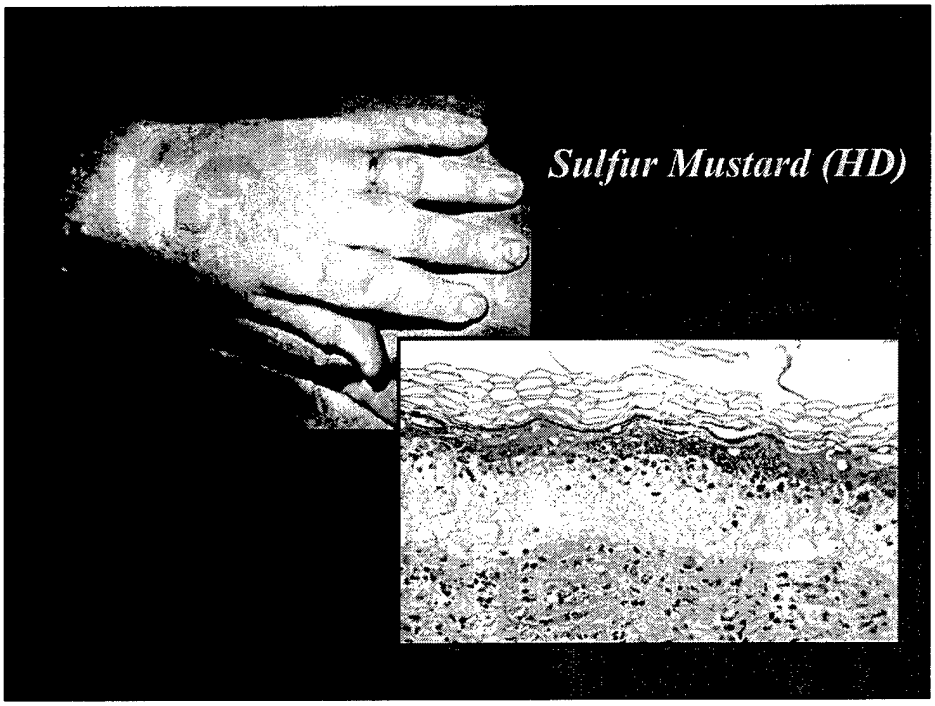

Several challenges present themselves here:

(1) No new human data

(2) Understanding of the mechanism of injury

(3) "high-fidelity" animal or other model

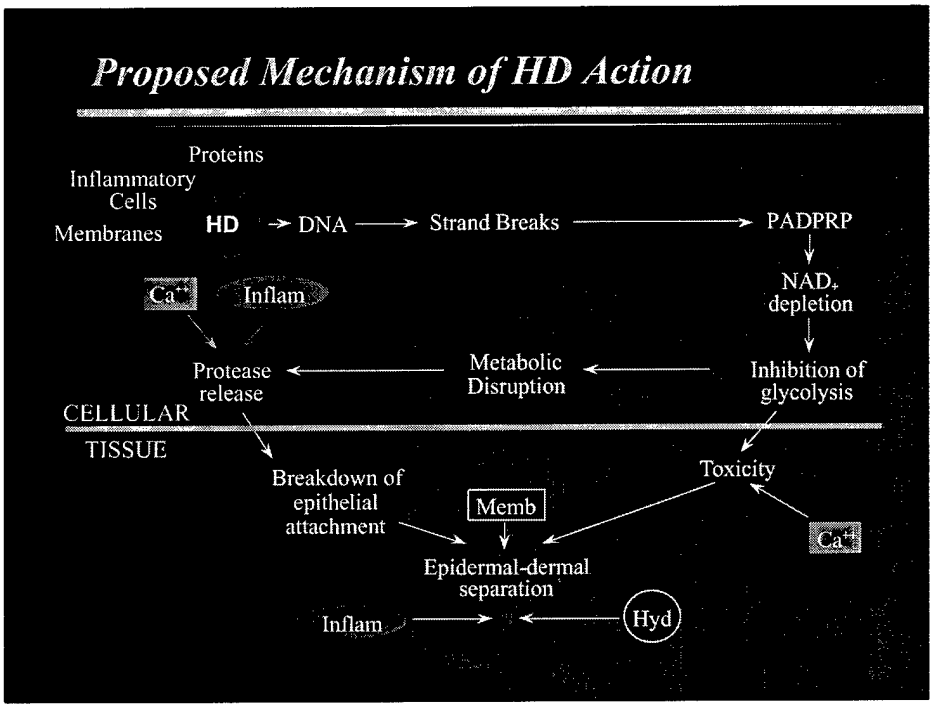

The cellular and tissue alterations induced by HD that are proposed to result in blister formation. HD can have many direct effects such as alkylation of proteins and membrane components (Memb) as well as activation of inflammatory cells. One of the main macromolecular targets is DNA with subsequent activation of PADP ribose. Activation of PARP can initiate a series of metabolic changes culminating in protease activation. Within the tissue, the penultimate event is the epidermal-dermal separation that occurs in the lamina lucida of the basement membrane zone. Accompanied by a major inflammatory response and changes in the tissue hydrodynamics(Hyd), fluid fills the cavity formed at this cleavage plane and presents as a blsiter.

The first breakthrough in HD by USAMRICD and its extramural collaborators was the development of a model. From this research, we were able to construct a schema of the major events of the pathological processes documented in cells and tissues exposed to HD. This schema was presented at numerous DoD and professional scientific forums, including the 20th Army Science Conference. The research findings of this program served as the core of a NATO sponsored monograph on HD research.

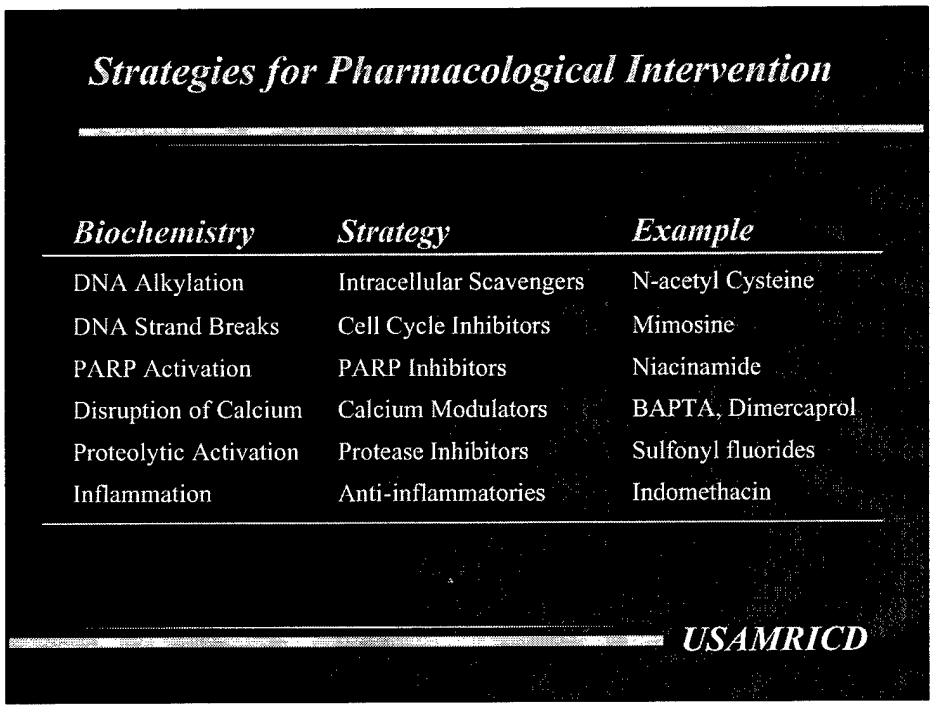

Over 500 candidate prophylactic compounds have been evaluated through the antivesicant DTN. Sixty-two compounds have demonstrated an ability to provide significant modulation of edema and/or histopathology caused by HD *in vivo*. Of these 62 compounds, nineteen have demonstrated at least 50% protection against the pathological indicators of mustard injury (Table 2). All of these 19 successful candidates fall into four of our six original proposed strategies: anti-inflammatories (7), antiproteases (3), scavengers (6), or PARP inhibitors (3).

An intermural partner often provided major injectors in each of these areas, e.g.

Prtease Inhibitors	Georgia Tech	Povers
Information	P&G, Dupont	Several PIs
PARP	Parke-Davis & others, Georgetown	Smulson
Scavenger	Porton, UTA	Ternay

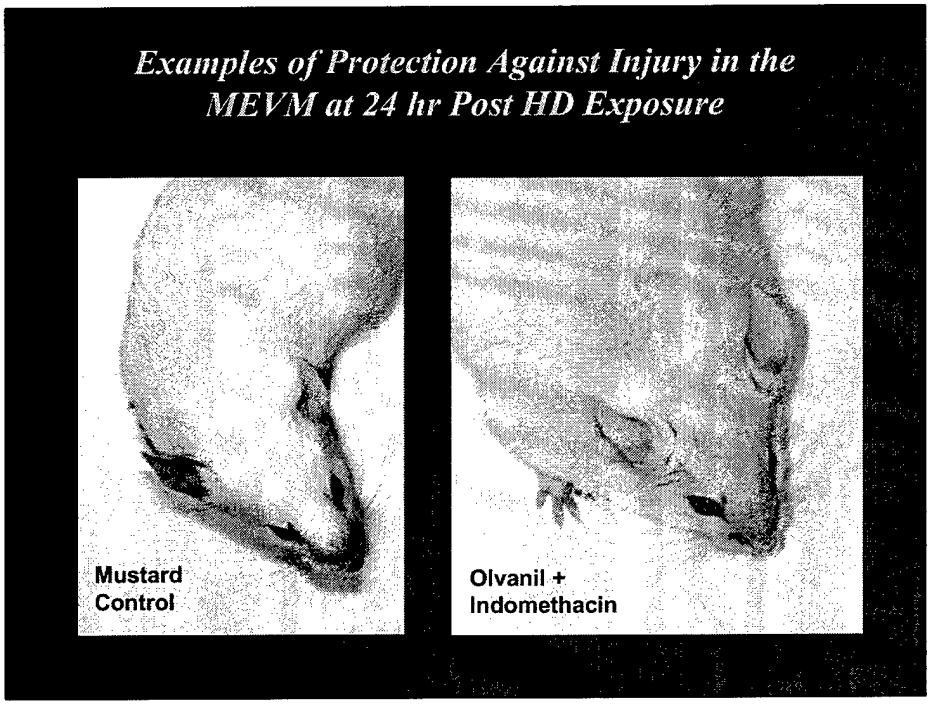

To show you how well our leading candiate antivesicant compounds work, we show here mice exposed to sulfur mustard as well as exposed mice treated with antivesicants. It is easy to see that the ears of treated mice look relatively normal compared to untreated mice.

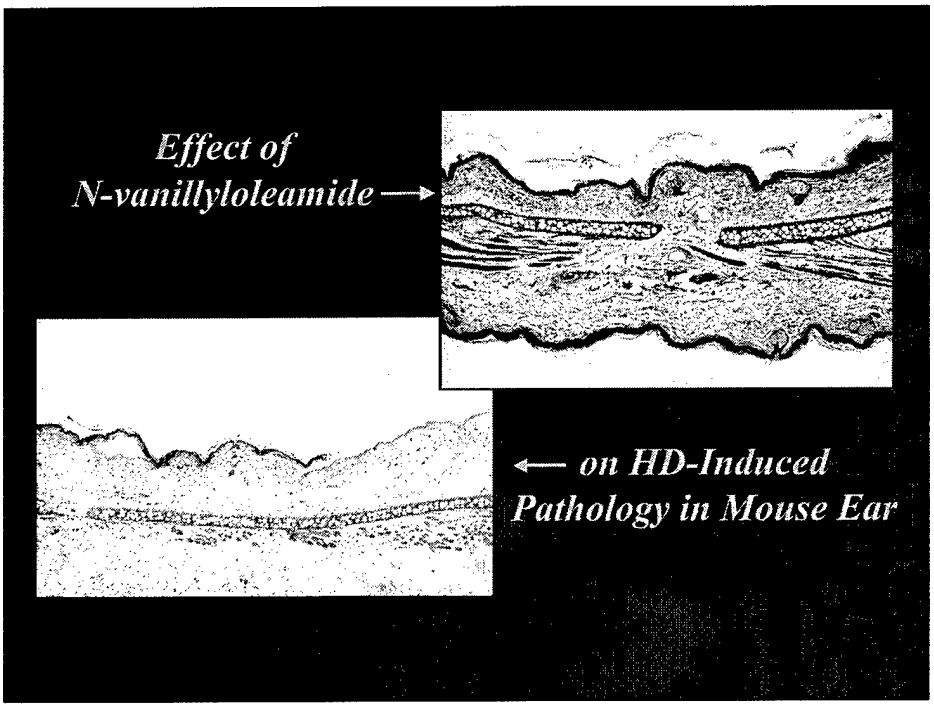

The findings of wet weight changes in mouse ear are corroborated histopathologically.

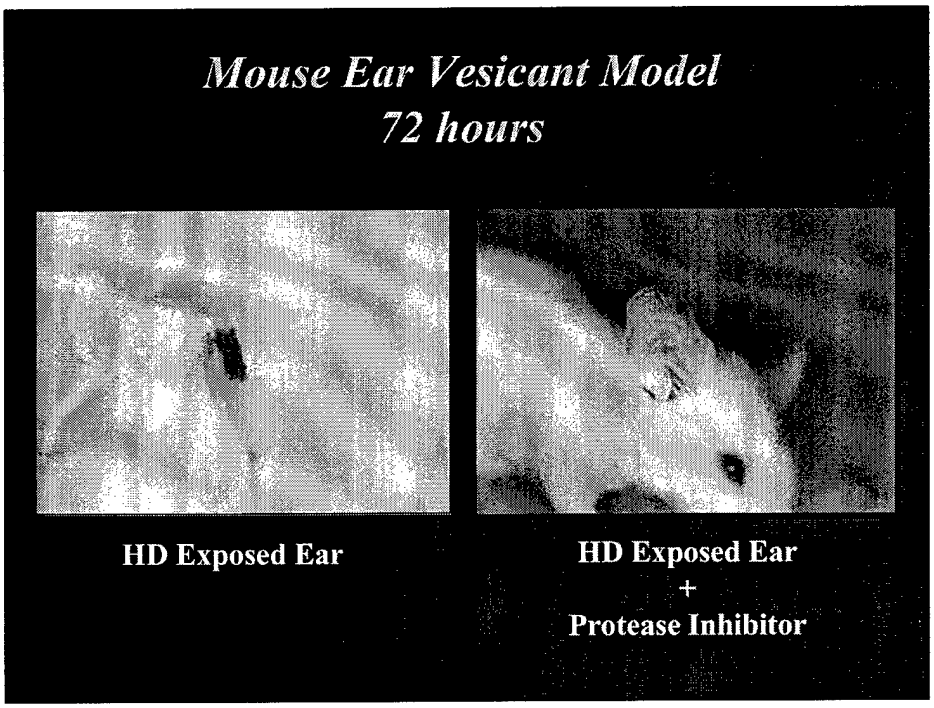

Protease inhibitors		
1-(40-aminophenyl)-3-(4-chlorophenyl) urea	1883	54%
N-(O-P)-L-Ala-L-Ala-benzy ester hydrate	2780	62%
Ethvl p-Guanidino Benzoate Hydrochloride	1578	62%

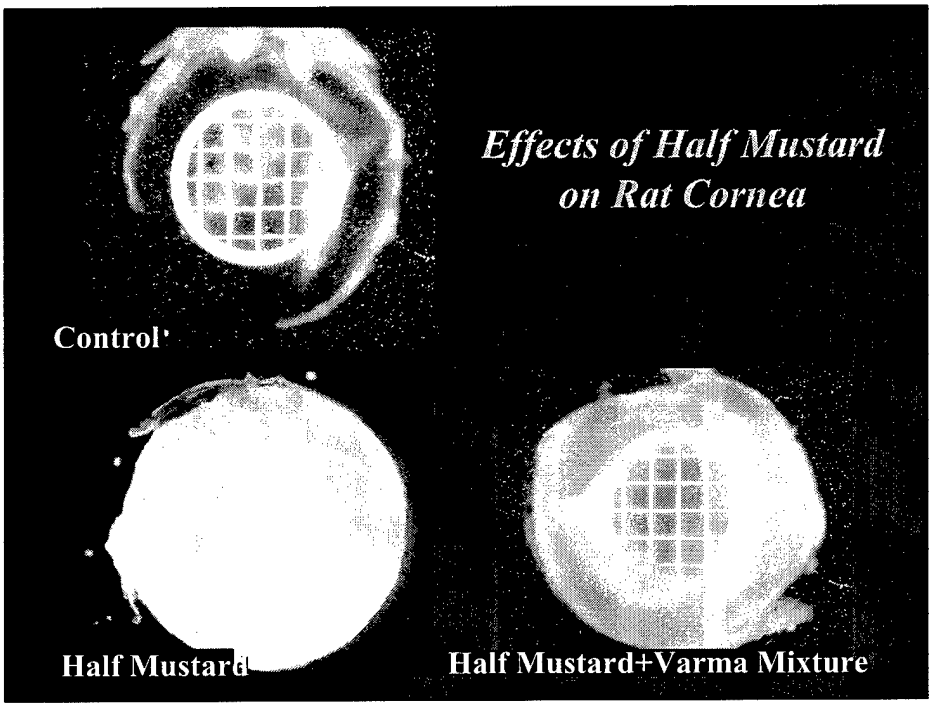
Effects of Half Mustard
on Rat Cornea
Control
Half Mustard
Half Mustard+Varma Mixture

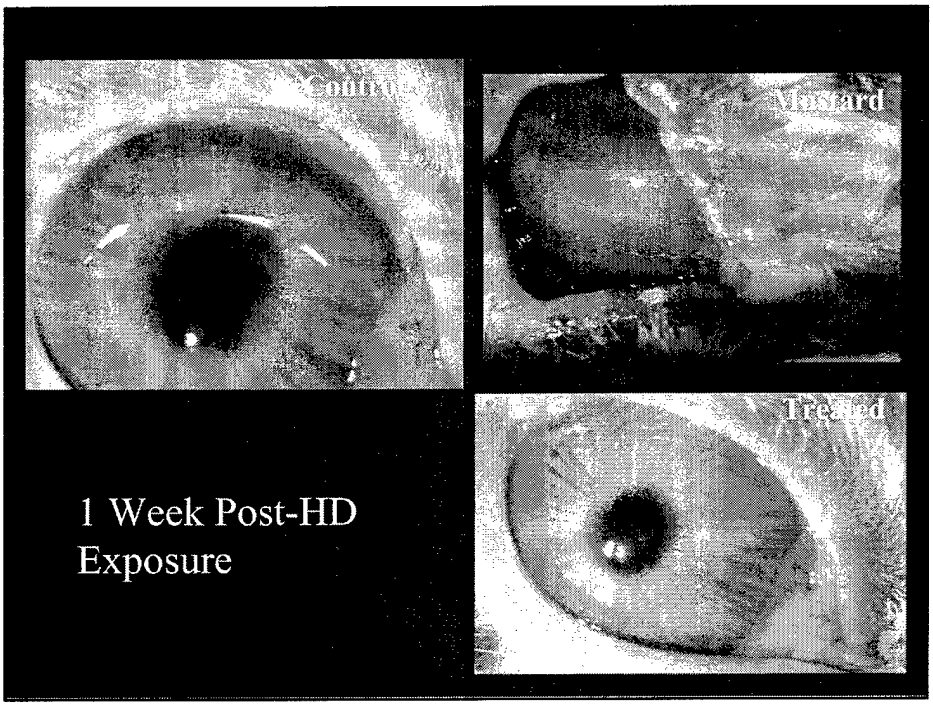

In this study we explored the use of two FDA approved medications (triamcinolone and cefazolin) as treatments for sulfur mustard injury. Female NewZealand White rabbits were divided into 5 groups: naïve controls (n=6), HD positive controls (n=14) and 3 treatment groups. Treatment groups received subtenons injection(s) of a combination of 20 mg triamcinolone and 15 mg cefazolin. Treatment group 1 (n=5) received a single injection 10 min after HD exposure. Treatment group 2 (n=6) received an injection 10 min after HD exposure plus a second injection 7 days later. Treatment group 3 (n=6) received an injection 10 min after HD exposure, a second injection 7 days later and a third injection 7 days after the second. Rabbits were observed for a total of 19 weeks after HD exposure. Pachymetry (cornea thickness) data and the presence or absence of neovascularization were recorded weekly for 6 consecutive weeks and then on weeks 15 and 19 post-exposure. Results show that a triamcinolone /cefazolin combination treatment is extremely effective in treating corneal injury from liquid HD exposure.

IMPACT - Vesicant Agent

Defense and Technology Objective (DTO)

Reactive Topical Skin Protectant Decontaminant

Demonstrate safety and efficacy of a reactive topical skin protectant

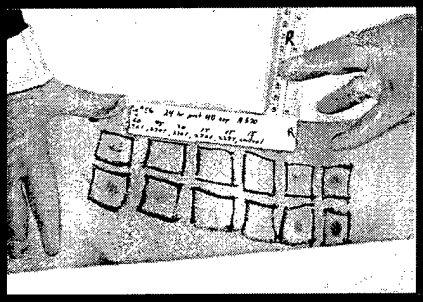

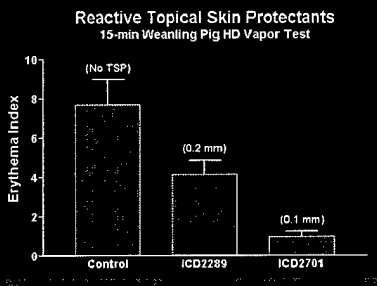

Accomplishments:

- Developed a TSP (NDA,Feb 00),
- Effective against HD, GD, TGD, VX, CS, T_2 and poison ivy toxins
- Identified reactive moieties
- rTSP provides significantly improved protection
- Met Milestone 0 (Feb 00)

Science and Technology Objective (STO)

Advanced Anticonvulsant

Demonstrate safety and efficacy for an advanced anticonvulsant

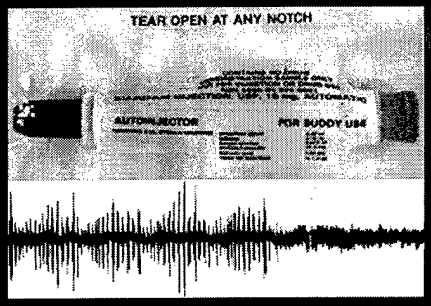

Accomplishments:

- Determined diazepam dose in NHP
- Identified compounds superior to diazepam
- Identified optimal treatment
- Milestone I
- Currently evaluating in NHP

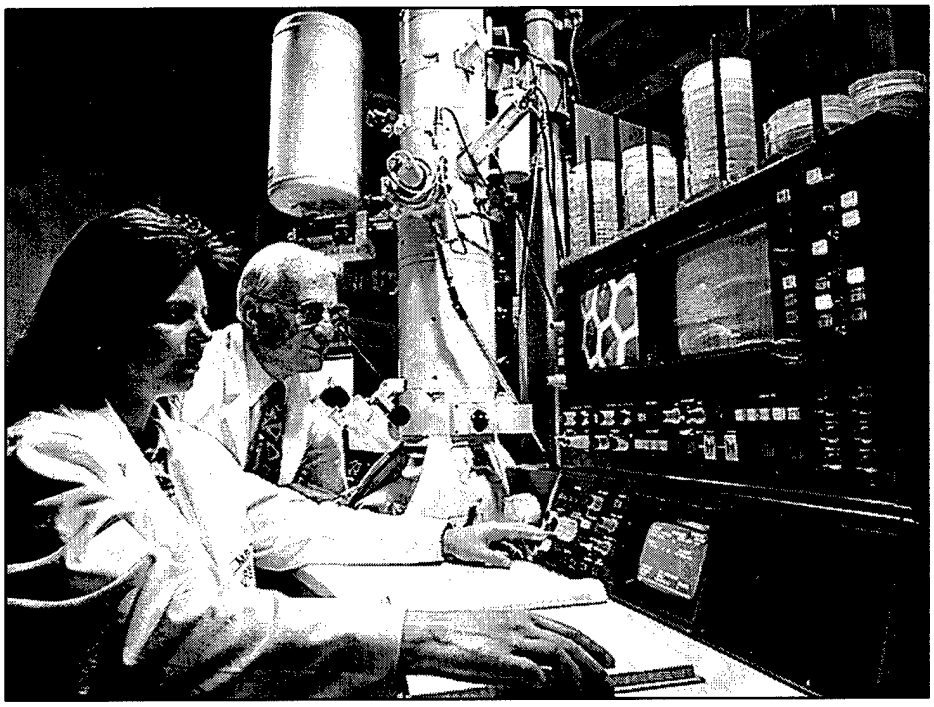

USAMRICD

"Research for the Warfighter"

United States Army Medical Research
Institute of Chemical Defense

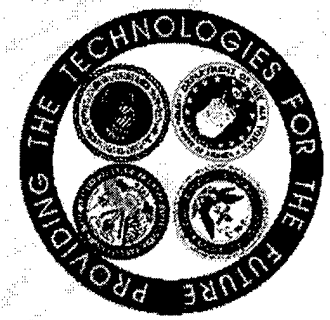

CHEMICAL BIOLOGICAL DEFENSE CONFERENCE

Dr. RAYMOND A. MACKAY
DIRECTOR
RESEARCH AND TECHNOLOGY DIRECTORATE

DoD Non-Med Tech Base Process

Joint Science and Technology Panel for Chemical / Biological Defense

- Addresses all phases of research in five commodity areas (modeling/simulation, detection, individual protection, collective protection, decontamination)
- Executed by Principal Investigators within Service labs
- Utilizes proposal-driven process focused by user-developed desired operational capabilities
- Responsive to development/acquisition program
- Managed as fully Joint Services program

Management Structure

Joint Science and Technology Panel for Chemical / Biological Defense

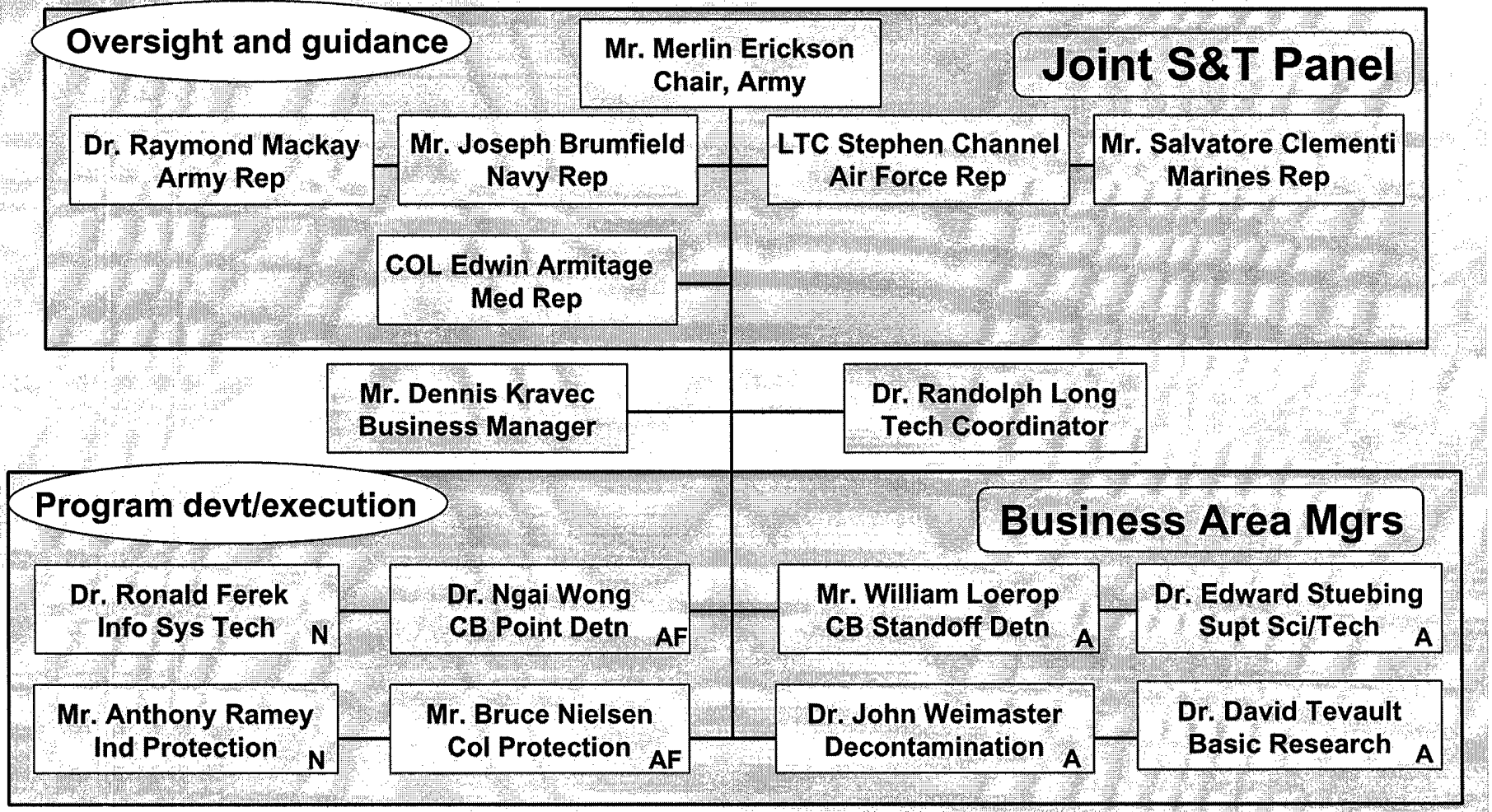

Joint Future Operational Capabilities Ranking: Driver for Investment

Joint Science and Technology Panel for Chemical / Biological Defense

1 BatMgt - Battle Management Systems	11 ConAvoid – Sensor Integration
2 ConAvoid - Biological Early Warning	12 Restore – Medical Diagnosis
3 BatMgt - Battle Analysis	13 ColProt – Mobile Applications
4 ConAvoid – Chemical Early Warning	14 Restore – Medical Treatment
5 BatMgt – Modeling & Simulations Training	15 ConAvoid – Radiological Early Warning
6 IndProt – Medical Prophylaxes	16 Restore – Equipment/Facilities/Large
7 ConAvoid – Biological Point Detection	17 Restore - Logistics
8 IndProt – Respiration & Percutaneous	18 ColProt – Fixed Site Applications
9 ConAvoid – Med Surveillance/ Vet Support	19 ConAvoid – Radiological Point Detection
10 ConAvoid – Chemical Point Detection	20 Restore – Personnel/Patient Decon

Non-Med CB Defense Program Taxonomy

Joint Science and Technology Panel for Chemical / Biological Defense

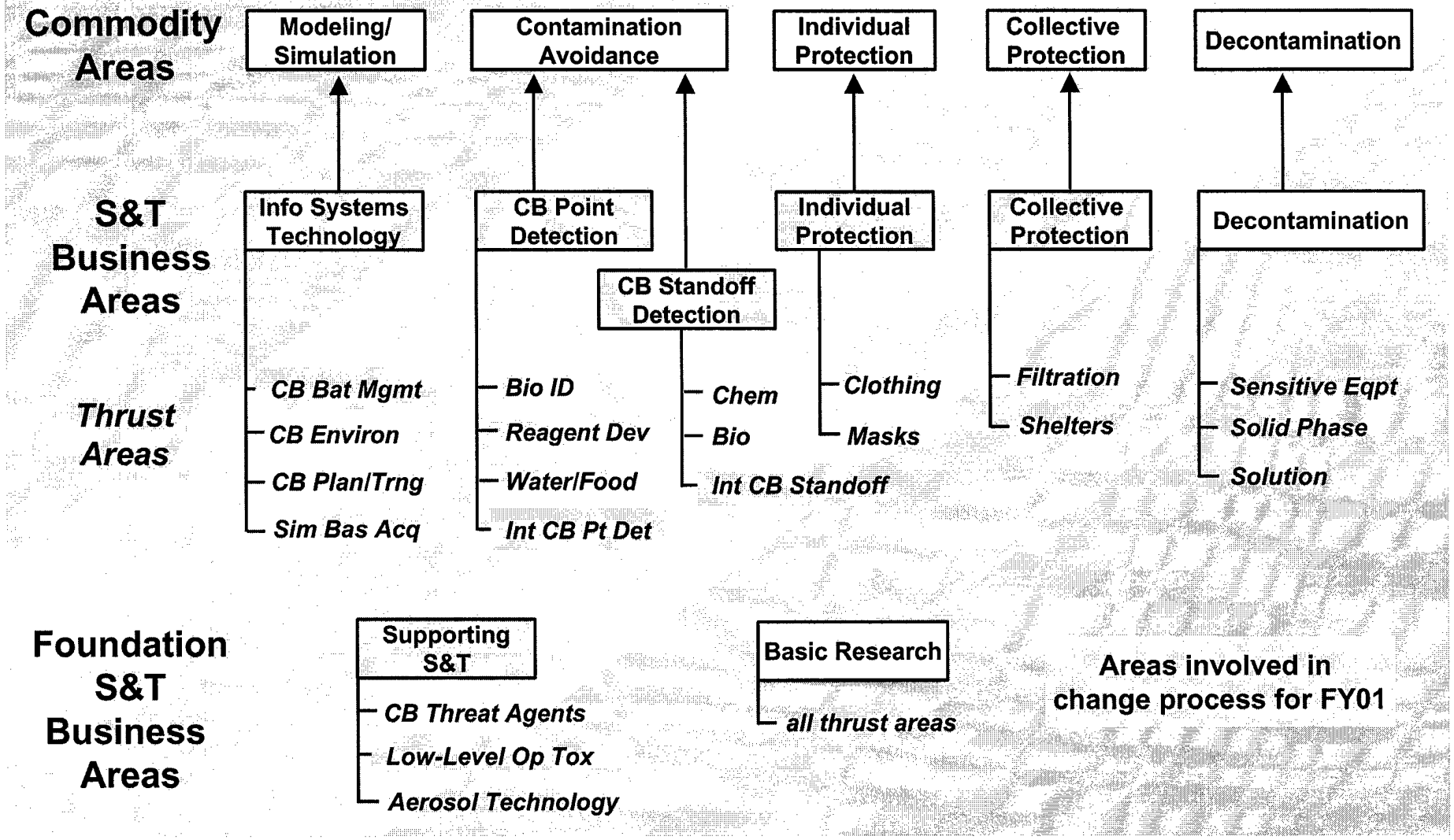

Near-Term Fielded vs Far Term Desired: An Example of the User's Challenge to S&T

Joint Science and Technology Panel for Chemical / Biological Defense

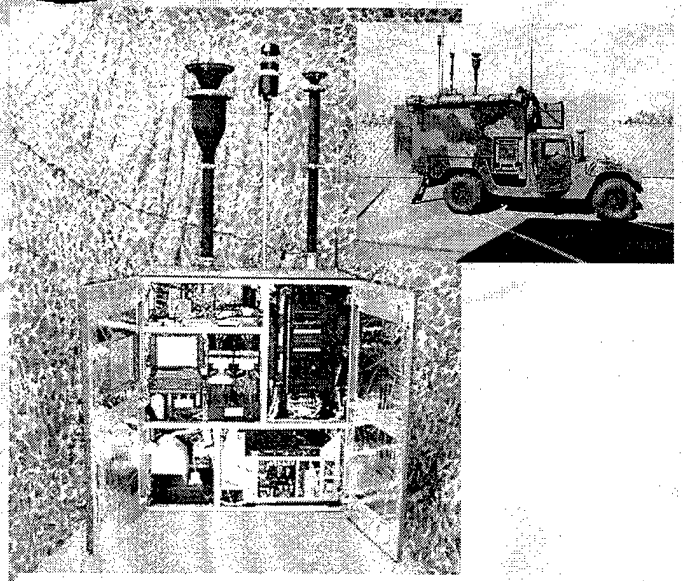

Joint Bio Point Detn System

- Fully Automated
- 12 Hour Continuous Operations
- 10 Agent ID within Minutes of Detection
- Sample Isolation
- < 30 Minute Set-up

Three years

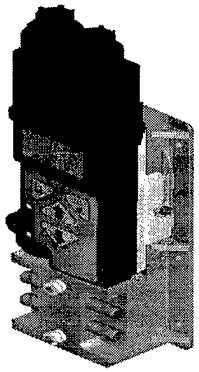

Joint Chem Agent Detector

- Hand size
- Miosis level detn of blister, nerve, blood
- Records dose
- Networked, remotely controlled

Twelve years

Joint Modular CB Detector

- Hand size (40 cu in)
- Identifies chemical agents
- Detects bio agents
- Networked

Information Systems Technology
Thrust Areas

Joint Science and Technology Panel for Chemical / Biological Defense

- ❖ New thrust area for FY01-02
- ❖ Sub-thrusts include
  - ➢ Sensor integration
  - ➢ Information management
  - ➢ Data fusion
  - ➢ Communications interfaces
  - ➢ Visualization approaches
- ▪ Panel of experts meeting is planned to refine/develop program objectives

- ➢ Disparate sensors – non-CB sensors that can provide info on CB events

FY01 activities:

6.2: Survey, characterize available potential sensors, e.g., acoustic, seismic sensors, FLIRs

6.3: Conduct field evaluation of radar as standoff CB event cueing device as well as sensors identified in 6.2; joint with PM-NBC

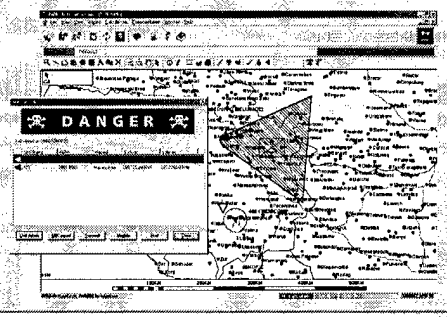

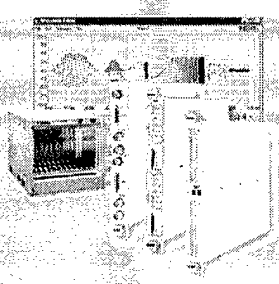

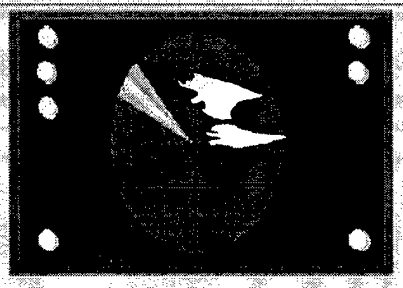

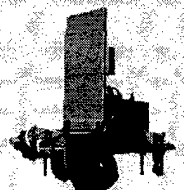

Q36/Q37

Information Systems Technology
Thrust Areas

Joint Science and Technology Panel for Chemical / Biological Defense

CBW Environment

Objective: Models to track evolution of CB threats from vapor, liquid, and solid agents across range of scales from individual to theater

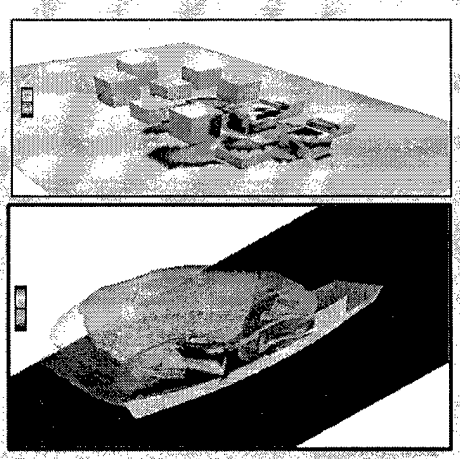

CBW-CFX Model

CB Planning/Analysis

Objectives: Models to describe effects of CBW on operations

Simulation Based Acquisition

Objective: Models supporting development of CBD equipment

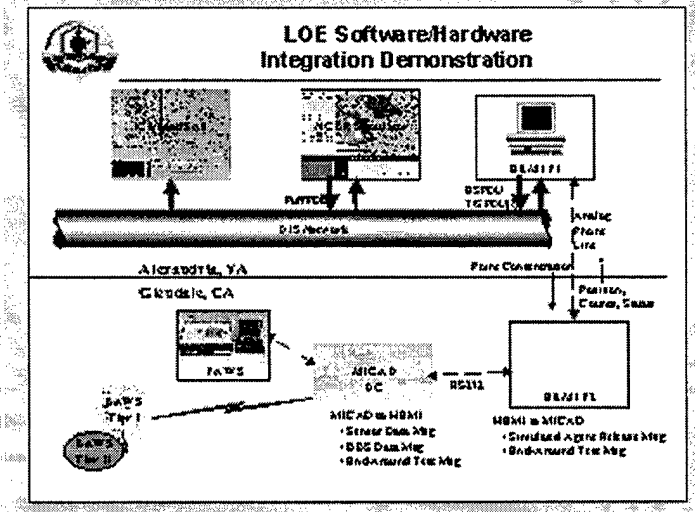

CB Point Detection
Thrust Areas

Joint Science and Technology Panel for Chemical / Biological Defense

Biological Identification

Objectives: Develop fully automated sample prep and analysis systems for unattended monitoring of air samples; transition FY02 to JBPDS

Challenges:
- **fluidics**
- **biomarker extraction/cleanup**
- **background interference**

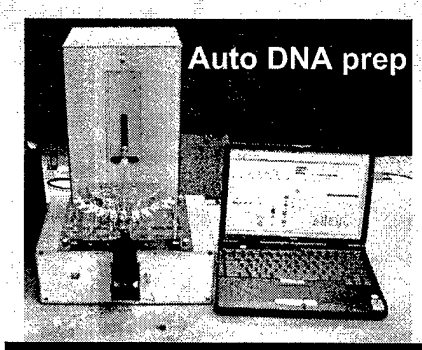

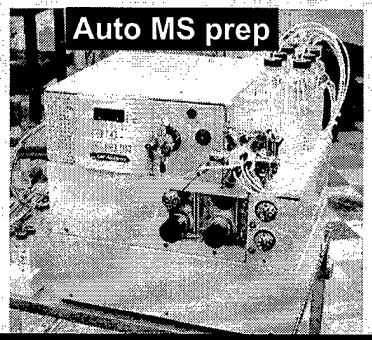

❖ ***Demonstrated detection of mass and genetic markers at JPBDS requirement levels; built 2 cu ft breadboards***

Reagent Development

Objectives: Develop improved reagent candidates for implementation in fielded and developmental identifiers via Critical Reagent Program

Challenges:
- **specificity**
- **shelf life**
- **reproducibility**

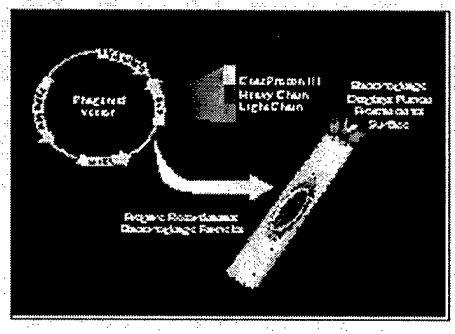

❖ ***Demonstrated improved sensitivity of recombinant antibodies vs available monoclonals; initiated assessment of combinatorial peptide***

CB Point Detection
Thrust Areas

Joint Science and Technology Panel for Chemical / Biological Defense

Detection in Water/Food

Objectives: Provide the capability to detect, identify, and quantify chemical and biological contamination in potable water

Challenges:
- **Non-traditional threat environment**
- **Immature technologies**
- **Sampling low level toxics**

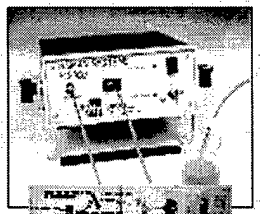

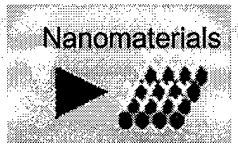

❖ ***Model technology downselect process utilized fair assessment of technology candidates from all sources***

Supporting Studies

Objectives: Assemble database of available ambient background data and analyze for key heuristics

Challenges:
- **multiple sources of data**
- **disparities in collection parameters**

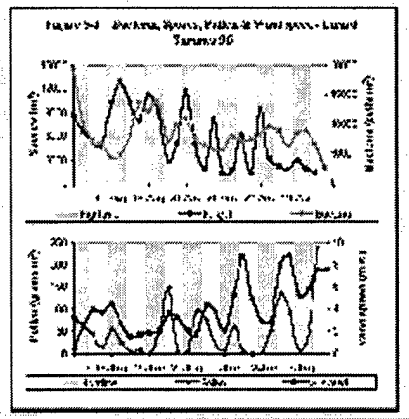

❖ ***Established joint DoD/DOE/TTCP website; data loading and analysis in process***

CB Point Detection
Thrust Areas

Joint Science and Technology Panel for Chemical / Biological Defense

Integrated Chem Bio Point Detectors

Objectives: Develop small, hand-size detectors to identify chemical agents and detect/discriminate biological agents

Challenges:

- Miniaturization of detector technologies
- Small, efficient air samplers
- Simultaneous optimization of size, selectivity, and sensitivity

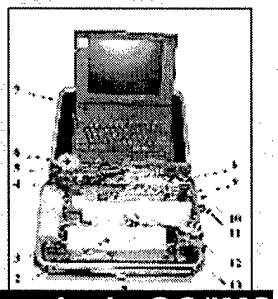

Pyrolysis-GC/IMS

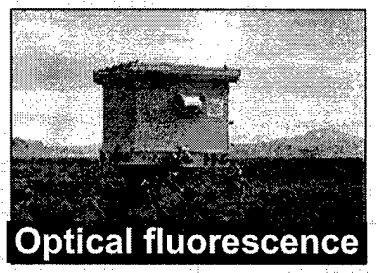

Optical fluorescence

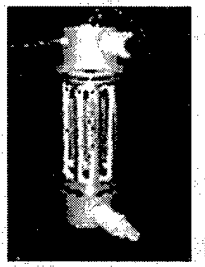

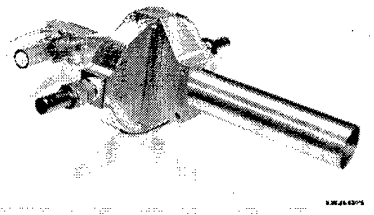

❖ *Py-GC/IMS demonstrated high detection probability and sensitivity relative to other candidates at JFT-6*

❖ *Air samplers evolving to smaller size with increased efficiency*

CB Standoff Detection
Thrust Areas

Joint Science and Technology Panel for Chemical / Biological Defense

Chemical Standoff Detection

Objectives: Develop and demonstrate passive and active concepts for remote detection, identification, ranging, and mapping of chemical clouds in all physical forms

Challenges:
- High speed interferometry; focal plane arrays
- Rapid data processing, software
- Laser technology to reduce size, weight of active systems

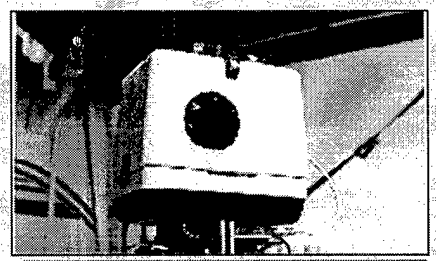

Chemical Imaging Sensor

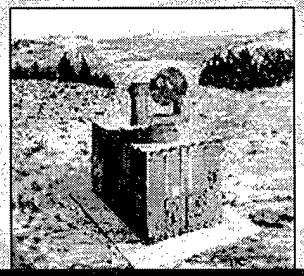

JS Warning ID Lidar

❖ *Demonstrated 100 scan/sec operation in field with 9-pixel array passive CIS spectrometer*

Bio Standoff Detection

Objectives: Develop and demonstrate concepts for remote detection, identification, ranging, and mapping of biological particulate clouds

Challenges:
- Laser technology to reduce size, weight of active systems
- Rapid data processing, software
- Spectroscopic technologies to enhance potential for classification

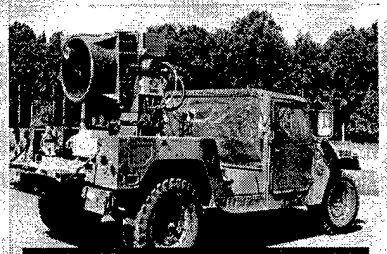

Short-range BSDS

❖ *Initiated panel of experts to develop and down-select concepts for exploration under Bio Standoff DTO*

CB Standoff Detection
Thrust Areas

Joint Science and Technology Panel for Chemical / Biological Defense

Integrated CB Standoff Detection

Objectives: Develop and demonstrate concepts for remote detection, identification, ranging, and mapping of chemical and biological clouds in all physical forms with a single sensor platform

Challenges:
- Laser technology to reduce size, weight of active systems
- Significant advances in spectroscopy
- Rapid data processing, software

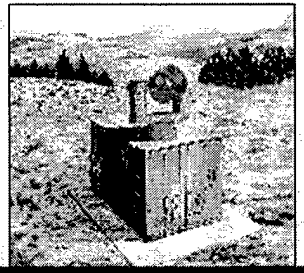

JS Warning ID Lidar

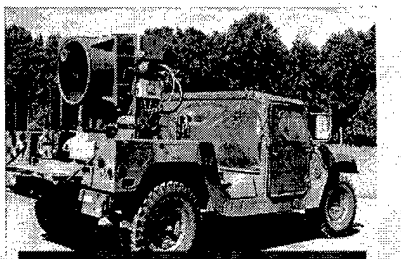

Short-range BSDS

Merge capabilities into a single small platform

?

Individual Protection
Thrust Areas

Joint Science and Technology Panel for Chemical / Biological Defense

Clothing

Objectives: Develop overgarments against CB agents that provide increased protection with decreased impediment of wearer's performance

Challenges:

- **Selectively permeable materials**
- **Interface of SPMs with garment fabric**
- **Testing**

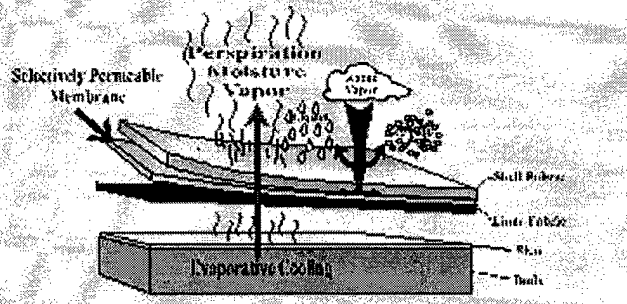

❖ Developed and demonstrated two SPM garments that outperform all fielded garments and are 50% lighter

Masks

Objectives: Demonstrate concepts that enhance respiratory and head protection against CB agents

Challenges:

- **Adsorbent materials**
- **End-of-service life indication**
- **TICs/TIMs**

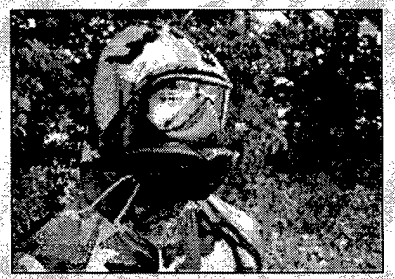

❖ Met or exceeded all JSGPM filter goals

Collective Protection
Thrust Areas

Joint Science and Technology Panel for Chemical / Biological Defense

Filtration

Objectives: Develop filtration approaches that reduce frequency of filter changes and are applicable to all toxic materials

Challenges:

- **residual life indicators**
- **filter regeneration**
- **biological filtration**

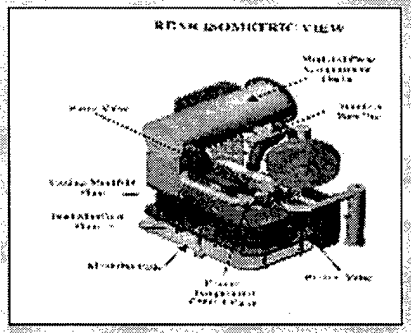

❖ *Completed evaluation of filter adsorbents against TICs*

Shelters

Objectives: Develop collective protection shelters with improved environmental isolation against threats from CB and toxic materials

Challenges:

- **Hermetic seals**
- **Rapid deployment**

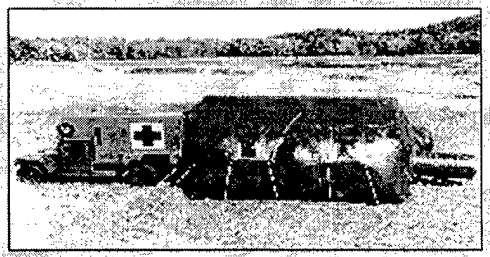

❖ *Transiitoned low cost tentage effort to JTCOPS*

Decontamination
Thrust Areas

Joint Science and Technology Panel for Chemical / Biological Defense

Sensitive Equipment

Objectives: Decontaminate sensitive equipment, interiors of combat vehicles and aircraft, and interiors on the move.

Challenges:
- **Identify freon alternatives**
- **Material compatibility**
- **Man-portable, on-the-move decon**
- **Agent destruction following removal**

❖ *Conducted technology assessment and identified leading candidates for JSSED program. Identified hydrofluoroether as freon alternative.*

Solid Phase

Objectives: Investigate and validate cost effective deactivation and destruction of CW agents rapidly by solid matrices. Extend technology to areas beyond sorbent decon.

Challenges:
- **Mass transfer constraints**
- **Enhance chemical reactivity**

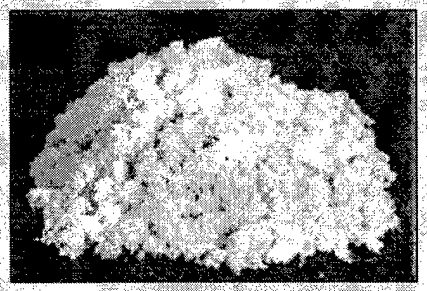

❖ *Measured kinetics of VX, GD, and HD on nanosize calcium oxide and aluminum oxide. Autocatalytic for HD elimination process.*

Decontamination
Thrust Areas

Joint Science and Technology Panel for Chemical / Biological Defense

Solution Chemistry

Objectives: Develop decon systems that supplement or replace existing systems used for immediate, operational and thorough decon and to replace DS2 and aqueous bleach in thorough decon applications.

Challenges:
- Optimize chemistry - co-solvents
- Stabilize the system
- Peroxide logistic issue

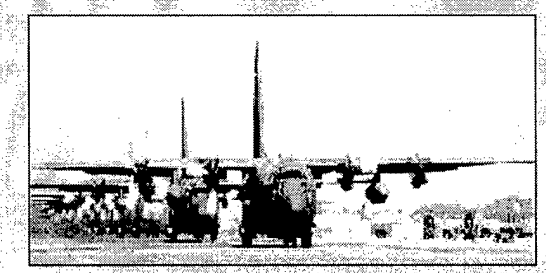

❖ *Candidate formulations have been identified that react rapidly and effectively for HD, GD, and VX.*

Enzyme Reactants

Objectives: Develop and demonstrate a new generation of CB warfare agent decontaminants that are non-toxic, non-corrosive, non-flammable, environ. safe and lightweight.

Sub-thrust to solution chemistry

Challenges:
- Identify appropriate enzymes
- Genetic engineering needed for large scale production
- Maintenance of catalytic activity

❖ *Increased activity on enzymes with activity for V-agents by 10-fold over baseline. Identified materials technology approach to destroy H-agents.*

Supporting Science and Technology
Thrust Areas

Joint Science and Technology Panel for Chemical / Biological Defense

Threat Agents

Objectives: Maintain awareness of evolving threat agent materials and conduct R&D studies to validate and characterize, and to assess fate of CB materials in environment

Challenges:

- ever expanding array of threats
- infrastructure issues
- identification of adequate simulants

VX (US)

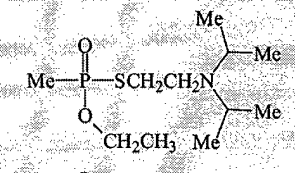

R-33 (Russian)

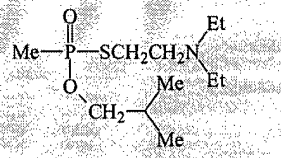

❖ *Conducted multiagency workshop on bioaerosol threat*

Low-Level Operational Toxicology

Objectives: Develop sound values for exposure levels having physiological impact below acute response levels to guide development of detectors and protective equipment

Challenges:

- Identifying physiological indicators of low level exposure
- Developing exposure methodologies
- Extrapolating to human response

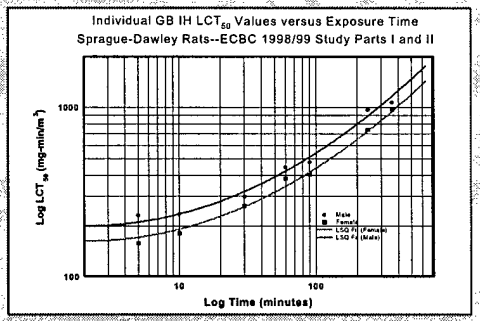

❖ *Extend CT range for acute effects*

Supporting Science and Technology
Thrust Areas

Joint Science and Technology Panel for Chemical / Biological Defense

Aerosol Technologies

Objectives: Characterize and test developmental air samplers/collectors; evolve new concepts toward next-generation small air samplers

Challenges:
- **high velocity test challenges**
- **size, power required to sample large volumes**

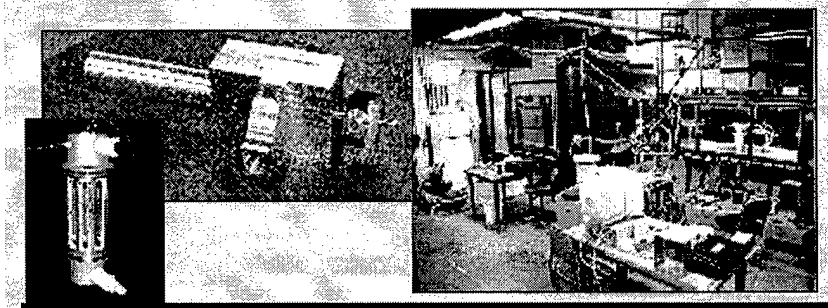

❖ ***Developed isokinetic, isoaxial reference reference sampler; developed new microslit transpirated impactor***

BIOSCAVENGERS AS A PRETREATMENT FOR NERVE AGENT EXPOSURE

David E. Lenz
US Army Medical Research Institute of Chemical Defense
3100 Ricketts Pt. Road
Aberdeen Proving Ground, MD 21010-5400

The use a bioscavenger has emerged as a new approach to reduce the in vivo toxicity of chemical warfare nerve agents. As an improvement of over current treatment, a biological scavenger should have no or minimal behavioral or physiological side effects, should provide protection up to a 5 LD50 exposure and should be devoid of any behavioral or physiological side effects. Studies with equine or human butyrylcholinesterase or fetal bovine serum acetylcholinesterase showed that none of these scavengers exhibited behavioral side effects when given alone to rats or monkeys. Furthermore, each was capable of providing protection against 2 to 16 LD50s of GD, GB or VX depending on the scavenger and the test species. The results to date support the value of this approach as the next generation of pharmaceuticals to afford protection against nerve agent poisoning.

The conventional approach to treatment of organophosphorus (OP) intoxication involves efforts to counteract the effects of acetylcholinesterase (AChE) inhibition. Cholinolytic drugs such as atropine are administered at the onset of signs of OP intoxication to antagonize the effects of the elevated acetylcholine levels that result from the inhibition of AChE (1). Additionally, an oxime nucleophile is given, which reacts with the inhibited (phosphonylated) enzyme to displace the phosphonyl group and restore normal activity (2). In the United States, the oxime of choice for treatment of nerve agent poisoning is the chloride salt of 2-PAM, usually referred to as 2-PAM Cl, although bis-pyridinium oximes may be more effective depending on the particular organophosphorus agent (3). Anticonvulsant drugs such as diazepam are also administered to control OP-induced tremors and convulsions. In conjunction with therapy, individuals at high risk for exposure to nerve agents are pretreated with a spontaneously reactivating AChE inhibitor such as pyridostigmine, which temporarily masks the active site of a fraction of AChE molecules and thus protects the enzyme from irreversible inhibition by the OP agent (4). Several nerve agents, including GF, sarin, and in particular soman, present an additional therapeutic challenge in that after they inhibit AChE, they undergo a second reaction in which the phosphonyl group attached to the inhibited enzyme is dealkylated. This process, known as aging, results in a phosphonylated AChE that is refractory to either spontaneous or oxime-mediated reactivation (5). The ineffectiveness of therapeutically administered oxime as a treatment for some nerve agents explains the continued research efforts aimed at alternative approaches to protection (6).

In contrast, recent efforts have focused on identifying proteins that can act as biological scavengers of organophosphorus compounds and can remain stable in circulation for long periods of time. This approach avoids the side effects associated with current antidotes (6, 7-14) and the requirement for their rapid administration, by prophylactically inactivating (through sequestration or hydrolysis) anticholinesterase agents before they can react with the target AChE. The time frame for this inactivation

to occur before endogenous AChE is affected is quite narrow (estimated to be approximately two minutes in humans (15). so especially for situations involving acute exposure, the scavenger function must be very rapid, irreversible and specific. Ideally, the scavenger would enjoy a long residence time in the bloodstream, would be biologically innocuous in the absence of nerve agent and would not present an antigenic challenge to the immune system and efforts have focused on enzymes of mammalian (usually human) origin.

Candidate bioscavenger proteins, in general, function either by stoichiometricly binding and sequestering the anticholinesterase or by catalytically cleaving the OP substrate into biologically inert products. In the former category are naturally occurring human proteins that bind nerve agents, including enzymes such as cholinesterases (ChEs) and carboxylesterases (CaEs), as well as antibodies specific for nerve agent haptens. Each of these stoichiometric scavengers has the capacity to bind one or two molecules of nerve agent per molecule of protein scavenger. While this approach has been proven to be effective in laboratory animals, it has the disadvantage that the extent of protection is directly proportional to the concentration of unexposed, active scavenger in the bloodstream at the time of nerve agent exposure.

Candidate enzymes with *bona fide* catalytic activity against nerve agents include the human organophosphorus acid anhydride hydrolases (OPAHs), such as paraoxonase (hu-Pon). Additionally, the ability to generate catalytic antibodies in response to appropriate transition state analogs (16,17) suggests that nerve agent-specific antibodies that catalyze hydrolysis of their ligands could be effective bioscavengers. Finally, the ability to engineer site-specific amino acid mutations into naturally occurring scavenger enzymes can allow investigators to alter the binding and/or catalytic activities of these enzymes. In general, the use of scavengers with catalytic activity would be advantageous because small amounts of enzyme, meaning lower concentrations in circulation, would be sufficient to detoxify both large amounts of nerve agent.

To be an improvement over the existing therapeutic approach for providing protection against nerve agent poisoning, a biological scavenger, either stoichiometric or catalytic, should satisfy three critical criteria. First it must be safe, producing no untoward effects in its own right. Secondly, it must provide an increase in efficacy or equal efficacy with no need for additional drugs, e.g., is easier to administer and is less time dependent in administration. Finally, it must produce an efficacious response with reduced level of behavioral or physiological incapacitation. Considerable effort has been made in the past five years in this area and currently there are a variety of proteins that meet these criteria

BEHAVIORAL EFFECTS OF SCAVENGERS ALONE

Several studies have examined the behavioral effects of the biological scavengers themselves in the absence of cholinesterase inhibitors (Table 1). Genovese and Doctor (18) reported that rats were trained to perform a passive avoidance task, a motor activity, and a scheduled-controlled behavior. The performance of animals before and after administration of purified equine-butyrylcholinesterase (eq-BuChE) at a dose that would be expected to provide protection against an exposure of several LD_{50}s of an organophosphorus compound was assessed. In all cases, the authors report that eq-BuChE did not disrupt performance of any of the learned tasks, did not upset the circadian cycle of light/dark activity, and had no effect on motor activity. These outcomes were in contrast to those observed when the standard cholinolytic, atropine, was administered. In a separate study also using eq-BuChE (19), rhesus monkeys were trained to perform a serial probe recognition (SPR) task. Once the animals became proficient at the task they received eq-BuChE in a dose similar to that reported by Broomfield et al. (20) as sufficient to afford protection against a 2 or 3 LD_{50} soman challenge. The authors reported that repeated administration of commercially prepared eq-BuChE had no effect on the behavior of the monkeys as measured by the SPR studies. Given the lack of behavioral effects and the relatively long *in vivo* half-life of the eq-BuChE, they concluded that this biological scavenger was potentially more effective than current chemotherapeutic treatments for organophosphorus intoxication.

TABLE 1. Protection from Organophosphorus Intoxication by Stoichiometric Bioscavengers.

Bioscavenger	Test Species	Nerve Agent	Protection (LD_{50})[a]	Serum $T_{1/2}$[b]	Reference
FBS-AChE	Rhesus Monkey	GD	2-5	30-40 Hrs	28, 29
"	Mouse	GD	2 (w/ Atropine + 2-PAM)	40-50 Hrs	24
"	"	GD	2 (after CBDP treatment)	~24 Hrs	30
"	"	GD	2-8	24-26 Hrs	21, 22, 26
"	"	MEPQ	4	~24 Hrs	22, 30
"	"	VX	2-3.6	~24-50 Hrs	24, 30
					22
eq-BuChE	Rhesus Monkey	GB	1	620 Hrs	20
"	"	GD	2 (4 w/ atropine)	"	20
"	"	GD	5	30-40 Hrs	29
hu-BuChE	Rhesus Monkey	GD	2	~30 Hrs	32
"	"	VX	1.5	"	32
"	Rat	GD	2-3	46 Hrs	23
"	"	VX	2	"	23
"	Mouse	GD	2.1	21 Hrs	32
"	"	GB	1.6	"	32
"	"	GA	1.8	"	32
"	"	VX	4.9	"	32
CaE[c]	Mouse	GD	16	N.D.[d]	37
"	Guinea Pig	GD	3.5	N.D.	37
"	Rabbit	GD	3	N.D.	37
"	Rat	GD	8-9	N.D.	28, 37
"	"	GB	8	N.D.	37
"	"	GA	4-5	N.D.	37
"	"	VX	1	N.D.	37
"	"	Paraoxon	2	N.D.	37

[a] Values represent multiples of median lethal doses (LD_{50}s) of nerve agent survived after scavenger administration. [b] Half-life of scavenger in blood circulation. [c] For each s the activity of the host's endogenous CaE was tested. [d] Not determined. Because CaE is an endogenous serum protein, the protection it offers was measured by comparing L values in untreated and CBDP-treated animals; 2 mg/kg CBDP completely abolishes endogenous CaE activity (28).

BEHAVIORAL EFFECTS OF SCAVENGER AND NERVE AGENT EXPOSURE

Studies on the behavioral effects that result from nerve agent exposure of animals pretreated with biological scavengers tend to include studies in both rodents and non-human primates (Table 2). The rodent data are, for the most part, limited to observations of animals after the experimental procedure (21-23) or to the ability of mice to respond to an inverted screen test (24, 25). Maxwell and co-workers (26) applied a mixture of tests including the inverted screen test as well as activity and motor function assays to mice given fetal bovine serum-AChE (FBS-AChE). In all of these studies, the authors report that animals pretreated with a scavenger, such as FBS-AChE, eq-BuChE, or human-BuChE (hu-BuChE), followed by exposure to soman or VX, exhibited no deficits in behavior. Animals that received no pretreatment all suffered notable impairment, and the time for recovery was on the order of days or longer. Brandeis et al. (27) examined the effects of soman on rats that either had or had not been pretreated with hu-BuChE and trained to perform the Morris water maze behavioral task. Rats given a sub-lethal dose of soman alone had significant impairments in cognitive function that manifested itself over a period of several weeks. Pretreatment with hu-BuChE provided substantial protection from these behavioral decrements; the performance of hu-BuChE-pretreated, soman-exposed rats was indistinguishable from that of control rats exposed only to saline. The authors also observed that rats administered the scavenger in the absence of soman were devoid of impairments in behavioral performance.

Studies in non-human primates have led to similar conclusions. Broomfield et al. (20) and Maxwell et al. (28), studying eq-BuChE and FBS-AChE respectively as scavengers, used the SPR task to evaluate the ability of these two scavengers to protect against behavioral decrements after soman poisoning. After eq-BuChE pretreatment followed by 2 LD_{50}s of soman, animals exhibited a transient performance decrement at 8 hours post-challenge. Thereafter they returned to baseline performance levels and were followed for up to six days. A related study in rhesus monkeys trained to perform a Primate Equilibrium Platform (PEP) task detected no performance decrements in animals given FBS-AChE alone, or pretreated with scavenger prior to a cumulative challenge of 4 LD_{50}s of soman. When eq-BuChE was the scavenger, transient performance decrements were observed when the soman challenge exceeded a cumulative dose of 4 LD_{50}s, although all of the animals survived this otherwise lethal dose. In no case were residual or delayed performance effects detected up to six weeks after nerve agent exposure in animals pretreated with either cholinesterase (29). A summary of the results from these primate studies can be found in Doctor et al. (30, 31).

Raveh and co-workers (32) described the protective effects of hu-BuChE in rhesus monkeys exposed to soman or VX. The monkeys were first trained on a spatial discrimination (SD) task and then pretreated with hu-BuChE before exposure to the organophosphorus nerve agents. The scavenger afforded protection against the lethality of soman or VX, but with respect to protection against behavioral deficits, the results were mixed. Despite less than ideal protection against performance decrements, the authors concluded that the hu-BuChE scavenger offered a high level of protection against soman-induced behavioral deficits. They also commented on the consistency of results across species for this type of pretreatment, and suggest that it should be possible to predict the extent of protection that would be afforded humans based on their own results (32) and the work of others.

BEHAVIORAL EFFECTS OF SCAVENGERS VERSUS CONVENTIONAL THERAPY POST EXPOSURE

Results reported using the SPR task as a measure of behavioral performance in non-human primates when scavenger pretreatment was followed by administration of multiple LD_{50}s of soman (20, 28, 33) can be compared with similar studies using conventional therapy (Table 2). Pyridostigmine pretreatment alone had no effect on SPR performance in trained animals. Following soman exposure and treatment with atropine and oxime either with or without diazepam, recovery of pre-exposure performance on the SPR task took from six (when co-administered diazepam) to 15 days (without the anti-convulsant; 34) The authors concluded that diazepam would be an excellent adjunct to the pyridostigmine pretreatment/atropine, oxime treatment regimen. The prolonged recovery time of six to 15 days after conventional therapy contrasts

dramatically with the results from bioscavenger prophylaxis. The lack of or presence of only a subtle, transient decrease in SPR performance, when a bioscavenger is used as a pretreatment (20, 28), offers impressive evidence for the value of this approach as affording protection against behavioral effects following nerve agent poisoning.

CONCLUSION

Organophosphorus nerve agents represent a very real threat not only to war fighters in the field but also to the public at large (35). Nerve agents have already been used by terrorist groups against a civilian population and, due to their low cost and relative ease of synthesis, are likely to be used again in the future (36). Current therapeutic regimes for nerve agent exposure are generally effective at preventing fatalities if administered in an appropriate time frame. Using bioscavengers would provide a capability for extended protection against a wide spectrum of nerve agents and would eliminate the need for extensive postexposure therapy. Work is currently underway to isolate gram quantities of BChE for safety and efficacy testing. The completion of this concept exploration phase should provide the data required for a program decision review pursuant to filing for an investigational new drug application.

TABLE 2. Protection from Behavioral Deficits by Bioscavengers or Conventional Therapy.

Protection	Test Species	Toxin	Dose (LD_{50})[a]	Behavioral Test(s)	Impairment[b]	Reference
Without Nerve Agents:						
Atropine	Rat	None	0	Passive Avoidance, VI56 s Schedule	Total	18
eq-BuChE	"	"	"	Passive Avoidance, Motor Activity, VI56 s Schedule	None	18
hu-BuChE	"	"	"	Morris Water Maze	None	27
Pyridostigmine	Rhesus Monkey	"	"	Primate Equilibrium Platform (PEP)	Substantial	38
eq-BuChE	"	"	"	Serial Probe Recognition (SPR)	None	19
"	"	"	"	Observation, SPR	Subtle SPR defect	33
"	"	"	"	"	None	19
hu-BuChE	"	"	"	Spatial Discrimination	Minor (1/4 had errors)	32
With Nerve Agents:						
Pyridostigmine & Atropine	Mouse	GD	8	Inverted Screen, Motor Function, Lacrimation, & Activity Level	Near Total	26
HI-6 & Atropine	"	GD	8	"	Near Total	"
FBS-AChE	"	GD	8	"	Very Minor	"
"	"	VX	2-3	Inverted Screen	Minor (1/10 failed)	24
PTE[e]	"	GD	3-4	"	None	25
eq-BuChE	Rat	MEPQ	> 1	VI56 s Schedule	Moderate (70% of control)[f]	18
hu-BuChE	"	GD	1.5	Observation	Minor (tremors in 1/6)	23
"	"	VX	1.4	"	None	23.
"	"	GD	1.5	Morris Water Maze	None	27
FBS-AChE	Rhesus Monkey	GD	5	Observation, PEP	None	29
"	"	GD	2.7	Observation, SPR	None	28
eq-BuChE	"	GD	2	"	Transient	20
"	"	GD	2	"	Subtle SPR defect[g]	33
eq-BuChE	"	GD	4	Observation, PEP	None	29
hu-BuChE	"	GD	3.3	Spatial Discrimination	Minor (1/4 had errors)	32
Pyridostigmine	"	GD	~0.4	Observation, PEP	Substantial	38
Pyridostigmine, Atropine & 2-PAM	"	GD	2	Observation, SPR	Substantial	20
"	"	GD	5	"	Substantial	34
Pyridostigmine, Atropine, 2-PAM & Diazepam	"	GD	5	"	Substantial	34

[a] Median lethal dose of nerve agent administered. [b] Behavioral impairment relative to untreated animals. [c] Not Determined [d] Phosphotriesterase from *Pseudomonas diminu*
[e] The VI56 s behavior is a food-reward based task. The authors speculate that nausea caused by nerve agent exposure, rather than a cognitive deficit, may have caused the behavioral impairment. [f] The sustained subtle defect was in addition to the short-term, substantial defect described by Broomfield, et al. (20)

REFERENCES

1. Heath, A. J. W. and Meredith, T., Atropine in the Management of Anticholinesterase Poisoning, in *Clinical and Experimental Toxicology of Organophosphates and Carbamates*, Ballantyne B. and Marrs, T. C., Eds., Butterworth, Oxford, 1992, 543.
2. Wilson, I. B. and Ginsburg, S., A powerful reactivator of alkyl phosphate-inhibited acetylcholinesterase, *Biochim. Biophys Acta.,* 18, 168, 1955.
3. Bismuth, C., Inns, R. H. and Marrs, T. C., Efficacy, toxicity and clinical use of oximes in anticholinesterase poisoning, in *Clinical and Experimental Toxicology of Organophosphates and Carbamates*, Ballantyne, B. and Marrs, T. C., Eds., Butterworth, Oxford, 1992, 555.
4. Gordon, J. J., Leadbeater, L. and Maidment, M. P., The protection of animals against organophosphorous poisoning by pretreatment with a carbamate, *Toxicol. Appl. Pharmacol.,* 43, 207, 1978.
5.Fleisher, J. H. and Harris, L. W., Dealkylation as a mechanism for aging of cholinesterase after poisoning with pinacolyl methylphosphonofluoridate, *Biochem. Pharmacol.,* 14, 641, 1965.
6. Dunn, M. A. and Sidell, F. R., Progress in medical defense against nerve agents, *J. Am. Med. Assoc.,* 262, 649, 1989.
7. Erdmann, W., Bosse, I. and Franke, P., Zur resorption und ausscheidung von toxigonin nach intramuskularer am menschen, *Dtsch. Med. Wschr.,* 90, 1436, 1965.
8. Wiezorek, W., Kreisel, W., Schnitzlein, W. and Matzkowski, H., Eigenwirkungen von trimedoxin und pralidoxim am menschen Zeitschr, *Militarmed.,* 4, 223, 1968.
9. Sidell, F. and Groff, W., Toxigonin: Blood levels and side effects after intramuscular administration in man, *J. Pharm. Sci.,* 59, 793, 1970.
10. Vojvodic, V., Blood levels, urinary excretion and potential toxicity of N,N'-trimethylenebis(pyridinium-4-aldoxime) dichloride (TMB-4) in healthy man following intramuscular injection of the oxime, *Pharmacol. Clin.,* 2, 216, 1970.
11. Wenger, G. R., Effects of physostigmine, atropine and scopolamine on behavior maintained by a multiple schedule of food presentation in the mouse, *J. Pharmacol. Exp. Ther.,* 209, 137, 1979.
12. Clement, J. G., HI-6 reactivation of central and peripheral acetylcholinesterase following inhibition by soman, sarin and tabun in vivo in the rat, *Biochem. Pharmacol.,* 31, 1283, 1982.
13. McDonough, J. H. and Penetar, D. M., The effects of cholinergic blocking agents and anticholinesterase compounds on memory, learning and performance, in *Behavioral Models and the Analysis of Drug Action. Proceedings of the 27th OHOLO Conference.* Spiegelstein, M. Y. and Levy, A., Eds., Elsevier, Amsterdam, 1982, 155.
14. Huff, B. B., Ed., *Physician's Desk Reference*, Medical Economics Co. Inc., Oradell, 1986, 1491.
15. Talbot, B. G., Anderson, D. R., Harris, L. W., Yarbrough, L. W. and Lennox, W. J., A comparison of *in vivo* and *in vitro* rates of aging of soman-inhibited erythrocyte acetylcholinesterase in different animal species, *Drug Chem. Toxicol.,* 11, 289, 1988.
16. Brimfield, A. A., Lenz, D. E., Maxwell, D. M. and Broomfield, C. A., Catalytic antibodies hydrolyzing organophosphorus esters, *Chem.-Biol. Interactions,* 87, 95, 1993.
17. Broomfield, C. A., Transition state analogs for catalytic antibodies. *Phosphorus, Sulfur and Silicon,* 109-110, 233, 1996.
18. Genovese, R. F. and Doctor, B. P., Behavioral and pharmacological assessment of butyrylcholinesterase in rats, *Pharmacol. Biochem. Behav.,* 51, 647, 1995.
19. Matzke, S. M., Oubre, J. L., Caranto, G. R., Gentry, M. K. and Galbicka, G., Behavioral and immunological effects of exogenous butyrylcholinesterase in rhesus monkeys, *Pharmacol. Biochem. Behav.,* 62, 523, 1999.
20. Broomfield, C. A., Maxwell, D. M., Solana, R. P., Castro, C. A., Finger, A. V. and Lenz, D. E., Protection of butyrylcholinesterase against organophosphorus poisoning in nonhuman primates, *JPET,* 259, 633, 1991.
21. Ashani, Y., Shapira, S., Levy, D., Wolfe, A. D., Doctor, B. P. and Raveh, L., Butyrylcholinesterase and acetylcholinesterase prophylaxis against soman poisoning in mice, *Biochem. Pharmacol.,* 41, 37, 1991.

22. Maxwell, D. M., Wolfe, A. D., Ashani, Y. and Doctor, P. B., Cholinesterase and carbo0.xylesterase as scavengers for organophosphorous agents, in *Cholinesterases: Structure, Function, Mechanism, Genetics and Cell Biology,* Massoulie, J., Bacou, F., Barnard, E., Chatonnet, A., Doctor, B. P. and Quinn, D. M., Eds., American Chemical Society, Washington, D. C., 1991, 206.
23. Raveh, L., Grunwald, J., Marcus, D., Papier, Y., Cohen, E. and Ashani, Y., Human butyrylcholinesterase as a general prophylactic antidote for nerve agent toxicity, *Biochem. Pharmacol.,* 45, 2465, 1993.
24. Wolfe, A. D., Rush, R. S., Doctor, B. P., Koplovitz, I. and Jones, D., Acetylcholinesterase prophylaxis against organophosphate toxicity, *Fund. Appl. Toxicol.*, 9, 266, 1987.
25. Broomfield, C. A., A purified recombinant organophosphorus acid anhydrase protects mice against soman, *Chem.-Biol. Interactions,* 87, 279, 1993.
26. Maxwell, D. M., Brecht, K. M., Doctor, B. P. and Wolfe, A. D., Comparison of antidote protection against soman by pyridostigmine, HI-6 and acetylcholinesterase, *J. Pharmacol. Exper. Therapeut.,* 264, 1085, 1993
27. Brandeis, R., Raveh, L., Grunwald, J., Cohen, E. and Ashani, Y., Prevention of soman-induced cognitive deficits by pretreatment with human butyrylcholinesterase in rats, *Pharmacol. Biochem. Behav.,* 46, 889, 1993
28. Maxwell, D. M., Castro, C. A., De La Hoz, D. M., Gentry, M. K., Gold, M. B., Solana, R. P., Wolfe, A. D. and Doctor, B. P., Protection of rhesus monkeys against soman and prevention of performance decrement by pretreatment with acetylcholinesterase, *Toxicol. Appl. Pharmacol.,* 115, 44, 1992.
29. Wolfe, A. D., Blick, D. W., Murphy, M. R., Miller, S. A., Gentry, M. K., Hartgraves, S. L. and Doctor, B. P., Use of cholinesterases as pretreatment drugs for the protection of rhesus monkeys against soman toxicity, *Toxicol. Appl. Pharmacol.*, 117, 189, 1992.
30. Doctor, P. B., Raveh, L., Wolfe, A. D., Maxwell, D. M. and Ashani, Y., Enzymes as pretreatment drugs for organophosphate toxicity, *Neurosci. and Biobehav. Rev.,* 15, 123, 1991.
31. Doctor, B. P., Blick, D. W., Caranto, G., Castro, C. A., Gentry, M. K., Larison, R., Maxwell, D. M., Murphy, M. R., Schutz, M., Waibel, K. and Wolfe, A. D., Cholinesterases as scavengers for organophosphorous compounds: Protection of primate performance against soman toxicity, *Chem.-Biol. Interactions,* 87, 285, 1993.
32. Raveh, L., Grauer, E., Grunwald, J., Cohen, E. and Ashani, Y., The stoichiometry of protection against soman and VX toxicity in monkeys pretreated with human butyrylcholinesterase, *Toxicol. Appl. Pharmacol.,* 145, 43, 1997.
33. Castro, C. A., Gresham, V. C., Finger, A. V., Maxwell, D. M., Solana, R. P., Lenz, D. E. and Broomfield, C. A., Behavioral decrements persist in rhesus monkeys trained on a serial probe recognition task despite protection against soman lethality by butyrylcholinesterase, *Neurotoxicol. Teratol.,* 16, 145, 1994.
34. Castro, C. A., Larsen, T., Finger, A. V., Solana, R. and McMaster, S. B., Behavioral efficacy of diazepam against nerve agent exposure in rhesus monkeys, *Pharmacol. Biochem. Behav.,* 41, 159, 1991.
35. Ember, L., Chemical weapons: plans prepared to destroy Iraqi arms, *Chem. Eng. News,* 19, 6, 1991.
36. Masuda, A. N., Takatsu, M., Morianari, H. and Ozawa, T., Sarin poisoning in Tokyo subway, *Lancet,* 345, 1446, 1995.
37. Maxwell, D. M., Brecht, K. M. and O'Neill, B. L., The effect of carboxylesterase inhibition on interspecies differences in soman toxicity, *Toxicol. Lett.,* 39, 35, 1987.
38. Blick, D. W., Murphy, M. R., Brown, G. C., Yochmowitz, M. G., Fanton, J. W. and Hartgraves, S. L., Acute behavioral toxicity of pyridostigmine or soman in primates, *Toxicol. Appl. Pharmacol.,* 126, 311, 1994.

NEUROPROTECTION FOR NERVE AGENT-INDUCED BRAIN DAMAGE

Jonathan Newmark, Gerald P.H. Ballough and Margaret G. Filbert
US Army Medical Research Institute of Chemical Defense
Postal address: CDR, USAMRICD, ATTN: MCMR-UV-ZM (COL Newmark),
3100 Ricketts Point Road,
Aberdeen Proving Ground, Maryland, 21010-5400, USA

SUMMARY

This presentation will explain the rationale behind the neuroprotection Science Plan which has been established at the US Army Medical Research Institute of Chemical Defense as part of the medical chemical defense program. This program attempts to address a need that has not been specifically addressed before in any country, which is specifically to save vulnerable neurons that have been damaged due to seizures secondary to exposure to nerve agents. Preliminary work in this laboratory has demonstrated proof of concept using a compound not yet approved for clinical use by the US Food and Drug Administration. We will continue work with neuropathological correlation and add a neurobehavioral component to the testing program to be able to exploit preparations developed by industry, particularly in neuroprotection for stroke. If successful we will be able to give field physicians a new treatment with an excellent chance of minimizing or preventing neurobehavioral dysfunction after nerve agent poisoning, should primary protection against exposure and acute therapy of exposure both fail and status epilepticus ensue. We intend by presenting this program at this forum to stimulate Canadian and European colleagues to consider work in this area.

PRÉCIS: Cette présentation veut expliquer la rationale fondamentale pour le nouveau Plan Scientifique de la Recherche (STP en anglais) que nous avons commencés a l'Institut de la Recherche Médicale de la Défense Chimique de l'Armée des États-Unis. Ce plan adresse un besoin que, en notre opinion, aucun pays n'a adresse avant que maintenant. Ce besoin est a sauver des neurones qui ont été blesses a cause des convulsions, qui sont, elles-mêmes, a cause de l'exposure aux agents nerveux. Le travail préliminaire complète dans notre laboratoire a montre la preuve de cette idée, mais seulement en employant des agents qui n'ont pas l'approbation de l'Administration des Aliments et des Drogues des États-Unis pour les humains. Nous continuons a travailler avec les agents approbés sur la relation neuropathologique avec l'effet de la traitement. Nous ajoutons du travail sur la relation avec le comportement en une modèle exemplaire animale. Nous voulons employer les préparations (les drogues) qui sont développés par l'industrie, en particulière, pour protéger les neurones du cerveau en cas de l'apoplexie. Si nous succédons, nous donnerions aux médecins militaires un nouveau traitement avec une grande probabilité de minimiser ou prévenir la perte de la fonction nerveuse après l'exposure toxique avec les agents nerveux, en le cas quand la prévention a l'origine et le traitement rapide ont tous les deux échoués, et le sujet est entré en status epilepticus ou les convulsions continuées. En présentant notre programme a cette conférence, nous intentons a stimuler les collègues canadiennes et européennes a considérer du travail en "neuroprotection" elles-mêmes.

Protection against brain damage produced by exposure to chemical nerve agents is of significant military concern. The currently fielded antidotal therapy for nerve agent poisoning on the battlefield--pretreatment with pyridostigmine bromide, atropine, oxime, and acute anticonvulsant therapy with diazepam--addresses only the acute, life-threatening consequences of nerve agent toxicity. Soldiers surviving initial life-threatening effects of nerve agents are likely to develop electrical seizure activity. Anticonvulsants such as diazepam can arrest chemical agent-induced seizures when administered shortly after seizure onset, but their effectiveness wanes after approximately twenty minutes, allowing seizures to recur. According to the McDonough-Shih hypothesis, this may reflect recruitment of other neurotransmitter systems beyond the original cholinergic crisis. Unless seizures are arrested, the currently fielded therapy does not afford protection against brain damage, specifically, apoptotic change and death of cortical neurons.

It may be practically impossible to distinguish on the battlefield between a casualty who is undergoing nonconvulsive status epilepticus, either because of the distribution of the seizure focus or, more likely, because ATP stores are depleted and thus no movement can be generated, and a casualty who is post-ictal, particularly if the casualty is wearing chemical protective gear. Since neither of these possibilities is associated with the usual movements seen with typical seizures, these victims are not likely to receive anticonvulsant treatment. Left untreated or refractory to anticonvulsants, nerve agent–induced seizures progress to status epilepticus, resulting in extensive neuronal death, particularly in cholinergically rich areas of cortex, and subsequent permanent neurological disability. Experience from the Tokyo subway attack demonstrated that cerebral hypoxia may well complicate this situation, which will worsen any damage to already vulnerable brain neurons. Thus, there is a clear need for a neuroprotective compound that is capable of preventing further neuronal damage, even when seizures have progressed to status epilepticus. Such a compound would greatly increase the window of opportunity to prevent or minimize neurologic dysfunction resulting from chemical agent-induced seizures and would augment the beneficial effects of currently fielded anticonvulsants.

A 1999 report prepared for the US Assistant Secretary of Defense for Health Affairs at the request of Congress concluded that brain damage from exposure to chemical warfare agents is one of the two major neurological threats on the modern battlefield. The other was neurologic damage due to head trauma. To address this problem, a new Science and Technology Plan (STP) for neuroprotection against seizure-related neuronal cell death has been established at the Medical Research Institute of Chemical Defense. The objectives of this STP are to develop an improved medical protection capability against neuronal loss and the resultant decrease in neurologic function resulting from prolonged seizures, status epilepticus and hypoxia caused by organophosphate nerve agents and to demonstrate that in the absence of other therapies, medical protection can be initiated to save neurons that have been subject to the excitotoxic effects of seizure activity. To ensure optimal neurological outcome, a neuroprotectant should have efficacy when administered one or more hours after seizure onset and have minimal detrimental side effects.

In terms of the echelons of medical care in the US military, the requirement for a candidate treatment to be efficacious when treatment is delayed as many as 4 hours is of great importance. By 3-4 hours after exposure and discovery on the battlefield, it is quite likely that a casualty will have been evacuated to what the US military calls Echelon II or III, at which level of care a physician or at least a physician assistant can manage his or her care. Although in the US a non-physician medic cannot use medications independently, a physician can do so. A drug approved for another use by the US Food and Drug Administration could be used "off label" by a physician.

The STP intends to exploit work already ongoing in the pharmaceutical industry for stroke. Unlike nerve agent poisoning, stroke has an enormous economic impact in all advanced countries. In the US it is the third leading cause of death and kills 960,000 people yearly. The

American Stroke Association estimated in 1999 that the direct and indirect cost of stroke care in the US is $45.3 billion. Stroke results in neuronal death in a small area of brain, but also creates a much larger ischaemic penumbra in which neurons are potentially salvageable. The only US Food and Drug Administration-approved acute therapy for stroke today is recombinant tissue plasminogen activator, which must be administered within 3 hours of stroke ictus. If delayed beyond that, outcome actually is worse. As a result, less than 5% of acute strokes in the US are receiving this treatment. Thus, many pharmaceutical companies are investigating neuroprotective compounds for stroke that might have a longer therapeutic window.

Potential stroke neuroprotectants come from many, unrelated drug classes. Classes including at least one product that has reached clinical trials in humans include calcium channel blockers (nimodipine, flunarizine, dextrorphan, selfotel, magnesium sulphate, eliprodil, GV150526); presynaptic glutamate release inhibitors (lubeluzole, fosphenytoin), antioxidants and free radical scavengers (trilazad, ebselen, nitrones), other ion channel inhibitors (clomethiazole, MBQX, GM1 ganglioside, Bay 3702), and some agents directed against delayed injury (BFGF, citicholine, enlimomab, piracetam). Unfortunately, several of these have proven disappointing in recent clinical Phase III trials. It is very likely that the reasons these drugs have not shown clinical effectiveness is that stroke itself are highly heterogeneous, both in terms of pathophysiology and also in terms of neuroanatomy. For example, a drug that acts at any receptor site is not likely to be useful in a white-matter or lacunar infarction, if only because white matter tracts contain few if any synapses. Bogousslavsky and others (Brott T and Bogousslavsky J. Treatment of acute ischemic stroke. New England Journal of Medicine 343:710-722, 2000) point out that, as stroke trials become more successful in isolating subpopulations of stroke by anatomy and physiology, it is much more likely that a putative neuroprotectant agent will prove efficacious than in the heterogeneous stroke populations so far studied. One or more of these compounds may well reach FDA approval in the next few years.

An approved neuroprotectant may prove useful in nerve agent toxicity as well, since in animals who have survived nerve agent challenge many of the neurons undergo apoptosis. Neurons that can be prevented from going into the apoptotic cascade in stroke models may well represent neurons that can be saved after nerve agent-induced status epilepticus, since the mechanism of cell death is identical.

Initial approaches in development of neuroprotectants include poly ADP-ribose polymerase (PARP) inhibitors such as benzamide and 3-amino benzamide. Benzamide showed neuroprotectant efficacy against soman when administered after seizure onset (Meier HL, Ballough GPH, Forster JS and Filbert MG. The poly ADP ribose polymerase inhibitor (PARPI) is neuroprotective against soman-induced seizure related brain damage. In: Trembly B and Slikker W, eds.: Fourth International Conference on Neuroprotective Agents. Annals of the New York Academy of Sciences 890:330-335, 1999). Other potential approaches are the use of scavengers of reactive oxygen species (ROS), such as the naturally occurring alpha lipoic acid, its reduced form dihydrolipoic acid, free radical traps such as nitrones and inhibitors of N-acetylaspartylglutamate (NAAG) peptidase to reduce the formation of glutamate from NAAG.

Neuroprotectant efficacy was demonstrated against soman-induced seizure-related brain damage with a nonpsychotropic cannabinoid, dexanabinol, or HU-211 (Filbert MG, Forster JS, and Ballough GPH. Neuroprotective effects of HU-211 on brain damage resulting from soman-induced seizures. In: Trembly B and Slikker W: Fourth International Conference on Neuroprotective Agents. Annals of the New York Academy of Sciences 890:505-514, 1999). When administered 40 min after onset of seizures and despite having no effect on the severity or duration of the seizure activity HU-211 reduced the lesion volume 70% (Ballough GPH, Cann FJ, Smith CD, Forster JS, Kling CE, and Filbert MG. GM1 monosialoganglioside pretreatment protects against soman-induced seizure-related brain damage. Molecular and Chemical Neuropathology 34: 1-23, 1998).

An interesting finding that has come out of these studies with dexanabinol is that lesion volume as measured at autopsy correlates very highly ($p<0.001$) with relative beta-2 activity on electrocorticography at 60 minutes after seizure onset. This time point coincides with the irreversible effects of intracellular calcium overload and may reflect that absolute window for preventing seizure-related neuronal death. This finding allows one to predict with certainty whether a putative neuroprotectant has indeed protected neurons long before subjecting the animal to sacrifice and full neuropathological examination (Ballough GPH, Jaworski MJ, Filbert MG and Newmark J. Electrocorticographic correlates of dexanabinol-induced neuroprotection following soman-induced status epilepticus. Neurology (suppl. 1), in press, 2001)

These preliminary studies demonstrate proof of concept that medical chemical defense against the delayed effects of nerve agents offers hope of decreased disability to victims of exposure to nerve agents.

We plan this year to begin both neuropathological and behavioral testing of a clinically approved agent, magnesium sulphate solution, which has the further advantage of being absurdly cheap ($0.08/dose). We will use the previous protocol shown above in the case of HU-211 to test the hypothesis that post-exposure treatment of a nerve agent-challenged, seizing animal can reduce the loss of neurons. At the same time, we also will test the ability of this agent to improve the mental functioning of an animal survivor of nerve agent challenge in a behavioral task. Although the first agent tested may not prove useful, this work will, if nothing else, establish these testing protocols as baseline in our laboratory. If either magnesium sulphate solution does prove to be neuroprotective in this situation, we may recommend it to field medical staff immediately for treatment of human nerve agent poisoning survivors with good basis for saying that it will reduce neurologic dysfunction.

How far into the business of research into neuroprotective agents should the military research establishment penetrate? In my opinion, most of the basic science and all of the safety work in new agents will be done by industry. The military research establishment should do that part of the work that industry will not fund, which, in this case, is the actual work with live nerve agents. Further, the military probably will do well to restrict itself to therapeutic agents already approved by the regulatory agency charged in a particular country with approving human drugs; in the US, this is the Food and Drug Administration. It will be extremely difficult to license a new neuroprotectant agent with no other clinical use, but it is not necessary, at least in the US, to get the FDA to approve the use of an already approved agent for a new indication. Although the US military cannot recommend it as a matter of doctrine, physicians are legally entitled to use any licensed product in any fashion "off-label" if there is good data to support its clinical use.

This area has not previously been considered a part of the military research effort into countermeasures for nerve agent exposure. NATO can contribute to this effort since many clinical trials of new neuroprotectants are being carried out in Canada or Europe before they are repeated in the US. One purpose of this presentation is to stimulate consideration of work in this area by those in countries where this has not yet been considered.

NOTE: The opinions expressed herein are solely those of the authors and not necessarily those of the United States Army, the United States Department of Defense, or the United States Army Medical Research Institute of Chemical Defense.

TRACE CHEMICAL VAPOR DETECTION BY PHOTOTHERMAL INTERFEROMETRY

Paul M. Pellegrino, Nicholas F. Fell, Jr., Scott D. Sarama, and James B. Gillespie
U.S. Army Research Laboratory, 2800 Powder Mill Road,
Adelphi, Maryland 20783-1197

ABSTRACT

Photothermal interferometry has been demonstrated for detection of vapors with extremely high sensitivity (parts-per-trillion). Our present research uses a photothermal detection scheme that incorporates tunable sources and a modified Jamin interferometric design to provide high selectivity and sensitivity for organo-phosphate vapor detection. Phase shifts on microradian levels have been detected. Trace chemical vapor detection is accomplished by introducing the tunable excitation laser along the path of one interferometer beam providing a phase shift due to absorptive heating. Preliminary results indicated parts-per-billion detection of both DMMP and DIMP using ~400mW of CO_2 laser power at appropriate wavelengths.

INTRODUCTION

Monitoring trace gases in our environment has many actual and potential uses. Escalating environmental awareness has led to more restrictive regulations on air quality in both the workplace and environment in general. Both industry and the military have expressed interest in development of more sensitive and adaptable trace gas analysis instrumentation. After the Tokyo subway sarin attack, the detection of CW agents became a crucial area of research in both the civilian and military arenas. Since many CW agents have low vapor pressures and are quite toxic, detection limits in the ng/mL range are required for fieldable systems. This detection limit highlights the need for extremely sensitive devices and techniques. A more general environmental application of trace gas detection can be seen in workplace monitoring for specific pollutants. An important example involves the detection of monomethylhydrazine (MMH) and unsymmetrical dimethylhydrazine (UDMH). These materials are common components in certain types of rocket fuel as well as etchants in microstructure fabrication. Typical National Institute for Occupational Safety and Health (NIOSH) exposure levels are 30-60 parts-per-billion (ppb)[1] depending on the form of the hydrazine. This example also demonstrates that the degree of sensitivity needed in certain circumstances can exceed the limits of detection for common monitoring systems.

Photothermal spectroscopy encompasses a group of highly sensitive methods that can be used to detect trace levels of gases using optical absorption and subsequent thermal perturbations of the gases. The underlying principle that connects these various spectroscopic methods is the measurement of changes in physical parameters (temperature, pressure, or density) as a result of photo-induced change in the thermal state of the sample. Photothermal methods in general are classified as indirect methods for detection of trace optical absorbance, because the transmission of the light used to excite the sample is not measured directly. Several

examples of these techniques include photoacoustic spectroscopy (PAS), photothermal lensing (PTL), photothermal deflection (PTD), and photothermal interferometry (PTI). In PAS the pressure wave produced by the sample heating is measured, while the other examples sense the refractive index directly changes in the refractive index or by use of combinations of probe sources and detectors. The photothermal method we have chosen to pursue is photothermal interferometry. Recent research suggests that trace gas detection at parts-per-trillion (pptr) levels is attainable with this photothermal technique.[2,3]

In the late 1960's it was recognized that optical absorption resulting in sample heating and subsequent changes in the index of refraction would induce a phase shift in light probing the heated region. McLean, Sica, and Glass[4] were the first to demonstrate use of an interferometer to measure these photo-induced index changes. Most PTI apparatus are based on laser sources for both excitation and probe. Later Stone[5,6] incorporated both coherent and incoherent excitation sources in a modified Jamin interferometer to measure trace absorption in liquid samples. Other notable contributions to PTI include measurements by Davis and Petuchowski,[7] who achieved a lower detection limit of the infrared absorption coefficient of 10^{-10} cm^{-1} for a gaseous sample in a windowless cell. Recent research by Owens *et.al.*[2] demonstrated atmospheric ammonia detection at pptr levels using an apparatus similar to the Davis designs[7]. The literature indicates that a trace gas sensor with high sensitivity can be constructed using interferometer designs similar to ones previously mentioned.[1-4,7,8]

We have designed, built, and are testing a new instrument for trace gas analysis in ambient air by PTI. The design uses a Jamin interferometer with a specialized optical coating, mid-IR excitation source, and HeNe probe source. Initial tests have established the ability to detect trace levels of two methylphosphonate compounds with modest amounts of CO_2 laser power. Methylphosphonates are well-studied simulants for nerve agents and pesticides. Our goals are to develop a PTI system with the ability to not only detect trace gases, but also to discriminate target gases from the normal atmospheric backgrounds and each other. Our work targets CW agent simulants to demonstrate the capabilities of PTI in this area. We have initially characterized the system performance with a waveguide CO_2 laser. We have also examined difference frequency generation (DFG) as a possible method for generating tunable light in the 8-12 μm region. The first literature demonstrating DFG as a tunable mid-IR source (2.2-4.2 μm) using CW laser was report by Pine in the mid-1970's[9]. Recent literature involving tunable diode lasers with and without amplifers have established this a possible foundation for a widely tunable infrared source[10-12]. Frequency agile sources such as DFG sources are of particular interest as they increase discrimination ability by providing absorbance information as a function of wavelength. A description of our DFG experiment will be given along with preliminary results.

THEORY

PHOTOTHERMAL THEORY

In this section the underlying physical principles of PTI will be described in relation to our experimental system. Since PTI relies on detection of phase shifts produced by photo-induced heating of a sample, having excitation sources that overlap the peaks in the absorption spectrum of analyte gases is extremely important. Also, focusing on wavelengths that provide unique spectral information about the sample strengthens the capabilities of the sensor. Due to these considerations we have chosen to probe the optical absorbance in the mid-infrared spectral region (8-12 μm). This region offers a wealth of information about the chemical structure of the CW agent simulants being investigated. A typical infrared absorption cross-section for one of these molecules, dimethyl methylphosphonate (DMMP), σ_{DMMP}, is approximately 44 atm^{-1} cm^{-1} near the 9P(26) CO_2 laser line. These large absorption cross-sections make the molecule well suited to absorption of the mid-infrared pump laser and subsequently convert the energy that is not re-emitted to heat after molecular relaxation, primarily through collisional relaxation. The collisional relaxation that occurs causes a temperature increase in the sampled gas according to,

$$\Delta T = \frac{P\sigma N}{2f\rho C_p \pi a^2}, \qquad (1)$$

where P is the IR excitation power, f is the laser modulation, ρ and C_p are the density and heat capacity of the sampled gas, respectively, N is the molecular number density, and a is the IR laser beam radius. The rate of relaxation of the organophosphonate analytes studied can be estimated to be in the sub-nanosecond region using general gaseous thermodynamic equations[13]. The conduction of the heated air in our sample is slow relative to the relaxation time for organophosphonate samples, and the displacement due to convection of the heated gas is small compared to the radius of the laser probe beam. This implies that we can regard the heating of the gas from the excitation source to be both instantaneous and localized within the probe beam. Modulation frequencies are chosen by considering both noise levels and the frequency dependence of the temperature change, as seen in equation (1). Given the quasi-static local heating in the probe beam, the modulated index of refraction change follows the Clausius-Mossotti equation and is given by,

$$\Delta n = -(n-1)\Delta T / T_{abs}, \tag{2}$$

where T_{abs} is the absolute temperature of the gas. The modulated index of refraction induces a modulated phase shift,

$$\phi_m = 2\pi l \Delta n / \lambda, \tag{3}$$

in the HeNe probe beam in one arm of the interferometer where l is the interaction path length, and λ is the wavelength of the interferometer laser. The complementary outputs of the interferometer are detected on two photodiodes. The difference in the intensities of the photodiode outputs is isolated by an instrumentation amplifier and the difference signal is sent to both the computer and a phase sensitive lock-in amplifier. The signal, S, is proportional to $\Delta\phi_m$, the difference between the complementary outputs of the interferometer, and is given by,

$$S = G\sin(\Delta\phi_m) = G(\Delta\phi_m), \tag{4}$$

with the final expression valid only for small $\Delta\phi_m$. The interferometer amplification factor, G, is a measure of the total system amplification.

DFG THEORY.

A brief description of the general principles underlying the theory involved in DFG will be discussed. Formal and more complete descriptions of the technique can be found in numerous texts and journal publications[10,14]. The basic process relies on the second-order nonlinear susceptibility $\chi^{(2)}$, which is normally associated with a limited number of nonlinear crystal types. The two higher frequency photons (ω_1, ω_2) enter the material and interact with the nonlinear polarizability of the crystal creating a photon at a lower frequency (ω_3) corresponding to the energy difference of the two input photons. Conditions regarding conservation of energy, momentum or phase matching, and transparency at all wavelengths must be meet. The phase matching method employed in our DFG technique uses the natural birefringence of the crystal and anglular orientation with respect to the optic axis to ensure matching of the wave vector constraints ($\Delta k = 0 = k_1 - k_2 - k_3$). The infrared power generated , P_3 ,in our mixing experiments can be approximated by the following equation,

$$P_3 = \frac{(32\pi\omega_3\chi_{15}^{(2)})^2}{n_1 n_2 n_3 c^3} P_1 P_2 \{^2/(w_1^2 + w_2^2)\}, \tag{5}$$

derived by Boyd and Ashkin in the near-field case[15]. Where P_i , n_i , w_i (i=1,2,3) are the power, refractive index and beam radius respectively and l is the crystal length described in equation 5. Initially, theoretical calculations using this equation to generate 10 μm infrared radiation yielded power estimates of 627 nW.

EXPERIMENTAL

PHOTOTHERMAL EXPERIMENTAL APPARATUS

The block diagram of the PTI beam paths and supporting analysis equipment is shown in Figure1. The border in the diagram corresponds to an acrylic enclosure that surrounds the interferometer portion of the system. This section also rests on a 2.5-inch thick optical honeycomb board. The beam from a stabilized HeNe laser (Spectra-Physics model 117A), the probe beam, is initially directed to a steering mirror before entering the first of two specially coated etalons. The etalons have anti-reflection (AR) coatings on the front surfaces except for a centered 50/50 beamsplitting (BS) stripe while the back surfaces have high-reflection coatings. All coatings are designed for the HeNe wavelength (632.8 nm) and S polarizations. The probe beam initially enters the first etalon, is reflected off the back surface, and is subsequently split by the BS stripe. One beam exits the optic while the other beam undergoes a second reflection off the back surface before exiting. Thus, the output of the first etalon is two equal intensity beams separated by ~12 mm edge to edge. These beams define the two interferometer arms and travel through an open-ended acrylic tube (32 cm long) en route to an identical second etalon 60 cm away. The second etalon acts to recombine equal amounts of both interferometer arms into two complementary outputs of the interferometer. The modified-Jamin interferometer design gives the system superior rejection of mechanically induced noise due to the common optical path of both arms and the lack of moving parts. The complimentary outputs are detected by two photodiodes (United Detector Technologies PIN 10DP). The signals are passed into a custom-fabricated instrumentation amplifier that provides the difference signal to both the lock-in amplifier (Stanford Research Systems SR510) and a personal computer running a LabVIEW (National Instruments) control program. The control program accepts inputs from the lock-in amplifier, instrumentation amplifier, and the power meter. A 1-second average of the DC component of the

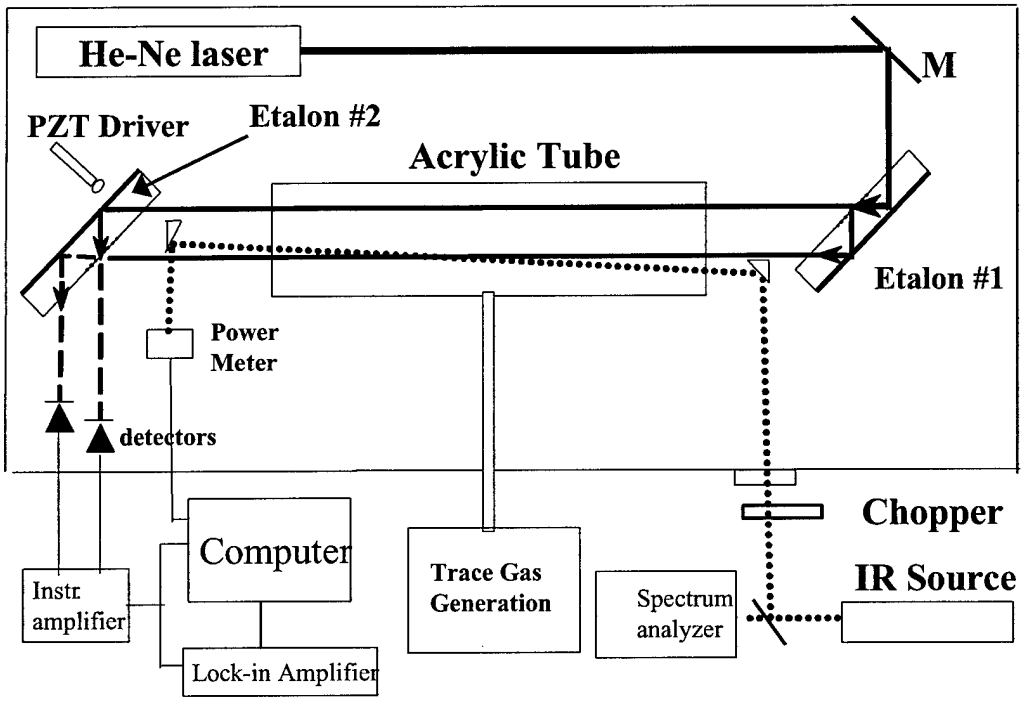

Figure 1. Experimental block diagram for modified-Jamin photothermal interferometer.

difference signal is used for feedback to control the piezo-electric (PZT)driven micrometer on the second etalon. This feedback control is used to maintain the interferometer in a quadrature position, which is the most sensitive position in relation to changes in the phase shift and the center of the linear response range. The lock-in signal and the measured IR power are used to provide an excitation power normalized signal. Pure trace gases are introduced into the acrylic tube via a trace gas generator (VICI-Metronics Dynacalibrator Model 190). The gas generator is set at 100°C and pure nitrogen flows of 0.1-1.0 L/min will produce trace levels of organo-phosphate from approximately 10 ppb – 1.0 ppm depending on the length of the permeation tube in the device and the flow. The IR excitation beam is introduced from a waveguide CO_2 laser (California Laser, circa. 1984) set at wavelengths corresponding to sizeable vapor absorption cross-sections. The beam is initially split with one part entering a spectrum analyzer (Optical Engineering 16A) to provide wavelength information. The other part is modulated by a chopper (f = 600 Hz) before entering the enclosure through an AR coated ZnSe window. This beam glances off the gold-coated hypotenuse of a prism making a shallow crossing angle with one arm of the interferometer. Using another coated prism, the beam is directed to broadband power meter. The effective path length is estimated at 10 cm with the IR beam diameter of 3-4 mm, with a probe beam diameter not exceeding 2 mm. This mismatch in beam diameters can be attributed to poor beam quality of the waveguide CO_2 laser. This is not an inherent quality of these types of lasers, but is related to the age of our laser system. The mismatch prevents the efficient use all of our IR excitation power.

DFG EXPERIMENTAL APPARATUS

Figure 2 is a block diagram of the DFG configuration used in our experiment. The output of a 852 nm distributed Bragg reflector (DBR) diode laser SDL-5722 and a tunable external cavity diode laser (ECDL) SDL-TC10-1393 operating in the 910-950 nm region for type II phase matching in $AgGaS_2$ were overlapped using a dichroic beamcombiner. The beams were focused using two cylindrical lenses and an aspheric lens for the ECDL and DRB lasers respectively. The 20-cm long AR coated nonlinear crystal was mounted on a on a motorized rotation stage to allow for angle tuning of the crystal to appropriately phase match the pump wavelengths. Calculations using published Selmier data[16] indicated a tuning range of 8-12 μm was possible by tuning the crystal approximately +/- 3 degrees from normal assuming a crystal cut of 44.15 degrees with respect to the optic axis. The infrared radiation generated in the nonlinear crystal was collected by a ZnSe lens and detected with a liquid-N_2-cooled HgCdTe detector (Electro-Optics Systems MCT012) after passing through a germanium plate and optical chopper.

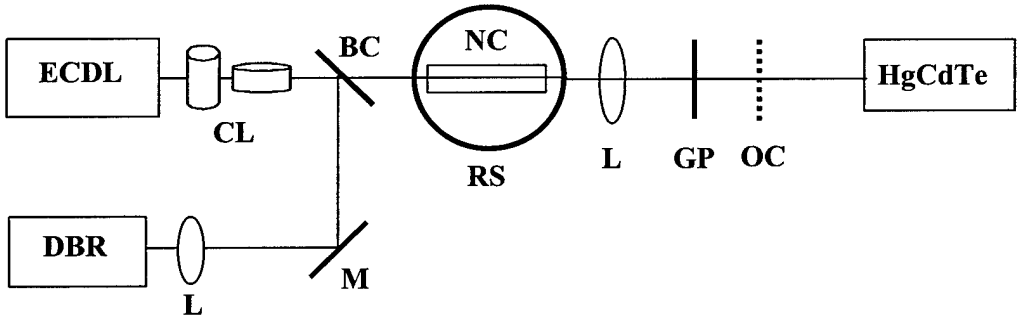

Figure 2. Block diagram of the difference frequency generation experimental set-up. L – lens, CL – cylindrical lens, M – mirror, BC – beam combiner, NC - nonlinear crystal, RS – rotation stage, GP – germanium plate, OC – optical chopper.

RESULTS AND DISSCUSSION

PHOTOTHERMAL

Initial trials were conducted by spiking the entire acrylic enclosure with minute volumes of methanol and methanol-glycerin mixtures. Using the methanol percentage, and known volumes of both the enclosure (169 L) and liquid, a partial pressure could be calculated. Figure 3 resulted from an 18-μL spike of pure methanol, which corresponds to 63 ppm partial pressure. The smooth line is a gaseous FTIR spectrum (EPA Public Gas Phase Database) overlaid on the experimental data taken with the PTI system. Despite gaps associated with the CO_2 laser this demonstrates the ability of the system to perform limited spectral discrimination using multiple lines of the grating-tuned CO_2 laser. Using methanol-glycerin mixtures and any of the 10P or 10R CO_2 lines as excitation, 1-ppm methanol levels were easily detected. Following these initial studies all beams were enclosed by the acrylic tube seen in Figure 1 and the trace gas generator was used to investigate responses from two organophosphonate compounds. Both dimethyl methylphosphonate (DMMP) and diisopropyl methylphosphonate (DIMP) permeation tubes of varying lengths were loaded in the generator. The tube lengths and calibrated flow range of our generation system limited the concentrations available for study to 10 ppb to 1 ppm. The power-corrected signal versus concentration is shown in Figure 4 for DMMP (σ_{DMMP}~ 44 $atm^{-1}cm^{-1}$) excited with the 9P(26) line (P = 575 mW). The log-log plot shows excellent linearity

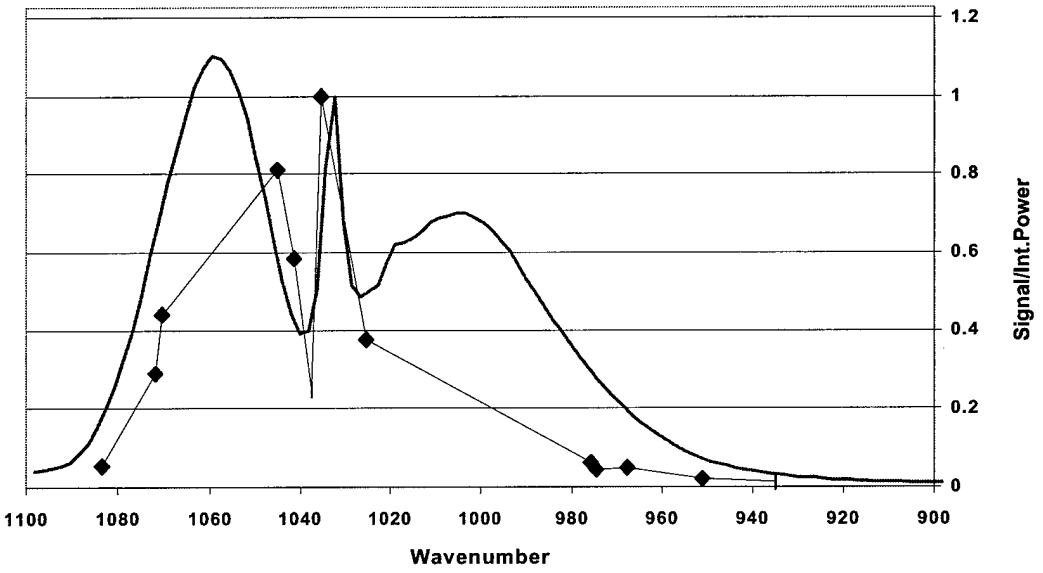

Figure 3. Spectrum of pure methanol excited with multiple CO_2 laser lines. The approximate concentration of the methanol is 63 ppm.

with a linear correlation coefficient (R^2) of 0.9987. The second organophosphonate studied provided more of a challenge to our system, due to the lack of available CO_2 lines at the maximum of the DIMP IR absorption spectrum. The DIMP absorption cross-section (σ_{DIMP}~ 27 $atm^{-1}cm^{-1}$) at the 10R(32) line is substantially weaker than the DMMP peak absorption, but was still measurable. The corrected signal versus concentration is shown in Figure 4 for DIMP excited with the 10R(32) line (P = 400mW). The log-log plot of the signal shows very good linearity with an R^2 of 0.9878.

The dynamic range of our trace gas generator and the PTI system noise floor dictate the limit of our measurements on both phosphonates. The electronic noise floor of 5-7 $\mu V/(Hz)^{-1/2}$ is still excessive considering the amplifier gains on the order of 10^4 V/A. This noise level is a factor of 60 above the shot noise limit of 10^{-7} $V/(Hz)^{-1/2}$ based on the systems standard parameters. Using an alternate amplified detector set (Thor Labs

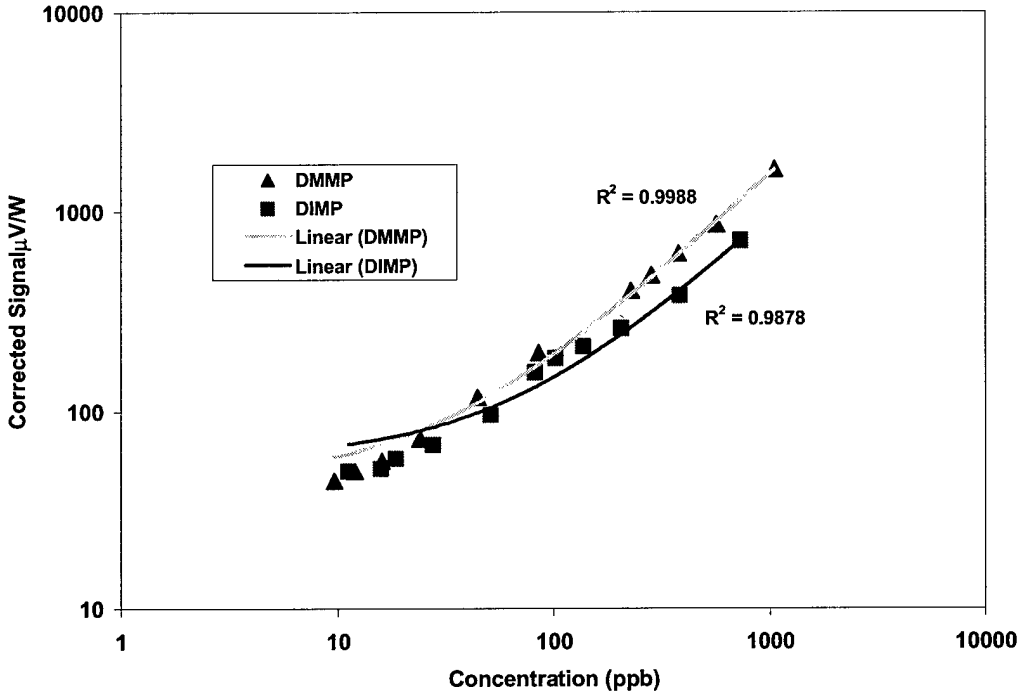

Figure 4. Log-log plot of corrected PTI signal versus DIMP and DMMP concentration.

PDA55) a calibration of the system phase sensitivity has been made. The calibration requires measurement of the interferometer as a function of PZT step, PZT step to applied voltage conversion, and finally known applied voltage to PZT drive input. Measurements were made piece-wise first recording interferometer response versus PZT step without active feedback followed by measurements of system response after known modulation was applied to PZT at normal detection frequencies. Using PZT step to applied voltage conversion factor and noise measurements the approximate phase sensitivity was calculated to be 1.85 µrad. Recent literature suggests that we can attain levels of noise that are factors of 3 to 4 above shot noise limits[3]. Other noise sources (acoustical and thermal) would probably prevent full realization of the shot noise limit. The second area that requires work is the CO_2 beam size and the shallow angle overlap. The CO_2 size should be less than or equal to the size of the probe beam to maximize use of the power that enters the interaction path. Insertion of an IR telescope to reduce the size and collimate the laser beam should make the system more efficient and aid in the alignment of the crossing.

DIFFERENCE FREQUENCY GENERATION

Result of our DFG ongoing effort to generate tunable infrared light as a source for PTI is described. Initial examination of ECDL beam showed astigmatism, which necessitated the use of two cylindrical lens to ensure co-located focusing of both vertical and horizontal directions. Use of two lens and beam combiner prior to the nonlinear crystal resulted in a beam radius that was approximately twice the optimal focus. Since the infrared output has a second-order dependence in the denominator of equation 5, the non-optimal focusing is results in an expected output that is reduced by a factor of 4. Initial attempts were centered on generation of an infrared output at 9.2 µm, which corresponds to normal incidence on a $AgGaS_2$ cut at 44.15 degrees. These attempts did not produce any measurable signal. Subsequent analysis with a version of equation 5 that includes

the walk-off term for critical (angular) phase matching[10] indicated the walk-off of our input beams could be sizeable. The walk-off of $AgGaS_2$ for our system was estimated at 22.7 mrad giving us an l_{eff} of approximately 4 millimeters. This reduced the effective length of the crystal to 20% of the total length. Conservative estimates with this effective length result in an experimentally realizable infrared output at 10-15 nW at a wavelength of 10 μm.

CONCLUSIONS

We have demonstrated the ability to detect trace amounts of organophosphonate vapor using PTI. This work focused on testing our detection system by incorporating a waveguide CO_2 as the excitation source. The measurement limits of 10 ppb for phosphonate vapors agree with the predicted sensitivity of several microradians of phase shift. Improvements on the system can be made in several key areas such as electronics and beam overlap. Initial studies on DFG for a highly tunable infrared source were performed. Experimental investigation suggests that the theoretical predictions were initially overestimated. Future work will concentrate on system improvements and continued study of difference-frequency-generation as highly tunable infrared source.

REFERENCES

1. D.L. Mazzoni and C.C. Davis, "Trace detection of hydrazines by optical homodyne interferometry," Appl. Opt. **30**, pp. 756-764, 1991.
2. M.A. Owens, C.C. Davis, and R.R. Dickerson, "A photothermal interferometer for gas-phase ammonia detection," Anal. Chem. **71**, pp. 1391-1399, 1999.
3. M.A. Owens, *Detection of Gas-Phase Ammonia Using Photothermal Interferometry*, University of Maryland, 1995 (dissertation).
4. E.A. McLean, L. Sica, and A.J. Glass, J. Appl. Phys. Lett. **13**, pp. 369, 1968
5. J. Stone, "Measurements of the absorption of light in low-loss liquids," J. Opt. Soc. Am. **62**, pp. 327-333, 1972.
6. J. Stone, Appl. Opt. **12**, pp. 1828, 1973.
7. C. C. Davis and S.J. Petuchowski, "Phase fluctuation optical heterodyne spectroscopy of gases," Appl. Opt. **20**, pp. 2539-2554, 1981.
8. S.E. Bialkowski, "Photothermal Spectroscopy Methods for Chemical Analysis," from *Chemical Analysis: A series of Monographs on Analytical Chemistry and Its Applications*, J.D. Wineforder, editor, Vol. 134, John Wiley & Sons, Inc., New York, 1996.
9. A.S. Pine, "Doppler-limited molecular spectroscopy by difference-frequency mixing," JOSA **64**, pp. 1683-1690, 1974.
10. U. Simon, Z. Benko, M. W. Sigrist, R. F. Curl, and F. K. Tittel, "Design considerations of an infrared spectrometer based on dfference-frequency generation in $AgGaSe_2$," Appl. Opt. **32**, pp. 6650-6655, 1993.
11. U. Simon, C. E. Miller, C. C. Bradley, R. G. Hulet, R. F. Curl, and F. K. Tittel, "Dfference-frequency generation in $AgGaS_2$ by use of single-mode diode-laser sources" Opt. Lett. **18**, pp. 1062-1064, 1993.
12. W. C. Eckhoff, R. S. Putnam, S. Wang, R. F. Curl, and F. K. Tittel, "A continuously tunable long-wavelength cw IR source for high resolution spectroscopy and trace-gas detection," Appl. Phys. B **63**, pp. 437-441, 1996.
13. F. Reif, *Fundamentals of Statistical and Thermal Physics*, Chapter 12, McGraw-Hill, New York, 1965.
14. R. W. Boyd, "*Nonlinear Optics*," Academic Press, New York, 1992.
15. G.D. Boyd and A. Ashkin, Phys. Rev. **146**, pp. 187, 1966.
16. D. A. Roberts, "Dispersion equations for nonlinear optical crystals: KDP, $AgGaSe_2$, and $AgGaS_2$," Appl. Opt. **35**, pp. 4677-4688, 1996.

PASSIVE STANDOFF DETECTION TEAM AT SBCCOM
RESULTS FROM THE OWL FIELD TEST
NEVADA TEST SITE
31 JULY THROUGH 11 AUGUST 2000

James. O. Jensen[a], Agustin I. Ifarraguerri[a], Alan Samuels[a], William R. Loerop[a], Richard Matta[b], Avishai Ben-David[c],
James W. Yang[d], Christopher Gittins[e], William Marinelli[e], Thomas Gruber[f], and Dustin Grim[f]

a. Passive Standoff Detection Team, U.S. Army SBCCOM, AMSSB-RRT-DP, APG, MD 21010-5424
b. Future Sensors Branch - Aerospace C2, Intelligence, Surveillance and Reconnaissance Center, AC2ISRC/C2RI, Langley AFB, VA 23665-1993
c. Science and Technology Corp. 500 Edgewood Road, Suite 205, Edgewood, Maryland 21040
d. Geocenters Inc, Bldg E3160, rm 48, APG, MD 21010-5424
e. Physical Sciences Corp, 20 New England Business Center, Andover, MA 01810
f. Mesh Inc, 129 Bechel Road, Oxford, PA 19363

ABSTRACT

An overview is presented of ongoing efforts in applied research by the Passive Standoff Detection Team at the U.S. Army Soldier Biological Chemical Command (SBCCOM). Passive infrared sensors such as the TurboFT, the High Sensitivity Field Fourier Transform Infrared Spectrometer (HISPEC), and the Adaptive InfraRed Imaging Spectroradiometer (AIRIS) will be described. The Owl Field Tests were held at the Nevada Test Site for a three-week period from 31 July to 18 August 2000. The AIRIS utilizes a Fabry-Perot tunable filter to spectrally resolve the image, which is captured on a 64x64-element HgCdTe focal-plane-array. The TurboFT uses a spinning crystal design to achieve scan speeds of up to 100 scans/sec with an ultimate goal of 360 scans/sec. The TurboFT utilizes a 16-element (2x8) focal-plane-array. The HISPEC is a single pixel sensor with extremely high sensitivity.

INTRODUCTION

The longwave infrared region (8 to12μm) of the EM spectrum has been used for some time at ECBC for passive detection of Chemical Warfare (CW) agents[1]. Passive LWIR detection utilizes small temperature differences between CW clouds and backgrounds for detection and alarm of a possible CW attack. This is shown in Figure (1).

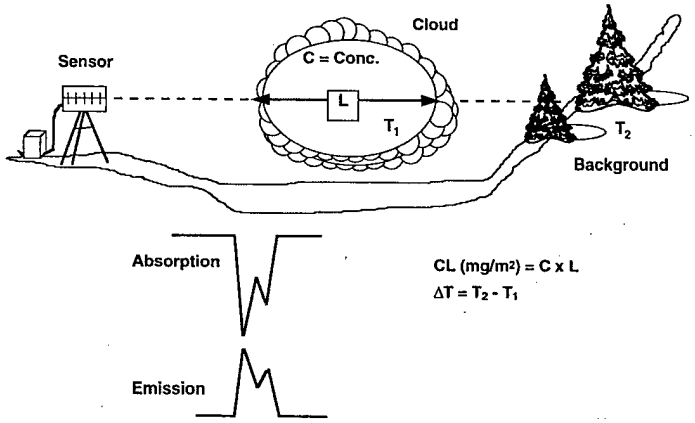

Figure 1. Principle of operation for the Chemical Imaging Sensor.

The Owl Field Tests were recently held at the Nevada Test Site. The Tests ran for three weeks from 31 July to 18 August 2000. The SBCCOM motor home spent 2 weeks in trailer park number 3, which is 1.5 kilometers form the release stacks. Three LWIR (8μm to 12 μm) passive sensors were tested. These are shown in Figure(2)

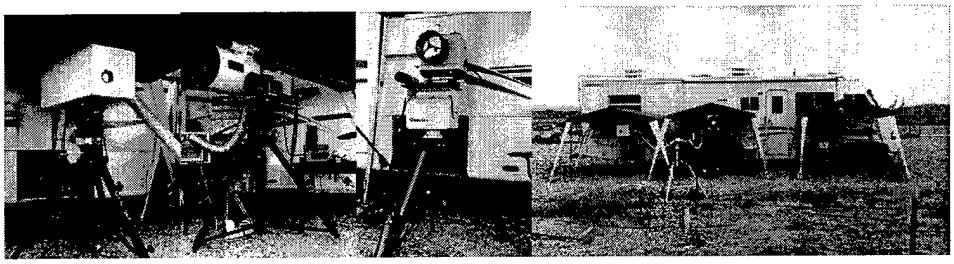

Figure 2. Three Sensors Tested – top from left to right, AIRIS, HISPEC, and TurboFT. Far right shows the three sensors as positioned next to the motorhome during the tests.

AIRIS– The AIRIS (Adaptive InfraRed Imaging Spectroradiometer) is comprised of a 64 x 64 element HgCd infrared focal-plane-array (FPA) which views the farfield through a tunable piezoelectric-actuated Fabry-Perot interferometer[2] placed in the afocal region of the imaging system. The AIRIS optical configuration is depicted in figure (3).

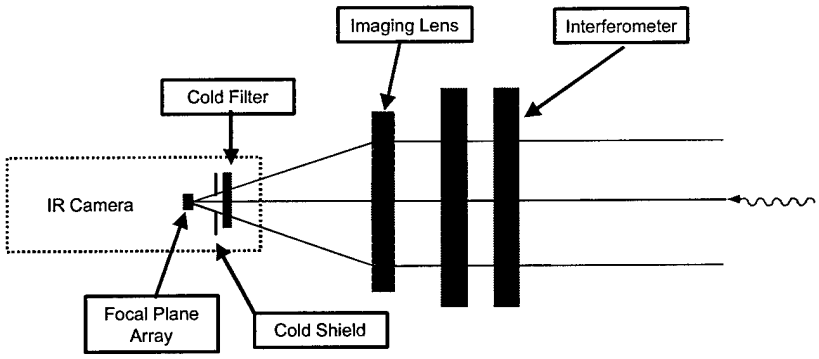

Figure 3. Diagram showing the Functioning of the AIRIS sensor.

The Fabry-Perot interferometer functions as a widely tunable, LWIR interference filter. The wavelength of light reaching the FPA is determined by the spacing of the two parallel mirrors. Light is transmitted when the mirror spacing, d, is equal to a half integer multiple of the wavelength, λ, i.e. $d = m\lambda/2$, where m is an integer. All other wavelengths are reflected. A cryogenically cooled optical filter allows only one of the transmitted wavelengths to reach the FPA.

Computer controlled selection of the transmitted wavelength takes advantage of the HgCdTe infrared focal-plane-array detector interface. The AIRIS is capable of using either sequential or selective sampling of wavelengths to build spectral data cube. Thus it is possible to tune the etalon to select wavelengths where expected chemical bands and background measurements can be made. Common pixel registry provides for simple processing for chemical cloud detection

The prototype AIRIS Spectrometer that was tested during the Owl Field Tests was manufactured by Physical Sciences Inc. The AIRIS has an operating Range from 900 cm^{-1} to 1250 cm^{-1}. (continuous coverage of full range) with a spectral Resolution of between 8 cm^{-1} and 10 cm^{-1}. The AIRIS has a per-pixel instantaneous field of view (IFOV) of 1.2 mrad. Noise Equivalent Spectral Radiance (NESR) of the AIRIS has been measured at 1 x 10^{-8} $W/(cm^2$ sr wavenumber), which is comparable to the best hyperspectral systems available in the LWIR region.

During single chemical and multi-chemical releases, the AIRIS successfully demonstrated simultaneous selective detection of individual and multiple species. AIRIS also demonstrated selective detection of single species at low column density. For example, Figure (4) represents the data taken during a DMMP release of 33 ppmv-m. At this low concentration DMMP could only be detected at a single pixel

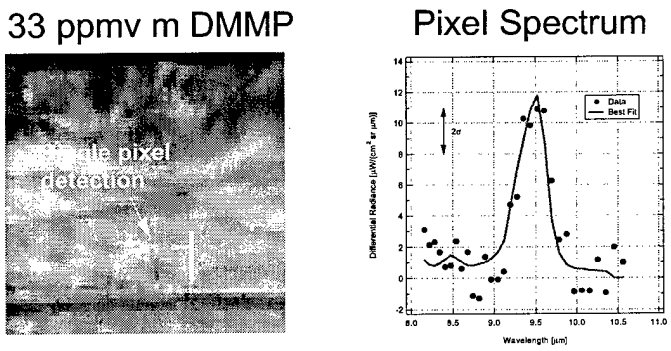

Figure 4. A 33 ppmv-m release of DMMP. The spectrum can be extracted.

A more concentrated release is shown in Figure (5). The plume remains hotter than background for about 10 meters. At that point the plume cools to the temperature of the mountain in the background. The Plume can be detected in absorption further downwind.

A Gaussian plume dispersion model was used to predict the plume temperature and DMMP concentration profile under four sets of release conditions. The output of the plume dispersion calculation was used as input for a multi-layer atmospheric radiative transfer model to predict the wavelength dependent radiance reaching the sensor. Figure (6) depicts the calculated differential radiance at 9.5 μm, corresponding the maximum in the DMMP emission spectrum, as a function of distance downwind of the DMMP plume release point along with the experimentally determined differential radiance. The plume rapidly cools and dilutes resulting in a rapid decrease in peak differential radiance. The measured plume radiance and detected plume length is consistent with local meteorological conditions (avg. wind velocity, Pasquill Class C (slightly unstable) atmosphere), plume release temperature, chemical concentration, and sensor NESR.

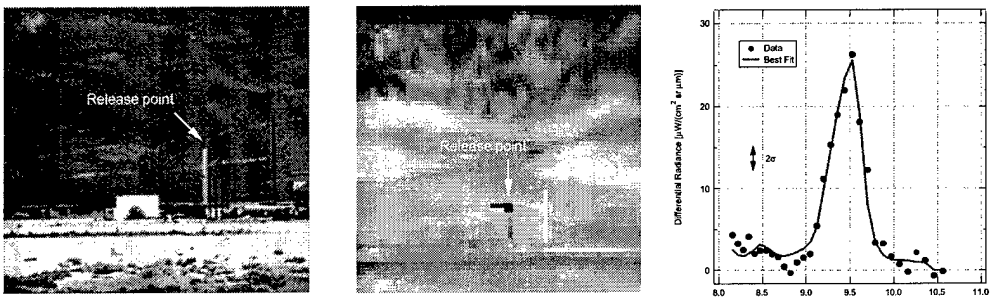

Visible image of chemical plume release stack

Broadband IR image w/automated plume detection

Spectrum of representative pixel w/DMMP detect

Figure 5. Release shown above is DMMP (~1800 ppmv, 160 deg C). Hot plume observed in emission (red = probable detect, yellow = possible detect) 8 frame avg., tint = 1.44 ms, 1.5 km stand-off.

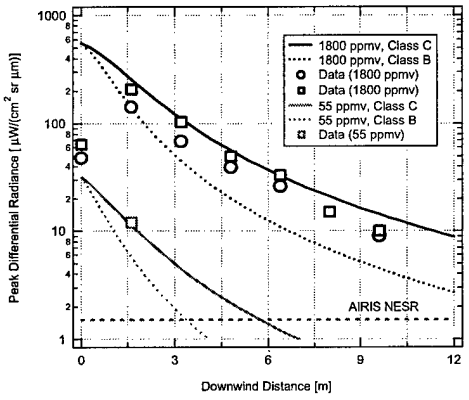

Figure 6. Four DMMP releases analyzed in detail. Meteorological station provides wind speed, direction near release point: 7 m/s avg. (12 m/s max, 3 m/s min), dir = SW. Measured plume radiance and detected plume length consistent with local meteorological conditions (avg. wind velocity, Pasquill Class C (slightly unstable) atmosphere), plume release temperature, chemical concentration, and sensor NESR.

TurboFT - The Chemical Imaging Sensor (CIS) is currently a sixteen-pixel system utilizing the TurboFT Spectrometer developed by Designs and Prototypes.[3] The major benefits of the TurboFT over other conventional Fourier Transform Spectrometer (FTS) designs is the extremely high-speed operation (hundreds of scans per second), the ability to run without a laser, and the very small size and low weight. The high speed is the direct result of the rotary scan technique using a mass balanced rotor design. A

comparison of the TurboFT design and a conventional Michelson FTS is shown in Figure (7). Since there is no scan direction reversal (a characteristic of the Michelson interferometer) in the TurboFT, the operation is very smooth and stable. Most vibrational disturbances, which would otherwise affect spectral quality, are eliminated. Speed of operation is limited more by constraints in signal electronics than by mechanical parameters. The laser-less operation is also a direct benefit of the rotary scan.

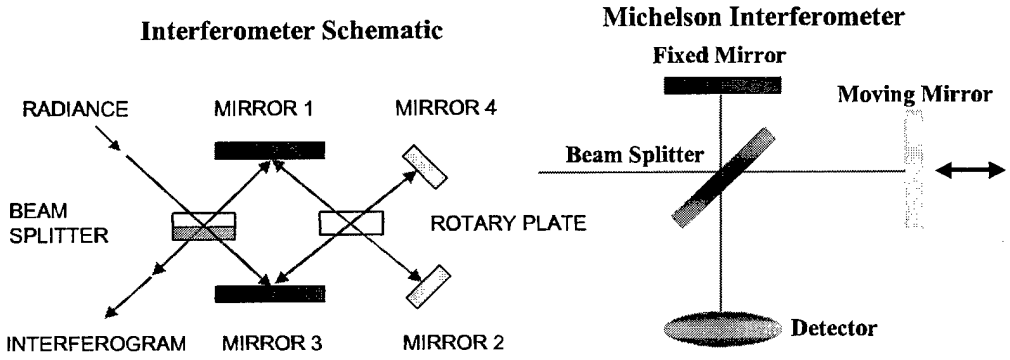

Figure 7. Comparison of the TurboFT interferometer vs. a traditional Michelson design. The TuboFT is very simple in its design. It has no laser and is very small and lightweight. It also is capable of operating at very high speeds.

The sixteen-element focal-plane array is shown schematically in figure 8 with its current pixel arrangement of 2 x 8. Each pixel represented a rectangle of approximately 2 meters by 10 meters when sensing from a distance of 1.5 Kilometers.

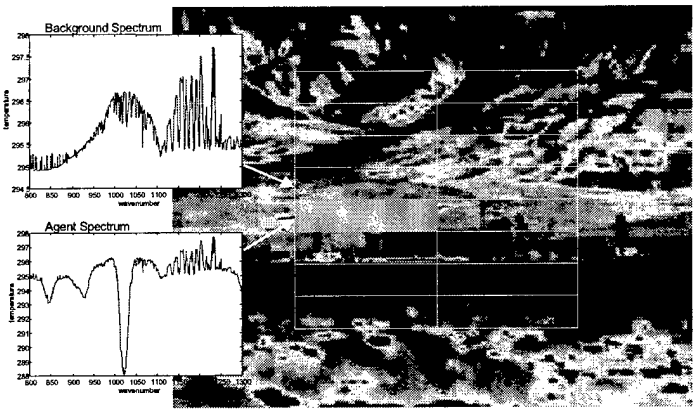

Figure 8. The current arrangement of the sixteen-element focal-plane array in the TurboFT. The current system is bore sighted with a visible camera. At a distance of 1.5 kilometers, each pixel covers an area of approximately 2 meters by 10 meters.

At the Owl Field Tests the TurboFT operated at very high speeds approaching 100 scans/sec with good results. Figure (9) represents the special ratio of some data taken on 4 August 2000. The Special Ratio is defined to be:

$$SR = \frac{release - blackbody}{background - blackbody}$$

As seen in Figure (9), the peak near 950 cm^{-1} can be attributed to the SF_6 in the release.

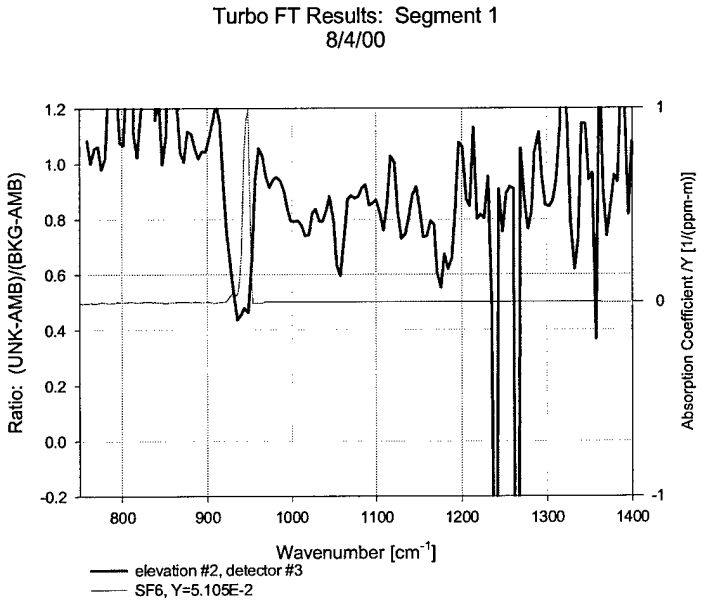

Figure 9. Special Ratio of data taken of an SF_6 release using the TurboFT at the OWL Field Tests.

Since the Chemical Imaging Sensor will be required to operate "on the move", we have been working on algorithms that do not require background subtraction. In Figure 10 we show the same data sets analyzed using the Mesh Algorithm.

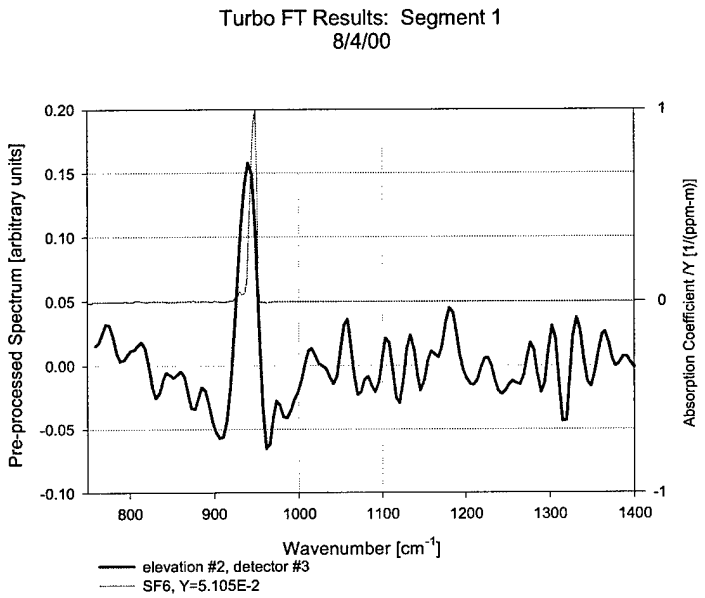

Figure 10. Analysis of data taken of an SF6 release using the TurboFT at the OWL Field Tests using the Mesh Algorithm.

HISPEC – The HISPEC (High Sensitivity Field Fourier Transform Infrared (FTIR) Spectrometer) is a traditional Michelson single-pixel field spectrometer. However the HISPEC was designed to be ultra-sensitive with an extremely low single scan NESR[4] (2 x 10^{-10} watts/(cm^2 sr wavenumber)). The HISPEC, manufactured by Block Engineering, is probably the most sensitive FTIR spectrometer in the world. This high sensitivity was achieved with several innovations. Notable among the unique properties of the HISPEC are the ultra-stable reference channel and its signal channel electronics.

The requirement of increased system sensitivity places an increased burden on the detector parameters and the signal channel electronics. Throughout the design of the signal channel, great care has been taken toward minimizing sources of performance-limiting noise and preservation of a large dynamic range. Since the HISPEC is envisioned for possible mass production at some time in the future, hand selection of components was avoided. Design parameters dictated that sensitivity improvements must be the result of improvements in the core design combined with better matching of the final sensor to a given application.

The primary factors involved in the sensitivity improvement are increased throughput (increased target photon collection), a detector carefully matched to the collection optics (throughput matching), increased dynamic range, and higher sampling stability. The

detector must also be matched with the signal channel electronics to take full advantage of the greater signal levels. This demands optimal detector cold shielding, a detector-noise-limited/wide dynamic range preamplifier, a post-amplifier with the correct bandwidth filtering and the equivalent of true 20+ bit analog-to-digital (A/D) converter performance.

In order to achieve maximum sensitivity, a properly designed signal channel must preserve the detector noise from the analog input throughout the digitization process (i.e. the noise introduced during the digitization process must not be significant relative to the detector noise). This means that the analog noise must be equal to or greater than the least significant bit in the A/D converter. If this condition is not met, then the A/D board is throwing away information and thus sensitivity. Modeling has shown that a standard 16-bit A/D board, commonly present in interferometers manufactured today, is not sufficient. In order to be "detector noise-limited" the dynamic range of the instrument must be increased.

The current HISPEC uses a gain-ranging technique to obtain an effective 22 bits of resolution. Thus, the centerburst of the interferogram is digitally captured while at the same time preserving resolution at the wings of the interferogram. This is shown in figure(11). This is accomplished by running two simultaneous analog post-preamplifier signal chains whose gains are set by a factor of sixteen (4 bits) apart. The system utilizes a single wide dynamic range preamplifier, which feeds the two different post amplifiers simultaneously. At the beginning of each scan, the analog multiplexer (MUX) connects the output of the low-gain post-amplifier to the A/D. At a selected point in the interferogram, the MUX switches to the high-gain post-amplifier and then presents the signal to the 18-bit A/D converter for conversion (after passing through an electronically programmable low-pass filter). The purpose of the programmable filter is to allow operation at more than one pre-selected retardation (spectral output) rate with the change in band of inteferometer frequencies that occurs. We have at the output of the A/D 18-bit words, which correspond to the 1X output up to the point where the counter/latch switches the MUX to the 16X gain output. At the corresponding time, the amplitude of the digital words taken at the higher gain is divided by 16. This is done by shifting the words 4 bits toward the least significant bit. In this way the interferogram is fully corrected and the change in gain is transparent to the computer and the user. Since the change in gain is done by multiplexing, no spurious signals are generated.

The high sampling stability of the interferometer is achieved by placing the optical reference signals (white light and HeNe laser) in the center of the optical axis, thus making them immune to mirror tilt. The result is significantly improved sampling and phase stability, which translates into higher sensitivity

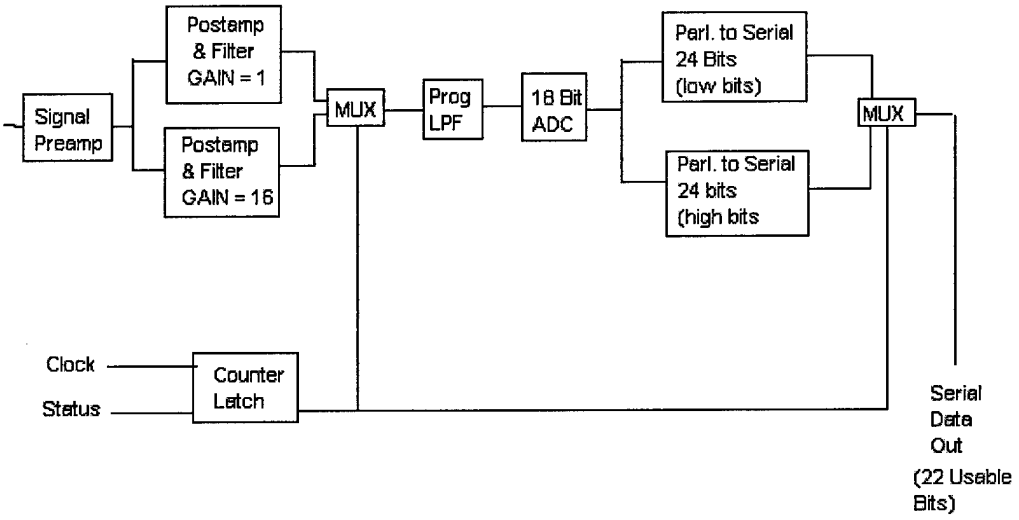

Figure 11. Digitizing Electronics in the HISPEC.

At the Owl Field Tests the pixel size of the HISPEC was approximately 10 meters square. While this does not match the stack size exactly, it gave some very good data. The detection of individual chemical species was performed using a matched filter technique. This is shown in Figure (12). After converting the radiance spectra to pseudo-transmission (i.e. un-scaled transmission), the influence of the atmospheric absorption was suppressed using the orthogonal projection operator:

$$\mathbf{P} = \mathbf{I} - \mathbf{U}\mathbf{U}^T$$

where **U** is the orthonormal matrix containing the first few principal vectors of the matrix formed by all the pseudo-transmission spectra for a given day of collection. Typically, **U** consists of either one or two column vectors, since the atmospheric transmission is the primary contributor to the spectra. The matched filter score is then obtained by:

$$score = \frac{\mathbf{x}^T \mathbf{P}\mathbf{t}}{\mathbf{t}^T \mathbf{P}\mathbf{t}}$$

where **x** is the column vector containing the pseudo-transmission and t is the target column vector obtained from a spectral library. A score of 1.0 or -1.0 represents an exact match (the sign indicates emission or absorption).

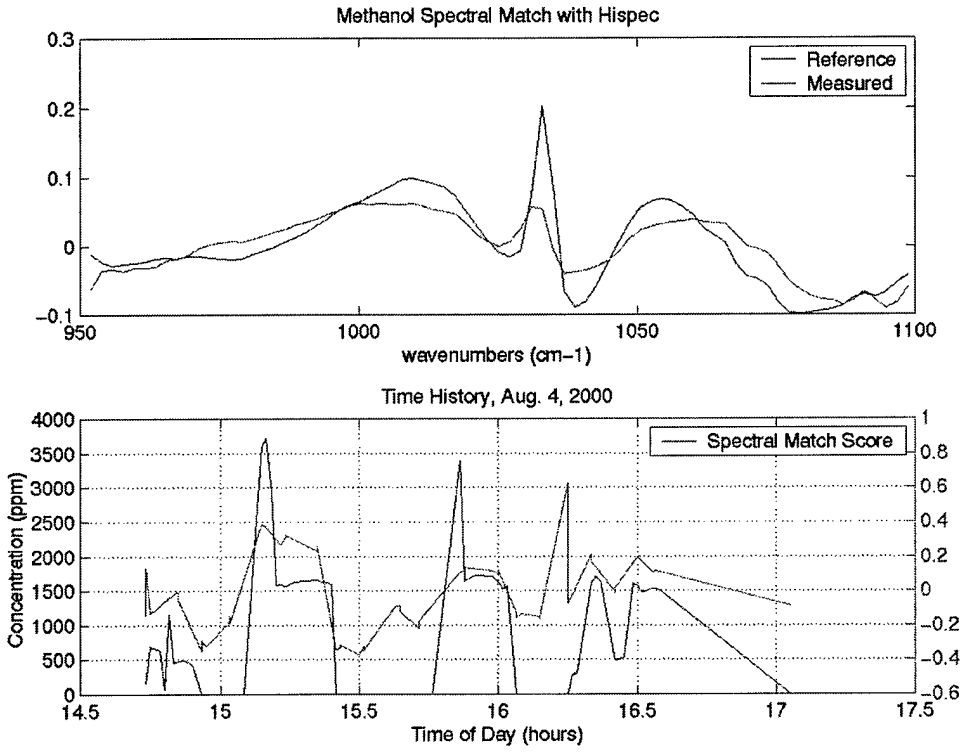

Figure 12. Top spectrum of methanol extracted from the HISPEC data. Below is the spectral match score, which gives an estimate of the concentration of methanol from the stacks.

SUMMARY AND CONCLUSION

The goal of the JSWAD program is to produce imaging spectrometers that maintain high chemical detection sensitivity while operating at very high acquisition rates. Detection "on-the-move" scenarios are very important to many DOD Joint Service applications, as is the ability to "look" everywhere at once without scanning. High sensitivity must be maintained in order to sense chemicals as relatively low concentrations a distances of up to several kilometers. Three sensors were recently tested at the Owl Field Tests at the Nevada Test Site in support of the Joint Service Wide Area Detection (JSWAD) Program. The TurboFT, AIRIS, and HISPEC spectrometers were evaluated with good success.

REFERENCES

1. W.R. Loerop, "Feasibility Of Detecting Chemical Agents Using a Chemical Imaging Interferometer From Low and High Altitude Platforms". U.S. Army Edgewood Research Development and Engineering Technical Report, ERDEC-TR-381, (1996)

2. C.M. Gittins, W.G. Lawrence, and W.J. Marinelli, "Frequency Agile Bandpass Filter for Direct Detection Lidar Receivers," Appl. Opt. **37**, 8327-8335 (1998); W.J. Marinelli, C.M. Gittins, A.H. Gelb, and B.D. Green, "Tunable Fabry-Perot Etalon-Based Long-Wavelength Infrared Imaging Spectroradiometer," Appl. Opt. **38**, 2594-2604 (1999)

3. W. Wadsworth and J.P. Dybwad, "Ultra High Speed Chemical Imaging Spectrometer", Proc. Of Electro-Optical Technology for Remote Chemical Detection and Identification II, Vol 3082, pp 148, SPIE, Bellingham, WA (1997); W. Wadsworth and J.P. Dybwad, "Chemical Imaging Spectrometer", Proceedings of the Fourth Joint Workshop on Standoff Detection, Williamsburg, VA, Science and Technology Corp., Oct. 1998.

4. T.G. Quinn, R.F. Conners, C. Fehser, J.A. Flanagan, D.E. Grover, E.R. Schildkraut, J.O. Jensen, and W.R. Loerop, "Optimized, High Sensitivity, Field FTIR Spectrometer – HISPEC", Proceedings of the Fourth Joint Workshop on Standoff Detection, Williamsburg, VA, Science and Technology Corp., Oct. 1998.

DEVELOPMENT OF A CB RESISTANT DURABLE, FLEXIBLE HYDRATION SYSTEM

Peyton W. Hall, Frank T. Zeller, John W. Bulluck, and Michael L. Dingus
Texas Research Institute, Austin, Inc.
9063 Bee Caves Road
Austin, Texas 78733

A durable, flexible hydration system resistant to contamination by contact with VX, GD, and HD chemical agents, as well as damage by the decontaminants sodium hypochlorite and DS-2 is being developed for aviator use. Decisions have been made regarding the often conflicting concerns of water potability and protection from chemical agents in compliant polymeric materials. Water potability and health concerns dictate the use of high purity thermoplastic resins with very limited use of lubricants, accelerators, antioxidants, and plasticizers. Flexible chemically resistant applications demand the use of highly crosslinked, permeation resistant, plasticized elastomers or thermosets. By using multilayer laminated and unlaminated polymer composites, as well as closely examining permeation properties, a balance has been reached to meet these conflicting requirements.

INTRODUCTION

The threat of chemical and biological warfare has accelerated the implementation of protective clothing for aircrew personnel. This protective clothing insulates aircrew personnel and accentuates the need for hydration during long or hot weather missions. Decline in mental performance with lack of proper hydration has been well documented and it is likely that physical performance is also affected[1]. Pilots must have the tools to hydrate in flight to maintain peak performance even in a CBW environment. Therefore, a personal hydration system designed for cockpit use is being developed to meet the hydration need, as well as provide CBW hardened protection of that water source from HD, GD, and VX agents.

The new hydration system was developed to exceed the capabilities of the previous generation two-quart canteen. The previous generation MIL-C-43603B two-quart canteen was designed neither for chemical and biological warfare use nor aviator use. This ethylene-vinyl acetate (EVA) canteen only provided a "disposable" CBW solution for ground forces. The new hydration system, consisting of a flexible water pouch, fill port, drink tube, and connecting hardware has been specifically designed for aviator use with the CBW protective ensemble. It has been designed to integrate with existing CBW aviator hardware and is unobtrusive in a tightly packed cockpit. Construction is modular and will allow adaptation to other military personal hydration configurations.

This paper will first discuss the mechanical design features of this cockpit-compatible hydration system. Next, material selection will be discussed. Finally, performance characteristics of prototype units will be presented. Performance was assessed using various mechanical, thermal, and chemical challenge tests.

MECHANICAL DESIGN

The CBW flexible hydration system was designed to integrate with existing aircrew hardware. First, it had to fit inside the AIRSAVE vest. This requirement necessitates flexibility because the water pouch is worn directly against the body, with several components mounted on the outside of the vest. The best way to ensure comfort for the pilot was to make the pouch completely compliant. Second, the pouch was required to connect directly to the M45 protective mask. The M45 mask connects to the M1 cap using an ethylene propylene diene monomer (EPDM) rubber tube and a metal drinking straw. The M1 cap, however, is a large, stiff component that will not fit comfortably inside a vest. Instead, a low profile fill port with a remote connection to the metal straw used with the M1 cap was designed. A comparison of these fittings is shown in Figure 1.

Without the connection for the metal straw provided by the M1 cap, a new location for the drink straw receptacle was required. This fitting was located on the end of a flexible tube that connects to the low-profile spout. The fitting was designed such that it can either be used with the drinkstraw, or in a non-CBW or emergency situation, can be drunken from directly. This situation might occur after a pilot has ejected and is awaiting rescue, but no longer wearing the M45 mask. Figure 2 shows the drink tube fitting connected to the metal drink straw.

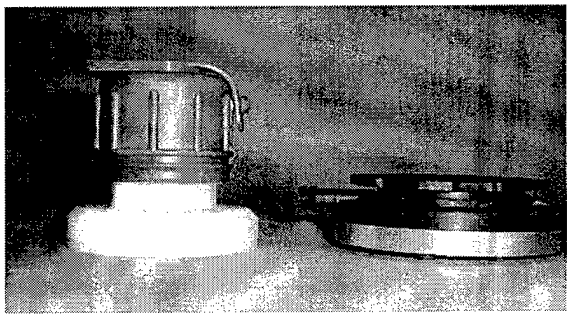

Figure 1. M1 cap and spout (l) and prototype low profile spout (r). The low profile spout was designed to lay flat against the body, preventing point pressure in the pilot's ribcage area.

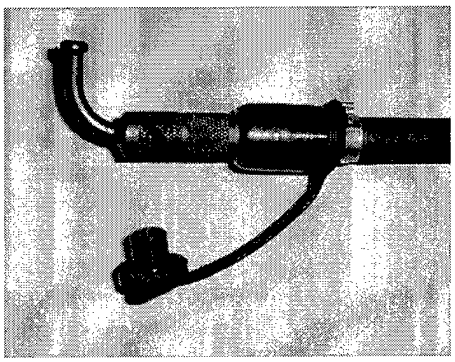

Figure 2. Metal drink straw connected to water pouch fittings. Tethered dust cap also shown. These fittings are sized for ease of placement in the vest, out of the windstream during ejection.

MATERIALS SELECTION

Aromatic thermoplastic polyurethane was selected as the inner bladder material to come in contact with the water for several reasons. First, it is flexible and tough over a wide temperature range without the use of plasticizers. Ultimate elongations of 500 to 600 percent are typical for urethanes without plasticizers. Other polymers such as PVC require additives to retain flexibility at room temperature, and still become brittle at near freezing temperatures. With regards to mechanical properties, the only other competing materials are elastomers, or rubbers. However, rubbers must be crosslinked by vulcanization using sulfur to obtain useful mechanical properties.

Unreacted sulfur or accelerators, even in very small amounts, imparts a foul taste to water that contacts it for any significant period of time. Additionally, typical rubbers must be chemically glued together, whereas polyurethane is a thermoplastic that readily forms strong thermal welds. Chemical bonding introduces another set of potentially toxic chemicals to drinking water and can be less reliable mechanically. The only problem with thermoplastic urethane is that it has relatively low resistance to permeation by chemical agents. An outer barrier is therefore required.

For the outer protective covering, a multilayer laminate already proven worldwide in industrial chemical protective applications is utilized. This laminate meets performance requirements, including permeation, flammability, and abrasion resistance, of the National Fire Protection Association (NFPA) 1991,1994 edition standard[2]. This proprietary laminate consists of several polymeric layers including a polyamide fiber reinforcement layer for strength, several rubber layers for permeation resistance, and a thermoplastic layer to allow for thermal welding. These materials are shown in Figure 3.

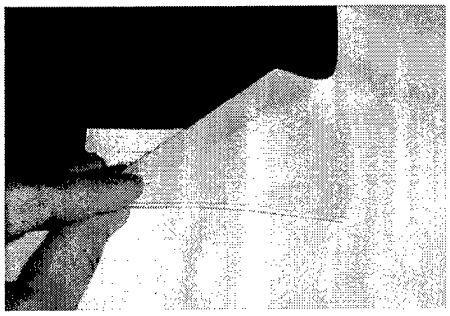

Figure 3. Bladder materials. The clear material is the inner water containing polyurethane, while the outer material is a multilayer laminate barrier.

The requirements for the tubing are not entirely similar to those for the pouch material. First, the tubing must be stiff enough to prevent collapse, but flexible enough to prevent kinking and allow ease of movement. Unfortunately, flexibility is usually related to permeability. Secondly, the tubing must be of a type approved for contact with potable water. It would seem the ideal tubing would consist of a layer of highly resistant fluoropolymer over a soft, flexible potable water formulated polymer. TFE fluoropolymers are inherently stiff and prone to kinking. Multilayer tubing is prone to difficulties with reliably sealing both tubes at the ends. A single layer tubing with the ability to both carry potable water and resist permeation and damage by both CBW agents and decontaminants was required. By choosing a flexible, chemical resistant tubing of a sufficient thickness to keep the permeation rate low, all requirements could be met.

Table 1 shows a listing of the most promising tubing materials. These were tested against dimethyl sulfoxide as an agent simulant. DMSO is polar aprotic solvent and is specified as a chemical agent simulant because it quickly permeates skin, similar to CBW agents, but has relatively low toxicity[3]. It thus provides a safe, worst case testing medium. Testing of tubing materials was performed by placing 20 ml of distilled water into 2 foot long sections of tubing, then immersing the center 12 inches of the tubing in a 50 vol% DMSO, 50 vol% water mix for 72 hours at room temperature and pressure. The water inside the tubes was then collected and tested for DMSO content using a Hewlett-Packard 5890 Series 2 gas chromatograph. Tubes were 1/4"ID by 7/16"OD unless otherwise noted. Table 1 also shows the advantages and disadvantages of each tubing material.

TABLE 1. Tubing material DMSO challenge test results and advantages and disadvantages of each material. Minimum level of detection was 10 ppm. Materials such as silicone rubbers and fluoropolymers were not tested because they were too permeable or too rigid.

Material	**72 hour water contamination by DMSO, ppm**	**Advantages**	**Disadvantages**
Tygon lined EPDM (ethylene propylene diene monomer)	<10	-flexible -highly resistant to permeation	extremely difficult to use with tube fittings
EPDM	<10	-single layer -works well with fittings -very flexible	imparts foul taste to water
Food grade Tygon, 3/8"OD	23 (average 0.005 ìg/cm^2/min)	-NSF approved-imparts no taste to water -flexible -single layer -works well with fittings	somewhat permeable
Food grade Tygon, 1/2"OD	<10	-same as above, but longer protection -will not kink	-difficult to use with standard fittings (too thick) -permeability
polyethylene lined ethyl vinyl acetate	<10	-tough and strong -cut resistant -low permeability -FDA compliant -seals well over barb fittings without hose clamps	-inflexible -can't use hose clamp valve to shut off flow -possible infiltration between layers
fluorinated ethylene propylene lined Tygon	<10	-flexible -low permeability	-kinks easily -cannot be used with barbed tube fittings or hose clamp valve

EPDM tubing has the best properties from a mechanical and CBW viewpoint, but the taste of water passing through this tubing is revolting. Personnel would most likely begin suffering the effects of dehydration before they would want to drink water that contacted this tubing or any other rubber materials. It is suspected that residual unreacted sulfur contained in the rubber contaminates water in contact with it. Although not toxic, it takes very little contact time to make the water undrinkable. The Tygon food and beverage tubing, by contrast, was found to add no detectable taste to water. Further testing of a thicker wall 1/4"ID by 7/16"OD food grade Tygon tubing for 96 hours in 50% percent DMSO revealed no contamination of the water inside. It is believed that the claimed exceptionally low porosity of this material keeps permeation rates low without excessive stiffness[4]. From the above data, it was decided that this thickness of food-grade Tygon tubing sufficiently resists permeation and damage by solvents and alkaline solutions, yet provides good flexibility and adds no taste to contacting water.

PERFORMANCE

At this time, the first of two developmental batches of pouch prototypes have been tested. Tests have been classified as mechanical, thermal, and chemical.

The first mechanical test of the water pouch was a drop test. A pouch was dropped from a height of eight feet onto a smooth concrete surface. This test was repeated for each of the 6 orthogonal directions relative to the water pouch as shown in Figure 4. No damage occurred.

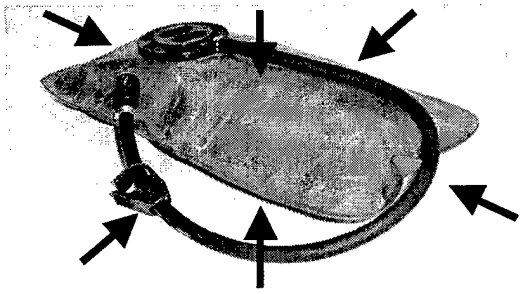

Figure 4. Drop test. The pouch was dropped such that impact occurred from all 6 directions.

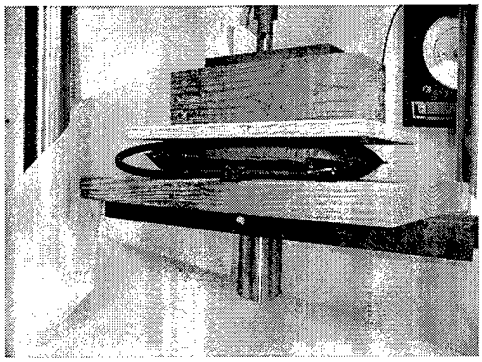

Figure 5. Crush test. In this configuration, the water pouch withstood a load of 1000 lbs with no damage.

The next test was a pressurization test for leakage. A pouch was submerged under 6 inches of water, then pressurized internally to 4.0 psi with air. No leakage occurred. Next, this pouch was placed in a hydraulic load frame as shown in Figure 5. In the configuration shown, a load was applied in displacement control at a rate of 0.5 inches/minute. When held at 1000 lbs. load for 30 seconds, no damage occurred. When the load was increased to 1200 lbs., slow, noncatastrophic separation of the heat sealed area of the outer barrier material occurred in one location. The chemically bonded tape did not separate, however, so no holes actually appeared in the outer layer and no leakage occurred at this location. Approximately 5 ml of water leaked from the spout during this testing. Upon subsequent air pressure testing of the same pouch as described above, a bubble appeared every 5 to 10 seconds at one location on the spout when pressurized to 3.5 psi due to slippage of the pouch material relative to the spout. Subsequent redesign included a reinforcing ring of double thickness polyurethane in the spout region to address this weakness, even though these tests far exceed previous durability expectations.

To address the possibility of breakthrough of the inner layer without visible damage to the outer layer, several puncture tests were conducted as shown in Figure 6 using both FTMS 101 M2065 (round tip probe) and ASTM D 4833 (cylinder tip probe) test equipment. To test the pouch material as a system, both layers were placed in the test apparatus in the same configuration as in the pouch. In these tests, puncture of the outer material always occurred first. In fact, the physical limits of the test apparatus were reached before puncture of the urethane material occurred.

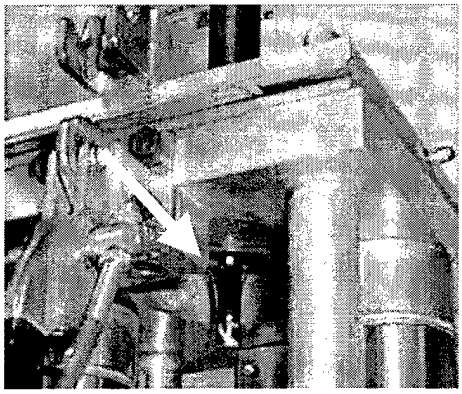

Figure 6. Puncture testing of the urethane/polymer laminate system. The puncture probes always broke through the outer layer, but not the inner urethane layer, even after 2 inches of displacement. The inner bladder cannot be punctured without visible damage to the outer material.

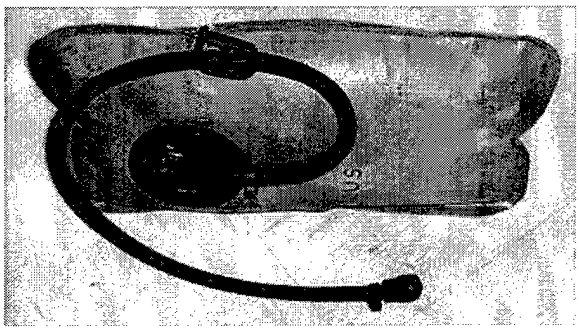

Figure 7. Frozen, filled water pouch. No damage occurred.

The final mechanical test was designed to address the possibility of decompression at high altitude during ejection or mechanical failure. The maximum change in pressure that is expected to occur in flight is from filling and sealing at sea level (14.7 psia) to a final cabin altitude after decompression of 40,000 ft (2.7 psia)[3]. To simulate this effect, a pouch was placed in a vacuum chamber and the pressure was reduced from atmospheric to 2.7 psia. Although rapid decompression (<15 seconds) was not difficult to reproduce and did not effect the pouch, explosive decompression (<0.1 seconds) is more difficult and has not yet been simulated. Due to the incompressibility of water and a vapor pressure of only about 0.5 psi at room temperature, the water pouch had to be filled partially with air for this test to be of any consequence. Because the pouch is flexible and there will only be a small quantity of air inside, it is expected that explosive decompression will also have very little effect on the pouch. Decompression effects will be negligible if air is removed from the pouch before sealing.

Thermal tests consisted of soaking and cycling between high and low temperatures. First, a filled pouch was placed in a freezer at 4°F until frozen solid (approximately 20 hours), as shown in Figure 7.

After thawing, the same pouch was placed in an oven at 149°F for 4 hours to simulate the hottest induced conditions expected, such as within an enclosed vehicle under bright sunlight on a hot day. Next the pouch was placed in a Tenney Environmental Test Chamber and exposed to 100 cycles between -13°F and 203°F at a rate of 2 cycles per hour for 100 hours. No damage occurred in any of these tests.

Although these water pouches have not yet been tested against actual chemical agents and decontaminants, testing of the complete pouches against a DMSO solution does provide a comparable measure of the ability of chemicals with high solvency to penetrate the materials and seals. Pouches were tested by immersing them in a 50% DMSO solution at room temperature for 24 hours. Samples were taken by withdrawing 15 ml aliquots through the drinking tube at exposure periods of 10 minutes, 2 hours, and 24 hours. Of three pouches tested, no DMSO contamination of the water contained inside was detected through 24 hours of exposure. Blind contaminated samples were used to verify the efficacy of the DMSO detection process.

CONCLUSIONS

A durable, flexible water pouch with the ability to resist contamination by exposure to chemical agents is being developed for aviators. The water pouch was designed to integrate with existing hardware such as the M45 mask and the metal drinkstraw for the M1 cap to form a complete hydration system. Many decisions were made regarding materials of construction to provide strength, flexibility, and resistance to chemical agents. It was found that a multi-layer configuration of thin barriers was appropriate for the main body of the pouch to provide water potability and chemical resistance, whereas a single thick material was appropriate for the drinking tube.

Currently, near production-ready prototypes have been tested. Pressure testing (including depressurization), drop testing, crush testing, thermal cycling, and thermal extremes testing have demonstrated the exceptional durability of the pouch. The water pouch has been characterized for permeation resistance using a chemical agent simulant, dimethyl sulfoxide. The pouch had no detectable permeation of the agent during a 24 hour period.

ACKNOWLEDGEMENTS

The authors wish to thank Dave Wheatley for the insight provided in many helpful conversations. This work was supported by the Naval Air Warfare Center under contract # N68335-99-C-0119.

REFERENCES

[1]Gopinathan, P. M., Pichan, G., and Sharma, V. M., "Role of Dehydration in Heat Stress-Induced Variations in Mental Performance", *Archives of Environmental Health* 43 [1] p. 15-17 (1988)
[2]Texas Research Institute Austin, Inc., Log Number 95025-84-05,06
[3]Spruance, S. L., McKeough, M. B. , and Cardinal, J. R., "Dimethyl Sulfoxide as a Vehicle for Topical Antiviral Chemotherapy", *Biological Actions and Medical Applications of Dimethyl Sulfoxide,* Ed. J. C. de la Torre, Annals of the New York Academy of Sciences, Vol. 411 (1983)
[4]MIL-STD-810F, Department of Defense Test Method Standard for Environmental Engineering Considerations and Laboratory Tests, 1 January 2000
[5]www.tygon.com/siterfrset.html, Tygon Tubing Product Overview, 2000 Saint-Gobain Performance Plastics Corporation

EVALUATION OF PERSONAL CHEMICAL VAPOR PROTECTION FOR PATROL AND TACTICAL LAW ENFORCEMENT

Dr. Paul D. Fedele
William L. Lake
Victor J. Arca
Stephen M. Marshall
US Army SBCCOM
5183 Blackhawk Road
APG, MD 21010-5424

COL David B. Mitchell
Superintendent, Maryland State Police
1201 Reisterstown Road
Pikesville, MD 21208-3899

ABSTRACT

In Domestic Preparedness efforts, the US Army Soldier and Biological Chemical Command and the Maryland State Police, have evaluated personal chemical protective systems for use in patrol and tactical functions in law enforcement. Various Level C, impermeable and charcoal impregnated, vapor-absorptive, air-permeable protective clothing ensembles, worn with the MSA Millenium respiratory protective mask/butyl hood, and seven-mil butyl rubber gloves, have been considered. In cooperation with the Maryland State Police Special Tactical Assault Team Element (STATE), these ensembles were tested using the man-in-simulant test (MIST) processes. The test results have been used to indicate the chemical hazards that protective system users can be expected to encounter, should they operate in chemical warfare agent vapor contamination. This information is helping law enforcement personnel select personal chemical protective equipment and design chemical incident response plans that can successfully manage chemical warfare agent risks.

INTRODUCTION

The military community has dealt with the threat of chemical and biological warfare for over 86 years[1]. Now, the civil community faces that threat, through possible terrorist attacks involving chemical and biological warfare agents. Although such incidents are expected to remain less likely than many other civil emergencies, without preparation and awareness, the potential consequences of chemical or biological terrorism are significant.

The Maryland State Police (MSP) and the US Army Soldier and Biological Chemical Command (SBCCOM) are participating in the Domestic Preparedness program to help civilian communities prepare to deal with terrorism involving chemical and biological warfare agents. The Domestic Preparedness program provides civilian responders with the training and awareness that they need to develop safe and effective operational procedures for responding to such incidents.

To help civilian responders develop safe operational plans for response to terrorism involving chemical warfare agents (CWA), the MSP and the Improved Response Program have evaluated the hazards faced by personnel using various individual chemical protective ensembles, in various roles of law enforcement. By testing chemical protective ensembles in operational use scenarios, analyses have been performed to indicate approximate exposure times that will begin to result in chemical effect hazards to persons using the protective ensembles in CWA vapors. This information is being used to help responders select chemical protective systems and develop safe and effective operational procedures for the equipment's use.

PATROL AND TACTICAL LAW ENFORCEMENT ROLES

The local law enforcement community will perform many functions associated with a CWA terrorism incident. At the scene of a chemical terrorism incident, local law enforcement patrol officers may evacuate downwind hazard regions and maintain perimeter security. Perimeter security involves controlling traffic and controlling entry to, and exit from, the scene of the incident.

Law enforcement tactical teams, or SWAT teams, often perform high-risk entries. In tactical situations, the MSP employ the Special Tactical Assault Team Element (STATE). The MSP STATE team may perform hostage rescue, raid a suspected chemical terrorist facility, or apprehend a suspected chemical terrorist. Two principle modes of operation are employed. The stealth mode is used to close-in on perpetrators, without making the perpetrators aware of the team's presence. It involves quiet, slow, deliberate actions and may be a prolonged operation, lasting for many hours. The STATE also uses the dynamic mode, in which a site is quickly moved into and through, securing it in minutes. Dynamic operations are fast. They are performed quickly, before the perpetrators recognize the situation, or are able to respond.

In patrol and tactical operations, personnel may encounter CWA contamination. Different levels of CWA hazards are expected in different roles. In a chemical release, the security perimeter is normally placed a safe distance from the site of the release. However, changing meteorological conditions and uncertainty regarding the chemical release may result in vapor hazards at the perimeter. A perimeter security officer also may contact liquid contamination carried from the scene by a contaminated victim or perpetrator. The amount of contamination expected at the perimeter is small. Tactical missions may involve higher levels of chemical contamination. Chemical warfare agents, in the form of liquids, vapors and aerosols, may be encountered as a tactical team enters an area. A perpetrator may attack a tactical team with CWA or disseminate CWA in an attempt to prevent the tactical team from reaching their objective.

Individual chemical protective equipment will help reduce the hazards of CWA exposures that might occur in these operations. This work does not address law enforcement roles in HAZMAT operations. It is limited to assessing protective capability against chemical warfare agent (CWA) vapors that may be encountered by law enforcement personnel engaged in the perimeter patrol and tactical operations described.

CHEMICAL PROTECTIVE SYSTEMS

For the perimeter control mission, various impermeable, chemical-resistant, hooded, protective overgarment clothing systems (Level C^2), were tested. All clothing systems were worn with the MSA Millenium Gas Mask/butyl hood, and seven-mil, butyl rubber gloves. In addition, the Maryland State Police Standard Duty Uniform was tested. The Maryland State Police Standard Duty Uniform also was worn under all Level C overgarments. The following clothing systems were tested for the perimeter control mission.

MSP Standard Duty Uniform
Tyvec ® Protective Wear ™ coverall
Dupont Tychem® 9400 suit
Kappler CPF®4 suit
Dupont Tychem® SL suit
Tyvek® Protech F suit

Figure 1 shows an MSP STATE officer donning a chemical protective suit in patrol tests. Details of each of these protective ensembles are available[3].

Figure 1. Donning personal protective system.

For tactical missions, the impermeable protective systems were found to create too much noise during movement. Air-permeable, charcoal-impregnated, military style, chemical protective systems appeared to be better suited for tactical missions. Tactical mission testing was performed with air-permeable, charcoal-impregnated, chemical protective overgarments and undergarments, including the following.

Hammer® Two-Piece Chemical Protective Overgarment
Saratoga® Chemical Protective Undergarment
Hammer® One-piece Chemical Protective Overgarment
Giat® SWAT One-piece Chemical Protective Overgarment
TOMPS® Two-Piece Chemical Protective Overgarment
LANX® Chemical Protective Undergarment

When the chemical protective overgarment included an integrated hood, the MSA Millenium mask hood was worn under the integrated hood, tucked fully beneath the overgarment. Chemical protective gloves were also worn, when supplied with the clothing ensemble. Details of these protective garments are available from their manufacturers.

Along with each of these protective systems, the MSP Special Tactical Assault Team Element (STATE) standard duty uniform, consisting of camouflaged fatigues and leather boots, was worn during each test. The MSP STATE team standard duty uniform was worn under the chemical protective overgarments and over the chemical protective undergarments.

OPERATIONAL TESTING PROCEDURES

The CWA protection offered by these chemical protective ensembles was measured using the Man-In-Simulant Test (MIST) procedure[4], at the Edgewood Area of Aberdeen Proving Ground. MIST fully assesses the protection offered by complete protective ensembles by measuring the absorption of chemical vapors at the surface of the skin, and compares that to the absorption that occurs at the skin without any protection. MIST is used by the US Army, in development of its personal chemical protective ensembles, and by the Domestic Preparedness program, in defining operational protective performance of personal protective systems[5].

MIST subjects wear full protective ensembles, in vapors, while performing activities that they would perform in an actual operation. MIST does not place people at risk of exposure to chemical agents because MIST uses a chemical simulant in place of chemical agent vapors. Standard fabric penetration measurements are used to identify simulants that penetrate protective systems at the same rates as chemical agent vapors. Such identified simulants are then be used to measure protective ensemble performance.

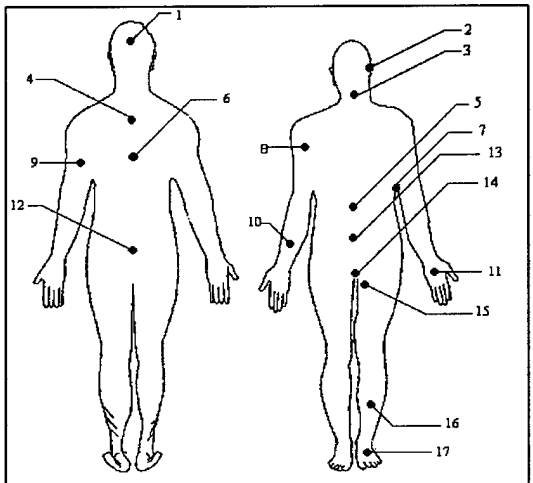

Figure 2. MIST sampler locations.

MIST uses passive samplers, which sample by absorption. These are placed on the skin, so they can accurately measure the absorption of the vapor at the skin surface. Sampler locations for these tests are illustrated in Figure 2. Figure 3 shows samplers being applied to MSP STATE team personnel before a test.

During MIST, volunteers perform actions specific to their operation. Tests last for 30 minutes. Specific detailed actions have been defined for the patrol officer tests[6]. Tactical team chemical protection was measured with the full MSP STATE team as they performed mock raids at an SBCCOM warehouse building. The warehouse was sealed so that it could contain a stable vapor concentration. The interior of the warehouse was configured with moveable partitions. The physical layout was altered to present a variable floor lay-out to the MSP STATE team. Each MSP STATE team member performed their normal functions during the test. During the first 3 minutes of exposure, the STATE team used dynamic tactics to sweep through the warehouse test area. In the following 27 minutes, stealth tactics were used. The Figures 4-6, below , show STATE team personnel during tests.

Figure 3. MIST samplers being placed on MSP STATE personnel.

After the 30 minute vapor exposure, protective clothing is removed. Vapor samplers are collected in a clean room. Analysis of each sampler yields the dosage received at the skin. The overall protective performance of the chemical protective system is determined by the Body Region Hazard Analysis[7].

Figure 4. Planning movement.

Respiratory protective mask performance was not measured for this study. Mask performance is represented by the NIOSH nominal protection factor (PF) for negative pressure respirators; 50[8] and by a PF value that is easily achieved by modern negative pressure respirators, 6666[9].

HAZARD ASSESSMENT ANALYSIS

Chemical hazards are determined by the chemical vapor concentration in the environment, the time spent in the concentration, the performance of the protective system, and the toxicity of the chemical agent vapor. By combining vapor concentration, protective system performance, and endpoint dosages for specified chemical agent effects, estimates of the exposure time required to reach the specified effect endpoint are obtained. Times required to reach specified effect endpoints are called stay times. At the stay time, exposures are not risk-free, but CWA effects are expected to be non-life-threatening.

Figure 5. Approaching the warehouse.

To determine stay times, values for endpoint dosages associated with chemical agent vapor effects, are taken from a recent review by elements of the National Research Council (NRC)[10].

Figure 6. Covering with shouldered weapons.

Stay times are assessed at three levels of chemical agent vapor concentration: perimeter, highly lethal, and saturation. The perimeter concentration corresponds to the maximum concentration expected at the down wind edge of the day-protect zone, as specified in the 2000 Emergency Response Guidebook[11], for a 55 gallon spill chemical agent. Details of dosage estimates for this situation are given by Stuempfle[12]. We refer to highly lethal concentrations as the concentration of chemical agent estimated to produce 95% lethality among unprotected persons exposed for 15 minutes. Lethal effect dosages recommended by the NRC are used to determine highly lethal concentrations. Worst-case vapor

concentrations are referred to as saturation concentrations and are taken as saturation at a temperature of 18°C (65°F).

With agent concentrations; NRC-recommended threshold effects endpoint dosages; and protective ensemble performance, we have calculated stay times for various protective clothing ensembles and respiratory protection levels, for various threshold effects. Results are shown in Table 1.

TABLE 1. Minimum Stay Times (Minutes).

Respiratory Mask PF	Perimeter (Day Protect Zone) Concentration	Highly Lethal Concentration	Saturation (at 65°F) Concentration
50	850	3	0.007
6666	1500	20*	1

*For nerve agents, the minimum stay time for the highly lethal concentration is 400 minutes.

Table 1 provides worst-case (shortest) stay times for worst case chemical agents when wearing worst case clothes for perimeter concentrations. Table 1 values for highly lethal concentrations were also calculated using worst-case parameters, however, the stand-alone standard duty uniform was excluded as it provides minimal skin protection. With a PF of 50, the protective respirator is the limiting factor when determining stay times, because of threshold effects associated with the eyes. At saturated concentrations, stay times remain limited by threshold eye effects due to exposure to GB, for both values of respiratory PF. This is because GB has a much greater volatility that HD.

CONCLUSIONS

Chemical hazards involve many variables. By performing a quantitative hazard assessment, these many variables can be combined to yield specific results that provide useful information that will make a difference in field operations involving chemical hazards. By determining minimum stay times under a range of field conditions, useful guidance can be developed. The assessed stay times and the limiting variables lead us to the following guidance. This guidance does not consider operational hazards posed by contact with liquid agents. These remain to be addressed. Chemical protective gloves are recommended for the most likely scenarios where liquid chemical agents may be contacted.

- On the perimeter of a CWA terrorism incident, chemical protective clothing systems are of secondary importance to respiratory protection for vapor protection.
- The negative pressure respirator, with a respiratory PF of 50, will be the limiting factor in CWA operations and initial operations-degrading symptoms will be eye effects.
- The impermeable suits that were tested made too much noise for stealth operations.
- The charcoal protective suits that were tested should be considered applicable for escape purposes only, if a CWA should be released in interior spaces, during tactical operations.
- None of the tested ensembles are suitable for tactical/stealth operations in enclosed spaces where CWA have been released.

REFERENCES

[1] SBCCOM, "A Brief History of the Edgewood Area, Aberdeen Proving Ground, MD", February 2001, January 2001, available at: EA History (PowerPoint Presentation), http://cbnet/INTRANET/WHATSNEW/menu.html

[2] US Department of Transportation, 2000 North American Emergency Response Guidebook, January 2001, available at: http://hazmat.dot.gov/erg2000/erg2000.pdf .

[3] SBCCOM, "Chemical Protective Clothing for Law Enforcement Patrol Officers and Emergency Medical Services when responding to Terrorism with Chemical Weapons", November 1999, available at: http://dp.sbccom.army.mil/fr/cw_irp_cpc_lepo_ems_report.pdf .

[4] Kocher, T., Man-In-Simulant Test (MIST) Test Operations Procedure (TOP), US Army Test and Evaluation Command, TOP 10-2-022, AMSTE-RP-702-107, 10 April 1996.

[5] Fedele, P, "Two Test Methods for Personal Protective Clothing Systems in Chemical Environments", October 1999, available at: http://dp.sbccom.army.mil/fr/cwirp_aero-mistdep-7.pdf .

[6] Ibid., Reference 3.

[7] Fedele, PD, and Nelson, DC, *A Method of Assessing Full Individual Protective System Performance Against Cutaneous Effects of Aerosol and Vapor Exposures*, US Army Edgewood Research Development and Engineering Center, APG, MD, October, 1995; Section 1-3 "Body Region Hazard Analysis Process" included in report for the JSLIST Program: Cronin, TD, *Final Report for the Development of the Man-In-Simulant Test (MIST) Method for Evaluation of Chemical/Biological (CB) Protective Garments*, TECOM Project No. 8-EI-825-ABO-004, US Army Dugway Proving Ground, Dugway, Utah, April 1996.

[8] NIOSH RDL, 78-108, 5-2000, K:\Bill\APFtable.

[9] Program Manager for NBC Defense, private communication, February 2001.

[10] Review of Acute Human-Toxicity Estimates for Selected Chemical-Warfare Agents, Subcommittee on Toxicity Values for Selected Nerve and Vesicant Agents, Committee on Toxicology, Board on Environmental Studies and Toxicology, Commission on Life Sciences, National Research Council, National Academy Press, Washington, DC, 1997, available at http://books.nap.edu/books/0309057493/html/index.html .

[11] Ibid., Reference 2.

[12] KL Stuempfle and AK Stuempfle, "Visual Comparison Of Perimeter Challenge Levels From Model Predictions of Chemical Incidents", Poster Paper, 2001 Chemical and Biological Defense Conference, March, 2001.

DEVELOPMENT OF SELF-DECONTAMINATING TEXTILES WITH MICROPOROUS MEMBRANES

John Walker, Heidi Schreuder-Gibson, Walter Yeomans, and Francis Hoskin
U.S. Army Natick Soldier Center, Natick, MA 01760-5020 USA

Tu-chen Cheng, U.S. Army Edgewood Chemical Biological Center,
Aberdeen Proving Ground, MD 21010

Ray Yin, U.S. Army Research Laboratory
Aberdeen Proving Ground, MD 21005

Craig Hill, Department of Chemistry, Emory University, Altanta, GA 30322 USA

ABSTRACT

Recently a number of compounds have been synthesized that can catalytically break down chemical warfare agents including G-type agents, VX and mustard. These compounds, including enzymes and polyoxometalates display significant level of hydrolytic and or oxidative activity against a wide spectrum of chemical warfare agents. Multispectral protection could be achieved if appropriate catalysts were combined into a clothing system. However, these compounds have been difficult to incorporate into textiles for use in self-decontaminating chemical protective clothing, as their reactivity is severely impacted by the method of attachment onto and into fabrics. We now report a breakthrough in the technology of fiber spinning that has enabled us for the first time to incorporate these catalysts directly into microporous membranes. The new microporous membranes have been developed at the U.S. Army Natick Soldier Center using the process of electrospinning. By electrostatically producing nanofibers from polymer/solvent spinning solutions at room temperature through the application of a high voltage electric field, we have demonstrated increased activity of the original catalyst alone in solution by incorporating the same catalysts into the nanofibers of these new membranes. Activities of enzymes, derivatized enzymes and inorganic catalysts are discussed. Durability of the catalyst with respect to daily use conditions is considered. Manufacturability of these new reactive membranes will be forecast.

INTRODUCTION

Electrospinning is a process for making extremely fine submicron fiber by a process of charging polymer solutions to thousands of volts. This method of manufacturing man-made fibers has been known since 1934, when the first patent on electrospinning was filed by Formhals.[1] Since that time, many patents and publications have been reported on electrospinning.

Electrospinning occurs when a polymer solution or melt is charged to high voltage to produce fibers. Voltages of 5kV to 30kV are sufficient to overcome surface tension forces of the polymer, and a free surface of charged polymer will produce fine jets of liquid that are rapidly drawn toward a grounded target. The jet splits a few times near the liquid surface, but before it reaches the target, substantial drawing is observed in a series of looping actions of the rapidly solidifying fiber.[2] The fiber is collected as an interconnected web of small filaments on the surface of a grounded target. The technique has been used for over a decade to produce ultra high efficiency filtration webs.[3-5] It is important to recognize that electrospinning can be used in many other products as well. For example, electrospinning provides the capacity to lace together a variety of types of polymers and fibers to produce ultrathin layers which are useful for protective clothing.[6] Depending on the specific polymer being used, a range of fabric properties, such as strength, weight and porosity, can be achieved. Fiber sizes of 10 nm and smaller have been reported, although lab scale apparatus normally produces fibers from 100nm to 500 to 1.0 μm in diameter. Commercial production size equipment produces fibers in the 0.5 to 10 μm diameter range. Fiber size depends upon solution viscosity, field strength, and field uniformity.[7]

SAMPLE PREPARATION

Various electrospun membranes have been prepared by charge induction of polymer solutions. A positively charged electrode is submerged in a pipette filled with a solution of polymer. In this configuration charged fibers are easily collected over a period of 1-2 hours from a single pipette onto a grounded screen.

The microstructure of an electrospun coating is shown in the scanning electron micrographs (SEM) in Figure 1, exhibiting a range of fiber size and porosities produced by different electrospun polymers. Pellethane fiber sizes range from 0.1-1.0μm in diameter. Estane fibers appear to be 10 times larger, due to the 10% additional enzyme in the material, which substantially thickens the spinning solution and produces larger fiber. Fiber production rates by inducted charge are on the order of 1g fiber per nozzle per hour, depending upon the polymer/solvent combination used. For comparison, cotton fibers are shown in Figure 1c with average fiber diameters of 20μm.

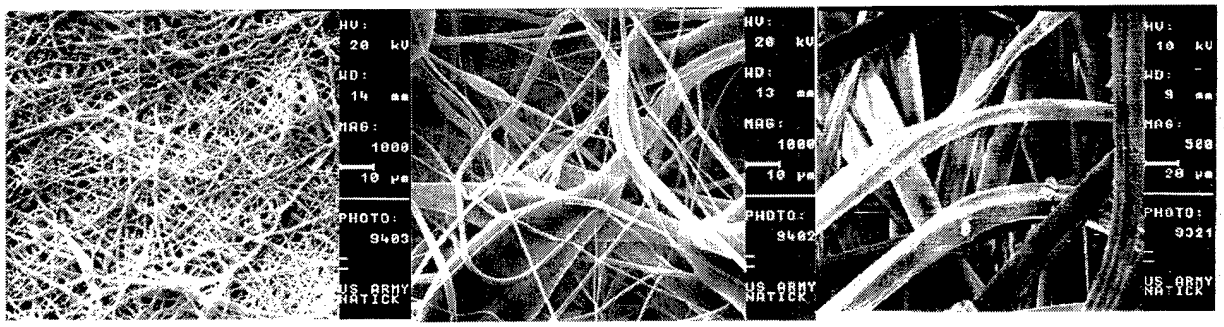

(a) (b) (c)

Figure 1. SEM micrographs at 100x of a) electrospun Pellethane; b) electrospun Estane containing 10% OPAA-C18; and c) cotton fibers at half the magnification of a & b.

Solutions for electrospinning were prepared by dissolving 10 wt% polyurethane in tetrahydrofuran (THF). Two types of polyurethanes were investigated: Pellethane 2103-70A from Dow Plastics, a polytetramethylene glycol ether based thermoplastic elastomer (TPE). Another polyether-based TPE was obtained from B.F. Goodrich Performance Materials, named Estane 58237-80A. Both polyurethanes produce tough, elastic fibers upon electrospinning and readily absorb moisture.

Enzyme was added to this solution immediately prior to electrospinning. Two types of enzymes were used: unmodified organophosphorus acid anhydrolase, OPAA, prepared as previously reported;[8] and OPAA-C18, a modified OPAA encapsulated with a hyperbranched polymer of polyethylene oxazoline with branches of 18-carbon chain lengths.

An inorganic catalyst of a polyoxometalate (POM) compound[9] was incorporated into polymer solutions of TPEs by dissolving 10 wt% POM and varying percentages of the co-oxidant benzoyl peroxide into the solution immediately prior to spinning. The chemical formula for the POM was $H_5PV_2Mo_{10}O_{40}$. Vanadium-based polyoxometalate compounds have been reported to catalytically oxidize thioethers directly to the sulfoxide, and have been under evaluation for the detoxification HD.

All catalyst-loaded TPE solutions were electrospun using 15kV at a target distance of 10 cm to produce a membrane of submicron fibers randomly aligned upon the surface of 5 cm circular aluminum targets. The final fiber mat was easily removed from the aluminum substrate and tested for catalytic activity against appropriate surrogates. OPAA and OPAA-C18 were tested for hydrolytic activity against diisopropyl fluorophosphonate (DFP), a G-agent surrogate. POM catalyst systems were tested for oxidation of 2-chloroethylethylsulfide (CEES), a mustard simulant.

A derivatized OPAA enzyme was used in an experiment to determine the efficiency of binding enzyme directly onto the surface of cellulosic fibers. An electrospun cellulose acetate fiber mat was used and compared to the enzyme binding efficiency of a cotton-based nonwoven fiber mat. Two nonwoven samples prepared by the University of Tennessee Textile and Nonwoven Development Center were used: each were spunbonded (SP) polypropylene (PP) webs with surface bonded cotton fibrils. A web containing 36% cotton was designated as SBPPC36, while a 30% cotton web was

SBPPC30. Cotton fiber sizes from SPPC30 are seen in Figure 1c. Cellulose acetate microfibers were prepared by electrospinning a solution of acetone and 10wt% cellulose acetate (Eastman Chemical sample CA380-30 with a degree of acetyl substitution of 2.5).

Each cotton nonwoven and the electrospun cellulose acetate samples were massed to 10 mg and exposed to a solution of suspended enzymes (protein concentration 71 μg/mL) of OPAA (non-binding) and CBD-OPAA. Cellulose binding domains (CBD) were added to the OPAA enzyme by use of a method of subcloning and preparation of the CBD-OPAA fusion protein from a Novagen (Madison, WI) CBD expression vector.[10] CBD-OPAA can be chemically bound to cotton, while OPAA cannot. After a one hour exposure of the celluosic fibers to the enzyme solutions at room temperature, the nonwovens and electrospun CA were removed, rinsed twice with buffer, and immersed in a solution of acetonitrile with p-nitrophenyl ethylphenyl phosphate (PNEPP), a colorimetric substrate that reacts in the presence of active enzyme.[11]

TESTING METHODS

CBD-OPAA enzyme activity against PNEPP was monitored by UV-VIS spectrometry at 412 nm over a period of 10 minutes. Reaction of the PNEPP substrate with enzyme on the fibers produces a light absorbing product with a molar extinction coefficient of 1300. Product concentration can be related to enzyme activity (rate constant) in mmoles of PNEPP hydrolyzed per gram of material per minute. We report this quantity as Units/g fiber.

In another (non-colorimetric) solution assay, hydrolysis of DFP by OPAA enzyme was measured by a fluoride sensitive electrode (Orion Model EA 940) by placing 1-10mg enzyme-containing material in a 10 mL beaker containing 3.5 mL 0.025M Pipes Buffer (pH 7) and 1.5 mL 0.01 M DFP in deionized water after first recording baseline spontaneous hydrolysis of DFP in water. Concentration of fluoride ion was recorded over a 10 minute period, and the slope of fluoride ion production with time was converted to μmoles of DFP hydrolyzed per minute per mg OPAA contained within the test material. This rate is reported herein as Units/mgOPAA for convenience.

Catalytic oxidation of CEES by POM/benzoyl peroxide (BP) blended into Pellethane fibers and film was determined by the following method. A solution 0.16M CEES was used for oxidation by the POM/BP catalyst systems. During reaction over a period of 24 hours, 1μL aliquots were injected for GC/MS determination of residual CEES concentrations.

RESULTS

1. ACTIVITY OF OPAA ENZYME ENCAPSULATED IN MICROFIBERS

Hydrolysis rates of DFP by OPAA were found to be lower than previously reported[10] due to pH differences. At neutral pH, neat, unmodified OPAA hydrolyzed DFP at an average rate of 7.87 +/- 3.9 Units/mgOPAA. A variation of up to 53% was found in the measurement of activity from run to run. Differences in reaction rates of

neat and modified enzymes are summarized in Table 1 for neat OPAA and OPAA-C18 enzymes in solution, and for enzymes that are encapsulated in electrospun fibers of Pellethane and Estane, or encapsulated in Pellethane film. The apparent activity of neat OPAA encapsulated in fiber is lowered by a factor of 36. When electrospinning neat enzyme in polymer solutions, enzyme does not disperse well and the resulting solution spins poorly, resulting in poor homogeneity in the fibrous membrane. Fiber spinning improves when the modified enzyme, OPAA-C18, is used. The apparent activity of OPAA-C18 in electrospun Pellethane increases 2-fold over the solution activity of the unspun OPAA-C18. When OPAA-C18 is incorporated into Estane and electrospun, the apparent activity increases 3-fold over the solution value for OPAA-C18. There is also a decrease in apparent enzyme activity for a film coating of OPAA-C18 in Pellethane. This indicates that the enzyme is more available for reactions in the electrospun fiber than in a cast film of the same material.

TABLE 1. Effect of Enzyme Encapsulation Upon Hydrolytic Activity.

Sample Treatment	Catalytic Activity (Units/mgOPAA)
Neat OPAA	7.87
OPAA-C18	6.70
Neat OPAA in Pellethane Nanofiber	0.212
Neat OPAA in Estane Nanofiber	1.77
OPAA-C18 in Pellethane Nanofiber	15.76
OPAA-C18 in Estane Nanofiber	18.92
OPAA-C18 in Pellethane Film	4.19

Electrospun enzyme ages and loses activity when encapsulated in polyurethane fiber. Figure 2 shows the effect of room temperature (30°C) aging upon OPAA-C18 apparent activity over a period of one month. Five weeks of aging causes a 4-fold drop in activity of OPAA-C18, falling to 40% of the activity of the original, unspun OPAA-C18.

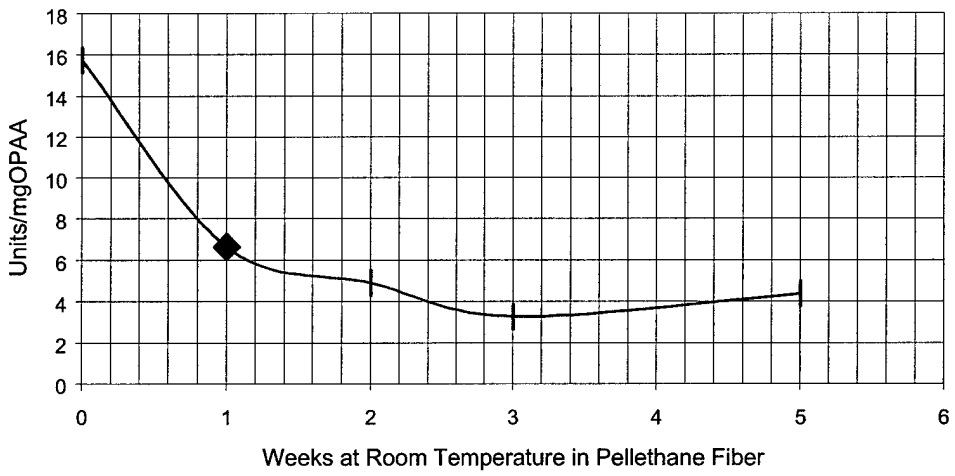

Figure 2. Effect of aging upon enzyme activity for 2% OPAA-C18 in Electrospun Pellethane.

In an effort to determine the fate of the enzyme in the electrospun fibers during hydrolytic reaction against DFP in buffered water, a re-immersion test was performed. A fiber mat of Estane containing 2.5% OPAA-C18 was immersed into a beaker containing buffered water and DFP as described above. After a 10 minute reaction, the fiber mat was removed and residual fluoride ion production in the absence of the enzyme fiber mat was measured. This residual activity was considered to be enzyme that had leached from the fiber mat into solution. The fiber mat from the first test was reimmersed in a new beaker with fresh buffered DFP, and fluoride ion production was measured a second time on the used sample. This reimmersion was repeated 3 times. Figure 3 shows the effect of multiple immersions of the enzyme-loaded fiber mat into the DFP reaction solution. Four immersions, or buffer washings, resulted in a 3-fold drop in apparent enzyme activity. While 16% of the enzyme activity leached into solution after the first immersion, very little leaching was seen after that.

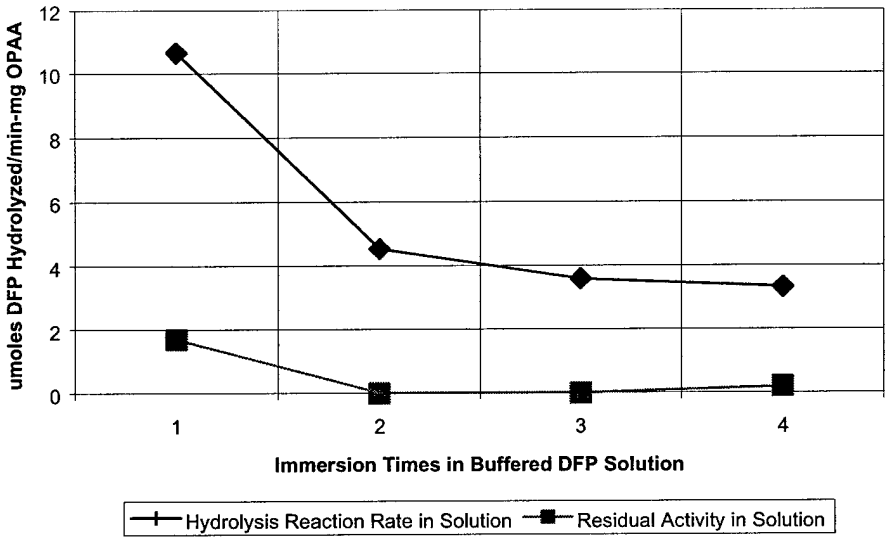

Figure 3. Effect of reimmersion on OPAA-C18 Estane fiber mat activity.

2. ACTIVITY OF CBD-OPAA ENZYME BOUND TO CELLULOSIC FIBERS

For surface bound CBD-OPAA, absorbances of reacted and unreacted PNEPP were monitored to determine a baseline effect of unreacted material. Shown in Figure 4, fibers treated with non-binding OPAA have the same flat slope as the blank solution of PNEPP with no enzyme treated fiber. However, the CBD-OPAA treated fibers react with the PNEPP and an increasing absorbance of PNEPP product with time is recorded.

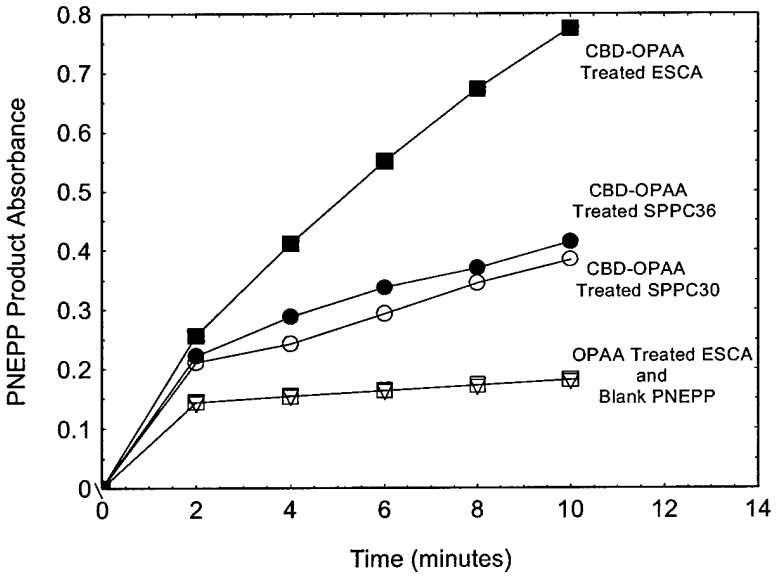

Figure 4. Effect of binding (CBD-OPAA) and non-binding (OPAA) enzyme on breakdown of PNEPP by enzyme-treated electrospun cellulose acetate (ESCA), SPPC36 (36% cotton) and SPPC30 (30% cotton) nonwoven fiber mats.

Table 2 shows the results of residual enzyme activity on the surface of the cotton samples after washing. There is appreciable activity, measured in Units/min-gram of fiber for the CBD-OPAA bound enzyme samples after exposure to PNEPP. Furthermore, there is an apparent increase in enzyme activity for the CBD-OPAA bound to the electrospun cellulose acetate (ESCA), compared to the cotton-surfaced nonwovens. However, further analysis of these results is needed to account for the actual percentage of reactive sites for the CBD-OPAA binding reaction in all three samples.

TABLE 2. Activity of Enzyme-Treated Cellulosic Fabrics Against PNEPP.

Sample	Activity CBD-OPAA (Units/g fiber)
ESCA	39.8
SPPC36	17.7
SPPC30	13.8

3. ACTIVITY OF POLYOXOMETALATE CATALYST IN ELECTROSPUN FIBERS AND CAST FILMS

Oxidation of CEES by POM-containing fibers and films was assessed. Data in Figure 5 show the depletion rate of CEES in solution in the presence of POM in three forms: 1) POM/BP alone in solution, 2) POM/BP in Pellethane cast films, and 3) POM/BP in electrospun Pellethane. We see that a POM to benzoyl peroxide weight ratio of 2:1 works well for the catalyst system alone in the CEES solution. For fibers and films containing the catalyst system, more BP (benzoyl peroxide) is required, possibly due to loss of the peroxide from the fiber and film to the solution. Electrospun fibers containing optimum ratios of POM to benzoyl peroxide will perform better in the catalytic oxidation of CEES in solution. Benzoyl peroxide alone in the nanofiber does not oxidize CEES.

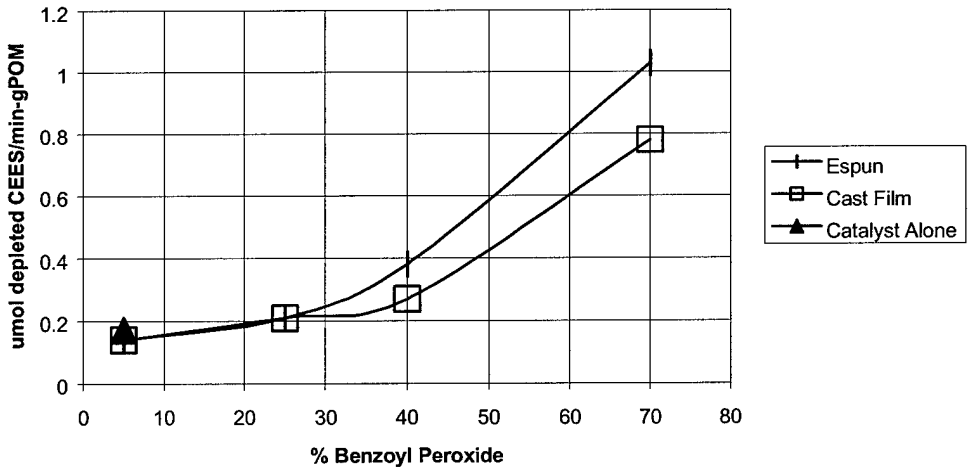

Figure 5. Depletion of CEES by POM/BP catalyst system over a 24-hour period.

CONCLUSIONS

Enzymes and polyoxometalate catalysts have been incorporated into films and nanofibers of polyurethanes. Increased catalytic activity against G-agent and HD surrogates have been found for catalysts encapsulated in nanofibers. Enzymes that have been encapsulated with a hyperbranched polymer are 15-20x more active within the nanofiber than unmodified enzymes. This activity is reduced by 40% after one month of aging. The encapsulated enzymes are not permanently bound in the fiber;16% of the enzyme activity leaches into an initial wash solution, but very little is lost after that.

Cellulose-binding OPAA enzyme has been found to bind effectively to both cellulose acetate and cotton fibers. Electrospun cellulose acetate is capable of binding a high level of enzyme due to the high surface area contained in the microfiber membrane.

Polyoxometalate-peroxide catalyst systems that were encapsulated in polyurethane nanofibers were also more active in the nanofibers, once the peroxide level was adjusted.

Electrospinning has been in use for over 50 years. Nevertheless, it is not used as a method to manufacture microporous membranes. Solvents used during the spinning process are a deterrent to this method of membrane production. Melt processing techniques such as fiber melt blowing might be an attractive option to electrospinning, but will produce much thicker fiber sizes, in the range of 10-100um fiber diameter. However, our preliminary results with enzymes in Estane suggest that these fiber diameters are not detrimental to the reaction of encapsulated catalysts with chemical agents in solution. Inorganic catalysts are continuing to be improved and have the potential to be melt processed into new self decontaminating textiles.

REFERENCES

1. Formhals, A., "Process and Apparatus for Preparing Artificial Threads," *U.S. Patent* 1,975,504 (1934).
2. Reneker, Darrell H.; Yarin, Alexander L.; Fong, H.; Koombhongse, S.; "Bending Instability of Electrically Charged Liquid Jets of Polymer Solutions in Electrospinning," *J. Appl. Phys.*, **9**, Part I, 87(2000).
3. Schmidt, K. "Manufacture and Use of Felt Pads Made from Extremely Fine Fibres for Filtering Purposes," *Melliand Textilber.*, **61**, 495 (1980).
4. Weghmann, A., "Production of Electrostatic Spun Synthetic Microfibre Nonwovens and Applications in Filtration," *Proceedings of the 3rd World Filtration Congress, Filtration Society*, London (1982).
5. Davis, M., "Electrostatic Melt Spinning Process Delivers Unique Properties," *Nonwovens World*, **9**, 51 (1987).
6. Baumgarten, P.K., "Electrostatic Spinning of Acrylic Microfibres," *J. Colloid Interface Sci.*, **36**, 71(1971).
7. Gibson, P.W.; Schreuder-Gibson; H.L, Pentheny, C.; "Electrospinning Technology: Direct Application of Tailorable Ultrathin Membranes," *J. Coated Fabrics*, **28**, 63(1998).

8. Cheng, T.C., Harvey, S.P. and Stroup, A.N. Purification and Properties of a Highly Active Organophosphorous Acid Anhydrolase from *Alteromonas undina*. *Applied and Environmental Microbiology*,**59** , (9), 3138 (1993).
9. Rhule, J.T., Hill, C.L., Judd, D.A. Polyoxometalates in Medicine. *Chemical Reviews*, **98**, (1), 327 (1998).
10. Cheng, T.C. and DeFrank, J.J., Wide-range Application of Alteromonas Prolidase for Decontamination of G-type Chemical Nerve Agents. *Proceedings of the Chemical and Biological Medical Treatment Symposia III*, in press (2000).
11. DeFrank, J.J., Cheng, T.C. Purification and Properties of an Organophosphorus Acid Anhydrase from a Halophilic Bacterial Isolate. *J. Bacteriology,* **173**, (6), 1938 (1991).

ACKNOWLEDGEMENTS

The authors wish to express their gratitude to Professor Darrell Reneker at the University of Akron for his expertise and generous sharing of knowledge about the physics and the mechanics of electrospinning.

STRUCTURE AND REACTIVITY OF THE PHOSPHOTRIESTERASE ACTIVE SITE

Morris Krauss
Center Advanced Research Biotechnology, Rockville, MD 20850

ABSTRACT

The structure and reactivity of the native, mutant, and metal substituted phosphotriesterase (PTE) is determined by *ab initio* quantum chemistry calculations. The x-ray structure for the Zn-Zn enzyme is leveraged into a catalytically competent active site in which a wide range of theoretical structures can be optimized for metal substituted and mutant active sites. The structural behavior of the active site is modeled using a new effective potential for representing the protein molecular environment (electrostatic, polarization, repulsive) interacting in the quantum Hamiltonian. The new methodology, effective fragment potentials (EFP), has been implemented in the GAMESS suite of electronic structure codes to make theoretical calculations on structure, spectroscopy, and reactivity tractable for systems involving many hundreds of atoms. Specific results on the structure of active site histidine to cysteine mutants, and a new proposal on the nucleophile for this hydrolase, will be presented.

INTRODUCTION

This study will focus on the theoretical analysis of the reactive behavior of organophosphorus hydrolase from *Pseudomonas diminuta*, phosphotriesterase (PTE), which catalyzes the hydrolysis of paraoxon, sarin, soman, and other inhibitors of acetylcholinesterase [1, 2]. This enzyme has been extensively studied with much emphasis on the effect on reactivity with metal substitution and mutations [3-8]. X-ray structures, of the bimetallic Zn-Zn [9] and Cd-Cd [10] enzymes, provide the basis for studying the detailed binding and mechanism. The molecular aspects of the mechanism can be deduced from the geometric and electronic structure of the reactant and transition state complexes with the enzyme active site. This information is very difficult to obtain experimentally. Structures of analogues of the reactant bound in the active site have been obtained [9, 11]. These structures provide insight into the possible binding modes. However, we suggest that not all binding modes have been catalogued even with new data showing several possibilities for simple substrates [11]. Even more important the arrangement of waters bound in the active site is poorly understood. Arrangements of the substituents in the active site are not consistent from substrate to substrate leading Benning et al to suggest "that nonproductive complexes are readily formed during the binding" and "one must proceed with caution when using x-ray structural data alone in the redesign of enzyme active sites" [11].

The structural basis for binding is still not clear since the three regions identified as interacting with the substrate have both hydrophobic and hydrophillic residues [9, 12, 13, 14]. The mutations engineered to alter chirality are considered to work on the basis of size of the binding pocket or the steric interactions of the residues with the substrate [14]. However, the importance of two histidines (H254, H257) and tryptophan (W131) in binding suggest that hydrogen bonding interactions are also possible. For example, W131 is hydrogen-bonded to the phosphonate inhibitor in the Zn-Zn enzyme crystal structure [9] (see fig.1). Modeling of paraoxonase into the active site also shows that the nitro group would be hydrogen bonded to H257. Mutations of the residues in the first shell [15], in near active site residues towards the protein interior [7], and near active site residues toward solution [6] modify activity and specificity. The molecular basis for these changes also has not been determined although an examination of the active site of the Zn-Zn enzyme shows that a combination of steric and hydrogen-bonded interactions are probable.

Experimental observations of the binding show only two binding arrangements so far. The substrate is hydrogen bonded to second-shell residues and also interacts with dispersion interactions but phosphoryl oxygen does not bind to the metal cation with the approach to the Zn2 atom not closer than 3.4 Å. The second binding arrangement does find the phosphoryl oxygen bound to the Zn2 with a distance of 2.1 Å. However, the presence of W131 makes the binding of substrates with bulky substituents to Zn2 difficult. The data would suggest that a substituent larger than a methyl group has steric interactions that impede direct binding to Zn2.

However, the observation of binding or near binding to Zn2 encouraged experimental suggestions that the hydrolysis initiated by binding to Zn2 which

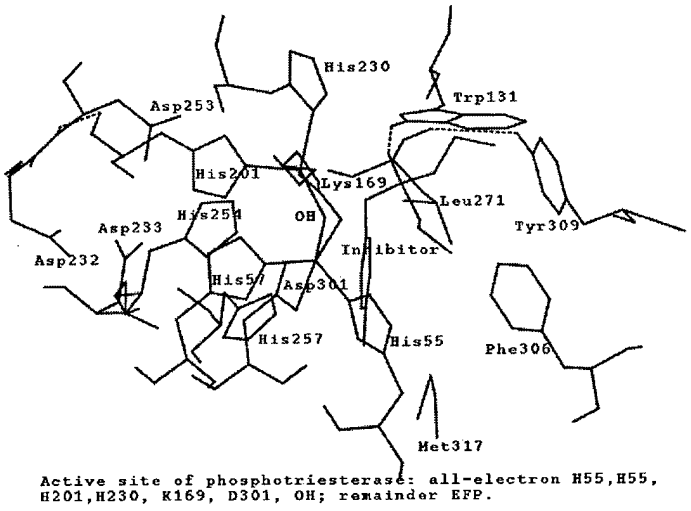

Figure1. Schematic of the active site of phosphotriesterase.

destabilized the hydroxide binding so it could act as the nucleophile [9]. However, recent structural data suggests that the binding of the phosphoryl oxygen does not destabilize hydroxide binding [11]. The theoretical calculations show that the direct binding of the phosphate to either Zn1 or Zn2 leaves the hydroxide as a bridging ligand. We suggest that waters bound to the active site will act as the nucleophile in either binding mode. Binding of water to the active site in the presence of the substrate is then part of the reactive substrate

complex but has not been studied either experimentally or theoretically.

Metal substitution is known to alter activity and specificity [3, 7] but the molecular and electronic basis is not known The accuracy with which molecular geometry must be known to provide insight into the electronic structure is also higher than is obtainable by x-ray crystal structure [16]. Differences of a few hundredths of an Å are significant in characterizing the electronic structure of the carboxylate bound to the metal in either the aspartate or carbamylate but several tenths of an Å is achieved at the resolution obtained for these enzymes. Kinetic isotope effects for the hydrolysis reaction for one substrate suggesting a late transition state have been obtained [4, 17]. However, there is evidence that for most substrates the rate is not limited by the chemical reaction [17, 18]. Theory can then contribute significantly to the understanding of the mechanism at the molecular level. We have recently developed a methodology for calculating the binding and energetic properties along the enzyme reaction path for selected catalytically competent protein structures leveraged from a single experimental structure to metal substituted or mutant structures [19-21]. Insight into the catalytic properties at the molecular level is obtained from the binding of the reactant and transition state in the active site of the enzyme. Preliminary results for phosphotriesterase already show that deductions on binding and the reaction path obtained from experiment do not completely cover the range of possible reaction paths. Accurate calculation of the Cd-Cd enzyme structure was used to validate the methodology for phosphotriesterase [20]. In this note HisXCys structures for all mutants in the active site are described. A specific reaction path in phosphotriesterase for the hydrolysis of trimethylphosphate has been calculated but the binding of trimethylphosphate and water only will be described very briefly due to the limitation on space.

METHOD

Application of *ab initio* methods is essential for accurate prediction of the properties of enzyme active sites and their role in catalysis. Although *ab initio* quantum methods have enjoyed great success in characterizing transition states and determining reaction paths *in vacuo*, the proper description of an enzyme active site can require hundreds of atoms making traditional all-electron methods intractable. An accurate picture of the binding and reactivity can be leveraged from limited experimental data with the use of effective fragment potentials (EFP) that make the calculation of the protein environment tractable [22]. The reactant, transition state, inhibitor, and product in the enzyme active site can now be optimized with a fully quantum chemical treatment of the interaction with the protein environment represented by the EFP in the hamiltonian. The EFP method provides insight into the electronic and geometric aspects of catalysis on the molecular level as well as the relative energetics along a reaction path for one of a range of catalytically competent conformations of the protein. Catalytically competent conformations are obtained from the crystal structure or from analysis of trajectories in a molecular dynamics simulation [21]. The number of waters bound in the active site or the arrangement of internal hydrogen bonds in the active site has been found to characterize different catalytic conformations for chorismate mutase. Preliminary evidence for water binding in phosphotriesterase suggests that activity in this enzyme similarly depends on water binding in the active site. Initial structures for EFP calculations are obtained from an x-ray structure, MD simulations, many-body classical mechanics [23], or semi-empirical quantum chemistry.

The effective fragment potential method was designed to model solvation effects [24-30] and is appropriately extended to describe protein interactions. The EFP are implemented in GAMESS [31] and have recently been applied to a variety of biomolecule problems [19-21, 32-37]. In the EFP method, the model of the enzyme active site is divided into two regions, an active (A) region and a spectator (S) region. The A region is treated all-electron and includes

any residues that are directly involved in the chemistry or whose movement is critical to catalysis. The S region, which influences A through electrostatic, hydrogen-bonded, and repulsive or steric interactions, is modeled by the EFP in the quantum hamiltonian. The directed electrostatics and distributed polarizabilities included in the EFP provide the local effective dielectric for the active site. Repulsive interaction-EFPs have been generated for a variety of protein residues [19] by fitting the repulsive interaction over a range of interactions found for the hydrogen-bonded conformations in the active site. All EFP are obtained at the Hartree-Fock level so that the calculation of the entire EFP and all-electron system is essentially a Hartree-Fock calculation for a very large system that can include much of the protein environment.

All geometry optimizations and transition state searches are done at the restricted Hartree-Fock level in GAMESS [31] using the effective core potential (ECP) to restrict the all-electron calculation to the valence electrons [38,39]. Since the number of all-electron atoms is relatively large, requiring a substantial basis set (~ 300-700) for the representation of the wavefunction, the calculation is restricted to a CEP 4-31G basis concomitant to the ECP. Polarized basis sets have not had a substantial effect on the structure of a single metal active site [40,41]. Structural calculations have been compared with a DFT calculation for phosphotriesterase with reasonable agreement for the native structures including zinc substitution by cadmium [16]. Using the EFP to analyze metal-substitution and protonation of the active site in phosphotriesterase has already proved accurate [20].

ACTIVE SITE STRUCTURE AND SUBSTRATE BINDING

All the structures for phosphotriesterase are leveraged from the Zn-Zn x-ray crystal structure [9]. The structure for the Cd-Cd enzyme is not used to initiate any calculations. The Cd-Cd active site structure is calculated from the Zn-Zn and shown to agree well with experiment for metal-ligand distances as well as angles within the first-shell [20]. This provides one test of the efficacy of the EFP for the determination of the structure of the active site. Although the metal-metal distance changes by over 0.4 Å from Zn-Zn to Cd-Cd, the increase is predominately obtained by distortion in the first-shell. The crystal structures show that the backbone atoms of the Zn and Cd enzymes superimpose within 0.2 Å. The differences in the *in vacuo* and EFP structures are found primarily in the orientation of the ligands that are constrained by the hydrogen-bonds to the interior residues. All metal substituted enzymes can be leveraged from the Zn-Zn using the EFP protein environment.

The active site of phosphotriesterase is described in fig.1 with the protein environment directly influencing the first-shell. The first-shell consists of the two metal cations and the following ligands: D301, H55, H57, H230, H201, K169 with the lysine carbamylated. All these residues are considered all-electron including all atoms back to the C_α atom. In one case, H230, the amide backbone is included since there are backbone hydrogen-bonded interactions to the interior protein. The residues represented by the by EFP are W131, D232, D233, D253, H254, H257, L271, M317, F306, and Y309. If all the atoms represented in the EFP calculation were represented by all-electron basis functions, there would be a total of 1244 basis functions rather than the 538 required. For the substrate binding calculations, W131, will also be considered all-electron and optimized since it can interact with the bound substrate. In the case of a paraoxon-like substrate, H257 would also be all-electron. H254 is chosen to be protonated because the arrangement of hydrogen-bonds suggests this is probable. H257 is found to be important in the chiral selection [14] but it probably functions through hydrogen bonding to the nitro group in the substituted paraoxons since such a hydrogen bond is easily modeled when the phosphonate inhibitor is converted into paraxon. In phosphotriesterase, the interior or protein has hydrophilic and hydrogen bonding interactions, which modify the charge distribution in the first shell by

polarization and charge transfer, while the exterior side toward solution determines how the protein shapes the hydrophobic box into which the substrate binds. Disruption of the pattern of hydrogen-bonds into the interior of the protein is the basis for structural and specificity changes that occur when mutations are made in the second and third shell around the active site [7].

HXC MUTANT STRUCTURE

The structures of all histidine to cysteine mutations in the first-shell of the active site in phosphotriesterase are optimized with the Cá frozen for all binding ligands. Although, the cysteine sulfur initially in the optimization can be as much as 4-5 Å from the zinc in the first shell, the active-site complex distorts sufficiently to permit ligand binding with a Zn-S distance of about 2.3-2.8 Å. Ligand binding of the cysteine was obtained with all four mutants with both bridging ligands maintained in the optimized structure. In an unconstrained optimization, the carbamylated lysine bond to Zn1 is strained and essentially broken for the H55C and H57C mutants. However, the strain in moving the Cá cannot be assessed at this time. The H55 and H57 structures only are shown in fig.2. Relevant bond distances for the active site are provided in Table 1.

The relative activities of all the HXC mutants for paraoxon have been determined [15]. The H55C mutant shows no activity while H57C activity increased over the native with a smaller reduction in the other two mutants. There are no obvious structural effects of the mutations that would affect activity. The relative effective charges at Zn1 and Zn2, however, do produce a surprise. In the native Zn-Zn enzyme, the Lowdin effective charge is comparable between Zn1 and Zn2. However, Zn1 is more positive than Zn2 for H57C, H201C, and H230C but it is less positive for H55C. The effective charges support the contention that Zn2 does not play a catalytic role in binding to the phosphoryl oxygen. The reactive conformation of paraoxon in the mutants will probably resemble the inhibitor structure in the Zn-Zn structure with no direct phosphoryl binding to the metal cations.

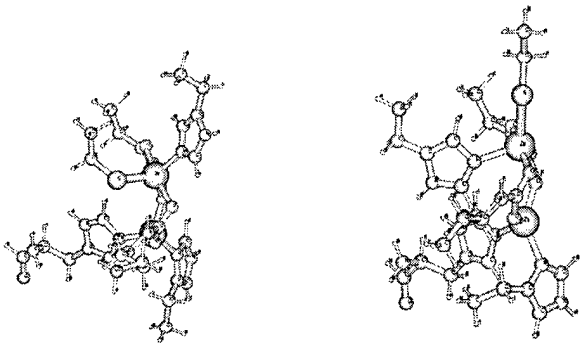

Figure 2. HXC mutant structure showing just the first-shell for a. H55, b. H57.

TABLE 1. Selected active site bond distances for HXC (Å).

	H55C	H57C	H201C	H230C
Zn-Zn	3.58	3.66	3.45	3.48
Zn1-Oasp	2.09	2.03	2.11	2.00
Zn1-OH	1.91	2.21	1.98	2.05
Zn1-Olys	2.47	2.84	5.71	5.20
Zn1-S	2.47	2.84	5.71	5.20
Zn2-OH	1.91	1.90	1.98	1.97
Zn2-Olys	1.97	1.99	2.07	1.98
Zn2-S	5.13	6.41	2.37	2.38

H257 and W131 are EFP in the present calculations. They play no role in the mutant structure but shifts in their positions could have an inordinate effect on paraoxon binding so they would have to be all-electron in any further calculation on the reaction path. The reactive conformations with bound waters are required to obtain insight into reactive behavior. Unconstrained optimizations also suggest that the carbamylated lysine bridge to Zn1 can be broken. This carboxyl anion can then assist the activation of a water for nucleophilic attack. The mutant geometrical and electronic structure is insufficient by itself to provide insight into the activity.

BINDING OF WATER AND TRIMETHYLPHOSPHATE

Calculation on the active site structure of phosphotriesterase finds ligated water or a water hydrogen-bonded to the first-shell active site ionic ligands is very polarized. In addition to the effects this has on the structure, we propose that this polarized water can act as the nucleophile. By including water hydrogen-bonded to the active site ionic center, this provides more room for docking the substrate without having to eject the water. Such a structure has been calculated for phosphotriesterase with a trimethylphosphate substrate. Trimethylphosphate was chosen as perhaps the simplest organophosphate and it is easy to generalize to other models where the methyl group is replaced by fluorine or the phosphate oxygen replaced by a sulfur. Trimethylphosphate probably reacts very slowly since there is no good leaving group. The triethyl phosphate is found bound to the active site but not directly to the metal [11]. Apparently any substituent larger than the methyl group will sterically interact with the tryptophan or phenyalanine that border the Zn2 site. Of course, a halogen substituent will fit easily. Two structures are found with water hydrogen bonded to the bridging hydroxide (3a) or the carbamylated lysine (3b). The O(P) distance to the Zn1 or Zn2 is about 2.2 Å while triethyl phosphate is observed to bind about 3.4 Å from the Zn2 or more solvent accessible site [11].

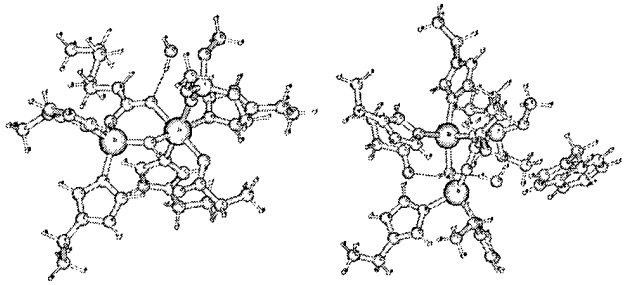

Figure 3. Binding of trimethylphosphate and water to phosphotriesterase, a. Water bound to carbamylated lysine, b. Water bound to bridging hydroxide.

The activation energy for hydrolysis of this relatively unreactive reactant is calculated at about 20 kcal/mol.The transition state is late and product-like as suggested by experiment. The methanol product is obtained by an intra-molecular proton transfer from the OH(P) to the methoxy oxygen which is comparable to the gas-phase attack of trimethylphosphate by hydroxide [42].

CONCLUSIONS

Theoretical calculations show that a single crystal structure of the Zn-Zn phosphotriesterase can be leveraged to determine the active site structure of the metal-substituted enzyme (Cd-Cd), low pH or protonated form of the active site, and mutants of active site residues (HXC). This provides a means of producing a wide range of active site structures relevant to the reaction or binding of interesting substrates by theoretical calculation. A new reaction pathway is also suggested by the calculations and critical analysis of the experimental crystal structures where the hydrolysis is initiated with an polarized water that is hydrogen-bonded to the active site ionic residues. Electronic structure of the native and mutant active sites suggest that a substrate with small substituents can bind equally well at either Zn1 or Zn2 sites. Binding of the simple organophosphate, trimethylphosphate, in the active site supports this contention. More complicated substrates will not bind at the metal sites but are suspended over the metals in the active site with the phosphate within easy distance of attack by a water hydrogen-bonded in the active site. The hydroxide will remain bridging but the carbamylated lysine bridge may open and be involved in the reaction.

REFERENCES

1.Rastogi, V.K., DeFrank, J.J., Cheng, T.C., Wild, J.R., *Enzymatic hydrolysis of Russian-VX by organophosphorus hydrolase.* Biochem.Biophys.Res.Comm., 1997. 241: p. 294-6.
2.Raushel, F.M., Holden, H.M., *Phosphotriesterase: an enzyme in search of its natural substrate.* Adv Enzymol Relat Areas Mol Biol., 2000. 74: p. 51-93.
3.Omburo, G.A., Mullins, L.S,, Raushel, F.M., *Structural characterization of the divalent cation sites of bacterial phosphotriesterase by 113Cd NMR spectroscopy.* Biochemistry, 1993. 32: p. 48-55.
4.Hong, S.B., Raushel, F.M., *Metal-substrate interactions facilitate the catalytic activity of the bacterial phosphotriesterase.* Biochemistry, 1996. 35: p. 10904-12.
5.Watkins, L.M., Mahoney, H.J., McCulloch, J.K., Raushel, F.M., *Augmented hydrolysis of diisopropyl fluorophosphate in engineered mutants of phosphotriesterase.* J.Biol.Chem., 1997: p. 25596-601.
6.Kuo, J.M., Chae, M.Y., Raushel, F.M., *Perturbations to the active site of phosphotriesterase.* Biochemistry, 1997. 36: p. 1982-8.
7.DiSioudi, B., Grimsley JK, Lai K, Wild JR., *Modification of near active site residues in organophosphorus hydrolase reduces metal stoichiometry and alters substrate specificity.* Biochemistry, 1999. 38: p. 2866-72.

8.DiSioudi, B.D., Miller, C.E., Lai, K., Grimsley, J.K., Wild, J.R., *Rational design of*

organophosphorus hydrolase for altered substrate specificities. Chem Biol Interact., 1999. 119-120: p. 211-23.
9.Vanhooke, J.L., Benning, M.M., Raushel, F.M., Holden, H.M., *Three-dimensional structure of the zinc-containing phosphotriesterase with the bound substrate analog diethyl 4-methylbenzylphosphonate.* Biochemistry, 1996. 35: p. 6020-5.
10.Benning, M.M., Kuo JM, Raushel FM, Holden HM., *Three-dimensional structure of the binuclear metal center of phosphotriesterase.* Biochemistry, 1995. 34: p. 7973-8.
11.Benning, M.M., Hong SB, Raushel FM, Holden HM., *The Binding of Substrate Analogs to Phosphotriesterase.* J.Biol.Chem., 2000. 275: p. 30556-60.
12.Hong, S.B., , Raushel, F.M., *Stereochemical constraints on the catalytic hydrolysis of organophosphate nerve agents by phosphotriesterase.* Phosphorus Sulfur, 1999. 146: p. 521-4.
13.Hill, C.M., Wu, F.Y., Cheng, T.C., DeFrank, J.J., Raushel, F.M., *Substrate and stereochemical specificity of the organophosphorus acid anhydrolase from Alteromonas sp JD6.5 toward p-nitrophenyl phosphotriesters.* Bioorg.Med.Chem.Lett., 2000. 10: p. 1285-8.
14.Wu, F.Y., Li, W.S., Chen-Goodspeed, M., Sogurb, M.A., Raushel, F.M., *Rationally engineered mutants of phosphotriesterase for preparative scale isolation of chiral organophosphates.* J.Am.Chem.Soc., 2000. 122: p. 1026-7.
15.Watkins, L.M., Kuo, J.M., Chen-Goodspeed, M., Raushel, F.M., *A combinatorial library for the binuclear metal center of bacterial phosphotriesterase.* Proteins, 1997. 29: p. 553-61.
16.Kafafi, S., Krauss,M., *Ab initio determination of the structure of the active site of a metalloenzyme: Metal substitutions in phosphotriesterase.* Int.J.Quantum Chem., 1999. 75: p. 289-99.
17.Caldwell, S.R., Newcomb, J.R., Schlecht, K.A., Raushel, F.M., Biochemistry, 1991. 30: p. 7438-44.
18.Shim, H., Raushel, F.M., *Self-assembly of the binuclear metal center of phosphotriesterase.* Biochemistry, 2000. 39: p. 7357-64.
19.Worthington, S.E., Krauss,M., *Effective fragment potentials and the enzyme active site.* Computers Chem., 2000. 24: p. 275-85.
20.Krauss, M., *Ab initio structure of the active site of phosphotriesterase.* J.Chem.Inf.Comp.Sci., 2000. 41: p. 8-17.
21.Worthington, S.E., Roitberg,A.E., Krauss,M., *An MD/QM study of the chorismate mutase catalyzed Claisen rearrangement reaction.* 2001.subm. J.Phys.Chem.B
22.Day, P.N.J., J.H.; Gordon,M.S.; Webb,S.P.; Stevens,W.J.; Krauss,M.; Garmer,D.; Basch,H.; Cohen,D, *An effective fragment method for modeling solvent effects in quantum mechanical calculations.* J.Chem.Phys., 1996. 105: p. 1968-86.
23.Gresh, N., *Inter- and intramolecular interactions. Inception and refinements of the SIBFA, molecular mechanics (SMM) procedure, a separable, polarizable methodology grounded on ab initio SCF/MP2 computations. Examples of applications to molecular recognition problems.* J Chim.Phys., 1997. 94: p. 1365-1416.
24.Chen, W., Gordon, M.S., *The effective fragment model for solvation: Internal rotation in formamide.* J.Chem.Phys., 1996. 105: p. 11081-90.
25.Krauss, M., Webb, S.P., *Solvation and the excited states of formamide.* J.Chem.Phys., 1997. 107: p. 5771-5.
26.Merrill GN, G.M., *Study of small water clusters using the effective fragment potential*

model. J.Phys.Chem.A, 1998. 102: p. 2650-7.
27.Webb SP, G.M., *Solvation of the Menshutkin reaction: A rigorous test of the effective fragment method.* J.Phys.Chem.A, 1999. 103: p. 1265-73.
28.Petersen, C.P., Gordon, M.S., *Solvation of sodium chloride: An effective fragment study of NaCl(H2O)(n).* J.Phys.Chem.A, 1999. 103: p. 4162-6.
29.Day PN, P.R., Gordon MS, Merrill GN, *A study of water clusters using the effective fragment potential and Monte Carlo simulated annealing.* J.Chem.Phys., 2000. 113: p. 2063-73.
30.Bandyopadhyay P, G.M., *A combined discrete/continuum solvation model: Application to glycine.* J.Chem.Phys., 2000. 113: p. 1104-9.
31.Schmidt, M.W., Baldridge,K.K., Boatz,J.A., Elbert,S.T., Gordon,M.S., Jensen,J.H.,Koseki,S., Matsunaga,N., Nguyen,K.A., Su,S.J., Windus,T.L., Dupuis,M., Montgomery,J.A., *General Atomic and Molecular Electronic Structure System.* J.Comp.Chem., 1993. 4: p. 1347-63.
32.Krauss, M., *Effective fragment potentials and spectroscopy at enzyme active sites.* Computers Chem., 1995. 19: p. 199-204.
33.Wladkowski, B.D., Krauss, M., Stevens, W.J., *Transphosphorylation catalyzed by RNase A: Computational study using effective fragment potentials.* J.Am.Chem.Soc., 1995. 117: p. 10537-45.
34.Krauss, M., Wladkowski, B.D., *Vanadate complex spectroscopy at the RNase A active site.* Int.J.Quantum Chem., 1998. 69: p. 11-19.
35.Luo, N., Ramadas, N., Krauss, M., Osman, R., *Molecular dynamics and quantum chemical study of uracil-DNA glycosylase: Specific recognition and catalytic mechanism.* Biophys.J., 1998. 74: p. A285-A285.
36.Krauss, M., Nirmala, R., Luo, N., Osman, R., *Molecular Dynamics and Quantum Chemical Study of Endonuclease V Catalytic Mechanism.* ACS Symposium Series 721 (Transition State Modeling for Catalysis), 1999. 721: p. 424.
37.Worthington, S.E., Krauss,M., *Claisen rearrangement of an unusual substrate in chorismate mutase.* 2001.subm. J.Phys.Chem.B
38.Stevens, W.J., Basch,H., Krauss,M., *Compact effective potentials and efficient shared-exponent basis-sets for the 1st-row and 2nd-row atoms.* J.Chem.Phys., 1984. 81: p. 6026-33.
39.Stevens, W.J., Krauss,M., Basch,H., Jasien,P.G., *Relativistic compact effective potentials and efficient, shared-exponent basis-sets for the 3rd-row, 4th-row, and 5th row atoms.* Can.J.Chem., 1992. 70: p. 612-30.
40.Krauss, M., *Ab initio determination of the structure of the active site of a metalloenzyme: Application to a metalloglutathione transferase.* Int.J.Quantum Chem., 2000. 76: p. 331-40.
41.Richter, U., Krauss, M., *Active site structure and mechanism of human glyoxalase I- An ab initio theoretical study.* subm., 2001.J.Am.Chem.Soc.
42.Chang, N.Y., Lim, C.,*An ab initio study of nucleophilic attack of trimethyl phosphate: Factors influencing site reactivity.* J.Phys.Chem.A, 1997. 101: p. 8706-13.

CRITIQUE OF TEST METHODOLOGIES FOR BIOLOGICAL AGENT DETECTION AND IDENTIFICATION SYSTEMS FOR MILITARY AND FIRST RESPONDERS

David Trudil
New Horizons Diagnostics, Columbia, MD 21045

Currently evaluations of the performance of various BW agent rapid detection or identification systems have primarily focused on defined aerosol samples released under favorable, controlled conditions or controlled samples assayed under laboratory conditions. Although these methods may provide information on the sensitivity, cross-reactivity, and some interferences, they may not provide sufficient information to adequately determine the effectiveness of the technology in the field conditions or when difficult environmental samples are analyzed.

Results with three different technologies currently utilized by various agencies in the field (Colloidal Gold - Hand Held Assays, generic DNA, and Luminescence) have demonstrated significant performance differences when evaluated with common environmental samples. Adulterants or interfering substances, which may be used by a terrorist, have also been tested, demonstrating additional potential problems.

In this study, salt, sugars, detergents, talc, phosphates, cross-reacting organisms (*Bacillus spp*), non-toxic material of biological origin (cereal), as well as very high concentrations of the specific organisms, were used to challenge the technologies. The purpose was to develop methods to determine both interference and potential pro-zoning issues. Results indicated that some of the immunological assays, including Anthrax, can give false positive results when a sample with high pH or ionic strength (salts) were evaluated. Moreover, a very high concentration of the antigen in a positive sample may cause a false negative result.

Utilizing testing challenges similar to those developed by the FDA, USDA, AOAC and other organizations, it is apparent the rapid detection systems developed for the battlefield "air samples" may not be applicable for other environmental samples including terrorist events. Collection and sample processing systems may aid in reducing potential problems with a sample, but the assay format should be evaluated with the specific samples to be tested in ensure reliable results. A modified Luciferase Assay provided an example of a case where minor sample processing significantly reduced interferences. Data as well as improved formats and processing systems will be presented.

INTRODUCTION

Numerous technologies have been considered for the rapid detection of Agents of Biological Origin (ABO). These include Immunoassay (EAI, gold, agglutination), light scattering, fluorescence, luminescence, culture, impedance, chip technology, GCMS, and others. Three of these technologies have been extensively utilized in rapid field tests for detection of ABOs. They have advantages as well as limitations, which have not always been fully appreciated. We have

performed various evaluations of assays that utilize these formats, delineating certain potential limitations or problem samples that may result in false or unclear results.

The three (3) technologies include:

1. Luminescence (ATP Bioluminescence)
2. Immunoassay (colloidal gold)
3. Fluorescence (DNA)

1. ATP BIOLUMINESCENCE:

Adenosine triphosphate (ATP) bioluminescence is a rapid alternative to the standard plate count for estimating microbial loads. ATP is the energy molecule in all living cells, including insects, plants, animals, bacteria, molds, or yeast. ATP bioluminescence is the technique of measuring ATP based on light emission during a bioluminescence reaction. The underlying premise of ATP bioluminescence is that the amount of ATP in a sample is proportional to the biomass. In the case of bacteria, there exists a strong correlation between cell number and ATP content. ATP can be measured using naturally occurring reagents from the firefly (*Photinus pyralis*) or genetically engineered. The reaction has been utilized with various samples from numerous sources including food, human, or environmental.

In the ATP bioluminescence reaction, luciferin is oxidized by the enzymatic reaction catalyzed in luciferase in the presence of magnesium and ATP. An end product of the reaction is energy in the form of yellow-green visible light (562nm). The emitted light , measured with a luminometer, is directly proportional to the amount of ATP in the reaction mixture. Data can be reported as the actual amount of ATP, however, in most cases it is reported as relative light units (RLU).

It is important to note that when measuring the ATP content of samples, one is measuring an average of the ATP content of the cells at that specific point in time. The ATP is in a constant state of flux and is species dependent. When comparing to culture, one must consider that the APC is growth based, where as the ATP assay measure a metabolite.

The ATP that is from non-microbial sources is termed somatic ATP. Generally, somatic cells have 100 to 1,000 times more ATP than bacteria cells. The ATP from an environmental sample may come from food, animals, plants, bacteria or even free ATP. This technology has become a standard tool for determining the "filth" or hygiene in a food plants. As such, this technique is a staple of many Hazard Analysis of Critical Control Point (HACCP) programs within the food industry worldwide (Cutter et al., 1996). Additionally, the ATP test with Luciferin Luciferase bound to a membrane (Model 4700) was included in the original Biological Integrated Detection System (BIDS) for the U.S. Army. This system detects the total ATP present in an air sample.

Most luminescence methods, however, neither differentiate between bacterial and non-bacterial ATP, nor correlate with standard culture methods. Also, it has been suggested that residual sanitizers as well as other substances may adversely affect the bioluminescence signal (Velazquez et al., 1996) by degrading Luciferin-Luciferase. Thus the presence of chemical residues on sampling sites could present a potential problem in underestimating or overstating the actual ATP signal and consequently affecting the decision tree.

A filtration-based bioluminescence technique which is able to separate bacteria from non-bacterial sources, thus able to detect bacterial ATP only (Siragusa et al., 1995, 1997), has been developed (Model 3550). Additionally, interfering substance were successfully removed. Evaluation studies performed on over 1000 food and environmental samples by researchers of the United States Department of Agriculture, Department of Defense, University of Michigan and others. A good correlation ($r = >0.92$) between the counts of bacteria on plates and the ATP from the luminometer for the same sample was obtained (Siragusa et al., 1995; 1997; Cutter et al., 1996; Stopa et al, 1998, 1999; Deininger et al, 1999).

To further expand the use of this technology, a unique heat incubation method was developed to identify spore samples within 20 minutes in a field setting. This method was able to reliably detect 10^5 CFU/ml of bacteria (Bartoszcze et al; Stopa et al 1999). A further modification of this Bioluminescence technique included the use of a Phage Associated Enzyme (PAE) for specific lysing and identification of bacteria.

2. COLLOIDAL GOLD TECHNOLOGY:

During the 1990s Hand Held Assays have developed which utilize a colloidal gold particle format to effect sensitive and selective detection of Agents of Biological Origin (ABO). Antibody (described below), specific to the agent of interest, is adsorbed on colloidal gold particles. Colloidal gold particles are discrete, electron-dense, non-fading, red-colored particles, approximately 20nm – 50nm in diameter. A 20nm gold particle adsorbs 20-30 antibody molecules (Figure 1). When antigens are combined with the colloidal gold-antibody conjugate, these complexes are concentrated on solid surfaces, either by capture antibody on nitrocellulose membrane or by immobilization on selective porous capture membrane, a distinct red spot is visualized by the naked eye. Labeled antibodies can be easily lyophilized (freeze dried) and reconstituted without losing activity or specificity which enables the product to be stored at ambient temperature.

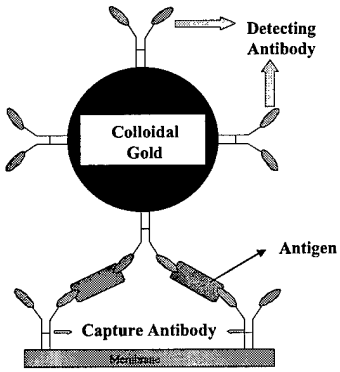

Figure 1. Gold Technology.

The two basic Gold Based assay formats are:

1. Flow Through
2. Lateral Flow

1. FLOW THROUGH COLLOIDAL GOLD PARTICLE CONCENTRATIONS:

Two variations of the Flow-Through Gold Technology utilize a colloidal gold particle concentration immunoassay to achieve sensitive and selective detection of biological materials, as illustrated in FIG. 2A and 2B. These are the Sandwich Assay (bacteria/toxin/virus) and the Charged Complex (spore). Antibodies specific to the agent of interest are conjugated to colloidal gold particles.

Figure 2A: For bacterial/toxin/virus samples, the antibody-antigen (Ab-Ag) complex is filtered and then concentrated onto a Nitrocellulose Membrane with capture-antibody. In the toxin or soluble antigen ticket format, the membrane is coated with a specific capture antibody to elicit binding of the antibody-antigen complexes to the membrane. The Control Spot utilizes antibodies derived from non-immune serum from the species of animal used to prepare the specific, active anti-serum. The complex is immobilized on the surface of the porous capture membrane and can be visually detected as a red spot. If the antigen is not present, the unbound colloidal gold reagents will diffuse through the membrane and will not be visually detectable. This assay does not require a washing step due to minimal interaction between the colloidal gold labeled antibody and the glass fiber capture membrane. However, in some cases, where there is a particularly dirty sample, the reaction area can be washed for better visualization.

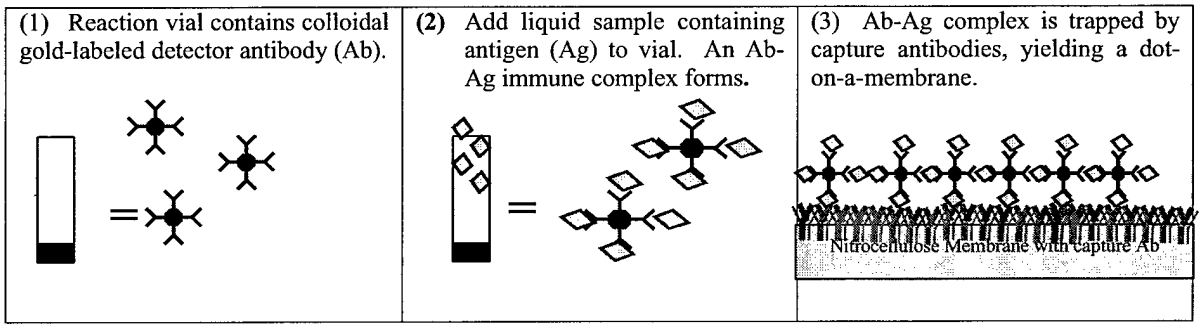

Figure 2A. Bacterial/Toxin/Virus: Colloidal Gold.

Figure 2B: For spores, the antibody-antigen (Ab-Ag) complex is filtered and concentrated onto a glass fiber membrane. The complex is immobilized on the surface of the porous capture membrane due to electrostatic attraction (charge) and can be visually detected as a red spot. If the antigen is not present, the unbound colloidal gold reagents will diffuse through the membrane and will not be visually detectable. This assay does not require a washing step due to minimal interaction between the colloidal gold-labeled antibody and the glass fiber capture membrane. However, in some cases, where there is a particularly dirty sample, the reaction area can be washed for better visualization. There is no Control Spot in the spore assay.

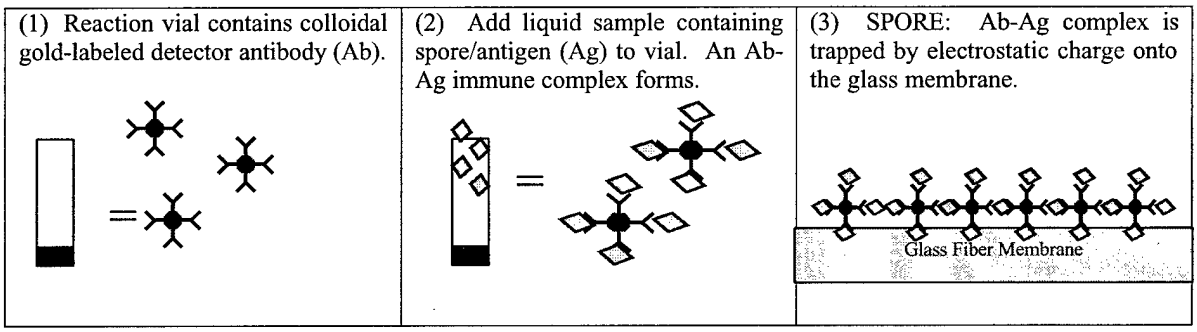

Figure 2B. Spore: Colloidal Gold Concentration Immunoassay.

2. LATERAL FLOW TECHNOLOGY:

In the Lateral Flow format, antibody coated colloidal gold particles are applied to a membrane surface and dried. When a test sample is applied, the gold conjugate reacts with any antigen that is present as it migrates across the length of the membrane to where it encounters a zone of capture antibody. Those antibody-gold conjugates, which have bound to antigen in the test sample, are then bound in the capture antibody zone, presenting a visually detectable line of color and indicating a positive test result (see Figure. 3). Sufficient antibody will be available to permit passage through the capture zone. These particles will then contact an area coated with an appropriate IgG fraction, where they will bind, producing a visible line of color.

1: Dry Strip

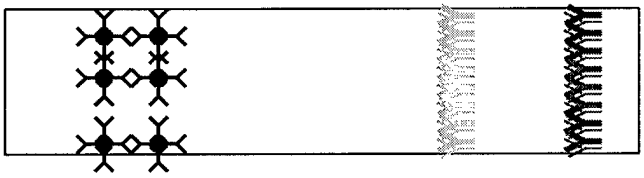

Capture, Control and Test antibodies

antigen

gold particle

TABLE 1.

complex

2: Add Sample (with Antigen)

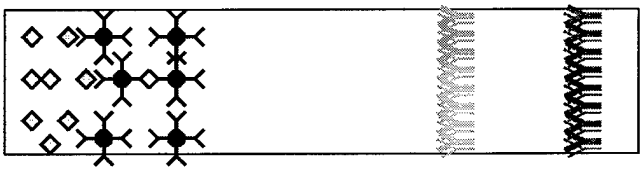

3: Sample flow moves particles; antigen form sandwich

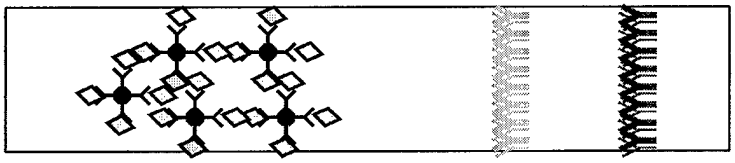

4: Dyed particles form colored lines for Positive test and Control

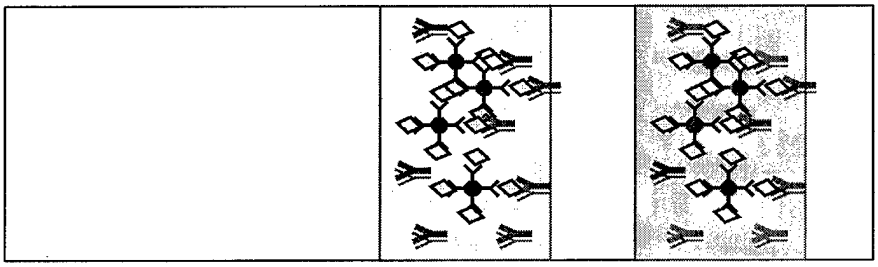

Figure 3. Chromatographic Strip Test (1 – 4).

The first Gold based tests developed and utilized during Desert Storm and subsequently the initial BIDS system employed the Flow Through technology (SMART I). Subsequent Hand Held Assays have been modified for the Lateral Flow technology as well. The lateral flow Technology, due to manufacturing and cost advantages, has become the format of choice for rapid medical, veterinary and environmental use as well.

FLUORESCENCE (DNA):

Fluorescence is a physical property of certain atoms and molecules. It is a molecule's ability to absorb light energy at one wavelength, then instantaneously re-emit light energy of another, usually longer, wavelength,. Each compound that fluoresces has a characteristic excitation wavelength, (the wavelength of light is absorbs) and a characteristic emission wavelength, (the wavelength of light that it emits when the molecules relax and return to their ground state). These excitation and emission wavelengths, (or spectra), are often referred to as the compound's fluorescence signature. Detecting and quantitating small amounts of DNA is important in a wide variety of biological applications. These include standard molecular biology techniques, such as synthesizing cDNA for library production and purifying DNA fragments for subcloning, as well as diagnostic and detection techniques, such as quantitating DNA amplification products and detecting DNA molecules in various samples (Turner Design, 2000).

The most commonly used technique for measuring nucleic acid concentration is the determination of absorbance at 260nm. Unfortunately, this absorbance method has limitations including; interference from contaminants found in nucleic acid preparations, inability to distinguish between DNA and RNA, lack of sensitivity and others. The use of a unique dye, PicoGreen ® (Molecular Probes) has resolved many of these problems and, as such, has been successfully utilized for the field detection of ABO (Stopa, et al., 1998).

TECHNOLOGY REVIEW

All three of these technologies (Luminescence, Colloidal Gold, and Fluorescence) have their advantages as well as disadvantages. During the course of development and in the haste to field an assay, there may be tendency to evaluate a test system in pristine laboratory conditions. Consequently, one may determine sensitivity by obtaining a pure sample and diluting the target analyte in a defined, controlled buffer until a negative result is obtained. Additionally, only a limited specificity panel of potential cross-reacting organisms may be performed. Obviously, in the case of human sample testing there are very defined criteria that must be met prior to issuance of an FDA 510(k) or PMA. In lieu of such criteria it is incumbent the potential user be aware of the limitations and capabilities of the assay system in question.

Awareness of the sensitivity, specificity, and known cross reactions is essential to the individual performing and interpreting the test results. These personnel must be familiar with each of these parameters for each assay performed to provide the decision makers/commanders with the appropriate information. In immunological assays, these factors are generally due to the properties of the antisera (polyclonal, monoclonal, avidity, affinity), or antigen from which the reagent is made; and therefore may change with new production materials.

A number of factors may also be of concern in the user of these tests. These include Prozoning and nonspecific cross reactions. Prozoning can occur when there is such an

overwhelming abundance of antigen/analyte that all antibodies sites are "flooded", not allowing for a "sandwich" (antibody-antigen-antibody) binding or allowing for latice formation. In this situation a false negative would be seen from what should have been a very strong positive sample. The non-specific reactions can be due to either a reaction to the chemistry of the test (not the antibody or detection system) or cross-reactions with other organisms.

Obviously, one would like an assay system that detects all positive samples without any false positives. This tends to be a lofty goal that can never realistically be achieved. Recognizing this, as a product is developed the intended use as well as the requirements of the intended user must be of primary importance. As an example, the original colloidal gold hand held assay was designed to detect a specific analyte from an air sample. The sample buffer and all other parameters were very well defined. The goal was to provide as much sensitivity in this defined buffer as possible. There was no requirement for determining interferences from various other environmental or human samples as, therefore, during the developmental process there was less of a need to balance sensitivity vs potential non-bacterial cross reacting substances. A good example would be Anthrax spore. Due to the nature of the spore and the antibody supplied, the most effect format was determined to be the Colloidal Gold Concentration Immunoassay as previously described. This assay system met sensitivity as well as specificity requirements when utilizing a defined air sample. The major drawback, however, was the lack of a negative control. However, as there were several test systems employing different formats, this limitation was incorporated in the decision tree and accounted for. Subsequently, however, attempts were made to utilize this "air sample" assay with various environmental or even hoax samples. As the assay was neither designed for nor tested with such samples, this created a problem fraught with unknowns. The unknown was further compounded by the lack of a negative control.

In another example of a human test system, the typical Limulus amebocyte lysate (LAL) agglutination assay can detect 1,000 gram-negative bacteria per ml. In untreated meningitis, there generally is 100,000 bacteria per ml, but significantly less in treated ones. Thus the sensitivity of the LAL test for untreated patients was 90%, whereas the sensitivity for treated patients was only 65-75%. This system would be intended for untreated patient samples, but would lacking when testing treated patient samples.

As there have been numerous studies of technologies utilizing air or pristine laboratory samples, we have focused primarily on filed samples. This includes both routine samples found in the environment, both microbial and chemical, as well as hoax or artificially dispensed material. Additionally, we have considered the other limitations of the technology employed such as pH, temperature, etc.

Another factor that was considered is the material or solutions utilized to collect the sample prior to performing the assay. The samples considered where primarily environmental, but in one case to emphasize microbial cross reactivity studies, human and clinical laboratory isolates were utilized.

MATERIALS AND METHODS

INTERFERING SUBSTANCES:

Trichloroacetic acid and sodium hypochlorite (bleach) at various concentrations, talc (baby powder), diet cola, plain sugar, ethanol, table salt, garlic powder, cinnamon, coffee creamer,

HCL, maltrin, heparin, sugar water, casein, EDTA, potassium phosphate, sodium phosphate, laboratory salt, trahalose in hepes, Dipel® (Ortho), laundry detergent, dish washer detergent, lawn fertilizer, lemon aide, road dust, soil, silica gel, gelatin, iron, foam cleaner, ammonium compounds, and various other compounds.

RAPID MICROBIAL ATP ASSAY (PROFILE®):
Microluminometer NHD Model 3550i (Fig.1), Filtravette™ (.45u and 5.0u), Somatic Cell Releasing Agent (SRA), Bacteria Cell Releasing Agent (BRA), Luciferin-Luciferase (LL), and cell concentrator with syringe.

STANDARD PROFILE® PROCEDURE:
A sample suspension is transferred to the Filtravette™ (.45u for bacteria). Three (3) drops of Somatic Cell Releasing Agent (SRA) are added. The mixture is pushed through the Filtravette™ by a positive pressure device. Three (3) more drops of SRA are added and pressure-filtered to ensure the removal of interfering substances, free ATP, and somatic cell ATP. The Filtravette™ is then placed into the drawer slide of the Microluminometer (PROFILE®). Two (2) drops of Bacterial Releasing Agent (BRA) are added into the Filtravette™ to extract the microbial ATP. Immediately after the addition of the BRA, 50µl of Luciferin-Luciferase (LL) is added and mixed by aspirating the fluid up and down three (3) times. The drawer slide is closed immediately. Light emission is measured with integration over ten (10) seconds. ATP is reported as Relative Light Units (RLUs), taken directly from the luminometer's digital readout (Fig 2-6).

STANDARD COLLOIDAL GOLD PROCEDURE:
Flow through:
A sample (100ul) is added to the gold conjugate tube. Two drops of buffer is added. Transfer the sample/gold mixture to the test device via a swab (provided). Close device wait 5-15 minutes (maximum 18hours). Open device, red dot is positive.

Lateral flow:
A sample (100ul) is added to the sample well of the test device. Add two (2) drops, wait for 15 minutes. Two red lines are positive. One (1) line in the control area indicates a negative result.

STANDARD FLUORESCENCE (DNA) PROCEDURE:
Add sample (50ul) to cuvette, add solution A (50ul). Add sample (50ul) to another cuvette, add solution B (50ul). Let both stand for 5 minutes. Place cuvette A into instrument and record result. Place cuvette B into instrument and record result. Reading cuvette B – reading of cuvette A = Fluorescence of DNA in sample.

ASSAY WITH INTERFERING SUBSTANCES:
A fifty (50) µL suspension of *S.aureus* and *E.coli* was transferred to the Filtravette™. Fifty (50) µl of substance was then added to the bacterial (.45u) Filtravette™ and the standard PROFILE® procedure was performed. The experiment was repeated with various concentrations and types of sanitizers. The expelled liquid filtrate was then assayed for bacteria utilizing the standard PROFILE® procedure.

The Colloidal Gold and Fluorescence assays were performed as per the standard sample protocol.

ASSAY WITH PHAGE ASSOCIATED ENZYME:

A 100ul sample of Group A Streptococci and Group B Streptococci was added to the Filtravette™. The standard SRA washing procedure was followed as per instructions of the PROFILE®. 100ul of PAE was then added in lieu of the standard BRA total lysing reagent. The standard PROFILE® procedure was then followed. To determine background, the PAE was tested with the addition of a sample.

ASSAY WITH SPORES:

The sample of the suspected spore is incubated in an equal volume of Trypticase Soy Broth (TSB) for 15 min at 37°C. The entire sample is removed and filtered through a cell concentrator containing the Filtravette™ and the standard Profile® procedure was then followed.

Table 1.

Efficacy of Filtration-Based
Bioluminescence to Remove Inhibitors

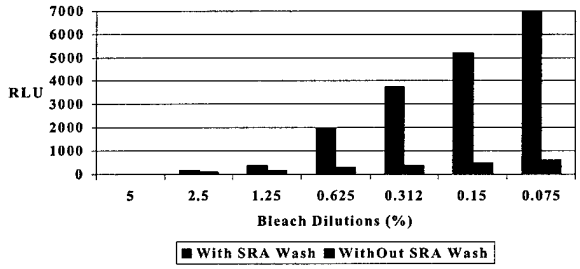

Table 2. Luminescence Interfering Substances.

SUBSTANCE	EFFECT
Ammonium compounds	Increase in signal
Bleach	Decrease in signal
Salt	Decrease in signal
Foam Cleaner	Decrease in signal
Iron	Decrease in signal

Velazquez, et al, JFP 1997

Table 3. Gold Interfering Substances.

Talc (Baby Powder)
Acid (HCl)
Ethanol
Heparin
Salts
Sugar
Detergent

Table 4. Modified Gold Test – Non-Interfering Substances.

Dipel	Baby Powder
Morton Salt	Sugar Water
Coffee Creamer	Sugar (plain)
Diet Coke	Cinnamon
Garlic Powder	Various Salts
Laundry Detergent	

Table 5. Cholera Gold Test Screened for Specificity.

Bacterial Strain	**No. of strains tested**	**% Positive**
V. cholerae O1	30	100
V. cholerae O139 (Bengal)	10	0
V. cholerae non-O1	20	0
V. vulnificus	4	0
V. parahaemolyticus	4	0
V. minicus	10	0
V. alginolyticus	2	0
V. campbelli	2	0
V. fluvialis	3	0
V. damsela	2	0
V. natriegens	2	0
V. pelagius	2	0
V. proteolyticus	2	0
Aeromonas hydrophila	5	0
A. veronii bv. Sobria	2	0
A. caviae	2	0
Shigella dysentariae	2	0
S. boydii	1	0
S. flexneri	1	0
S. sonnei	1	0
Escherichia coli	3	0
Salmonella typhimurium	2	0
S. thompson	1	0
S. hadar	1	0
S. berta	1	0
S. johannesburg	1	0
Klebsiella pneumoniae	2	0
Serratia marcescens	2	0
Citrobacter freundii	2	0
Proteus vulgaris	2	0
Enterobacter aerogenes	2	0
Pseudomonas aeruginosa	2	0
Plesiomonas shigelliodes	2	0

Table 6. Fluorescence (DNA) Interference.

Silica Gel	Dish Detergent
Gelatin	Phosphate
Baby Powder	Sugar
LemonAid	Road Dust
Lawn Fertilizer	*Stopa et. al 6th CBW Prot. Symp.*

Table 7. Effective pH Range.

Luminescence	7.75
Colloidal Gold	6.0 – 8.5
Fluorescence	7.50

Table 8. Effects of Interfering Substances.

Interfering Substances	ATP Protocol	Protein Protocol	DNA Protocol
Pollens/Mold Spores	N	Y^4	N
Household/Laboratory Detergents	N	Y^3	N
Household Food Items	N	Y^2	N
Household Chemicals/Detergents	N	Y^3	Y^3
Laboratory Nutrient Media	N	Y^2	Y^2
Laboratory Chemicals	N	Y^3	N
Color Producing Substances	N	Y^4	Y^4
Large Particles in Sample	N	Y^4	N

N = No interference seen

Y^2 = Result was high due to a natural presence of substance being analyzed.

Y^3 = Inhibition/enhancement of reaction due to interaction between reagents and interfering substance. High concentration of detergents causes a false positive with the protein test.

Y^4 = Physical interference caused by particles in the sample, discoloring reagents, or mechanically dispersing or reflecting instrument light. *Stopa et al 6th CBW Prot. Symp.*

Table 9. Prozone Effect.

	50ng	100ng	500 ng	1000 ng	5000 ng
SEB	**2+**	**4+**	**2+**	**1+**	**Neg.**

RESULTS AND DISCUSSION

LUMINESCENCE (ATP)

It has been widely reported that basic ATP assessment although sensitive is subject to variability and when compared to standard culture methods is not accurate. As previously mentioned, these issues are due to various factors not the least of which is due to the presence of interfering substances, somatic ATP, and free ATP mixed with microbial ATP. It is interesting to note that these factors could cause false positives as well as false negatives. (Cutter et al, 1996; Siragusa et al, 1995, 1997; Velazquez et al, 1997; Stopa et al, 1999).

The filtration-based bioluminescence method was challenged to perform with various samples under pristine, as well as stressed environments. The assay performed well; correlating to culture for bacteria directly from various samples. The filtration method employed also demonstrated satisfactory performance when confronted with high salts, detergents, cleaners, ammonium compounds and metals of the type normally found in the environment or samples presented to a first responder.

Utilizing sodium hypochlorite (bleach) and trichloroacetic acid, a reduction of 94 to 96% in the bioluminescence signal was observed when concentrations higher than 1% were used in conjunction with the standard non-filtered ATP method (Table 1). It was further demonstrated that when the SRA wash filtration step was employed, this quenching effect was significantly reduced or removed expanding the utility of this method. It was also interesting that some compounds (ammonium) actually increased the RLU signal overstating the result, potentially leading to a false positive result if this filtration step was not implemented (Velazques et al,1997) [Table 2]. This method also tends to keep the pH at the optimum 7.75 {Table 7) and minimizes the effect of temperature variability.

Testing with a pure culture of *S. aureus* this method with a Model 3550 luminometer (New Horizons) could readily detect 10^5 CFU/ml with a 50 µl sample size. When the sample size increased to 2 ml, there was a 1 log increase in sensitivity. Subsequent testing has indicated sensitivity can be further improved by increasing the sample size as well as adjusting the voltage setting of the instrument.

The method described detects and enumerates generic bacteria or yeast. Several modifications can be employed that will allow specific identification. These may include antibody coated beads, chemiluminescence, or the use of specific lysing reagents. Recent preliminary data has demonstrated that a specific bacteria phage enzyme (PAE) may be employed in lieu of a generic bacterial releasing agent (BRA) to selectively lyse a target organism. The Group A Streptococci phage enzyme was chosen due to the long history of use and complete definition of the phage and bacteria. This method may be useful not only for the routine identification of various bacteria, but also as a rapid environmental monitoring tool to determine the effectiveness of cleaning or identification of potential problem areas.

As spores are deficient in ATP, an incubation method was developed whereas the spore would convert to the vegetative state. During this phase ATP is produced at sufficient levels to be detected by the model 3550 luminometer. Although spores are detectable after less than 10

minutes, a 15 minute incubation was utilized to insure consistent agreement to standard methods. Data demonstrates a detection limit of 10^5-10^6 can be achieved with a normal sample size of less than 1 ml.

COLLOIDAL GOLD

The standard colloidal gold based assays has gone through dramatic changes since New Horizons introduced the first tests in the late 1980's. Improved membranes, sample pads, conjugate pads and gold chemistries have allowed for continued improvement in the overall performance of this format.

The initial flow through colloidal gold particle concentration technique offered the advantages of ease of use and ambient storage with improved sensitivity compared to the agglutination or rapid EAI tests. The sensitivity improvement came not only as a result of the gold chemistries, but due to the transfer of virtually 100% of the sample/gold complex and focusing this complex at a small point (small hole in the laminant). Sensitivity ranged from 10^4 for Group A strep to $5x10^5$ for many ABO tests. The primary variable, however, was the antibody.

As a answer to the issues of improved ease of use (1 less step), decrease cost of goods, and decreased antibody usage; the lateral flow assays were developed. The primary issue that had to be resolved was sensitivity. With the improvements mentioned above this format was off and running.

The first lateral flow assays were designed for medical applications and as such the samples were fairly consistent. The entry into the environmental and first responder arena, however, precipitated other issues. The standard gold based assays are optimized for a sample with a pH of from 6.0-8.5 (dependent on the test) [Table 7]. Also, various samples can cause the gold to "crash" causing a deposition on the membrane giving the indication of a positive. Alternatively, some sample may cause no or slow flow of the complex leading to an invalid result (Ethanol, trahalose). Some of these interfering substances are listed in Table 3.

To resolve these, the chemistries and membranes of the lateral flow assays were modified. It is interesting to note that typically there is no one fix, but each assay must be developed separately, utilizing a panel of potential interfering substances (Table 4). This is further complicated if the antibody changes in any significant manner - as may be the case with polyclonal antibodies from different sources.

In addition to the various chemical compounds, the assay systems must be tested for potential cross reactions for other organisms. This again, is primarily due to the specificity of the antibody utilized in the test. Table 5 is a sample of some of the specificity data for a gold based Cholera O1 test. As this assay is for human use, this as well as other testing was necessary for FDA 510(k) submission. Here it is importance to have an understanding of which potential organisms may cause cross reactions with the target analyte. As another example, Anthrax spore antibody may also react with (false positive for an Anthrax spore test) other *Bacillus* species such as *Bacillus cereus* and *Bacillus thuringiensis* (BT). This is of critical importance as these are very common in the soil and the BT is common used to kill insects such as the gypsy moth. The commercial form of the BT is sold under the name Dipel® (Ortho). This further complicates

testing of an assay as a test system that may function very well in a desert situation where these organisms are not present, may not be fully usable in the US where they are very common.

Another issue that is known in the human clinical laboratory is the effect of prozoning. In this situation an excess of a specific analyte will cause a false positive. The most striking example of this phenomenon is SEB. I this example, a 5000ng sample reacted as a negative but further dilutions gave a 4+ reaction at 100ng (Table 9).

It is important to verify the assay system will detect all levels of expected ABO. This further underscores the intended use. Clearly for the battlefield, the commanders want immediate answers therefore underscoring the need for sensitivity with minimal concern about sample overload (sampling an air sample). The first responder who may obtain a large packet of powder may be more concerned about a false negative due to prozoning.

FLUORESCENCE (DNA)

The fluorescence assay is a good tool to assist in determining the presence of a virus, however, it has similar limitations as other technologies. Clearly the pH is optimized for the dye utilized (Picogreen® – 7.5). Additionally any substance of biological origin may cause interference. The system is further by other easily obtained substances such as phosphates, detergent, sugar, baby powder , etc. (Table 4). Obviously, these effects must be taken into account when analyzing a sample. The effects of general interfering substances for ATP, DNA as well as protein are seen on Table 8.

INHIBITORY PROPERTIES OF COLLECTION DEVICES

From the studies conducted it is apparent that common compounds such as ammonium, phosphates, salts and various sanitizers may interfere with some assays. Additionally, these may also inhibit the growth or even kill bacteria. Cellulose sponges and even some swabs may contain sulfur, ammonium, and other compounds. These compounds are utilized in the manufacturing process to break down wood fibers from which these sponges are made. Studies have shown that significant bacterial loads could be reduced to zero (0) in a little as 4 hours (Perry and Ballou, 1997). Additionally, it has been demonstrated that bacteria and bacterial antigens tend to be absorbed by the wooden shaft swabs. Also, bacteria are not as freely released from cotton swabs as opposed to dacron or rayon swabs (Becton Dickinson, personal communication).

When expands this further to the collection fluid it becomes apparent that all facets of the system should be verified (collection, processing, detection) . Consequently, a Phosphate Buffered Saline solution should be evaluated for over effects on recovery and detection with assay systems employed.

Recognizing these factors a collection system has been developed for different samples. One for a large surface sample, a second for a powder/small surface sample, a third for a liquid sample and the fourth for an air sample. Additionally a sample processing packet has been designed for cleaning up a "dirty" sample as well as submitting for further testing. All components have been tested with the testing formats described.

CONCLUSION

- Presence of salts, sugars, ammonium compounds, metals or other chemicals could present a potential problem by interfering with some luminescence, colloidal gold (hand held assays), and fluorescence (DNA) tests systems.

- In determining the acceptance of an assay system one should consider the sensitivity (including prozoning), specificity, and potential cross reacting substance based upon the manufacturers intended use as well as the users requirements.

- Employing filtration-based bioluminescence technique, interfering residues could be removed/reduced to a level that does not significantly inhibit the bioluminescence signals. Consequently, the actual bacterial status of a sample is obtained.

- The filtration-based system detects Bacteria in less than two (2) minutes while providing good correlation (>90%) with conventional culture methods which require as long as 4-7 days.

- The major variable with immunological (antibody) based systems is the antibody. Care should be taken to fully evaluate the total system for other potential cross reactants of biological origin as well as method to insure lot to lot reproducibility.

- Evaluations performed on similar assay systems but with different intended use should be reviewed carefully for potential limitations.

- Further advances in this system allow for increased detection limits as well as specific identification including the use of Specific Phage Associated Enzymes (PAE).

- The measurement of the ATP from a sample prior to and after incubation demonstrated the presence of a spore (i.e. *Bacillus spp.*) in less than 15 minutes

- Collection devices and processing buffers should be carefully considered to insure compatibility with assay systems as well as effective recovery of target analyte.

REFERENCES

1. Cutter, C. N., W. J. Dorsa, and G. R. Siragusa. 1996. A rapid microbial ATP bioluminescence assay for meat carcasses. Dairy, Food & Environ. San. 16 (11) p. 726-736.
2. Hasan, J.A.K., S. Garg, L. Loomis, D. Miller, and R.R. Colwell. 1997. A rapid surface-monitoring method for bacteria employing ATP bioluminescence. Abstr. No. I-026, 97th General Meeting of Am. Soc. Microbiol.
3. Siragusa, G. R., C. N. Cutter, W.J. Dorsa, and M. Koohmaraie. 1995. Use of a rapid microbial ATP bio- luminescence assay to detect contamination on beef and pork carcasses. J. Food Protec. 58 (7), p.770-775.

4. Siragusa, G. R., W. J. Dorsa, C. N. Cutter, L. J. Perino, and M. Koohmaraie. 1996. Use of a newly developed rapid microbial ATP bioluminescence assay to detect microbial contamination on poultry carcasses. J. Biolumin. Chemilumin (11), p. 297-301.
5. Velazquez, M., H. Chan, A. Kirumira, and J. Feirtag. 1996. Quenching and enhancement effect on the ATP bioluminescence signal using different ATP extractants and sanitizers. Abstr. No. 73. In program and abstract book, 83rd Annual Meeting of IAMFES, p. 50.
6. Northcutt, J., and S. M. Russell. 1996. Making HACCP happen in your plant. Broiler Industry, July p 24-35.
7. Russell, S. M. 1995. Sanitation procedures and HACCP. Broiler Industry, October, p. 22-38.
8. Perry, J.L. and D.R. Ballou, Inhibitory Properties of a Swab Transport Device. J. Clinical Micro 35 (12):3367-3368
9. Stopa, P.J.,P.A. Coon, A.T. Seitzinger, D. Paterno, D. Tiemanm, and M. Milton. 1998. Proc. 6th CBW Int. Symp: suppl. 229
10. Stopa, P.J., D. Tieman, P. Coon, M. Milton, and D. Paterno. 1999. Detection of Biological Aerosols by Luminescence. Field Anal. Chem.& Tech.3 (4-5):283-290
11. Deininger, R.A. and J. L. Lee. 1999. A Rapid Method for Detecting Bacteria in Drinking Water. J. Rapid Methods & Auto. Micro.7: 135-145.

CONTACT: David Trudil, NEW HORIZONS DIAGNOSTICS CORPORATION,
9110 Red Branch Road, Columbia, MD 21045
410-992-9357 / email: NHDiag@aol.com

DETECTION OF BIOLOGICAL AEROSOLS BY MALDI ON-LINE AEROSOL TOF MS

Ben L.M. van Baar,[1] Michael A. Stowers,[2] Arjan L. van Wuijckhuijse,[2] Charles E. Kientz,[1] Brian Scarlett,[2] Jan C.M. Marijnissen,[2] and Ruud W. Busker[1]

1. TNO Prins Maurits Laboratory, P.O. Box 45, NL-2280 AA Rijswijk (ZH), The Netherlands.
2. Delft University of Technology, Faculty of Applied Sciences, Julianalaan 136, NL-2628 BL, Delft, The Netherlands.

ABSTRACT

Matrix-assisted laser desorption/ionisation (MALDI) mass spectra were obtained from single biological aerosol particles using an aerosol time-of-flight mass spectrometer (ATOFMS). The inlet to the ATOFMS was coupled with an evaporation/condensation flow cell that allowed the aerosol to be coated with matrix material as the sampled stream entered the spectrometer. Mass spectra were generated from aerosols of gramicidin-S, erythromycin, insulin and cytochrome c, or of *Bacillus subtilis* var niger spores. The results give a proof of principle that MALDI ATOFMS can provide nearly real-time identification of biological aerosols.

INTRODUCTION

Single particle aerosol mass spectrometry has developed since the late 1980s.[1] A system for aerosol mass spectrometry, was originally constructed at the Delft University of Technology.[2] This system, the ATOFMS, consists of a particle-beam like aerosol inlet, a HeNe laser for particle sizing and ionization triggering, an UV ionization laser and a time-of-flight mass analyzer. This system was recently further modified to achieve bio-aerosol detection, with the ultimate goal of establishing a generic bio-aerosol alarm.

RESULTS

First, a device was constructed for the on-line coating of aerosol particles with a matrix compound. This allowed more efficient ionization, through on-line aerosol MALDI MS.[3] Low mass peptides, erythromycin (~700 Da) and gramicidin S (~1,040 Da) and glycan type material from *Bacillus subtilus* var niger spores (~1,230 Da) was observed in typical MALDI-ATOFMS mass spectra.

Next, the upper mass range limit of 2000 Da was extended by instrument modifications to the mass spectrometer. With the extended mass range and matrix addition, spectra of larger peptides were obtained; in Figure 1, an example is shown of a spectrum obtained from cytochrome c aerosol.

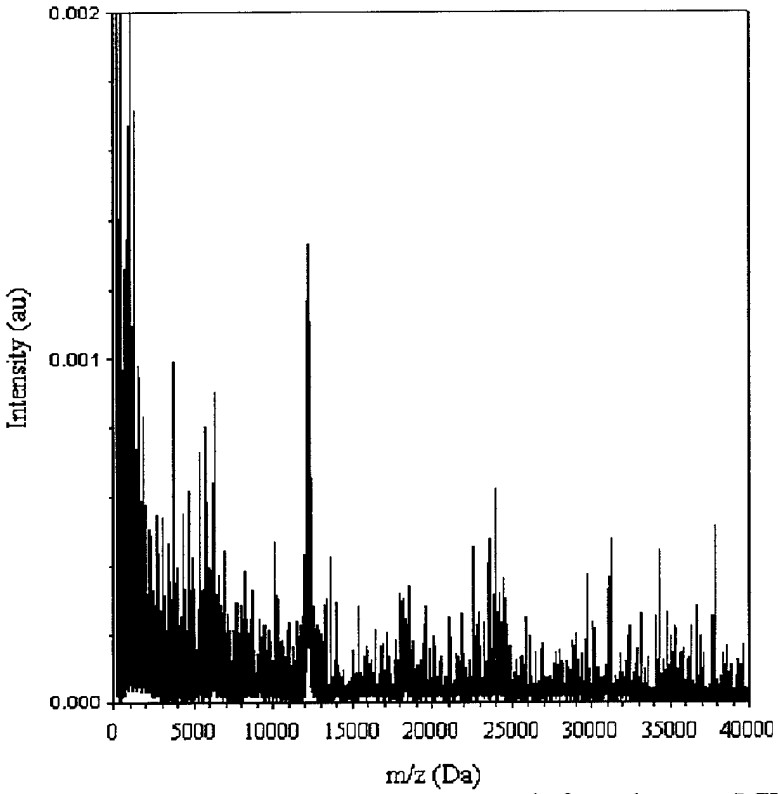

Figure 1. MALDI-ATOFMS spectrum obtained from an aerosol of cytochrome c (MW_{av} 12,270 Da), premixed with ferulic acid matrix.

Most biomarker signals from bacteria, as observed in common MALDI MS, fall in the mass range up to 30,000. Therefore, observations of proteins in this range, with the MALDI-ATOFMS, is a proof of principle that bacteria fingerprints can be obtained in real-time (seconds).

Currently, the MALDI-ATOFMS system is being modified for selective ionization of bio-aerosol particles, by on-the-flight distinction of biological particles from common organic and inorganic particles. This selective ionization will be used to increase the detection efficiency for bio-aerosol particles.

ACKNOWLEDGMENT

The authors thank The Netherlands Ministry of Defence for continued support to the project (under number 98A420).

REFERENCES

[1] D.T Suess and K.A Prather, Chem. Rev. **99** (1999), 3007-3035.
[2] O. Kievit, M. Weiss, P.J.T. Verheijen, J.C.M. Marijnissen, B. Scarlett, Chem. Eng. Commun. **151** (1996), 79-100; and M. Weiss, P. Verheijen, J.C.M. Marijnissen, B. Scarlett, J. Aerosol Sci. **28** (1997), 159-171.
[3] M.A. Stowers, A.L. van Wuijckhuijse, J.C.M. Marijnissen, B. Scarlett, B.L.M. van Baar, C.E. Kientz, Rapid Commun. Mass Spectrom. **14** (2000), 829-833.

DEVELOPMENT OF MEDICAL COUNTERMEASURES TO SULFUR MUSTARD VESICATION

William J. Smith, Michael C. Babin
US Army Medical Research Institute of Chemical Defense
Aberdeen Proving Ground, MD 21010-5400

Robyn C. Kiser, Robert P. Casillas
Battelle Memorial Institute
Medical Research and Evaluation Facility
Columbus, OH 43201-2693

ABSTRACT

Sulfur mustard (HD) is an alkylating agent with cytotoxic, mutagenic and vesicating properties. Its use on the battlefield results in debilitating injuries to skin, eyes and the respiratory system (1, 2). To elucidate the toxic sequelae that follow cutaneous exposure to HD, the United States Army Medical Research Institute of Chemical Defense (USAMRICD) has undertaken a broad-based research program encompassing both intramural and extramural research. This report summarizes our current understanding of the toxicology of human exposure to HD based on *in vitro* and *in vivo* experimental models.

INTRODUCTION

While many of the toxic manifestations that follow HD exposure have been defined, the actual mechanisms of pathology remain elusive. Much of the research in this area has been conducted in the Pharmacology and Drug Assessment Divisions of USAMRICD, the laboratories of our NATO allies and laboratories funded through the Medical Research and Materiel Command extramural contract program. Based on the technological database developed, through this program, we have been able to generate a unifying hypothesis for cellular and tissue events that explains the formation of cutaneous blisters following exposure to HD. Studies of individual toxic events, such as alkylation of cellular macromolecules, formation of DNA strand breaks, activation of poly(ADP-ribose) polymerase (PARP or PADPRP), disruption of calcium regulation, proteolytic activation and tissue inflammation, have together led to the formulation of six strategies for therapeutic intervention (3, 4). The proposed pharmaceutical strategies are intracellular scavengers, DNA cell cycle modulators, PARP inhibitors, calcium modulators, protease inhibitors and anti-inflammatory compounds.

These compound classes are currently being evaluated as medical countermeasures against HD dermatotoxicity. We have validated four *in vitro* testing modules for compound screening: solubility, direct toxicity, protection against HD-induced cytotoxicity and protection against HD-induced depletion of cellular nicotinamide adenine dinucleotide (NAD+) levels. Two additional *in vitro* modules, preservation of cellular adenosine triphosphate (ATP) levels and inhibition of proteolysis, are in the final stages of validation. For *in vivo* screening, we have utilized the mouse ear vesicant model (MEVM) with associated histopathological evaluation (5) and cutaneous vapor exposure in hairless guinea pigs (6). For systemic drug therapy, we are validating a hairless mouse cutaneous vapor exposure model.

EXPERIMENTAL DESIGN

DECISION TREE NETWORK (DTN)

A DTN has been devised to outline the selection process used to evaluate candidate pretreatment or treatment compounds. This DTN consists of pathways through *in vitro* and *in vivo* compound screening modules based on known characteristics of the compounds being evaluated.

IN VITRO SCREENING MODULES

As compounds are placed in the Drug Assessment Compound Tracking System, they are assigned to specific functional categories. Based on their categorization, they are evaluated through a series of assays such as aqueous solubility, direct cytotoxicity in human lymphocytes (PBL), protection of PBL against the cytotoxicity of HD, depletion of metabolic factors (NAD+ or ATP), and inhibition of HD-induced proteolysis. Results from these assays are used to prioritize movement of candidate compounds into the *in vivo* screening modules.

IN VIVO SCREENING MODULES

Compounds passing the *in vitro* modules or compounds from classes not applicable to *in vitro* screening (i.e., anti-inflammatory compounds) are tested in the MEVM for edema and histopathologic (i.e., epidermal-dermal separation and epidermal necrosis) evaluation. Other *in vivo* assays available for additional testing as required include cutaneous HD vapor exposure in the hairless guinea pig or the domestic swine and cutaneous HD vapor and liquid exposures in the hairless mouse. These modules usually employ topical treatment with candidate compounds, but new modules are being designed for systemic treatment regimes.

RESULTS AND DISCUSSION

BASIC RESEARCH

After its introduction onto the battlefield in World War I and through the 1940's, most of the research efforts directed toward HD focused on defining the histopathological sequeale of exposure in humans. Attempts were also made to establish relevant animal model systems. Beginning in the 1950's, research turned more toward the biochemical effects of HD and empirical studies were conducted with the aim of identifying therapeutic modalities. While the biochemical studies led to significant inroads for our understanding of the toxic mechanisms, the therapeutic approaches were futile. In the 1960's and 70's, HD research focused mostly on DNA damage and repair, cytotoxic mechanisms and mutagenesis.

Around 1990, the US Army decided to focus it efforts for developing medical intervention strategies for HD injury through the formulation of an Army Science and Technology Objective (STO) titled *Medical Countermeasures Against Vesicant Agents.* This STO presented three technical milestones: by 1996, define technological and pathophysiological databases and establish pharmacological intervention strategies for the HD injury; by 1997, show efficacy of a candidate medical countermeasure in an animal model; and by 2000, prepare a Milestone 0 drug development decision.

The first technical milestone for 1996 was met through the research efforts of the USAMRICD, the extramural contract program of the US Army Medical Research and Materiel Command (USAMRMC), and the medical research programs of our allied nations. From this research, we were able to construct a schema of the major events of the pathological processes documented in cells and tissues exposed to HD (Figure 1). This schema was presented at numerous Department of Defense and professional scientific forums, including the 20th Army Science Conference (3). The research findings of this program served as the core of a NATO sponsored monograph on HD research (7).

The second part of the 1996 milestone, i.e., define strategies for pharmacological protection against the vesicant injury, was met by utilizing the information developed for the pathology schema. We identified 6 specific areas of the pathologic mechanism that could serve as points of pharmacological intervention into the HD injury. These were presented along with the pathology schema at numerous meetings and are presented in Table 1 along with prototypic compounds, in each area, that have been shown to be efficacious against HD toxicity in various model systems.

The 1997 technical milestone called for the demonstration of efficacy by a candidate countermeasure in an animal model. This was first met by research in hairless guinea pigs by Yourick et al. (6) and subsequently confirmed in the MEVM (5, 8).

CANDIDATE COMPOUND SCREENING

In FY97, the program was converted from an Army STO to a Defense Technology Objective (DTO),CB.22, and while the technical milestones remained intact, a new metric was imposed on the drug development effort. Rather than identifying compounds that just significantly reduced our pathological endpoints, we were required to attain at least 50% reduction of indicators of morbidity.

Over 500 candidate prophylactic or therapeutic compounds have been evaluated through the antivesicant DTN. Sixty-two compounds have demonstrated an ability to provide significant modulation of edema and/or histopathology caused by HD *in vivo*. Of these 62 compounds, nineteen have demonstrated at least 50% protection against the pathological indicators of mustard injury (Table 2). All of these 19 successful candidates fall into four of our six original proposed strategies: anti-inflammatories (7), antiproteases (3), scavengers (6), or PARP inhibitors (3).

With these compounds as proof of concept we received approval for transition to Concept Development in November 2000. A new DTO (CB.30) has been approved and work has been initiated to drive the drug development process through Concept Exploration toward a transition to Advanced Development in the FY03/04 time period.

FUTURE

Having established proof of concept for the potential development of a medical countermeasure against vesicant agents, we will move the 19 most successful candidate compounds from Basic Research into the Concept Exploration phase of the drug development process. Through a downselection process currently underway we will present to the US Army Medical Materiel Development Activity the optimal candidate, route of administration and timing of dosage for transition to advanced drug development within 3 years.

Proposed Mechanism of HD Action

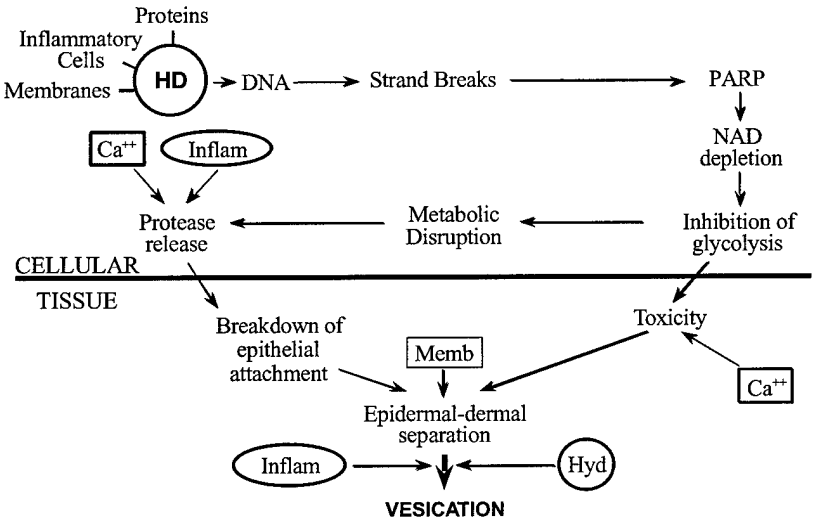

Figure 1. The cellular and tissue alterations induced by HD that are proposed to result in blister formation. HD can have many direct effects such as alkylation of proteins and membrane components (Memb) as well as activation of inflammatory cells. One of the main macromolecular targets is DNA with subsequent activation of poly(ADP-ribose) polymerase (PARP). Activation of PARP can initiate a series of metabolic changes culminating in protease activation. Within the tissue, the penultimate event is the epidermal-dermal separation that occurs in the lamina lucida of the basement membrane zone. Accompanied by a major inflammatory response and changes in the tissue hydrodynamics (Hyd), fluid fills the cavity formed at this cleavage plane and presents as a blister.

TABLE 1. Strategies for Pharmacologic Intervention of the HD Lesion.

Biochemical Event	Pharmacologic Strategy	Example
DNA Alkylation	Intracellular Scavengers	N-acetyl cysteine
DNA Strand Breaks	Cell Cycle Inhibitors	Mimosine
PARP Activation	PARP Inhibitors	Niacinamide
Disruption of Calcium	Calcium Modulators	BAPTA*
Proteolytic Activation	Protease Inhibitors	AEBSF*
Inflammation	Anti-inflammatories	Indomethacin; Olvanil

*BAPTA is a calcium chelator; AEBSF is a sulfonyl fluoride compound

TABLE 2. Candidate Countermeasures With Greater Than 50% Efficacy In Mouse Ear Model.

Total # of Positive Compounds = 19

	ICD #	% reduction in pathology
Anti-inflammatory drugs		
fluphenazine dihydrochloride	2040	50
Indomethacin	2086	96
olvanil	2723	91
olvanil (saturated)	2974	53
retro olvanil	2976	84
olvanil (urea analog)	2977	81
octyl homovanillamide	2980	100
Scavenger drugs		
2-Mercaptopyridine-1-oxide	1304	66
6-Methyl-2-Mercaptopyridine-1-oxide	1307	56
4-Methyl-2-Mercaptopyridine-1-oxide	1308	94
dimercaprol	2525	78
Na 3-sulfonatopropyl glutathionyl disulfide	3195	64
Hydrogen Peroxide gel, 3%	2828	58
Protease Inhibitors		
1-(40-aminophenyl)-3-(4-chlorophenyl) urea	1883	54
N-(0-P)-L-Ala-L-Ala-benzy ester hydrate	2780	62
Ethyl p-Guanidino Benzoate Hydrochloride	1579	62
PARP Inhibitors		
3-(4'-Bromophenyl)ureidobenzamide	1548	74
Benzoylene Urea	1796	54
4-amino-1-naphthol hydrochloride tech	2059	80

CONCLUSIONS

This research has been directed at meeting the Medical Chemical Defense DTO *Medical Countermeasures Against Vesicant Agents*. Based on results to date, we have met every milestone of the DTO, i.e., "to develop a technological database and define therapeutic strategies that protect against the vesicant injury," and "demonstrate efficacy in an animal model." Having identified at least 19 compounds that are capable of protecting against the *in vivo* pathology of HD, we now have the means to move from the research phase of pharmaceutical investigation into the Concept Exploration phase of drug development. This work, the combined efforts of Army, academic, industrial and contracted research laboratories, has set the stage for development of a fielded medical countermeasure against HD. For the first time since HD's introduction onto the battlefield more than 80 years ago, we have the true potential to protect our warfighters against this insidious weapon through pharmacological therapy.

REFERENCES

1. Papirmeister, B, Feister, AJ, Robinson, SI and Ford, RD. *Medical Defense Against Mustard Gas: Toxic Mechanisms and Pharmacological Implications*, CRC Press, Boca Raton, FL, 1991.

2. Smith, WJ and Dunn, MA. "Medical Defense Against Blistering Chemical Warfare Agents," *Arch Dermatol*, Vol 127, pp. 1207-1213, 1991.

3. Smith, WJ, Martens, ME, Gross, CL, Clark, OE and Cowan, FC. "Therapeutic Approaches to Cutaneous Injury by Sulfur mustard," *Proceedings of the 20th Army Science Conference*. Vol 2, pp. 699-703, 1996.

4. Smith, WJ, Martens, ME, Gross, CL, Clark, OE, Cowan, FC and Yourick, JJ, "The Use of In Vitro Systems to Define Therapeutic Approaches to Cutaneous Injury by Sulfur Mustard." In *Toxicity Assessment Alternatives: Methods, Issues, Opportunities*, Salem & Katz, eds. Humana Press, Totowa, NJ, pp. 205-212, 1999.

5. Casillas, RP, Mitcheltree, LW and Stemler, FW. "The Mouse Ear Model of Cutaneous Sulfur Mustard Injury." *Toxicology Methods*, Vol. 7. pp. 381-397, 1997.

6. Yourick, JJ, Clark, CR and Mitcheltree, L. "Niacinamide Pretreatment Reduces Microvesicle Formation in Hairless Guinea Pigs Cutaneously Exposed to Sulfur Mustard." *Fundam Appl Toxicol* Vol. 17, pp. 533-542, 1991.

7. Smith, WJ and Mol, MAE. "Progress and Future Direction of Research into the Toxicity and Treatment of Sulfur Mustard Exposure." NATO Technical Report AC/243 (Panel 8) TR/19, 1997.

8. Smith, WJ, Casillas, RP, Gross, CL and Koplovitz, I. "Therapeutic Approaches to Dermatotoxicity by Sulfur Mustard." *US Army MRMC Bioscience Review*, Baltimore, MD, May-June 1998.

MIDAZOLAM: AN IMPROVED ANTICONVULSANT TREATMENT FOR NERVE AGENT-INDUCED SEIZURES

John H. McDonough, Ph.D.
Pharmacology Division, U.S. Army Medical Research Institute of Chemical Defense
3100 Ricketts Point Rd., Aberdeen Proving Ground, MD 21010-5400 USA

ABSTRACT

The drug midazolam has been recommended to replace diazepam as the immediate anticonvulsant treatment for nerve agent-induced seizures. This recommendation marks the latest decision in an ongoing program to improve medical countermeasures to treat nerve agent poisoning. Extensive rodent screening studies first identified midazolam as the most promising compound to focus on for advanced testing. Midazolam was then evaluated directly with diazepam for the ability to terminate nerve agent seizures in a nonhuman primate model. In all animal tests midazolam was twice as potent and more rapidly acting than diazepam, thus minimizing the possibility of seizure-induced brain damage.

INTRODUCTION

In November of 1990 the U.S. Army fielded the anticonvulsant drug diazepam in the Convulsant Antidote, Nerve Agent (CANA) autoinjector for the immediate field treatment of nerve agent-induced seizures. Each CANA injector contains 10 mg of the drug diazepam. Military personnel are issued one CANA injector in addition to the three MARK 1 antidote kits, each of which contains autoinjectors of atropine (2 mg/injector; total = 6 mg) and the oxime 2-PAM Cl (600 mg/injector; total = 1800 mg). The diazepam in the CANA injector is to be administered by the casualty's buddy or a medic at the onset of severe effects from a nerve agent (when the casualty's condition warrants the use of three MARK 1's at the same time), whether or not seizure activity is among the effects. Additional CANA autoinjectors are available to the combat medic to treat severely poisoned individuals; the medic is authorized to give up to two more 10-mg injections of diazepam to convulsing casualties (total allowed dose = 30 mg diazepam).[1]

The fielding of CANA marked the end of research and development efforts that first started in the early 1980's. At that time it was already recognized that diazepam and other benzodiazepine-type drugs provided significant improvements in preventing the lethal effects of nerve agent exposure when used as an adjunct treatment in conjunction with the standard anticholinergic and oxime therapy. Then came reports that exposure to nerve agent, primarily soman, produced brain lesions in survivors of intoxication.[2,3,4] Throughout the mid-1980's researchers investigated the three most prevalent hypotheses that were advanced to account for this brain pathology: a direct neurotoxic effect of the agent, the result of brain hypoxia/anoxia/ischemia coincident with the effects of acute intoxication, or the result of prolonged seizures triggered by the agent intoxication. Numerous studies were performed to evaluate these different hypotheses, and by 1987 it had been concluded that the brain damage was primarily the result of prolonged seizure activity that was triggered by intoxication by the agent.[5] Some of the major studies contributing to this conclusion were those that showed that treatment of animals with diazepam or other benzodiazepine

anticonvulsant drugs, in conjunction with the standard atropine and oxime therapy, minimized or prevented the development of brain lesions as well as enhanced survival following nerve agent exposure.[6,7,8,9,10,11]

By the late 1980s it was decided that anticonvulsant protection against nerve agent-induced seizures was critical for complete therapeutic protection of nerve agent casualties.[12] The logical drug to develop at that time was diazepam. It was the drug most frequently used in nerve agent protection studies and was already approved for clinical use by the U.S. Food and Drug Administration (FDA) with an indication for treatment of status epilepticus seizures. Diazepam was a significant improvement over previous medical defense capabilities since it provided the ability to deliver immediate anticonvulsant treatment that may stop or minimize the neurotoxicological effects of nerve agent-induced seizures.

However, experimental findings showed that diazepam may not be the optimal compound for anticonvulsant protection against nerve agent-induced seizures. First, while diazepam reduced the incidence and severity of neuropathology in nerve agent-intoxicated animals, the protection was never complete.[6, 7,11,13] Secondly, it was found in primate models that the dose of diazepam needed to control soman-induced convulsions might be greater than first estimated.[11,14,15] Finally, there were continuing concerns from clinicians that the IM route of dosing would not achieve therapeutic levels of diazepam sufficient to stop seizures.

In addition to doubt about the sufficiency of diazepam, research studies showed that at least two other classes of drugs exerted strong control of nerve agent-induced convulsions and seizures. Drugs that act as antagonists of the glutamate receptor, in particular the N-methyl-d-aspartate subtype and to a much lesser extent the AMPA subtype, proved to provide substantial protection against nerve agent-seizures and brain damage.[16,17,18,19,20] In addition, antimuscarinic anticholinergic drugs with strong central activity also produced robust anticonvulsant effects against nerve agent-induced seizures.[21,22,23,24,25] These findings contributed to a growing realization that there were still gaps in our understanding of the basic neuropharmacological mechanisms of nerve agent seizures and the production of neuropathology and raised the question of the suitability of diazepam as the best anticonvulsant treatment for nerve agent-induced seizures. In reaction to these questions, the development of an advanced anticonvulsant treatment was formally adopted as an Army Science and Technology Objective (STO) in 1993.

1. INITIAL ADVANCED ANTICONVULSANT DEVELOPMENT RESEARCH EFFORTS.

In the 1993-1995 time frame, the major research efforts were arrayed along five lines. First, the standard drugs used clinically to treat epilepsy or seizure disorders were evaluated for the potential to moderate nerve agent-induced seizures. This work showed that, with the exception of the benzodiazepines (diazepam and midazolam) and barbiturates, the standard antiepileptic drugs were unable to stop ongoing nerve agent seizures.[26] Secondly, there were a variety of compounds that different authors had championed as being capable of stopping or moderating nerve agent seizures (e.g., memantine, clonidine) that had been evaluated by observational procedures only. Additionally, there were a number of research discrepancies based on the animal model and/or the procedure used to evaluate anticonvulsant effectiveness (i.e., observation vs EEG) that needed resolution. Close evaluation of several drugs that exerted a purported anticonvulsant effect against nerve agent seizures showed that these were primarily due to a profound muscle relaxation (e.g., memantine, neuroactive steroids; EEG seizures were still evident) or required such a narrow dose range or specific treatment conditions that development of them as a field treatments would be impractical (e.g., clonidine, huprazine, ivermectin; worked over narrow dose range and only as pretreatments). Other studies showed differences in the anticonvulsant effectiveness of diazepam and centrally acting anticholinergics depending upon the animal model used; both failed to produce an anticonvulsant effect in rat when given 40 min after seizure onset, whereas they did in a guinea pig model. The third major thrust was to evaluate in greater depth the contribution of the glutamatergic system to nerve agent seizures, nerve agent-induced brain damage, and the therapeutic potential for use of antiglutamate drugs to antagonize these effects. These studies showed that antagonists of the AMPA subtype of the glutamate receptor produced very weak anticonvulsant effects by themselves.[26] Evaluation

of compounds that acted as antagonists at the NMDA subtype of the glutamate receptor showed they produced robust anticonvulsant activity against nerve agent seizures, but this class of compounds had several drawbacks that will be discussed in more detail below. The fourth major effort was to evaluate the potential antiglutamatergic properties of a variety of potent, centrally acting, anticholinergic drugs that had shown robust anticonvulsant activity in a rat nerve agent seizure model. This study showed that a number of anticholinergics possess NMDA antagonist activity at high doses and thus had dual therapeutic effects against nerve agent seizures[27]. Finally, a thorough review of the literature was performed and a review paper that evaluated and synthesized this broad research area was prepared. It was presented in an abbreviated form at the NATO RSG-3 meeting in Porton Down in 1995, and after undergoing a series of revisions, it was published.[5] This review has provided a theoretical framework within which to direct development efforts of anticonvulsant treatments as well as possible neuroprotectant drugs.

2. FOCUSING OF ADVANCED ANTICONVULSANT RESEARCH EFFORTS – DOWN-SELECTION OF CANDIDATE COMPOUNDS.

By 1995-1996, research showed that only three classes of drugs exerted strong anticonvulsant activity against nerve agent seizures: benzodiazepines, anticholinergics, and NMDA antagonists. At that point a decision was made to no longer concentrate on NMDA antagonists (e.g., MK-801, TCP, phencyclidine) for development as immediate field treatment of nerve agent seizures. Although these compounds had shown marked anticonvulsant activity against nerve agent-induced seizures as well as seizures produced by other experimental manipulations, they had several drawbacks that would make ultimate development very difficult if not impossible. NMDA antagonists are potent psychomimetic compounds, at high doses they are capable of producing morphological damage to brain neurons,[28] and, despite intense development efforts of several major drug companies, no drug of this class has been approved for human use by the FDA with the exception of ketamine.

At this time we were also performing studies to compare the anticonvulsant therapeutic efficacy of a variety of anticholinergic drugs against the current standard, diazepam. Ultimately, 11 anticholinergic compounds were investigated using a guinea pig model. Unlike previous results using rats[22,26], most of the tested anticholinergics were effective when given either shortly (5 min) or after a substantial delay (40 min) following seizure onset. However, the doses needed to achieve an anticonvulsant effect when treatment was delayed (40 min following seizure onset) were almost a log unit greater than those required of the same drugs when treatment was given shortly after exposure[29]. This indicated that there was a narrow therapeutic treatment window for producing an anticonvulsant effect with clinically relevant doses of anticholinergic drugs. The results also showed (again, unlike previous results with rats) that diazepam continued to produce anticonvulsant effects at equivalent doses when given either shortly or delayed after seizure onset. However, the anticonvulsant action of diazepam given IM in the guinea pig was very slow (~50 min) and required high doses of the drug. The implications of these results were that anticholinergics most likely could never serve as the sole anticonvulsant treatment for nerve agent-induced seizures since in most operational situations it could not be guaranteed that all casualties would receive immediate treatment. It was decided to investigate whether other benzodiazepine drugs had the same broad therapeutic activity as diazepam, and whether some may have a more rapid time to effect following IM dosing. Five benzodiazepines (avizafone, clonazepam, loprazolam, lorazepam, midazolam) were then tested using the guinea pig model.[30] The results of that study showed that all tested benzodiazepines showed equal efficacy (equivalent ED50s and latencies to seizure control for each compound) when given at 5 or 40 min after seizure onset. However, there were differences in potency of the different drugs, and there were marked differences between drugs in how rapidly seizures were controlled following IM injection. Of the compounds tested, midazolam had the "best" therapeutic profile – it was about twice as potent as diazepam and was the most rapidly acting compound of the drugs tested. These initial results were available for the Milestone 0 meeting in July 1997.

3. MILESTONE 0.

The Milestone 0 meeting is a programmed decision point in the development process where proof of concept is demonstrated. In attendance are the scientific proponent, the MRICD science and technology coordinator; the commander of the U.S. Army Medical Research and Material Command; the U.S. Army Medical Material Development Activity, the agency with ultimate responsibility to perform advanced development of a medical product; the Army Medical Department Center and School, the combat developer that sets doctrine (policy) as to how medical items are to be used; and a representative of Army Logistics, to determine the logistic support requirements of proposed new items.

The Milestone 0 meeting for the advanced anticonvulsant was held in July 1997. A summary of the scientific information to date reiterated much of what was discussed above. In short, both midazolam and several potent anticholinergic drugs (biperiden, scopolamine, trihexyphenidyl) appeared to be viable candidates for development. It was decided at that point that an advanced anticonvulsant could reasonably be achieved and the program then entered a concept development phase with midazolam as the lead candidate compound. A target date of FY00 was established for the Milestone 1 review of this project. In addition, specific exit criteria were established that delineated goals/tasks that needed to be met/accomplished to consider that Milestone 1 had been achieved. These exit criteria are listed below.

Exit Criteria:

1. Identify one preparation to be recommended to the MS1 review body for transition.
2. Determine metabolism and distribution of compounds/preparation either by reference to existing literature or by conduct of appropriate nonclinical studies.
3. Provide sufficient pre-clinical (animal and any relevant human experience with similar compounds) data to permit a preliminary assessment of the safety and efficacy of the identified preparations.
4. During Phase 0 a scientific committee will identify valid surrogate endpoints, present valid support for these endpoints, and develop a plan for getting the product through FDA review.
5. A Scientific Steering Committee will consider all possible side effects from the use of these compounds.
6. Preparation of a Transition Information Paper suitable for use in development of an Investigational New Drug application for submission to the FDA.
7. Coordinate with the Combat Developer to insure availability of a draft Operational Requirements Document (ORD) containing a milestone schedule.
8. Perform an administrative review of any patent issues.

4. CONCEPT DEVELOPMENT – NONHUMAN PRIMATE STUDIES.

Following the accomplishment of the Milestone 0 review, the major research activity involved the development of a nonhuman primate model of nerve agent exposure and seizures to evaluate the anticonvulsant effectiveness of midazolam in comparison with diazepam.[31] The key features of this model were to faithfully approximate the field medical doctrine for use of pretreatment (pyridostigmine) and therapy (atropine and 2-PAM Cl) drugs, evaluate and document seizure control using EEG recording, and to concurrently determine blood levels of treatment compounds to estimate human dose levels. In this study, male rhesus monkeys were surgically prepared with cortical electrodes and a transmitter that allowed for continuous telemetry monitoring of EEG activity. On the day of exposure the animals were pretreated IM with 0.024 mg/kg pyridostigmine, which achieved ~25% inhibition of red blood cell cholinesterase at the time of exposure. At 42 min after pyridostigmine the animals were challenged with 15 ug/kg, IM, of the nerve agent soman (2 x LD_{50}) and 1 min later were treated with 0.10 mg/kg (diazepam study) or 0.20 mg/kg (midazolam study; 3 diazepam treated animals), IM, atropine and 25.7 mg/kg, IM, 2-PAM Cl. The pyridostigmine dose produced cholinesterase inhibition equivalent to that provided by pyridostigmine pretreatment tablets, and the doses of atropine and 2-PAM Cl were mg/kg equivalent doses provided by 3

MARK 1 antidote kits to a 75 kg human. All animals developed EEG seizure activity in 5-9 min following exposure. One min after the appearance of epileptic EEG activity, individual animals were treated with one of two doses of diazepam, 0.40 or 0.63 mg/kg, or one of two doses of midazolam, 0.18 or 0.32 mg/kg, IM. Following diazepam or midazolam treatment, serial blood samples were taken to determine drug pharmacokinetics. Treatment with the 0.40 mg/kg dose of diazepam (N = 8) either failed to terminate EEG seizure activity (N=6) or failed to do so in a clinically relevant time frame (N=2). Treatment with the 0.63 mg/kg dose of diazepam (N = 6) terminated seizure activity ($X \simeq 70$ min). Three animals recovered normally; in the other 3 animals the seizures returned after 2-3 hr. Diazepam pharmacokinetic estimates show that the 0.40 mg/kg dose produced a mean maximum plasma concentration of 202 ng/ml with a time to maximum concentration of 21.37 min, while the 0.63 mg/kg dose produced a mean maximum plasma concentration of 415 ng/ml with a time to maximum concentration of 18.80 min. With midazolam treatment, the 0.18 mg/kg dose failed to control seizures (N=3), while the 0.32 mg/kg dose rapidly stopped seizures (X = 32 min) in all animals tested (5 permanently, 1 temporally). Determinations of midazolam plasma pharmacokinetic estimates showed that the 0.18 mg/kg dose produced a mean maximum plasma concentration of 167 ng/ml with a time to maximum concentration of 28.4 min, while the 0.32 mg/kg dose produced a mean maximum plasma concentration of 195.6 ng/ml with a time to maximum concentration of 18.5 min. The results showed that the current recommended maximum field dose of diazepam (0.40 mg/kg) was insufficient to stop seizures induced by soman in a clinically meaningful time. Although the 0.63 mg/kg dose of diazepam could terminate soman-induced seizures, the time for seizure control was slow. Midazolam terminated seizures at a lower dose and more rapidly than diazepam. With both drugs, seizures could reoccur after a period of anticonvulsant effect, and if seizures were not completely terminated the animal never regained consciousness.

This study shows that the dose of diazepam needed to terminate ongoing nerve agent-induced seizures had been underestimated and that the maximum allowable dose needed to be increased by at least 50% to produce a reliable anticonvulsant effect. These doses are concordant with blood levels of diazepam reported clinically to control status epilepticus seizures[32] and correspond to doses that were reported to be effective in treating sarin- and VX-induced seizures in patients of the Japanese terrorist attacks.[33,34,35] In addition, the time it took to terminate seizures in the nonhuman primate model following diazepam injection was >1 hr, and in 2 of 5 animals the seizures recurred 1.5-2 hr following an initial period of anticonvulsant effect. In contrast, midazolam was effective in terminating seizures at roughly half the dose necessary for diazepam, the time for seizure termination was ~30 min, and seizure activity recurred in only 1 of 6 animals.

5. CONCEPT DEVELOPMENT: GUINEA PIG STUDIES AND OTHER ACTIVITIES.

Concurrent with this nonhuman primate work, two other rodent studies were performed. First, midazolam was evaluated in parallel with diazepam for ability to stop seizures produced by all threat nerve agents (GA, tabun; GB, sarin; GF, cyclosarin; GD, soman; VX; VR, the Russian analog of VX).[36] The results show, much like previous studies, that midazolam was both significantly more potent and rapidly acting than diazepam in controlling seizures elicited by each of these threat nerve agents. A second study evaluated combination treatments of the benzodiazepines (diazepam or midazolam), along with one of the anticholinergic drugs (biperiden, scopolamine, trihexyphenidyl) for controlling soman-induced seizures.[37] Results from the combination study showed that either of the two benzodiazepines could be paired favorably with the anticholinergics, and there was strong evidence of anticonvulsant synergism especially when treatment was delayed (40 min) after seizure onset. In addition to these laboratory efforts, an exhaustive review of the clinical epilepsy literature was performed and identified 32 published studies where midazolam was used to treat status eiplepticus or serial seizures. Midazolam successfully controlled seizures in 89% (506 of 568) of the reported cases, and the success rate was virtually identical when the drug was given IM (92% 168 of 182 cases).

6. MILESTONE 1 – TRANSITION TO ADVANCED DEVELOPMENT.

All this information, especially the data from the nonhuman primate study, solidified the decision to transition midazolam to advanced development. Midazolam acts by the same mechanism of action as diazepam. It is an FDA approved drug with a substantial history of safe use. In addition to its efficacy in treating nerve agent-induced seizures in both rodents and nonhuman primates, midazolam also has a documented history of use in the clinical treatment of status epilepticus. All these features, along with other administrative scientific tasks that were being performed concurrently with the experimental efforts, met the established exit criteria and culminated in the successful Milestone 1 review in early Sep 00.

Product development is guided by the U.S. Army Medical Material and Development Agency. The science and technology coordinator and Scientific Steering Committee continue to address scientific issues that arise as this development process goes on. Within the immediate future the major effort will involve pre-investigational new drug (IND) meetings with the FDA to outline research findings to date and explore the most effective way to have midazolam approved for treatment of nerve agent-induced seizures. This will be the most critical aspect of the development process because, unlike the development of other types of drugs, clinical efficacy trials cannot be performed against nerve agent-induced seizures in humans. Animal data will have to suffice for demonstration of efficacy against nerve agents.

REFERENCES

1. Medical Management of Chemical Casualties Handbook. Third Edition. USAMRICD. Aberdeen Proving Ground, MD.1999.
2. Petras, J.M. Soman neurotoxicity. Fundam Appl Toxicol, 1:242, 1981.
3. Lemercier, G., et al. Histological and histochemical changes in the central nervous system of the rat poisoned by an irreversible anticholinesterase organophosphorus compound. Acta Neuropathol. (Berlin) 61:123-129, 1983.
4. McLeod, C.G., et al. Acute neuropathology in soman poisoned rats. NeuroToxicol. 5:53-58, 1984.
5. McDonough, J.H., Shih, T-M. Neuropharmacological mechanisms of nerve agent-induced seizures and neuropathology. Neurosci. Biobehav. Rev. 21:559-579, 1997.
6. Singer, A.W. Effect of Valium and atropine on mortality and pathology in guinea pigs exposed to soman. U.S. Army Medical Research and Development Command 4th Annual Chemical Defense Bioscience Review, Ft Detrick , MD, 1984.ADB089975
7. Martin, L.J., et al. Protective effect of diazepam pretreatment on soman-induced brain lesion formation. Brain Res, 325:287-289, 1985.
8. Domino, E.F. Comparative seizure inducing properties of various cholinesterase inhibitors: antagonism by diazepam and midazolam. Neurotoxicol. 8:133-122, 1987.
9. Morelis, P., et al. Le loprazolam, benzodiazepine anticonvulsivante hydrosoluble, ameliore la therapetique de l'intoxication du cobaye par le soman. Paper presented at NATO Research Study Group Panel VIII/RSG-3, Ghent, Belgium, 27-30 Apr 1987.
10. Riotte, M., et al. Efficacite de quelques benzodiazepines administrees a titre curatif chez le singe et le cobaye intoxiques par le soman. Paper presented at NATO Research Study Group Panel VIII/RSG-3, Washington DC, USA, 25-29 Sep 1988, 204-216.
11. Hayward, I.J., et al. Decreased brain pathology in organophosphate-exposed rhesus monkeys following benzodiazepine therapy. J. Neurol. Sci. 98:99-106, 1990.
12. Dunn, M.A., Sidell, F.R. Progress in medical defense against nerve agents. J.A.M.A. 262:649-652, 1989.
13. Clement, J.G., Broxup, B. Efficacy of diazepam and avizafone against soman-induced neuropathology in brain of rats. NeuroToxicol. 14:485-504, 1993.
14. Castro, C.A., et al. Behavioral efficacy of diazepam against nerve agent exposure in rhesus monkey. Pharmacol. Biochem. Behav. 41:159-164, 1991.

15. Murphy, M.R.; et al. Diazepam as a treatment for nerve agent poisoning in primates. Aviat. Space Environ. Med. 64:110-115, 1993.
16. Braitman,D.J., Sparenborg,S. MK-801 protects against seizures induced by the cholinesterase inhibitor soman. Brain Res. Bull. 23:145-148, 1989.
17. Sparenborg, S., et al. Dizocilpine (MK-801) arrests status epilepticus and prevents brain damage produced by soman. Neuropharmacol. 31:357-368, 1992.
18. Carpentier, P., et al. Anticonvulsant and antilethal effects of the phencyclidine derivative TCP in soman poisoning. NeuroToxicol. 15: 837-852, 1994.
19. Lallement, G., et al. Antiepileptic effects of NBQX against soman-induced seizures. NeuroRep. 5:425-428, 1994.
20. Lallement,G., et al. Modulation of soman-induced neuropathology with an anticonvulsant regimen. NeuroRep. 5:2265-2268, 1994.
21. Capacio, B.R., Shih, T.-M. Anticonvulsant actions of anticholinergic drugs in soman poisoning. Epilepsia, 32:604-615, 1991.
22. McDonough, J.H., Shih, T.-M. Pharmacological modulation of soman-induced seizures. Neurosci. Biobehav. Rev. 17:203-215, 1993.
23. Sparenborg, S., et al. Pharmacological dissociation of the motor and electrical aspects of convulsive status epilepticus induced by the cholinesterase inhibitor soman. Epilepsy Res.14:95-103, 1993.
24. Anderson, D.R., et al. Efficacy of injectable anticholinergic drugs against soman-induced convulsive/subconvulsive activity. Drug Chem.Toxicol., 17: 139-148, 1994.
25. Anderson, D.R., et al. Efficacy comparison of scopolamine and diazepam against soman-induced debilitation in guinea pigs. Fundam. Appl. Toxicol., 22:588-593, 1994.
26. Shih, T-M., et al. Anticonvulsants for soman-induced seizure activity. J. Biomed. Sci. 6:86-96, 1999.
27. McDonough, J.H., Shih, T.-M. A study of the N-methyl-d-aspartate antagonist properties of anticholinergic drugs. Pharmacol. Biochem. Behav. 51:249-253, 1995.
28. Olney, J.W., et al. NMDA antagonist neurotoxicity: mechanism and prevention. Sci. 254:1515-1518, 1991.
29. McDonough, J.H., et al. Anticonvulsant treatment of nerve agent seizures: anticholinergics versus diazepam in soman-intoxicated guinea pigs. Epilepsy Res. 38: 1- 14, 2000.
30. McDonough, J.H., et al. Comparative evaluation of benzodiazepines for control of soman-induced seizures. Arch.Toxicol. 73:473- 478, 1999.
31. McDonough, J.H., et al. Benzodiazepine dosage necessary to terminate soman-induced seizures in a rhesus monkey model. U.S. Army Medical Defense Bioscience Rev. Abs., p.65, 2000.
32. Shorvon, S. Status Epilepticus: its clinical features and treatment in children and adults. Cambridge University Press, Cambridge, 195-213, 1994.
33. Morita, H., et al. Sarin poisoning in Masumoto, Japan. Lancet, 346:290-293, 1995.
34. Nozaki, H., et al. A case of VX poisoning and the difference from sarin. Lancet 346:698-699, 1995.
35. Okumura, T., et al. Report on 640 victims of the Tokyo subway sarin attack. Ann. Emerg. Med. 28:129-135, 1996.
36. Shih, T.-M., McDonough, J.H. Organophosphorus nerve agents, electrographic seizures, anticonvulsants, neuropathology and acute lethality. U.S. Army Medical Defense Bioscience Rev. Abs., p.63, 2000.
37. Koplovitz, I., et al. Combination anticonvulsant treatment for nerve agent seizures. U.S. Army Medical Defense Bioscience Rev. Abs., p.64, 1998.

CONTROL OF NERVE AGENT-INDUCED SEIZURES IS CRITICAL FOR NEUROPROTECTION AND SURVIVAL

T.-M. Shih, S.M. Duniho and J. H. McDonough
Pharmacology and Comparative Medicine Divisions
U.S. Army Medical Research Institute of Chemical Defense
Aberdeen Proving Ground, MD 21010-5400 USA

ABSTRACT

All six nerve agents studied were capable of producing prolonged seizures (*status epilepticus*) and neuropathology, and all 5 tested drugs were capable of terminating seizure activity. This presentation focused on the aspect of the influence of seizure activity, whether it was or was not terminated by any of the drug treatment, on neuropathological consequence and on mortality. Regardless of doses and drug treatment, control of seizure was strongly associated with protection against acute lethality and brain pathology, while failure to stop seizures was associated with increased lethality and more frequent and severe brain pathology. Thus, effective anticonvulsant treatment of a nerve agent casualty is critical to immediate and long-term recovery.

INTRODUCTION

The chemical warfare nerve agents, such as tabun, sarin, soman and VX, are organophosphorus (OP) cholinesterase inhibitors. Exposure to these agents causes a progression of toxic signs (Taylor 1985). In addition to hypersecretions, fasciculations, tremor, convulsions and respiratory distress, prolonged seizures (*status epilepticus*) can begin rapidly after nerve agent exposure in animals and humans. Animal studies show these seizures can result in neuropathology and long-term behavioral deficits if not promptly controlled (McDonough et al. 1995; McDonough and Shih 1997). A combined treatment regimen of prophylaxis and therapy is now generally agreed upon as the most effective medical countermeasure for dealing with the threat of nerve agent poisoning (Dunn and Sidell 1989; Moore et al. 1995; Sidell 1997). Pretreatment with carbamate cholinesterase inhibitors, such as pyridostigmine, binds a small fraction of cholinesterase in the periphery and reversibly shields it from irreversible inhibition by the nerve agent. In the event of poisoning, an anticholinergic drug, such as atropine sulfate, is used to antagonize the effects of excess acetylcholine at muscarinic receptor sites, and an oxime, such as pralidoxime chloride (2-PAM Cl), is used to reactivate any unaged inhibited enzyme (Moore et al. 1995). However, this treatment regimen does not control the development of nerve agent-induced seizures (McDonough et al. 1999).

Although diazepam or a water soluble prodrug form of diazepam, avizafone (Clement and Broxup 1993), is the drug that has been adopted by most military forces for the immediate treatment of nerve agent seizures (Moore et al. 1995), research has demonstrated that diazepam is not always completely effective in protecting animals against nerve agent-induced neuropathology (Hayward et al. 1990; McDonough et al. 1995). Thus, there has been continuing debate as to whether diazepam is the best drug to use for the treatment of nerve agent seizures (McDonough and Shih 1997). Much of this debate has centered around pharmacokinetic issues, since diazepam, or for that matter any emergency treatment drug used by the military for nerve agent poisoning, must be given intramuscularly (im) by automatic injectors. This is necessitated by the fact that all personnel must be able to receive immediate treatment in the event of exposure. Therefore, there is a continuing need to find better drugs to treat seizures elicited by OP nerve agents. Our research effort was initially focused on soman exposure and protection (Shih et al. 1991; McDonough et al. 1999). However,

during the past several years this effort has been extended to include many other threat nerve agents, such as tabun, sarin, GF, VR and VX (Shih and McDonough 1999).

We have recently completed a study on the effectiveness of several anticholinergic (atropine sulfate, biperiden HCl, or trihexyphenidyl HCl) and benzodiazepine (diazepam or midazolam) drugs to terminate epileptiform seizures produced by six threat OP nerve agents (tabun, sarin, soman, GF, VX and VR) in a guinea pig model that closely approximates the use of pretreatment and therapy drugs as medical countermeasures for nerve agent exposure (Shih and McDonough 2000). Specifically, anticonvulsant ED_{50}s were determined for each drug treatment at 5 min after the onset of EEG seizures after nerve agent exposure. The animals in these tests thus could be subdivided into those in which seizure activity was successfully terminated by the drug treatment and those in which seizure activity continued. The present report describes the analysis of the relationship between seizure termination and neuropathology, and between seizure termination and lethality.

Male Hartley guinea pigs (Crl: (HA) BR COBS; Charles River Labs, Kingston, NY, USA) of 250-300 g body weight at the start of the study served as subjects. They were prepared approximately one week before experimentation with cortical stainless steel screw electrodes using previously described procedures (McDonough et al.1999). EEG recordings were made using QND software and amplifiers supplied by Neurodata Inc. (Pasadena, CA) (low frequency filter = 0.3 Hz; high frequency filter = 40 Hz; sampling rate = 128 Hz) and displayed on a computer monitor. During EEG recordings, all animals were housed in individual plastic recording chambers that allowed free movement with the exception of the recording leads attached to the electrode connector on the top of the head.

On the day of the experiment, guinea pigs were continuously monitored for EEG activity. After a 15-min recording of baseline EEG measures, animals received pyridostigmine (0.026 mg/kg, im) to produce ~30% whole blood ChE inhibition (Lennox et al. 1985). Thirty min later, animals were challenged with 2 x LD_{50} subcutaneous (sc) dose of tabun (240 ug/kg), sarin (84 ug/kg), soman (56 ug/kg), GF (114 ug/kg), VR (22 ug/kg) or VX (16 ug/kg). One min after nerve agent challenge, all animals were treated with atropine sulfate (2 mg/kg, im) plus 2-PAM (25 mg/kg, im). Five min after the onset of EEG seizure activity, different doses of the anticholinergic drug atropine sulfate, biperiden HCl, trihexyphenidyl HCl, or the benzodiazepine drug diazepam or midazolam were given intramuscularly. Animals were observed continuously for the first hour following exposure and treatment and periodically thereafter for at least 6 hr. EEGs were monitored continuously throughout this time and for 30 min at 24 hr. Seizure onset was operationally defined as the appearance of $\geq$10 sec of rhythmic high amplitude spikes or sharp wave activity in the EEG. Each animal was rated as having the seizure terminated (OFF) or not terminated (NOT OFF) based on the overall appearance of the EEG record at the end of the experimental day and during the 24-hr observation. (Note: An animal was rated as OFF if the seizure was terminated and the EEG remained normal at all subsequent observation times.)

Surviving animals at 24 hr after nerve agent exposure were deeply anesthetized with pentobarbital (75 mg/kg, ip) and perfused through the aorta with saline followed by 10% neutral buffered formalin. The brain was blocked, embedded in paraffin, cut 6-10 microns thick, stained with hematoxylin and eosin and then evaluated by a board certified pathologist who was unaware of the experimental history of a given subject. The procedures and criteria used for pathological evaluation have been published (McDonough et al. 1995, 2000). Briefly, six brain areas (cerebral cortex, pyriform cortex, amygdala, hippocampus, caudate nucleus, thalamus) were evaluated in each animal; each area was given a score that described brain lesion severity based on the approximate percentage of tissue involvement: 0=none; 1=minimal, 1-10%; 2=mild, 11-25%; 3=moderate, 26-45%; 4=severe, >45%. For each animal, a total neuropathology score was obtained by summing the scores of the six brain areas. The criterion used to characterize the lesion/pathology was neuronal necrosis, e.g., shrunken ensinophilic neurons with dark, round, pyknotic nuclei.

The proportion of animals surviving as a function of successful control of the seizure, as well as the incidence of neuropathology as a function of seizure control, was evaluated using the Chi-square procedure with Yates correction (Winer, 1971). The latency to seizure termination was evaluated between drugs using the Kruskal-Wallis one-way analysis of ranks. The total neuropathology scores were categorized by whether seizure was turned OFF vs. NOT OFF and by drug and then was evaluated by a two-way analysis of variance.

All six OP nerve agents were capable of inducing brain seizure activity in this model. When drug treatment failed to stop the seizure, epileptiform activity was evident continuously throughout the 6-hr experimental period and could still be observed in some animals 24 hr after nerve agent exposure.

TABLE 1. Acute (24-h) Survival as a Function of Seizure Control.

	24-h Survival		
	ALIVE	DEAD	TOTAL
SEIZURE OFF	411 (96%)	16 (4%)	427
SEIZURE NOT OFF	232 (58%)	169 (42%)	401

Table 1 shows the strong relationship between the control of seizures and protection against the lethal effect of nerve agent exposure. Animals were categorized by seizure outcome (OFF, NOT OFF) and lethality (ALIVE, DEAD) at 24 hrs following nerve agent exposure. Less than 4% of the animals that had their seizures successfully controlled (OFF) died, whereas 42% of animals that failed to have the seizures controlled (NOT OFF) died. This result was highly significant ($\div^2 = 173.5$, df = 1, $p < 0.001$). Analysis of the individual drugs showed this was a consistent and robust finding.

The brains of 593 animals were available for pathological evaluation. All the nerve agents were capable of producing neuropathology under the conditions of this study. No drug completely protected against neuropathology development, but control of seizure clearly had an influence on the incidence and severity of neuropathology (Tables 2 and 3). Animals that had their seizure successfully controlled (OFF) had significantly higher numbers of brains that displayed no neuropathology ($\div^2 = 81.14$, df = 1, $p < 0.001$). Again, analysis of the individual drugs showed that this was a consistent and robust finding with each compound.

TABLE 2. Incidence of Neuropathology as a Function of Seizure Control.

	No pathology	Pathology	TOTAL
SEIZURE OFF	284 (78%)	77 (22%)	361
SEIZURE NOT OFF	55 (24%)	177 (76%)	232

Table 3 displays the average brain lesion scores for individual brain areas. The data are collapsed across all nerve agents and then categorized by whether the seizure was rated OFF or NOT OFF and listed by treatment drug. The data clearly show that failure to control the seizure resulted in significantly greater numbers of animals with brain lesions, and in general the severity of the lesion was greater than in animals in which the seizures were successfully controlled by the treatment drug. The data also show that the cortex and amygdala were the brain areas most likely to experience the greatest damage.

CONCLUSION

The present study shows that all six nerve agents tested can induce prolonged brain seizures (*status epilepticus*) and have the potential for producing neuropathology in our guinea pig model. These results provide strong evidence that the prolonged seizure activity elicited by the nerve agents was the major factor in lesion production (McDonough et al. 1995). Animals that had seizures controlled by the different anticonvulsant treatments (OFF) were significantly more likely to be totally free of neuropathology or, if it did occur, to have it greatly reduced in both incidence and severity. This is in agreement with previous findings in both rodents (Lallement et al. 1994; McDonough et al. 2000) and nonhuman primates (Hayward et al. 1990; Lallement et al. 1997, 1998) that any treatment that can reduce or terminate seizure activity in nerve agent-exposed animals has a protective effect on the development of neuropathology.

TABLE 3. Mean brain lesion score by brain area collapsed across all nerve agents and categorized by seizure control and treatment drug.

Mean Brain Lesion Scores*

		Brain Area					
	Drug	Cortex	Amygdala	Pirifo rm	Hippocampus	Caudate	Thalamus
OFF	ATR	1.5(6)	1.4(3)	1.8(4)	1.1(8)	1.0(5)	1.7(3)
	BIP	1.1(26)	1.7(10)	1.1(8)	1.1(7)	1.2(5)	1.1(15)
	THX	1.0(5)	3.0(3)	0(0)	1.4(5)	1.0(1)	1.0(1)
	DIZ	1.3(9)	2.0(8)	1.0(5)	0(0)	0(0)	1.0(2)
	MDZ	1.1(7)	2.4(7)	0(0)	1.4(5)	0(0)	1.0(1)
	Total	1.2(53)	2.1(31)	1.2(17)	1.5(25)	1.1(11)	1.1(22)
NOT OFF	ATR	1.2(14)	2.6(11)	1.8(12)	1.0(8)	2.0(8)	1.9(14)
	BIP	3.5(43)	3.8(41)	2.0(38)	1.1(33)	3.0(41)	3.3(34)
	THX	2.9(20)	3.8(21)	1.7(13)	1.3(18)	3.2(18)	2.0(19)
	DIZ	2.8(54)	3.3(55)	1.7(48)	1.0(2)	1.7(19)	1.7(44)
	MDZ	2.3(36)	3.7(33)	1.6(25)	1.5(15)	2.9(21)	1.7(28)
	Total	2.7(167)	3.5(161)	1.8(136)	1.2(76)	2.7(107)	2.1(139)

*number in parenthesis indicate number of animals involved.

Another interesting aspect of these results was the strong association between anticonvulsant effect of the treatment and protection from the acute lethal effects of the nerve agents. Such association has been seen in previous studies from our laboratory with both anticholinergic as well as benzodiazepine drugs using soman challenge in this guinea pig model (McDonough et al. 1999, 2000) and has also been observed in nonhuman primate studies of anticonvulsant treatment of soman exposure (Lallement et al. 1997, 1998). Such an association between mortality and status epilepticus is well recognized in the clinical medical literature (Towne et al. 1994; Krumholz et al. 1995). The fact that control of nerve agent seizures is so strongly linked to protection from the lethal effects of nerve agents may explain the requirement for such high doses of atropine that have been routinely used in studies of the protective effects of carbamate pretreatment (Dirnhuber et al. 1979; Maxwell et al. 1988) or oxime therapies (Melchers et al. 1994; Worek et al. 1994; Koplovitz et al. 1995). These findings lend perspective to the older reports that inclusion of a benzodiazepine to standard atropine and oxime therapy would increase the protective ratios against OP nerve agent exposure (Johnson and Wilcox 1975; Boskovic 1981).

In summary, animals that had seizures successfully terminated by an anticonvulsant drug were significantly more likely to survive and were more likely to be totally protected from or experience only mild forms of brain pathology. These data indicate the importance of immediate anticonvulsant drug treatment in combination with traditional atropine and oxime therapy in OP nerve agent poisoning.

REFERENCES

Boskovic B (1981) The treatment of soman poisoning and its perspectives. Fundam Appl Toxicol 1: 203-213.

Clement JG, Broxup B (1993) Efficacy of diazepam and avizafone against soman-induced neuropathology in brain of rats. NeuroToxicology 14: 485-504.

Dirnhuber P, French MC, Green DM, Leadbeater L, Stratton JA (1979) The protection of primates against soman poisoning by pretreatment with pyridostigmine. J Pharm Pharmacol 31: 295-299.

Hayward IJ, Wall HG, Jaax NK, Wade JV, Marlow DD, Nold JB (1990) Decreased brain pathology in organophosphate-exposed rhesus monkeys following benzodiazepine therapy. J Neurol Sci 98: 99-106.

Johnson DD, Wilcox WC (1975) Studies on the mechanism of the protective and antidotal actions of diazepam in organophosphate poisoning. Eur J Pharmacol 34: 127-132.

Koplovitz I, Menton, R, Matthews, CM, Shutz, MB, Nalls, C, Kelly, SA (1995) Dose response effects of atropine and HI-6 treatment of organophosphorus poisoning in guinea pigs. Drug Chem Toxicol 18: 119-136.

Krumholz A, Sung GY, Fisher RS, Barry E, Bergey GK, Grattan LM (1995) Complex partial status epilepticus accompanied by serious morbidity and mortality. Neurology 45: 1499-1504.

Lallement G, Pernot-Marino I, Baubichon D, Burckhart M-F, Carpentier P, Blanchet G (1994) Modulation of soman-induced neuropathology with an anticonvulsant regimen. NeuroRep 5: 2265-2268.

Lallement G, Clarencon D, Brochier G, Baubichon D, Galonnier M, Blanchet G, Mestries JC (1997) Efficacies of atropine/pralidoxime/diazepam and atropine/HI-6/prodiazepam in primates intoxicated by soman. Pharmacol Biochem Behav 56: 325-332.

Lallement G, Clarencon D, Masqueliez C, Baubichon D, Galonnier M, Burckhart MF, Peoc'h M, Mestres JC (1998) Nerve agent poisoning in primates: antilethal, antiepileptic and neuroprotective effects of GK-11. Arch Toxicol 72: 84-92.

Lennox WJ, Harris LW, Talbot BG, Anderson DR (1985) Relationship between reversible acetylcholinesterase inhibition and efficacy against soman lethality. Life Sci 37: 793-798.

Maxwell DM, Brecht KM, Koplovitz I (1997) Characterization and treatment of the toxicity of 0-isobutyl S-(2-(diethylamino)ethyl)methylphosphonothioate, a structural isomer of VX, in guinea pigs. J Am Coll Toxicol 15(Suppl. 2): S78-S88.

McDonough JH, Dochterman LW, Smith CD, Shih T-M (1995) Protection against nerve agent-induced neuropathology, but not cardiac pathology, is associated with the anticonvulsant action of drug treatment. NeuroToxicology 15: 123-132.

McDonough JH, McMonagle J, Copeland T, Zoeffel D, Shih T-M (1999) Comparative evaluation of benzodiazepines for control of soman-induced seizures. Arch Toxicol 73: 473-478.

McDonough JH, Shih T-M (1993) Pharmacological modulation of soman-induced seizures. Neurosci Biobehav Rev 17: 203-215.

McDonough JH, Shih T-M (1997) Neuropharmacological mechanisms of nerve agent-induced seizures and neuropathology. Neurosci Biobehav Rev 21: 559-579.

McDonough JH, Zoeffel LD, McMonagle J, Copeland TL, Smith CD, Shih T-M (2000) Anticonvulsant treatment of nerve agent seizures: anticholinergics versus diazepam in soman-intoxicated guinea pigs. Epilepsy Res 38: 1-14.

Melchers B, Philippens IHCHM, Wolthius OL (1994) Efficacy of HI-6 and HLo-7 in preventing incapacitation following nerve agent poisoning. Pharmacol Biochem Behav 49: 781-788.

Moore DH, Clifford CB, Crawford IT, Cole GM, Baggett JM (1995) Review of nerve agent inhibitors and reactivators of acetylcholinesterase. In: Quinn DM, Balasubramanian AS,

Doctor BP, Taylor P (eds) Enzymes of the Cholinesterase Family. Plenum Press, New York, pp 297-304.
Shih T-M, Koviak TA, Capacio BR (1991) Anticonvulsants for poisoning by the organophosphorus compound soman: Pharmacological mechanisms. Neurosci Biobehav Rev 15: 349-362.
Shih T-M, McDonough JH (1999) Organophosphorus nerve agents-induced seizures and efficacy of atropine sulfate as anticonvulsant treatment. Pharmacol Biochem Behav 64: 147-153.
Shih T-M, McDonough JH (2000) Efficacy of biperiden and atropine as anticonvulsant treatment for organophosphorus nerve agent intoxication. Arch Toxicol 74: 165-172.
Sidell FR (1997) Nerve Agents. In: Sidell, FR, Takafuji, ET, Franz, DR (eds) Textbook of Military Medicine, Part I: Medical Aspects of Chemical and Biological Warfare, Office of the Surgeon General, Department of the Army, Washington, DC, pp 129-179.
Taylor P (1985) Anticholinesterase agents. In: Gilman AG, Goodman LS, Rall TW, Murad F (eds) The Pharmacological Basis of Therapeutics, 6th ed. Macmillan, New York, pp 110-129.
Towne AR, Pellock JM, Ko D, DeLorenzo JR (1994) Determinants of mortality in status epilepticus. Epilepsia 35: 27-34.
Winer BJ (1971) Statistical Principles in Experimental Design. McGraw-Hill, New York.
Worek F, Kirchner T, Szinicz L (1994) Treatment of tabun poisoned guinea-pigs with atropine, HLo 7 or HI 6: effect on respiratory and circulatory function. Arch Toxicol 68: 231-239.

Utility of respiratory vaccination with recombinant subunit vaccines for protection against pneumonic plague.

Douglas S. Reed & Jennifer Smoll
Department of Aerobiology & Product Evaluation
Division of Toxinology & Aerobiology,
U.S. Army Medical Research Institute of Infectious Diseases

Plague
Causative agent: *Yersinia pestis*

- a.k.a. "The Black Death"
- Endemic disease worldwide
- Normally infects rodents
- Three forms: bubonic, septicimic, and pneumonic plague
- Plague can be aerosol transmitted, has a rapid onset and high mortality (100%)

Respiratory vaccination:

Why vaccinate via the respiratory tract?

- Immunity at mucosal sites can prevent pathogen infection of the host.
    - A) oral poliovirus vaccine
    - B) inhaled influenza vaccine
    - C) kennel cough & Newcastle vaccines (pets & livestock)
- Inhaled vaccines could be easily administered in the field.

Plague vaccine:

Recombinant subunit vaccine for plague: a fusion protein that combines the F1 capsular protein and secreted V protein (F1-V). When given intramuscularly (i.m.) with alhydrogel, F1-V protects mice against a lethal pneumonic plague challenge.

Mucosal adjuvant: monophosphoryl lipid A (MPL), in an aqueous formulation (MPL-AF)

Respiratory Vaccination: Proof-of-Principle Experiments

Species: *Mus musculus*, Swiss/Webster strain, adult, both sexes

Experiment outline:

- One or two doses of vaccine, spaced 4 weeks apart
- Fourteen mice per group; four for BAL/sera collection
- 6 weeks after final vaccination - collect BAL/sera, challenge (100 LD_{50} of aerosolized *Yersinia pestis* CO92)
- Monitor mice for 20 days after challenge
- BAL & sera measured for antibody titers against F1 & V using the fluorescent microsphere immunoassay (FMIA). FMIA allows for simultaneous measurement of antibody to F1 & V.

IgG titers against F1 and V in BAL of F1-V vaccinated mice.

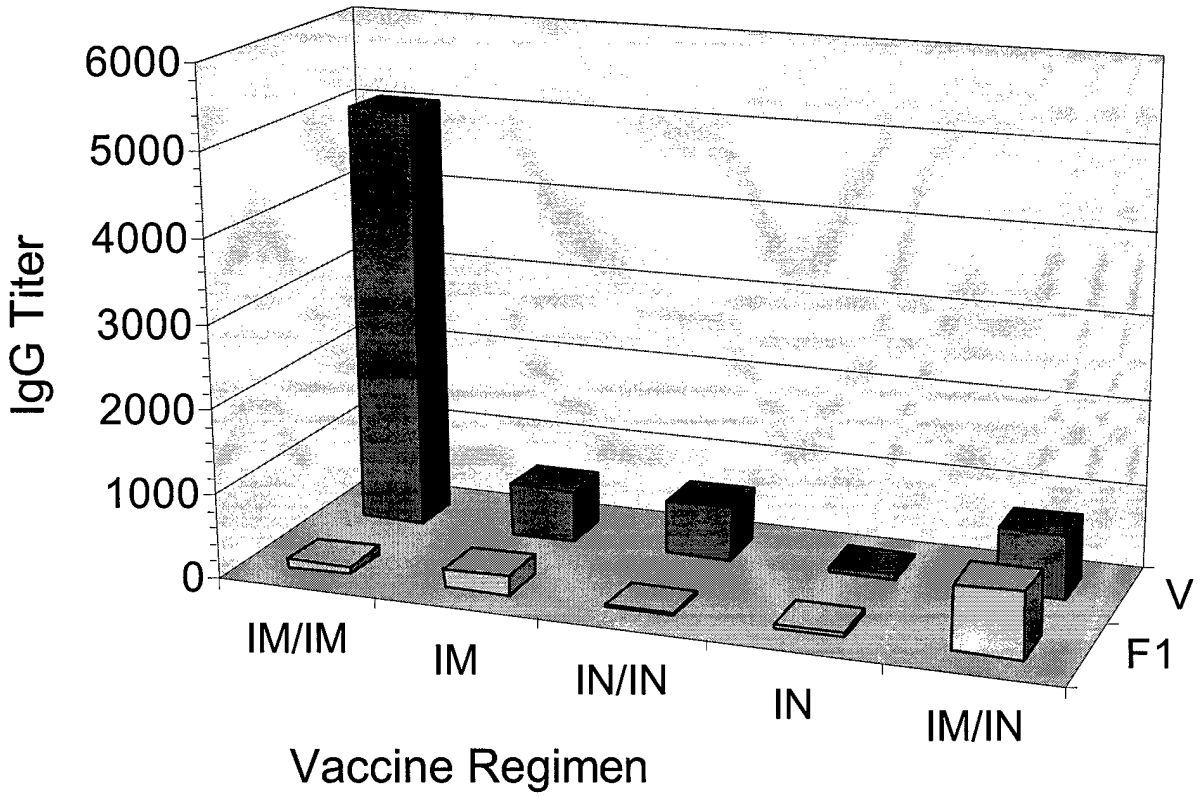

Intranasal vaccination fails to protect mice against aerosolized *Yersinia pestis*

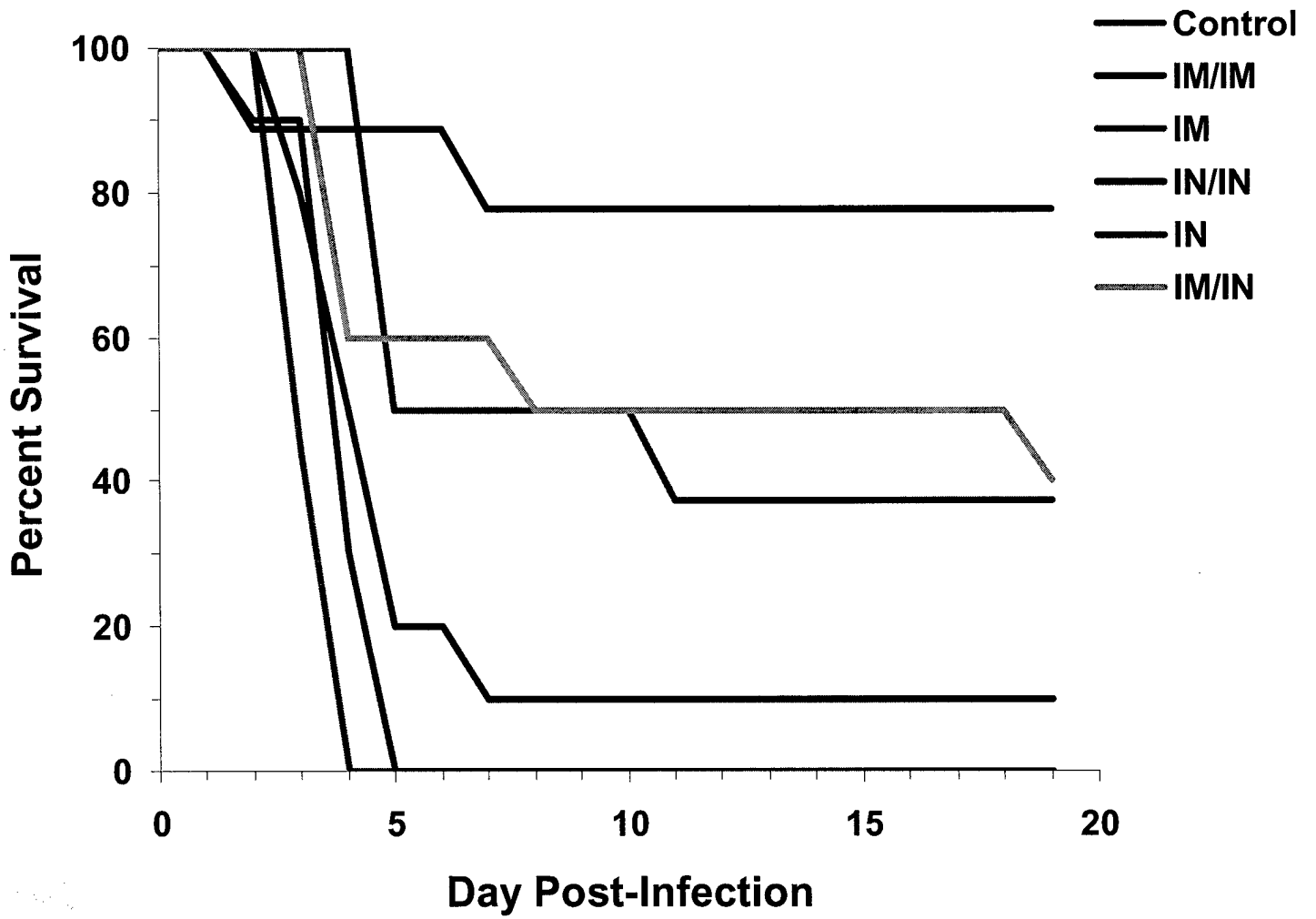

Challenge strain: *Yersinia pestis* CO92
Challenge dose: 100 LD_{50}

IgG titers after vaccination using intranasal F1-V as a booster.

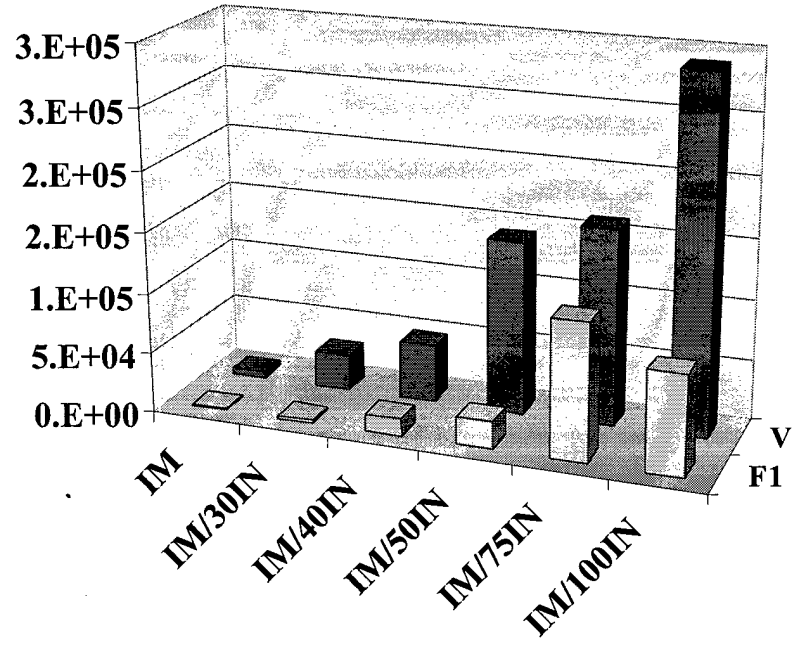

Sera

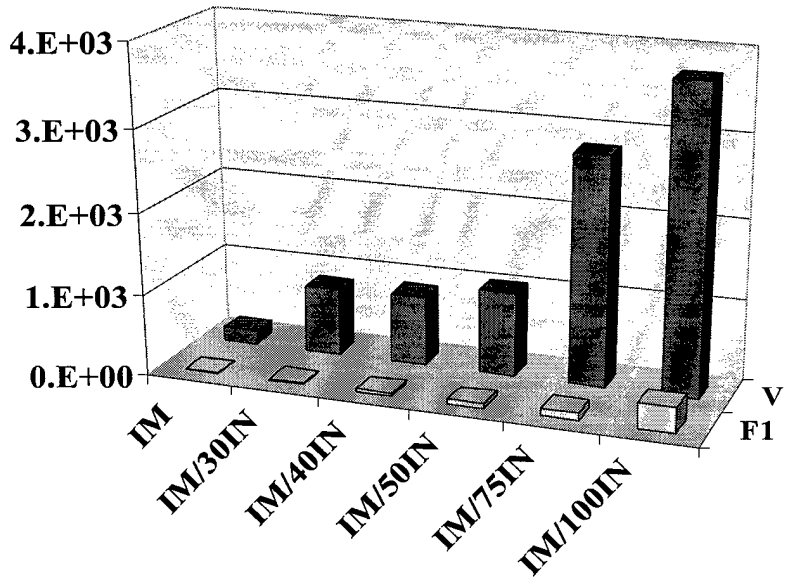

BAL

Intranasal vaccination elicits protective immunity when used as a booster.

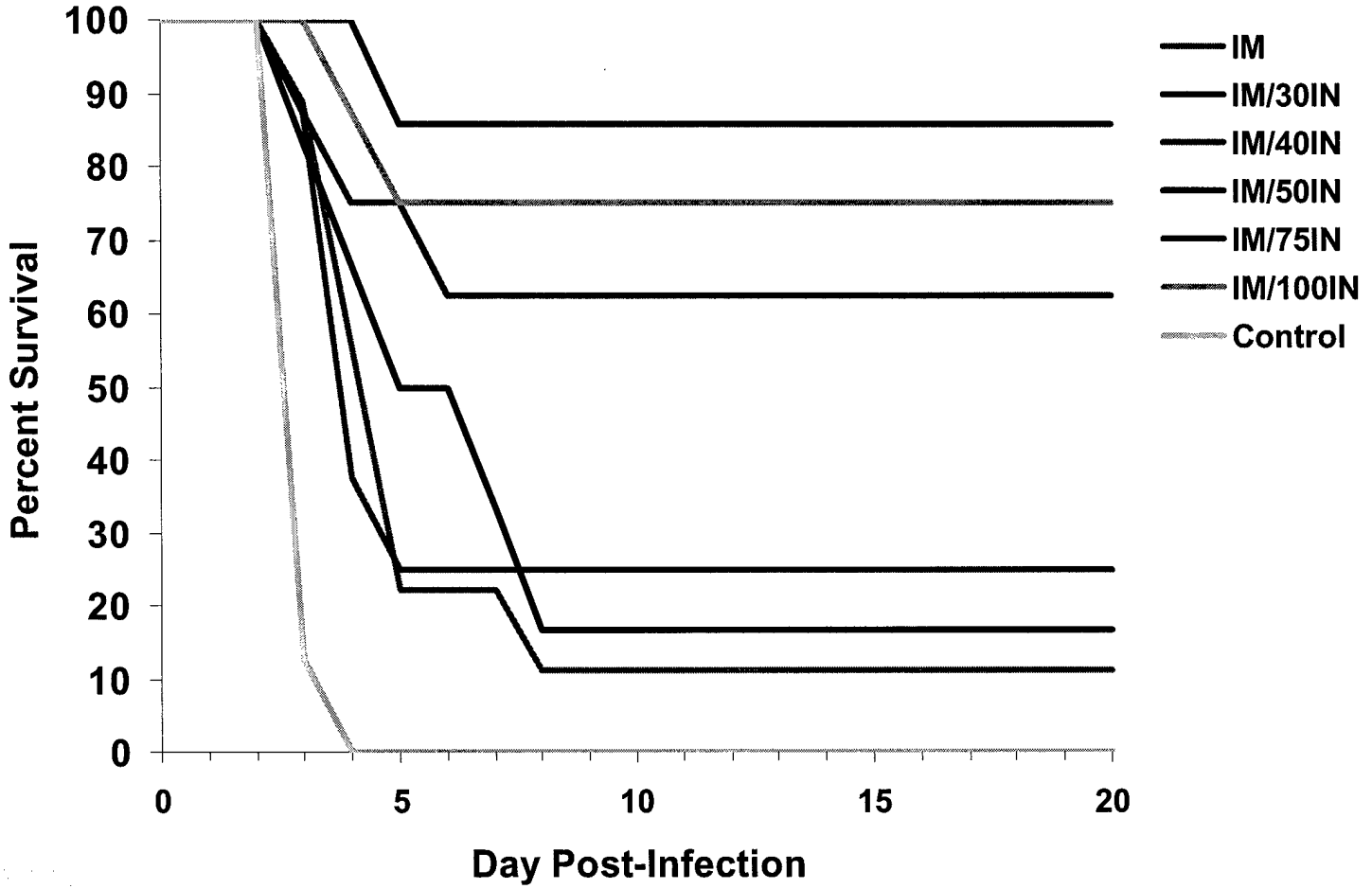

Challenge strain: *Yersinia pestis* CO92
Challenge dose: 100 LD_{50}

Percentage change in body weight after challenge.

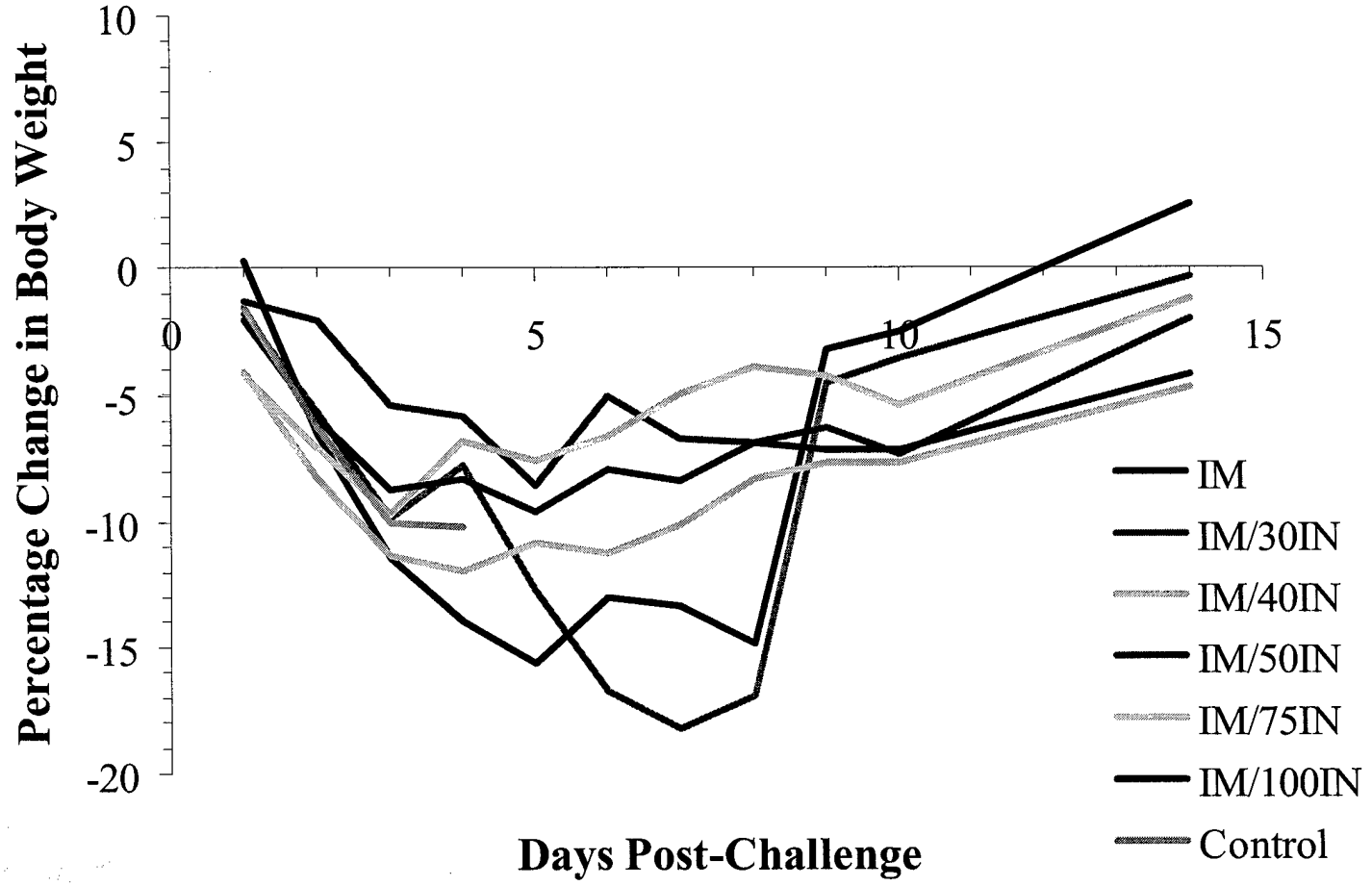

Severe pneumonia in lungs of vaccinated mice that succumb to infection.

Original magnification, 20X.

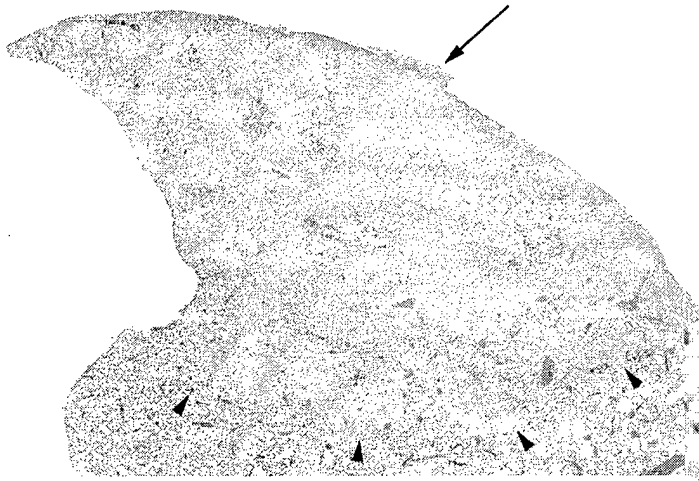

Original Magnification, 600X.

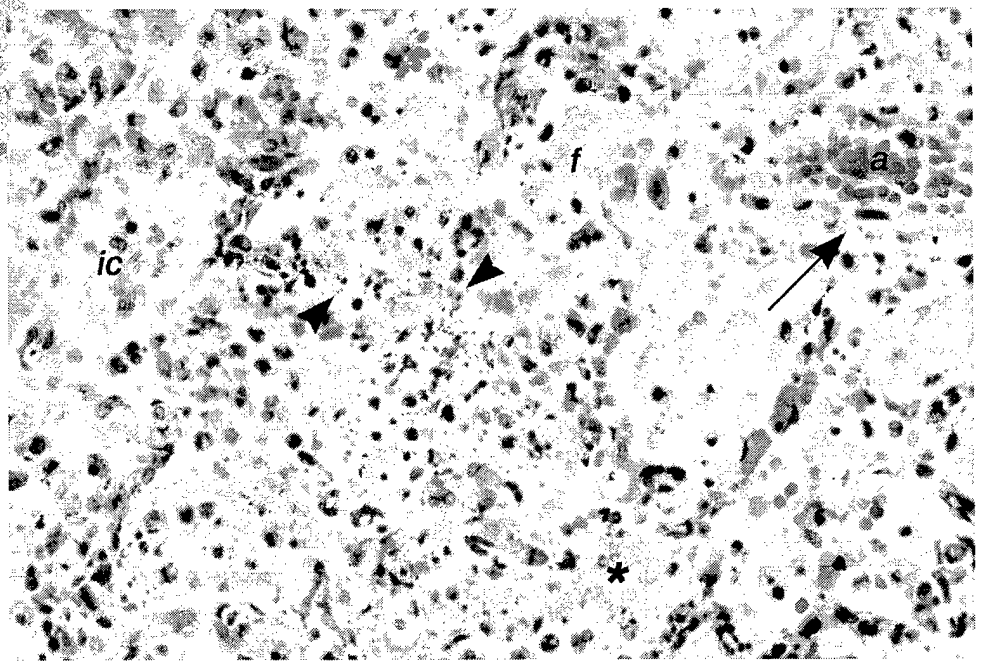

Lungs of control mice that succumb to infection are essentially clear.

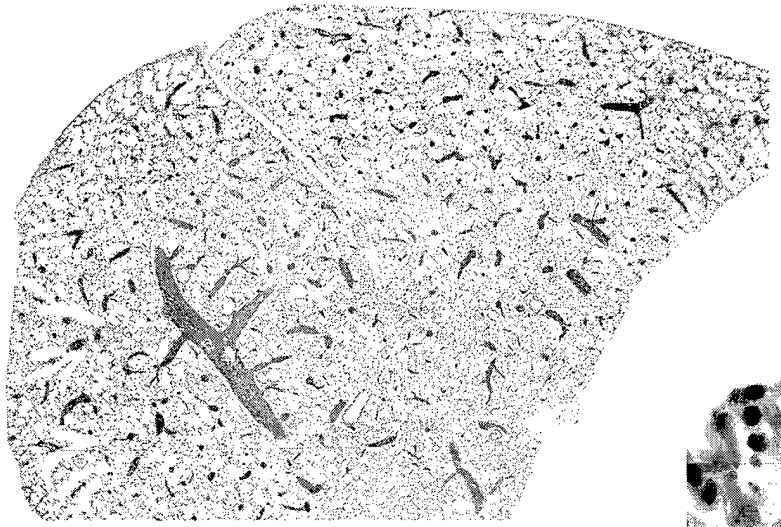

Original magnification, 20X.

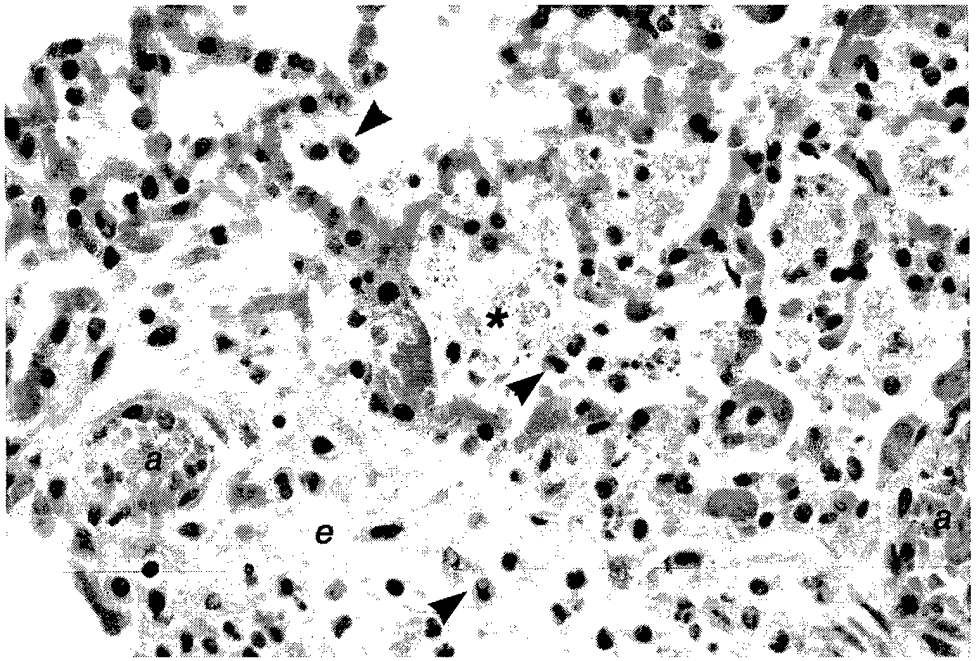

Original Magnification, 600X.

Conclusions:

- Intranasal vaccination alone failed to elicit a good immune response and did not protect mice against pneumonic plague challenge.
- Intranasal administration of F1-V + MPL-AF can serve as a booster to primary immunization with F1-V + alhydrogel injected i.m.. The levels of both systemic and mucosal immunity is determined by the dose of F1-V given as an intranasal boost.
- The data from the second experiment suggests that both systemic and respiratory immunity are necessary for protection against pneumonic plague. Systemic immunity prevents dissemination of *Yersinia pestis* while respiratory immunity prevents development of fatal pneumonia.

Future Plans:

- Vaccinate mice using aerosolized F1 with MPL-AF to target the lower respiratory tract.

Acknowledgments

Toxinology & Aerobiology
- Louise Pitt
- Chad Roy
- Mike West

Bacteriology
- LTC Gerry Andrews
- Sue Welkos

Veterinary Medicine
- CPT Lloyd Phinney
- Ron Lind & Carlton Rice

Pathology
- LTC Mark Martinez

DETERMINATION OF THIODIGLYCOL IN GROUNDWATER USING SOLID PHASE EXTRACTION FOLLOWED BY GAS CHROMATOGRAPHY WITH MASS SPECTROMETRIC DETECTION IN THE SELECTED ION MODE

Bruce A. Tomkins[1] and Gary A. Sega

Organic Chemistry and Separations Section
Chemical and Analytical Sciences Division
Oak Ridge National Laboratory[2, 3]
P. O. Box 2008
Oak Ridge, TN 37831-6120

Fax: (865)-576-7956

Version of June 4, 2001

An original contribution submitted to the 2001 Scientific Conference on Chemical & Biological Defense Research

6-8 March, 2001

Marriott's Hunt Valley Inn, Hunt Valley, MD

---

[1] To whom correspondence should be addressed. E-mail address: tomkinsba@ornl.gov

[2] Research sponsored by the Rocky Mountain Arsenal, DOE No. 1989-H077-A1 with the US Department of Energy. Oak Ridge National Laboratory is managed by UT-Battelle, LLC, for the US Department of Energy under contract DE-AC-05-00OR22725.

[3] The submitted manuscript has been authored by a contractor of the US Government under contract DE-AC05-00OR22725. Accordingly, the US Government retains a nonexclusive, royalty-free license to publish or reproduce the published form of this contribution, or allow others to do so, for US Government purposes.

DETERMINATION OF THIODIGLYCOL IN GROUNDWATER USING SOLID PHASE EXTRACTION FOLLOWED BY GAS CHROMATOGRAPHY WITH MASS SPECTROMETRIC DETECTION IN THE SELECTED ION MODE

Bruce A. Tomkins and Gary A. Sega

Organic Chemistry and Separations Section, Chemical and Analytical Sciences Division, Oak Ridge National Laboratory, P. O. Box 2008, Oak Ridge, TN 37831-6120

A highly-sensitive analytical procedure is described for determining thiodiglycol in groundwater. Samples are initially fortified with 3,3'-thiodipropanol (surrogate), then both species are extracted using sequential solid phase extraction with C_{18} and Ambersorb 572 columns in tandem. The C_{18} column, which removes extraneous groundwater components, is discarded; the Ambersorb 572 column is dried thoroughly before eluting polar components with a small volume of dichloromethane. The extract is taken to dryness using dry flowing nitrogen, and the resulting residue is derivatized using MTBSTFA and pyridine. The derivatized products are diluted to a final volume with toluene, chromatographed using a fused-silica capillary column, and detected with a quadrupole mass spectrometric detector in its selected-ion mode. Two independent statistically unbiased procedures were used to evaluate the detection limits for thiodiglycol; the values ranged between 4 and 16 $\mu g\ L^{-1}$ groundwater.

INTRODUCTION

Sulfur mustard (HD, *syn.* bis-(2-chloroethyl)sulfide, CAS Registry No. [505-60-2]) is an organosulfur blister agent that was first deployed in World War I and has been used occasionally worldwide ever since. It was manufactured by several agencies during World War II, including the US Army Rocky Mountain Arsenal between December 1942 and May 1943[1]. Sites such as the Rocky Mountain Arsenal are currently being remediated and converted to non-military uses. In order to ensure that the final site contains soil and groundwater with contaminant levels below those maximum levels allowed by the regulatory agencies, rigorously-tested analytical methods must be available that will (a) demonstrate the presence or absence of HD at regulatory levels in soil or groundwater samples, (b) be readily implemented by most commercial analytical laboratories, (c) be rapid and convenient to use, and (d) generate minimal final quantities of chemically-hazardous waste. The determination of traces of HD and its decomposition products is crucial to support efforts in the remediation of contaminated sites at many military installations and the verification of arms control agreements in compliance with the Chemical Weapons Convention.

The primary environmental fate mechanism of stored or buried HD is hydrolysis[2]. Although HD is rapidly hydrolyzed (half-life of 8.5 min at 25°C)[3], its rate is limited by the slow rate of dissolution. The hydrolysis mechanism is complex and, depending upon the availability of water, occurs by two routes, both of which lead to the initial formation of thiodiglycol (TDG, *syn.* 2,2'-thiodiethanol, CAS Registry No. [111-48-8]) and hydrochloric acid. Hence, the presence of TDG in a groundwater sample is an

excellent indicator of legacy HD manufacture or storage. The current Target Reporting Limit (TRL) set by the US Army Rocky Mountain Arsenal for TDG in groundwater[4] is 5 $\mu g\ L^{-1}$.

The open literature describes a variety of analytical procedures for TDG in aqueous matrices, but few exhibit both the required sensitivity and selectivity required and ready availability within most commercial analytical laboratories. Some of the high-pressure liquid chromatography-based methods reported for this purpose employ sulfur flame photometric detectors[5,6], capillary electrophoresis with UV detection[7], and mass spectrometric detectors employing either electrospray[8,9] or atmospheric pressure chemical ionization[10,11]. Methods based on gas chromatography are particularly attractive when combined with a derivatization step both to reduce tailing of thiodiglycol and to improve sensitivity and selectivity. For example, Black and Read[12] converted the urinary metabolites of sulfur mustard, including TDG, to their corresponding bis(pentafluorobenzoate) derivatives prior to gas chromatography-tandem mass spectrometry (GC-MS-MS) or electron-capture negative ion chemical ionization mass spectrometry in the selected ion monitoring mode[13]. TDG present in the urine of exposed rats or guinea pigs has been derivatized with heptafluorobutyric anhydride prior to gas chromatography with mass spectrometric detection, with excellent results[14,15].

The present method expands the work of Leong et al.[16] to provide a viable method for quantitating TDG and 3,3'-thiodipropanol (TDP, CAS Registry No. [10595-09-02]), a proposed surrogate, in groundwater at low µg/L (ppb) concentrations. The detection limits and recoveries for both derivatized species were rigorously determined using protocols mandated by both the US Army Rocky Mountain Arsenal and the US Environmental Protection Agency. The final chemical waste produced requiring disposal did not exceed 1 mL per sample.

REAGENTS, APPARATUS, AND INSTRUMENTATION

Thiodiglycol (*syn.* 2,2'-thiodiethanol, CAS Registry No. [111-48-8]), 3,3'-thiodipropanol (CAS Registry No. [10595-09-02]), and *N-(tert*-butyldimethylsilyl)-*N*-methyltrifluoroacetamide (MTBSTFA, CAS Registry No. [77377-52-7]) with 1% *t*-butyldimethylchlorosilane (TBDMS-Cl, CAS Registry No. [18162-48-6]) were purchased from the Aldrich Chemical Co. at 99+% purity. Silylation grade pyridine (CAS Registry No. [110-86-1]) was obtained from Sigma. Toluene (CAS Registry No. [108-88-3]), HPLC-grade water, acetonitrile (CAS Registry No. [75-05-8]), and dichloromethane (CAS Registry No. [75-09-2]) were purchased in HPLC grade or better purity from J. T. Baker or Allied Signal, Inc., Burdick & Jackson. Reagent-grade sodium chloride and anhydrous sodium sulfate were procured from Fisher Scientific, Inc., and EM Scientific. All chemicals were used without further purification.

Ambersorb 563 and Ambersorb 572 (20-50 mesh) were purchased from Supelco, Inc. These sorbents were packed as required into empty 6-mL capacity surgical polypropylene columns (J. T. Baker) with customary 20 µm porosity Teflon® frits. Columns (6-mL) containing 500 mg Envi-Carb were obtained from Supelco. Disposable 6-mL columns packed with 500 mg Bakerbond spe™ octadecyl C_{18} and 75-mL empty surgical polypropylene sample reservoirs were purchased from J. T. Baker.

All groundwater samples were extracted using a 12-position solid phase extraction manifold with Teflon® valves and needles and vacuum applied from the stainless steel top, rather than the side, of the glass chamber (Burdick & Jackson, part no. 9400). Dichloromethane extracts were collected and derivatized (as described below) in 8-mL shell vials and sealed using 15-425 plastic black caps with open tops and PTFE-faced silicone rubber septa. Derivatized and diluted residue was ultimately transferred to 2-mL amber silanized automatic sampler vials bearing hole caps with Teflon®-silicone rubber-Teflon® septa.

Two Multi-Block Heaters were used during sample preparation. One, which was used strictly for extract concentration, was positioned underneath a nine-port Reacti-Vap™ Evaporator attached to a nitrogen cylinder (99.999% purity). The usual cast aluminum heating block was turned over, enabling shell vials to stand under the vanes of the evaporator in full view of the analyst. The block temperature was maintained at 45°C. The second, which was used strictly for derivatization, was maintained at 105°C and employed a heating block drilled for 12/13 mm diameter vessels (i.e., 8 mL shell vials) and a thermometer.

A Hewlett-Packard Model 5890 Series II gas chromatograph interfaced to a Hewlett-Packard Model 7673 automatic sampler and Hewlett-Packard Model 5989A quadrupole mass spectrometer was used for all measurements. The injector was equipped with a double-gooseneck injector sleeve. The fused-silica gas chromatographic column was an HP-5MS Ultra Low Bleed (5% diphenyl-95% dimethylsiloxane), 30 m x 0.25 mm i.d., 0.25 μm film thickness. The head pressure of the carrier gas (helium, 99.99% purity) was 54 kPa (7.8 psi). The automatic sampler syringe was flushed twice each with methanol and toluene before injecting 1 μL sample into the gas chromatograph.

The injector, detector, and mass transfer line temperatures for the gas chromatograph were 250, 280, and 280°C, respectively. The column oven temperature was increased linearly from 100°C (hold for 3 min) to 270°C (hold for 1 min) at 10°C/min. The mass spectrometer operated at source and quadrupole temperatures of 200° and 100°C, respectively, and a source manifold pressure less than 8×10^{-6} torr. The ionization mode was electron impact (70 eV), with an electron multiplier voltage of 50 V above the "tune" voltage. The "solvent delay", or the time after the start of a given analysis until the mass spectrometer was turned on, was 14 min. The GC/MS system was operated in its "selected ion monitoring" (SIM) mode, in which the mass-to-charge ratio (m/z) monitored for TDG was 293, while those monitored for TDP were 321 and 363. The selected ions for TDG were scanned between 14 and 16.5 min, while those for TDP were scanned between 16.5 and 19 min. The "dwell time", or time spent monitoring a given m/z value, for 293, 321, or 363 was 400, 400, or 100 msec, respectively. The "low mass resolution" feature was "on", allowing a mass peak width of 0.9 amu. The increased peak width (normally 0.5 amu) increased sensitivity with little loss in specificity.

EXPERIMENTAL PROCEDURES

An aliquot of calibrating solution (normally 10 to 100 μL) was combined with 100 μL each pyridine and MTBSTFA with catalyst in a 2-mL silanized automatic sampler vial. The vial was capped and heated to 105°C for 1 hr, then cooled to room temperature. The contents of the vial were diluted to 1 mL with toluene, then analyzed for TDG and TDP by GC-MS-SIM according to the parameters noted above. If reanalysis of the extracts is either expected or desired, the vials may be recapped and stored at 4°C for at least seven days. Daily calibration of the mass spectrometer with derivatized standards is recommended.

100 mL portions of model groundwater (100 mg/L each in chloride and sulfate as their sodium salts in ASTM Type II water)[17] were fortified to a desired concentration of TDG (2-100 ng TDG/mL). In addition, each groundwater sample was fortified with TDP (surrogate, 25 μg TDP/L).

The solid phase extraction column train was prepared as follows: The C_{18} "guard" column was conditioned with two column volumes each of methanol and HPLC-grade water, while the "extraction column" (100 mg Ambersorb 572) was conditioned with a single column volume of methanol and two column volumes of HPLC-grade water. *Once the column conditioning process has begun, neither the C_{18} nor the Ambersorb 572 column should be allowed to go dry.* The solid phase extraction column train consists of (a) 75 mL reservoir, (b) C_{18} "guard" column filled with water, and (c) Ambersorb 572

extraction column filled with water, all connected using the hardware supplied with the reservoirs. The completed train is then mounted on the solid phase extraction manifold. The fortified groundwater sample is added to the reservoir, and liquid flow is adjusted to a flow of 2-3 mL/min, with vacuum applied as required. (Note that some groundwater samples may contain an excessive quantity of particle fines that will clog the "guard column" rapidly. In that case, "off-line" filtration of the fortified sample may be required prior to solid phase extraction.) After the entire 100 mL sample has passed through the Ambersorb 572 column, the train is disassembled and the Ambersorb 572 column is dried under full vacuum for at least one hour.

Materials collected on the Ambersorb 572 column are eluted, slowly if possible, into an 8-mL shell vial using three 3-mL portions of dichloromethane (typically, 8 mL dichloromethane extract are recovered). A 100 µL aliquot of pyridine is added to the extract as a "keeper", and the resulting solution is taken to dryness both by warming the bottom of the shell vial (to 45°C) and by using dry flowing nitrogen. The resulting residue is derivatized in the 8-mL shell vial at 105°C for 1 hr with 100 µL each additional pyridine and MTBSTFA with catalyst. After the derivatized mixture has cooled, it is diluted to a final volume of 1 mL with 800 µL toluene, transferred to a 2-mL automatic sampler vial, and analyzed for TDG and TDP by GC-MS-SIM using the parameters described above. If reanalysis is either expected or desired, the vials may be recapped and stored at 4°C for at least seven days.

The measured integrated peak area for either TDG or TDP is calculated using the "integrate" function of HP 5989A mass spectrometer data system. The peak areas from the derivatized standards were fit to a quadratic calibration curve of the form $C = aA^2 + bA + c$, where C is the concentration of analyte in the extract in µg/mL, A is the measured peak area, and a, b, and c are regression constants, all of which should be considered statistically significant. The extract concentration was later corrected in the usual manner for the groundwater sample volume, 100 mL.

RESULTS AND DISCUSSION

In principle, TDG could be removed and concentrated from aqueous samples using either liquid-liquid or solid-phase extraction. Both approaches exhibited deficiencies and challenges. TDG is so soluble in water that partitioning with a variety of organic solvents, e.g., ethyl acetate and dichloromethane, produced overall recoveries not greater than approximately 20% at a test concentration range of 20-120 µg/mL. This situation persisted even when the pH of the aqueous sample was adjusted to <1 and salt (~25% w/v) was added. To compound the problem, liquid-liquid extraction generated a considerable quantity of organic solvent waste. For all of these reasons, this approach was set aside.

An alternative approach involved the adsorption of TDG onto a carbonaceous sorbent(s), with subsequent elution and analysis. Several sorbents were evaluated, i.e., Ambersorb 563, Ambersorb 572, and Envi-Carb. Ambersorb 572 was an attractive choice because it has been used successfully for the determination of other small water-miscible analytes, such N-nitrosodimethylamine, in groundwater[18]. Envi-Carb is available commercially in small prepacked columns and would be convenient for routine analyses. Small columns packed with 500 mg of each sorbent were challenged with 100 mL model groundwater samples fortified to 2-50 µg TDG/mL. The analyte was eluted with a variety of solvents, including dichloromethane, ethyl acetate, methanol, and acetone. The nominal eluting condition was three 3-mL portions of each solvent, which were pooled. The resulting extract was taken to dryness and derivatized with MTBSTFA, as described below.

It became clear that passing the sample through Ambersorb 572 and eluting TDG with dichloromethane was the preferred choice of sorbent and eluting solvent. Ambersorb 563 was less successful than Ambersorb 572, while the Envi-Carb sorbent never retained TDG at all. Even with an

optimized sorbent and desorbing solvent, the recoveries of TDG were both low and inconsistent. Subsequent experiments demonstrated that the lengthy concentration periods using dry flowing nitrogen, often more than 1 hour, were slowly and irreproducibly volatilizing trace quantities of TDG, a compound normally considered "nonvolatile". By adding a small quantity (100 µL) of pyridine as a "keeper" and warming the bottom of the shell vial slightly (to 45°C), the sample concentration time was reduced to approximately 30-45 min, while the analyte recovery was increased to approximately 40% at test concentrations ranging between 0.25-2 µg TDG/mL. We believe, but cannot prove, that the effectiveness of Ambersorb 572 in this method is related to its specific surface area that, at 1100 m^2/g, is the highest of the three sorbents evaluated.

The use of a carbonaceous adsorbent presented several additional challenges and considerations. First, such a sorbent is nonselective and will retain any non-ionic neutral analyte present in an authentic contaminated groundwater sample. Having all of these materials present in the final extract would provide an excessive and unwanted level of interferences, even for the most selective detectors. For that reason, a guard column was placed in tandem and ahead of the Ambersorb 572 column. The initial choice for the guard column was a 500 mg C_{18} octadecyl SPE column, which would be capable of retaining modest quantities of nonpolar interferences. Other guard columns might be more appropriate, depending upon further characterization of the interferences. Second, it is very difficult to elute the desired analytes quantitatively from an adsorption column with a small volume of organic solvent, although that is commonly done with a reversed-phase column. For example, when we attempted to elute TDG from a 500 mg Ambersorb 572 cartridge (test conditions, 0.25-2 µg TDG/mL, 100 mL sample) using three 3-mL aliquots of dichloromethane, significant quantities (up to 25% of the expected mass) of TDG were observed in the combined second and third aliquots.

Two approaches to improve the overall recovery and convenience were investigated. First, an alternative and more powerful eluting solvent was considered. This approach was immediately set aside because we had found no common organic solvent that was more effective for stripping TDG from Ambersorb 572 than dichloromethane. Second, reducing the bed mass would prevent TDG from migrating further into the bulk sorbent upon elution and possibly becoming re-adsorbed. For that reason, adsorption columns containing 500, 200, and 100 mg Ambersorb 572 were evaluated. When each of these was challenged with a 100 mL model groundwater sample containing 0.25-2 µg TDG and TDP/mL, the recoveries observed in the initial 3-mL dichloromethane extract were similar, and ranged between 25-40%, regardless of the bed mass. Based on these data, we hypothesize that the adsorption of TDG and TDP on Ambersorb 572 is basically a surface phenomenon, occurring on the very top of the adsorption column. As long as the expected concentration of TDG is trace-level and the capacity of the surface sorbent is not exceeded, the rest of the bed mass is extraneous and, in fact, inhibits quantitative recovery of analyte. For that reason, further work focused on Ambersorb 572 columns employing a 100 mg bed mass. Three 3-mL column washes with dichloromethane were employed to ensure that the sorbent was thoroughly exposed to solvent while simultaneously allowing a high ratio of eluting solvent to sorbent bed volumes. At the same time, further significant improvements in overall recovery are not expected unless advanced instrumentation featuring extraction under elevated temperature and pressure conditions (Accelerated Solvent Extraction™) is employed.

Because most commercial service analytical laboratories would possess GC-MS capabilities, the current method emphasizes derivatization of TDG with a reagent that would convert the analyte into a stable and volatile species amenable to highly-selective and sensitive selective ion monitoring. Of the reagents available, MTBSTFA was particularly attractive, for the following reasons: (a) neutral volatile by-products are produced; (b) the butyldimethylsilyl ether products are stable to hydrolysis; and (c) simple readily-predicted mass spectra feature an $(M-57)^+$ ion, which represents loss of a tertiary butyl group, and is both diagnostic and of medium to high intensity.

In spite of the obvious advantages, there are additional considerations when using MTBSTFA. Because water, not the analytes, will preferentially react with MTBSTFA, it is important that the Ambersorb 572 bed be completely dry prior to dichloromethane elution. The recommended drying time for the Ambersorb 572 bed is at least one hour. In addition, it is important that *both* hydroxyl groups present on either TDG or TDP be derivatized. Insufficient reaction time or temperature produces both a singly-derivatized species, whose presence reduces the apparent recovery of analyte, as well as the doubly-derivatized entity. For that reason, both a derivatization time (1 hr) and temperature (105°C) higher than normal for such reactions is recommended. Derivatized standards or extracts are reasonably stable to hydrolysis. They may be stored at 4°C and re-analyzed reliably within seven days, as needed. Both the standards and derivatized extracts were ultimately dissolved in toluene, rather than an aprotic polar solvent such as acetonitrile, to minimize peak splitting on the nonpolar HP-MS5 gas chromatographic column.[19]

The performance of the proposed method was evaluated using two statistically-unbiased protocols, viz., those of the US Army Rocky Mountain Arsenal[20] and the US Environmental Protection Agency[21], to determine the Method Reporting Limit (MRL) and the Method Detection Limit (MDL), respectively. The former is equivalent to determining a "found" concentration so that both the false positive and false negative errors are both 5%.[22, 23] By contrast, the latter is the minimum concentration that can be measured and reported with 99% confidence that the analyte concentration is greater than zero.

The MRL was evaluated using a procedure established by the US Army and discussed in detail elsewhere[24]. Briefly, 100 mL portions of model groundwater were fortified to 2.5-100 µg TDG/L, or 0.5 to 20 times the Target Reporting Limit (TRL) of 5 µg/L. Each test sample was also fortified with 25 µg/L TDP, which served as a candidate surrogate. Samples were spiked, extracted, derivatized, and analyzed as described above, and the resulting model groundwater concentrations calculated using calibration data obtained on each of two method certification days. The MRL values were calculated using the current version of software recommended by the Program Manager Rocky Mountain Arsenal[25]. Candidate analytical methods employing GC-MS-SIM are considered to be "self-confirming", in that the identity of a given compound is established using both its retention time and mass spectrum or selected ions within. No independent confirmatory method was required. The slope of the calculated linear regression line representing the relationship between the analyzed ("found") and spiked ("true") values may be taken as a measure of analyte recovery. The calculated MRL value for TDG was 16.2 µg/L, with a corresponding recovery of 38%.

MDL values were calculated for both TDG and TDP, the proposed surrogate compound. A single set of nine 100-mL model groundwater samples (seven required) were independently fortified to 25 µg/L in each of TDG (five times the TRL) and TDP, then processed as described above. The resulting concentrations and sample standard deviation for each analyte were calculated. The latter values were multiplied by the appropriate value of the Student's-t distribution, 2.896, representing 99% confidence and (n-1) degrees of freedom (here, 8), where n is the number of data values available. The resulting value is the MDL; it is 3.5 and 1.2 µg/L for TDG and TDP, respectively. The average recoveries for TDG and TDP are 23 and 17%, respectively, and reflect the difficulty in extracting these water-miscible species from a groundwater matrix. However, the recoveries are clearly consistent and reproducible. Similar recoveries were reported for the determination of N-nitrosodimethylamine, which is also a small, highly-polar, water miscible analyte, from aqueous samples using Ambersorb 572 as the extraction sorbent[26,27]. The extraction and derivatization behavior of TDP tracks that of TDG closely, and is therefore an acceptable surrogate compound.

CONCLUSIONS

Thiodiglycol (TDG), a major hydrolysis product of sulfur mustard, may be extracted from groundwater samples using a small column packed with Ambersorb 572, a synthetic carbonaceous sorbent. The analyte is ultimately is derivatized with MTBSTFA, diluted with toluene, and analyzed by GC-MS-SIM. The detection limits for this procedure ranged between 3.5 and 16 μg TDG/L groundwater. Thiodipropanol (TDP) exhibited an extraction behavior and detection limit (1.2 μg TDP/L) similar to that of TDG, and was considered to be an acceptable surrogate compound. The method recovery for both analytes is modest, ranging between 20-40%, and reflects the difficulty in extracting water-miscible analytes from a groundwater sample.

The typical sampling rate for the proposed method is approximately twelve to sixteen groundwater samples per eight-hour working day. Calibration standards may be prepared concurrently with the groundwater extracts, and should also be analyzed daily. It is strongly recommended that all sample preparation be performed during an eight-hour shift, and that all subsequent GC-MS-SIM determinations be performed independently using an instrument equipped with an automated sampler.

ACKNOWLEDGMENTS

The research described in this paper was sponsored by the US Army Rocky Mountain Arsenal, DOE No. 1989-H077-A1, US Department of Energy under contract DE-AC05-00OR22725 with Oak Ridge National Laboratory, managed by UT-Battelle, LLC. The submitted manuscript has been authored by a contractor of the US Government under contract DE-AC05-00OR22725. Accordingly, the US Government retains a nonexclusive, royalty-free license to publish or reproduce the published form of this contribution, or allow others to do so, for US Government purposes.

REFERENCES

[1]D. Parks, The Analysis of Army Chemical Agents; GB, VX, Mustard, and Lewisite in Soil at Rocky Mountain Arsenal, presented to the 15th Annual Waste Testing and Quality Assurance Symposium, Arlington, VA, 1999.

[2]N. B. Munro, S. S. Talmage, G. D. Griffin, L. C. Waters, A. P. Watson, J. F. King, V. Hauschild, Environ. Health Perspectives 107 (1999) 933.

[3]S. J. Lundin (ed), *Verification of Dual-use Chemical under the Chemical Weapons Convention: The Case of Thiodiglycol,* Oxford University press (1991) 4-23.

[4]Personal communication between Dr. Bruce A. Tomkins, Oak Ridge National Laboratory, and Mr. Steve Baca, US Army Rocky Mountain Arsenal, Commerce City, CO, June 2000.

[5]E. W. J. Hooijschuur, C. E. Kientz, U. A. Th. Brinkman, J. of Chromatogr. A 849 (1999) 433.

[6]E. W. J. Hooijschuur, C. E. Kientz, A. G. Hulst, U. A. Th. Brinkman, Anal. Chem. 72 (2000) 1199.

[7]R. L. Cheicante, J. R. Stuff, H. D. Durst, J. Capillary Electrophor. 2 (1995) 157.

[8]P. A. D'Agostino, L. R. Provost, J. R. Hancock, J. of Chromatogr. A., 808 (1998) 177.

[9]G. R. Asbury, C. Wu, W. F. Siems, H. H. Hill, Anal. Chim. Acta 404 (2000), 273.

[10]R. W. Read, R. M. Black, J. of Chromatogr. A, 862 (1999) 169.

[11]R. W. Read, R. M. Black, Proc. ERDEC Sci. Conf. Chem. Biol. Def. Res. (1998), D. A. Berg, Ed., 897.

[12]R. M. Black and R. W. Read, J. Chromatogr. B. 665 (1995) 97.

[13]R. M. Black and R. W. Read, J. Chromatogr. 449 (1988) 261.

[14]E. M. Jakubowski, C. L. Woodard, M. M. Mershon, T. W. Dolzine, J. Chromatogr. 528 (1990) 184.

[15] "Verification of Sulfur Mustard Exposure – Measuring Thiodiglycol in Urine by Gas Chromatograph/ Mass Spectrometer" in *TB Med 296. Assay Techniques for Detection of Exposure to Sulfur Mustard, Cholinesterase Inhibitors, Sarin, Soman, GF, and Cyanide.* Washington, D.C., Technical Bulletin Headquarters, Department of the Army, 22 May 1996. Internet address: http://chemdef.apgea.army.mil/tbmed296/chap02.htm.

[16]W. Y. Leong, E. H. Teo, C. H. Lim, Y. L. Tan,Wat. Sci. Tech. 38 (1998) 139.

[17] Chemical Quality Assurance Plan, Rocky Mountain Arsenal, Version 1.0, July, 1989.

[18]The Determination of N-Nitrosodimethylamine (NDMA) in Water by Gas Chromatography-High Resolution Mass Spectrometry (GC-HRMS), Etobicoke, Ontario, Canada, Ministry of Environment, Laboratory Services Branch, Quality Management Unit (1997), method no. NDMA-E3291A.

[19]J. G. Purdon, J. G. Pagotto, R. K. Miller, J. Chromatogr. 47 (1989) 261.

[20]Program Manager for Rocky Mountain Arsenal Chemical Quality Assurance Plan, Version I, September 1993, 2nd ed., April 1996.

[21]Appendix B to Part 136—Definition and Procedure for the Determination of the Method Detection Limit—Revision 1.11, Code of Federal Regulations: Protection of the Environment, Pars 100-149, Title 40, US GPO, Washington, DC. Revised July 1, 1990.

[22]A. Hubaux and G. Vos, Anal. Chem. 42 (1970) 849.

[23]C. L. Grant, A. D. Hewitt, T. F. Jenkins, Am. Lab. 23 (1991) 15.

[24]B. A. Tomkins, W. H. Griest, C. E. Higgins, Anal. Chem. 67 (1995) 4387.

[25]The Rocky Mountain Arsenal Method Reporting Limit Program, Version 1.0.0, Users Guide.

[26]S. W. D. Jenkins, C. J. Koester, V. Y. Taguchi, D. T. Wang, J.-P. F. P. Palmentier, K. P. Hong, Environ. Sci. Pollut. Res. Int., 2 (1995) 207.

[27]V. Y. Taguchi, S. W. D. Jenkins, D. T. Wang, J.-P. F. P. Palmentier, E. J. Reiner, Can. J. Appl. Spectrosc. 39 (1994) 87.

INTERACTION OF EXPOSURE CONCENTRATION AND DURATION IN DETERMINING ACUTE TOXIC EFFECTS OF SARIN VAPOR IN RATS

R. Mioduszewski, J. Manthei, R. Way, D. Burnett, B. Gaviola, W. Muse, S. Thomson,
D. Sommerville, and R. Crosier
U.S. Army Edgewood Chemical Biological Center
ATTN: AMSSB-RRT-TT (E3150)
5183 Blackhawk Road
Aberdeen Proving Ground, MD 21010-5424
USA

ABSTRACT

These studies were conducted as part of the "Low Level Operational Toxicology" program which began by addressing the question of how low do chemical agent detectors need to go to measure toxicologically significant effects of the classical chemical warfare (CW) agents. Initial phases of the program have focused on GB vapor. The objective of these studies was to 1) identify threshold exposure conditions at which toxicologically significant effects occur in the rat and 2) develop models for predicting dose-response effects of low CW agent concentrations as a function of exposure duration. Sarin (GB) vapor exposure is associated with both systemic and local toxic effects occurring primarily via the inhalation and ocular routes. These studies examined the effects of varying exposure concentration and duration on the probability of lethality occurring in rats exposed to Sarin (GB) vapor. Groups of male and female rats (Sprague-Dawley) were exposed to one of a series of GB vapor concentrations for a single duration (5- 360 minutes) in a whole-body dynamic chamber. The onset of clinical signs and changes in blood cholinesterase activity were measured with each exposure. Separate effective concentrations for lethality (LC50) and miosis (EC50) in 50% of the exposed population and corresponding dose-response slopes were determined for each exposure (duration) by the Bliss probit method. A predictive model derived from multifactor probit analysis describing the relationship between exposure conditions and probability of lethality in the rat is presented. Contrary to that predicted by Haber's rule, LCt_{50} values increased with exposure duration (i.e., the CT for 50% lethality exposed population and corresponding dose-response slope was not constant over time). A plot of Log (LCt50) versus Log (Exposure Time) showed significant curvature. To account for this curvature, an interactive term, Log (C)*Log(T), was added to the toxic load model. Overall, female rats were more sensitive to GB vapor toxicity than male rats over the range of exposure concentration and duration studied. Miosis was the initial clinical sign noted following the start of GB vapor exposure. Although blood cholinesterase activity was significantly inhibited by GB vapor exposure, poor correlation between cholinesterase inhibition and exposure conditions or cholinesterase inhibition and severity of clinical signs was noted

INTRODUCTION

Acute whole-body exposure to Sarin (GB) vapor results in both systemic and local toxic effects, which are primarily mediated via inhalation and ocular routes, respectively. In order to assess the acute health hazards of such an exposure, the probability of GB-induced biological effects must be quantitatively related to exposure parameters, including both atmospheric concentration (C) and exposure time (duration) (T).

Historically, it has been standard practice to use a linear time-integrated concentration (i.e., C x T, CT, or dosage) to predict mortality-response relationships for chemical vapor exposures. The above concept has persisted as an accepted principle in military hazard assessment, currently serving as the basis for estimating injury from exposure to chemical warfare (CW) agents. This measure of exposure was first attributed to Haber (1924), who found that for certain poison gases (e.g. phosgene) used in the First World War, the toxic effects appeared to be correlated with the dosage (at least between 5 min and 8 hr durations). Haber's law or rule, as commonly understood in inhalation toxicology, states:

$$C \times T = k \qquad [1]$$

with regard to the incidence of a particular biological effect. A linear time-integrated concentration implies concentration and duration are equally important components in quantifying the toxic potential of an exposure.

Alternatively, ten Berge et al., (1986) demonstrated that:

$$C^n T = k \qquad [2]$$

correlates well with the degree of injury; where C is the (constant) concentration, T is the exposure time, and n is an index (the so-called *toxic load* exponent) that depends on the particular gas or aerosol, and exposure scenario. In general, for most gases for which experiments have been conducted, n was found greater than one. In order to determine the value for n, an experiment must be designed such that both exposure concentration and duration are varied in the same study. If the above concepts for quantifying health risks of toxic gases are also true for chemical nerve agents, the traditional use of "dosage" (i.e., C x T) in estimating casualty/risk is not appropriate. Military deployment operations, or handling, storage, and destruction of chemical agents as well as emergency response procedures will require the most accurate and up-to-date assessment of agent-related health hazards.

A major objective of the present study was to determine the relationship between GB vapor exposure concentration (C), duration of exposure (T) and the probability of a toxic effect (lethality). Prior to this study, the range of exposure times cited in the literature for mammals was limited to relatively short acute exposures (from seconds to several minutes) (Yee, 1996). The present study examined acute exposure times from 5 to and including 360 min, for which little data has been published. Data generated from this study were used in formulating concentration-exposure time-response models for more accurately estimating the probability of lethality given a combination of exposure concentration and duration. Future studies will extend this approach to characterize responses to other nerve agents for which data gaps exist, biological responses to very low concentrations of chemical nerve agents, as well as differences among mammalian species.

MATERIALS AND METHODS

GB Vapor Generation. Sarin (GB) samples (97.2 ± 0.2% purity by NMR ^{31}P) were obtained from the US Army Egewood Chemical Biological Center. A modified spray atomization system produced GB droplets (<15μ) that quickly evaporated into vapor which was drawn through a 750-liter dynamic air-flow inhalation chamber constructed of stainless steel with Plexiglas windows.

Vapor Sampling/Anaysis. Three methods were used to sample/monitor and analyze GB vapor concentration in exposure chamber: a) *"Edgewood" bubblers* (containing hexane)/ gas chromatograph with flame photometric detection (GC-FPD) b) *solid sorbent tubes* (Tenax-TA)/gas chromatograph with flame ionization detection (GC-FID) and c) a *phosphorus monitor* (HYFED, Model PH262) provided a

continuous strip chart record of rise, equilibrium, and decay of the chamber vapor concentration during an exposure.

Animal Exposures and Measures of Clinical Response. Sprague-Dawley rats (8-10 weeks old from Charles River Laboratories) were confined in stainless steel compartmentalized cages (20" x 14" x 4") with each rat free to move within a separate compartment. Male (10 rats/exposure group/concentration) and female (10 rats/exposure group/concentration) rats were exposed (whole body, dynamic mode) to a fixed concentration of GB vapor for a fixed duration. Rats were exposed to one of five concentrations (2 – 56 mg/m^3) of GB vapor for one of seven exposure times (5, 10, 30, 60, 90, 240 or 360 min). Lethality and sub-lethal clinical signs (e.g., miosis, tremors, salivation, labored breathing and convulsions) were monitored during and after exposure. Lethality was counted as the fraction of each exposure group which died within 14 days after exposure. Blood cholinesterase (AChE and BuChE) activity was measured (Ellman, 1961) from pre and post-exposure blood samples collected from a tail vein. The effects of GB vapor exposure on pupil size (diameter) were assessed pre- and post-exposure under a 100 ft candle light source using a simple microscope (Bausch & Lomb, 20x) with a reticule eyepiece insert.

Data Analysis. A probit analysis program (MINITAB®, Version 13) was used to generate a separate dose-response curve (with slope, intercept and 95% fiducial limits) for each duration of exposure tested and to determine if gender differences exist in the sensitivity to the toxic effects of GB vapor exposure. Binary normal regression (multifactor probit analysis) was used to model the relative effects of exposure concentration and duration on probability of lethality or miosis. Differences in pre-exposure vs. post-exposure cholinesterase levels were expressed as a percent change resulting from treatment. This graded response was plotted against CT using linear regression in order to determine if correlations exist as indicated by significant regression coefficients.

RESULTS

LC_{50}, LCT_{50}, 95% fiducial limits, and slopes are listed for each exposure duration in Table 1. Plots of LC50 vs time are shown in Figure 1. In the first phase of this study, exposure conditions were optimized for estimating LC_{50} and LCt_{50}. The study design was not optimized for estimating EC_{50}s for sublethal signs.

Blood AChE and BuChE activities (expressed as percent of pretreatment) were inhibited as a result of exposure to various combinations of GB vapor concentration and time. Most responses (for 10, 30, 90 and 240 min exposures) appeared to fall between 5 and 30% of pretreatment baseline (Figure 2). AChE and BuChE activity (percent of pretreatment) was poorly correlated with exposure conditions (CT) in the lethal range of exposures. Median pretreatment levels of BuChE activity were consistently higher ($P< 0.001$) in female (1750 U/ml) than in male rats (424 U/ml), as determined by the Mann-Whitney Rank Sum test. However, no differences were noted between pretreatment male and female AChE activity.

All combinations of GB vapor exposure concentration and time resulted in complete miosis (pinpoint pupil) in male and female (Figure 3) rats as measured at the first hour post-exposure. This was followed by a transient mydriasis (dilated pupil) between 24-48 h post-exposure ($p < 0.01$) lasting several days. At 7 days post-exposure pupil diameters were decreasing in size ($p <0.01$) but still greater ($p <0.01$) than pre-exposure sizes.

DISCUSSION

Predicting lethality with exposure concentration models. Adequacy of exposure concentration models (Haber's rule and "toxic load") for predicting GB vapor-induced lethality were tested by regressing log(LCT50) on log(Time) and [log(Time)] squared. The statistical significance of the squared term in log (Time) shows that the plot of log(LCT50) versus log(Time) (Figure 1) is not a straight line with slope other than -1 (as predicted by the toxic load model) nor a straight line with a slope of –1 (Haber's rule) but instead a curved line. Given that the resulting squared term was statistically significant, there was adequate evidence, from a statistical point of view, to reject both Haber's rule and the toxic load model.

Starting with 12 terms [constant, C, T, C^2, T^2, C*T, Sex, Sex*C, Sex*T, Sex*C^2, Sex*T^2, and Sex*C*T, where C = centered log(Conc), T = centered log(Time), C^2 = C*C, etc., and Sex = 1 (male) and –1 (female)], the least significant term (largest p value) was deleted followed by reanalysis. This process was reiterated until all terms were significant ($p < 0.05$) in order to reduce the multicollinearity in the model. The model produced from this process is described below. The backwards elimination procedure described above resulted in the following significant terms (Table 2):

TABLE 1. Summary of LC50, LCT50, slopes and fiducial limits for GB Vapor-induced lethality (14 days post exposure) at each of seven exposure durations.

Exposure Duration (min)	Sex	LC50 (mg /m3)	95% F.I.	Slope	Sex	LC50 (mg /m3)	95% F.I.	Slope
5	F	32.8	29.8 –36.6	10.3	M	45.9	40.0 – 51.3	9.4
10	F	18.1	16.3 - 20.4	11.9	M	22.6	20.8 – 24.8	16.4
30	F	8.51	7.79 - 9.31	12.9	M	8.84	8.20 - 9.47	21.6
60	F	6.39	5.72 – 6.95	13.0	M	7.55	*	6.1
90	F	4.46	4.24 - 4.69	22.1	M	4.81	4.58 - 5.12	21.5
240	F	3.03	2.66 - 3.37	9.9	M	4.09	3.66 - 5.00	8.0
360	F	2.63	2.44 - 2.82	14.9	M	2.89	2.69 - 3.15	13.2
Exposure Duration (min)	Sex	LCt50 (mg. min/m^3)	95% F.I.	Slope	Sex	LCt50 (mg. min/m^3)	95% F.I.	Slope
5	F	164	149 -183	10.3	M	230	200 - 257	9.4
10	F	181	163 - 204	11.9	M	226	208 - 248	16.4
30	F	255	234 - 279	12.9	M	265	246 - 284	21.6
60	F	383	343 - 417	13.0	M	453	*	6.1
90	F	401	382 - 422	22.1	M	433	412 - 461	21.5
240	F	727	638 - 809	9.8	M	982	878 - 1200	8.0
360	F	947	878- 1015	14.9	M	1040	968 - 1134	13.2

*-Not able to calculate due to non-significant slope at 95% level.

TABLE 2. Summary of Binary Normal Regression Fitted Coefficients, Associated Errors and Statistical Significance for the Interaction Model [3].

Predictor	Coef.	S.E. Coef.	z	p
Constant	0.669	0.1686	3.97	0.000
Sex	-0.4238	0.0934	-4.53	0.000
cLogC	11.171	1.5000	7.45	0.000
cLogT	6.7223	0.9097	7.39	0.000
cLogCcLogT	1.8936	0.4156	4.56	0.000
Sex*cLogC	-0.3813	0.1783	-2.14	0.033

Thus, for probability of lethality let Y= normit (Probit -5):

$$Y = 0.6691 - 0.42381*Sex + 11.171*cLogC + 6.7223*cLogT + 1.8936*cLogC*cLogT - 0.3813*Sex*cLogC; \quad [3]$$

for males, this reduces to

$$Y = 0.2453 + 10.7897*cLogC + 6.7223*cLogT + 1.8936*cLogC*cLogT, \quad [4]$$

and for females, to

$$Y = 1.0929 + 11.5523*cLogC + 6.7223*cLogT + 1.8936*cLogC*cLogT. \quad [5]$$

$$cLog(X) = Log\ X - Mean\ Log\ (X);\ where\ X = C\ or\ T \quad [6]$$

Means for centering: Log(C) = 0.951702; Log(T) = 1.67781.

Predicted LCT_{50} values from Equations 4 and 5 are plotted in Figure 4. Equations 4 and 5 are an extension of the toxic load model. They are referred to here as the "interaction" model because of the presence of the interaction term, clogC*clogT.

Male vs. Female Sensitivity to GB Vapor-induced Lethality. Female rats were more sensitive to the lethal effects of GB vapor than males in the present study based on the significance of the Sex term in Equation 3 ($p<0.001$). In addition, a review of the clinical sign data suggests that clinical signs of toxicity appeared earliest in females, as a group, and progressed to more severe levels than in male rats. These findings are consistent with those of Callaway and Blackburn (1954) (for 1 min exposures) who reported that female rats were almost twice as sensitive to the lethal effects of GB vapor than males. McPhail (1953) reported that the male mouse was more sensitive to GB vapor than the female but the reverse was true for the hamster and the rat. In addition, female rats have been shown to be more sensitive than males to the lethal effects of Soman (Sket, 1993). In female rats, the LD50 for Soman was only about half that of males. This pattern was also reported for lethal exposure of rats to some organophosphate insecticides (Sheets et al., 1997).

GB Vapor Effects on Blood AChE and BuChE.. The most commonly accepted mechanism by which nerve agents are believed to induce acute toxicity is by inhibition of AChE activity in target tissues. Although red blood cell (RBC) and plasma cholinesterase activities are routinely monitored as a sensitive index of exposure to anti-cholinesterase agents, they by no means imply anti-cholinesterase intoxication (Koelle, 1994). In a review of theories and therapy of intoxication by potent AChE compounds, Ellin (1981) suggested that poor correlation exits between the clinical picture of poisoning by OP compounds and levels of ChE activity. According to Ellin et al. (1981), solutions to this problem might be obtained in pharmacodynamic studies which relate to binding of OP compounds to ChE and other esterases in tissue and blood as well as their rates of elimination. Symptoms and treatment of patients accidentally

exposed to ChE inhibitors, Sarin and Soman, are discussed by Sidell (1992). He suggests that activity of the circulating ChE does not parallel the activity of ChE in tissue and that tissue function can be reasonably normal even with minimal ChE activity. If an OP compound is administered in low concentration levels over a long period, blood levels of an animal can drop to near zero, yet the animal survives. This was observed in the present study (Figure 2). If blood levels are caused to drop to zero rapidly, the animal dies.

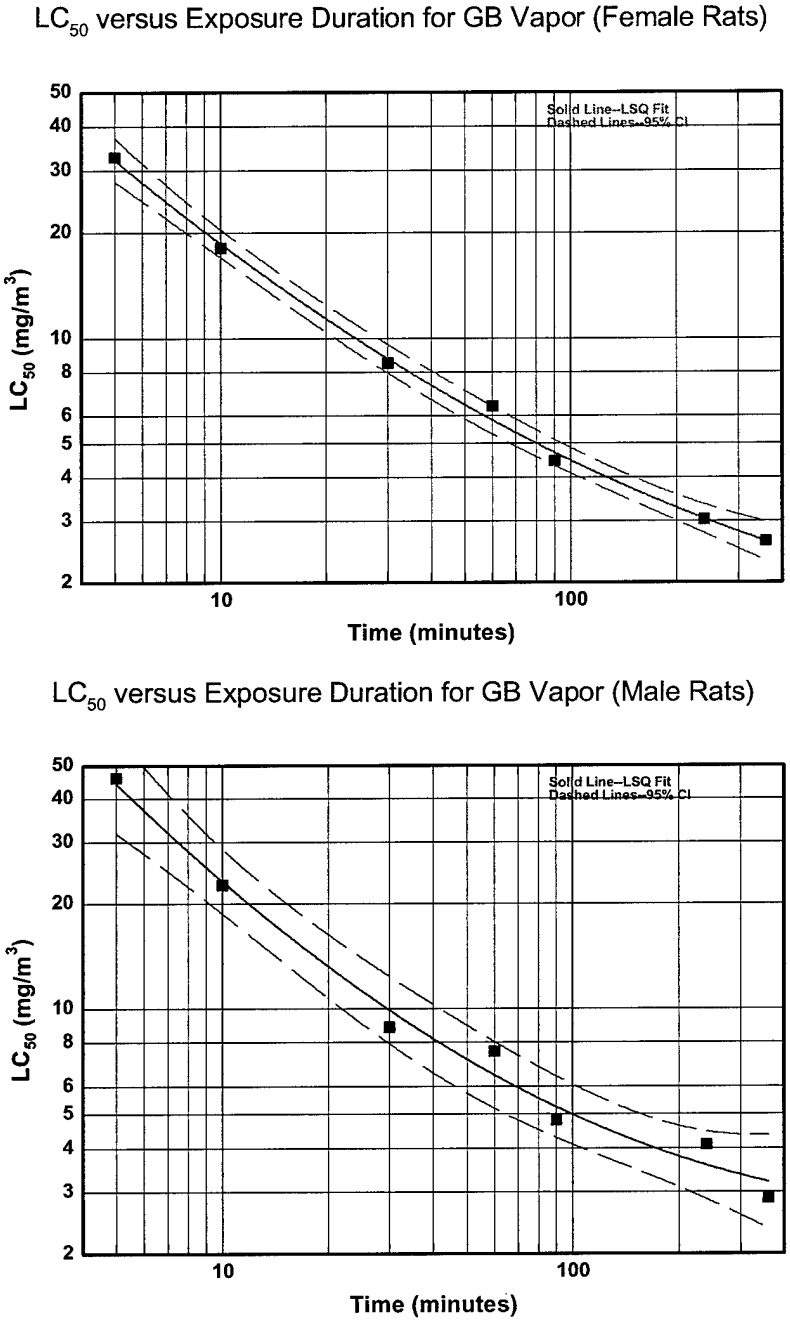

Figure 1. LC_{50} vs. Duration (minutes) of GB Vapor Exposure in Rats.

Pupil Responses to GB Vapor Exposure. Given that the exposure concentrations tested in this study were selected to optimize LC50 responses, it is not surprising that maximal miosis was seen in all exposed rats over the first 48-hrs post exposure. However, the marked and consistent reversal of this response progressing to a limited duration of mydriasis was not expected. Such responses are rarely, if ever, reported in the literature. Perhaps pupil effects were seldom monitored beyond the onset of miosis and the return to a pupil diameter within the pretreatment range. GB vapor-induced changes in pupil size of the present study are likely a local effect of GB on the eye. Presumably, GB exposure altered the balance between sympathetic vs. parasympathetic control over the pupil size, which changed over time following exposure. In proposing an explanation, it can be speculated that sometime during and following (within 48 hrs) exposure, the cholinergic component would likely predominate in the absence of AChE activity, resulting in miosis. At longer periods (4-6 days post exposure) cholinergic input would be desensitized thus leaving the noradrenergic component with predominant control resulting in mydriasis until the opposing mechanisms return to normal function and the balance is restored

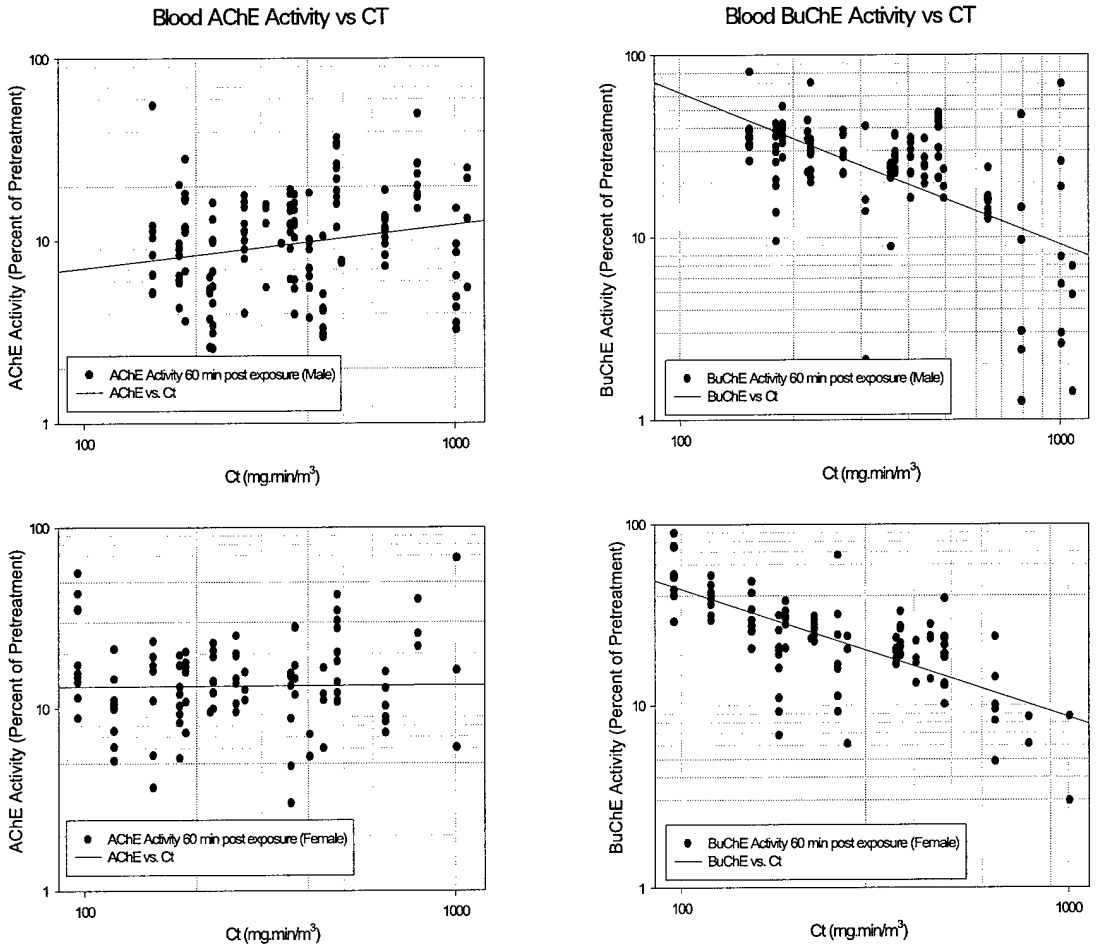

Figure 2. Blood AChE and BuChe (percent of pretreatment activity) vs. CT in GB vapor exposure (for 10, 30, 90 and 240 min exposures).

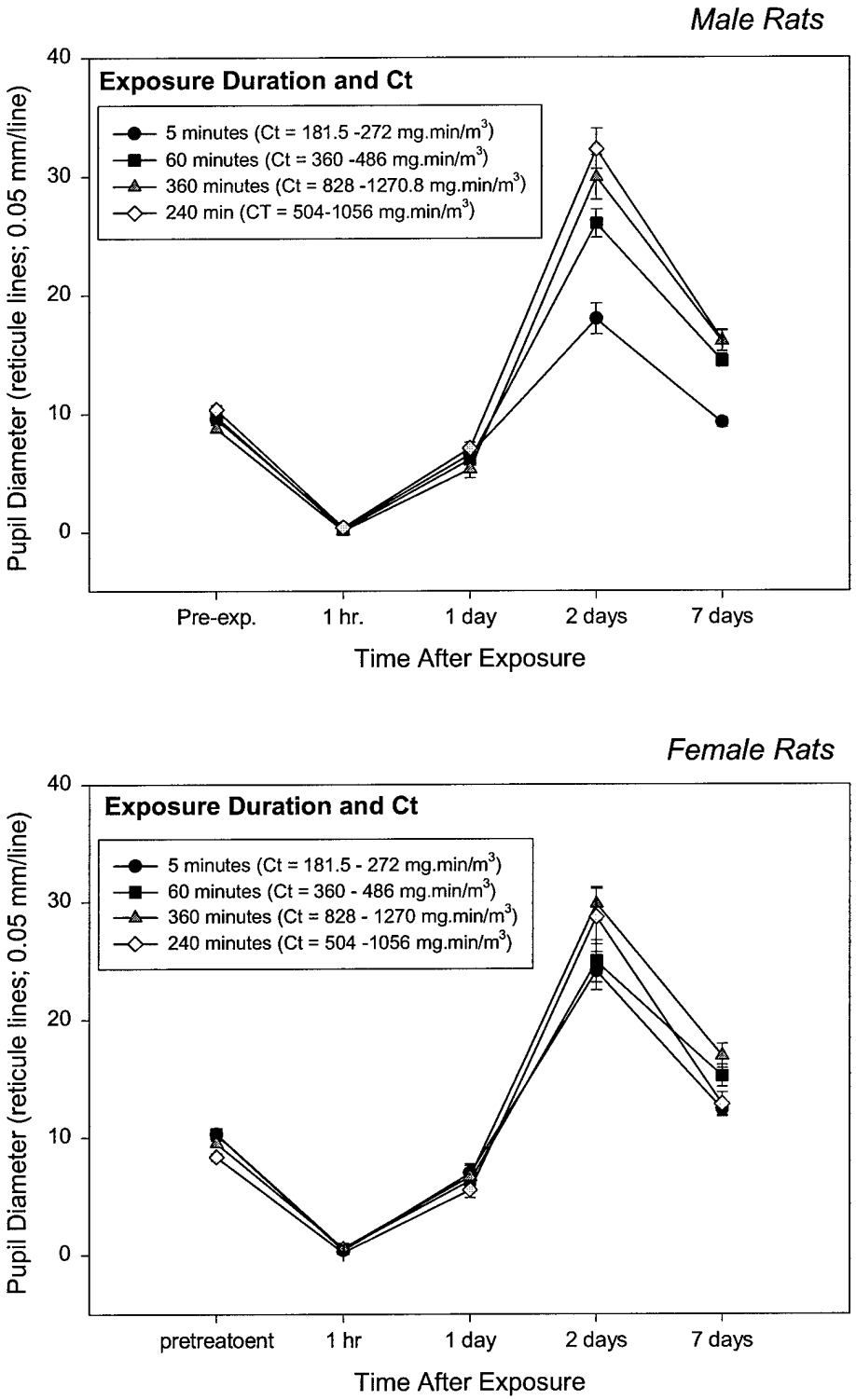

Figure 3. Effects of GB Vapor Exposure (240 min) on Pupil Diameter.

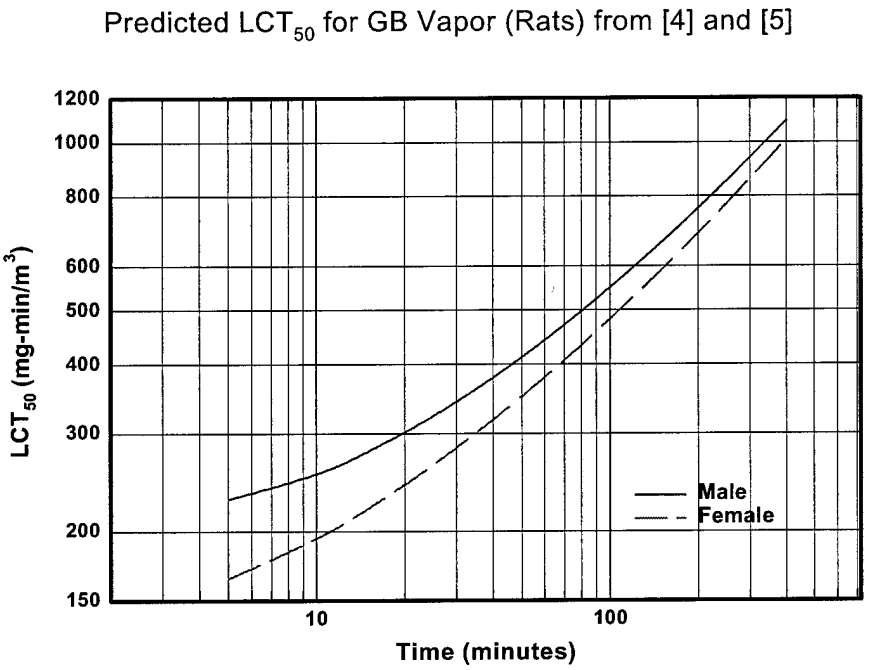

Figure 4. Predicted LCT_{50} versus Exposure Time.

CONCLUSIONS

This study examined the relationship between exposure concentration-time and lethal response in rats exposed to GB vapor. It was found that neither Haber's rule nor the toxic load model adequately explain the relationship between exposure conditions and probability of lethal response in the rat. An analysis of the randomized Part-II data led to the interaction model Y = b0 + b1* Log(C) + b2* Log (T) + b3* Log (C)*Log(T) as an extension of the toxic load model. Overall, female rats appeared to be more sensitive to GB vapor toxicity than male rats over the concentration and time range studied. Various sub-lethal clinical signs (miosis, salivation, tremors, convulsions, and blood cholinesterase activity) were also observed, but since the exposure conditions were optimized for lethality, effective concentrations (e.g., ECt_{50}) could not be determined. Miosis was maximal at all combinations of GB vapor concentration-time studied, and appeared to be the most sensitive clinical sign of GB exposure recorded. Miosis briefly progressed to mydriasis before returning to pupil sizes closer to the normal range. Although GB vapor exposure concentration (Ct) was correlated with the inhibition of blood cholinesterase activity, this correlation can not be used for estimating the level nor clinical severity of GB vapor exposure.

REFERENCES

Bliss, C.I., The method of probits, Science 79:38-39 (1934).

Callaway, S., and Blackburn, J.W., A comparative assessment of the vapour toxicities of GB, GD, GF, T.2132, T.2137 and T.2146 to male and female rats. PTP 404, CDE, Porton Down (1954).

Ellin, R. I., Anomalies in theories and therapy of intoxication by potent organophosphorus anticholinesterase compounds. Biomedical Laboratory Special Publication USABML –SP-81-003. APG, MD, April (1981).

Ellman, G. L., Courtney, K.D., Andres, V., Jr., and Featherstone, R.M., A new rapid colormetric determination of acetylcholinesterase activity. Biochem. Pharm. 7:88-95 (1961).

Finney, D.J. Probit Analysis. Third Edition, University Printing House, Cambridge, 1971).

Haber, F.R., Zur geschichte des gaskrieges. In *"Funf Vortrage aus Jahren 1920-1923"*, Spinger, Berlin (1924).

Koelle, G. B., Pharmacology of organophosphates, Journ. Appl. Toxicol. 14(2):105-109 (1994).

Larsen, R.I., Gardner, D.E., and Coffin, D.L., An air quality data analysis system for interrelating effects, standards and needed source reductions: part 5 (NO2 mortality in mice), Journal of the Air Pollution Control Association 29:133-137 (1979).

McPhail, M.K. Sex and the response to G agents. Suffield Technical Paper No. 38, (Unclassified Report) Suffield Experimental Station, Ralston Alberta, CA (1953).

MINITAB®, Version 13, Minitab Inc., State College, PA (1999).

Sidell, R. F.,"Clinical considerations in nerve agent intoxication," In Somani, S.M., ed., Chemical Warfare Agents, New York, NY: Academic Press (1992).

Sheets, L.P., Hamilton, B.F., Sangha, G.K., and Thyssen, J.H. Subchronic neurotoxicity screening studies with six organophophate insecticides: an assessment of behavior and morphology relative to cholinesterase inhibition. Fund. Appl. Toxicol. 35:101-119 (1997).

Sket, D., Efficacy of antidotes against soman poisoning in female physostigmine-protected rats. Pharmac. Toxicol. 72: 25-30 (1993).

ten Berge, W.F., Zwart, A., and Appelman, L.M., Concentration-time mortality response relationship of irritant and systemically acting vapours and gases. Journal of Hazardous Materials 13:301-309 (1986).

Witschi, H. Some notes on the history of Haber's law. Toxicological Sciences 50, 164-168 (1999).

Yee, E., A non-linear dose-response model with an application to the reconstruction of the human mortality response surface from acute inhalation toxicity with sarin. DRES-SM-1476 (unclassified report) (1996).

ANALYSIS OF RAT BLOOD SAMPLES FOR AGENT BIOMARKERS AFTER GB INHALATION EXPOSURE

E.M. Jakubowski, L.S. Heykamp,
EAI Corporation, 1308 Continental Dr, Suite J, Abingdon, MD 21009.

R.J. Mioduszewski, J. Manthei, D.C. Burnett, R. Way, B. Gaviola, W. Muse, J. Anthony, C. Crouse, H.D. Durst, S.A. Thomson
Research and Technology Directorate, U.S. Army ECBC, APG-EA, Edgewood, MD 21010.

ABSTRACT

A method was developed for the analysis of a GB nerve agent biomarker in blood that is very sensitive, selective, and applicable for archived samples. The biomarker resulting from sample acidification and in the presence of fluoride ion was regenerated GB (rGB) which was found in rat blood after inhalation exposures ranging from miosis to lethal levels. The method utilized a C18 solid-phase extraction (SPE) followed by quantification using a gas chromatograph with either a flame photometric detector (GC-FPD) or a mass spectrometer (GC-MS). Samples were concentrated by injecting the SPE extract on a Tenax -TA sorbent tube along with 100 pg of decadeuterated diethyl ethyl phosphonate as the internal standard followed by thermal desorption GC-FPD analysis and GC-MS confirmation. The method detection limit was 6 pg of agent and the working range was 20-200 pg GB on column. Quality control samples were analyzed and yielded spike recoveries greater than 95%.

INTRODUCTION

There is the need to be able to verify and model nerve agent exposure for medical, tactical, and political reasons. Current methods such as those based on cholinesterase activity are inadequate. Symptoms of exposure are not specific to the chemical warfare agents. Our objective was to find and/or develop analytical methods capable of quantifying low level nerve agent inhalation exposure in biological matrices such as blood and tissue using available instrumentation. The strategy to obtain the needed methods could be summarized in three steps which were: 1) Search the literature for potential methods, 2) Further develop methods as necessary, and 3) Validate using agent spiked matrices and inhalation exposure samples.

The literature search for nerve agent methods produced one very promising candidate method which served as a starting point. In this method, GB was regenerated from bound sites in the serum/plasma by relatively simple sample matrix manipulation followed by solid-phase cartridge extraction (Polhuijs et al. Toxicology and Applied Pharmacology 146, 156-161, 1997). This method served as a starting point. Modifications were made to the method in accordance with the instrumentation, standards, and objectives of our laboratory and research goals.

EXPERIMENTAL

MATERIALS

GB and VX were CASARM grade prepared and analyzed at ECBC and diluted with isopropyl alcohol or hexane. Decadeuderated diethyl ethylphosphonate ($^2H_{10}$DEEP)were synthesized at ECBC using an mixture of ethylphosphonic dichloride, Ethyl-$^2H_5$-alcohol, and N,N-diisopropylethylamine (Aldrich, Milwaukee, WI) in a 1:2:2 molar ratio, respectively, in acetonitrile, cold filtered to remove the resulting amine hydrochloride, and analyzed by GC-FPD and GC-MSD. The C_{18} SPE cartridges were 200mg and 500 mg (Waters Associates, Millipore Corp., Milford, MA) capacity. Acetate buffer

(pH3.5)was prepared from 5.41 mL glacial acetic acid and 0.4435 g sodium acetate diluted to 500 mL with deionized water. Potassium fluoride was ACS reagent grade (Aldrich, Milwaukee, WI) dilute with deionized water to approximately 2 M. All other chemicals were procured commercially at ACS reagent grade or higher.

SAMPLE PREPARATION

Serum (human, guinea pig, rat sera from Sigma, St.Louis, MO) was spiked with dilute GB or VX to 1 ug/mL. The exposed sera were filtered using 500 mg C_{18} SPE cartridges to separate the free from the bound nerve agent. The free agent was eluted with 1 mL ethyl acetate, collected over sodium sulfate and saved for analysis. The resulting positive control sera was then analyzed for regenerated agent using acetate buffer and fluoride ion. For inhalation exposure samples, whole blood from GB exposed rats was collected (with and without EDTA) and centrifuged at 15,000 rpm for 3 min. The resulting cell pack and serum/plasma was analyzed for regenerated agent by the addition of acetate buffer and fluoride ion. Archived sample from 1998 were in the form of packed cells. The sample preparation steps were as follows :

1) Weigh Sample (0.1-0.5 g)
2) Add and mix(vortex): 1.5 mL acetate buffer pH 3.5, and 0.02 mL(plasma) or 0.4 mL (packed cells) of KF solution.
3) For packed cell samples centrifuge 4000 rpm for 10 min,
4) Transfer liquid to conditioned C18 SPE column (conditioned with 1 mL isopropanol followed by 1 mL acetate buffer),
5) Elute with 1-1.5 mL ethyl acetate over sodium sulfate
5m) For miosis levels: concentrate ethyl acetate to ~100uL
6) Spike 0.010-0.200 mL ethyl acetate on DAAMS tube (Tenax-TA), and then spike tube with internal standard (100 pg of $^2H_{10}$-DEEP), flush with N_2 for 3 min at 75 cc/min
6m) For miosis levels:spike entire contents of vial and wash vial with 2x50uL of ethyl acetate adding wash to DAAMS tube

INSTRUMENTAL

Samples were analyzed on either a Hewlett-Packard 5890 GC-FPD (dual flame photometric detectors) or a Hewlett-Packard 6890 GC-5973 MSD (Newark, DE). Sample inlet was by Tenax® solid sorbent tube (Depot Area Agent Monitoring System (DAAMS) tube: Dynatherm Inc, Oxford, PA) using an ACEM 900 (Dynatherm Inc, Oxford, PA) desorber interfaced to the GC column via butt-connector. The GC column was a 30 m x 25 mm x 0.5 um thickness DB-5 MS (J&W Scientific, Avondale, CA). The ACEM 900 temperature program was as follows: Dry 60 °C for 1 minute, Tube Heat 200°C for 3minutes, Cool for 1minute, Trap Heat 275 °C for 3 minutes. The GC oven temperature program was as follows: Initial 40 °C for 2 minutes, ramp to 160 °C at 15 °C/minute, ramp to 260 °C at 40°C/minute and held for 3 minutes. The MSD was used in the electron ionization mode with selected ion monitoring at m/z 81, 99, 125. After the sample was desorbed on the GC column the sorbent tube was reconditioned by backflushing using 100 mL/min flow of dry nitrogen at 280-300 °C for five to eight minutes to decrease the high boiling point interference from the serum samples. Backflushing of the sorbent tube prevents degradation of the instrument and column producing a stable baseline despite the complex nature of the sample matrix.

RESULTS

The GC-FPD or MSD(EI) with Dynatherm inlet to allows injection volumes from 1-400 uL(above 200 uL in MS). Volumes above 200 uL tended to decrease FPD sensitivity but were useful for GC-MSD analysis in some cases. The working range was 20-200 pg GB on column. The method detection limit was 0.006 ng/mL for GB(FPD). Positive controls were developed for human, guinea pig, and rat blood cells and serum. The extraction efficiency was determined to be better than 90%. The optimum levels of fluoride needed for regeneration varied among species and types of sample (serum vs blood cell fraction). VX-G which could represent an interference was baseline resolved from GB as shown in Figure 1.

GB inhalation rat packed cell samples stored at 5°C for a year produced regenerated GB in the range of 1-10 ng/g with a mean of 4.88 ng/g and a standard deviation of 2.28 (n=38). Pre-exposure samples produced no GB. Immediately analyzed GB inhalation rat packed cell samples produced regenerated GB in the range of 2-36 ng/g with a mean of 18.6 ng/g and a standard deviation of 8.08 (n=48). Again, pre-exposure samples produced no GB. Serum samples that were analyzed soon after exposure produced regenerated GB in the range of 0.4-8 ng/g with a mean of 2.0 and standard deviation of 1.7 (n=11). Packed cell concentrations of regenerated GB were typically greater than serum/plasma levels at the higher Ct exposures, as shown in Figure 2

The mean percent GB standard spike recovery [(Found GB/Target level)100] was 98.3 +/- 11.2% (n=10). The mean percent GB standard matrix spike recovery (on-tube spikes) mean was 97.3 +/-7.44% (n=6). In general, regenerated GB levels in serum were lower than the cell fraction. Also, preliminary data from LCt50 level exposures indicated that female rats produce higher initial blood levels of regenerated GB than males depending on exposure level. However, after 14 days male and female levels appear similar, Figure 3.

DISCUSSION

The results indicate that GB can be verified from blood and tissue samples using GC-FPD or GC-MSD. In LCt50 experiments, recovered quantities of GB in samples from the cell fraction consistently exceeded by a factor of four or more those seen in the serum/plasma. This is possibly due to the presence of other binding sites such as carboxyesterases or possibly non-esterase related sites. Miosis level samples showed relative amounts of GB were greater in plasma/serum then packed red cells by a factor of six. Overall, there appears to be a better relationship between Ct and rGB concentration than Ct and cholinesterase activity given the data analyzed, Figures 4 and 5.

CONCLUSIONS

Methods for the quantification of low-level chemical nerve agent biomarkers after inhalation exposure has been developed that will allow exposure verification and blood/tissue concentration to be determined. The advantages are simplicity and speed of analysis, the ability to look at archived samples for evidence of exposure, applicability to all G and V agents, detection limits lower than miosis level exposure, and yield more information than cholinesterase-based metrics. The major disadvantage is that the original leaving group of the agent is not known but this is also true in the case of using agent metabolites as indicators of exposure.

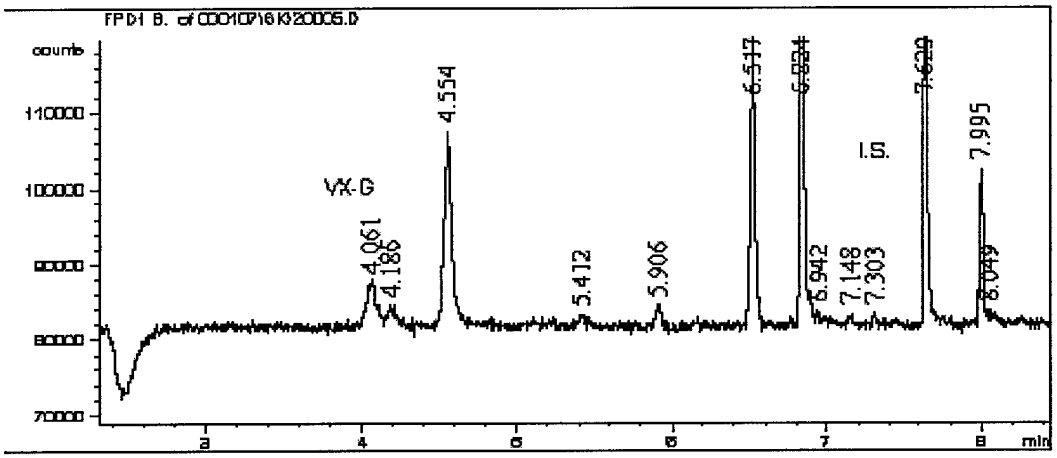

Figure 1. Chromatogram of VX-G(4.039 min) Spiked GB(4.535 min) Sample.

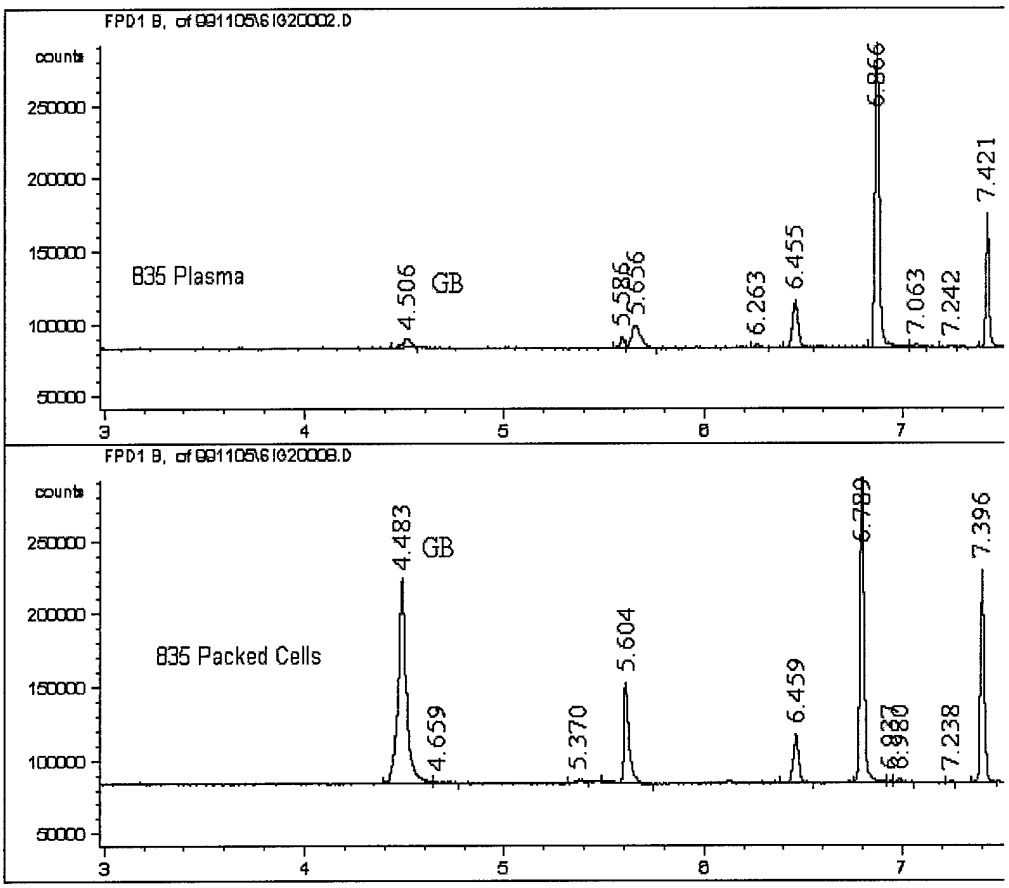

Figure 2. Chromatograms Comparing Response for GB in Plasma and Packed Cell Samples (Ct=1076mg min/m^3).

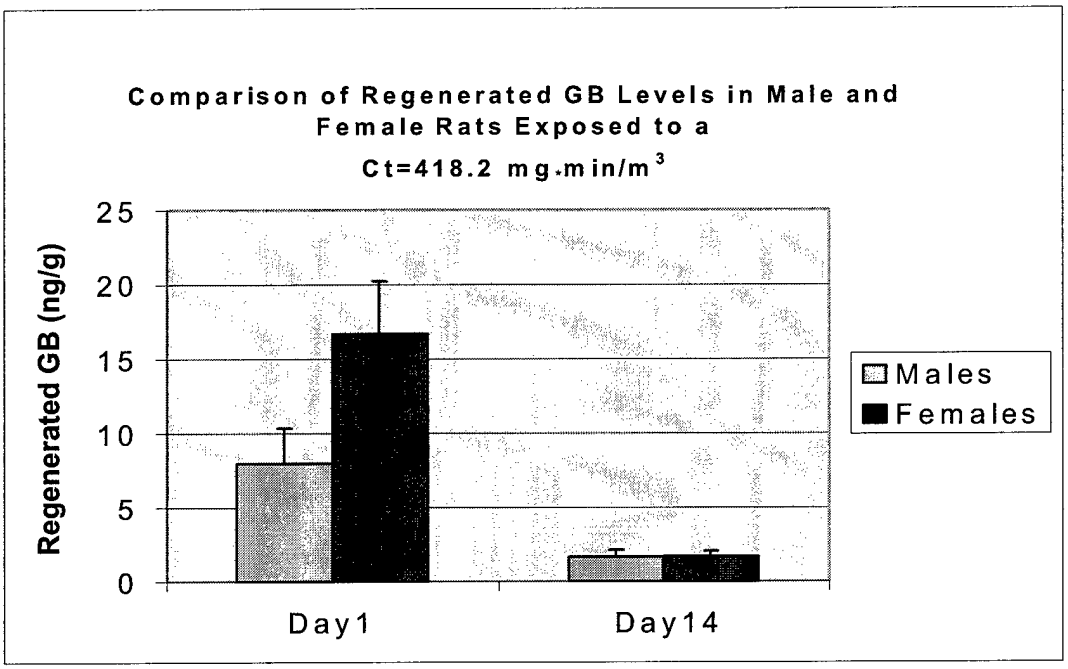

Figure 3. Comparison of GB Levels (6 hr test, Ct=418.2 mg min/m3): Day 1 *vs* Day 14.

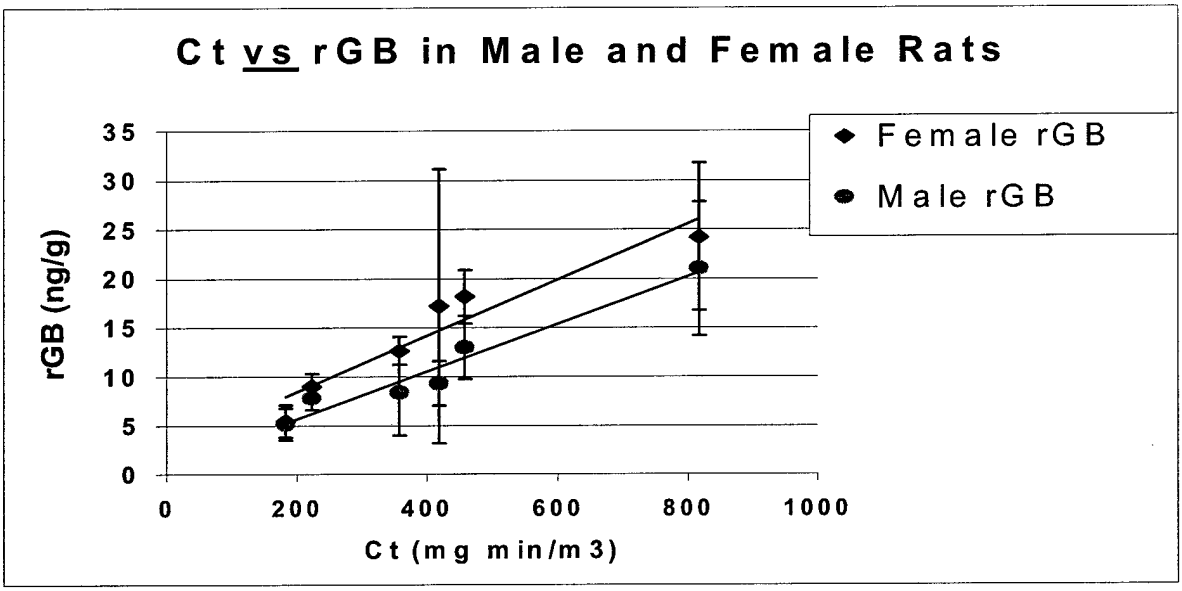

Figure 4. Ct versus rGB in male and female rats after inhalation exposure.

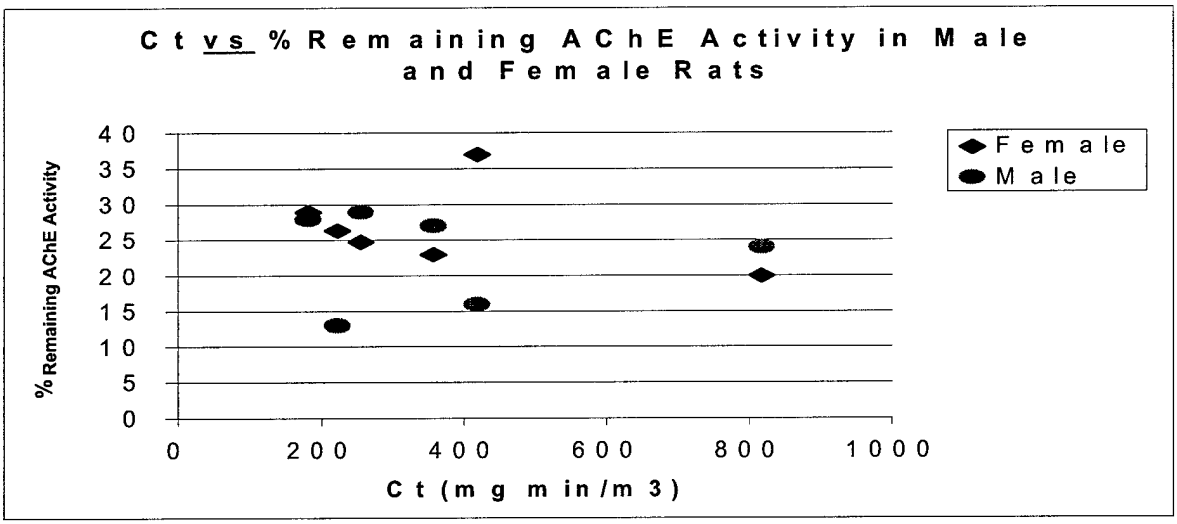

Figure 5. Ct versus AchE activity in male and female rats after inhalation exposure.

NOVEL PHOTOCATALYSTS AND PROCESSES FOR THE DESTRUCTION OF CHEMICAL WARFARE AGENTS (CWA)

Panagiotis G. Smirniotis
Department of Chemical Engineering, University of Cincinnati, Cincinnati, OH 45221-0171

ABSTRACT

The present research project aims at developing novel photocatalysts for the destruction of chemical warfare agents to innocuous products in gas and liquid phases. The project focuses on understanding the chemistry involved during photodegradation of selected simulants, which can effectively represent chemical warfare agents such as HD, G-type (GA, GB, GD) and VX. Studies addressing the destruction of toxic organics found in other military activities (solvents, purification centers, etc.) will be performed as well. The project combines the synthesis and characterization of novel catalysts, catalytic evaluations with probe molecules and kinetic studies to understand the lability of certain bonds (C-S, C-P, P=O, etc..). Moreover, the project focuses on the development of effective slurry and gas phase reactors including "closed cycle" systems, photocatalysts, which operate with visible/solar radiation and finally use of novel processes such as ultrasound to enhance the photochemical transformation and avoid formation of any toxic intermediates.

This paper describes the initial work and research tasks undertaken for testing selected categories of photocatalysts for destruction of organics and CWA simulants, utilization of ultrasound for enhancement of reactant transformation and elimination of byproducts, and development of photocatalysts for operation with visible light. More specifically, we present the initial work we performed on the photodegradation of diethylsulfide (DES) in gas phase (C_2H_5-S-C_2H_5) as a simulant of mustard gas (HD) over various titanias utilizing UV light. The main routes of DES degradation are C-S cleavage, S oxidation, α-C and β-C oxidation were revealed. The liquid phase photodegradation of organics in the presence of ultrasound aiming at the enhancement of catalyst reactivity and elimination of any byproducts was studied as well. Effective photocatalysts for operation with visible light were synthesized based on transition metal substituted and loaded MCM-41. Extensive work is being performed involving the use of the above approaches for CWA simulants such as diethylsulfide, 2-chloro ethyl-ethyl-sulfide ($Cl(CH_2)_2SCH_2CH_3$) and dimethyl-methyl-phosphonate (DMMP).

INTRODUCTION

Over the last decade, numerous studies have been performed aiming at the development of novel technologies for the successful and economic destruction of CWAs to benign products. In view of the seriousness of the problem, the National Research Council (NRC) recommended a new research program [1] to address the chemical neutralization and biodegradation of CWAs. Since then, several attempts combining different methods have been performed. The existing state-of-the-art on this subject has been reviewed in detail by Yang and coworkers [2, 3].

The present research project is a multiyear effort and aims at developing novel photocatalysts, reactors and processes for the destruction of chemical warfare agents to innocuous products in gas and liquid phases. The project focuses on understanding the chemistry involved during photodegradation of selected probe molecules which can effectively represent chemical warfare agents such as HD, G-type (GA, GB, GD) and VX. The project combines the synthesis and characterization of novel catalysts, catalytic evaluations with probe molecules and kinetic studies to understand the lability of certain bonds (C-S, C-P, P=O, etc..). Moreover, the project focuses on the development of highly

effective slurry and gas phase reactors including "closed cycle" systems, photocatalysts, which operate with visible/solar radiation and finally use of novel processes such as ultrasound to enhance the photochemical transformation and avoid formation of any toxic intermediates. This paper describes the initial work and research tasks undertaken for testing selected categories of photocatalysts for destruction of CWA simulants, utilization of ultrasound for enhancement of reactant transformation and elimination of byproducts, and development of photocatalysts for operation with visible light.

EXPERIMENTAL

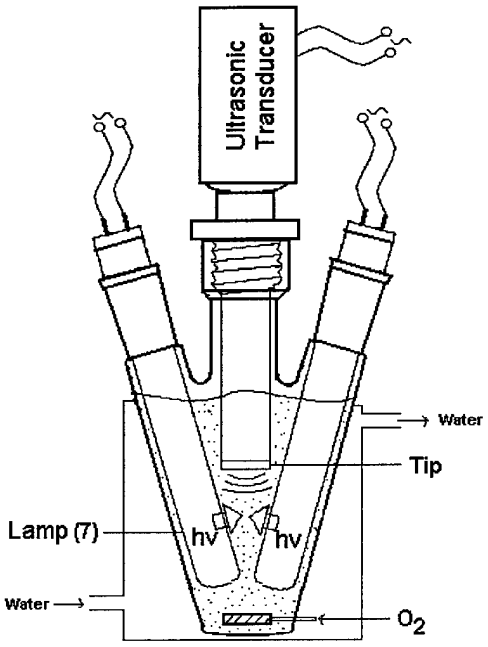

Figure 1. Sonophotocatalytic reactor for the degradation of organics.

Preliminary photocatalytic experiments were performed using four different samples of titanium dioxide: Hombikat UV 100 (Sachtleben Chemie GmbH), Degussa P25 with 50 m^2/g, Degussa P25 with 75 m^2/g, and homemade TiO_2. Diethyl sulfide (Fluka) as a simulant of HD and deionized water were used. Photocatalytic degradation of diethyl sulfide over a thin film of photocatalysts was accomplished in a flow reactor. The set up used in this study has been described in detail in our earlier work [4]. The reactor was a stainless steel cylindrical vessel illuminated through a Pyrex window placed on the top of the reactor. Two types of light sources were employed to illuminate the catalyst: two 4 W fluorescent lamps (Wiko, Japan) and 450 W mercury lamp (Hanovia). This type of experiments constitutes the initiation of research for understanding the kinetic pathways for the destruction of HD simulants in gas and liquid phases. The first results are described in [5]. Additional work involving CWA simulants such as diethyl-sulfide (DES) and dimethyl-methyl –phosphonate (DMMP) in liquid phase is being performed [6].

The photocatalytic activity of the selected titania powders was evaluated using salicylic acid in oxygenated aqueous suspensions in order to test the effect of ultrasound. Salicylic acid (Fisher) and titania used in the study were of reagent grade. Photocatalytic experiments were performed in a custom-made ultrasonic reactor presented in Figure 1, which contained seven pyrex immersion wells hosting the UV lamps. The reactor consisted of a working volume of 1 L and was surrounded by a glass jacket to allow circulation of cooling water to maintain the reaction temperature at 30±2°C. Seven UV-irradiated black light fluorescent lamps (4 W each) with a peak intensity at 375 nm were used and were placed inside the pyrex immersion wells (cutoff wavelength 320 nm). The agitating action of a stirrer and ultrasound assured adequate mixing of the suspension of titania particles inside the reactor. The ultrasonic tip (1x7 cm) delivered 100 W of ultrasound into the reaction space at the frequency of 20 kHz. Pure oxygen gas (Wright Brothers, 99.5%) was sparged through the vessel utilizing a stainless steel bubbler at a rate of 500 cm^3/min. The experiments involving CWA simulants and ultrasound are being performed and very promising results are collected [6].

Transition metal substituted MCM-41 supports with Si/Me=80 and Si/Ti=40 were synthesized using Ludox HS-40 (DuPont) as the source of silica. The precursors used for the incorporation of transition metal oxides in the framework of MCM-41 were vanadia: $VO(C_3H_7O)_3$ (Alfa); chromia: $CrCl_3$ (Fisher); iron (III) oxide: $Fe_2(SO_4)_3$ (Fisher); titania: titanium isopropoxide (Aldrich). All samples were prepared in the presence of hexadecyltrimethylammonium bromide (Fluka) as a template. The final mixtures were stirred together for 30 minutes, then transferred into polypropylene

bottle and treated under autogenous pressure without stirring at 90 - 100°C for 3 days. The resulting solids were filtered, washed, dried, and calcined at 550°C for 10 hours under air flow. The support (typicaly 1.5 g) was dispersed in ~100 ml of isopropanol, and titanium isopropoxide was added to achieve 25 % loading. The system was dried while stirring at ambient temperature. It was then placed in the oven to dry at 100°C for 1 hour and later were calcined at 450°C for 3 hours.

The photocatalytic testing included the degradation of organic compounds, which was performed in a batch round flat-plate reactor using 200 W medium pressure mercury lamp (Ace Glass) as the light source. A 0.25" thick plexiglas filter was utilized for the purpose of excluding ultraviolet radiation when conducting visible-light experiments. Several reactants were tested for the photocatalytic degradation: 2,4,6-trichlorophenol (Fisher), chlorophenol (Aldrich), formic acid (Fisher).

RESULTS AND DISCUSSION

No dark reaction of DES degradation was detected over all catalysts studied at room temperature. The second type of blank experiment was carried out in order to check the possibility of photochemical transformation of diethyl sulfide under the light. No conversion of diethyl sulfide was

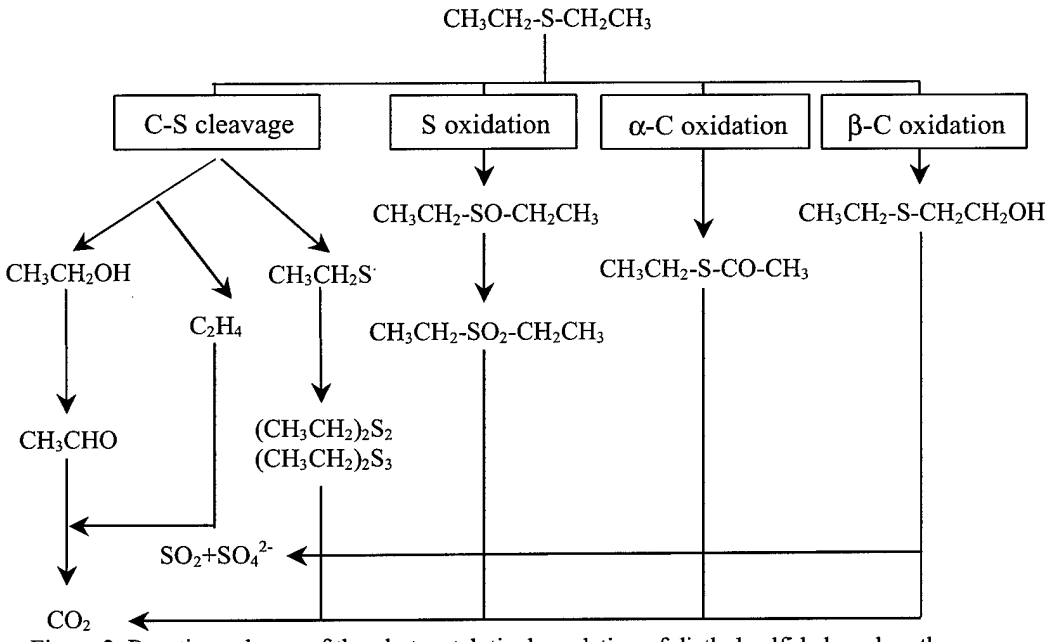

Figure 2. Reaction scheme of the photocatalytic degradation of diethyl sulfide based on the products detected.

detected during this test at air humidity 25% (21°C). Hence, only heterogeneous photocatalytic processes cause all the transformation of diethyl sulfide over TiO_2 under ultraviolet light in the system applied. Switching on the lamps of the reactor initially led to high initial conversion of diethyl sulfide (up to 90%). Photocatalytic destruction of diethyl sulfide resulted in the formation of the same gaseous products in different proportions over all catalysts tested in the current work. Gaseous products comprised ethylene, carbon dioxide, acetaldehyde, ethanol, sulfur dioxide, S-ethyl ethanethioate, and diethyl disulfide. The extract in isopropanol from the surface of TiO_2 Hombikat UV 100 operated during 23 hours at humidity 19% and temperature 26°C in diethyl sulfide destruction contained the following products: diethyl sulfoxide and smaller quantities of diethyl disulfide, diethyl sulfone, 2-ethylthioethanol, and diethyl trisulfide. Acid products and salts (such as sulfates), which are produced at the final stage of the oxidation of sulfur in diethyl sulfide were not detected because of their extremely low volatility. Only diethyl disulfide was detected in both gaseous and surface products. Other products distributed between gas and surface according to their volatility.

On the basis of the set of detected products it is possible to derive conclusions about the routes of diethyl sulfide destruction (Fig. 2).

Such products as ethanol and ethylene clearly testify to the contribution of C-S bond cleavage (corresponding branches in Fig. 2). The cleavage can be deemed to proceed through hydrolysis to form ethanol and rearrangement to form ethylene. However, the intermediate product of hydrolysis (ethylthiol) was not detected in the products. This may be related to the high lability of this intermediate at the reaction conditions. Dimerization of surface $CH_3CH_2S^{\bullet}$ species results in diethyl disulfide. Further C-S bond cleavage in this disulfide and interaction of $CH_3CH_2SS^{\bullet}$ and $CH_3CH_2S^{\bullet}$ surface species can explain the formation of diethyl trisulfide. It should be noted that although diethyl disulfide was present in the initial diethyl sulfide feed, its concentration in the reactor effluent was well beyond its initial concentration, especially in experiments with high light intensity (as will be shown later in the study).

The second obvious route of diethyl sulfide photocatalytic destruction is the oxidation of sulfur atom. The products of this oxidation pathway (sulfoxide and sulfone) resided on the surface of catalyst, where they could be further oxidized leading to the formation of inorganic compounds. The third route is the oxidation of the α-carbon, which resulted in the formation of low concentrations of CH_3CH_2-S-CO-CH_3 in the gas phase. Such route was also present in the photocatalytic degradation of the oxygen analog of diethyl sulfide, diethyl ether, and led to the formation of ethylacetate [7]. The last route of diethyl sulfide photocatalytic oxidation is the oxidation of the β-carbon. Small quantities of $CH_3CH_2SCH_2CH_2OH$ were detected on the surface of catalyst, which signifies the presence of this fourth route of degradation. The proposed above four routes of the photocatalytic destruction of diethyl sulfide represent only initial stages of transformation. During further deeper reaction, these routes can intersect each other. For example, after oxidation of β-carbon the oxidation of sulfur could take place. Finally, the photocatalytic oxidation results in inorganic oxides, H_2O, CO_2, and SO_2.

The phenomena of cavitation *i.e.* the nucleation, growth and collapse of bubbles in a liquid are due to the chemical effects of ultrasound [8, 9, 10]. The collapse of the bubbles induces localized supercritical conditions: high temperature, high pressure, and electrical discharge effects. The consequences of these extreme conditions are the cleavage of dioxygen molecules and water molecules forming $H^{\bullet}$ and $^{\bullet}OH$ radicals. From the reactions of these entities ($O^{\bullet}$, $H^{\bullet}$, $^{\bullet}OH$) with each other and with H_2O and $^{\bullet}O_2^-$, $HO_2^{\bullet}$ radicals and H_2O_2 are formed. Therefore, the combination of photocatalytic and ultrasonic irradiation can enhance the degradation of organic pollutants in water by the species, notably $^{\bullet}OH$ radicals.

$$H_2O \xrightarrow{))))} H^{\bullet} + {}^{\bullet}OH \qquad (1)$$

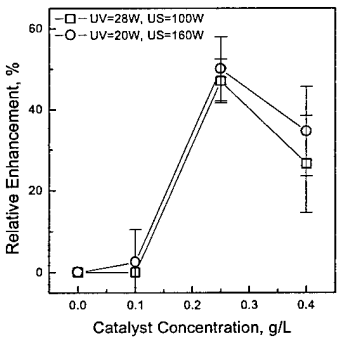

Figure 3. Enhancement by ultrasound for Hombikat UV 100.

The photodegradation of salicylic acid was employed to test the simultaneous effect of photodestruction and sonication [11]. Salicylic acid was the probe molecule we used originally, but currently we are studying selected CW simulants [6]. With salicylic acid we found that ultrasound augments the chemical transformation. More specifically, we found that the use of ultrasound eliminates the organic byproducts, something which is unique for the effective destruction of organics since organic byproducts resulting during the photodegradation can be equally toxic with the reactants themselves.

Now let us study the effect of the catalyst mass by comparing the behavior of HK at 0.1, 0.25, and 0.4 g/L concentration. As expected, the conversion after 3 hours is the greatest for the larger concentration of the catalyst and the smallest for the smallest concentration of the catalyst. For some systems (as described in [14]) the reaction rate decreases with the increase in the catalyst concentration after a certain threshold value. However, we observed that this threshold value of

catalyst concentration has not been achieved for the system HK/salicylic acid, since the rate increases monotonically in the sequence 0.1, 0.25, and 0.4 g/L of titania with and without the ultrasound. Moreover, comparing the enhancement of the reaction rate (defined as the absolute difference between the two reaction rates divided by the rate of photocatalysis alone) imparted by the presence of ultrasound reveals a different trend (Figure 3).

The enhancement is negligible for the low concentration of the catalyst (see Figure 2a). This is due to the insufficient number of centers of bubble disruption in the solution since the presence of solids significantly enhances this process [12]. As a result, the ultrasound passes through the slurry without imparting energy into it and with little formation of active radicals. On the other hand, relatively low concentrations of solids usually correspond to smaller aggregate sizes [13], which are more difficult to break in order to expose more surface area to the light. The enhancement of the activity is the largest for the intermediate concentrations of titania (0.25 g/L) as shown in Figure 3. This is a combined effect of the full attenuation of light [14], aggregate breakage by ultrasound due to the action of its shear stress, and generation of radicals by the ultrasound itself upon impingement onto solid particles. The low value of enhancement by ultrasound for higher concentrated suspensions can be explained by the fact that the working volume of the slurry becomes low [15]. Indeed, from the high values of the extinction coefficients one cannot expect the light to penetrate far into such an optically dense medium. As a result, there is no enhancement due to aggregate breakage, as the zone of action of light is far away from the zone of action of ultrasound. Therefore, one has to use higher ultrasound power and less attenuating powders to achieve adequate enhancement of photocatalytic activity in highly concentrated suspensions.

Photocatalysts for the operation in visible light (potential utilization of solar radiation) are employed. We have initiated an effort in this direction and our original results utilizing simple organic probe molecules are very promising [16]. Our catalysts are based on a methodology we developed to synthesize transition metal incorporated MCM-41 molecular sieves loaded with titania. Ongoing research in our labs focuses on testing the most effective photocatalysts for the destruction of CWA simulants utiliziang visible light. The time course of the photodegradation of formic acid on visible-light irradiated catalysts is shown in Figure 4.

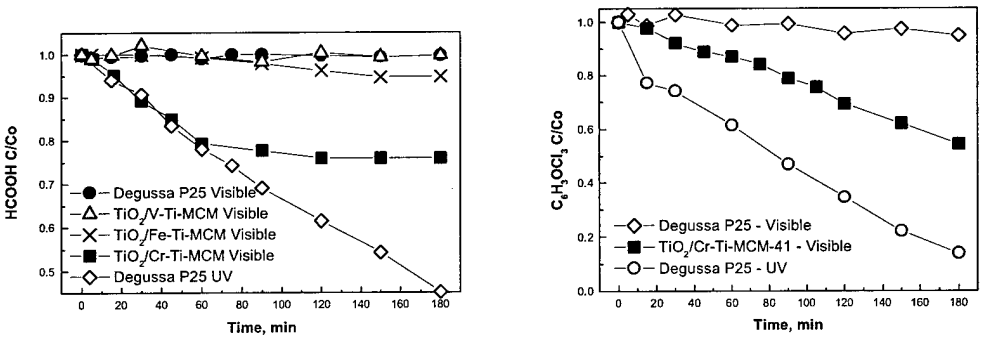

Figure 4. Time course of the photodegradation of formic acid (left) and 2,4,6-trichlorophenol (right) in visible light on transition metal substituted titania loaded MCM-41 materials.

Non-reduced (as calcined) chromium substituted MCM-41 with loaded titania did exhibit activity comparable with that of Degussa P25 in UV (Fig. 4). For the TiO_2/Cr-Ti-MCM-41 the concentration of formic acid decreases steadily for about 60 min, then levels off at approximately 25 % of conversion. This behavior is unexpected, since from a physics point of view the altervalent cations (especially with the oxidation state of +5) would serve best as dopants [17], but we will see later that the primary doping species in the above catalysts is Cr^{+6}. Iron substituted MCM-41 sieves loaded with titania also exhibit some photoactivity (Fig. 4). The concentration of formic acid monotonically decreases and levels off at about 6 % of conversion, which was proved in three independent experiments. The maximum degradation rate is considerably lower than that of neat titania (P25) in UV. Such behavior can be explained on the basis of the structure of neat Fe-Ti-MCM-41. The activity

of TiO_2/V-Ti-MCM-41 was also explored under identical operation conditions (Fig. 4). However, no discernible conversion of formic acid under visible light was detected.

The performance of the most active catalyst (TiO_2/Cr-Ti-MCM-41) was also tested for the photodegradation of phenolic compounds in visible light. As seen from Fig. 4, the above specimen exhibits photoactivity to decompose 2,4,6-trichlorophenol. This is also the case for 4-chlorophenol (not shown). The activity for the degradation of these reactants in visible light is not as high as that of Degussa P25 in UV. As in the case of Degussa P25, the activity acquires lower values with the smaller number of chlorine atoms in the reactant molecule, primarily due to the lesser generation of secondary active chlorine radicals [18]. No deactivation is observed for the above two reactions in visible light, contrary to the photodegradation of formic acid. Apparently, the chlorine atoms help to re-activate the catalyst.

In order to explain the general trend in the activity of the catalysts employed in visible light, one may note that the lowest activity (close to zero) was exhibited by the V-Ti-MCM-41 based powder. It should be noted that the oxidation state of five is the most stable for vanadium at ambient conditions. Furthermore, its transformation into other oxidation states in aqueous solution is very unlikely. This is the primary reason for low activity. This is because no effect of doping took place. Indeed, considering the absorption spectrum of V-doped catalysts (not shown) reveals that they lack shoulders corresponding to dopant levels. As a result, the sublevel allowing for double photon excitation is not observed. Such double step excitation would promote the electron to the conduction band of titania by the absorption of two low-energy quanta in visible range. On the contrary, the most active catalysts (TiO_2/Cr-Ti-MCM-41 and to a much lesser extent TiO_2/Fe-Ti-MCM-41) have two stable oxidation states (Cr^{+3} and Cr^{+6}, Fe^{+2} and Fe^{+3}) both of which are found inside and outside the framework of MCM-41, which was also shown by our own XPS results. Only ions that are in the framework can act as dopants for titania, as they are atomically dispersed, unlike bulk oxides outside the framework. Furthermore, in our materials we have two types of heterojunctions: framework ions (V, Cr, or Fe)–titania and extra-framework metal oxide-titania. The first type allows to excite the photocatalyst by absorbing two photons in the visible part of the spectrum (reaction 2). The second type can consume the trapped electrons produced by the doped titania, wherein the dopant is represented by the transition metal ions in the framework (reaction 3). Finally, the free hole reacts with the aqueous medium to form active radicals (reaction 4):

$$MeTiO_x \rightarrow h^+ + e^- \text{ (trapped)} \quad (2)$$

$$e^-\text{(trapped)} + MeO_x \rightarrow MeO_{x-0.5} \quad (3)$$

$$h^+ + OH^- \rightarrow \bullet OH \quad (4)$$

where Me is the transition metal employed.

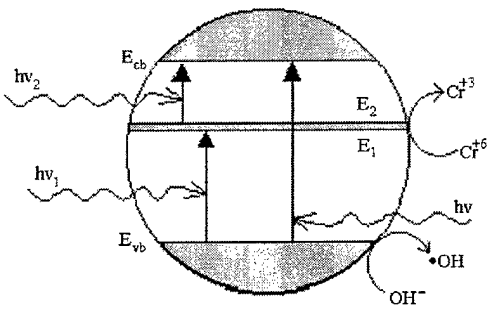

Figure 5. Mechanism of the photodegradation on transition metal substituted MCM-41.

The trapping of electrons and holes by the dopant was detected in doped titania [19]. This phenomenon is deleterious for the photocatalytic activity. However, we propose that the presence of a reducible oxide (for example, CrO_3) in close proximity allows to scavenge the trapped electrons (as shown in Fig. 5). For the case of chromium substituted MCM-41, such oxide was detected by our own XPS studies. As the result, the extra-framework transition metal oxide attains the lower oxidations state (for example, extra-framework CrO_3 becomes Cr_2O_3). At the same time, the valence band holes of titania become available to oxidize water and produce hydroxyl radicals (reaction 4), which constitute the major oxidant in aqueous heterogeneous photocatalysis. The maximum activity obeys the following pattern: Cr > Fe >> V. This clearly corresponds to the difference in the number of electrons between the two stable oxidation states of each transition metal. It is three for chromium and one for iron.

CONCLUSIONS

The distribution of diethylsulfide products strongly suggests that the two main pathways of the degradation are the oxidation of sulfur and carbon atoms and hydrolysis of the C-S bond. The products of the complete oxidation (SO_2 and CO_2) were detected in very small quantities, most of the products correspond to C-S bond cleavage and partial oxidation. Further efforts should be devoted to make photocatalytic oxidation suitable for the complete mineralization of reduced sulfur compounds. Other CWA simulants are being tested by using simultaneously photocatalysis and somication aiming at rapid destruction of the reqctants and complete elimination of organic byproducts.

Several transition metal based titania loaded MCM-41 (Si/Me=80, titania content – 25 wt%) materials were tested for the degradation of organics in visible light. The chromium substituted MCM-41 was found to serve as the best support for titania to achieve the highest degradation rates of formic acid, 2,4,6-trichlorophenol, and 4-chlorophenol. The change in the state of the catalyst during the reaction was observed for Cr substituted molecular sieves, which led to its deactivation. XPS revealed increased surface concentrations of Cr ions upon the loading of TiO_2, which at the same time allows to minimize the leaching of chromium ions. The mechanism of the photodegradation in visible light on titania loaded transition metal substituted MCM-41 is proposed. It consists of double step excitation by visible light, as opposed to conventional single step excitation by UV light

ACKNOWLEDGEMENTS

The authors wish to thank the following agencies for their finantial support: DoA (40414/CH/YIP), NRC (COBASE), and NATO (SfP-974209).

REFERENCES

1. NRC: Recommendations for Disposal of Chemical Agents and Munitions, *National Acad. Press.*, Washington, DC, 1994
2. Yang, Y.C., Baker, J.A., and Ward, J.R., *Chem.Rev.*, **92**, 1729 (1992)
3. Yang, Y.C., *Chem.&Ind.*, 334 (1995)
4. A.V.Vorontsov, E.N.Savinov, P.G.Smirniotis, *Chem. Eng. Sci.*, **55** (2000) 5089.
5. A.V.Vorontsov, E.N.Savinov, L. Davydov, and P.G.Smirniotis, *Appl.Catal. B:Env.*, in press (2001)
6. L.Davydov, E.P.Reddy, and P.G.Smirniotis, *US Patent Appication.*, to be submitted April 2001
7. A.V.Vorontsov, E.N.Savinov, G.B.Barannik , V.N.Troitsky and V.N.Parmon, *Catalysis Today*, **39** (1997) 207.
8. H.G. Flynn, in *Physical Acoustics,* ed. W.P. Mason, Acad. Press, New York, 1964, vol. 1, pp. 58
9. A.J. Walton, and G.T. Reynolds, *Adv. Phys.*, **33** (1984) 595
10. I. Hua, R.H. Hoechemer, and M. R. Hoffmann, *J. Phys. Chem.*, **99** (1995) 2335
11. L.Davydov, E.P.Reddy, and P.G.Smirniotis, *Appl.Catal.B:Env.*, in press (2001)
12. L. Thompson and P. Doraiswamy, *Ind.Eng.Chem.Res.*, **38** (1999) 1215
13. S. Friedlander in *Smoke, Dust and Haze,* Wiley and Sons Press, 1969
14. L. Davydov, P.G. Smirniotis, and S.E. Pratsinis, *Ind. Eng. Chem. Res.*, **38** (1999) 1376
15. G. Heit, and A.M. Braun, *Wat. Sci. Tech.*, **35** (1997) 25
16. L. Davydov, E.P.Reddy, P.France, and P.G.Smirniotis, *J.Catal.*, submitted (2001)
17. Karakitsou, K.E. and Verykios, X.E., *J.Phys.Chem.*, **97**, 1184 (1993)
18. Hoffmann, M.R., Hua, I., and Hochemer, R., *Ultrason. Sonochem.*, **3**, S163 (1996)
19. Hoffmann, M.R., Martin, S.T., Choi, W., and Bahnemann, D.W., *Chem.Rev.*, **95**, 69 (1995)

DECONTAMINATION AND DETOXIFICATION WITH SPONGES

Richard K. Gordon[†], Shawn R. Feaster, Alper T. Gunduz, and Bhupendra P. Doctor
Division of Biochemistry, Walter Reed Army Institute of Research,
503 Robert Grant Road, Silver Spring, MD 20910-7500

David E. Lenz, Donald M. Maxwell, Rudy C. Macalalag, Edward D. Clarkson, and John P. Skvorak
United States Army Medical Research Institute of Chemical Defense,
Aberdeen Proving Ground, MD 21010

Michelle C. Ross
Defense Threat Reduction Agency/CB, Washington, DC 20301-3050

ABSTRACT

One of the serious problems that may be encountered while caring for personnel contaminated with organophosphate (OP) chemical warfare nerve agents is the possibility that there will be cross-contamination to the medical personnel. Secondly, during combat or terrorist acts, individuals might be exposed to chemical toxins before they don their protective gear. Therefore, we have attempted to develop an enzyme immobilized polyurethane foam which can effectively decontaminate the skin and other such exposed surfaces of the organophosphate toxins. Antidotal therapy using cholinesterases (ChE) to scavenge the toxicity caused by OP chemical toxins is an effective parenteral pretreatment in animals against a variety of OP compounds. To continuously detoxify OPs, the ChE is combined with an oxime so that the catalytic activity of OP-inhibited ChE is continuously restored. In addition to this *in vivo* antidotal therapy, the *in vitro* reactivation of OP-inhibited ChEs by oximes also has important applications for the decontamination of skin. We have demonstrated the rapid *in-situ* copolymerization of ChEs at room temperature, and that ChE-sponges exhibit high activity and stability. In addition to the decontamination of skin and personnel, the enzyme-sponges can be utilized for preventing cross-contamination of medical and clinical personnel. The source of OP contaminants in the environment could be enclosed and detoxified if the ChE-sponge were incorporated into firefighting foams. Indeed, the sponge should be suitable for a variety of detoxification and decontamination schemes for both chemical weapons and civilians exposed to pesticides or highly toxic OPs such as sarin, or for first responders who could be exposed to OPs resulting from a terrorist act.

[†]Telephone: 301 319 9987; fax: 301 319 9571 DSN: 285 9987
e-mail: Richard.Gordon@na.amedd.army.mil

INTRODUCTION

It was previously demonstrated that a variety of enzymes exhibited enhanced mechanical and chemical stability when immobilized on a solid support, thus producing a biocatalyst. The study of degradation of organophosphates by immobilized enzymes dates back to Munnecke (1), who attempted to immobilize a pesticide detoxification extract from bacteria by absorption on glass beads. The absorbed extract retained activity for a full day. Wood and coworkers (2), using isocyanate-based polyurethane foams (Hypol®), found that a number of different enzymes could be covalently bound to this polymer and retain their activity; after that Havens and Rase (3) successfully immobilized parathion hydrolase.

More recently, the enzyme bioscavenger approach (4, 5) has been shown to be effective against a variety of OP compounds *in vitro* and *in vivo*; pretreatment of rhesus monkeys with fetal bovine serum (FBS) acetylcholinesterase (AChE) or equine serum butyrylcholinesterase (BChE) protected them against a challenge of up to 5 LD_{50} of soman. While the use of cholinesterase (ChE) as a single pretreatment drug for OP toxicity provided complete protection, a stoichiometric amount of enzyme was required to neutralize the OP *in vivo*.

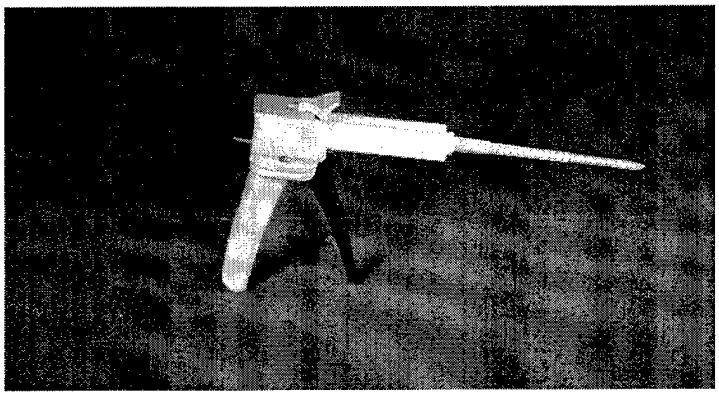

Figure 1. Apparatus for mixing enzymes in aqueous buffer and prepolymer.

To increase the OP/enzyme stoichiometry, enzyme pretreatment was combined with oximes such as HI-6 so that the catalytic activity of OP-inhibited AChE is rapidly and continuously restored before irreversible aging of the enzyme-OP complex can occur. Thus, the OP is continuously detoxified. Based on the two above observations, (a) that polyurethane foams are excellent adsorption materials for OPs (6), and (b) that soluble ChEs and oxime together have the ability to detoxify OP compounds, we combined these components in a porous polyurethane foam formed *in situ* from water-miscible hydrophilic urethane prepolymers and the enzymes. Thus, we envision a reusable immobilized enzyme sponge of cholinesterases and oximes for OP decontamination.

METHODS

SPONGE SYNTHESIS AND ASSAY.

The immobilized enzyme-sponge can be synthesized and cured in less than 20 minutes at ambient temperature and molded into the shape of any container (7). A new technique (8) was utilized to mix the prepolymer (Hypol prepolymer TDI 3000, Hampshire Chemical, Lexington, MA) and enzyme in buffer containing 1% surfactant (Pluronic P-65, BASF Specialty Chemical, Parsippany, NJ). This method replaces the rapid mixing by an electric drill with a mixing stator (a stationary plastic disposable tube for two-component mixing) to effectively reduce high shear stress and partial denaturation of the enzymes during mixing of the two components, prepolymer and enzyme (Figure 1). In addition to simplicity and easy scale-up, the activity of the ChEs coupled to the prepolymer increased by using the mixing stator compared to the high-speed drill mixing (data not shown). Depending on additives to the prepolymer, different size and length mixing stators were used to promote effective mixing. The decontamination sponge containing the immobilized enzymes were molded in a Tupperware® container to the size of a human hand as is shown in figure 2. A modified Ellman method was used to determine the effects of temperature, environment, inhibition by OPs, and reactivation by oximes on the ChE activity of the sponges (4,8).

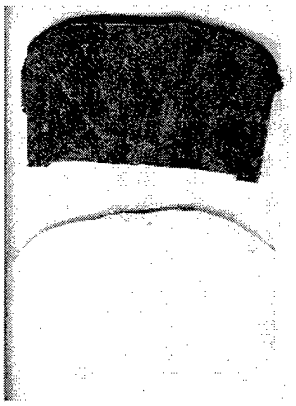

Figure 2. Top sponge, activated carbon incorporated during synthesis; bottom sponge, immobilized AChE sponge.

BACK-TITRATION MONITORING OF SPONGE DECONTAMINATION OF GUINEA PIG SKIN.

After the guinea pig skin was wiped with the sponge(s), each sponge was placed in a separate 50 mL capped polypropylene tube and thoroughly mixed by vortexing. Then, an aliquot was removed and placed in 1 mL

tubes containing 0.05% bovine serum albumin and 50 mM potassium phosphate buffer pH 8. The samples were sequentially diluted in the same buffer. Aliquots of all the dilutions were next transferred to a 96-well microtiter plate containing acetylcholinesterase (typically, 0.055 units). After incubation of the diluted soman with the known quantity of cholinesterase, 10 iL was removed to a second 96-well

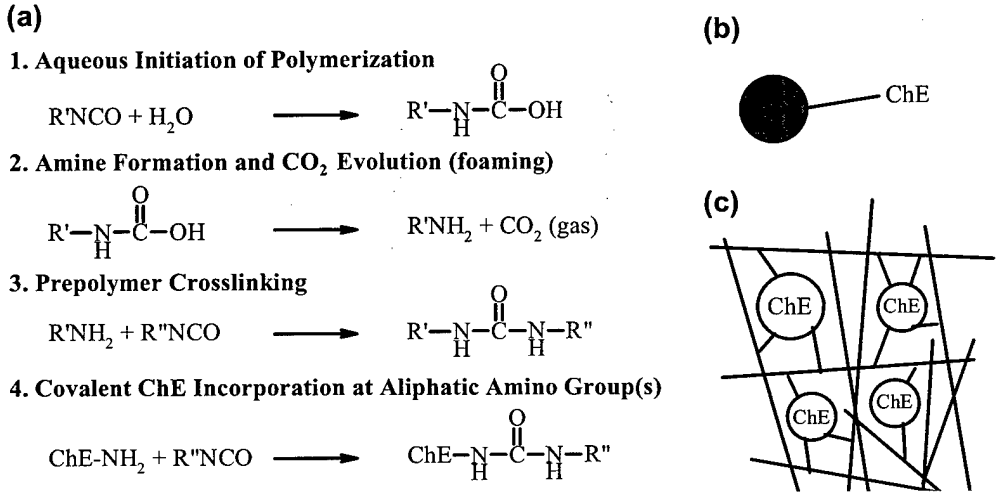

Figure 3. (a) Reactions 1-4 show the interaction of the prepolymer with water and free amino groups on the surface of cholinesterases (ChEs) or any protein. (b) Classical covalent linkage to a preformed solid support is shown in the upper right, where the enzyme is distant from the support. (c) In contrast, the result of *in situ* polymerization with enzyme is depicted in the lower right, where the enzyme becomes cross-linked to and a part of the matrix during synthesis. In this manner, the enzyme gains some of the structural integrity of the cross-linked polymer, including resistance to environmental denaturating conditions.

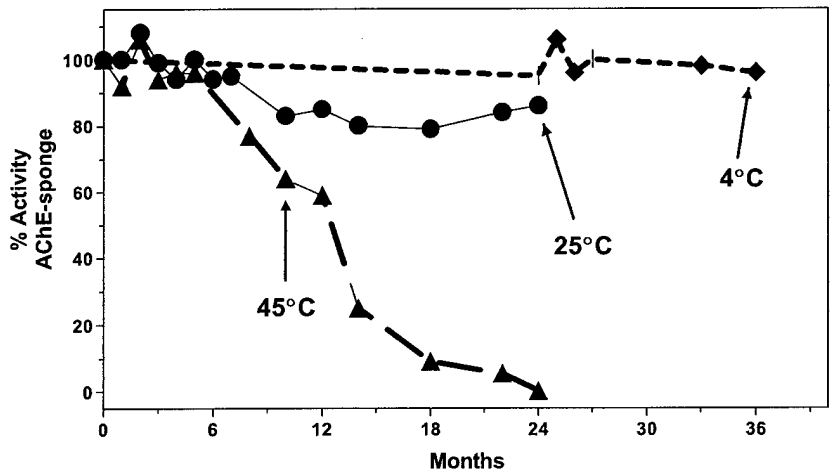

Figure 4. Immobilized AChE after continuous exposure to the indicated temperatures.

microtiter plate and inhibition determined using a Molecular Devices Plate Reader and a modified Ellman procedure as previously described (4,8). In this manner, the soman samples were diluted between 10^5 and 10^{11} fold, permitting quantification of the resulting inhibition of the cholinesterase (10-90% activity remaining) in at least one of the dilutions.

GUINEA PIG DECONTAMINATION.

Animal use: The protocols for the animal experiments were approved by the U.S. Army Medical Research Institute of Chemical Defense Committee on Animal Care and Use, and research was conducted in compliance with the Animal Welfare Act and other Federal statutes and regulations relating to animals and experiments involving animals, and adheres to principles stated in the Guide for the Care and Use of Laboratory Animals, National Research Council, NRC publication 96-23, 1996 edition.

M291 decontamination kit: The sedated and shaved guinea pigs were cutaneously exposed to neat soman on their sides. One minute after the exposure, an M291 pad, previously removed from the M291 kit and cut it in half, was held in forceps and the guinea pig was decontaminated using five counter clockwise swipes. The second half of the pad was used to perform an additional five clockwise swipes.

Sponge: The sedated and shaved guinea pigs were cutaneously exposed to neat soman on their sides. One minute after the exposure, a sponge wrapped around a pair of forceps was moved across the guinea pig's side; then the forceps were rotated 180 degrees, so that the clean surface of the sponge was pointed at the animal. Three more passes were taken from the rear towards the front. An identical procedure was used when the protocol required an additional second sponge to decontaminate the animal.

RESULTS

Previously, we described the development of a product, composed of cholinesterases (ChEs), oxime, and polyurethane foam (PUF) combinations, for the decontamination of organophosphorus compounds (OPs) from sensitive biological surfaces such as skin. Fetal bovine serum-AChE and equine-

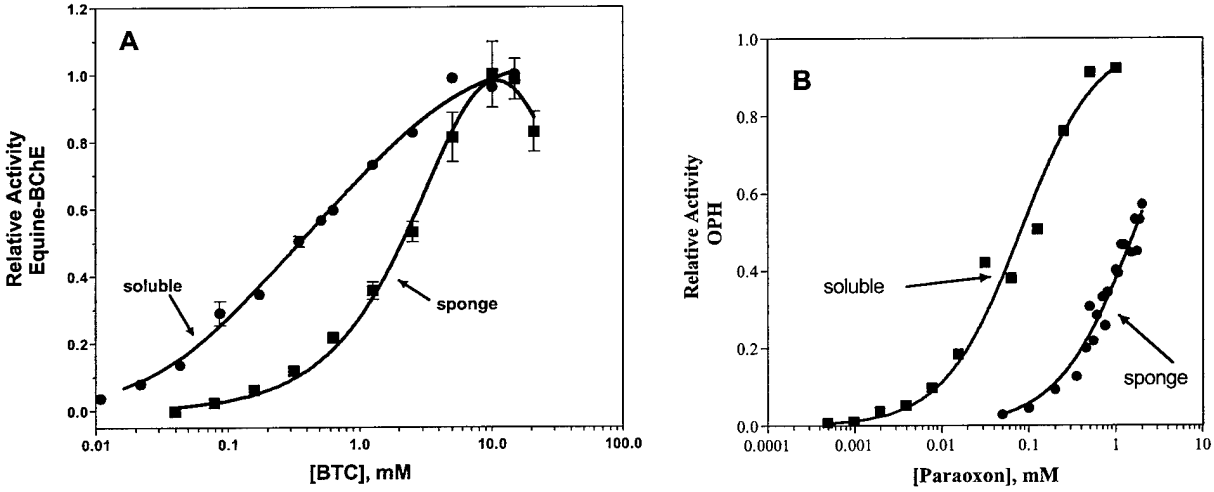

Figure 5. Substrate and activity curves for soluble and immobilized BChE and OPH. Note the shift to right for the immobilized enzymes (BChE and OPH) in the sponge compared to the soluble form of the enzymes.

BChE, which were purified using procainamide-Sepharose 4B affinity chromatography to apparent homogeneity, were immobilized by covalently linking the enzymes to polyurethane foams yielding a product having the consistency of sponges. We have demonstrated that the ChEs are covalently linked to the polyurethane matrix since immobilized ChEs showed little leakage from the PUF matrix. This linkage has the added benefit of enhancing the thermal stability of the ChEs to elevated temperatures (7). We now report further studies of the immobilized enzymes and characterization of the polyurethane foams.

Our recent results now demonstrate the following characteristics of sponges containing immobilized AChE. We evaluated different polymers for immobilization of the enzymes. Originally, we used tolyl diisocyanate (TDI, 5%, scheme shown in Figure 3) and methylenedi-phenyl diisocyanate (MDI, 5%) polyether prepolymers. The TDI prepolymer proved more suitable to enzyme immobilization, presumably due to its flexible structure, and the TDI yielded ChE-sponges with enhanced resistance to environmental denaturation. We have now evaluated prepolymers containing 3% TDI and 5% isophorone diisocyanate. The latter prepolymers yielded about the same efficiency for covalently coupling AChE and retained a high degree of esterase activity. The TDI polyurethane and enzyme matrix results in a ChE sponge of remarkable enzymatic stability. Specifically, ChE-sponges retained their original activity after 3 years at $0^{o}C$ and after 2 years at $25^{o}C$, and more than 50% activity after more than 6 months at $45^{o}C$ (Figure 4).

The K_m values for immobilized BChE and immobilized OPH (Figure 5A and 5B, respectively) were about 10-fold greater than for the corresponding soluble enzymes, as demonstrated by the rightward shift of the substrate (in mM) vs. activity curves. Note that while immobilized BChE yielded substrate inhibition, in contrast, the soluble form of BChE lacked substrate inhibition. These observations suggest that covalent binding of the polymer to surface residues of ChEs and OPHs caused changes to be transmitted to the active site region of the bound enzymes. On the other hand, there were no significant shifts in the pH profiles of either OPH or BChE enzymes, and the bimolecular rate constants for the inhibition of AChE and BChE in soluble or immobilized forms of the enzymes remained unchanged (8). Therefore, OPs interacted similarly with soluble and immobilized ChEs.

We also found that the OPs diisopropylfluorophosphate (DPF) or MEPQ (7-(methyl-ethoxyphosphinyloxy)-1-methylquinolinium iodide) inhibited the activity of ChE-sponges, as was observed for non-immobilized ChE in solution. The oxime HI-6 restored activity of the AChE-sponge until the molar concentration of MEPQ reached approximately 1000 times that of the cholinesterase active site. However, the AChE-sponge could be recycled many times by rinsing the sponge with HI-6 in the absence of OP. In this case, most of the original ChE activity could then be restored to the sponge. Therefore, the bioscavenger approach (Figure 6) can be used externally: the sponge would soak up organophosphate decontaminating the OP contaminated skin. Then the ChE sponge and oxime would detoxify the OP in the sponge. We have found that the ability of the immobilized enzymes and HI-6 to detoxify the OP MEPQ was dependent upon the efficiency of the sponge to decontaminate particular surfaces.

Experiments were performed with sponges lacking enzyme so that we could directly evaluate the ability of the sponge to decontaminate the skin. The sponge alone could remove and decontaminate more than 97% of the MEPQ from non-porous plastic and stainless steel surfaces (Figure 7), and an AChE-sponge with HI-6 detoxified the removed MEPQ. However, the sponge without enzyme was not more effective than the M291 decontamination kit for removing neat soman (GD) applied to guinea pig skin (figure 8). We therefore evaluated additives to the polyurethane matrix, both during synthesis and post synthesis, to improve the removal and extraction of OPs from guinea pig skin.

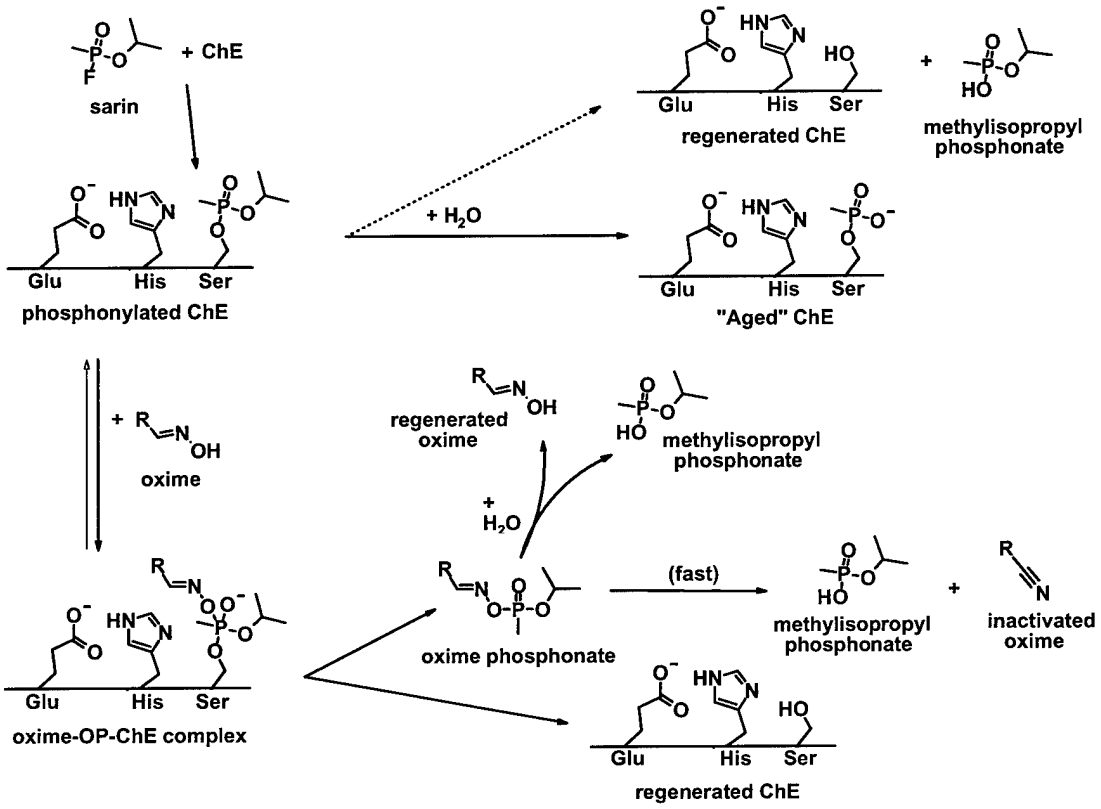

Figure 6. Inhibition of soluble or immobilized cholinesterase by organophosphate (sarin) and reactivation of the alkylphosphonylated enzyme by oxime.

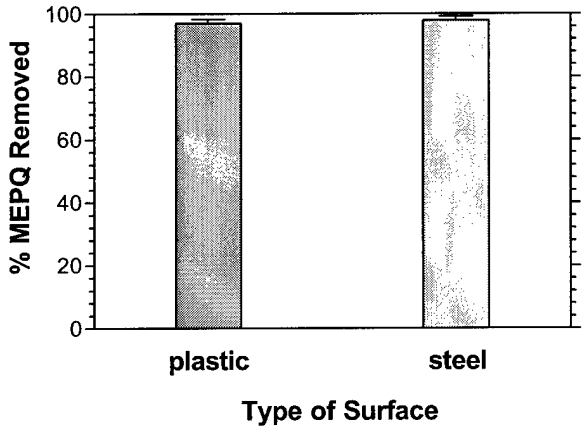

Figure 7. Removal of the organophosphate MEPQ from solid surfaces.

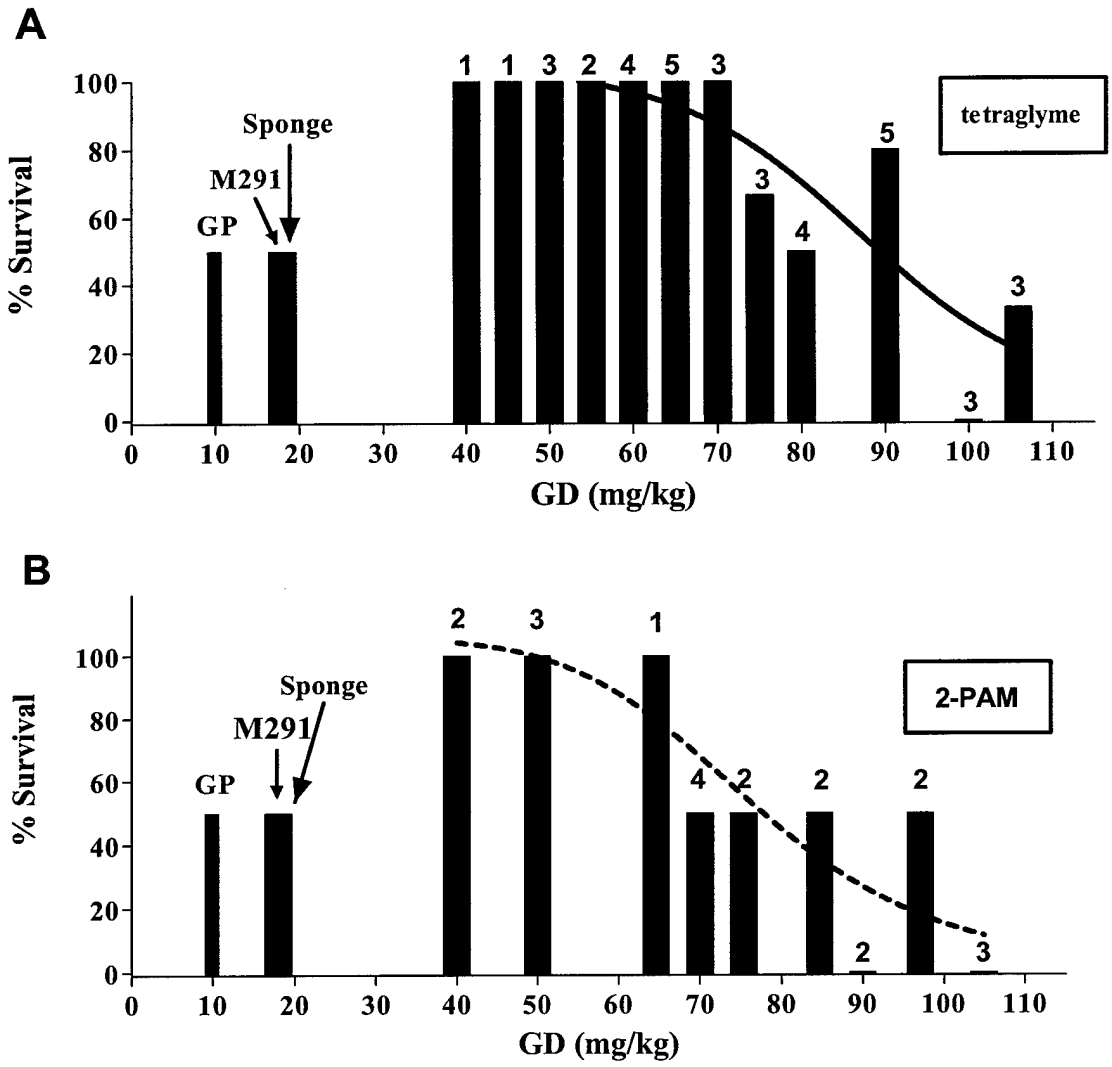

Figure 8. Detoxification of neat soman on guinea pig skin by the M291 decontamination kit, sponge without enzyme or additives, and sponge with additives. The values above the bars indicate the number of animals tested.

We were unable to modify the prepolymer since currently there is no formulation of prepolymer with an increased hydrophobic nature that might be expected to absorb the OP more effectively. Liquid additives possessing surfactant properties, zwitterion and buffers, and partial organic solubilizing characteristics were tested, including centrimide, 18-crown-6, iso-octane, kryptofix 222, polyethylene glycol 6000, triacetin, and tetraglyme. We found that most solutions provided no significant benefit over the original phosphate buffer included in the sponge that was optimized for enzyme activity. However, both triacetin and tetraglyme (Figure 8A) provided additional ability to remove soman from the skin, protecting guinea pigs about four to five-fold better than the M291 kit. In addition, sponges were synthesized so that activated carbon would be incorporated into the polymer matrix. The addition of carbon (Figure 2) did not interfere with the immobilization of ChEs. Sponges containing the oxime 2-PAM also showed increased protection to soman skin toxicity compared to the M291 kit, at least four-fold (Figure 8B and Table 1).

The capacity of sponges to remove GD from guinea pig skin was determined using the back-titration method (see *Methods* section). The line labelled Tube shows the validation of this technique (figure 9). The slope of this line is in effect 1 and it extrapolates through the origin (where $x = 0$, $y = 0$), demonstrating that the mg of GD added to the Tube yielded a 1:1 ratio to the amount of GD found in the titration assay. The line depicting the amount of GD removed by sponge containing tetraglyme (Sponge-TG) exhibited a shallower slope (0.66), indicating that this combination did not remove all the GD from guinea pig skin. Sponge composed of only activated carbon (Sponge-carbon) was less effective than the Sponge-TG in removing soman from the animal's skin (slope = 0.55). In neither case were the sponges saturated with GD because the data did not curve at the higher amounts of GD, and both of these curves also extrapolated to the origin. In part, the inability of Sponge-TG to remove all the GD might reflect the rapid penetration of GD through skin and that tetraglyme cannot extract this fraction.

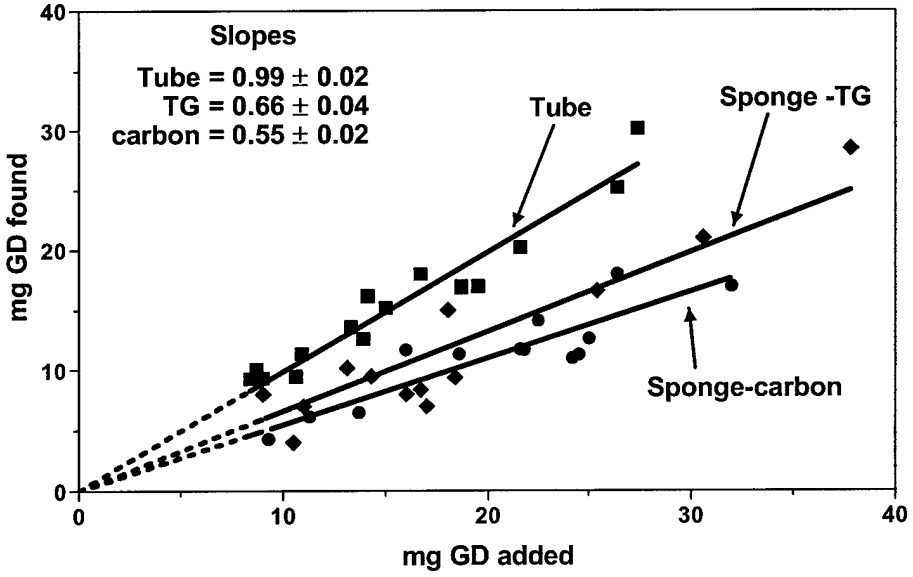

Figure 9. Determination of GD removed from guinea pig skin by different sponges based on the back-titration assay described in *Methods*: Sponge-TG, sponge with tetraglyme; Sponge-carbon, sponge synthesized with activated carbon; Tube, GD placed directly into tubes with buffer.

TABLE 1. Protective ratio of the M291 kit and sponge with additives.

Additive to sponge	LD_{50} (mg/kg)	Protective Ratio
HI-6 (oxime)	**79**	**8.0**
2-PAM (oxime)	**76**	**7.7**
Tetraglyme	**88**	**8.9**
2-PAM + Tetraglyme	**137**	**13.8**
Reference values		
M291 decon kit	**17.7**	**1.8**
Soman alone	**9.9**	**-**

Next, we evaluated the combination of oximes with tetraglyme. In this decontamination treatment using sponges containing 2-PAM and tetraglyme, the protective ratio of the sponges over the M291 kit increased to more than 7-fold, and the LD_{50} of soman increased to 137 mg/kg (Table 1). This compares to LD_{50} values of 9.9 and 17.7 mg/kg for untreated animals (not decontaminated) and the M291 kit, respectively.

CONCLUSIONS

We have demonstrated the rapid *in-situ* copolymerization of ChEs at room temperature, and the ChE-sponges exhibit high activity and stability, making them suitable for a wide variety of decontamination tasks. We have evaluated decontamination schemes using the sponge alone by incorporating additives to aid in the removal of OPs from biological surfaces, rather than smooth and solid objects. Then, detoxification of the OP in the enzyme-sponge pad with oxime would take place, in so doing preventing secondary contamination. In addition, in the presence of oxime, the enzyme-sponge would be reusable. The sponges should be suitable for a variety of biological surface detoxification and decontamination schemes for both chemical weapons and pesticides directed against ChEs.

ACKNOWLEDGEMENTS

The technical expertise, guidance, and thoughtful conversations of the following individuals is gratefully acknowledged: Brian Lukey, PhD, Roy Railer, Mary Schons, Susan Schulz, Mike Shutz, Simon Strating, Patrick Herron II, Erik Lowe, Keith LeJeune, PhD, and Alan Russell, Ph.D.

REFERENCES

1. Munnecke, D. M. (1979) Residue Rev. 70, 1-26.
2. Wood, L. L., Hardegen, F. J., Hahn, P. A., U.S. Patent 4,342,834 (1982).
3. Havens, P. L., and Rase, H. F. (1993) Ind. Eng. Chem. Res. 32, 2254-2258.
4. Caranto, G. R., Waibel, K. H., Asher, J. M., Larrison, R. W., Brecht, K. M., Schutz, M. B., Raveh, L., Ashani, Y., Wolfe, A. D., Maxwell, D. M., and Doctor, B. P. (1994) Biochem. Pharmacol. 47, 347-357.
5. Maxwell, D. M., Castro, C. A., De La Hoz, D. M., Gentry, M. K., Gold, M. B. Solana, B. P., Wolfe, A. D., and Doctor, B. P. (1992) Toxicol. Appl. Pharmacol. 115, 44-49.
6. Turner, B. C. and Glotfelty, D. E. (1977) Analy. Chem. 49, 7-10.
7. Gordon, R. K. Gunduz, A. T., Feaster, S. R., Doctor, B. P, Lenz, D. E., .Maxwell, D. M., Macalalag, R. M., Clarkson, E. D., and Skvorak, J. P. "Polyurethane Sponges and Immobilized Cholinesterases to Decontaminate and Detoxify Nerve Agents" (May 2000), *in* Proceedings of the Bioscience Review.
8. Gordon, R. K. Feaster, S. R., Russell, A. J., LeJeune, K. E., Maxwell, D. M., Lenz, D. E., Ross, M., and Doctor, B. P. (1999) Chemico-Biolog. Interac. 119-120, 463-470.

Concepts for Injectable Nanoparticles for *In Vivo* Removal of Overdose Toxins from Blood

Richard Partch, Dinesh Shah, Chuck Martin
NSF Engineering Research Center

Donn Dennis, Timothy Morey
College of Medicine

University of Florida, Gainesville, FL 32611, USA

ERC
Particle Science & Technology

- This paper represents an interdisciplinary effort recently started by a group of engineers, medical doctors and scientists at the University of Florida, an effort designed to mediate the loss of life by a large number of people who have become overdosed internally or externally with toxic chemicals.

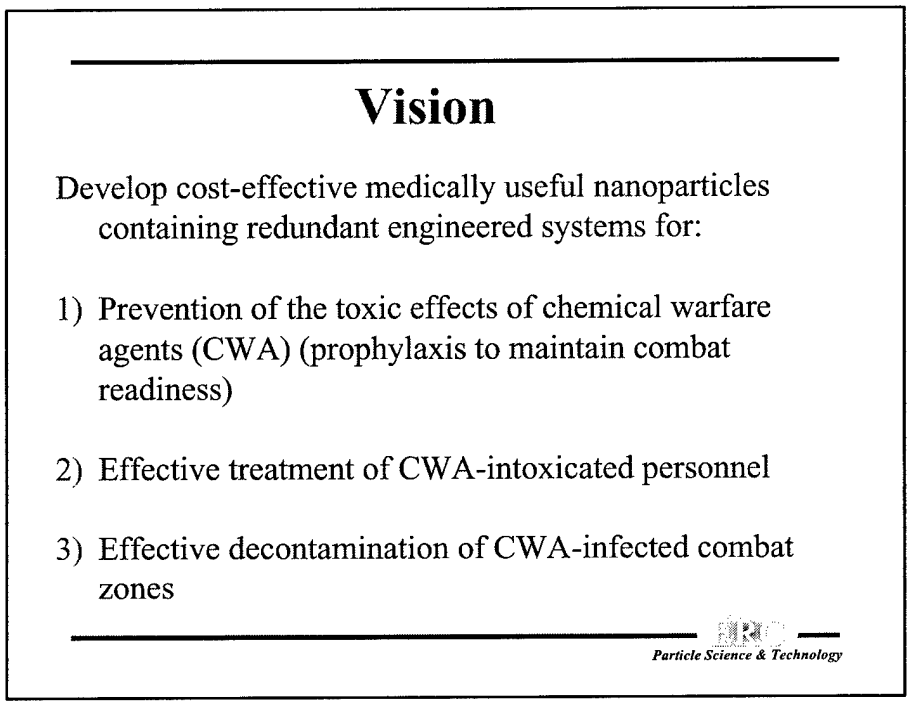

- The vision for the technology to be developed, controlled and selective toxic chemical removal, is that it will serve to fill the void that exists in emergency medical treatment for overdosed persons and contaminated environments. The technology will be equal in importance to but opposite in concept to controlled release delivery of pharmaceuticals.

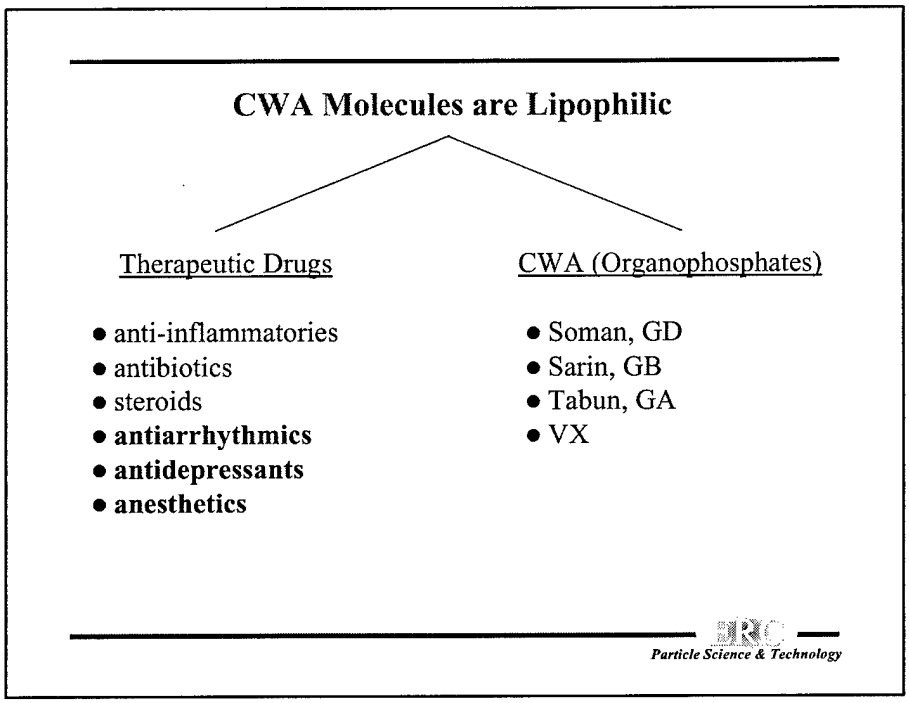

- The toxic chemicals of concern include prescription therapeutics such as antiarrythmic, antidepressant and local anesthetic drugs, as well as terrorist and warfare agents. All are lipophilic.

Drugs currently being investigated

Amiodarone	Amitriptyline	Bupivacaine
Antiarrhythmic	Antidepressant	Anesthetic

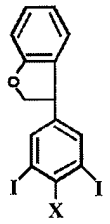

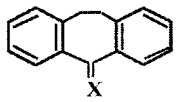

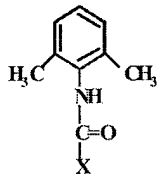

where X = aminoalkyl (similar to VX)

- Initially, the research will focus on creating nanoparticles to efficiently remove three therapeutic drugs which cause thousands of deaths each year. All are aromatic and basic due to an aminoalkyl group pendant to a benzene ring. It will be demonstrated that the pi electron density in at least bupivacaine is high enough to allow its selective binding to a pi acceptor aromatic, hence a means for detoxification. Chemical warfare agents are typically nonaromatic so their removal will rely on their lipophilicity and partitioning from blood onto hydrophobic particles or into oil-in-water microemulsions.

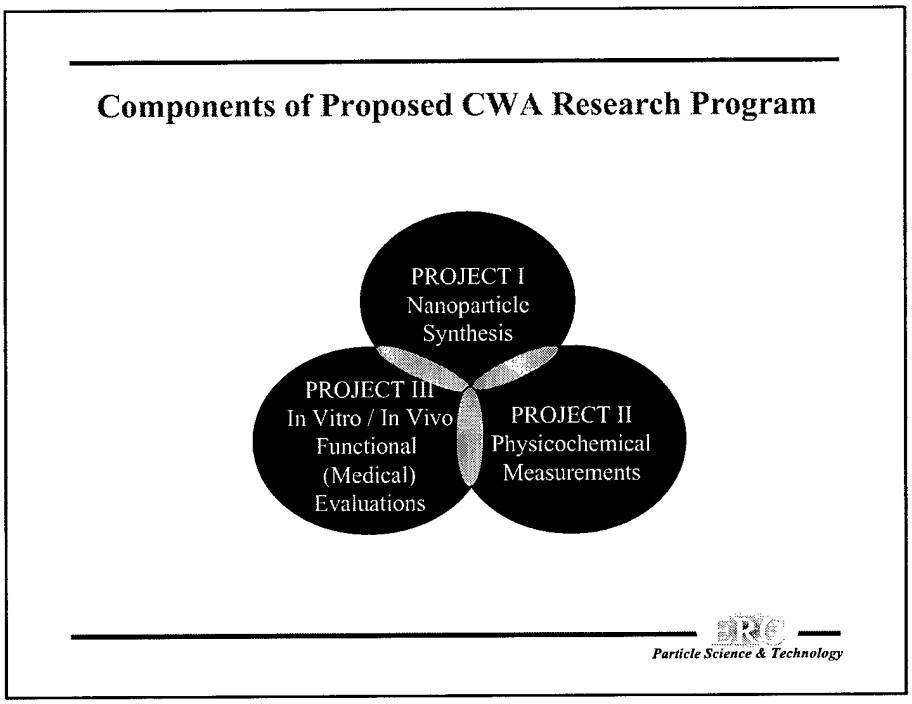

- The overall goal will be achieved through three areas of investigation: nanoparticle synthesis; physicochemical characterization and evaluation of the types of nanoparticles generated; and in vitro and in vivo testing of toxic chemical removal capabilities.

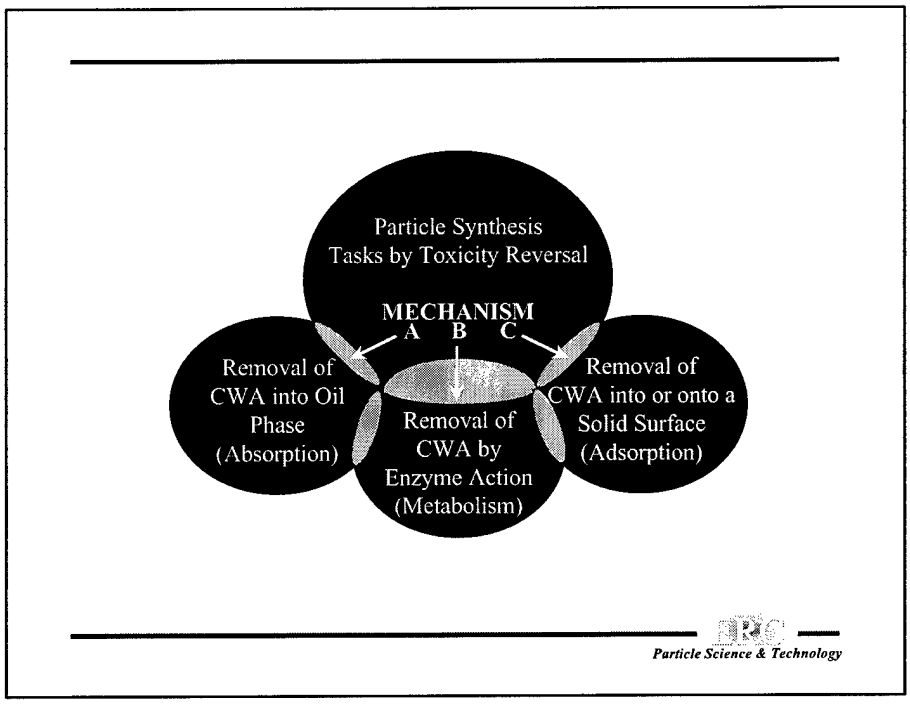

- Removal of overdose toxins from the blood stream is considered to be possible using one of three mechanisms: (A) partitioning or absorbing the generally lipophilic toxins into nano and micro emulsion oil droplet reservoirs; (B) degrading or metabolizing the toxins using natural or more active expressed enzymes; and (C) adsorbing the toxins onto solid nanoparticle surfaces. These mechanisms might be employed singly or in some combination.

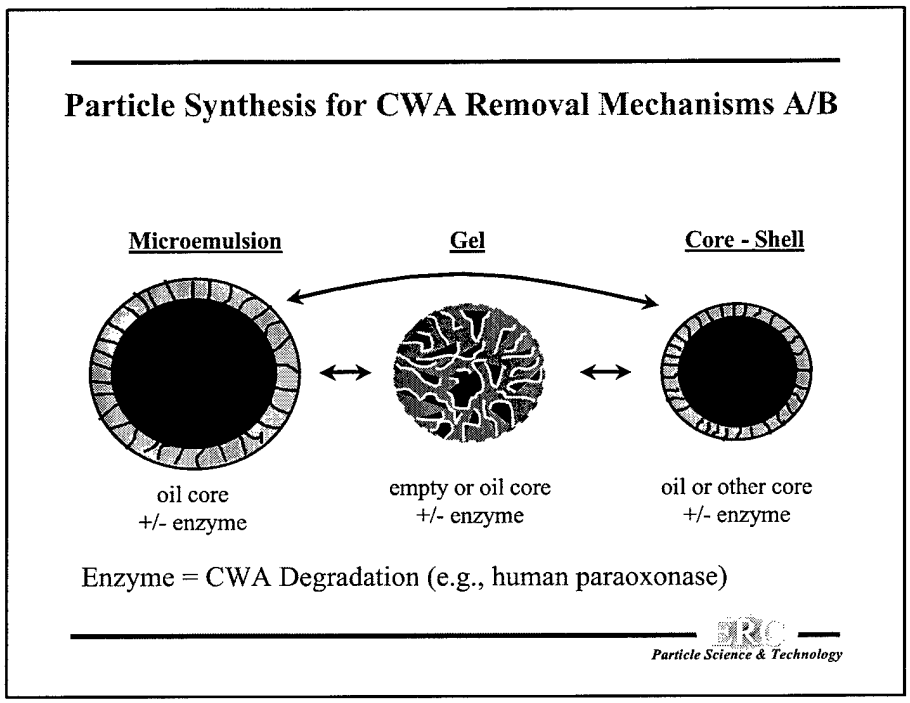

- Particles envisioned for use by removal mechanisms (A) and (A)/(B) are microemulsions where the oil core is stabilized by one or more of several biocompatable surfactants. Alternatively, the oil-like cores to be evaluated may be in gel form. The oil or gel cores may be encapsulated in a rigid shell, the latter of which may be prepared with molecularly templated pores to allow selective passage of one or other of the small toxins but not macromolecules contained in blood. Finally, the enzyme if included may be natural or expressed and be selected for a given target toxin.

Effect of pluronic L-44 micelles and microemulsions (ME) to reduce the concentration of amitriptyline in human plasma

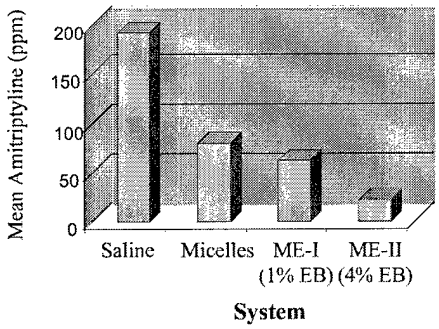

Particle Science & Technology

- Proof of concept that oil-in-water microemulsion droplets are effective in removing the antidepressant drug from blood plasma has been established (Shah). The efficiency of removal depends on the way the microemulsion is prepared. The oil in this study was ethyl butyrate.

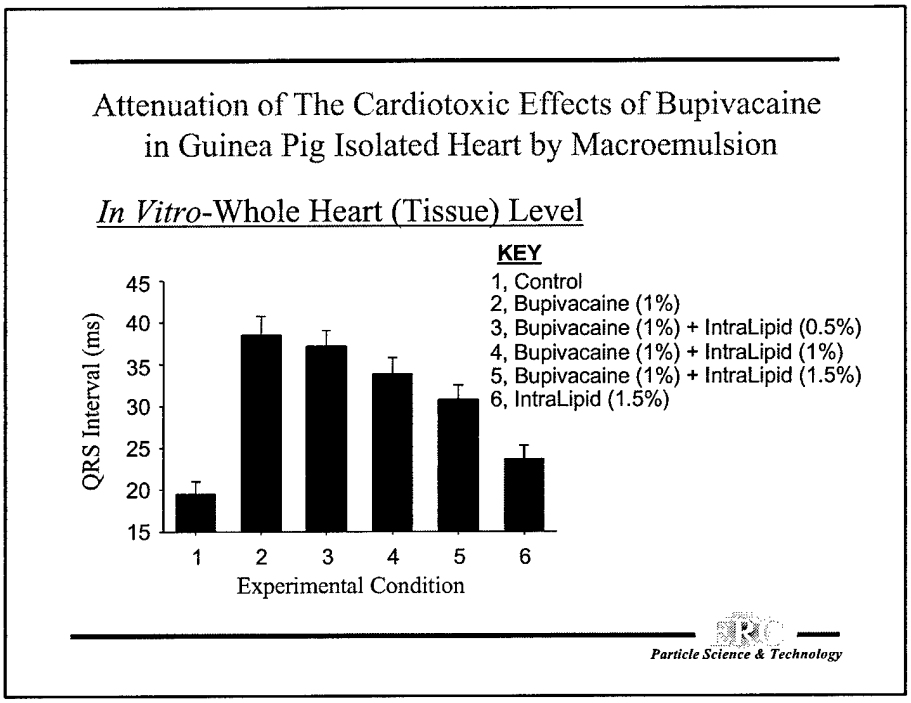

- In vitro tests on reduction in concentration of the toxic anesthetic bupivacaine in heart muscle by a natural oil-in-water emulsion have been successful (Dennis and Morey).

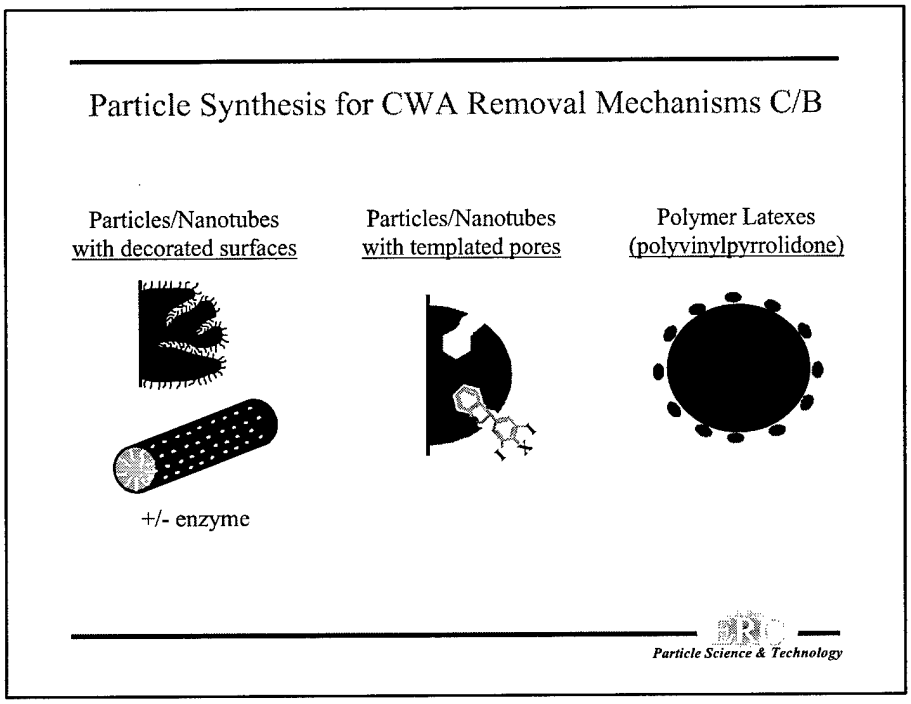

- Nanoparticles envisioned for use by removal mechanisms (C) and (C)/(B) are solids having different shapes, porosities and decorated surfaces. Particles and nanotubes may have hydrophobic molecules attached capable of acting as oil-like sites into which the lipophilic toxins will migrate. The attached molecules may have additional features for selective binding with toxins. The nanotubes may have such attachments either or both on the inside or outside. Solid nanoparticles will be prepared with pores templated for the specific toxin to be removed. Templating of inorganic metal oxides and of organic polymers has precedent and will be applied to the nanoparticles of interest in this research (Partch). In the center example one hexagonal end of amiodarone is shown fitting into a templated pore. Finally, solid latex cores composed of polymer known for drug delivery will be adapted for use. PVP is one such polymer which, due to its water solubility, will be encapsulated or otherwise altered for toxin removal studies (Partch).

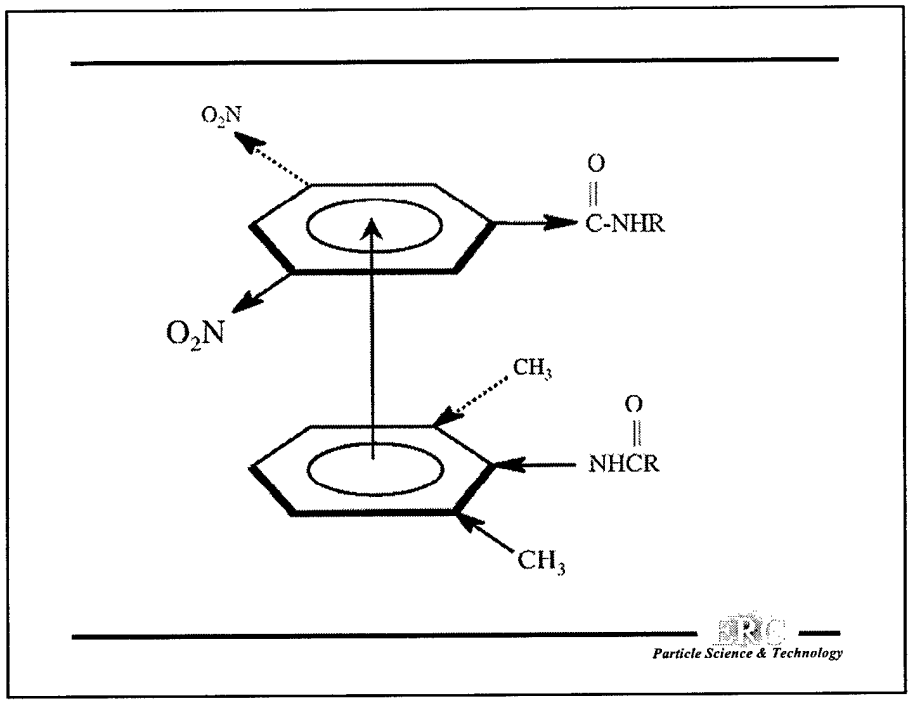

- Benzene rings having opposite degrees of pi electron electron density form complexes with each other. Here the upper ring substituted with -NO2 and -C=O groups is electron deficient. It attracts (vertical arrow) pi electron density from the lower ring substituted with -CH3 and -NH groups. It should be noted that the lower ring structure is identical to that in the toxin bupivacaine where R = aminoalkyl. The upper acceptor ring is designed for easy covalent attachment to a silica nanoparticle (R= -(CH2)n-SiO2 .

Values of Δ for Donor-N-Methyl-3,5-dinitrobenzamide Complexes[a] in Chloroform-d			
Donor	Resonance	Δ (ppm, acceptor)	Direction
2,6-Dimethylaniline	Triplet	0.0874	Upfield
	Doublet	0.0779	Upfield
2,6-Dimethylacetanilide	Triplet	0.0156[b], 0.1584	Upfield
	Doublet	0.00775[b], 0.0055	Downfield, Upfield
Bupivacaine (salt)[c]	Triplet	0.0891	Upfield
	Doublet	0.0275	Upfield
[a]Donor : Acceptor = 60 : 1, except case b where D : A = 1 : 1; [c]Studied in 50 : 50 D_2O : CD_3CN			

- Proof of concept has been demonstrated that the pi-donor pi-acceptor molecules selected form a complex (Partch). The table shows previously unknown data for the change (delta) in NMR proton chemical shift values of the doublet and triplet signals for the pi-acceptor dinitrobenzamide derivative. The upfield direction and magnitude of the changes compares with literature values when trinitrobenzene was the pi-acceptor for various aralkyl compounds.

Scanning Electron Micrograph of the SiO_2 Nanotubules After Dispersion and Collection by Filtration

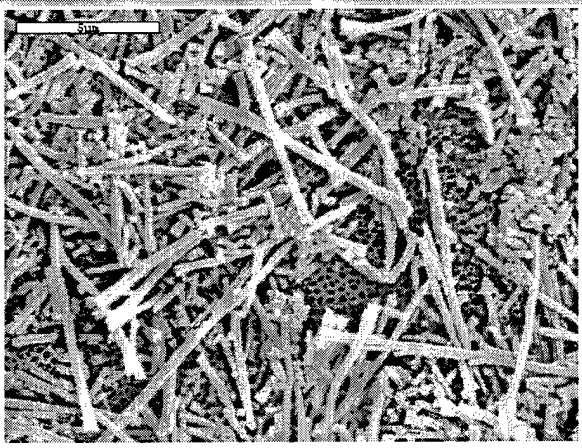

Particle Science & Technology

- Preliminary results on use of 30 nm diameter silica nanotubes decorated with either C18 chains or with an enzyme on their interiors are encouraging (Martin). Shown are the tubes before undergoing internal surface modification. After treatment the tubes showed effective removal of a tricyclic aromatic from solution, and glucose oxidation by tethered oxidase enzyme.

Project II - Physicochemical Characterization of Nanoparticle-CWA Interaction

Applicable Analytical Techniques

- Spectroscopy
- Chromatography
- Liquid Scintillation
- Ultrafiltration

Phenomena to be Observed

- Kinetics of CWA capture
- Nanoparticle-CWA interactions with blood components
- Equilibrium distribution of CWA between solutions and nanoparticles

Particle Science & Technology

- During and after the nanoparticle synthesis, all microemulsions, gels and decorated particles will be fully characterized as to composition, morphology and affinity for removing various toxins from synthetic solutions and blood plasma.

Project III - *In Vitro* and *In Vivo* Functional Assessment of Nanoparticles

Biological Tests for NSF Detoxification Program (drugs = amiodarone, amitriptyline, bupivacaine, i.e., 1° toxicity is heart-related)

***In Vitro* Studies**

- Isolated hearts
  - --His bundle electrograms (heart conduction)
  - --Monophasic action potentials (heart repolarization)
- Isolated heart cells (ventricle)
  - --Currents (e.g., Na current)

***In Vivo* Studies (Whole animal)**

- EKG
- Arterial pressure

ERC
Particle Science & Technology

- The biomedical efficacy of the types of nanoparticles under preparation for removal of the three toxic therapeutic drugs will be evaluated both in vitro and in vivo (Dennis, Morey).

Project III - *In Vitro* and *In Vivo* Functional Assessment of Nanoparticles for CWA Detoxification

Biological Tests for Proposed CWA-nanoparticle program

- modified approach necessary

Assessment of CWA toxicity in 3 major organ systems:

- Central Nervous System – EEG (Seizure activity)
- Cardiovascular System – EKG (Arrhythmias)
- Respiratory System – Ventilatory status (Paralysis)

Other Measures of Nanoparticle Efficacy

- Survival and LD_{50} estimates

Particle Science & Technology

- The ability of the nanoparticle systems to remove warfare and terrorist chemicals requires slightly different in vitro and in vivo medical protocols than the assessments for the therapeutics (Dennis, Morey). For the CWA toxins CNS and respiratory activity will be monitored using appropriate organs.

What is the potential of nanoparticles to safely and effectively deal with CWAs?

2 illustrative examples of what nanoparticles can offer:

1. Substrate Concentration Effect for CWAs

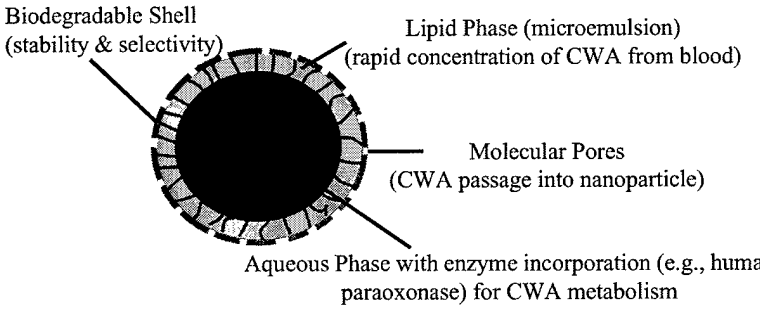

Particle Science & Technology

- Two examples are envisioned for how the selected nanoparticles might function to reduce overdose toxins. The first is illustrated here where the idealized nanoparticle is composed of several core-shell compartments. Note this example employs a water-in-oil core surrounded by functional shells.

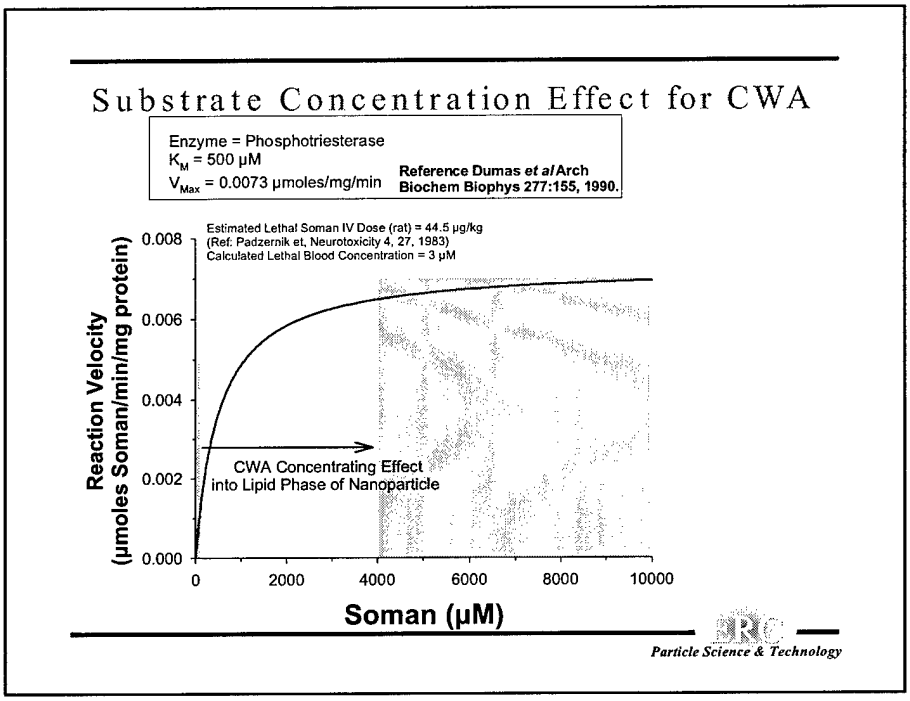

- The design of the previously shown and described idealized particle is such that it is intended to be a reservoir in which the toxin will be concentrated over 1000X above the lethal dose (3 uM for Saran) and thereby facilitate the rate of enzyme attack and toxin destruction.

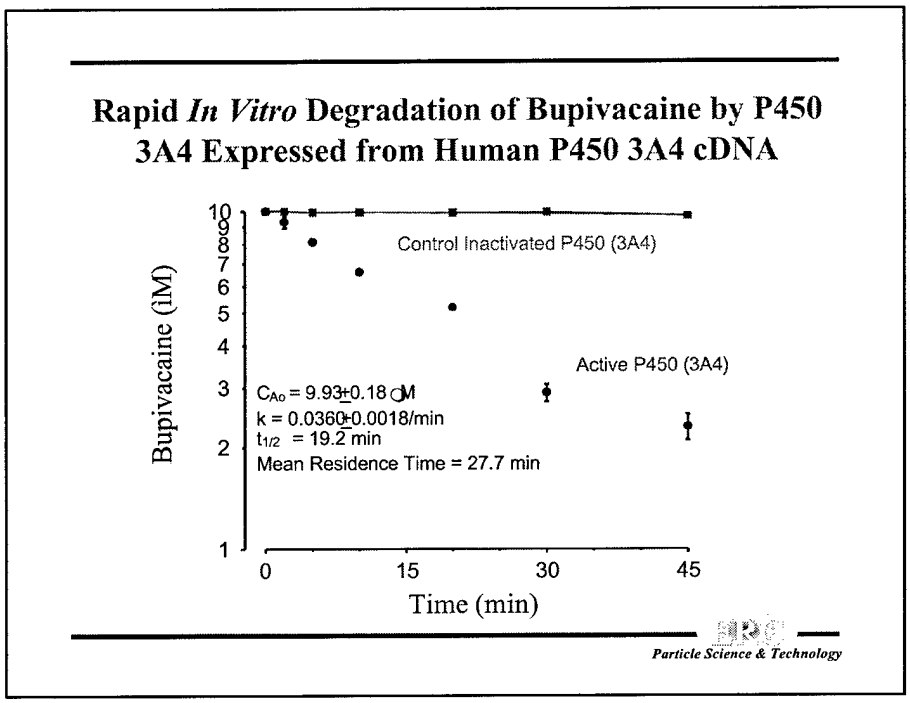

- Representative of enhanced activity by expressed enzyme are the rates of degradation of bupivacaine toxin shown in the figure. The half-life is much reduced from its value when natural P450 is used.

What is the potential of nanoparticles to safely and effectively deal with CWAs?

2. Adsorption of CWAs onto Nanoparticles ("nanobodies")

Particles/Nanotubes with decorated surfaces

Particles/Nanotubes with templated pores

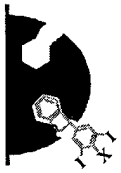

- Similar to antibodies in their function (e.g., digibind)
- Potential to bind CWAs and excrete them from body via kidneys (nanoparticles ⊙5 nm diameter)

Particle Science & Technology

- The second example of how the nanoparticle may function to detoxify blood is to employ adsorption using solids having either decorated surfaces or molecularly templated pores.

Conclusions

Nanoparticle technology offers unprecedented cost-effective opportunities to maintain combat readiness in CWA zones by providing:

- A therapeutic approach to safely and efficaciously prevent (and treat) CWA toxicity

- An approach to safely, rapidly and effectively cleanse CWA-contaminated combat zones

THE ARMY'S UNIVERSITY AFFILIATED RESEARCH CENTER CHEMICAL/BIOLOGICAL COUNTERMEASURES

Steven Kornguth[1], Walter Zielinski[1], Gordon Boezer[2], James Valdes[3]
[1]The University of Texas at Austin, [2]The Institute for Defense Analyses, [3]The US Army SBCCOM

In 2000, a National Biological and Chemical Countermeasures Program was created involving three major institutions: The University of Texas (UT), The University of South Florida, and Texas Tech University. This report considers the structure and technical achievements of The University of Texas University Affiliated Research Center (UARC) component and describes research activities from four UT campuses (Austin, Galveston Medical Branch, San Antonio and South West Medical School Dallas), the Texas Department of Health, the 6th Civil Support Team of the Texas National Guard, Austin Office of Emergency Management, and the Institute for Defense Analyses. The major research efforts are in sensors for threat agents, biomedical responses, and communication. During the first year rapid progress was achieved in several areas, including: the production of high affinity antibodies against anthrax toxin and brucella presented on external surfaces of bacteria; the production of antibodies against multiple pathogenic components; and identification of aptamers that bind ricin and recognize nuclear factors involved in inflammatory responses to threat agents. Intelligent software agents are being developed for belief maintenance and resource allocation. The integration of this effort with the Texas State Health Alert Network (HAN) and archival health data sets initiates our efforts in fusing countermeasures with biosurveillance responses.

INTRODUCTION

In the event of an actual CB attack, the components needed for a successful response will include: human and material resources needed to validate that an incident has occurred (e.g., sensor systems); physical and medical countermeasures (technologies for the rapid diagnosis and treatment of exposed targets or environments); novel counter-agents (antidotes, vaccines) that will be able to defeat the validated biological or chemical agent; health care and triage related to the treatment of people in the area of the affected target; effective communication; and an effective system that integrates these requirements. A team with expertise in all of these areas has been assembled which includes scientific components at the University of Texas. This integrated team is designed to assist the Department of Defense and relevant government agencies in comprehensively addressing the challenges ensuing from a biological/chemical incident. This team has expertise in antibody, genome, and aptamer based sensors, in rapid scale-up vaccines, the effect of B agents on experimental animals, hierarchical computer based communications, clinical diagnostics, and public health delivery response. The unique contributions of this program are the presence of leading edge research teams coupled with application teams that will transition discoveries to meet military needs and requirements.

The Objective of the UARC Biological/Chemical Countermeasures Program is to disencumber the US Army Objective Force from operational and combat capability constraints posed by these threats. Three elements of this effort are sensor development, medical countermeasures and communications.

DISCUSSION

Our research team has been developing high affinity binders of threat agents and exploring platforms upon which the binders can be placed effectively. The high affinity binders include antibodies with $K_d<10^{-10}$, polynucleotide aptamers and cDNA probes. The laboratory of George Georgiou and Brent Iverson has developed a technology by which randomized portions of the variable region of immunoglobulins are expressed on the external surface of bacteria. The bacteria producing highest affinity antibody fragments against anthrax toxin and brucella are selected using fluorescent tagged antigen and a fluorescent activated cell sorter. The cells with the highest affinity binders were then grown to produce 10^7 cells that could bind antigen (Figure 1).

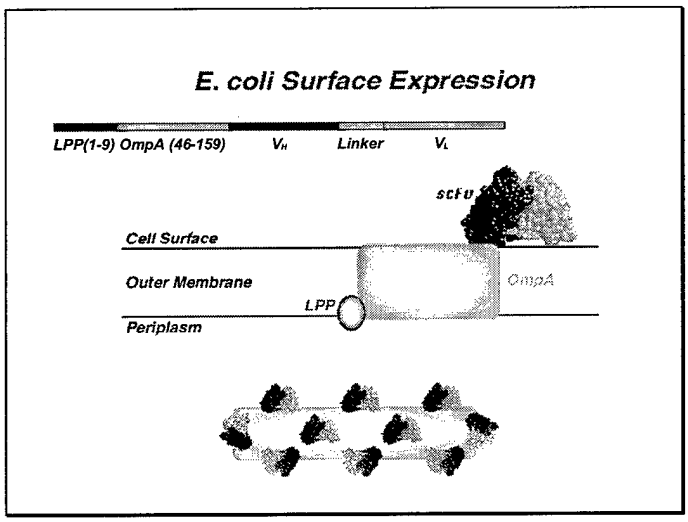

Figure 1. Expression of variable region of antibodies on E.coli surface.

The advantage of this technique is that the highest affinity antibodies against threat agents may be rapidly assessed for utility in field hardened sensor systems. The bacterial systems are stable and can be grown to requirements in a short period of time.

A different binding system has been explored by researchers in the laboratory of Andrew Ellington using polynucleotide aptamers (approximately 31 nucelotides in length) that have good affinity for the toxin ricin. The aptamers are low molecular weight materials that are synthesized in the laboratory and may be attached to various matrices used in sensor systems. In addition to serving as sensor elements, such compounds may have therapeutic value if the bound toxin is rendered inactive in the host. Figures 2a and 2b illustrate the technology.

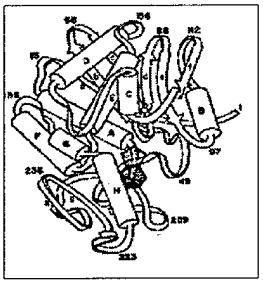

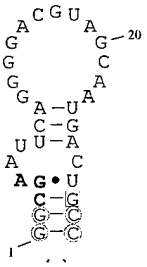

Anti-ricin aptamer

Aptamers against biological warfare targets

Schedule:

FY01: Aptamer against pathogenicity island
Aptamer against B. anthracis
Antibody against Botulinum toxin A

Figure 2a. Polynucleotide aptamers to ricin.

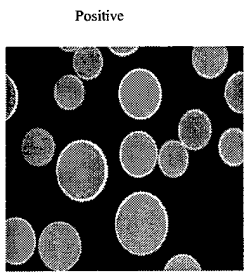

Positive

1. Avidin coupled agarose
2. Biotinylated-DNA
3. Labelled DNA complement

Negative

1. Avidin coupled agarose
2. Labelled DNA complement

Figure 2b. Visualization of aptamer target complexes.

The laboratory of Robert Shope is developing polynucleotide aptamers that bind transcription nuclear factors in macrophages (NFkB) involved in the initiation of inflammatory response following infection with a variety of biological agents including Pichinde virus. The nuclear factors are activated when stimulated by virulent agent but not avirulent material (Figure 3). The resulting thioaptamers are anticipated to have utility in the design of biologicals that can prevent massive inflammatory response and thereby protect forces from toxic shock resulting from threat agents.

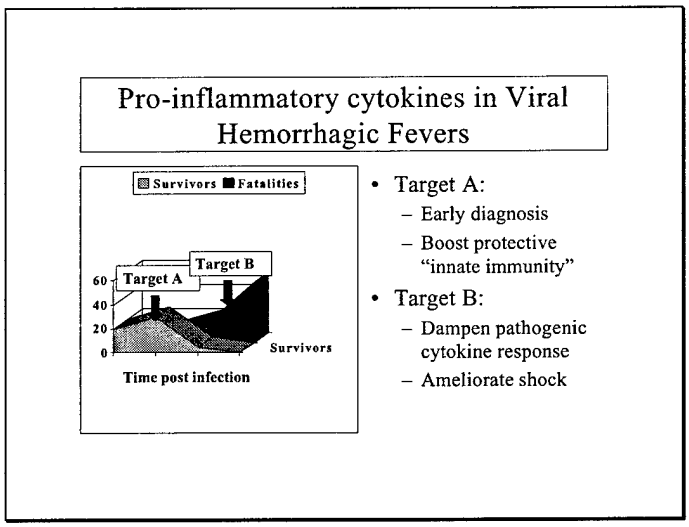

Figure 3. Aptamers for therapeutics against pro-inflammatory cytokines.

A fourth example of the progress made in sensors by the UARC is represented by the successes of Shelley Payne and colleagues. The genetic determinants that lead to pathogenicity of bacteria are factors that increase adhesion of bacteria to target tissues or increase transport of nutrients essential for the organism to grow in particular environments. These virulence factors are present in pathogenic shigella and E Coli ColV (Figure 4). The Payne group has sequenced the virulence factor aerobactin genes responsible for transport of heme iron.

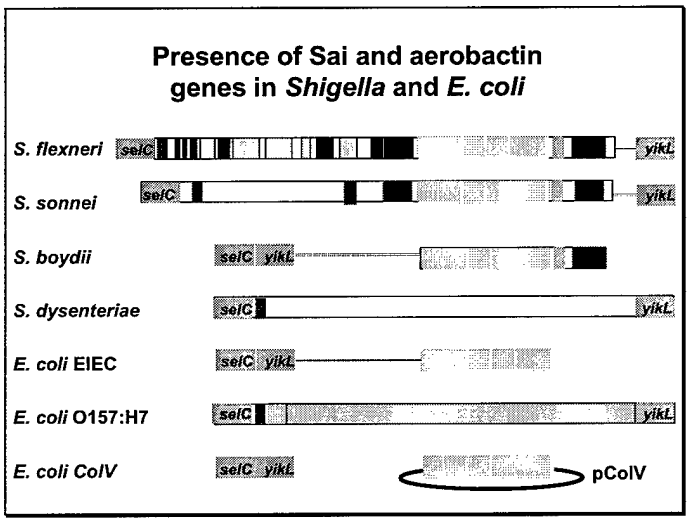

Figure 4. Virulence factors in Shigella and E. coli.

Three platforms for sensors are currently in exploration. One is designed by the team of John McDevitt and Eric Anslyn and is called the electronic tongue; a second utilizes a redox system that will detect polynucleotide complexes in a gel matrix designed by the group led by Adam Heller; and the third is an apatmer based sensor developed by James Chambers of UT San Antonio. The Chambers design has

utilized an anti-ricin aptamer constructed by Andrew Ellington. The McDevitt electronic tongue has shown utility in detecting an antigen-antibody complex.

An intelligent software system is being designed by K. Suzanne Barber. This has the attributes of addressing belief maintenance and resource allocation in a manner similar to that of the Encompass Program created by DARPA. A critical component of the Countermeasures Effort is to evaluate the credibility of incoming information and create a network that will enable distribution of the information. An illustration of this component is shown in Figure 5.

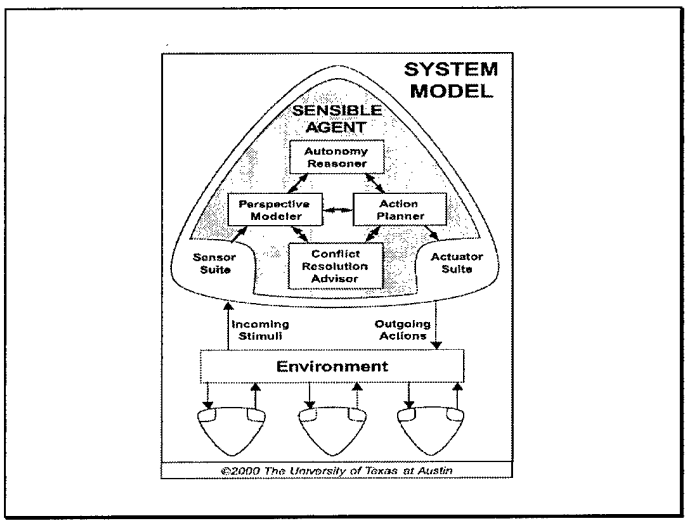

Figure 5. Intelligent software agents.

This communication system, as it develops, interfaces the sensors programs with the Texas Department of Health. The 6th Civil Support Team can provide secure means for transmission of critical information.

During the first year of funding the program has experienced rapid progress in all areas (Table 1).

TABLE 1. UARC accomplishments in first year.

Sensors	• Generated high affinity Ab's-anthracis toxin • Designed aptamer bases MEMS chip • Developed anti-ricin aptamers for detector elements • Detect 10^8 copies/microliter of 70 base DNA in 20 min; S/N ratio 7 • Characterize heme transport gene in pathogenicity island
Bio-Med	• Demonstrated new vaccine against multiple pathogens • Identified potential signatures for early alert disease outbreak • Developed compounds with potential protective properties against Pichinde virus
Communication	• Defined B/C Incident constituencies and their unique communications requirements • Identified "signature" flags in health system for early warning of B/C event • Identified ER facility and faculty at Hermann Hospital, Houston, with leading edge electronic data entry for surveillance

CONCLUSIONS

This integrated team is designed to assist the Department of Defense and other US government agencies in comprehensively addressing the challenges ensuing from a chemical/biological incident. This team has recognized expertise in antibody, genome, and aptamer based sensors, in rapid scale-up of vaccines, in knowledge of the effect of B agents on experimental animals, in hierarchical computer based communications and telemedicine, in clinical diagnostics, and in public health delivery response. The unique contributions of this program are the presence of leading edge research teams coupled with application teams that will transition discoveries to meet military needs and requirements.

ACKNOWLEDGEMENTS

The UARC is thankful for the support received from our sponsors at DTRA (Terry Creque and George Balunis), SBCCOM (James Valdes and William Lagna), and ARL (Buck Tanner).

This work was supported by the U.S. Army Research Laboratory (ARL) under contract DAAA21-93-C-0101.

DEVELOPMENT OF A GENOME FINGERPRINT DATABASE TO IDENTIFY GENETICALLY ENGINEERED MICROBES

Luther E. Lindler, Ph.D. and Xiaozhe Huang, Ph.D., Department of Bacterial Diseases, Division of Communicable Disease and Immunology, Walter Reed Army Institute of Research, Silver Spring, MD 20910

ABSTRACT

The development of recombinant DNA technology and the current state of bioscience has for the first time made the laboratory creation of new biological weapons a real possibility. A critical part of any countermeasures is the ability to identify strains that are unlike previous strains that have been isolated, i.e. are "outside the box" of known genetic variability for the organism. A database of this type will help medical care providers plan an appropriate course of treatment and aid strategic decisions as to the possible origin of the new isolate. Such a database should be capable of including many types of data including source characterization and be capable of determining the phylogenetic relationship of any new isolate to the data contained in the database. We are using the Bionumerics software package and *Yersinia pestis* as our test organism. We examined 37 isolates from the United States (CONUS) and 20 isolates obtained from four different continents (OCONUS) that span a time period of 100 years. We examined our group of strains using a variety of techniques selective housekeeping gene sequencing and pulsed field gel electrophoresis (PFGE). We compared these methods with the established plague typing technique of ribotyping with ribosomal RNA gene probes. All of the CONUS strains belonged to a single ribotype. Chromosomal gene sequencing revealed that *Y. pestis* coding regions are highly stable and have not varied in any of the OCONUS strains. In contrast, PFGE was able to distinguish 46 strains (CONUS and OCONUS) that were derived from different parents. All CONUS strains were at least 70% similar to each other and could be divided into four groups that were greater than 90% similar. Furthermore, PFGE could distinguish one of two *Y. pestis* strains that were isogenic except for a single uncharacterized 14 kilobase pair insertion. Taken together, our results demonstrate that the *Y. pestis* genome is variable at the macromolecular level and that this instability is useful for determining the phylogenetic relationship between isolates and identification of potentially engineered BW strains.

INTRODUCTION

The likelihood that we will face the use of Genetically Engineered Microbes as biological weapons (BW) is significant (8). In order to counter this possibility one critical asset will be an information resource that can be used to identify strains that are different from previous isolates and have the capability of determining the geographic origin of the new isolate. The development of a genetic fingerprint database will support clinical investigation/treatment of patients as well as support strategic decisions pertaining to any possible military response. Several different laboratories associated with the Department of Defense, Department of Energy or Health and Human Services are conducting research to characterize the utility of various genetic techniques for the ability to discriminate between isolates. These techniques include variable number tandem repeats, DNA Sequencing of selected genes, pulsed-field gel electrophoresis (PFGE) and

amplified fragment length polymorphism (2, 7, 9, 13). Accordingly, given the diversity of techniques being used, the analysis package and database software must be capable of incorporating many types of data for phylogenetic analysis. Together, we have chosen the Bionumerics software package by Applied Maths (Kortrijk, Belgium) as the framework for our fingerprint database.

We have chosen *Yersinia pestis* as our model BW threat organism. Little is known about *Y. pestis* genetic variability and the only current technique used to categorize isolates is ribotyping using 16S and 23S ribosomal DNA probes. Ribotyping is not satisfactory because there are only 20 described patterns following analysis of hundreds of isolates from different continents (5, 6). Previously, PFGE was used to determine the size of the *Y. pestis* genome (10). We have combined this technique with selected housekeeping gene sequencing (4) in order to begin to characterize the natural genomic variability of *Y. pestis*. Here, we report the results of those studies and the utility of these techniques for analysis of new plague isolates.

MATERIALS AND METHODS

Growth of bacteria and preparation of genomic DNA for analysis.

Bacteria were grown in Brain Heart Infusion (Difco Laboratories, Detroit, MI) broth supplemented with 2.5 mM $MgCl_2$ at 30^{0}C. When growth on solid medium was required the broth was supplemented with 1.5 percent agar. Whole-cell DNA was prepared from undiluted overnight cultures. Total genomic DNA was isolated using the Puregene DNA isolation kit (Gentra Systems, Minneapolis, MN).

Genomic DNA for PFGE was prepared by diluting overnight cultures one to five with like medium. Plugs for PFGE were prepared by removing 1 ml of diluted overnight culture (OD_{600} ~ 0.2) and centrifuging at 5,000 x g for 5 minutes. The cells were washed once in ice cold PETT IV+E (1 M NaCl, 10 mM Tris, 20mM EDTA, pH 7.6) and suspended in 0.5 mls of like buffer. The cells were warmed at 37^{0}C for 1 minute and an equal volume of 1.4 percent PFGE sample preparation grade agarose (Biorad Laboratories, Richmond, CA) pre-warmed to 52^{0}C was added. The agarose-cell suspension was mixed rapidly and 100 µl aliquots were placed in the wells of disposable plug molds (Biorad) then allowed to solidify at 4^{0}C for 10 minutes. Groups of 10 similar samples were treated with 10 mls of lysis buffer (6mM Tris, 100mM EDTA, 1M NaCl, 1 mg/ml Lysozyme, 0.5% Sarkosyl, 0.2% Sodium Deoxycholate, pH 7.6) for 1 hour and 15 minutes at 37^{0}C. The samples were suspended in 10 mls of ESP buffer (500 mM EDTA, 1% Sarkosyl, 1 mg Proteinase K/ml, pH 9.2) and incubated at 55^{0}C for 6 hours to overnight. The ESP buffer was removed and the samples were washed twice with 10 mls of 10 mM Tris, 1 mM EDTA, 1 mM PMSF, pH 7.5 for one hour at room temperature. Finally, the samples were washed three times with storage buffer (10mM Tris, 50 mM EDTA, pH 8) for thirty minutes at room temperature before being stored at 4^{0}C.

Separation and analysis of genomic DNA by PFGE.

Genomic DNA prepared in agarose plugs was digested with *Spe*I restriction endonuclease overnight and fractionated by PFGE using a CHEF-DRII apparatus (Biorad). Electrophoresis was carried out in 0.5 X Tris-Borate-EDTA buffer (45 mM Tris-borate, 1 mM EDTA, pH 8.3). Genomic fragments were separated on 1% agarose gels for 24-48 hours at 200 volts with a ramp from 10s to 30s. Gels were maintained at 7^{0}C for the length of the electrophoresis. Following electrophoresis, gels were stained in a solution of 1 µg/ml ethidium bromide for one hour followed by rinsing for 1 hour in water before visualization. PFGE patterns were analyzed for phylogenetic relationships with the Molecular Analyst software package (Biorad).

PCR amplification and sequencing of *Y. pestis* genes.

The oligonucleotide primers used to amplify the *Yersinia sp.* 16S rDNA, 16S-23S rDNA intergenic region, *mdh, asd, gyrA* and *galE* genes are listed in Table 1. The DNA sequences

TABLE 1. Primers used for amplification of *Y. pestis* gene sequences.

Gene	Primer Name and Sequence	Product Size[a] (bp)	GenBank Accession Number of *Yersinia* Sequences[b]	Source or Reference[c]
16S rDNA	8F AGTTTGATCATGGCTCAG 1448R CCATGGCGTGACGGGCAGTGTG	1407	AF282306, AF282307, AF282308	(14)
16S-23S Intergenic region (IGR)	UNI-1 CACACCGCCCGTCACACCAT UNI-2 TTAGCACGCCCTTCATCGCCTCTG	735	AF282218, AF282219, AF282220	BLAST of *Y. pestis* genome with *E. coli* 16S rDNA sequence (J01695)
mdh	MDH-1 TGGCCCGCAGGATGAGC MDH-2 TCTGCGATAGTAATGAGAATGTT	1452	AF282309, AF282310	BLAST of *Y. pestis* genome with *E. coli mdh* (Y00129)
galE	GALE-1 TGGCGTGCTATCTTTATT GALE-2 ATGAGGCGAGACCAATAC	1158	AF282311, AF282312, AF282313	BLAST of *Y. pestis* genome with *E. coli galE* (X06226)
gyrA	GYRA-51 ATGAGCGACCTTGCGAGAG GYRA-31 TGTTCCATCAGCCCTTCAATG	632	AF282314, AF282315	*E. coli gyrA* (X06744.1)
asd[d]	ASD-1 TCATATGCGGCTGTTTCC ASD-2 AGGCTACTGGCGTTTTCG	1894	AF282316, AF282317, AF282318	BLAST of *Y. pestis* genome with *E. coli asd* (V00262)

a- The PCR product size predicted following amplification of *Y. pestis* genomic DNA is indicated.

b- Accession numbers for *Y. pestis galE* sequences from the Angola, pestoides A and pestoides F strains (see Table 2) have not yet been deposited in GenBank.

c- GenBank accession numbers used to search the unfinished *Y. pestis* genome sequence are indicated in parenthesis.

d- Oligonucleotide primer pair asd13F (CCACGACACTATGCGACG) and asd18R (CCGCAACCCCCACTTACA) were used to amplify *Y. pseudotuberculosis* strains PB1/+ and 43 *asd* sequences. No PCR product was obtained with these bacteria when ASD1 and ASD2 primers were used in amplification reactions.

for *Y. pestis mdh, asd* and *galE* were obtained by searching the unfinished genome sequence at http://www.sanger.ac.uk/Projects/Y_pestis/blast_server.shtml with the *E. coli* protein sequences that correspond to the translated products for each of these genes. The sequence of the 16S-23S intergenic region (IGR) of the *Y. pestis* rDNA operon was obtained by searching the above genome database with the *E. coli rrnB* operon sequence. All BLAST (3) searches produced probability values of $6.3e^{-126}$ or greater. Amplification of the 16S rDNA sequences of *Y. pestis* was with previously described primers (14). Oligonucleotide primers for the amplification of *Y. pestis gyrA* were selected from the *E. coli* gene sequence. PCR primer pairs were selected from the *Y. pestis* sequences such that flanking DNA as well as the complete gene sequences would be

amplified. Amplification primer pairs and DNA sequencing primers were selected using PrimerSelect (Lasergene, Madison, Wisconsin) software. DNA sequencing reactions were performed using Perkin Elmer Applied Biosystems (ABI) dRhodamine Terminator Cycle Sequencing Ready Reaction Kit with AmpliTaq DNA polymerase FS. Sequencing reactions were analyzed on an Applied Biosystems Incorporated (ABI) model 377XL DNA sequencer. DNA sequences were edited and assembled using Sequencher 3.0 software (Gene Codes Corporation, Ann Arbor, Michigan). Sequence alignment and phylogenetic tree building were with Megalign (Lasergene) using the Clustal method.

RESULTS

Genetic variation of *Y. pestis* strains at the nucleotide level.

All of the strains characterized in this study are listed in Table 2.

TABLE 2. List of isolates characterized in this study.

Strains[a]	Geographic origin or comments[b]	Biovar[c]	Year of isolation	Ribotype[d]	PFGE [e] group	*galE* Allele
Yersinia pestis						
KIM (pgm$^-$)	Iran	M	unknown	F	ND	1
A1122	CA, US	O	1939	B	ND	ND
NM59-BENZ	Bernalilo, NM, US	O	1959	B	2	ND
NM61-DURAN	Santa Fe, NM, US	O	1961	B	2	ND
NM66Jaramillo	Bernalillo, NM, US	O	1966	B	1	ND
AZ70-130-1	Apache, AZ, US	O	1970	B	1	ND
TX79-0209	Canyon, Texas, US	O	1979	B	2	ND
NM81-3387-684	NM, US	O	1981	B	2	ND
NM82-0395	Rio Arriba, NM, US	O	1982	B	2	ND
NM83-0854	San Miguel, NM,US	O	1983	B	ND	ND
NM85-4298-585	Bernalillo, NM,US	O	1985	B	ND	ND
NM87-2987-614	Cibola, NM, US	O	1987	B	2	ND
NM87-1298	Rio Arriba, NM, US	O	1987	B	2	ND
NM87-2007	McKinley, NM, US	O	1987	B	2	ND
NM95-1065	Santa Fe, NM, US	O	1995	B	ND	ND
NM95-1100-276	Santa Fe, NM, US	O	1995	B	3	ND
CO96-3188CAT	Larimer, CO, US	O	1996	B	4	ND
NM96-3002-658	Bernalillo, NM, US	O	1996	B	2	ND
CO96-3188	Larimer, CO, US	O	1996	B	4	ND
NM96-2968	Bernalillo, NM, US	O	1996	B	3	ND
CO96-1214	El Paso, CO, US	O	1996	B	3	ND
NM96-3404	Bernalillo, NM, US	O	1996	B	2	ND
NM96-2970	Bernalillo, NM, US	O	1996	B	2	ND
NM97-2129-373	Santa Fe, NM, US	O	1997	B	2	ND
NM97-2129-374	Santa Fe, NM, US	O	1997	B	2	ND
NM97-2072-344	Santa Fe, NM, US	O	1997	B	3	ND

NM97-2064-338	Santa Fe, NM, US	O	1997	B	2	ND
NM97-2070-345	Santa Fe, NM, US	O	1997	B	3	ND
NM98-0152	Albuquerque, NM	O	1998	B	ND	ND
NM98-2993	Santa Fe, NM, US	O	1998	B	2	ND
NM98-2993Org	Santa Fe, NM, US	O	1998	B	2	ND
NM98-2446 Small	Santa Fe, NM, US	O	1998	B	2	ND
NM98-2446 Large	Santa Fe, NM, US	O	1998	B	2	ND
NM98-2252	Santa Fe, NM, US	O	1998	B	4	ND
NM98-0510-86	Santa Fe, NM, US	O	1998	B	2	ND
NM98-0511-87	Santa Fe, NM, US	O	1998	B	2	ND
NM98-1714	Santa Fe, NM, US	O	1998	B	2	ND
CO99-1133	Larimer, CO, US	O	1999	B	2	ND
Angola	Angola	ND	<1985	ND	ND	2
PEXU 2	Brazil	O	1966	B	ND	1
Harbin 35	China	M	1940	F	ND	1
195/P	India	O	1898	B	ND	1
17721	India	O	1994	ND	ND	1
516	Nepal	ND	1969	F	ND	1
F361/66	South Africa	ND	1966	ND	ND	1
16-34	Vietnam	ND	1970	G	ND	1
ZE942122	Zimbabwe	ND	1994	B	ND	1
219	Vietnam	O	?	ND	ND	1
A16	Belgian Congo	O	?	ND	ND	1
CO92	Colorado	O	1992	ND	ND	1
La Paz	Bolivia	O	?	ND	ND	1
PMB9	Burma	O	1984	ND	ND	1
Stavropol	Russia	O	?	ND	ND	1
Antigua	Belgian Congo	A	1954	ND	ND	1
PKR108	Kurdistan	M	?	ND	ND	1
Yersinia pestoides						
15-91	Russia	?	1960	ND	ND	1
Pestoides A	Russia	?	?	ND	ND	4
Pestoides F	Russia	?	?	ND	ND	3
Yersinia pseudotiberculosis						
PB1/+	Type 1 strain	NA[f]	?	NA	NA	6
43	Type III	NA	?	NA	NA	5

a. For all US isolates (except A1122), the first two capital letters represent states. The number following that represents the year the organism was isolated. The number after the first dash represents the ID number of the patient or animal. Two dashes indicate that the isolates were from fleas with the number after the second dash indicating the flea ID number.

b. NM=New Mexico; CO=Colorado; TX=Texas.

c. The Biotyping information was provided by Dr. P. Worsham, USAMRIID, Frederick, MD. O=Orientalis; M=Medievailis.

d. Ribotyping is according to a method described previously (5).

e. ND= not determined.

f. NA= not applicable.

We examined the *mdh, galE, gyrA, asd,* 16S rDNA and IGR gene sequence variation for a diverse group of *Y. pestis* strains. In the first group of experiments, we determined the DNA sequence of

all of these genes in nine OCONUS *Y. pestis* islolates and two different strains of *Yersinia pseudotuberculosis*. The plague strains were PEXU2, Harbin, 195/P, 17721, 516, F361/66, 16-34, ZE94-2112 and KIM5 listed in Table 2 and were obtained from Dr. May Chu at the Centers for Disease Control, Fort Collins, Colorado. The total number of basepairs analyzed was approximately 65,000 and we did not identify a single nucleotide change within this group of *Y. pestis* strains. Single nucleotide polymorphisms (SNP) were identified when the *Y. pestis* and *Y. pesudotuberculosis asd, galE* and *gyrA* sequences were compared. In contrast, the 16S rDNA and IGR sequences between these two species were identical. Next, we examined a larger group of strains obtained from Dr. Patricia Worsham in the Bacteriology Division, U.S. Army Research Institute of Infectious Disease (USAMRIID). The second group of *Y. pestis* strains examined for SNP was Angola, 219, A16, CO92, La Paz, PMB9, Stavropol, Antigua, 15-91, pestoides Type A, pestoides Type F and PKR108 listed in Table 2. None of these strains encoded any SNP within *mdh* compared to the first group of *Y. pestis* we examined. However, *galE* encoded nucleotide changes at four positions. Combinations of these changes resulted in six different alleles of *galE* within these *Y. pestis* and *Y. pseudotuberculosis* strains as indicated in Table 2. The most predominat DNA sequence of *galE* was designated as allele number 1. The only *galE* sequence variation within *Y. pestis*-like organisms was seen in strains Angola, pestoides Type A and pestoides Type F. Figure 1 shows a phylogenetic tree of the *galE* sequences we derived. All of the "atypical" *Y. pestis* strains were found to fall between the majority group of typical strains and *Y. pseudotuberculosis*.

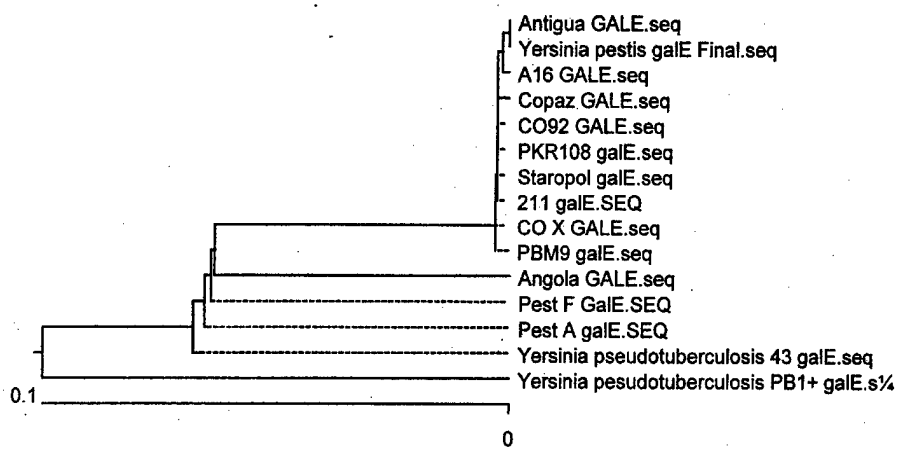

Figure 1. Dendogram of *Yersinia galE* DNA sequences. Allele numbers were assigned from the majority group at the top to the most distant member shown at the bottom of the tree. Sequence alignment was with Megalign (DNAStar) and the Clustal algorithm.

PFGE analysis of CONUS and OCONUS *Y. pestis* strains.

We analyzed most of the *Y. pestis* strains listed in Table 2 by PFGE as described in the Materials and Methods above. All of the OCONUS plague strains we examined displayed a unique PFGE profile as shown in Figure 2 below.

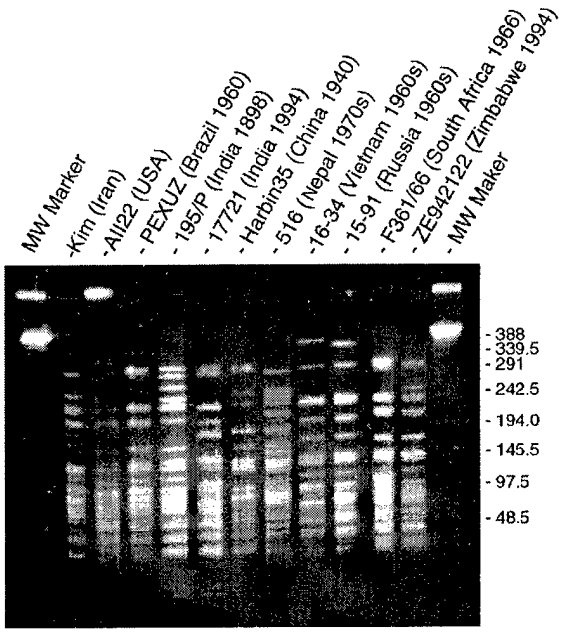

Figure 2. PFGE of representative *Y. pestis* strains of diverse origin. Genomic DNA in agarose plugs was digested overnight with *Spe*I and separation was as described in the Materials and Methods. Electrophoresis was for 24 hours. Molecular weight (MW) marker was applied to the first and last lane with the sizes of the individual fragments shown at the right of the figure. Sizes of the MW marker fragments are in kb.

The amount of heterogeneity seen when we examined our group of CONUS strains using similar conditions to those used in Figure 2 was much lower. Many of the strains displayed more than 90% similarity. Most of the CONUS strains fit within four groups as shown in Figure 3 below. The only strains within the CONUS group that could not be differentiated were ones that either originated from the same parent or were isolated from the same region in the same year, i.e. were clones of each other. These results suggested that the genome is highly variable in the natural environment but that the variation seen in laboratory sub-culture is very low. Evidence of the independent evolution of the genotypes of *Y. pestis* can be seen in Figure 3. For example, the PFGE pattern of NM98-2252 is very different from NM98-1714 yet both isolates originated from Santa Fe in 1998. This apparent independent evolution of PFGE patterns may be due to the natural endemic foci of plague in the US. Specifically, *Y. pestis* is endemic in Prairie Dog colonies and these groups may not intermingle with other groups. Humans become exposed to plague by infected fleas from these colonies and therefore the human isolates would be expected to carry the genotype of the organism from the colony that caused the infection. The number of possible genotypes may be limited. Examination of the data shown in Figure 3 reveals that some geographically diverse strains encoded similar PFGE profiles. For example, comparison of strain TX79-0209 with NM98-1714 revealed that these isolates greater than 90% similar but were obtained 19 years apart and from two different states. We found that regional strains did not group together, i.e. strains obtained from a particular city were interspersed with strains isolated from other cities (Figure 3).

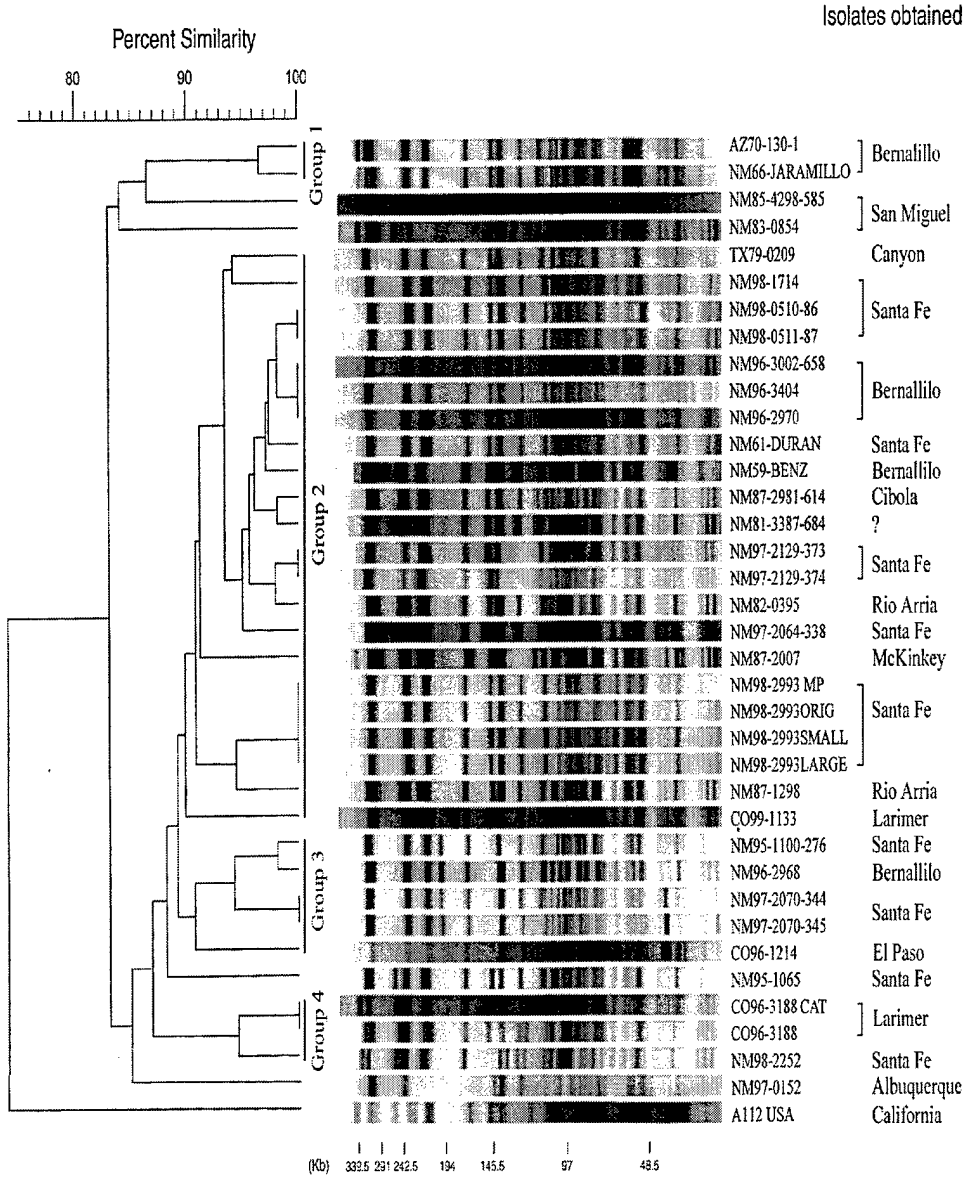

Figure 3. Dendrogram from digitized PFGE patterns for the 37 domestic *Y. pestis* isolates digested with *Spe*I was constructed by cluster analysis using the Dice coefficient and the Molecular Analyst Software Version 1.6 (BIO-RAD Laboratories, Richmond CA). Percentage of similarity is shown above the dendrogram. The patterns are ordered from least similar to most similar (left to right). The position tolerance was 1.4%. The ID numbers of the US isolates are as listed in Table 2.

Detection of genetically modified strains of *Y. pestis*.

Since one of the principle goals of this project was to determine if we could identify potentially modified BW agents we examined two *Y. pestis* mutants generated in our laboratory. These mutants were generated by random mutagenesis of *Y. pestis* KIM5 with Tn10-*lacZ* using bacteriophage λ as a delivery vehicle (15). TN10-*lacZ* is approximately 14 kb in size and was

inserted randomly in the *Y. pestis* KIM5 genome. Approximately 10,000 mutants were screened for pH-regulated β-galactosidase expression at 37°C and two mutants were identified that displayed this phenotype. The mutants were designated numbers 13 and 15 and have not been further characterized. We compared the PFGE pattern of mutants 13 and 15 with the pattern produced by the isogenic parental *Y. pestis* strain KIM5 and identified a single restriction fragment that was not present in mutant 15 as shown in Figure 4 below. The loss of the approximately 230 kb fragment in mutant 15 was accompanied by a gain of an approximately 240 kb fragment. These same strains have been analyzed by the VNTR technique in the laboratory of Dr. Paul Keim at the University of Northern Arizona (2) and were found to be identical by this technique (Paul Keim personal communication). Accordingly, PFGE was able to distinguish a genetically modified *Y. pestis* strain from the parental strain in contrast to more modern PCR-based techniques.

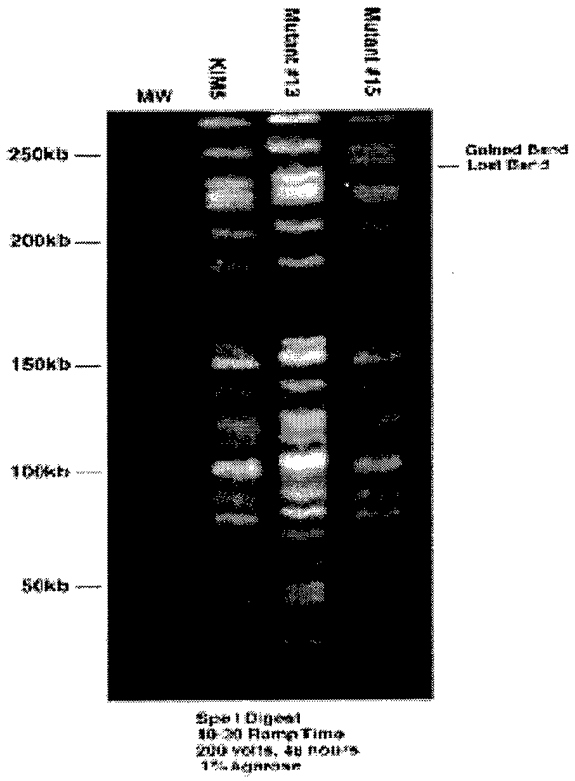

Figure 4. PFGE analysis of TN10-*lacZ* insertions in *Y. pestis* KIM5. The contents of each lane is labeled above gel. Electrophoresis conditions are shown below the image and the size of molecular weight (MW) markers is shown to the left. The DNA fragment that differentiated mutant 15 from the parent strain is indicated to the right of the image.

CONCLUSIONS

We have examined the genetic variability of *Y. pestis* within a diverse as well as homogeneous group of strains by PFGE and by DNA sequencing of selected housekeeping genes. Our analysis indicates that the organism is highly variable at the whole genome level since PFGE profiles of geographically close isolates could be distinguished in most cases. One area of concern we identified was the similarity between a few isolates obtained from geographically dissimilar

regions. This may indicate that the *Y. pestis* genome is not infinitely plastic at the whole genome level. The reason for similar PFGE profiles obtained from geographically dissimilar strains remains unclear however it must be considered that the strains in our phylogenetic comparison shown in Figure 3 were all obtained from the continental US. Unfortunately the PFGE patterns obtained for our OCONUS strains were analyzed using different conditions than the CONUS strains. Accordingly, a more comprehensive comparison of PFGE patterns has not been possible to date but is planned for the near future.

Our finding that *Y. pestis* is very homogeneous at the nucleotide level must be considered in light of the whole genome fingerprint variability noted above. SNP has been used routinely with other enteropathogens to determine clonal and phylogenetic relationships (12). However in the case of the analysis of the genetic relationship of *Y. pestis* strains by this technique all of the "typical" isolates would be considered one clone. Furthermore, the "atypical" strains (Angola and the two pestoides types) are intermediate between *Y. pestis* and *Y. pseudotuberculosis* as might be predicted by earlier studies (1). Our demonstration that "atypical" *Y. pestis* strains are more related to *Y. pseudotuberculosis* by housekeeping gene sequencing is in agreement with other PCR-based techniques (2 and DR. Patricia Worsham personal communication).

Our demonstration that PFGE can differentiate at least some genetically modified BW agents is encouraging. However, the choice of restriction enzyme and the conditions of the fragment separation directly influence the ability of this technique to identify small changes in otherwise isogenic strains. We must therefore increase our experience with PFGE conditions as well as obtain a comprehensive dataset of profiles against which we can compare future isolates.

To date we have used the Molecular Analyst software marketed by Bio-Rad Laboratories for our genetic relationship analysis. However, we are migrating our data to the Applied Maths Bionumerics suite for a more comprehensive ability to incorporate different types of data into our ability to distinguish strains that are significantly different from previous isolates, i.e. have emerged as new clones or are geographically "out of place". This same software package is in use by CDC as part of their Pulsenet program to monitor *Escherichia coli* O:157 isolates for newly emerging strains (11). This package is suitable for a Biodefense database because it has the ability to accommodate many types of data including gel patterns of any kind, biochemical characteristics, antigenic profile and DNA sequences. Furthermore, investigators at remote sites can deposit their data as well as perform analysis using data contained in the central database. We are currently working with Dr. Ted Hadfield at AFIP and Dr. May Chu at CDC in Fort Collins, CO to begin to build our database capabilities for many of the BW bacterial pathogens.

ACKNOWLEDGEMENTS

The authors would like to thank Dr. May Chu, Dr. Patricia Worsham and Dr. Ted Hadfield for providing strains and DNA for these analyses. We would also like to thank SPC Sydney Lee and Ying Liu for database work and technical assistance, respectively.

REFERENCES

1. **Achtman, M., K. Zurth, G. Morelli, G. Torrea, A. Guiyoule, and E. Carniel.** 1999. Yersinia pestis, the cause of plague, is a recently emerged clone of Yersinia pseudotuberculosis. Proc Natl Acad Sci U S A. **96:**14043-8.
2. **Adair, D. M., P. L. Worsham, K. K. Hill, A. M. Klevytska, P. J. Jackson, A. M. Friedlander, and P. Keim.** 2000. Diversity in a variable-number tandem repeat from Yersinia pestis. J Clin Microbiol. **38:**1516-9.
3. **Altschul, S. F., W. Gish, W. Miller, E. W. Myers, and D. J. Lipman.** 1990. Basic local alignment search tool. J Mol Biol. **215:**403-10.

4. **Boyd, E. F., K. Nelson, F. S. Wang, T. S. Whittam, and R. K. Selander.** 1994. Molecular genetic basis of allelic polymorphism in malate dehydrogenase (mdh) in natural populations of Escherichia coli and Salmonella enterica. Proc Natl Acad Sci U S A. **91:**1280-4.
5. **Guiyoule, A., F. Grimont, I. Iteman, P. A. Grimont, M. Lefevre, and E. Carniel.** 1994. Plague pandemics investigated by ribotyping of Yersinia pestis strains. J Clin Microbiol. **32:**634-41.
6. **Guiyoule, A., B. Rasoamanana, C. Buchrieser, P. Michel, S. Chanteau, and E. Carniel.** 1997. Recent emergence of new variants of Yersinia pestis in Madagascar. J Clin Microbiol. **35:**2826-33.
7. **Huang, X., M. Chu, D. M. Engelthaler, and L. E. Lindler.** 2001. Genotyping of a homogeneous group of *Yersinia pestis* strains isolated in the United States. J. Clinical Microbiology. **submitted:**.
8. **Hughes, J. M.** 1999. The emerging threat of bioterrorism. Emerg Infect Dis. **5:**494-5.
9. **Lindler, L. E., T. L. Hadfield, E. Hilyard, and X. Huang.** 2001. Genotyping of *Yersinia pestis*: examination of heterogeneous isolates at the nucleotide and whole genome levels. Journal of Clinical Microbiology. **Submitted:**.
10. **Lucier, T. S., and R. R. Brubaker.** 1992. Determination of genome size, macrorestriction pattern polymorphism, and nonpigmentation-specific deletion in Yersinia pestis by pulsed-field gel electrophoresis. J Bacteriol. **174:**2078-86.
11. **Ransom, G., and B. Kaplan.** 1998. USDA uses PulseNet for food safety [news]. J Am Vet Med Assoc. **213:**1107.
12. **Swaminathan, B., and G. M. Matar.** 1993. Molecular typing methods: Definition, applications and advantages, p. 26-50. *In* D. H. Persing, T. F. Smith, F. C. Tenover, and T. J. White (ed.), Diagnostic molecular microbiology. ASM Press, Washington, D. C.
13. **Velappan, N., J. L. Snodgrass, J. R. Hakovirta, B. L. Marronea, and S. Burde.** 2001. Rapid identification of pathogenic bacteria by single-enzyme amplified fragment length polymorphism analysis. Diagn Microbiol Infect Dis. **39:**77-83.
14. **Warner, C. K., and J. E. Dawson.** 1996. Genus- and species-level identification of *Ehrlichia* species by PCR and sequencing, p. 100-105. *In* D. H. Persing (ed.), PCR protocols and emerging infectious diseases. ASM Press, Washington, DC.
15. **Way, J. C., M. A. Davis, D. Morisato, D. E. Roberts, and N. Kleckner.** 1984. New Tn10 derivatives for transposon mutagenesis and for construction of lacZ operon fusions by transposition. Gene. **32:**369-79.

ASSESSMENT OF THE THERMAL LOAD ATTRIBUTABLE TO PROTECTIVE MASKS

David M. Caretti
U.S. Army Edgewood Chemical Biological Center
Attn: AMSSB-RRT-PR (E5604)
5183 Blackhawk Road
Aberdeen Proving Ground, MD 21010-5424

Two studies were performed to quantify the thermoregulatory responses to mask wear during heat exposure with and without chemical protective (CP) clothing. A powered air-purifying respirator was worn in one study whereas a negative pressure respirator was worn in the second test. Results suggest that there is no measurable thermal load attributable to just a mask in the absence of CP clothing. Unmasked and masked results during wear of CP clothing differed for each mask type and did not clearly indicate a thermal effect of a mask. Additional findings suggest that the protective suit may be the greatest contributor to physiological thermal load during heat exposure.

INTRODUCTION

There are many possible criteria to use for respirator design. For the U.S. military, recent development efforts advocate, among others, designing for a reduced respirator thermal load. However, quantitative data that defines the thermal load attributable to a respirator in and of itself is limited. Respirator designers need to know the amount of heat load due to a respirator under various conditions of work and environmental exposures before the issue can be addressed in the development of next generation respirator systems. Technical shortcomings of many thermal stress studies that have reported mask-only thermal burden data make it difficult to determine just how much thermal stress is associated with wearing a respirator.[1-3] In addition, the issue of respirator thermal load may be further clouded by the effects of wearing encapsulating chemical and biological protective clothing.[4] Therefore, two studies have been performed to quantify the effects of respirator wear on the physiological responses during heat stress. Specifically, one study assessed thermoregulatory responses to wear of a tight-fitting, powered air purifying respirator (PAPR) during heat stress, whereas the second study measured thermoregulatory responses during wear of a full facepiece, negative pressure respirator.

EXPERIMENTAL METHODS

1. PAPR HEAT STRESS TEST (TEST 1)

Five healthy male subjects aged 32 to 39 years volunteered for this study. Subject characteristics were as follows (mean ± standard deviation (SD)): age, 36.0 ± 2.9 years; weight, 87.7 ± 3.4 kg; height, 178.7 ±

5.2 cm; maximal oxygen consumption, 2.41 ± 0.44 L · min^{-1}; and trait anxiety, 27.7 ± 5.0. A written statement of voluntary consent was obtained from each volunteer before testing began. Each subject then completed a test to determine maximal oxygen consumption ($\dot{V}O_{2\,max}$) using an incremental treadmill exercise protocol. Treadmill speed and grade required to elicit between 40-45% of subject's $\dot{V}O_{2\,max}$ were estimated following each test. Once subjects recovered from their $\dot{V}O_{2\,max}$ test, they were asked to walk on the treadmill for up to 10 minutes so that determinations of speeds and grades needed to elicit 40-45% of $\dot{V}O_{2\,max}$ could be determined.

Subjects received instructions on the techniques that they would use to complete the computer-based tasks selected for this study. The three computer-based applications used in this study were the Walter Reed Performance Assessment Battery (PAB),[5] the State-Trait Anxiety Inventory (STAI),[6] and a flight simulation application. The PAB was configured to include a mood scale, serial addition/subtraction, logical reasoning, four-choice serial reaction time, and 10-choice reaction time task. The State-Trait Anxiety Inventory comprises separate self-report questionnaires for measuring state and trait anxiety. Jane's® Longbow Anthology flight simulation software package was used as a low-intensity computer operation task for this investigation.

The Aircrew Eye/Respiratory Protection (AERP) protection equipment was used for mask wear trials. The AERP equipment consisted of a chemical protective mask-hood assembly, a nose-cup breathing subsystem, and a blower subsystem. The AERP mask-hood assembly is best classified as a tight-fitting, powered air-purifying respirator (PAPR). The blower supplied filtered air at ambient temperature.

The following heat exposure trials were completed in random order: no mask with cotton coveralls, the AERP with coveralls, no mask with the Joint Service Lightweight Integrated Suit Technology (JSLIST) protective overgarment, and wear of the AERP with the JSLIST. Test days were separated by at least 24 hours. On the evening prior to a scheduled test, subjects ingested a telemetric temperature sensor or pill (CorTemp™, HTI Technologies, Inc.) that was used for monitoring body core temperature (T_c). Upon arrival to the laboratory, a data receiver/logger (CorTemp™ 2000 Ambulatory Recorder, HTI Technologies, Inc.) was used to confirm that the subject had indeed ingested the temperature pill as instructed and to ensure that the device was functioning. Temperature readings were recorded during every minute of heat exposure and later downloaded to a computer after completion of data collection.

An initial nude (i.e., dressed only in underwear) body weight was then obtained using a calibrated electronic scale (DIGI Grand Scale, DIGI Matex, Inc., accuracy ± 10 g) and subjects were prepped for heart rate monitoring. Heart rate and rhythm were monitored continuously throughout heat exposure trials using a telemetry system (Eaton Medical Telemetry System 4Si, EatonCare). Following placement of heart rate electrodes, subjects were fitted with temperature thermistor probes (Model 409B, YSI, Inc.) for recording skin surface temperatures. Mean weighted skin temperature (MWST) was calculated from surface temperatures recorded from the chest, arm, and calf using the Burton[7] equation. Skin temperatures were recorded every five minutes of testing using a scanning thermistor thermometer (Cole-Parmer 5-Channel Thermistor Thermometer, Cole-Parmer).

Once dressed for the scheduled test configuration, subjects performed a regimen of treadmill walking and completion of computer test batteries in an environmental chamber. The environmental chamber was set for 35°C dry bulb temperature for all trials. At the beginning of a heat exposure session, subjects entered the chamber and were seated in front of a computer. Once seated, baseline measurements of T_c, skin temperatures, and heart rate were recorded. Subjects were then asked to provide baseline subjective

ratings of perceived exertion (RPE)[8] and thermal sensation[9] using specific subjective scales. Subjective RPE and thermal sensation scores were obtained following initial donning of the clothing and/or respirator at 10-minute intervals throughout each heat exposure session.

After baseline data were obtained, timing of the two-hour heat exposure trial began once subjects initiated the first session of the PAB test battery and completion of the state anxiety questionnaire. This first task period lasted for 10 minutes. Subjects were seated during performance of the PAB/state anxiety test period and remained seated if the tasks were completed before the 10-minute period transpired. Following this initial 10 minutes of heat exposure, subjects completed 20 minutes of treadmill walking at an exercise intensity of 40-45% of $\dot{V}O_{2\,max}$. After treadmill exercise, subjects were again seated before the computer and performed the tasks of the selected flight simulation software package for 30 minutes. The PAB/state anxiety session, treadmill walk, and flight simulation tasks were then repeated.

An experimental heat exposure session was terminated when the 120-minute test period transpired, a subject reached a predetermined endpoint criteria for T_c (39.0°C), heart rate exceeded 180 beats·min^{-1}, or a subject requested to terminate the session or was unable to continue. Following cessation of the second flight simulation period, subjects completed one final PAB/state anxiety session. Subjects then exited the climatic chamber and were assisted with removal of the test clothing and/or mask. A final nude body weight was then obtained and subjects were free to drink ad libitum.

Subjects drank approximately 300 ml of water every 20 minutes throughout the heat exposure period to prevent excessive loss of body weight and dehydration during exercise. Canteen weights were recorded to the nearest 0.01 g using a calibrated scale (Sartorius Balance L2200 S, Brinkmann Instruments Co.) before and after each drinking period and total water replacement was calculated after each test session. Total body sweat production and sweat rate were calculated as the difference between a subject's final and initial nude body weights, adjusted for fluid intake.

Heart rate and rhythm were monitored continuously throughout heat exposure trials and recorded on-line in five-minute intervals using a telemetry system. The rate of body heat storage for each mask and clothing configuration was calculated using the formula of Craig *et al.*[10]

Physiological and cognitive responses during heat exposure periods were analyzed using an analysis of variance ANOVA for the independent variables of time and mask condition. Scheffe's *post-hoc* analysis was computed to determine significant differences between group means if a significant *F* statistic was initially obtained. Independent-samples t-tests were conducted for comparisons of unmasked and masked group means for pre and post-test data. All statistical computations were performed using SPSS 10.0 for Windows. Statistical significance was accepted at the $p<0.05$ level. Unless otherwise stated, data are presented as means ± SD.

2. NEGATIVE PRESSURE RESPIRATOR TEST (TEST 2)

Four male subjects aged 32 to 39 years volunteered for this study. All subjects were healthy and free of coronary risk factors, as determined by completion of a medical history questionnaire and physical examination. Subject characteristics were as follows: age, 36 ± 3 years; weight, 89.1 ± 1.2 kg; height, 179.9 ± 5.2 cm; maximal oxygen consumption, 2.6 ± 0.3 L · min^{-1}; and trait anxiety, 26 ± 5. A written statement of voluntary consent was obtained from each volunteer before testing began.

Testing procedures for determination of treadmill speeds and grades needed to elicit 40-45% of $\dot{V}O_{2\,max}$ for each subject were identical to those performed in Test 1. Likewise, methods and procedures

utilized for recording thermoregulatory and subjective responses to heat stress were the same. However, the mask condition for Test 2 was the M40A1 negative pressure respirator. In addition, Test 2 involved longer periods of walking (30 min) and did not include the flight simulation task. Heat exposure sessions were still limited to 120-min duration. Statistical analyses of the results were completed independent of the analysis done for Test 1 using the same techniques.

RESULTS

1. TEST 1

Core temperatures were statistically similar between the masked and unmasked coverall conditions at each minute for the entire measurement period. Core temperatures were statistically similar between the masked and unmasked JSLIST conditions at each minute of heat exposure up to 109 min. However, T_c was significantly higher under AERP wear conditions compared to unmasked conditions after 110 min of heat exposure.

Comparisons of T_c between clothing conditions without mask wear (i.e., coveralls vs. JSLIST) indicated that T_c was generally higher under JSLIST conditions for the duration of the heat exposure sessions; however, minute-by-minute averages were not statistically different. Analysis of T_c responses for the two AERP wear conditions showed that T_c was significantly higher for the AERP with JSLIST condition compared to the AERP with coveralls condition from the beginning of the second treadmill walk until the end of the heat exposure period (i.e., 70 min to 120 min) (Figure 1).

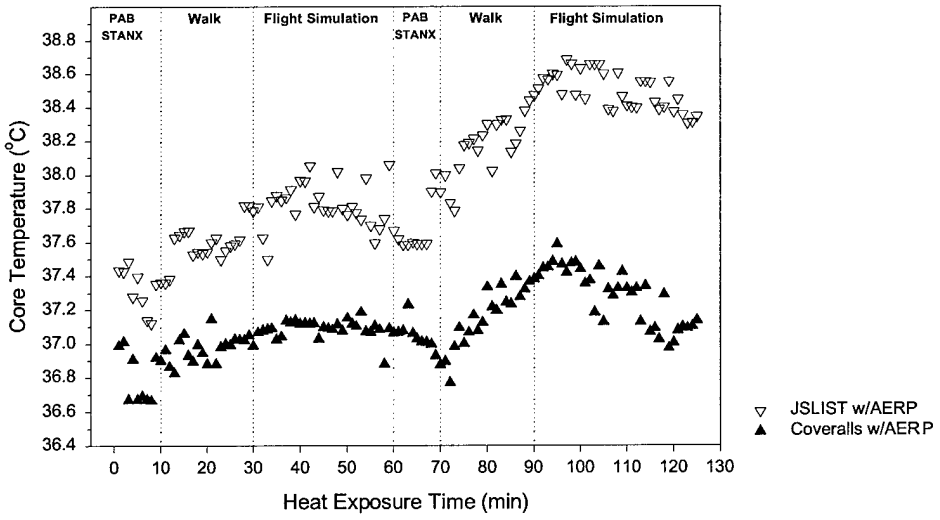

Figure 1. Average T_c responses with and without the JSLIST during wear of the AERP.

Average MWST were statistically similar between the masked and unmasked conditions for both the coverall and JSLIST garments at all measurement periods. MWST were higher for both JSLIST conditions compared to the coverall conditions and the highest MWST were recorded for the AERP with JSLIST configuration. MWST were significantly higher for the AERP with JSLIST condition compared to the AERP with coveralls condition from 95 minutes to the end of heat exposure. Average heart rate

responses for the masked and unmasked experimental conditions followed a pattern similar to MWST and no differences were found between conditions throughout the heat exposure sessions.

No statistical differences in sweat rates or heat storage rates were found between the masked and unmasked coverall or between the masked and unmasked JSLIST conditions following heat exposure. However, average heat storage rate was significantly greater for the AERP with JSLIST condition (46.9 ± 15.8 kcal· m^{-2}· h^{-1}) compared to the AERP with coveralls condition (15.5 ± 5.8 kcal· m^{-2}· h^{-1}). No interactive effects of experimental condition with the different heat exposure tasks were found on subjective data related to RPE and thermal sensation of the face and body.

2. TEST 2

Core temperatures were statistically similar between the masked and unmasked JSLIST overgarment conditions throughout the entire measurement period. Core temperatures were also similar between the masked and unmasked coverall conditions at each minute for the entire measurement period and did not differ statistically from the beginning to the end of testing.

Without the M40A1 mask, increases in T_c were similar for the JSLIST and coveralls garments up to 96 minutes of testing (Figure 2). With the exception of the data recorded at 117 minutes ($P = 0.07$), T_c were statistically higher during wear of the JSLIST garment compared to the coveralls for the remainder of the 120-minute heat exposure session. During mask wear, increases in T_c were similar for the JSLIST and coveralls garments up to 101 minutes of testing. Thereafter, T_c values were statistically higher during wear of the JSLIST garment compared to the coveralls.

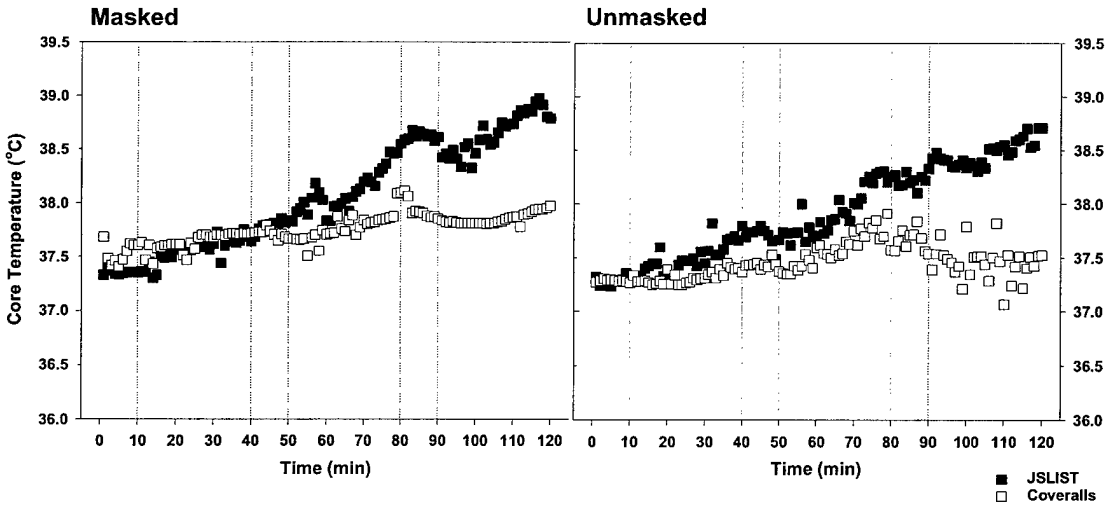

Figure 2. Minute average T_c for masked (M40A1) and unmasked test conditions with and without the JSLIST suit.

For the most part, average heart rate responses were similar between experimental conditions. However, heart rate was significantly lower for the unmasked JSLIST condition compared to the masked JSLIST condition at 110 min (125 ± 6 vs. 156 ± 5 beats· min^{-1}), 115 min (125 ± 4 vs. 156 ± 6 beats· min^{-1}), and 120 min (125 ± 4 vs. 159 ± 4 beats· min^{-1}) of heat exposure. Heart rate tended to be

higher during JSLIST wear compared to conditions of coverall wear for both masked and unmasked conditions, but no significant differences were found.

Average MWST did not differ between any of the masked and unmasked experimental conditions at any time during the 120-min heat exposure tests. However, with the exception of data recorded at 45 min, MWST were significantly higher for the M40A1 JSLIST condition compared to the M40A1 coverall condition between 35 and 100 min of testing. After 100 min, the differences between conditions persisted but did not reach significance. Without the mask, MWST were also significantly higher during JSLIST wear compared to coverall wear after 35 min of testing. Independent of time, average MWST were significantly greater for all JSLIST conditions compared to both conditions of coverall wear.

Sweat rates and heat storage rates did not differ between the masked and unmasked coverall conditions or between the masked and unmasked JSLIST conditions following heat exposure. In addition, no differences were observed between the masked coverall and masked JSLIST conditions or the unmasked coverall and unmasked JSLIST results. Subjective RPE scores and thermal sensation ratings for the face and whole body did not differ between experimental conditions at any time during the test session.

DISCUSSION

This study attempted to quantify the effects of respirator wear in and of itself on select physiological and psychological responses during heat stress. Several previous studies have made attempts to do the same with differing results. For tests that were conducted without the use of protective overgarments, others have reported that wear of a full facepiece, negative pressure respirator with an impermeable hood elevates whole body sweat rate and mean skin temperatures above no mask conditions during exercise.[1-3] Likewise, most reports state that heart rates tended to be higher with a mask on. However, we found no statistical differences in sweat rates, heart rates, or MWST between the masked and unmasked coverall conditions of either Test 1 or Test 2. In addition, T_c responses between the unmasked and masked coverall conditions were similar in both tests and total body heat accumulation and heat storage rates did not differ between conditions. Collectively, these findings suggest that there is no measurable thermal load attributable to just a mask in the absence of CP clothing, regardless of mask type.

Masked and unmasked thermoregulatory responses for trials that involved wear of the JSLIST CP overgarment were, for the most part, similar for both Tests 1 and 2. No differences in sweat rates or MWST were found between masked and unmasked conditions with the JSLIST in either test. In Test 1 with the AERP mask, heart rate responses were similar between the unmasked and masked JSLIST conditions. However, in Test 2 with the M40A1 mask, heart rate was significantly lower for the unmasked JSLIST condition compared to the masked JSLIST condition after 110 min of heat exposure. A similar difference in T_c responses was not observed between the unmasked and masked JSLIST conditions. Interestingly, the opposite T_c and heart rate responses were observed between the unmasked and masked JSLIST conditions of Test 1. In brief, average heart rates were identical between conditions and T_c were significantly higher under AERP wear conditions after 110 min of heat exposure. Whether or not these findings indicate that mask wear causes a certain degree of thermal burden in and of itself during wear of CP clothing is difficult to say considering the differing heart rate and T_c responses observed in our tests. However, the limited test sample population sizes of each study highlights the need for additional testing to reach a more definitive conclusion on the thermal load of a mask.

Despite the inconclusive results evident between masked and unmasked JSLIST conditions, the results of both Tests 1 and 2 demonstrated a thermal load effect of the CP clothing ensemble, a finding that has

been reported elsewhere.[4] Wear of the JSLIST resulted in higher T_c, MWST, and heat storage rates compared to the coverall conditions whether or not a mask was worn and the masked JSLIST condition tended to result in the higher values for all thermoregulatory parameters. The differences between T_c and MWST for the coverall and JSLIST conditions were significant for each test, although at different times during heat exposure.

CONCLUSIONS

The thermoregulatory effect of wearing a PAPR or negative pressure respirator without CP clothing appears to be similar to that produced when no respirator is worn. In contrast, differing heart rate and core temperature responses between masked and unmasked conditions suggest that mask wear may cause some degree of additional heat stress when worn in combination with CP overgarments. However, thermoregulatory responses observed for the CP clothing by itself suggest that the protective suit may be the greatest contributor to physiological thermal load during heat exposure. Therefore, designing for a reduced respirator thermal load should not be a significant focus for future mask development efforts.

REFERENCES

1. Martin, H. deV., and Calloway, S., An Evaluation of the Heat Stress of a Protective Face Mask. *Ergonomics* 17: 221-231 (1974).
2. Martin, H. deV., and Goldman, R., Comparison of Physical, Biophysical and Physiological Methods of Evaluating the Thermal Stress Associated with Wearing Protective Clothing. *Ergonomics* 15: 337-342 (1972).
3. Robinson, S., and Gerking, S.D., *Heat Stress Imposed by Gas Masks*, Report #26, Office of Scientific Research and Development, U.S. War Research Agency, Washington, D.C., 1945.
4. Montain, S., Sawka, M.N., Cadarette, B.S., Quigley, M.D., and McKay, J.M., Physiological tolerance to uncompensable heat stress: effects of exercise intensity, protective clothing, and climate. *J. Appl. Physiol.* 77(1): 216-222 (1994).
5. Thorne, D.R., Gesner, S.G., Sing, H.C., and Hegge, F.W., The Walter Reed Performance Assessment Battery. *Neurobehav. Toxicol. Teratol.* 7: 415-418 (1985).
6. Spielberger, C.D., Gorsuch, R.L., and Lushene, R.E., *The State-Trait Anxiety Inventory Manual,* Consulting Psychologist Press, Palo Alto, CA, 1983.
7. Burton, A.L., Human Calorimetry. *J. Nutrition* 9: 261-279 (1935).
8. Borg, G., Psychophysical Bases of Perceived Exertion. *Med. Sci. Sports Exerc.* 14: 377-381 (1982).
9. Gwosdow, A.R., Nielsen, R., Berglund, L.G., DuBois, A.B., and Tremml, P.G., Effect of Thermal Conditions on the Acceptability of Respiratory Protective Devices on Humans at Rest. *Am. Ind. Hyg. Assoc. J.* 50: 199-195 (1989).
10. Craig, F.N., Garren, H.W., Frankel, H, and Blevins, W.V., "Heat Load and Voluntary Tolerance Time," *J. Appl. Physiol.* Vol. 6, p 634 (1954).

IMMOBILIZED FILTERS FOR AIR FILTRATION

John J. Mahle
U.S. Army SBCCOM

Saeed Zaiee
University of Delaware, Center for Composite Materials

This study will determine the feasibility of creating an immobilized bed of adsorbent particles using adhesives. The immobilized adsorbent will be designed for gas phase filtration in military respirators, in order to provide enhanced moldability (settling performance) and attrition resistance. The fabricated filter samples will be analyzed in order to determine the physical and chemical factors affecting mechanical strength and chemical filtration.

Five different resin systems were studied in this work; epoxy/amine, vinyl-ester, water-borne epoxy/amine and two water-borne urethane pre-polymer. The first two resins are organic but epoxy/amine system is more hydrophilic than vinyl-ester. Samples were cured through temperature cycles appropriate for their corresponding resin. Optical microscopy was used to look at the samples and determine the extent of dispersion of resin with the activated carbon particles. Compressive and flexural properties of samples of activated carbon particles with water-borne resin systems were evaluated. This effort was focused on distinguishing between brittle failure and ductile failure of the samples.

INTRODUCTION

Gas phase, adsorption based separation processes are usually conducted in cylindrical vessels under axial or radial flow. This symmetry offers several advantages in filter design. Restraining of the granular adsorbent material is facilitated because only one spring plate is required. Also uniform flow patterns are established. Cylindrical filter bed designs are employed almost exclusively in high pressure adsorber vessels because stresses are evenly distributed. Personal protective mask canisters and ventilation filters on the other hand are typically operated at ambient pressure allowing non-cylindrical designs to be considered. Respirator canister designs have been developed which have a reduced profile. Such filters would not be used as an external canister but rather as an integrated element, closely molded to the cheek or placed in some less cumbersome location.

If under rough handling or settling the adsorbent bed develops leak paths or regions of low density, premature breakthrough could result. An unrestrained bed can also result in increased particle attrition. When a unidirectional spring plate is no longer feasible, one solution would be to make the adsorbent structure self-supporting. Particles would be bonded together creating larger effective particles. High adhesive content in the interstices, on the surface or in the pores would result in additional mass transfer, and flow resistance and performance degradation relative to the un-immobilized material.

A recent patent, which specifically addressed the fabrication of filter canisters, concluded that dry mixing of adsorbent and binder worked best for small particles and wet mixing for large particles. Verification by microscopy was suggested. Polymer should be selected based on wetting ability, where more wetting of adsorbent would result in coating rather than contacting

the adsorbent. This work identified the best candidates as polyurethane, ethylene-vinyl acetate, and polyethylene. Binder particles sizes between 40 to 400 mesh were appropriate to minimize coating and pressure drop effects. One interesting observation was that samples prepared under compression could have high bulk densities as much as 110 percent of a loose packed bed of the same adsorbent.

The principal adsorbent considered here is a military specific material for chemical warfare protection, ASZM-T, which is an activated carbon, impregnated with metal oxides to promote detoxification of adsorbed chemical agents. This adsorbent is used for CW protection in a variety of filter sizes. The activated carbon adsorbent is formulated from microparticles, which are agglomerated with a petroleum, or pitch based binder. The short-range structural strength of the binder can be broken which would form dust. The cost advantage of granular ASZMT at $9/lb versus up to $200/lb for novel materials such as activated impregnated carbon cloth suggests that further use of the granular material is highly favored for disposable items such as respirator cartridges.

Performance properties of the adsorbent can be determined by a series of tests. Vapor filtration performance is measured by challenging the adsorbent under flow with both a strongly adsorbed simulant vapor, DMMP, to measure physical adsorption properties and a weakly adsorbed reactive vapor, cyanogen chloride (CK), to asses the activity of the chemical reaction based impregnant formulation. In addition, pressure drop across the filter and accumulated dust measurements are important performance parameters.

The ASZM-T utilizes an impregnant formulation of metal oxides to react with weakly adsorbed acid gases. The separation is accomplished by reaction between the toxic gas and metallic compounds (reference report) deposited into the pores and onto the surface of the particles. To enhance the physical adsorption of catalysts, triethylenediamine known as TEDA, was applied to the activated carbon particles. This limits the upper temperature for processing samples to approximately 80°C. Since the porosity of these particles greatly enhances their separation capacity, processing factors that affect porosity and/or accessibility of the pores are critical to the overall performance of the material.

The ASZMT material must be processed in a moderate temperature range. This limits the number of polymers that are possible to consider. The binder must contact the surface of the adsorbent but not coat it. The breakthrough testing provides a severe challenge to assess the extent of surface coverage.

Polymers are divided into two main categories; thermoplastics and thermosets. In thermoplastics, physical interactions and entanglements create the cohesion between polymer chains. In thermosets, chemical bonds between chains / crosslinks, in addition to physical bonding, create a network that cannot be significantly reshaped unless some chemical bonds are broken. Both thermoplastics and thermosets exhibit a softening temperature named glass transition temperature, Tg. Below Tg, both types of polymer are rigid / glassy. Above Tg, thermoplastics become liquid like; flow under their own weight, however, thermosets exhibit rubbery behavior. Thermoplastics can lose their shape, cohesion, and all their mechanical attributes when heated above their softening point while thermosets retain some of their useful properties

Most thermoset resin systems consist of a viscous liquid prepolymer and a hardner, whose mixture gels and solidifies upon heating. The liquid state of the mixture before curing allows for ease of processing of these materials. Therefore, the initial experiments were focused

on using thermosets as the adhesive for immobilizing the activated carbon particles. Moreover, some useful mechanical properties; such as elasticity, ductility, and fracture toughness of thermosets have wider range than those of thermoplastics do. Further mechanical advantages of thermosets will be discussed later in this report.

It is expected that low resin loading would have less adverse effect on the porosity and packing of the particles. Therefore, good dispersion of resin over activated carbon particles is desired. This implies that the resins should have low viscosity for effective mixing. For this reason, three water-borne resin systems were tested in this work. It is also desired that the organic resin not fill the micropores of activated carbon during processing. One approach is to fill the micropores with water; thus limiting the accessibility of organic molecules to the pores by taking advantage of the incompatible nature of organic and aqueous phases, and then to mix the particles with resin. To this end, activated carbon particles, both dry and saturated at 50°C and 85% relative humidity, were tested with five resin systems. Initial work will entail selecting the resin systems for evaluation, including both thermosets and thermoplastics. The potential exists for these organic materials to alter the adsorbent characteristics of the activated carbon. Water-borne systems are often used for coatings and in this case would limit the need for organic solvents and could potentially provide a method for limiting pore filling while still providing adequate bonding of particles. Thus emphasis will be placed on water-borne systems for this investigation.

This study will determine the feasibility of creating an immobilized bed of adsorbent particles using adhesives. The immobilized adsorbent will be designed for gas phase filtration in military respirators, in order to provide enhanced moldability (settling performance) and attrition resistance. The fabricated filter samples will be analyzed in order to determine the physical and chemical factors affecting mechanical strength and chemical filtration.

MATERIALS

Five different resin systems were studied in this work; epoxy/amine, vinyl-ester, water-borne epoxy/amine and two water-borne urethane prepolymer. The first two resins are organic but epoxy/amine system is more hydrophilic than vinyl-ester. Dry activated carbon particles and particles saturated at 50°C and 85% relative humidity were mechanically mixed with these resin systems at different loadings to determine the minimum required resin content for good adhesion. Samples were cured through temperature cycles appropriate for their corresponding resin. Optical microscopy was used to look at the samples and determine the extent of dispersity of resin with the activated carbon particles. Compressive and flexural properties of samples of activated carbon particles with water-borne resin systems were evaluated. This effort was focused on distinguishing between brittle failure and ductile failure of the samples. Samples cut out of cartridges produced by the 3M company were tested for their flexural strength and the results were compared to those obtained using the water-borne resins. The applicability of a spraying technique was tested using one of the water-borne urethane prepolymers sprayed on the activated carbon particles. Experiments were conducted to determine the effect of the viscosity of the resin on this technique.

RESULTS

Micrographs of the bonded samples can be instructive of the extent and efficiency of the contact. Figure 1 presents a 20X view of the un-immobilized adsorbent sample. Figure 2 presents

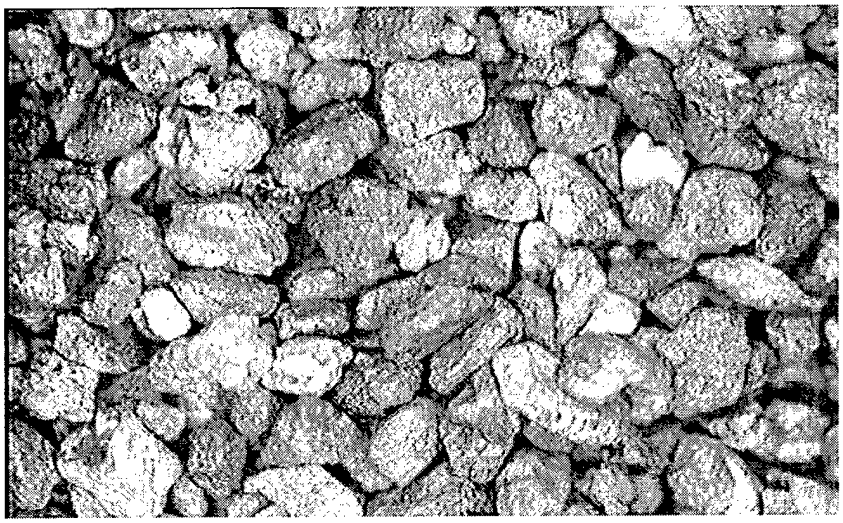

Figure 1. Activated carbon particles, ASZM-T, as received.

Figure 2. Sample of dry activated carbon with 10% water-borne epoxy/amine resin.

the results for a sample prepared with 5% water-borne epoxy/amine. The contact points between the particles are seen to be randomly oriented. Thus approaches which coat the surface are highly inefficient. Figure 2 indicates that the waterborne samples result is excessive coverage.

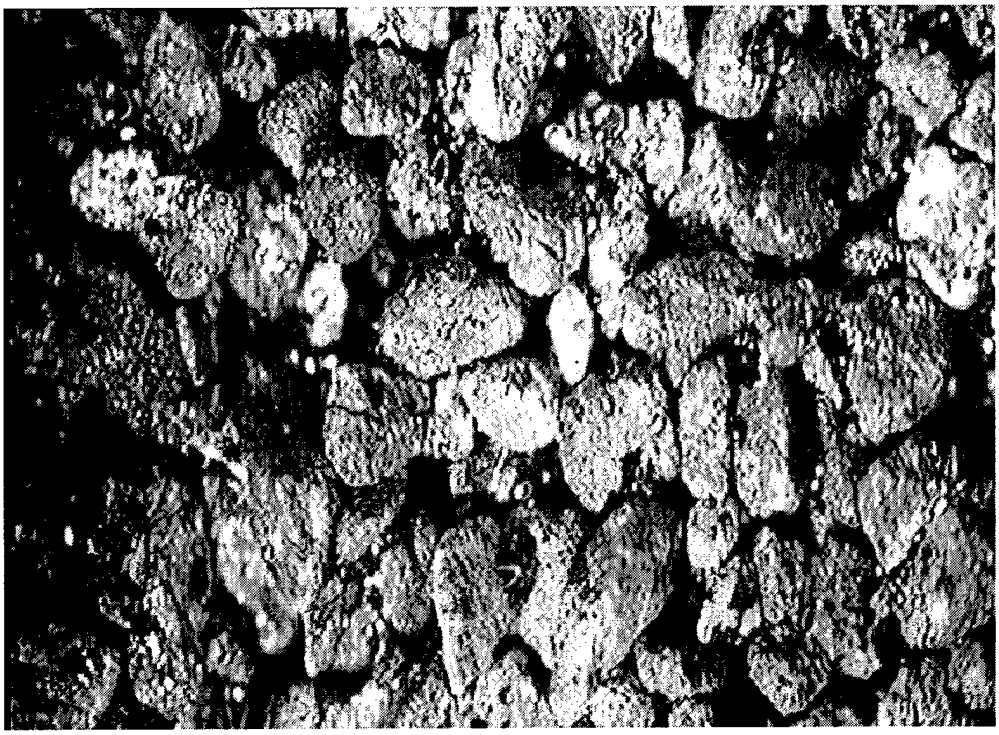

Figure 3. Sample of dry activated carbon with 15% cured 50 mesh thermoplastic.

It can be seen that a sample bonded with granular adsorbent produces less surface coverage than waterborne samples. The effect of bed packing is seen in figure 4. A 30% decrease in breakthrough time results from a loosely packed bed due to tamping.

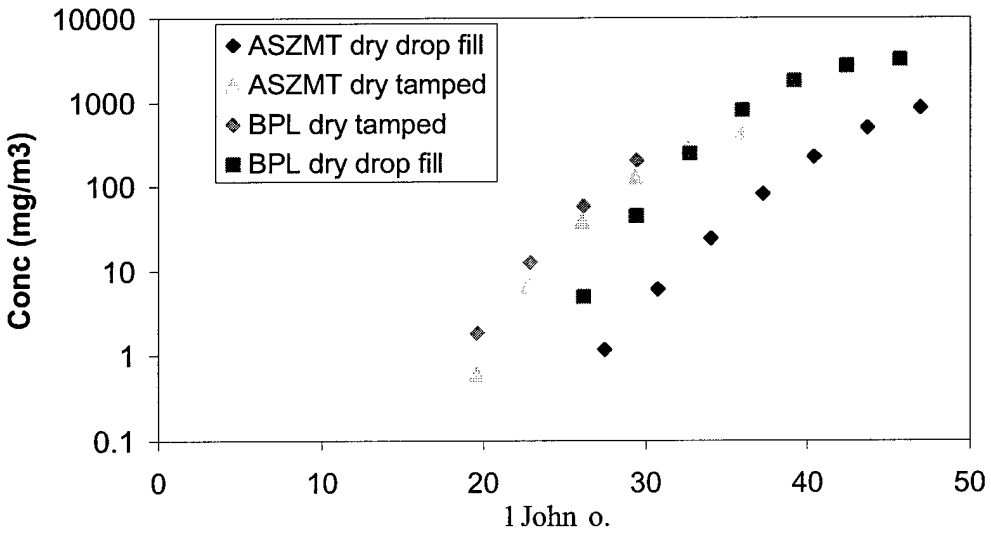

Figure 4. Sample of dry activated carbon with 15% cured 50 mesh polyester.

The mechanical properties of immobilized beds were assessed using three techniques: stress/strain, compression and attrition. Figure 5 illustrates the effect of loading on compressive strength. Epoxy samples are stronger in compression while urethane samples give better flexural properties. Attrition effects are measured by weight loss on a vibration table.

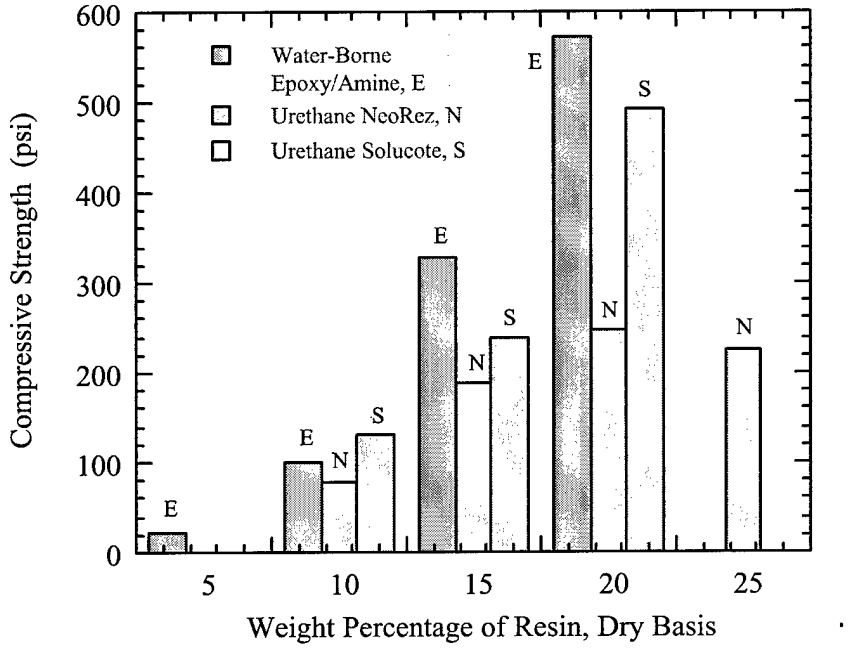

Figure 5. Comparison of compressive strength versus resin content for samples of dry activated carbon with water-borne epoxy/amine, urethane Solucote and urethane NeoRez.

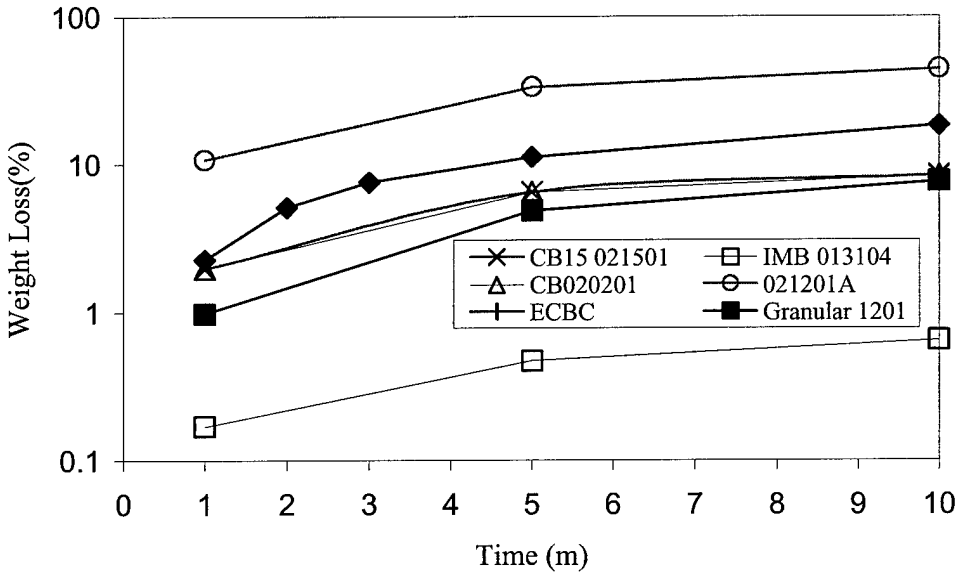

Figure 6. Attrition weight loss for several immobilized samples at 15% loading.

The change in rate of attrition is demonstrated in figure 6. The initial rate is affected by loose granules and edge effects. This rate decreases with time.

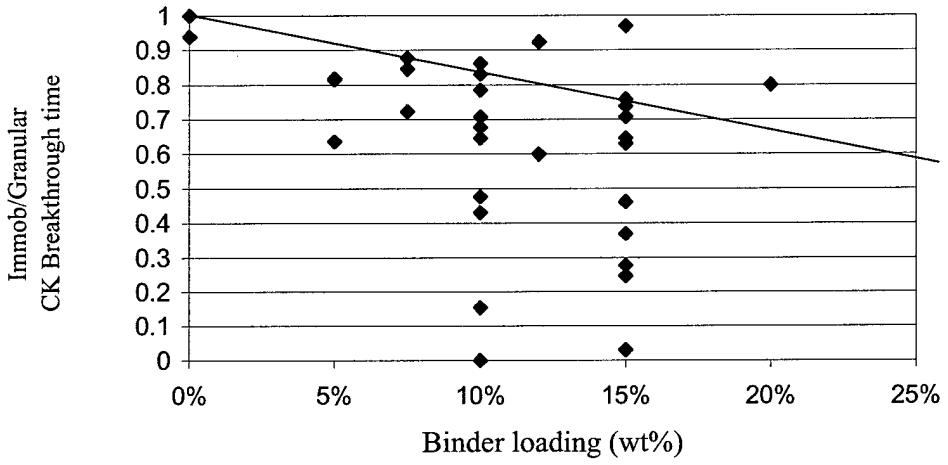

Figure 7. Effect of loading on breakthrough behavior.

The breakthrough results for bonded samples are presented in figure 7. Despite the large scatter in the data there appears to be a linear trend the breakthrough time reduction with increasing loading. The increase in bonding strength as related to this filtration reduction must be addressed by some optimization scheme.

CONCLUSIONS

Immobilized samples of granular activated carbon have been fabricated with strong mechanical properties, attrition resistance and light gas filtration performance loss of 10-20%. The wet techniques using waterborne epoxy and urethane result in significant surface coverage with associated loss of filtration performance.

CITATIONS

1. Mahle, J.J., Palmese, G., Ziaee, S., "Filter Immobilization Studies Part 1. Polymer Screening", U.S. Army, APG MD, ECBC-TR-060, (1999).

FOUR PORTRAITS OF THE PLAGUE ORGANISM

Millard M. Mershon

Science Applications International Corporation
Biomedical Modeling and Analysis Program

Yersinia pestis organisms have infective and self-protective features that are expressed or suppressed to fit different conditions. The *Y. pestis* bacteria respond selectively to a variety of signals (which occur inside or outside of diverse hosts and cells) by expressing products that ultimately promote the multiplication and survival of the organisms. This paper briefly outlines the dynamics and time courses of the warfare between invading bacteria and susceptible hosts. At least four different sets of products and mechanisms are described as characteristic of natural life cycles of wild-type *Y. pestis* in non-human hosts. This information is used to project likely hazards for human beings, design of effective vaccines, and selection of other countermeasures.

INTRODUCTION

This paper resulted from a requirement to estimate human hazard levels (and probable consequences) of feasible military attacks involving weaponized *Y. pestis* organisms[1]. Such requirements pose severe problems. In such cases, experimental data collection is impractical. Experimental methods would require unavailable human subjects, inappropriate use of animals, or unreasonable resources. Computer-aided modeling offers alternatives, but (as with other modeling) usefulness depends upon effective projection of realities in the field of interest. Modeling of biological warfare hazards involves realities of organism or toxin characteristics, and their interactions with live environments. Since potential enemies do not share data on characteristics of weaponized *Y. pestis* organisms, it was necessary to base estimates on parameters of (and experience with) wild-type *Y. pestis.* Accordingly, it became necessary to project consequences from human inhalation of an organism adapted for success in promoting infections of fleas and rodents. This necessity led to extrapolations of conclusions drawn by plague specialists. Such interpretations were strongly dependent upon perspectives provided in two comprehensive reviews by Dr. Robert Brubaker[2,3] and one by Drs. Robert Perry and Jacqueline Fetherston[4]. In lieu of extensive citations, references to these reviews are implied or used wherever possible, below. A few citations are provided indirectly as references listed in modeling reports[1,5]. In some cases these indirect modeling references are localized to one of 40 numbered paragraphs (ex.:[1-40]) or a section (ex.:[5-4.1]) of the cited report. Papers by Dr. Joseph Hinnebusch, *et al.*[6-8] illustrate flea anatomy and relationships of *Y. pestis* properties to pathophysiology in fleas. Photographs of a blocked flea and *Y. pestis* in tissue have been related to biological warfare by Drs. Thomas McGovern and George Christopher[9]. Initial capitals are used, in this paper, to distinguish protein products from their genes (ex.: Ymt vs. *ymt*).

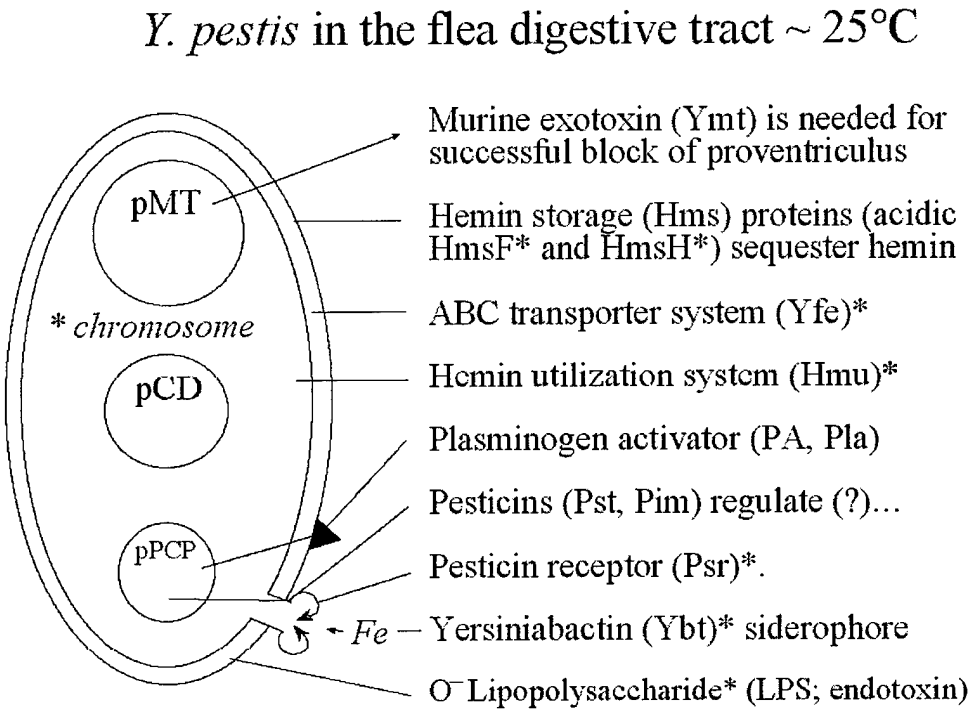

Figure 1. The virulence of *Yersinia pestis* bacteria has been associated with proteins encoded by genes in chromosomal DNA and three plasmids. As represented above, the pMT1 (murine toxin) plasmid is the largest. The mid-sized pCD1 (calcium dependence) plasmid is not expressed in fleas. Although it is small, the pPCP (pesticin, coagulase, plasminogen activator) plasmid is active in both fleas and their hosts. Hinnebusch et al.[8] report that Ymt exotoxin is primarily expressed at flea temperatures, and is important for survival of *Y. pestis* (for transmission via the flea) but it is not required to kill mice. Perry[10] observes that "Pathogens must acquire iron from the iron-deficient environment of their mammalian hosts to survive and cause disease...the siderophore-dependent yersiniabactin (Ybt) iron transport system is required during the early stages of plague infections. An independent Yfe iron transport system functions later in the infectious process to acquire the iron essential for growth. [Another *Y. pestis* system allows use of] heme-containing proteins...a temperature-regulated hemin-storage [Hms system] absorbs hemin to the outer membrane...and is required for transmission of the disease from fleas to mammals." Hinnebusch et al.[7] found that Hms proteins are required for blockage of the flea proventiculus with *Y. pestis* that are regurgitated into flea bite wounds in hosts. They concluded that sequestered hemin of *Y. pestis* outer membranes causes them to be "...extremely aggregative and hydrophobic." Such bacteria stick to each other sufficiently to 'gum up' spines of the proventiculus a few days after infection occurs in the flea midgut[8]. This action was shown as independent of the plasminogen activator (Pla). Pla is now believed to aid host uptake of bacteria from a bite wound, rather than affecting the flea[8]. It appears that some of the *Y. pestis* iron-acquiring mechanisms are also expressed in the flea primarily in readiness for use in a host. This may be true for LPS, Yfe, Hmu, and the pesticin receptor (Psn) system, including pesticin (Psn), its inhibitor (Pim), and Ybt.

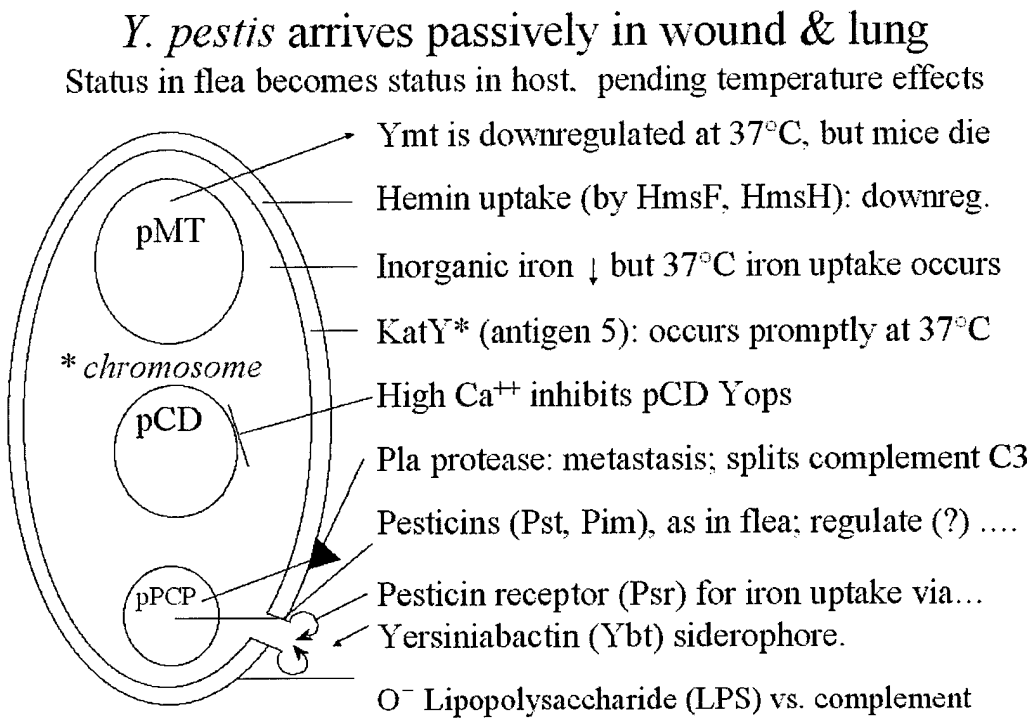

Figure 2. Continued Ymt exotoxin export may be useful but not necessary at 37°C. However, the key to *Y. pestis* success in warm bodies is temporary vulnerability[1-27]. *Y. pestis* present as a harmless Trojan horse to be taken inside host macrophages, which are then sabotaged. This stage may last for ¼4 hrs [1-9,24]. Perhaps only the bacteria prepared for survival in a macrophage are relevant for infection; Finegold[1] found only about 100 *Y. pestis*/lung at 12-16 hrs after an inhalation exposure. Prepared bacteria will have features primarily needed in the flea, but specific products of iron storage may have a brief role. Already stored hemin may be needed for *Y. pestis* survival of destruction from H_2O_2 in the macrophage[1-32]; the KatY in periplasm[3] may provide a second line of catalase defense. Extracellular blockade of pCD prevents an attack by *Y. pestis* before they are safely within the macrophage. Pre-existing Pla is ready to lyse clots or membranes that might isolate extracellular *Y. pestis* from local macrophage intake, or transfer to lymph nodes. Pla protects *Y. pestis* from phagocyte chemotaxis[1-9] or opsonization[1-14] by C3 complement protein in blood. The unornamented (O^-, sidechain free) LPS[1-6] of *Y. pestis* also prevents placement of the complement membrane attack complex. It appears that some iron-related processes are temperature specific to meet changing conditions. It is less clear why and when given systems are needed. After mentioning the Ybt, Yfe, and Hmu systems, Perry[10] states, "All three of these uptake systems are expressed only when needed and we are examining the regulatory mechanisms which control their expression." It is known that Psr binds both Pst and Ybt. Iron delivered to Psr by Ybt is handled by a cytoplasmic iron transfer protein known as TonB, under control of a feedback regulator known as Fur[1-30]. This iron transfer system is found in other *Y. pestis* iron uptake systems[4]. Brubaker[2] observed that Psn may aid iron uptake, but lack of Psn does not reduce virulence of *Y. pestis* in the presence of iron. Psn kills Psn-deficient mutants. Brubaker[11] suggests that Psn kills *Y. pestis* mutants that might arouse effective host immune responses. However, Psn might induce toxic levels of iron if not regulated by Pim. This would explain Psn killing of bacteria without Pim.

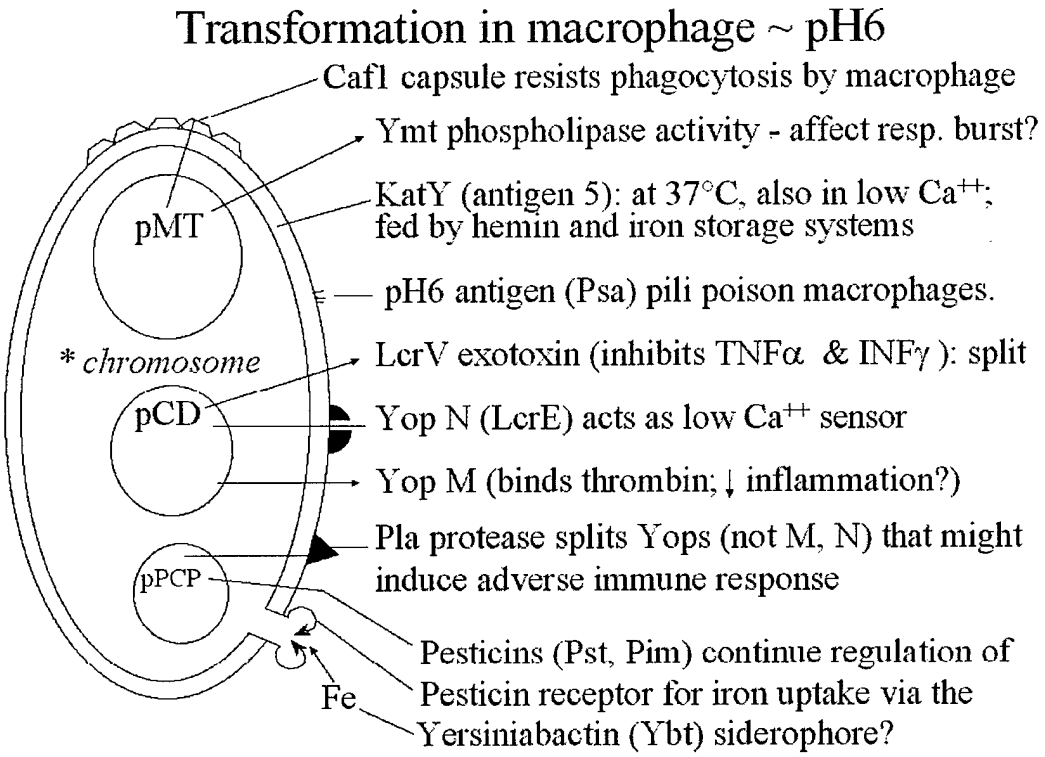

Figure 3. Caf1 (F1 capsular antigen of Plague Vaccine, USP[1-7]) is freely expressed by *Y.pestis* in cultures at 37°C, but probably not before macrophage uptake *in vivo*[1-27]. However, Davis et. al.[4] have shown that capsules do not impede virulence of cultured *Y. pestis* inhaled into monkey lungs. This is important because acidic alveolar macrophage lysosomes may have relatively weak oxidative bursts[1-26], making them easy targets for *Y. pestis* to parasitize. The Ymt phospholipase activity inhibits cell respiration in mice[1-7]. Such activity and/or suppression (Bauldry[1]) of tumor necrosis factor (TNFα) may depress phagocyte respiratory bursts. Such suppression could be slow (or hemin insufficient) to neutralize lysosomal H_2O_2. Rapid deployment of more catalase (Fe+KatY) may provide defense-in-depth[1-32]. *Y. pestis* not only survive but adapt, multiply and escape from macrophages[1-31]. They adapt to very acidic conditions (pH 4.6-4.8[1-34]) within the lysosome by expressing fibers (pili) of pH 6 antigen (Psa). Pili are cytotoxic to macrophages, preventing antigen presentation or antibody formation[1-34]. Further suppression of host immune defenses is made potentially possible by the activation of transcription factor LcrH (under intracellular conditions) to express some Yersinia outer proteins (Yops)[2,3,4]. However, LcrV inside cells is destroyed by Pla protease. Presumably LcrE is needed, and LcrV and Yop M become exotoxins, only after the multiplied *Y. pestis* burst from macrophages. As in the flea, the *Y. pestis* bacteria must simultaneously flourish in their current intracellular environment and be preparing for transition to the next. Although handling of iron is critical (more than 10% of *Y. pestis* membrane protein is involved with this function[1-28]), it is not clear how iron handling takes place within the macrophage. One guess is that internal status directs change. Hemin retention and KatY may dominate while *Y. pestis* must resist oxidation under acid conditions in the lysosome. When the lysosome is disabled, the multiplying *Y. pestis* may use other systems to reprocess iron stored by the initial organism. Then the bacteria may use Ybt to scavenge iron from macrophage cytoplasm poisoned by pili. Finally, systems must be in place for survival during extracellular transit (in lymph or blood) to nodes, liver, or spleen.

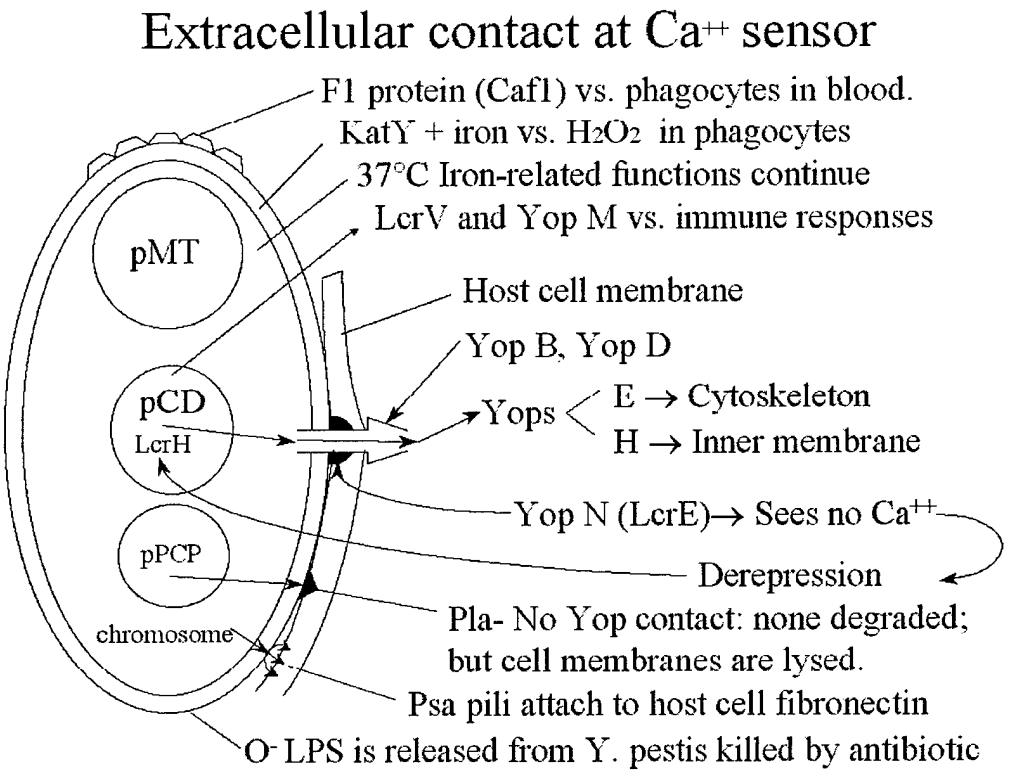

Figure 4. In macrophages, synthesis of Psa was detected after 90 min. and pili after 4hrs, but F1 capsular antigen caught up after 18 hrs[1-33]. Assembled Caf1 subunits[1-7] largely shield pili in culture. This may represent the extracellular state in which Caf1 repels phagocytosis. KatY is expressed abundantly at 37°C, and it may scavenge H_2O_2 in foci made necrotic by *Y. pestis*[3], but virulence is unaffected by deletion of genes for KatY[11] or Caf1[1,3]. The diverse iron-acquisition system assures uptake of the iron required for massive extracellular multiplication of *Y. pestis*[4]. LcrV is expressed independently of cytotoxicYops to serve as an exotoxin that suppresses usual immune responses to foreign protein or bacteria[3,4]. LcrV does this by blocking upregulation of inerferon gamma (IFNγ) and tumor necrosis factor alpha (TNFα). As noted by Brubaker[4], these cytokines "...fill indispensable roles in non-specifically activating professional phagocytes and mediating formation of protective granulomas...[*Y. pestis*] maintains the illusion that the host has no cause for alarm. In short, plague is a disease of stealth." Yop M helps to maintain that illusion by interfering with inflammatory responses involving thrombin and platelets. It has been suggested that this blocks mediators of chemotaxis, histamine release, vascular permeability, and migration of leukocytes[1-16]. *Y. pestis* use Psa and a type III secretory pathway[2] as follows: "...while employing pili to pin their opponents, at close quarters the invaders deploy syringes and dispatch host cells by injecting cytotoxic Yops. Gaining strength from captured nutritional assets...the invading masses cause focal necrosis and...terminal levels of bacteremia...with endotoxin shock.[1]" The roles of Yops B, D, E and H (and other cytotoxins) in this process (and external disabling of phagocytes) have been illustrated in more detail elsewhere[2,4]. However, it should be noted that Psa pili permit *Y. pestis* to adhere both to fibronectin of host membranes and mucin of mucous membranes[1-36]. LcrE needs close contact to exclude extracellular Ca^{++}. Pla binds collagen[2] and "...promotes adherence[4...]" until its proteolytic action opens membranes. According to Finegold et al.[1], LPS may be under-rated as a cause of death from *Y. pestis*. Others have observed that antibiotics may kill *Y. pestis*, then their LPS kills with henorrhagic shock[1].

TABLE 1. Relative Impacts of Conceivable Vaccine Antigens on *Y. pestis* virulence.

Antigens	Attenuation Factor*	References
Pgm (pigmentation: useage of iron)	10^8	Kutyrev, *et al.* (1989, 1992)[4]
Lcr (transcription of all Yops)	10^7	Une & Brubaker (1984)[4]
LcrV (V exotoxin)	10^7	Brubaker (1996)[1]
pPCP (pesticins + Pla)	10^7	Brubaker, *et al.* (1965)[1]
Pla (plasminogen activator)	10^6	Sodinde *et al.* (1992)[4]
Yops E, H, KL or Lcr (cytotoxicity)	10^6	Straley & Bowmer (1986)[4]
Yop M (binds thrombin)	10^5	Leung *et al.* (1990)[4]
pH6 (Psa) antigen (pili)	10^4	Lindler *et al.* (1990)[4]
Yop D (cytotoxicity)	10^3	Andrews *et al.* (1999)[3]
Yop N (LcrE; Ca^{++} sensor)	1	Andrews *et al.* (1999)[3]
Caf1 (F1 protein)	1	Pitt, *et al.* (1990)[1]
Kat Y (catalase)	1	Brubaker (2001)[11]
Psr (pesticin receptor)	?	-
O^- Lipopolysaccharide (endotoxin)	?	-

* Approximated attenuation factors given as *Y. pestis* log dose reduction with antigen deleted, rounded to nearest log; studies may not be completely comparable.

Table 1. A substantial portion of the human population does not develop effective antibodies to a given vaccine. Accordingly, trivalent vaccines (such as the annual influenza vaccine) are used in hope that seroconversion failure will not occur with all antigens. This prompted thoughts of a future trivalent plague vaccine[5]. Kutyrev *et al.* (1989)[4] list the minimal requirements for *Y. pestis* pathogenicity as functioning Pgm and LcrV. This idea is supported by successful long term Russian use of live *Y. pestis* in human vaccination programs[1,5]. Such vaccination relies on absence of the multiple Pgm genes from *Y. pestis* strain EV-76. Brubaker[3] has reported apparent success of experimental vaccines that incorporate LcrV as a subunit antigen. He also mentioned hearsay of Russian success with a vaccine using Pla as the antigen[5-3.5]. This table might suggest that targeting of Yops could be effective. However, antibodies need access to an antigen displayed on the bacterial surface, like capsular antigen of Plague Vaccine USP. Figures 3 and 4 show that most Yops are expressed when and where they are not readily accessible to antibodies. As secreted exotoxins, LcrV is (and Yop M may be) accessible. LcrE is the only other Yop reported as resistant to proteolysis by Pla. The report of Andrews *et al.*[4] suggests that Y. pestis has alternatives to use of LcrE for activation of the type III secretory pathway. Vodop'ianov *et al.* (1995)[5] found that cytotoxic effects of Psa pili prevented attempts to induce antibodies to this surface-displayed antigen. It appears that a surface-displayed member of the Pgm family might be a promising candidate. KatY is primarily located in periplasm and otherwise unpromising[4,11]. This leaves the pesticin receptor as a candidate for evaluation. It remains to be seen whether components of other iron-related systems are available to antibodies. However, it is possible that antigen accessibility should be assessed for *Y. pestis* in the form considered in Figure 4. A review[1] of human pneumonic plague transmission suggests that this is the form of *Y. pestis* that was inhaled. Russian investigators[5-3.6] claim success with vaccination by inhalation of dry *Y. pestis* strain EV-76. Butler (1996)[5] has developed monoclonal antibody anti-endotoxins. It is not clear that O^- LPS, as displayed on the surface of *Y. pestis*, has been tried in a vaccine.

SUMMARY

The plague organism presents in at least four distinctively different forms, depending upon its current environment. Since biological warfare is likely to involve inhalation exposures[9], it follows that a future anti-plague vaccine should be optimized to prevent pulmonary macrophage access by either passive or pneumonic forms of *Y. pestis*. Presently available data suggest that a future inhalable trivalent vaccine might beneficially include subunit antigens for LcrV, Pla, and Psr and/or other iron-related *Y. pestis* antigens.

ACKNOWLEDGEMENTS

This paper is a result of research (under Contract No. DAMD17-93-C-3141) directed by COL Gerald Parker, (then) Deputy for Medical, Chemical, and Biological Defense, U.S. Army Medical Research and Materiel Command, Fort Detrick, MD 21702-5012, with initial project management by (then) MAJ George Korch and subsequent support by (then) LTC Kelly Davis.

REFERENCES

1. Hursh, S.R., Mershon, M.M. and Fanzone, J.F., Jr. *Yersinia pestis* Battlefield Challenge and Contagious Hazard Modeling with Medical and Non-Medical Countermeasures. Technical Report MCBDRP 97-1 (1997). Medical Biological Defense Research Program, U.S. Army Medical Research and Materiel Command, Fort Detrick, Frederick, MD.

2. Brubaker, R.R. Factors Promoting Acute and Chronic Diseases Caused by *Yersiniae*. *Clinical Microbiological Reviews*, July 1991; 4:309-324.

3. Brubaker, R.R. *Yersinia pestis* and Bubonic Plague. In: M. Dworkin, S. Falkow, E. Rosenberg, K.-H. Schliefer, and E. Stackelbrandt (Ed.), The Prokaryotes, an Evolving Electronic Resource for the Microbiological Community, On Line. Springer Verlag, New York, 2000.

4. Perry, R.D. and Fetherston, J.D. (1997) *Yersinia pestis*--Etiologic Agent of Plague, *Clinical Microbiological Reviews*, January 1997; 4:309-324.

5. Mershon, M. M. *Yersinia pestis* Properties and Countermeasures. Special Report MCBDRP 98-1 (1998). Medical Biological Defense Research Program, U.S. Army Medical Research and Materiel Command, Fort Detrick, Frederick, MD.

6. Hinnebusch, B.J., Perry, R.D. and Schwan, T.G. Role of the *Yersinia pestis* Hemin Storage (hms) Locus in the Transmission of Plague by Fleas. *Science*, July 1996, 273:367-370.

7. Hinnebusch, B.J., Fischer E.R., and Schwan, T.G. Evaluation of the Role of the *Yersinia pestis* Plasminogen Activator and Other Plasmid-Encoded Factors in Temperature-Dependent Blockage of the Flea. *Journal of Infectious Disease*, November 1998, 178:1406-1415.

8. Hinnebusch, B.J., Cherpanov, P., Du, Yi, Dixon, J.D., Schwan, T.G. and Forsberg, A. Murine Toxin of *Yersinia pestis* is Not Required for Virulence in Mice.

9. McGovern, T.W. and Christopher, G.W. Biologic Warfare and Its Cutaneous Manefestations. http://telemedicine.org/BioWar/biologic.htm, April 2001.

10. Perry, R.D. Current Projects. http://jenner.mi.uky.edu/perry.htm, April 2001.

11. Brubaker, R.R. Personal communication, April 2001.

PROTECTION AGAINST CHEMICAL AGENT-INDUCED, SEIZURE-RELATED NEURONAL CELL DEATH

Gerald P. H. Ballough
La Salle University
Philadelphia, PA 19141-1199

Margaret G. Filbert*
US Army Medical Research Institute of Chemical Defense
Aberdeen Proving Ground, MD 21010-5400

INTRODUCTION

Organophosphorus nerve agents are the most toxic chemical warfare agents that present a threat to the warfighter. Irreversible inhibition of acetylcholinesterase, by nerve agents leads to accumulation of the neurotransmitter acetylcholine (ACh) at cholinergic synapses (Taylor, 1996). Currently fielded MARK I nerve agent antidote for treatment of nerve agent poisoning protects against life threatening consequences (Dunn and Sidell 1989). When (ACh) accumulates in excess amounts it can initiate seizure activity. Soldiers surviving the initial life threatening effects of nerve agent poisoning are likely to develop seizure activity. Seizures perturb other neurotransmitter systems and release the excitatory animo acid (EAA) glutamate. The EAA then assumes control of the seizures and progression to status epilepticus (SE) (McDonough and Shih, 1993) . Sustained release of glutamate and excessive stimulation of EAA receptors triggers delayed secondary excitotoxic biochemical changes involving a complex cascade of factors such as intracellular calcium overload, lipid peroxidation and free radical development, all of which contribute to neuronal cell death (Olney *et al.,* 1983).

Control of seizure activity is the most critical factor in development of brain damage following nerve agent poisoning. While seizure-related brain damage can be prevented by administration of an anticonvulsant drug, battlefield conditions may preclude prompt administration of the convulsant antidote for nerve agents (CANA). The currently fielded CANA is diazepam. Diazepam may not prevent or arrest seizures in all individuals. At the present time there is no capability for measuring seizure activity on the battlefield. Unconscious battlefield victims may undergo silent seizures without convulsive behavioral manifestations. Delays or failures to locate casualties are to be expected on a battlefield. Left untreated, seizures progress to status epilepticus and become more refractory to anticonvulsant therapy. There is a military need for neuroprotective adjunct drugs capable of preventing development of delayed neuronal cell death when administered one or more hours after onset of seizures.

We have investigated the effects of a synthetic nonpsychotropic derivative of tetrahydrocannabinol (THC), HU-211 (dexanabinol, 7-hydroxy-Δ^6– tetrahydrocannabinol-1, 1-dimethylheptyl; Pharmos Ltd, Rehovot, Israel) on soman-induced seizure-related brain damage. HU-211 was reported to have neuroprotectant effects in neurons exposed to excitotoxins in culture (Eshhar *et al.,* 1993). Binding studies revealed that HU-211 blocks N-methyl-D-aspartate (NMDA) receptors in a stereospecific manner at binding sites that are distinct from MK-801 and TCP binding sites (Feigenbaum *et al.,* 1989). HU-211 was observed to attenuate cell damage produced by nitric oxide and to be a peroxy radical scavenger protecting neuronal cells in culture from free radical generators (Eshhar *et al.,* 1995). Mechoulam *et al.,* 1998 proposed that the mechanism of action of HU-211 is blockage of the NMDA-operated calcium channel. HU-211 has been reported to act as a neuroprotectant in animal models of head injury, optic nerve crush and ischemia. A single injection of HU-211 conferred a significant increase in neuronal survival after the above insults (Mechoulam *et al.*, 1989).

METHODS

Male Sprague-Dawley rats (CRL: CD[SD]-BR: Charles River Labs, Wilmington MA), weighing between 250-300 g were anesthetized with sodium pentobarbital (35 mg/kg, i.p.) and positioned in a sterotaxic apparatus. Three holes were drilled through the skull into which screw electrodes were placed for electrocorticographic ECoG recordings. Electrodes were connected to a standard small-animal headpiece and secured by dental cement. One week later, the animals were connected to an ECoG recording system and allowed 30 min to acclimate. Baseline ECoG activity and behavior were

monitored for at least 15 min. Following baseline recordings, animals were injected (i.p.) with 125 mg/kg of the oxime HI-6. This was followed 30 min later by injection of 180 μg/kg soman (1.6 LD_{50}, s.c.) or sterile saline. Within one min following soman or saline injection, animals were injected (i.m.) with 4-mg/kg atropine methylnitrate (AMN). The quaternary compounds, HI-6 and AMN, were administered to protect against the peripheral effects of soman and to ensure survival. HU-211 was injected (25 mg/kg in Miglyol) at 5 or 40 min following onset of seizures as determined by ECoG recordings. In a small group of animals 20 mg/kg, (i.p.) diazepam was administered 40 min after seizure onset or 20 mg/kd diazepam + 25 mg/kg HU-211 were given at this same time.

Twenty-eight hours after soman administration, rats were given an injection of pentobarbital (100 mg/kg, i.p.) and euthanatized via transcardial perfusion with ice cold 4% paraformaldehyde in 0.1M phosphate buffer, pH 7.4. Brains were immediately excised and longitudinally divided into left and right hemispheres. Alternate hemispheres were postfixed by immersion in a second solution of ice-cold 4% paraformaldehyde in 0.1M phosphate buffer for 4-6 hr. The hemispheres were subsequently sucrose-saturated (30% sucrose in 0.1M buffer for 72 hr) and coronally sectioned at 40 μm. Serial sections were collected directly onto polylysine-coated slides for staining or cryoprotected and stored at –20° C pending immunocytochemical staining for microtubule associated protein 2 (MAP2). The remaining hemispheres were paraffin processed, sectioned at 4 μm and stained with hematoxylin and eosin (H&E). Morphometric image analysis of MAP2 stained sections was performed according to the procedure described by Ballough *et al.,* (1995).

Group means for temporal lobe lesion volumes obtained from MAP2-stained sections were compared using t-tests. ECoG data were grouped according to treatment, post-seizure onset delay, frequency band and absolute or relative powers. Group means were compared using one-way analysis of variance (ANOVA), followed by the Student-Newman-Keuls (SNK) multiple range test. Chi-square analysis was used to assess the relative power distributions across frequency bands in the 24 hr ECoG data. Regression analysis was used to extract ECoG correlates of seizure-related brain damage or neuroprotection by comparing all powers and relative powers of all frequencies to lesion volumes at 28 hr following soman injections. Values for $p < .05$ were considered significant.

RESULTS

All soman-treated rats exhibited sustained seizures and status epilepticus for several hr with or without HU-211 treatment. This determination was based on the presence of ECoG amplitudes greater than four times baseline. Proconvulsive behavioral signs of soman intoxication included repetitive chewing, facial clonus, forepaw clonus, motor stereotypy and wet-dog shakes. Overt motor convulsions were characterized by rhythmic clonic jerks of both head and forepaws, rearing, salivation and Straub tail. Seizure activity was evident in these animals when assessed 24 h post-soman administration. ECoGs from non-soman control rats showed no evidence of seizures and there was no histological evidence of neuropathology in H&E- and MAP2-stained brain sections from these animals.

Histopathological evaluations of H&E-stained brain sections from rats that received soman but not HU-211 revealed severe region-specific brain damage, i.e., some regions exhibited severe lesions, while others were virtually unaffected. This damage was bilaterally symmetrical and characterized by widespread tissue necrosis, neuronal loss, chromatolysis, vacuolization, pyknosis and gliosis. The most severe damage was consistently observed in the piriform cortex, entorhinal cortex, dorsal endopiriform nucleus and the laterodorsal thalamic nucleus. Pronounced damage was seen in perirhinal cortex, amygdaloid complex, hippocampus and midline thalamic nuclei. This pattern of soman-induced seizure-related brain damage is consistent with previous reports (Ballough *et al.,* 1995, 1998: McDonough *et al.,* 1998).

Histopathological damage rating for H&E-stained brain sections are based on the presence of necrotic neurons and/or the absence of a defined neuronal population. In this study, piriform cortical brain damage was significantly ($p = .008$) reduced in the soman + HU-211-treated animals compared to soman controls.

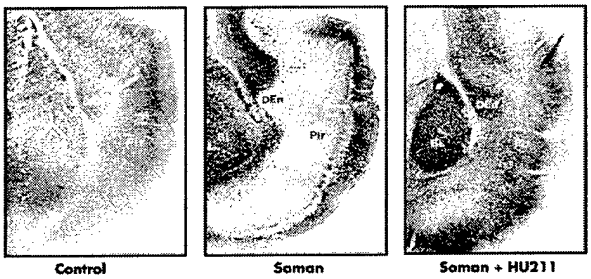

Figure 1. MAP2 immunohistochemical staining of the rat temporal lobe. **Control**: saline-injected animal; **Soman**; soman-induced lesions after 4-5 hr status epilepticus; **Soman + HU-211**: neuroprotection produced by treatment with HU-211. BL: basal lateral amygdala; Den: dorsal endopiriform nucleus; Pir: piriform cortex. Black letters indicate damaged areas.

Figure 1 (Control) shows the MAP2 immunostaining of the rat temporal lobe. In control animals, MAP2 staining was localized in the neuronal perikarya and proximal dendrites. MAP2 immunostaining was not observed in areas composed of white matter, except in small numbers of scattered neurons. The loss of the neuron-specific MAP2 marker indicates severe neuronal damage and provides clear demarcation of widespread neuronal necrosis (Ballough *et al.,* 1995). In this study severely damaged brain regions were easily identified by an almost total absence of MAP2 immunostaining (Fig 1, soman). Clearly demarcated macroscopic lesions (MAP2-*negative* immunostaining) were consistently observed in the piriform, perirhinal and entorhinal cortices, endopiriform nucleus, postiolateral cortical amygdaloid nucleus, laterodorsal, mediodorsal, ventromedial and lateroposterior thalamic nuclei of the soman control group. Along the anterior-posterior axis of the temporal lobe, cross-sectional areas of necrosis were greatest at bregma –3.3± 0.2 mm, irrespective of lesion volume. These lesions often extended dorsally to include the perirhinal cortex. Medially, the area of damage often included the endopiroform nucleus while sparing the lateral and basolateral amygdaloid nuclei. In the most severe cases, the necrotic core included these nuclei as well. In the penumbra, surrounding the necrotic core, MAP2 immunostaining was elevated above controls. Control animals showed no evidence of MAP2 loss in any of the above brain regions. And the MAP2 immunostaining was consistent between individuals and exhibited the normal staining pattern described previously (Ballough *et al.,* 1995, 1998).

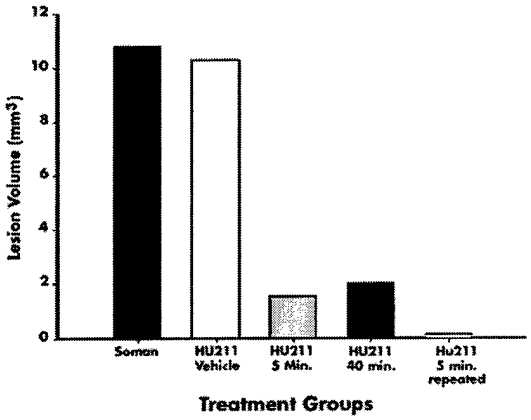

Figure 2. Histogram depicting median lesion volumes of temporal lobe necrosis (mm^3). Morphometric image analysis was used to assess MAP2-*negative* staining in the piriform cortex and contiguous regions. HU-211 reduced median lesion volume 86% when administered 5 min after seizure onset; 81.5% at 40 min and repeated administrations (5 min then @ 6 hr) produced a 99% reduction in lesion volume.

HU-211 provided considerable neuroprotection against soman-induced seizure-related brain damage, (Fig 1, soman + HU-211). When administered 5 min after seizure onset, unilateral temporal lobe macroscopic lesion volume was significantly reduced ($p = .006$) in the soman + HU-211 treated group 86% (Fig 2).

When administered 40 min after seizure onset, HU-211 reduced the median lesion volume of necrosis 81.5%. In a small group of animals ($n = 6$) the HU-211 was given 5 min after seizure onset and then every six hr for the next 24 hr. In this group, median lesion volume was reduced 99% (Fig 2).

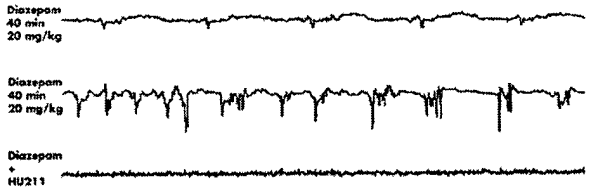

Figure 3. ECoG recordings from animals given 1.6 LD_{50} soman and 20 mg/kg diazepam 40 min after seizure onset. The lower tracing is from an animal that received diazepam at 40 min as above and 25 mg/kg HU-211 immediately after the diazepam.

Figure 3 shows the ECoG records at 24 hr after soman injection of three animals that were given diazepam or diazepam + HU-211 at 40 min after seizure onset. It has been shown by McDonough (personal communication) that diazepam is not effective in arresting seizures when given 40 min after seizure onset even at very high doses, e.g., 20 mg/kg. When HU-211 was administered immediately following the diazepam, seizure activity abated.

Statistical analysis of ECoG total power (i.e., sum of all frequencies) revealed no differences between the soman control and the soman + HU-211 groups at any of the sampling periods. Spectral power analysis revealed that relative Delta-1 power (0-0.5 Hz) in soman controls increased more than three fold over the baseline value of this frequency. In the soman + HU-211 group, the 24 hr relative delta-1 power was not significantly different from the baseline value.

The most striking fluctuation in the ECoG power of all frequency bands was seen in relative beta-2 (21-31.5 Hz). Chi square analysis of the relative power distributions across frequencies revealed a significant shift of the entire ECoG spectrum toward the lower frequencies in the soman control group compared to the HU-211 protected group at the 24 hr time period. Regression analysis provided evidence of a shift in the entire ECoG spectrum: there was a good correlation ($R^2 = 84.4$, $p < .001$) between decreased relative beta and increased relative delta in the soman control group. Of 109 regression analyses, using ECoG powers and relative powers of all frequency bands and total power at all time points as predictors of subsequent lesion volume at 28 hr, only 15 frequency/time points had correlations coefficients above 20. There were 5 frequency/time-points with correlations above 30, and 2 with correlations above 34.5, i.e., relative beta-1 ($R^2 = 58.5$, $p < .01$) and relative beta-2 ($R^2 = 90.6$, $p< .001$) at 60 min after onset of seizures (Fig 4).

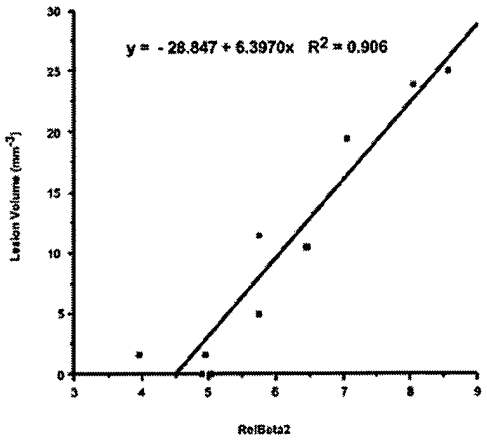

Figure 4. Correlation of median lesion volumes observed at 27 hr after soman injection with relative beta-2 frequency power at 60 min after seizure onset ($P < .001$).

DISCUSSION

As see in Fig 1, HU-211 conferred considerable protection against brain damage resulting from soman-induced seizures without diminishing the intensity or duration of the seizures. MAP2 volumetric assessments revealed an 86%

reduction in temporal lobe macroscopic lesions in the HU-211-protected group compared to soman controls. This observation was supported by H&E histopathological evaluations where the HU-211-treated animals showed a significant reduction in piriform cortical damage. The HU-211 group showed only a mild neuronal loss (11-25%) compared to soman controls which had severe neuronal loss (> 45%).

Earlier reports have shown that NMDA antagonists such as ketamine and MK-801 protect thalamic neurons from seizure-related brain damage without preventing seizure activity (Clifford et *al.*, 1990). These authors suggested that these NMDA antagonists may have prevented seizure-related damage by blocking NMDA receptor ion channel complexes on the dendrosomal surfaces through which glutamate excitotoxicity is expressed and that the seizure activity can be maintained by other neurotransmitter systems without NMDA receptor participation.

The high correlation of lesion volume with relative power of beta-2 frequency observed at 60 min after seizure onset may indicate that this is the absolute window for preventing seizure-related brain damage. This time point coincides with the irreversible effects of intracellular calcium overload that leads to cell death (Randall and Thayer, 1992).

Interestingly, neither HU-211 nor diazepam administered at 40 min after seizure onset stops the seizure activity when administered alone. But when given together, seizures were arrested suggesting a synergistic interaction between these two compounds. This synergy may have produced augmentated hyperpolarization of post synaptic memebranes by the combined HU-211 antagonnism of NMDA receptors and agonistic modulation of the GABA receptors by diazepam.

The results presented here demonstrate that pharmacological interventions can prevent or minimize delayed brain damage resulting from chemical warfare agent-induced seizure activity. Such intervention is most important where administration of countermeasures for chemical warfare agents is delayed. HU-211 or other neuroprotectant drugs may be useful adjuncts for medical management of chemical casualties on the battlefield.

ACKNOWLEDGEMENTS

The authors wish to thank Dr.s. Anat Beigon and George Fink of Pharmos for the most generous gift of HU-211 and the skillful assistance of JS Forster, M. Jaworski, and Joe Jaworski in conducting these experiments.

REFERENCES

Ballough G., Martin, L., Cann, F., Graham, J., Smith C., Kling, C., Forster, J., Phann, S. and Filbert, M., "Microtubule-associated Protein 2 (MAP2): A Sensitive Marker of Seizure-related Brain Damage. J. Neurosci. Meth., Vol 61, pp. 23-332, 1995.

Ballough, G., Cann, F., Smith, C., Forster, J., Kling, C., and Filbert, M., "GM! Monosialoganglioside Pretreatment Protects Against Soman-induced Seizure-related Brain Damage." Molec. Chem. Neuropath. Vol 34: pp1-23, 1998.

Clifford, D., Zormumski, C. and Olney, J., "Ketamine and MK-801 Prevent Degeneration of Thalamic Neurons Induced by Focal Cortical Seizures. Exp. Neurol. Vol 10: pp. 272-279, 1989.

Dunn, M. and Sidell, F., "Progress in Medical Defense Against Nerve Agents." J. Amer. Med. Assoc., Vol 262, pp. 649-652, 1989.

Eshhar, N., Striem, S. and Biegon, A., "HU-211, a Non-psychotropic Cannabinoid Rescues Cortical Neurons from Excitatory Amino Acid Toxicity in Culture." NeuroReport Vol 5: pp. 237-240, 1993.

Eshhar, N., Streim, S., Kohen, R., Tirosh, O. and Biegon, A. "Neuroprotectant and Antioxidant Activities of HU-211, a Novel NMDA Receptor Antagonist." Eur. J. Pharmacol., Vol 283: pp. 1-3, 1989.

Feigenbaum, .J., Bergmann, F, Richmond S., Mechoulam R., Nadler, V., Kloog, Y and Sokolovsky M., "Nonpsychotropic cannabinoid Acts as a Functional N-methyl-D-aspartate Receptor Blocker. Proc. Natl. Acad. Sci., USA Vol 86: pp. 9584-9687, 1989.

McDonough, J.H., Jr., and Shih, T.-M. "Neuropharmacological Mechanisms of Nerve Agent-Induced Seizure and Neuropathology." Neurosci. Biobehav. Rev. Vol 21: pp. 559-579, 1997.

McDonough, J., Clark, R., Slone, T., Zoeffel, D., Brown, K., Kim, S. and Smith, C., "Neural Lesions in the Rat and Their Relationship to EEG Delta Activity Following Seizures Induced by the Nerve Agent Soman. NeuroToxicol. Vol 19: pp. 381-392, 1998.

Mechoulam, R., Hanue, L., and Fride, E., "Towards Cannabinoid drugs- Revisited." Prog. Med. Chem. Vol 35: pp. 199-243, 1998.

Olney, J.W., De Gubareff, T. and Labuyere, J., "Seizure-Related Brain Damage Induced by Cholinergic Agents." Nature, Vol 301: pp 520-522, 1983.

Randall, R. and Thayer, S., "Glutamate-induced Calcium Transient Triggers Delayed Calcium Overload and Neurotoxicity in Rat Hippocampal Neurons." J. Neurosci. Vol 12: pp. 1882-1895, 1992.

Taylor, P. "Anticholinesterase Agents. *In* Goodman & Gilman's The Pharmacological Basis of Therapeutics. 9th edition. Hardman, J.G., Limbird, L.E., Molinoff, P.B., Ruddon, R.W. & .Gilman, A.G., Eds.: pp 161-176. McGraw-Hill, New York. 1996.

SELECTIVE, SPECIFIC, AND VERSATILE PERSONAL BIOSENSORS TO ORGANOPHOSPHATE CHEMICAL TOXINS COMPOSED OF POLYURETHANE IMMOBILIZED ENZYMES

Richard K. Gordon†, Alper T. Gunduz, Shawn R. Feaster, and Bhupendra P. Doctor
Division of Biochemistry, Walter Reed Army Institute of Research,
503 Robert Grant Road, Silver Spring, MD 20910-7500

Tracy Cronin
Chemical Biological Radiological and Nuclear Countermeasures,
Technical Support Working Group, Ft. Washington, MD

ABSTRACT

Organophosphorus (OP) nerve agents are a serious threat to military and civilian personnel, so rapid detection of OP compounds in all of these forms is of paramount importance to prevent casualties. Recently, we combined porous polyurethane foam formed *in situ* from water-miscible hydrophilic urethane prepolymers and enzymes such as ChEs. One of the advantages of this technique imparted to the *immobilized* enzymes is resistance to denaturing events. Most important, the enzyme will not leach from the polyurethane support so the ChE-badge can now be used to sample for OPs in diverse environments such as soil and large bodies of water, as well as conventional sources such as air. In addition, immobilized enzyme badges are being designed with a unique attribute not present in the current non-immobilized detectors: a rapid field system to identifying which OP is present. For instance, organophosphorus hydrolase (OPH) hydrolyzes sarin more readily than soman, while laccase hydrolyzes the VX agent preferentially over the G agent OPs. Currently, we are evaluating polyurethane immobilized laccase for long-term stability and kinetic properties of VX hydrolysis. Thus, the immobilized sensor can provide new features and testing of more diverse environments than the M256A1 and M272 kits combined. Also, the ability to identify the OP toxin in real-time using the immobilized differential detector would aid in treatment and securing the contaminated area, in the identification of the use of OPs, and permitting first responders to identify the OP present in a civilian terrorist act.

†Telephone: 301 319 9987; fax: 301 319 9571
E-mail: Richard.Gordon@na.amedd.army.mil

INTRODUCTION

Traditional analysis of cholinesterase inhibitors is performed using gas and liquid chromatography and mass spectrometry (Witkiewicz, et al., 1990). These techniques have significant drawbacks when considering an individual kit for field deployment, including lack of portability, simplicity, cost, and rapid results. An alternate technology is a biosensor. Biosensors have been widely used to de-

Covalent ChE Incorporation at Aliphatic Amino Group(s)

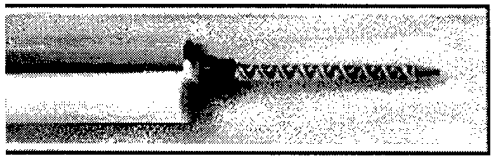

Figure 2. Apparatus for combining enzymes in aqueous buffer and prepolymer. Complete mixing is evident at the end of the mixing stator by the uniform and consistent gray (right).

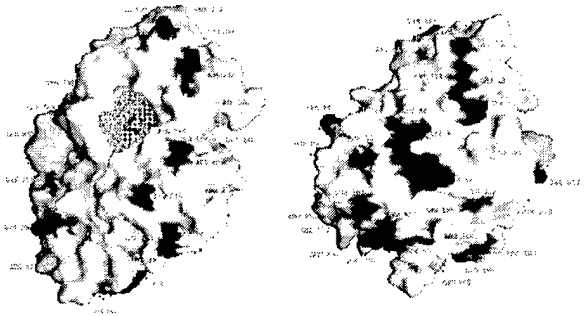

Figure 3. Computer model of the surface of butyrylcholinesterase based on the x-ray crystal structure. Left model: A speckled area in the middle represents the active site gorge through which substrate and OP must pass to get to the active site. Lysine residues on the surface of the enzyme (shown in black) are possible coupling sites for cross-linking to the prepolymer, and do not interfere with the gorge. Right model: 180° rotation shows the backside of the enzyme and additional coupling sites to lysine moieties.

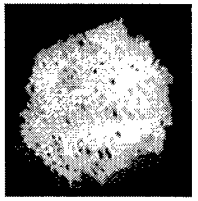

Figure 4. Biosensor, consisting of immobilized AChE and polyurethane polymer. The biosensor depicted here is about the size of a pencil eraser.

covalently have been prepared by a variety of processes (Ghindilis, et al, 1996). The drawback to these methods includes lack of enzyme stability at ambient conditions, leaching from the surface, sensitivity to denaturating conditions, and short half-life when in solution. Currently fielded spot chemical agent detector kits and even water test kits use dry eel ChE non-covalently applied onto fiber or ion-exchange paper. It can only be exposed to air/vapor or at most several drops of aqueous solutions. Wood and coworkers (Wood, et al., 1982), using isocyanate-based polyurethane prepolymers (Hypol®), found that a number of enzymes could be covalently bound to this polymer, and that every enzyme retained activity to varying degrees. We have combined a porous polyurethane foam formed *in situ* from water-miscible hydrophilic urethane prepolymers and enzymes such as ChEs, producing immobilized enzyme sponges (Gordon, et al., 1999; Ember, 1997; Medlin, 1998). In this method, the enzyme becomes an integral part of the solid support (figure 1). Some of the advantages of this technique include retention of similar kinetic characteristics as the soluble form of the enzyme. Most important, the immobilized enzyme retains high activity after prolonged storage, and it is resistant to the detrimental effects of low and high temperatures, and long exposure to the environment. In addition, because the enzymes are covalently attached to the polyurethane, they will not leach from this polymer support so that the product - an OP badge - can now be used to sample for chemical weapons and pesticides in anything from soil, water, to air.

METHODS

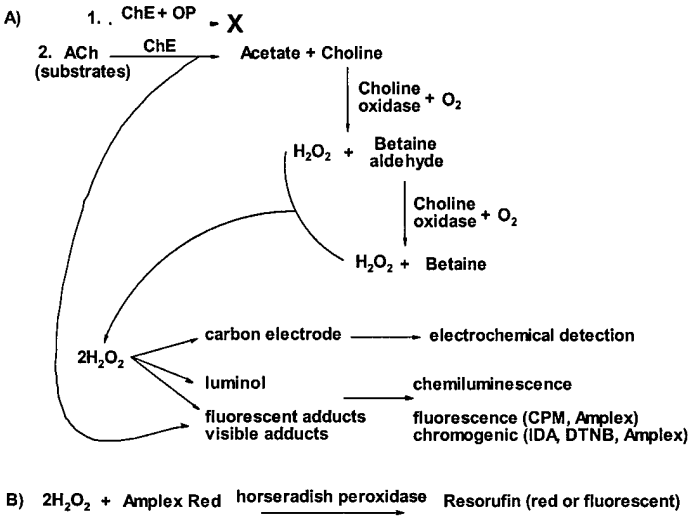

Figure 5. A) Schemes for detecting cholinesterase activity of the biosensor including visible, fluorescent, chemiluminescent, and electrochemical methods. In reaction 1, the biosensor ChE reacts with OP, and the enzyme is inhibited, so no change in color is generated. In reaction 2, uninhibited ChE cleaves the substrate, and can produce a variety of detection results. B) Specific mechanism for the biosensor to yield resorufin, both a visible red and a fluorescent indicator.

BASF, Specialty Chemicals, Parsippany, NJ) and an equivalent volume of water miscible prepolymer (TDI Hypol 3000 prepolymer, Dow Chemical, Lexington, MA). The 2-phase system, enzyme and prepolymer, is mixed by a method we modified from the adhesive industry. The mixing apparatus uses a 1:1 ratio double barrel chamber and a mixing stator (figure 2, CPA, Inc., 21 Starline Way, Cranston, RI 02921). The isocyanate functional group of the Hypol prepolymer reacts with the surface amine groups of enzymes (figure 1and 3; Gordon, et al., 1999; Ember, 1997).

Figure 3 depicts possible cross-linking sites between BChE surface lysine groups and the prepolymer. Similar computer models of AChE, OPH, and laccase demonstrate cross-linking sites that would not interfere with the active site of the enzymes. The mixed material ejected from the mixing stator can be ejected into a mold to form any size or shape product. Alternatively, the immobilized product can be spotted (as a dot of glue) onto a paper or rigid plastic backing, generating the immobilized ChE biosensor ticket. A 5 mg biosensor is shown in figure 4 (not to scale).

Determination of immobilized enzyme activity: Several different techniques to determine the activity of the immobilized ChE enzymes in the biosensor are shown in the scheme in figure 5. Detection can be performed qualitatively by the human eye for visible chromagens, or dark-adapted eyes for chemiluminescent chromagens (Parari, et al, 1993; Birman, 1985; Okabe, et al., 1977). Detection can also be performed quantitatively using portable handheld devices, which measure fluorescence, chemiluminescence, and visible chromagens. Typically, reactions of the immobilized enzymes were monitored spectrophotometrically, e.g., by the Ellman assay for ChEs (De La Hoz,, et al., 1986), in a cuvette containing a stir bar and the biosensor.

RESULTS

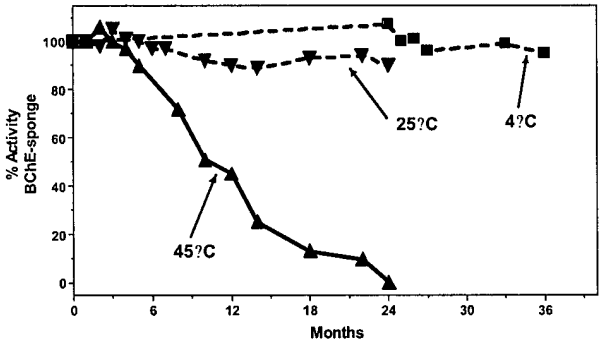

Figure 6. Long-term stability of BChE biosensor after continuous exposure to various temperatures.

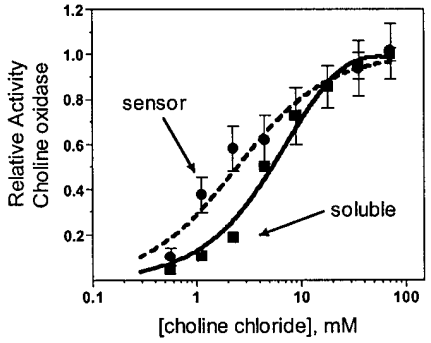

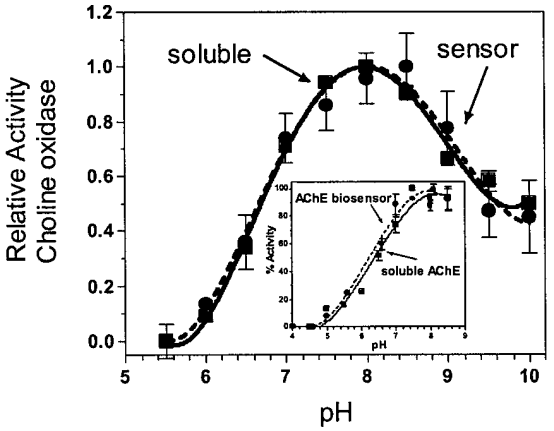

Figure 7. Top: Immobilized choline oxidase and soluble form of the enzyme display similar kinetic properties. Bottom: pH profiles of soluble and immobilized choline oxidase are identical and exhibit the same pH optimum as the AChE biosensor or soluble AChE.

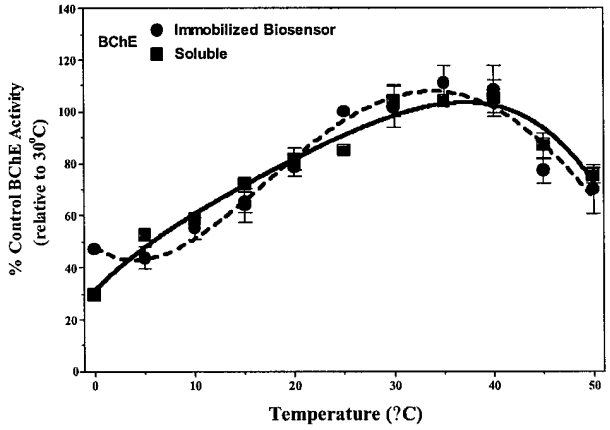

Figure 8. Relative reaction rates of soluble BChE and biosensor BChE at different temperatures relative to 30°C.

Capacity of biosensor for multiple immobilized enzymes and coupled reactions: We found that the polymer badge has a significantly higher loading capacity for ChEs than the amount of purified BChE or AChE we added. Therefore, adding larger quantities of enzyme during synthesis could increase the final ChE activity of the biosensor. When increasing amounts of a nonspecific protein, such as bovine serum albumin that contains no ChE activity, were added to a constant amount of purified AChE and the mixture

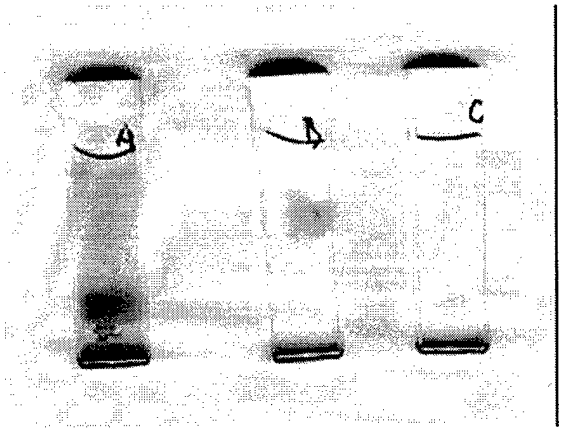

Figure 9. Immobilized AChE biosensor after exposure to OP in aqueous solution using the resorufin indicator reaction. Tube A and B have AChE immobilized sensor. Tube B sensor was poisoned with OP prior to using the indicator; color developed was observed in tube A, but is lacking in tube B.

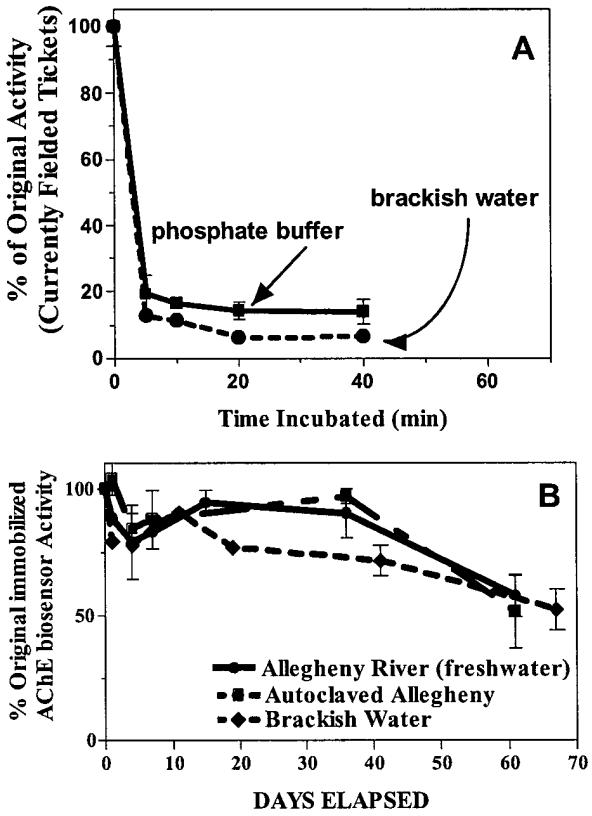

Figure 10. Comparison of a current *non-covalent* ChE ticket (A) and immobilized AChE biosensor (B) after exposure to aqueous solutions. Note that the time scale (x-axis) is minutes for the existing tickets and days for the immobilized AChE biosensor.

8), the coupled reactions depicted in the multiple assay scheme (figure 5) can be simultaneous optimized for both immobilized enzymes.

As expected for similar kinetic parameters, the relative rate of substrate hydrolysis and generation of color is identical for the soluble and immobilized ChEs, as shown in figure 8. While the enzyme is stable at significantly lower temperatures, both enzyme forms demonstrate temperature dependence.

Sensor color reactions: Figure 9 is an example of the biosensor poisoned by OP (tube B, middle), bio-

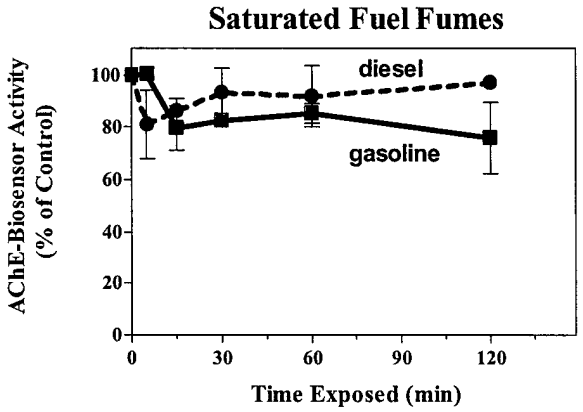

Figure 11. The biosensor (immobilized AChE) is resistant to false positives caused by continuous exposure to organic vapors, such as diesel and gasoline fumes.

TABLE 1. Time-Dependent Inhibition of ChEs by MEPQ

ChE	Enzyme Form	Bimolecular rate constant (M^{-1} min^{-1}) ± SD
AChE	soluble	$1.59 \pm 0.52 \times 10^8$
	biosensor	$1.00 \pm 0.28 \times 10^8$
BChE	soluble	$4.15 \pm 0.78 \times 10^7$
	biosensor	$4.21 \pm 2.00 \times 10^7$

do not dissociate (leach) from the polymer support. Therefore, the immobilized enzyme biosensor can be used to test water or even left in liquid or other environments for long-term monitoring.

Existing fielded OP tickets from the United States and other countries contain eel cholinesterase dried (not covalently attached) onto an ion-exchange filter paper. These tickets lost more than 80% of their original activity in less than *5 minutes* in various aqueous conditions, including pH 8 phosphate buffer or brackish water (figure 10A). Therefore, these tickets can only detect OPs in vapor or a *drop* of solution placed on the paper. In contrast to these tickets, the AChE activity in the immobilized biosensor was stable for almost 60 *days* in continuous immersion in aqueous samples including Allegheny River (fresh water, figure 10B) or brackish water. Since the results were identical for autoclaved and untreated river water, the immobilized enzymes were also resistant to microbial induced proteolytic degradation. Also note that the same biosensor was assayed multiple times over many days, so it is evident that the immobilization process confers dramatic stability to covalently coupled AChE, and provides further evidence that the enzymes do not leach from the polyurethane matrix.

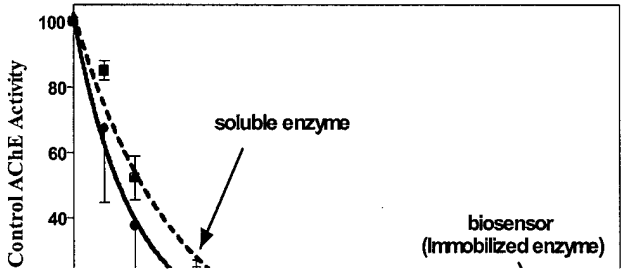

The biosensor is less sensitive to events that cause false positives: In addition to robustness to temperature extremes and washout by aqueous environments, the biosensor is

Biosensor Sensitivity to Organophosphates: The biosensor composed of immobilized ChE and the soluble form of the enzyme exhibited the same titration curve to OP, as illustrated in figure 12. Furthermore, time-dependent inhibition of AChE and BChE by the organophosphate MEPQ yielded the same bimolecular rate constants of inhibition for soluble or immobilized AChE or BChE (Gordon, et al., 1999) (Table 1). These data demonstrate that the immobilized ChEs react to and detect OPs in the same manner as the soluble form of the ChEs, even though the biosensor has increased stability to adverse environmental assaults and is cross-linked to the polymer (figure 1).

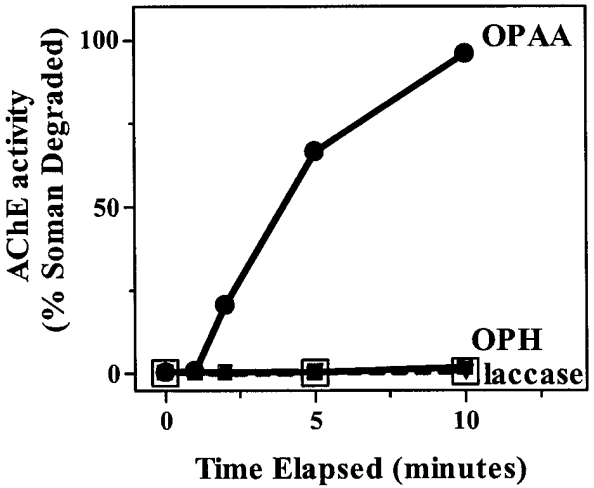

Figure 13. Differential hydrolysis of the OP soman. Soman is not rapidly hydrolyzed by OPH or laccase, which hydrolyze sarin and VX, respectively. In contrast, after 10 min OPAA hydrolyzed the soman completely so that now an AChE biosensor was no longer inhibited.

Differential OP Biosensor: The sensors we propose will have an additional unique attribute: We are developing a field system capable of differential identification of the type of OP contamination that occurred, e.g., sarin or soman. This would aid in the decontamination and treatment of OP contaminated individuals and permit tracking of OPs from a terrorist organization without removing samples to a central laboratory. The badge would be subdivided into compartments; each containing immobilized enzymes that behave uniquely to the different OPs (Gordon, et al., 1999). For instance, one strain of OPH hydrolyzes sarin more readily than soman, while OPAA hydrolyzes soman, and laccase hydrolyzes VX. To this end, we have successfully immobilized OPH, OPAA, and laccase using the same Hypol TDI prepolymer and conditions used for ChE immobilizations. In the first step, the solution containing a suspected OP (either in water, dirt, or after swabbing) would be added to a series of these differential immobilized enzymes. After 10 min, these enzymes would be removed as they are immobilized to the polyurethane, and the ChE-biosensor added. An uninhibited biosensor would indicate that an enzyme hydrolyzed the OP, and therefore which OP was present. This procedure can be seen in figure 13: The OP present was soman, based on time-dependent hydrolysis by OPAA, but not laccase or OPH.

CONCLUSIONS

We have demonstrated a unique immobilized enzyme biosensor system for the detection of OP contamination. This biosensor is versatile, durable, and reusable for sampling water and air or almost any environment. We have shown that the immobilized enzyme is active over 60 days, whereas existing OP

These immobilized enzyme badges have an additional unique attribute not present in the existing non-immobilized detectors: a rapid field system capable of identifying which OP is present. This is possible because the immobilization process stabilizes the enzymes that behave uniquely to different OPs. For instance, organophosphorus hydrolase (OPH) hydrolyzes sarin more readily than soman, while laccase hydrolyzes the OP VX preferentially over G-agent OPs.

The immobilized polyurethane enzymes will make versatile biosensors for detecting organophosphates. These badges, by virtue of their high capacity for most enzymes, stability, specificity, sensitivity, and resistance to harsh environmental conditions, can be used under diverse conditions encountered by troops in the field. These badges should be suitable for a variety of sensor schemes for both chemical weapons and pesticides. These badges should be suitable for first responders, Navy seals, and also civilian populations gathered in large numbers such as sports activities, subway stations, airports, crop dusters and farmers. They could be incorporated into the telemedicine initiative as electrochemical organophosphate probes when mated to an automatic reader.

ACKNOWLEDGEMENTS

This work was supported in part by the Office of Special Technology

REFERENCES

1. Witkiewicz, Z., Mazurek, M., and Szulc, J. "Chromatographic analysis of chemical warfare agents." *J. Chromatogr.* Vol. 503 pp. 293-357, 1990.
2. Ghindilis, A. L., Morzunova, T. G., Barmin, A. V., and Kurochkin, I. N. "Potentiometric biosensors for cholinesterase inhibitor analysis based on mediatorless bioelectrocatalysis." *Biosensors Bioelectronics* Vol. ll pp. 873-880, 1996.
3. Wood, L. L., Hardegen, F. J., Hahn, P. A., Enzyme Bound Polyurethane. U.S. Patent 4,342,834, 1982.
4. Gordon, R K., Feaster .S R., Russell, A. J., LeJeune, K. E., Maxwell, D. M., Lenz, D. E., Ross, M., and Doctor, B. P. "Organophosphate skin decontamination using immobilized enzymes." *Chemico-Biological Inter.* Vol. 119-120, pp. 463-370, 1999.
5. Ember, L. "Detoxifying Nerve Agents", *Chemical & Engineering News*, pp. 26-29, (September 15, 1997).
6. Medlin, J. F. "Super Sponges." *Environ. Health Perspect.* 106:A182-A184, 1998.
7. De La Hoz, D., Doctor, B. P., Ralston, J. S., Rush, R. S., and Wolfe, A. D. "A simplified procedure for the purification of large quantities of fetal bovine serum acetylcholinesterase." *Life Sci.* Vol. 39, pp. 195-199, 1986.
8. Gan, H.K., Smolen, A., Eckerson, H.W., LaDu, A "Purification of human serum paraoxonase/arylesterase. Evidence for one esterase catalyzing both activities." *Drug. Metab. Disp.* Vol. 19, pp. 100-106, 1991.

STUDIES IN THE FORMATION OF ETHYL METHYLPHOSPHONOFLUORIDATE FROM RAT AND HUMAN SERUM EXPOSED TO VX AND IN THE PRESENCE OF FLUORIDE ION

E.M. Jakubowski, L.S. Heykamp
EAI Corporation, 1308 Continental Dr, Suite J, Abingdon, MD 21009.

H.D. Durst, S.A. Thomson
Research and Technology Directorate, U.S. Army ECBC, APG-EA, Edgewood, MD 21010.

ABSTRACT

A method has been developed for the analysis of a VX nerve agent biomarker in blood that is very sensitive and selective. VX was detected in spiked human and rat sera by the generation of its corresponding G-series derivative, ethyl methyl phosphonofluoridate (VX-G). This method utilizes a C18 solid-phase extraction (SPE) followed by quantification using a gas chromatograph with either a flame photometric detector (GC-FPD) or a mass spectrometer (GC-MS). VX-G was completely resolved from sarin (GB) and the method has the potential to resolve other nerve agents in the VX series of cholinesterase inhibitors. The method detection limit was 10.5 pg of agent on column.

INTRODUCTION

The ability to verify nerve agent exposure and to determine the degree of exposure is extremely important for medical, tactical, and political reasons. Current verification methods depend on establishing either a significant depression in cholinesterase activity and/or the presence of nerve agent metabolites. Cholinesterase activity is known to fluctuate significantly within a population and even within individuals. A simple correlation between cholinesterase depression and severity of exposure is not always evident. Nerve agent metabolites such as the alkylmethylphosphonates are not easily observable and currently require derivatization for low-level GC analysis which adds time and complexity to the sample analysis scheme. Our goal was to find or develop analytical methods capable of quantifying VX exposure in biological matrices such as blood and tissue using available instrumentation. A literature search for nerve agent methods produced one very promising candidate method which served as a starting point. In this method, GB was regenerated from bound sites in the blood by relatively simple sample matrix manipulation (addition of fluoride at pH 4) followed by solid-phase cartridge extraction.[1] This method has never been used with VX analogs and it may prove useful as a tool to study VX exposures. VX itself would not reform from under the conditions of the assay. The product would likely be methyl ethylphosphonofluoridate.

EXPERIMENTAL

CHEMICALS AND MATERIALS

Rat and human sera were purchased from Sigma (St. Louis, Missouri). Potassium fluoride (CAS No. 7789-23-3) and sodium sulfate (anhydrous, CAS No. 7757-82-6) from Aldrich Chemical Company (Milwaukee, Wisconsin). Silver fluoride pads were purchased from CMS (OI Analytical, Birmingham, AL). Waters (Waters Associates, Millipore Corp., Milford, MA) Sep-Pak® 500 mg and 200 mg C_{18} solid-phase extraction (SPE) cartridges were used for extractions. Ethyl acetate and 2-propanol were pesticide grade from Aldrich Chemical Company (Milwaukee, Wisconsin). Aqueous acetate buffer (pH 3.5) was prepared from acetic acid (0.189 M) and sodium acetate (10.8 mM). The internal standard was decadeuterated diethyl ethylphosphonate which was synthesized at ECBC using standard methods.

SAMPLE PREPARATION

Human and rat sera (Sigma, St.Louis, MO) was spiked with dilute VX (in 2-propanol) at 147.3 ng/mL and 176.6 ng/mL, respectively. The exposed serum was filtered using a 500 mg C_{18} SPE cartridge (conditioned first with 1.5 mL 2-propanol and then with 1.5 mL acetate buffer) to separate the free from the protein bound nerve agent. The free agent was eluted with 1.5 mL ethyl acetate, collected over sodium sulfate and saved for analysis. For the standard assay, the resulting spiked human serum was then analyzed in 0.25-mL aliquots by addition of both 0.75-mL acetate buffer and 0.2 mL of potassium fluoride solution. Rat serum required only acetate buffer. The resulting treated serum was extracted using a 200-mg C_{18} SPE cartridge (conditioned first with 1.0 mL 2-propanol and then with 1.0 mL acetate buffer) and the analytes were eluted with 1.0 mL ethyl acetate. Sodium sulfate was added to dry the extract that was then analyzed by GC-FPD. Evaluation of the relative importance of the reagents was assessed by substituting saline for one or both reagents. In addition, extracts in some cases were injected through the silver fluoride pad.

INSTRUMENTAL

Samples were analyzed on either a Hewlett-Packard 5890 GC-FPD or a Hewlett-Packard 6890 GC-5973 MSD (Newark, DE). Sample inlet was by Tenax® solid sorbent tube (Depot Area Agent Monitoring System (DAAMS) tube: Dynatherm Inc, Oxford, PA) using an ACEM 900 (Dynatherm Inc, Oxford, PA) desorber interfaced to the GC column via butt-connector. The GC column was a 30 m x 25 mm x 0.5 um thickness DB-5 MS (J&W Scientific, Avondale, CA). The ACEM 900 temperature program was as follows: Dry 60 °C for 1 minute, Tube Heat 200°C for 3minutes, Cool for 1minute, Trap Heat 275 °C for 3 minutes. The GC oven temperature program was as follows: Initial 40 °C for 2 minutes, ramp to 160 °C at 15 °C/minute, ramp to 260 °C at 40°C/minute and held for 3 minutes. The MSD was used in the electron ionization mode with selected ion monitoring at m/z 111, 99, and 82. After the sample was desorbed on the GC column the sorbent tube was reconditioned by backflushing using 100 mL/min flow of dry nitrogen at 280-300 °C for five to eight minutes to decrease the high boiling point interference from the serum samples. Backflushing of the sorbent tube prevents degradation of the instrument and column producing a stable baseline despite the complex nature of the sample matrix.

A standard curve was established by sequentially injecting five VX standards from 17.66 ng/mL to 176.6 ng/mL on a silver fluoride pad. The silver fluoride pad was connected to a Tenax® DAAMS tube while a flow of air at approximately 100 mL/min as determined by an inline ball flowmeter was pulled through the system by vacuum. A collection time of two minutes was used to transfer the G-analog from the silver fluoride pad to the DAAMS tube. Prior to analysis, tubes were spiked with 94 pg of internal standard separately using a flow of nitrogen of approximately 100 mL/min. The peak-area-ratio (PAR) for

each standard was plotted against the mass of VX-G injected to yield a linear relationship with a correlation coefficient of greater than 0.99.

RESULTS AND DISCUSSION

Standard curves were created by sequentially injecting five VX standards from 17.66 to 176.6 pg through a silver fluoride impregnated fiber pad. The efficiency of VX conversion to VX-G using this method has been reported to be better than 75% depending on the age and condition of the silver fluoride pad.[2] Noting changes in the daily VX standard results can assess degradation of the pad. Analysis of an 88.3 pg VX standard through a single pad over six days produced a mean recovery of 86.3 pg with a standard deviation of 8.10 and a percent relative standard deviation of 8.29 percent. An estimate of the MDL was obtained by the analysis of seven replicate 20 pg VX injections. The MDL was approximately 10.5 pg of VX.

For this method to be useful, it should be able to distinguish between closely related molecules within the G-series of nerve agents. GB differs by only a methylene group from VX-G and presents an important potential interference. Using this method GB was clearly resolved from the VX-G and would not interfere with the method.

The importance of fluoride ion and acidification were assessed as well as the use of the silver fluoride pad on spiked serum samples. Table 1 lists the analysis results of spiked serum prepared under various conditions of buffer and fluoride ion. Variations of sample preparation and analysis included the following treatments: 1) analysis of the initial 500 mg C_{18} SPE cartridge filter eluent by injecting through silver fluoride pad, 2) substitution of saline for all reagents added to the filtered spiked serum followed by another SPE step, 3) substitution of saline for all reagents added to the filtered spiked serum followed by another SPE step and injection through a silver fluoride pad, 4) addition of buffer and saline (no KF) to the filtered serum followed by another SPE step, 5) addition of buffer and saline (no KF) to the filtered serum followed by another SPE step and injecting through a silver fluoride pad, 6) addition of KF and saline (no buffer) to the filtered serum followed by another SPE step, 7) addition of KF and saline (no buffer) to the filtered serum followed by another SPE step and then injecting through a silver fluoride pad, and 8) addition of KF and buffer to the filtered serum followed by another SPE step.
According to Table 1, treatments six and seven indicated that the addition of buffer to adjust the pH to approximately four was not absolutely necessary to produce some VX-G if fluoride was present in large abundance. Only approximately 47% and 85% as much VX-G was formed without pH adjustment in the rat serum and human serum, respectively (rat: [1.85/3.95]100=46.8%, human: [3.06/3.60]100=85%) for treatment six. The effect of fluoride ion on the spiked human serum was noticeably greater than on the rat serum possibly because rat serum has significant levels of endogenous fluoride.

TABLE 1. VX-G Recovered (ng/mL) from Rat and Human Sera Spiked with VX.

	ng/mL VX-G Recovered							
Treatment	1 Excess VX on Filter	2 Saline only	3 Saline + Pad	4 Saline + Buffer	5 Saline + Buffer + Pad	6 Saline + KF	7 Saline + KF+ Pad	8 Buffer + KF
Rat Serum	165*	0	0	3.29	***	1.85	1.68	3.95
Human Serum	88.2**	0	5.63	0	4.05	3.06	12.7	3.60

* Spike level = 176.6 ng/mL, injected through silver fluoride pad.
** Spike level = 147.3 ng/mL, injected through silver fluoride pad.
*** Rat serum not analyzed

The results when the extract of the human serum was not treated with KF but injected through the AgF pad indicated a substantial amount of VX-G was formed without the presence of aqueous fluoride ion. Since the source of fluoride in these cases was provided by the silver fluoride pad, a precursor of VX-G must have been present in the ethyl acetate extract. The precursor could have been VX or a breakdown product of VX that was still capable of reacting on the silver fluoride pad to generate VX-G. Excess VX was extracted using a 500 mg C18 SPE cartridge the same as was used with the rat serum. Moreover, the amount spiked in the case of the human serum was less than that of the rat serum therefore the capacity of the SPE cartridge was likely not exceeded. Proportionately less excess VX was recovered from the initial SPE cartridge with human serum than the rat serum which indicated that the VX was either binding to sites in the human serum and being carried through the SPE cartridge or that VX was degrading faster in human serum. However, the degradation product was still capable of forming VX-G when it came in contact with the silver fluoride pad and/or aqueous fluoride ions. In theory, any breakdown product of VX that retains the general O-ethyl methyl phosphonothioate structure can produce VX-G. The existence of degradation products capable of this conversion have been shown in samples of stored VX.[3]

In the event of a possible nerve agent exposure, a method would be needed to analyze for both G-agents and V-agents in biological matrices. Treatment eight was similar to a method previously used on archived serum samples to confirm human exposure to GB.[1] In the present case of VX spiked human serum this method produced the corresponding VX-G in measurable amounts indicating this method can be used to detect both the G and V series of nerve agents. Treatment eight also produced slightly higher amounts of VX-G in rat serum (3.95 ng/mL) as compared to treatment four which depended on endogenous fluoride levels (3.29 ng/mL).

Treating VX spiked human serum with KF and injecting the ethyl acetate through the silver fluoride pad yielded the highest amounts of VX-G (treatment seven, 12.7 ng/mL) which is probably a combination of free VX-G precursors and enzyme bound VX-G precursor. Rat serum extract did not produce the same effect upon injection through the pad.

Addition of buffer, which acidifies the sample to pH 4, appears to decrease the free VX-G precursor in the case of human serum as illustrated by the drop from 5.63 to 4.05 ng/mL. One possible explanation for this drop is the ionization of a VX-G precursor lessens its affinity for the C_{18} SPE

cartridge. For example, the amine group in VX would be ionized to a greater extent at pH 4 than at pH 7 creating a larger percentage of charged molecules that would be less likely to bind to the SPE media. The question of how VX or some closely related molecule survives the initial C_{18} SPE cartridge in the case of human serum and not rat serum is not clear. Additional investigation is required to elucidate this phenomenon.

Rat serum spiked at 176.6 ng/mL VX yielded 165.4 ng/mL of VX as G-analog in the filtrate of the SPE cartridge. This filtrate was injected on the silver fluoride pad and represents unbound or excess VX added to the serum. Aliquots of 0.25 mL of the filtered serum were then analyzed after being treated with reagents. These samples produced approximately 3.95 ng/mL of VX as G-analog. This represents the bound form of the nerve agent. The sum of both unbound and bound VX gives a reasonable mass balance of 169.4 ng/mL which accounts for 95.9% of the agent. It was noted that omission of the fluoride reagent in the preparation of the rat serum does not drastically effect the resulting VX-G production from the spiked samples as seen in Table 1 (3.29 ng/mL without fluoride versus 3.95 ng/mL with fluoride). This observation is in agreement with earlier reports that noted rat serum had endogenous levels of fluoride sufficient to regenerate Soman (GD) on addition of acetate buffer.[4,5]

CONCLUSIONS

A method for the verification and quantification of a nerve agent biomarker was developed for VX. VX exposure can be verified as G-analog in serum samples. This analysis is simple and quick using instrumentation available in field laboratories and air monitoring facilities and it is applicable to G-series and V-series nerve agents. The major disadvantage is that the original leaving group is not known but this is also true in the case of the agent metabolites.

REFERENCES

1. M.Polhuijs, J.P.Langenberg, H.P.Benschop, Toxicol. Appl. Pharmacol., **146**, 156-161, (1997).
2. W.K. Fowler, J.E. Smith Jr, J. Chromatogr., **478**, 51-61, (1989).
3. P.A. D'Agostino, L.R. Provost, J. Visentini, J. Chromatogr., **407**, 221-232, (1987).
4. L.P.A.De Jong, C. Van Dijk, Biochem. Pharmacol.. **33**, 663-669, (1984).
5. H.P.Benschop, E.C.Bijeveld, M.F.Otto, C.E.A.M.Degenhardt, H.P.M.Van Helden, L.P.A.De Jong, Analytical Biochem., **151**, 242-253, (1985).

TREATMENT OF M1 AND M8 HYDROLYSATES WITH HD/TETRYTOL ADAPTED IMMOBILIZED CELL BIOREACTORS

Dr. Joseph J. DeFrank, Mark A. Guelta, Mark V. Haley
U.S. Army Edgewood Chemical Biological Center
Aberdeen Proving Ground, MD 21010

Dr. F. Stephen Lupton
Honeywell
Des Plaines, IL 60017

Under U.S. law and the terms of the Chemical Weapons Convention (CWC), the U.S. Army is required to destroy its stockpile of 30,000 tons of chemical warfare agents by April 2007. While incineration has been the baseline method used for demilitarization of these materials, public and political opposition lead to the evaluation of alternative technologies, including biodegradation. Hot water hydrolysis followed by biodegradation has been shown to be an effective means of disposing of the blister agent sulfur mustard (HD). The ability of this type of immobilized cell bioreactors (ICB's) to deal with a mixture of hydrolyzed HD and Tetrytol (Tetryl and TNT) was evaluated under the Assembled chemical Weapons Assessment (ACWA) program and shown to be quite promising. The work in this presentation deals with a laboratory-scale examination of the ability of ICB's to deal with the hydrolysates of energetics M1 and M8 after grown on HD/Tetrytol. Two sets of ~ 600 ml ICB's in series were inoculated with sewage sludge and biomass from a large-scale ICB and fed a mixture of HD and Tetrytol hydrolysates. After establishment of the cultures, the feed was switched to increasing concentrations of either M1 or M8 hydrolysates as a sole carbon source. The ICB effluents were monitored for COD removal, nitrogen and phosphorus levels, suspended solids and aquatic toxicity. The results of the two systems in respect to their ability to make the changeover from HD/Tetrytol to M1 or M8 and other parameters will be compared and discussed.

INTRODUCTION

One effort currently underway by ACWA is the demonstration of a combined neutralization/ biodegradation process as an alternative to the baseline "incineration" process. A fairly strict application of this process is for siting at the Pueblo Chemical Depot, Pueblo Co. The Pueblo Chemical Depot maintains a stockpile of assembled HD chemical rounds in projectiles and cartridges. The 4.2-inch Mortar and 155mm projectile are examples of these rounds. For a technology to be considered as an alternative to baseline, it must represent a complete solution for the weapon destruction. ACWA has successfully demonstrated the ability of neutralization/biodegradation of the chemical and explosive

components of these chemical rounds. One process still incomplete is disposition of the rounds propellant charge.

The propellants used in these chemical rounds are the M1 and M8 solid propellants. For this study each of the solid propellants have been hydrolyzed in a 6% NaOH solution. These propellant hydrolysates were fed to two separate laboratory-scale ICB reactors. To closely simulate a likely operation of a proposed full-scale facility, the ICB culture was seeded from biomass removed from the ACWA HD/Tetrytol pilot-scale ICB. The culture was grown-up on HD/Tetrytol hydrolysate feed. After the culture was established the feed was switched to each of the propellant hydrolysates. After the acclimation period and feed concentration run-up, a validation period was started. Samples were taken to measure the biodegradability of the propellant feeds.

METHODS

The M1 and M8 propellants are mixtures of compounds. The propellant materials supplied were removed from 155mm projectiles and shipped to ECBC just prior to the hydrolysate production. The composition of each propellant prior to hydrolysis is listed in Table 1. The propellant hydrolysates have not been completely characterized as of this writing.

TABLE 1. Composition Of M1 And M8 Propellants.

M1 Propellant Composition		**M8 Propellant Composition**	
Compound	% wt/wt	Compound	% wt/wt
Nitrocellulose	85	Nitrocellulose	52.15
Dinitrotoluene	10.0	Nitroglycerine	43.0
Dibutylphthalate	5.0	Diethylphthalate	3.0
Diphenylamine	1.0	Potassium nitrate	1.25
		Ethyl centralite	0.60

The M1 and M8 propellant hydrolysates were prepared by neutralizing in 6% NaOH solution by heating and stirring in laboratory flasks over an 8-hr period. After cooling and coarse filtration the hydrolysates were prepared as bio-feed in 4-liter batches as required. The standard bio-feed formula at full concentration is listed in Table 2.

TABLE 2. Propellant Hydrolysate Feed Formulation.

Compound	**Amount**
Propellant Hydrolysate (M1 or M8)	800 ml
Potassium phosphate di-basic	0.64 gm
Wolin salts	20 ml
Distilled/Deionized Water	To volume (4L)
Neutralize with HCl to pH 7.5	As required for pH=7.5

The laboratory ICB's used for this study are glass cylinders of approximately 1 Liter internal volume. In an ICB the culture grows on an expanded foam media. Spacers mixed with the foam keep the culture from becoming plugged and allow air and aqueous media mixing within the ICB. The actual M8 ICB is shown in Figure 1 below. The expanded foam and spacer packing materials are shown in Figure 2. Under normal growth conditions the working volume of the ICB decreases to approximately 600-ml. Air to supply the culture enters the ICB through a glass fret in the bottom and exits through a tube inserted into a butyl rubber stopper as the top of the ICB. Effluent leaves the ICB through an overflow. For this study two ICB were operated in series for each of the two propellant hydrolysate feeds.

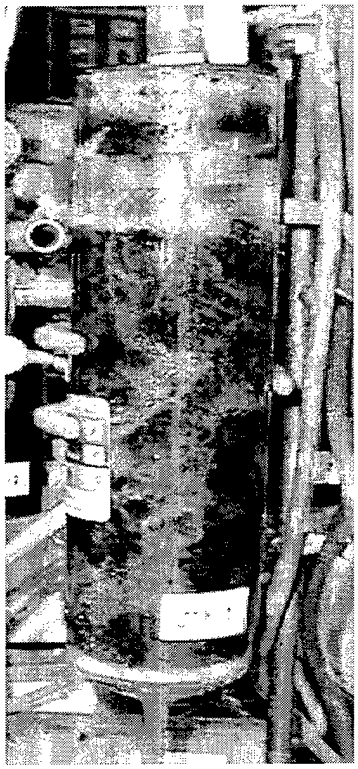

Figure 1. The M8 Propellant ICB.

Figure 2. The ICB Expanded Foam And Spacer Media.

The propellant hydrolysate bio-feed was pumped continuously into the ICB at 300 ml/day. Approximately 300 ml/min of air was supplied to each ICB by diaphragm pumps. The media pH was continuously monitored and controlled with acetic acid early in testing to provide additional carbon, and hydrochloric acid during the second half of the 80-day validation period. Process monitoring samples were taken 3-times per week and analyzed for chemical oxygen demand (COD), nitrogen ammonia and phosphate. Samples of the effluent were taken near the end of each feed batch and screened for aquatic toxicity using a MICROTOX Assay.

The MICROTOX (MTX) Bioassay exposes a bioluminescent marine bacterium (*Vibrio fischeri*) to a sample of unknown toxicity and measures the change in light output as the means of determining effects on the organism. A reduction in light output is a direct indication of metabolic inhibition. The assays were performed in glass cuvettes in temperature-controlled wells of a photometer. The assay must have a minimum of four dilutions exhibiting a dose response for optimum accuracy in predicting toxicity. The addition of bacteria was referred to as time zero. Five minutes after time zero the control cuvette was used to calibrate the photometer to 100% light output. The control and treatment cuvettes were returned to the incubator and measured again at 15 minutes. Data was analyzed with the MTX Test Protocol software to determine the EC_{50} (the effective concentration causing a 50% reduction in light out put).

RESULTS AND DISCUSSION

The COD measurement is used as a near real-time measure of the degree of utilization of degradable compounds by the bio-culture. The COD is advantageous in that analysis can be completed in just over two hours. This information is useful in assessing the cultures effectiveness at degrading the propellant feed until more complete analysis is available. At this writing processing monitoring samples

provided the only analytical available. The COD does not indicate degradation or utilization of any one compound of interest, although the COD is mostly associated with carbon compounds and to lesser degree nitrogen containing compounds. The COD of the effluents and the COD removal efficiency of each of the propellant reactors are presented in Figures 3 and 4.

Figure 3 represents the effluent COD results and feeding schedule for the M1 reactor. The culture was inoculated with bacteria from the HD/Tetrytol pilot-scale. The culture was grown-up on HD/Tetrytol feed. On day 150 just prior to changing to propellant feed the COD removal efficiency of the reactors was very good at approximately 90 %. The propellant feed was started on day 153, and is represented by the vertical bars. COD removal efficiency decreased dramatically even though the feed load was greatly decreased. The culture COD removal efficiency improved as the culture adapted even when feed loading was increased. On day 181, additional activated sludge from a local treatment plant was added to supplement the culture. The spike in the effluent COD is a result in adding the carbon rich activated sludge. COD removal efficiency stabilized near day 190. Removal efficiency began dropping even though feed COD decreased as exogenous carbon was gradually removed from the feed and pH control systems.

The 80-day validation period began on day 204. Validation sampling of the effluent began on day 204. Validation sampling results will contain more detailed analysis for the constituents of the ICB effluents and propellant hydrolysate including measures of volatile organic compounds (VOC), metals and mercury, TOC, energetics and nitroglycerine, total dissolved solids, total suspended solids and volatile suspended solids and the Toxic Characteristic Leaching Procedure (TCLP).

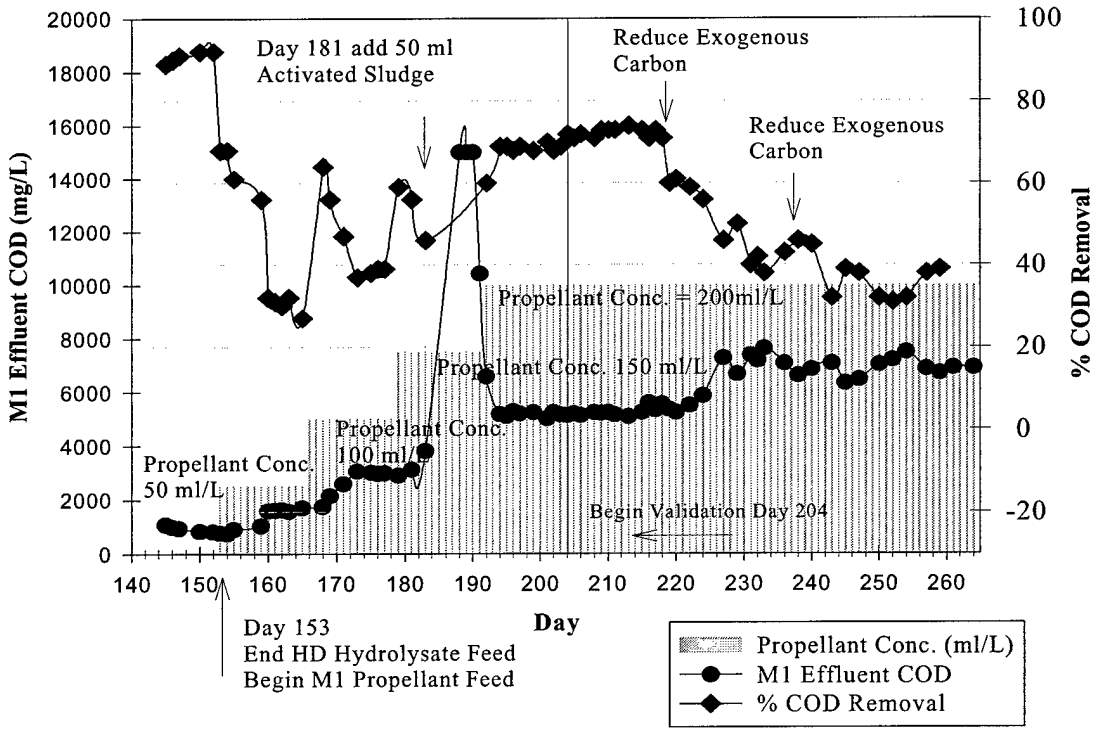

Figure 3. M1 Effluent COD, COD Removal Efficiency and Feed Schedule.

Figure 4 represents the M8 effluent COD, COD removal eficiency and feeding schedule. Like the M1 ICB in figure 3, the M8 ICB was grown on HD/tetrytol feed from an initial innoculumn from the HD/Tetrytol pilot-scale ICB. Change-over to propellant feed and incremental feeding schedule are the same as with the M1 ICB. All changes in pH control, sludge addition, validation start date and exogenous carbon removal are the same. However, the M8 reactor received less exogenous carbon than the M1 reactor due to M8 bio-feed's lower acid requirement for neutralization to pH of 7.5. The M1 feed received 5.4 ml/L acetic acid, while the M8 feed received only 2.5 ml/L acetic acid in the feed.

The effect of change-over to propellant feed, sludge addition and incremental increases in feed loading to each reactor had similar effects on COD removal efficiency. However, the COD removal efficiency of the M1 reactor decreased more dramatically than it did in the M8 reactor.

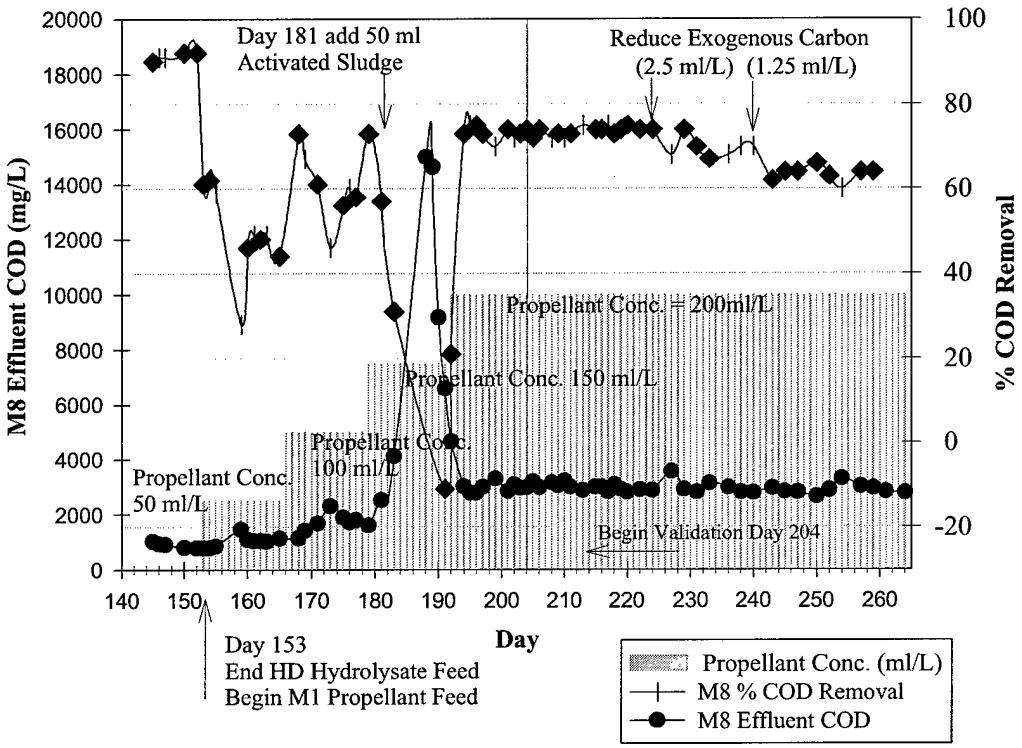

Figure 4. M8 Effluent COD, COD Removal Efficiency and Feed Schedule.

Microtox assays were performed on the propellant feed and ICB effluents during the study. Figure 5 represents the comparative toxicities of the propellant feed at each incremental propellant hydrolysate concentration. The Microtox results for the HD feed are also included for comparison. Microtox results indicated the M1 feed is more toxic than the HD feed at full strength than at the M1 lowest propellant concentration. The M1 at 50 ml/L, its lowest concentration, is more toxic than the M8 feed is at 200 ml/L.

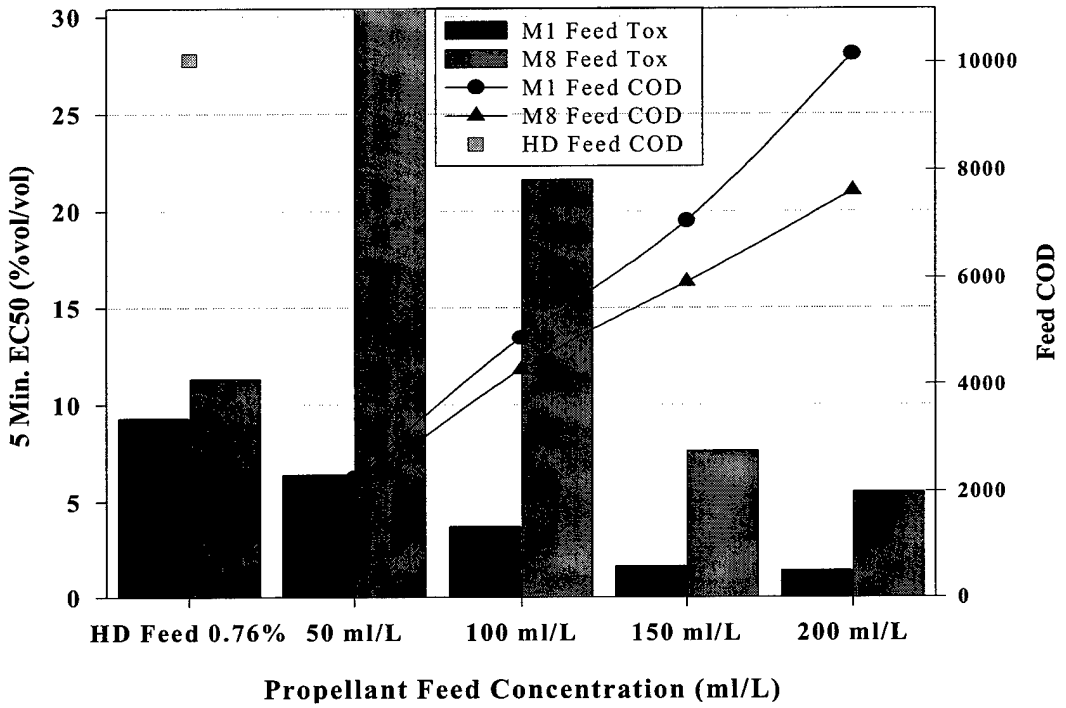

Figure 5. Chart of Microtox And COD Results For ICB Propellant And HD Feeds.

The Microtox Assay results are presented in Figure 6 below. A 5 min. EC50 of greater than 70 is considered non-hazardous. The effluent generated in each of the reactors while being feed the HD hydrolysate is quite low. The toxicity increases immediately after the switch to propellant hydrolysate feed. The M8 reactor recovers shortly after addition of acetic acid to neutralize the feed. The M1 reactor does not do as well with the M1 propellant feed. Once at the target concentration of 200ml/L hydrolysate the M1 reactor effluent becomes quite toxic and hasn't recovered as of day 230, shortly before this writing. The decrease in carbon added through acetic acid seems to have a negative effect on the M8 effluent toxicity, even though COD removal is still quite good (Figure 4.)

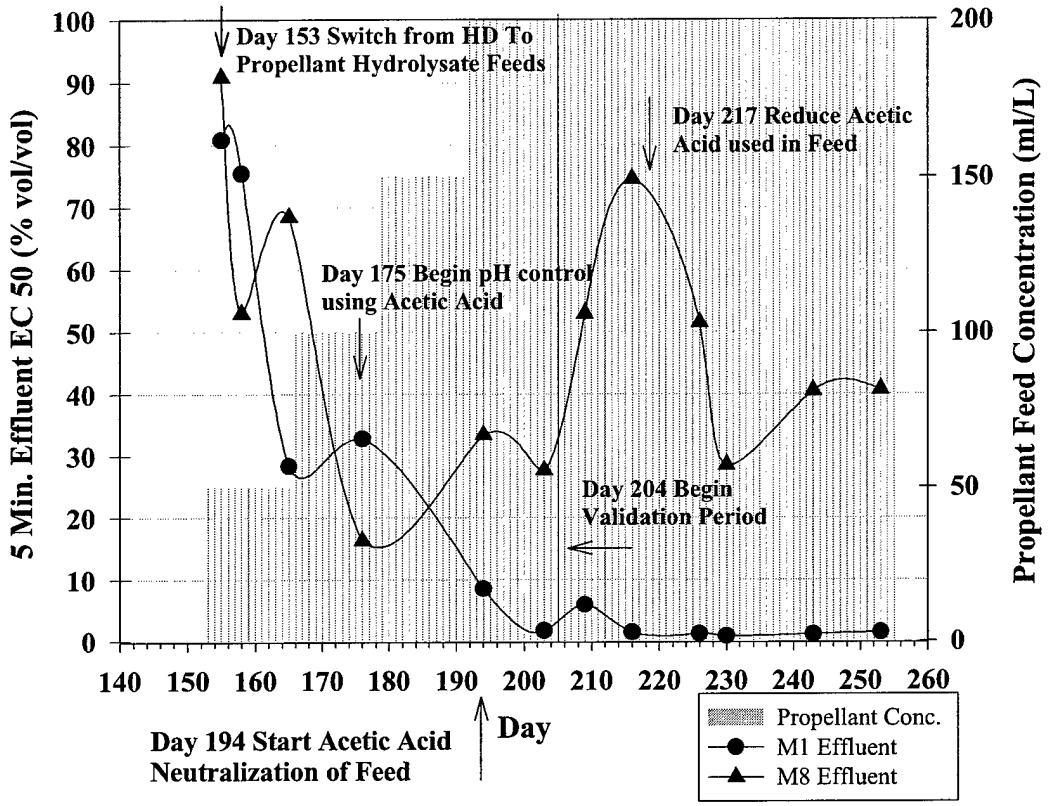

Figure 6. MICROTOX Assay Results For The M1 and M8 ICB Effluents's.

CONCLUSION

As of this writing, planned, in-depth chemical analysis of the propellant hydrolysate and ICB effluents have not been received. We look forward to receiving this data and confirming the performance indicated by our process monitoring data.

The intent of this study was to assess the ICB's ability to degrade the M1 and M8 propellant hydrolysates in to less toxic compounds. The proposed total solution for HD chemical rounds stored at Pueblo Chemical Depot presently under consideration by ACWA limits the flexibility of operating conditions for the reactors. Since the projectile propellant is not considered an agent or Schedule-2 compound under the CWC, it is not subject to a strict destruction deadline. It can therefore be removed from the projectile and stored until after destruction operations for the HD and Schedule-2 compounds are complete. In that scenario, the propellant hydrolysates would be processed separately. The process under consideration also restricts the ICB media carbon to what is already present in the propellant hydrolysates. This study follows that scenario in that it limits the addition of a carbon source that could help in further degrading the nitrogen containing compounds.

From the limited data available from this study, we can see that the ICB culture is able to remove at least 70% of the COD from the feed, indicating that degradation is occurring. Data show that the M8 propellant was degraded to a relatively non-toxic level, as indicated by Microtox assay, while the culture was supplied with an external carbon source. An interesting observation is that since lowering the added carbon the COD removal efficiency has changed little yet the toxicity of the effluent has changed. The

effluent produced since reducing the acetic acid carbon source has become more toxic, confirming an expected relationship between effluent toxicity and carbon availability. The culture still may adapt further to this low carbon condition during the remainder of the study and effluent toxicity may improve.

The M1 reactor effluent has shown consistent increases in toxicity since the switch from HD hydrolysate to the M1 propellant hydrolysate. As of this writing the M1 effluent shows little improvement in toxicity over that of the M1 feed as measured by Microtox Assay. Interestingly the COD removal efficiency of the M1 reactor has declined since removing the external carbon source, a different effect than that observed in the M8 reactor. This effect of decreased carbon and relatively high effluent toxicity still could change over the second half of the study.

Data indicate a need for additional external carbon. A potentially favorable scenario would be to combine the two hydrolysates incorporate them into the HD degradation process, since that process requires the addition of nitrogen compounds to work efficiently. Finally, the addition of a denitrification step to the process could degrade nitrogen containing compounds, releasing previously unavailable carbon for degradation and lessening effluent toxicity.

HIGH SENSITIVITY DETECTION OF BACTERIAL ENDOSPORES VIA TB PHOTOLUMINESCENCE ENHANCEMENT

Nicholas F. Fell, Jr.*, Paul M. Pellegrino, and James B. Gillespie
U.S. Army Research Laboratory, Optics Branch
2800 Powder Mill Rd., Adelphi, MD 20783

ABSTRACT

Detecting bacterial endospores is a critical challenge to bioanalytical chemistry, since a number of serious diseases and health problems are caused by members of the spore-forming genera *Bacillus* and *Clostridium*. We have developed a highly sensitive method for their detection and have demonstrated detection limits of less than 5000 CFU/ml. Our method is based on the presence of a marker compound in bacterial endospores, dipicolinic acid (dpa). When complexed with Tb and excited in the UV, the dpa enhances the photoluminescence emission of Tb by several orders of magnitude.

We have investigated the potential for interference from other biological materials and chemicals and found that nothing other than bacterial endospores will give us a positive response to this test. Our investigation also showed that the presence of phosphate or organophosphate ions will reduce the observed signals. We have been able to overcome this problem through the addition of $AlCl_3$. The results of our interference studies and phosphate studies will be presented.

Since only 10% or less of the dpa is released when the endospores are suspended in aqueous buffer, we have also examined methods for enhancing the release of dpa. Our results from both mechanical and chemical methods to enhance dpa release will be presented. The best we have achieved is a 20-fold increase in dpa release from *B. globigii* endospores in 2 minutes through the addition of dodecylamine and heating to 80°C.

INTRODUCTION

The detection of bacterial endospores is a significant challenge in bioanalytical chemistry. The endospore is a dormant stage in the life cycle of some members of the genera *Bacillus* and *Clostridium*. A number of these species can cause disease, food poisoning, or food spoilage, so their detection is important in both the civilian and military sectors. The method we describe in this paper is intended for first-alert use. In this intended deployment the method is

used to monitor the background and when the signal level increases significantly, an alert is issued to trigger other more specific and time-consuming techniques.

Our method is based on the presence of calcium dipicolinate (Ca(dpa)) in the endospore casing and the release of some of this dpa into solution. Endospores contain 2 to 15% by weight[1] of dpa,[1] depending on species and other factors. Addition of Tb^{3+} to the aqueous solution will result in complexation with the dpa^{2-} released from the spore. When irradiated with UV light at the dpa absorption maximum, $[Tb(dpa)_n]^{3-2n}$ exhibits a greatly enhanced luminescence compared to Tb^{3+} alone. The observed luminescence is shifted far from the excitation wavelength and is narrower than normal molecule luminescence signatures. Detection of the Tb^{3+} luminescence signature is therefore a unique marker for the presence of dpa and thus bacterial endospores. In our experiments we use an excess of Tb^{3+}, so the form of the complex is $[Tb(dpa)]^{+}$. Previous research has determined that energy transfer from the ligand (dpa^{2-}) to the terbium excited states leads to this enhancement.[2,3] In this method, a small amount of an aqueous suspension of the analyte is added to a buffered $TbCl_3$ solution. Any samples containing particulates are filtered to isolate the water-soluble compounds. The sample is then irradiated with a wavelength corresponding to the dpa absorption maximum and the luminescence emission spectrum is collected. Any sample that exhibits stronger emission intensity than Tb^{3+} alone contains bacterial endospores.

Our research has been divided into three major studies. First was the examination of various chemical and biological materials for interference with our detection method.[4] This involved investigating both false positive and negative results. False positive testing checked for responses for samples that do not contain bacterial endospores. False negative testing investigated cases where the reduction or elimination of signal from samples containing bacterial endospores occurred. The second study concerned finding an additive to reduce the deleterious effect of phosphate, the primary interferent with our technique.[6] Finally, we have investigated methods to release more dpa from the bacterial endospores in order to improve the limit of detection. In this phase of our work we examined several mechanical and chemical methods to extract more dpa.

EXPERIMENTAL

The experimental procedures and optical arrangement are described in detail in our previous publications.[4-6] The samples in each group of experiments are brought to a constant volume with buffer and the level of Tb and *B. globigii* are held constant within each set to permit proper comparisons. All of the samples were made in aqueous Trizma buffer at pH 7.6. Three replicate measurements are made on each sample and the average value for the three replicates is used for succeeding calculations and in all plots. The signal from each set of samples is normalized to a standard with the same bacterial endospore concentration and total volume.

RESULTS AND DISCUSSION

INTERFERENCE STUDY. We have examined materials in three classes to determine their effect on our bacterial endospore detection technique.[4, 5] We checked nine organic chemicals, seven inorganic salts, and fourteen biological materials for both false positive and false negative responses. A false positive occurs when a material other than a bacterial endospore give a signal above the Tb background. None of the materials we examined gave a

false positive signal. In fact, the only materials that yielded a positive response were bacterial endospores, as seen in Figure 1. Figure 1 includes the responses for two samples of *B. globigii*

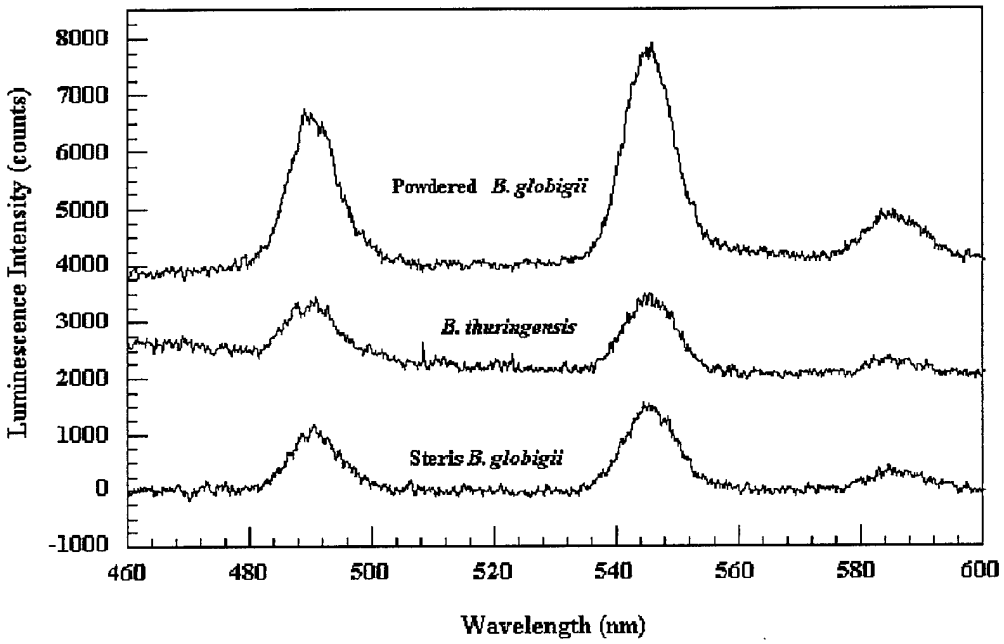

Figure 1. Positive responses from bacterial endospores. Top-powdered *B. globigii* 6.165×10^8 CFU/mL, intensity offset by + 4000; Middle-Thuricide®, containing 0.8 % *B. thuringensis*, diluted by a factor of 40, intensity offset by + 2000; Bottom-Steris *B. globigii* 1.3×10^9 CFU/mL.

and a commercial insecticide containing 0.8% *B. thuringensis*. The Steris *B. globigii* was washed by centrifugation and we were still able to detect the signal from the dpa remaining in the spores.

Several of the materials in the test set did result in reductions in the signals we observed from a fixed amount of *B. globigii*. Some difficulties were also observed with a number of the pollens and molds, but these materials can be removed through size-selective sampling since they are much larger than bacterial endospores. The worst case occurred with addition of phosphate-containing chemicals. K_2HPO_4 had the most deleterious effect on our signals. Barela and Sherry have reported that phosphate buffer has a similar inhibiting effect on the photoluminescent emission from terbium dipicolinate.[7] Two explanations are possible for this observation. The first is that the phosphate anion has a high affinity for Tb^{+3} and may displace dpa from it. Secondly, the phosphate anion may quench the excited dpa molecules before they transfer their energy to the Tb^{+3}. These results demonstrated the need for a method to deal with phosphate interference.

PHOSPHATE INTERFERENCE. Our next set of experiments[6] focused on finding a method to reduce or eliminate the deleterious effect of phosphates described in the previous section. We found that *B. globigii* samples from Dugway Proving Ground were less susceptible to phosphates than dpa alone. It is possible that this resistance is due to the additional

components[8] in those samples as a result of their growth and processing. Despite the additional "protective" components, samples of Dugway *B. globigii* still experienced a decrease in signal of up to 15% when exposed to 85 μM K_2HPO_4. At the same concentration of K_2HPO_4, dpa alone suffered up to a 65% decrease in signal strength.

The next step in our investigation was to examine the use of various inorganic salts to reduce the interference of phosphates. Figure 2 shows the results of this examination. We

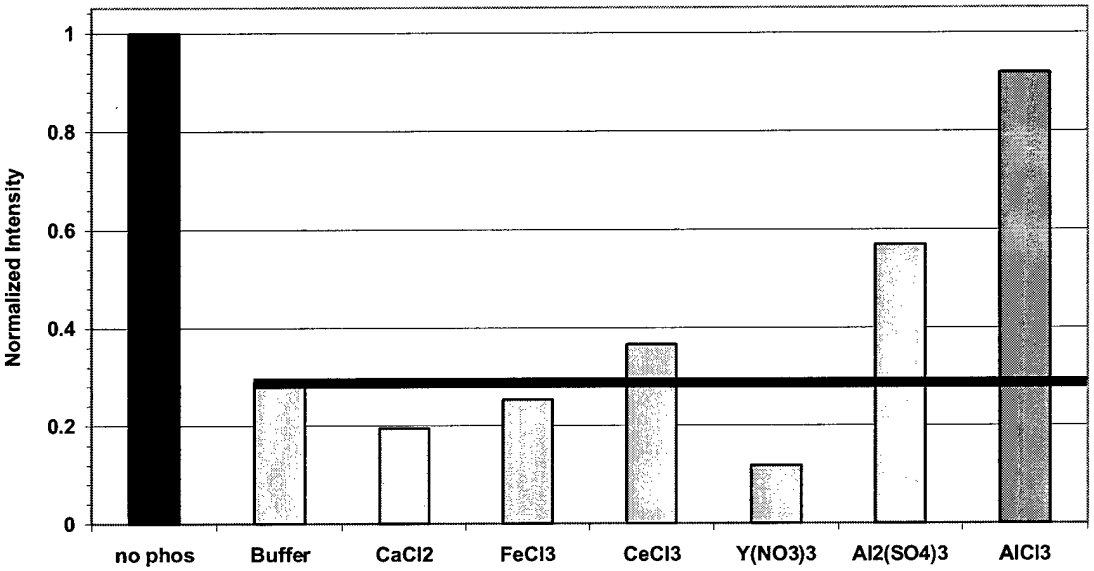

Figure 2. Signal recovery on addition of salt solutions. The signal is normalized to the intensity (no phosphate) of the Tb/dpa stock with buffer added to compensate for the volume of salt solution added. Buffer represents the normalized signal level of the Tb/dpa/phosphate stock with buffer added to compensate for the volume of salt solution added. The beneficial effects of $Al_2(SO_4)_3$ and $AlCl_3$ are clear.

concentrated on salts with cations with a +3 charge. It has been reported that Al^{+3} is used in water processing facilities to remove phosphate ions.[9] The utility of this approach is clearly evident from these results. The salts with anions containing a negatively charged O were not effective and served to reduce the signal or hinder the beneficial effects of the cation. This is a direct result of the high affinity of Tb^{+3} for negatively charged oxygens.[2,3] When $AlCl_3$ was added to samples containing dpa or Dugway *B. globigii*, the signal level was reduced by up to 15% for dpa and maintained for the Dugway *B. globigii* on exposure to 85 μM K_2HPO_4, provided that the dpa was added before or at the same time as the phosphate. This graphically shows the beneficial effect of addition of $AlCl_3$.

DPA RELEASE ENHANCEMENT. We have focused our most recent efforts on determining the best method of enhancing the release of dpa from the bacterial endospores, since less than 10% of the available dpa is released by suspension in aqueous buffers. In this study we used a washed commercial suspension of *B. globigii* that had a significantly lower level of readily available dpa upon suspension in aqueous buffer than the Dugway *B. globigii* did. We have examined both mechanical and chemical means of extracting more dpa from the endospores. Table 1 summarizes the results of these experiments.

TABLE 1. Summary of DPA release methods. The maximum enhancement is the ratio of the maximum signal achieved and the room temperature standard with the same concentration of bacterial endospores.

Method	Maximum Enhancement	Time to Max. Signal
Glass Beads	6.3	2 min.
Diatomaceous Earth	4.8	12 min.
Cetyltrimethylammonium bromide	7.4	120 min.at 50°C
Amino Acid/Sugar	5.8	180 min. at R.T.
Dodecylamine	20.5	2 min. at 80°C
Boiling	18.3	15 min. at 100°C

Among the mechanical means we have attempted are sonication, sonication with glass beads (40 nm and 200 nm), shaking with glass bead and diatomaceous earth, and heating. Sonication and shaking with glass beads was intended to crush the endospores between the glass beads. Shaking with diatomaceous earth abraded the endospores on the sharp facets of the diatomaceous earth. It has been reported in the literature[1, 10] that boiling endospores for 15 minutes will extract all of the dpa from them. We have found that sonication with or without glass beads was ineffective on our samples. Agitation in a Wig-L-Bug with glass beads or diatomaceous earth increased the extracted dpa by a factor of 6.3 and 4.8, respectively. One of the difficulties with the diatomaceous earth required 10-15 minutes of settling time after being agitated in order to extract a sample of the suspension.

We also examined three chemical means of extracting more dpa. The first was to mix a solution of cetyltrimethylammonium bromide (CTAB) with a sample of the bacterial endospore suspension and heat the mixture to 50°C. Samples were removed at set time intervals, mixed with Tb solution, and the photoluminescence emission collected. This method took two hours to reach its maximum release and increased the dpa by a factor of 7.4. We also attempted to coax the endospores into germinating, since the first step in that process is the expulsion of all of the dpa from the endospore. This was accomplished by adding a mixture of alanine, asparagine, and glucose to a sample of the endospore suspension, sampling at intervals, and collecting the photoluminescence emission. This method released 5.8 times the initial dpa concentration and took three hours. Later experiments, in which the endospores are pre-heated, have achieved almost complete release of dpa from the spores with either alanine alone or the alanine-asparagine-glucose cocktail, but it still required 2 hours to 3 hours to reach the maximum level of dpa release. Neither of these methods resulted in acceptable release rates. The last chemical method we have examined is addition of dodecylamine (DDA) to endospores suspensions. This was done in a similar manner to the CTAB addition. The DDA was able to release all of the dpa (as determined by boiling) from the bacterial endospores in 2 minutes at 80°C. The dpa release with DDA is a strong function of relative endospore-to-DDA concentration and temperature.[11] Once a threshold level of DDA is reached, the rate of dpa release is independent of endospore-to-DDA ratio. The rate also increases as a function of temperature, as one would expect. Clearly, DDA addition is the best method for releasing more dpa from bacterial endospores.

DISCUSSION. The release of all of the dpa from the endospores permits the most sensitive possible detection of bacterial endospores with this technique. Based on our un-

enhanced limit of detection of 83,000 CFU/mL of suspension for *B. globigii*,[11] we can detect less than 5000 CFU/mL with DDA release. We have experimentally detected less than 10,000 CFU/mL of BG using the DDA treatment with a signal-to-noise ratio of greater than 6, indicating that our LOD will be less than 5000 CFU/mL. This level of detection permits detection at the 10 agent-containing particle per liter of air level in less than 10 minutes of sampling at the 500 L/minute rate and concentration to 1 mL. Commercial samplers with this rate of collection are available permitting extremely sensitive detection of bacterial endospores from the atmosphere. With a commercial fluorescence system and no processing, Dugway *B. globigii* has been detected at a level of 1900 CFU/mL.[12] Improvements in our system may permit us to reach this level of detection and with the DDA treatment reach detection limits of less than 200 CFU/mL. One area of concern to quantitative use of this technique is the reproducibility of sampling from a suspension. This results in a 15% relative standard deviation for replicate samples[6] and limits quantitative use of the method. Despite this limitation, our technique is well-suited to use as a first alert warning system.

CONCLUSIONS

The results we have reported clearly indicate the high sensitivity of our method for bacterial endospore detection. We are able to detect less than 5000 CFU/mL of endospores in less than 5 minutes with DDA for enhanced release of dpa from the endospores. Our method is immune from false positive responses. Through the use of $AlCl_3$ to complex any phosphate present in a sample, we have eliminated the only significant interference with this technique. While quantitative use of the method is limited, it is more than sufficient for first-alert use.

ACKNOWLEDGEMENTS

The authors wish to acknowledge several sources of samples and support for this work. We would like to recognize the effort of our summer research assistant, Ms. Carrie DiGeralamo (2000), and our STARS student, Ms. Lola Kelly (1999, 2000), who performed a number of the experiments described here. Some of this work was performed while Dr. Paul Pellegrino held a National Research Council-U.S. Army Research Laboratory Research Associateship and Dr. Nicholas Fell held an American Society for Engineering Education-U.S. Army Research Laboratory Postdoctoral Fellowship. We also thank the U.S. Army Edgewood Chemical Biological Center, especially Ms. Dottie Paterno, for providing some of the bacteria samples used in this study. In addition, we appreciate the assistance of Dr. Dan Martin of Dugway Proving Ground, UT, for his descriptions of the composition of the impurities present in our BG samples. Finally, we would like to acknowledge the helpful suggestions of and our discussions with Dr. David L. Rosen of the U.S. Army Research Laboratory, who initially developed this method.

REFERENCES

1. G. W. Gould and A. Hurst, The Bacterial Spore (Academic Press, New York, 1969).
2. F.S. Richardson, *Chem. Rev.* **82**, 541 (1982).
3. D. H. Metcalf, J. P. Bolender, M. S. Driver, and F. S. Richardson, *J. Phys. Chem.* **97**, 553 (1993).
4. P. M. Pellegrino, N. F. Fell, Jr., D. L. Rosen, and J. B. Gillespie, *Anal. Chem.* **70(9)**, 1755 (1998).
5. D. L. Rosen, U.S. Patent 5,876,960, 1999.
6. N. F. Fell, Jr., P. M. Pellegrino, and J. B. Gillespie, *Anal. Chim. Acta* **426(1)**, 43-50 (2001).
7. T. D. Barela and A. D. Sherry, *Anal. Biochem.* **71**, 351-357 (1976).
8. Dr. Daniel Martin, U.S. Army Dugway Proving Ground, UT, private communication.
9. R. H. Petrucci, General Chemistry Principles and Modern Application, 4th ed., Macmillan, New York, 1985, p 659.
10. L. J. Rode and J. W. Foster, *Archiv für Mikrobiologie* **36**, 67-94 (1960).
11. N.F. Fell, Jr. and P. M. Pellegrino, unpublished results, manuscript in preparation.
12. N.F. Fell, Jr., ARL and V. Vullev, Boston University, unpublished results.

BIOHAZ: BIOLOGICAL DETECTION FOR EMERGENCY RESPONDERS

David L. Gray [1], Randall R. Bright [1], Peter J. Stopa [2], Philip A. Coon [2], David Trudil [3]
[1]EAI Corporation, 1308 Continental Drive, Abingdon, Maryland, 21009, USA; [2]The US Army Soldier, Chemical, and Biological Command, Aberdeen Proving Grounds, Maryland, 21010, USA; [3]New Horizons Diagnostics Corporation, 9110 Red Branch Road, Columbia, Maryland, 21045, USA

ABSTRACT

There exists an urgent need for emergency responders to rapidly detect the presence of biological materials in a suspect sample. The BioHAZ™ Kit has been recently developed to fill such a need. It is intended to give the emergency responders an integrated capability to collect an environmental sample and to rapidly screen that sample on site for the presence of biological material. This allows the incident commander to be aware of a potential biological hazard and call for the proper response to the situation.

This kit consists of both sampling and detection equipment. It has a variety of sample collection and processing packets to obtain solid, liquid, or air samples. Samples are then screened using multiple, complimentary technologies that are well-proven to determine the presence of biomarkers such as ATP, DNA, and protein within the samples. A simple algorithm allows the operator to determine if the sample may contain bacteria, spores, or protein. Samples can then be further analyzed on site with immunoassay tickets before being sent to a laboratory.

This system provides the emergency responders with a capability that they do not have. The adoption of this kit could result in savings of time and money by debunking biological hoaxes and providing timely warning of the presence of actual biological materials. The BioHAZ™ Kit may also deter the use of biological agents when used as part of a system to mitigate the effects of a biological incident.

INTRODUCTION

As the result of an increasing number of bioterrorism hoaxes and incidents throughout the United States, there is a recognized deficiency among the emergency response community to rapidly detect the presence of biological materials at the site of an incident that is suspected of involving a biological agent. In the late 1990s, the U.S. Army Edgewood Chemical and Biological Center initiated an effort to develop an expedient capability for first responders to sample, detect, and identify the presence of hazardous biological materials in the environment.

The first step in this effort was to identify user requirements and to develop a concept of operations for the use of the kit. Design goals and performance specifications were then established with assistance from the responder community to develop the first prototype, called the Biological Detection Kit (BDK). The performance goals of the BDK were adopted from the first generation Biological Integrated Detection System (BIDS) that is currently fielded by the US Army for biological detection. The requirements of the kit were that it should be able to collect all forms of samples, but work primarily with surface samples to answer the question: "Does that device contain a biological material? If it is bacteria,

is it viable?" Additional goals of the development effort were that the total cost of the kit should not exceed $20,000 apiece, that all of the components had to be commercially available, and that the entire kit had to be portable.

DEVELOPMENT OF THE BIOHAZ KIT

MARKET SURVEY AND APPROACH

A market survey to identify technologies that would meet the mission requirements of the BDK was performed and, upon completion, the problem was re-evaluated. It was then decided to change the focus of the effort. The original concept consisted of a kit with sampling devices and a library of immunoassay test tickets for identification purposes. The concept was changed to a more generic approach for a variety of reasons, some of which were:

1. A limited library of test tickets capable of identifying "military threat" biological agents is available. The tests may miss other pathogenic biological materials that could be used by a terrorist but might not otherwise be thought of as a battlefield biological agent.
2. Immunoassay test kits have to be used within concentration and pH guidelines. Tests of samples that are outside of these guidelines may give erroneous results. It would be more useful for field analysis to have the means to determine if the sample was within these guidelines necessary for accurate use of the test kits.
3. Genetic engineering of organisms or other treatments may compromise the ability of antibody-based or nucleic acid probe-based tests to detect and/or identify pathogenic materials.

Based on the market survey, a BIDS-like approach was then adopted in which multiple, complimentary technologies are used as generic tests for biological traits. By comparison, the BIDS uses a particle counter to measure fluxes in the quantity of threat sized particles (1-10 μm) in the environment. Upon alerting to a spike in the particle flux, the BIDS operators collect a sample and analyze the sample for adenosine tri-phosphate (ATP) content and for deoxyribonucleic acid (DNA) content. If the sample possesses certain criteria, it is subjected to immunoassay techniques for further analysis. This scheme is based on the:

1. Particle size and count determination. Most intentionally man-made particles that have viable organisms and/or biological activity are typically above three microns (3 μm) in diameter.
2. ATP determination - detects the presence of living things.
3. DNA test - most all biological materials have DNA. Although purified proteins are assumed to contain no DNA, they are often contaminated with sufficient residue DNA from the protein source to be detectable.
4. Immunoassay test - the antibody-antigen reaction of immunoassay tests give a confirmation of the presence of specific biological agents within the available library of tests.

Tests similar to those are used in the BIDS are used in the BioHAZ kit, but because of cost, size, and weight constraints, the approach on how these tests are used was changed. For example, the BIDS uses a flow cytometer to do DNA detection. This instrument is capable of distinguishing between spore and vegetative cell DNA. The cytometer weighs 300 pounds and has a price tag of $100,000. The BioHAZ approach will detect DNA in the sample using a hand-held fluorometer, but does not distinguish what type. The BioHAZ luminometer is similar to the one in the BIDS. The BIDS luminometer measures total ATP and cannot differentiate among non-bacterial ATP, vegetative bacterial ATP, and spore ATP. The model used in the BioHAZ Kit has the capability to differentiate among these sources of ATP. Therefore, the BIDS uses the cytometer to differentiate among types of biological material and the BioHAZ Kit does it with the luminometer. Unlike the BIDS, a generic protein detection capability was added to the BioHAZ Kit for detection of proteinaceous toxins, such as Botulinum toxin and Ricin. Also, the design of the BioHAZ Kit eliminated the use of the particle counter used in the BIDS. With the BIDS, this instrument is used as a real-time aerosol sampler to trigger further actions of sample collection and subsequent analysis. The use profile of the BioHAZ Kit presumed that, if a biological attack had

occurred in conjunction with an incident that resulted in an emergency response, any biological materials disseminated as an aerosol would have precipitated onto surfaces from which they can be collected using the surface sampling components of the kit.

Since there are a variety of sampling systems in the commercial marketplace for use in different applications, it was decided to integrate some of these into the kit for specific purposes. Individually sealed, expendable sample collection kits were developed to enable the user to collect environmental samples in various forms. Specific kits are included to collect samples from large surfaces (Swipe-1 Kit), small surfaces (Swipe-2 Kit), liquids (Swipe-3 Kit), and from air using filter systems designed either for air sampling or asbestos monitoring (Swipe-4 Kit). In addition, sample processing kits (SPK) were added to allow the user to refine the collected sample for testing on site.

TECHNICAL CONSIDERATIONS

Hand-held particle counting instruments. Small, hand-held particle sizers, including: the Met-One models 227A (2 channel) and 237A (6 channel) and the Bio-Test AG (4 channel) were obtained and evaluated for use in the BDK. They were tested extensively during several joint field trials held in the U.S. They compared relatively well to some of the more expensive instruments currently available. As the approach for the BioHAZ Kit differed from that of the BIDS and the original BDK development, the use of a particle counter Kit was eliminated from further consideration.

ATP luminescence detection instruments. Three luminometers were evaluated for detection of bioluminescence: the IDEXX Lightning System, the New Horizons Diagnostics Model 4700, as it is used in the BIDS, and the New Horizons Diagnostics Model 3550. Although other systems exist and are mainly used in food safety and sanitation monitoring, these three units offered some distinct advantages. The IDEXX system has all of the reagents packaged in a swab device. The Model 4700 is used in the BIDS and would be representative of some of the other luminometers that read total ATP. The Model 3550 has a separation step that allows the operator to eliminate non-bacterial sources of ATP. This process was further used to develop a test capable of detecting spores. This test could not be easily achieved with the other instruments. The New Horizons Diagnostics Model 3550 was therefore implemented for the following reasons:

1. Tested by the USDA and several other organizations [1, 2, 3] under field conditions and found to be the only luminometer that showed good correlation with culture results.
2. Approved by the FDA for detection of bacteria in human urine.
3. Used by several commercial companies to measure bacterial contamination in process control measurements.
4. Shown to be the least prone to interferences.
5. Allows the operator to use a variety of sample volumes for analysis.

DNA detection. For DNA determination, the Hoefer DNA Quantitation Kit from Pharmacia Chemicals, Inc., was initially evaluated. The instrument analyzes in the UV. It was not sufficiently rugged to be of use in the field and the dye was highly prone to interferences from the sample that could not be controlled. The PicoGreen dye kit from Molecular Probes was also evaluated [4]. This kit is readily available and gives detection limits at the required level. It is routinely used in reference labs to quantify DNA in samples prior to PCR analysis. It does not seem to be prone to matrix interferences and has a related dye that detects RNA (single-stranded nucleic acids). To utilize the PicoGreen dye, the Turner Designs TD-360 fluorometer was initially considered for the BDK. It performed well within the required detection limits. The BioHAZ Kit incorporates the newer, smaller Turner Designs instrument, TD-00, which operates at the same performance specifications as the TD-360.

Protein detection. The Coomassie Blue protein test was initially evaluated, since it was the only protein test that met the time and other mission requirements. Other tests either took one hour or required boiling of the sample. Interference from detergents was found with this test. Field experiences with the test showed that an adoption of a cut-off of 10 µg/ml of protein from surface samples was necessary to minimize false positive test results. Likewise, a value of 2.5 µg/ml protein was chosen as the cut-off

value for air samples. Several colorimeters were evaluated for use, types that are used for water analysis and typically range in price from $200-600. The ChemMetrics VVR colorimeter was initially accepted for use with the BDK. An improvement with the BioHAZ Kit is the replacement of the Coomassie Blue reagent and the colorimeter with the colorimetric protein test strips commonly used for urinalysis. Although the detection limit is increased to about 50 µg/ml with Bovine Serum albumin, these strips are less prone to interference, far less expensive, and easier to perform than the Coomassie test.

Instrument integration. At the conclusion of the laboratory development phase, the instruments were given to emergency responders for field trials. Based on their experience and advice, it was decided that an integrated instrument housing both the luminometer and the fluorometer functions should be built. The resulting instrument is depicted in Figure 1. Since this dual instrument consists of the Model 3550 luminometer and the TD-00 fluorometer components in a single outer housing, the performance of each instrument is the same as the original components.

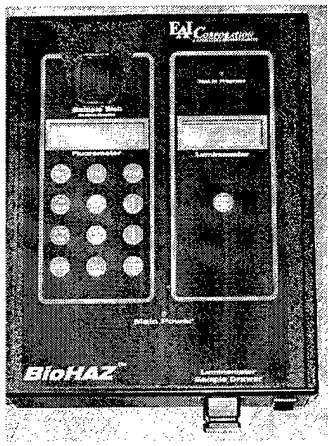

Figure 1: BioHAZ instrument.

SUMMARY OF TESTING RESULTS

A variety of tests were performed both in the laboratory and in the field [5]. The luminometer was evaluated with five different types of bacteria, including gram positive spores, cocci, and bacilli, and gram negative bacilli and cocci. Laboratory tests showed that using the BioHAZ system protocols, the luminometer could routinely detect 10^5 colony forming units of vegetative bacteria per milliliter of solution (CFU/ml), 10^6 CFU/ml of spores using the spore test procedure, and could differentiate between spore forming and non-spore forming bacteria. This was demonstrated during a recent joint field trail in the U.S. Interferences from common household, laboratory, and environmental chemicals were also evaluated. The ATP test showed no interference from any of these materials, although timing was crucial as to when the sample was tested relative to when it was collected. The DNA test did exhibit false positive results when tested with phosphates; however, in the scenarios under which the kit would be used, this should not be a problem since the presence of phosphate may be another indicator of biological material. The urinalysis test strips were not subject to interference from these materials.

The results in Table 1 list the performance capabilities of the BioHAZ Kit for each test. Table 2 shows a comparison of the BioHAZ Kit to the BIDS.

TABLE 1: BioHAZ testing performance capabilities.

Original Goal	ATP Test (1)	DNA Test	Protein Test
Bacteria - $5x10^5$ CFU/ml	$<10^5$ CFU/ml (vegetative) $\sim10^6$ CFU/ml (spores)	$\sim10^5$ CFU/ml (vegetative) $\sim10^6$ CFU/ml (spores)	N/A
Viruses - 10^6 PFU/ml	N/A	$\sim10^7$ PFU/ml	N/A
Toxins - 500 ng/ml	N/A	See note (2)	~50 µg/ml

Notes: CFU: Colony forming units; PFU: plaque forming units.

(1) The ATP test measures only live bacteria. The DNA test can measure the presence of either live or dead bacteria. It was also noted that the signal increases, hence the detection limit decreases, if detergents are used to disrupt the bacteria.

(2) At protein concentrations greater than 10 µg/ml, there is detectable DNA present that is typically $1/1000^{th}$ of the protein concentration.

TABLE 2: Comparison between BIDS and BioHAZ Kit.

Specification	NDI BIDS	BioHAZ Kit
Measure changes in biomass	Measure total ATP with Model 4700 luminometer	Measure change in DNA concentration with fluorometer
Differentiate vegetative cells and spores	Uses DNA dye with flow cytometer	Measures ATP flux with luminometer after incubation
Bacterial detection limit	$5x10^5$ CFU/ml	$<10^5$ CFU/ml
Generic detection	Bacteria , probably virus, no protein	Bacteria , probably virus, protein
Cost	~$1,300,000	$20,000
Size and weight	1-1/4 ton HMMWV (~12,500 lbs.) with trailer (generator)	~ 50 lbs., ~5 cu. ft. total

These results indicate that the BioHAZ Kit sufficiently meets the specifications to do what it is designed for, to indicate the presence or absence of biological materials, and it does so for a much lower cost than the BIDS, after which it was designed.

USING THE BIOHAZ KIT

The emergency responders at an incident may be called upon to use the BioHAZ Kit. There are several reasons or scenarios that might prompt an Incident Commander to initiate the use of this kit, but the end result will be to provide additional information about the possibility of biological materials being present at the incident scene. Responders and other operators can use the kit to check specific locations for suspected agents (e.g., the material inside of an anthrax letter or the area surrounding the release of a suspected biological agent), survey areas of interest for hot spots, determine the extent of contamination, measure the relative effectiveness of decontamination operations, monitor water, or for other inspection purposes. If the kit indicates the presence of biological materials, this information can help to:

1 Determine the extent of additional response required. For example, there may be requirements for protection, decontamination, or evacuation of potentially exposed personnel for medical evaluation.

2. Determine the type of biological materials that are present. This information can be passed to supporting medical facilities to help them decide on treatment protocols for the victims and to supporting laboratories to narrow their efforts in identifying the specific biological agent used.

3. Determine the type of immunoassay that can be performed on site. The results of these assays help to identify or eliminate specific biological agents from further consideration.

If the BioHAZ Kit tests indicate that no biological materials are present, the Incident Commander can scale back the response efforts toward termination of the incident. This is the case with the responses to hoaxes, such as the ubiquitous anthrax scare letters.

Using the BioHAZ Kit is a simple process of collecting the samples, processing them for testing, testing the samples for biological materials, and evaluating the results for further action. Sample collection is facilitated by the use of individually sealed collection kits. One example is pictured in Figure 2. Once the sample has been collected, the operator can elect to forward the sample to a federal agency, or to test it on site with the BioHAZ Kit testing components. The kit contains the necessary components to package samples for transfer off site and to process samples for testing on site. A sample to be tested is refined into a clear, aqueous solution suitable for testing by using the SPK. The operator then performs quick tests using the instrument and the test strips. Table 3 indicates the type of

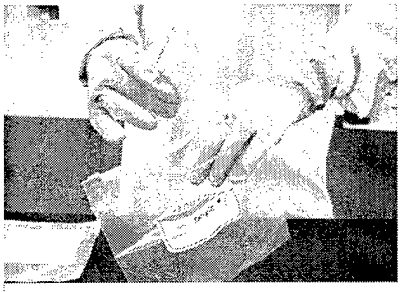

Figure 2: Swipe sampling kit.

results that can be expected from using the test equipment of the BioHAZ Kit. Depending on the results, the operator can perform assays specific to the type of biological materials found in the sample. For example, if toxin were likely to be present, assays for toxins (e.g., Ricin, etc.) would be used in lieu of other available assays. So too, if spore-forming bacteria were found, the appropriate assay (e.g., anthrax) would be warranted.

TABLE 3: Expected results of testing.

Indicates Sample Contains	ATP Test	DNA Test	Protein Test
Bacteria	Positive	Positive	See note (1)
Virus	Negative	Positive	See note (1)
Toxin	Negative	See note (2)	Positive

Notes:

(1) Possibly present from culture media or lysed cells.

(2) If protein concentration is above 10 μg/ml, will probably detect contaminating DNA.

The final results of any field testing must be verified by a laboratory. Even if an immunoassay indicated the presence of a specific biological agent, these results must be confirmed for positive identification. If other agents not detected by the available assays were used, the BioHAZ Kit will detect and categorize their presence but not provide any further information. For emergency response purposes, this indication alone is sufficient to determine the next series of response actions.

CONCLUSIONS

The BioHAZ Kit successfully does exactly what it was designed to do. It can provide emergency responders and other users the means to rapidly screen and determine the operationally significant presence or absence of biological materials in suspect samples.

REFERENCES

1. Cutter, Catherine N. et al., 1996, A Rapid Microbial ATP Bioluminescence Assay for Meat Carcasses, Dairy, Food, and Environmental Sanitation 16: 726-736.
2. JiYoung, Lee et al., 1999, A Rapid Method for Detecting Bacteria in Drinking Water, Journal of Rapid Methods and Automation in Microbiology 7: 135-145.
3. Stopa, Peter J. et al., 1999, Detection of Biological Aerosols by Luminescence Techniques, Field Analytical Chemistry and Technology 3: 283-290.
4. Singer, Victoria et al., 1997, Characterization of PicoGreen Reagent and Development of a Fluorescence-Based Solution Assay for Double-Stranded DNA Quantitation, Analytical Biochemistry 249: 228-238.
5. Stopa, Peter J. et al., 2000, BioHAZ: a Concept for First Responders, presented in the International Symposium for Chemical and Biological Defense in Sweden

QUANTIFICATION OF LEWISITE IN AIR BY LIQUID CHROMATOGRAPHY MASS SPECTROMETRY (LC/MS)

Wesley Ercanbrack, Sherry Sheffield, Steve Freudenberger, Aaron Jenkins
Science and Technology Corporation

ABSTRACT

It has been determined that lewisite will hydrolyze and oxidize under ambient conditions to form chlorovinyl arsonic acid (CVRA) which is an As+5 compound. Most published methods for the analysis of lewisite require the derivatization of lewisite with a dithiol compound to produce a compound that can be analyzed using a gas chromatograph. The derivatization methods generally have poor reproducibility and precision which is due to the fact that the CVRA compound will not be derivatized by the dithiol compound. The authors have established an air monitoring method that will account for both lewisite and CVRA sampled from the air during various sampling periods. Both lewisite and CVRA are extracted off a solid sorbent tube and analyzed by liquid chromatography/mass spectrometry.

INTRODUCTION

Lewisite (2-chlorovinyldichloroarsine) is a toxic arsenical compound. Since it is categorized as a suspected carcinogen, vapor concentrations must be monitored to protect worker safety in areas where the chemical is stored and where the compound is going to be neutralized. Several different air-monitoring methods have been developed and all have employed some sort of derivativization technique to quantify the amount of lewisite. The derivativization techniques rely on a chemical reaction of lewisite with dithiol to produce a compound that is more amenable to gas chromatography. These techniques have been plagued with poor precision and accuracy, particularly with aspiration times beyond two hours.

Research performed by the authors at the United States Army Chemical Agent Munitions Disposal System (USACAMDS) has culminated in a method with improved accuracy and precision compared to existing twelve hour methods. The method employs a glass solid sorbent tube packed with TenaxTA(60/40 mesh) that collects a vapor sample over a period of twelve hours at 0.5 liters per minute. Lewisite is collected on the sorbent tube, extracted with hexane and methanol and oxidized by adding 6% hydrogen peroxide. The extract is quantified by LC/MS.

BACKGROUND

The chemistry of Lewisite will be discussed along with some of the experiments that were conducted to validate the reactions.

LEWISITE REACTIONS

Lewisite undergoes several different reactions. The most rapid is hydrolysis.

$$\underset{\text{Lewisite}}{ClCHCHAsCl_2} + H_2O \rightarrow \underset{\text{Chlorovinyl arsonous acid (CVAA)}}{ClCHCHAs(OH)_2} + HCl$$

This reversible reaction can occur with a very small amount of water. CVAA can also lose a water molecule and form lewisite oxide (chlorovinylarsineoxide).

$$\underset{\text{CVAA}}{ClCHCHAs(OH)_2} \rightarrow \underset{\text{lewisite oxide (LO)}}{ClCHCHAsO} + H_2O$$

This reaction will only occur in the absence of water. The lewisite oxide will then polymerize. The polymerization reaction occurs slowly.

Lewisite is not easy to oxidize directly, but after it has hydrolyzed to CVAA oxidation occurs readily.

$$\underset{\text{CVAA}}{ClCHCHAs(OH)_2} + O_2 \rightarrow \underset{\text{Chlorovinyl arsonic acid (CVRA)}}{ClCHCHAsO(OH)_2}$$

LEWISITE OXIDATION TO CVRA

The authors found that lewisite spiked on a sorbent tube that was aspirated over a period of time tended to have poor recovery (<30%). It was theorized that the poor recovery was attributed to the oxidation of CVAA. Humidity was hydrolyzing the lewisite to CVAA and the oxygen was oxidizing it to CVRA. To test this theory, stannous chloride pre-filters were placed at the sampling end of the tubes. Stannous chloride was used because of its ability to absorb the oxygen from the air. The samples were aspirated in the same manner as before and the lewisite recoveries were much improved (>90%).

LEWISITE OXIDATION PATHWAY AND RATE

To further test the theory and to find the reaction pathway and rate, two experiments were performed. The first was to determine if hydrolysis had to occur prior to oxidation. A set of glass impingers filled with water and another set filled with methanol were each spiked with 1 ug of lewisite. Compressed air was bubbled through the impingers at 0.5 liters per minute for one hour. The samples were analyzed for lewisite by HPLC/MSD. The impingers filled with methanol had a recovery of 90%. The impingers filled with water had a recovery of <10%. The results conclude that hydrolysis of the lewisite to CVAA is the first step in oxidation.

The second test was to estimate a reaction rate for the oxidation of Lewisite to CVRA. A set of sorbent tubes were spiked with 1080 ng of lewisite and aspirated for 5 minutes at 1

liter per minute. Another set of tubes were spiked with 1080 ng of lewisite and aspirated for 12 hours at 0.5 liters per minute. Each sample was analyzed for lewisite and CVRA. This process was repeated for 2 hours, 1 hour, 30 minutes, and 15 minutes. Based on the data, oxidation begins to occur between 5 minutes and 15 minutes of aspiration and then levels off after 15 minutes (see Figure 1). This is most likely due to the oxidation reaction reaching an equilibrium due to the concentration of oxygen in the air.

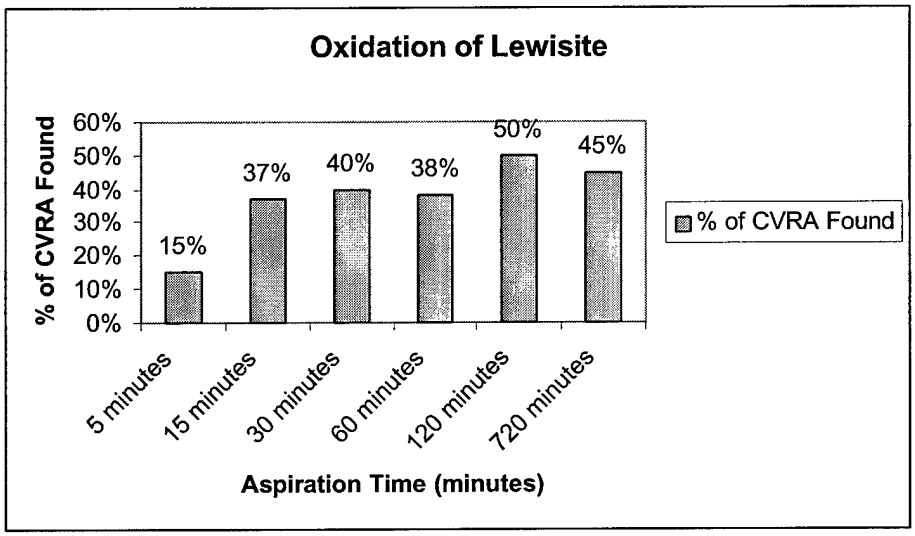

Figure 1. Oxidation of lewisite on a solid sorbent tube.

CVRA HEADSPACE TEST

Approximately 1 gram of felt pads were soaked in 697 ug/mL CVRA/methanol. The pads were placed in a heated chamber. The headspace was sampled with a sorbent tube for 1 hour. The sample was analyzed for CVRA by LC/MS. The entire procedure was performed at ambient temperature, 70 C and 150 C. There was < 0.1% CVRA found in the headspace, which draws a conclusion that CVRA is essentially not a vapor hazard.

The entire experiment was repeated using 897 ug/mL lewisite/methanol and a significant amount of lewisite was found on the tube. To compare the vapor pressure of CVRA with that of a known chemical agent, the experiment was again repeated using 425 ug/mL VX/isopropanol. The VX was analyzed by GC/FPD and a significant amount was recovered.

The authors believe that lewisite/CVAA will only oxidize on a substrate. So although CVRA is not a significant vapor hazard, it is a contact hazard and could be spread through the air by depositing on dust particles and being carried by air current.

METHODOLOGY

After reviewing the results of the previous experiments, specifically that lewisite will hydrolyze in air due to humidity and then oxidize as a function of time, the authors proposed a 12 hour air monitoring method that would work whether the lewisite was oxidized or not. Therefore a more accurate representation of the lewisite concentration in the sampled air would be obtained. The precision and accuracy study that was performed to validate the method is outlined below.

ASPIRATION

Twelve sorbent tubes were spiked in duplicate at 0, 216 ng, 540 ng, 864 ng, 1080 ng and 1620 ng. The spikes corresponded to 0.2, 0.5, 0.8, 1.0, 1.5 times the time weight average of 0.003 mg/m3. The tubes were aspirated for twelve hours at 0.5 liters per minute. This process was repeated for four days for a total of 48 samples.

EXTRACTION

Samples are extracted using a modified solid phase extraction system. The system consists of an extraction manifold, a vial rack and a vacuum pump. Plastic pipette tips are used to fit the sorbent tubes into the vacuum manifold (see Figure 2). The tip is inserted into the manifold and the sorbent tube is placed into the plastic tip. All extraction port valves are closed and the vacuum pump is switched on.

An aliquot 0.25 mL of hexane is applied to the top of the sorbent tube (see Figure 3) and slowly allowed to be pulled through the tube by opening the valve slightly. The tube is allowed to air dry for approximately 10 seconds after which the valve is closed. An additional 0.25 mL aliquot of hexane is applied to the top of the sorbent tube and allowed to flow through the sorbent in the same manner. The analyst moves on to the next tube in the rack.

After all tubes have been extracted with hexane, the analyst performs the same extraction procedure with 4 aliquots of methanol. Two different solvents are used because hexane extracts any lewisite present on the tube but will not extract CVRA and methanol extracts CVRA but will not adequately extract lewisite.

After the tubes have been extracted, 0.25 mL of 6% hydrogen peroxide is added to each vial. This oxidizes any lewisite or CVAA present into CVRA.

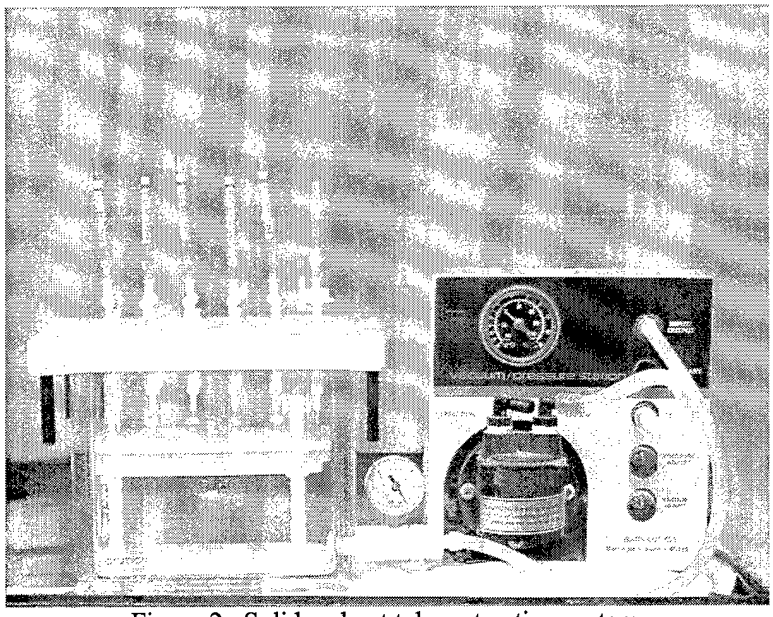

Figure 2. Solid sorbent tube extraction system.

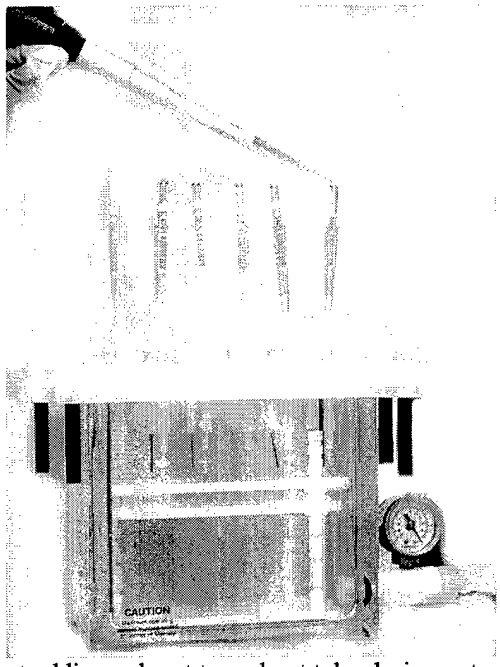

Figure 3. Analyst adding solvent to sorbent tube during extraction procedure.

ANALYSIS

Samples are analyzed on an Agilent Technologies 1100 HPLC/MS. The mass spectrometer has a single quadrapole with atmospheric pressure ionization electrospray source (see Table 1 for list of set points). The sample analysis is performed in negative mode using

selective ion monitoring for ions 184.9 m/z, 186.9 m/z, 148.9 m/z and 122.9 m/z). The resulting data is identified by retention time and mass spectra ion ratios and quantified using the total ion chromatogram. Each set of 12 samples, are divided into two sets of 6, with each set being analyzed by a different analyst.

CALIBRATION

A standard solution of Lewisite at a concentration of 216 ug/mL Lewisite in methanol is used to calibrate the HPLC-MSD. Calibration curves are prepared by spiking solid sorbent tubes in duplicate with 216 ng, 1080 ng, and 1620ng of lewisite. After each injection of the standard solution, the sorbent tubes are aspirated for 5 minutes at approximately 1.0 liters/minute. The sorbent tubes are extracted and analyzed using the procedures defined above. The ChemStation software is used to record the calibration curve data and to quantify analyzed samples.

STATISTICAL RESULTS

All 48 data points were pooled into a single group and entered into a statistical analysis program called Certify. The program was used to plot the target concentration versus the found concentration for the data population. The average recovery of the samples was 92 %. The uncertainty in found mass was 38.04 %.

FIELD ACCEPTANCE

To test the long term stability of the new method a 30 day baseline study was performed. Every 12 hours a spiked tube (1080 ng Lewisite) and a blank tube were aspirated, extracted and analyzed following the procedures in the method. This process was repeated 5 days a week for 4 weeks. The agent recoveries are summarized in Figure 4.

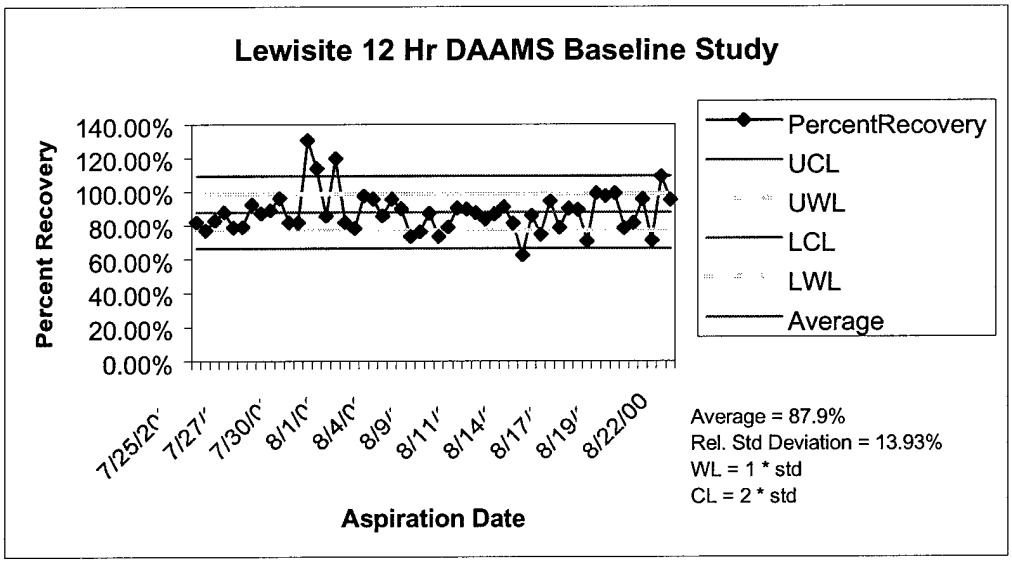

Figure 4. 12 Hour Baseline Summary.

INSTRUMENT CONFIGURATION

The following (Table 1) is a summary of the instrumentation used to develop the method and the key set points for the instrument.

TABLE 1. Instrument Set-points.

Instrumentation
Agilent Technologies 1100 High Performance Liquid Chromatograph with G1946B Mass Spectrometer using an Atmospheric Pressure Ionization Electrospray source.

Instrument Set Points for CVRA Method
Column: Agilent Technologies Extend C-18 2.1mm x 150 mm, 5 um
Pump Flow: 0.2 ml/min
Mobile Phase: 75/25 0.02 M NH4OH/Methanol
Diode Array Detector: Not Used
MSD Ionization Mode: API-ES
Time Filter: Enabled
Peakwidth: 0.10 min
SIM Ion: 122.9 Fragmentor: 90
SIM Ion: 148.9 Fragmentor: 70
SIM Ion: 184.9 Fragmentor: 50
SIM Ion: 186.9 Fragmentor: 50
EMV Gain: 1.0
MSD Gas Temp: 350C
MSD Drying Gas: 12.0 L/min
MSD Nebulizer Pressure: 35 psig
MSD VCap: 4000 V
Injection Volume: 10 uL
Column Thermostat: 25C
Expected Retention Time: 1.7 minutes

FUTURE ENDEAVORS

After reviewing each of the procedures in the method the greatest chance of induced error is during the extraction. It is a detail oriented task where analysts need to have good training and practice to produce precise and accurate results. Currently the issue is being addressed by developing an automated extraction system that would minimize the determinate error.

CONCLUSION

Derivatization methods are only reliable when Lewisite or CVAA is present. Most methods do not account for the loss of lewisite due to oxidation. If the lewisite is oxidized, the derivatization reaction will not work. The end result is low lewisite recoveries especially during longer aspiration times (>2 hours). Field-testing this method has demonstrated a viable new method of detection for lewisite with good precision and accuracy.

ACKNOWLEDGMENTS

The authors would like to thank the U.S. Army for the use of the Chemical Agent Munitions Disposal System facility and also Steve Mallen and Dallen Cox for support in making this research possible.

REAL TIME BIODETECTION OF INDIVIDUAL PATHOGENIC MICROORGANISMS WITH A RUGGED, SUB-BRIEFCASE-SIZED SYSTEM

Paul E. Johnson, Michael L. Lund, Amanda S. Votaw, and Jerome E. Swanson
Department of Physics and Astronomy, University of Wyoming, Laramie, WY 82071

Richard W. Shorthill and William Asprey
SoftRay, Inc., 519 South 5th Street, Laramie, WY 82070

Julie L. Kellogg
Department of Chemical Engineering, University of Wyoming, Laramie, WY 82071

Dehua Zhao
Department of Computer Science, University of Wyoming, Laramie, WY 82071

ABSTRACT

The objective of this research is to test the feasibility of an innovative approach to rare cell detection: using a CCD to image an entrained flow through a rectangular glass tube. This approach is especially useful for the detection of rare cells where a high volumetric flow rate is desired. We present the results of our work with Nile red labeled 1-micron polystyrene beads as labeled cell simulants. This technique has key advantages over current alternatives, including: (1) high volumetric flow rate, 2) capability of detecting single microorganisms (3) automatic operation, and (4) easy implementation in a rugged, portable system.

INTRODUCTION

Rapid biodetection of specific pathogenic microorganisms at very low concentrations usually requires immunofluorescence detection with an epifluorescence microscope or conventional flow cytometer. We present an immunofluorescence detection approach that lends itself to low-cost detection in a rugged, miniature package. While conventional flow cytometers are essential for making accurate photometric measurements of light scattering from cells, simpler means may be used where only cell identification is necessary. This research was based on use of a two-dimensional or panoramic CCD (charge-coupled device) detector, which allows for a much greater signal-to-noise ratio (S/N) than conventional photomultiplier or photodiode systems.

A second important achievement of this research was successful demonstration of a "sheathless" (or core-flow-only) flow cell, providing for simpler construction and operation of the flow cytometer and

potentially far greater volumetric flow rate than the conventional cylindrical core/sheath flow device. This was accomplished by using a "*ribbon flow*": flowing the sample through a rectangular, transparent tube, large enough to inhibit clogging, yet small enough to enable imaging all of the target particles flowing through it.

APPROACH

The SoftRay approach to biodetection is an unconventional form of flow cytometry (patents pending) based on:

- a sample flow entrained by a rectangular glass tube to deliver the total volume of solution being sampled into the laser beam for detection,
- fluorescent labels to provide high selectivity, and
- use of a CCD with time delayed integration (TDI)[1] to provide the highest signal-to-noise (S/N) and the possibility of spectral discrimination for simultaneous identification of more than one species. This technique is called time delayed integration because the CCD is read out continuously, one line at a time, in sync with a moving image, as opposed to reading the entire image at once. TDI allows for detection in real time, with a reduction in background noise, as explained later.

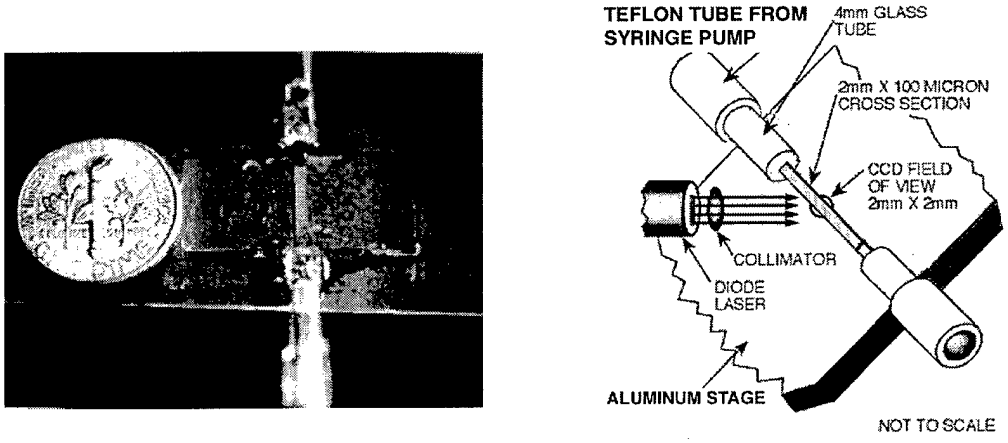

Figure 1. A schematic of the SoftRay flow cytometer used to test the concepts of TDI with a ribbon-flow geometry. On the left is an early version of our miniature flow cell, consisting of a 1 mm x 50 μm flow channel mounted on a microscope slide and connected to Teflon tubing through two short 3 mm glass tubes. A drawing of our current design is shown on the right. This version of our instrument employs a 4.0 mW Nd:YAG laser, a 2.0 mm x 100 μm rectangular flow tube, a 4x-microscope objective, an inexpensive, uncooled CCD camera, and an IBM-compatible PC for data collection. An image made from a similar flow cell is shown in Fig. 4.

In this research, a fully operational TDI/CCD flow cytometry apparatus was assembled and tested with 1-micon Nile red fluorescent microbeads (Molecular Probes, Eugene, OR). The flow cell and the laser source are shown in Fig. 1. This device enabled the flow cytometry feasibility demonstration and established the suitability of the TDI/CCD flow cytometer to *effectively detect single pathogenic microorganisms*. Emphasis was placed on signal-to-noise enhancement. In this detection system, SoftRay successfully used "sheathless" ribbon flow geometry. Fluid is transported through a transparent rectangular flow tube that is large enough (2mm x 100 μm) to prevent clogging (Fig. 1). Our imaging technique allows measurement of individual cells while they transit this flow cell.

A fundamental difficulty with conventional flow cytometry is embodied in the competing requirements of high flow rate, to provide near-real-time detection of microorganisms, and high sensitivity. High sensitivity is predicated on having a fluorescing microorganism in the detection region long enough to provide for a high S/N ratio, and having an optical design that limits background from scattering and fluorescence from unbound dye, which can dominate the background. The optimal device is a flow cytometer with a small excitation beam, a high flow rate, and detection electronics that allow for collection of enough photons from a microorganism for reliable detection. Time delayed integration with a CCD camera can provide such a system. TDI allows for detection in real time (in seconds) but with a significant reduction in background noise, as explained below and in Fig. 3. The time delayed integration (TDI) technique was first discussed by Barbe[1] and developed by Wright and Mackay for astronomy[3].

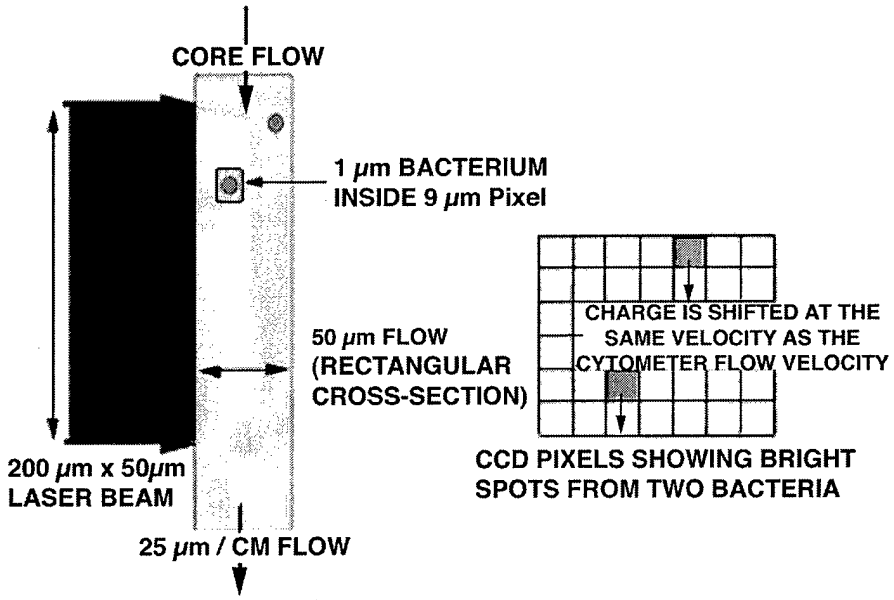

Figure 2. The detection signal-to-noise is improved with imaging TDI. Left panel: two bacteria (circular) are shown in the core flow illuminated by a laser beam from the left. Right panel: the image, at the CCD surface, where pixels illuminated by the two previous bacteria are shaded. The charge packets associated with these illuminated spots are shifted down the CCD at the same rate as the bacteria move in the cytometer flow. The result is that a moving volume 9 μm × 9 μm × 50 μm is imaged onto the CCD and read out as a pixel. Using a single, conventional detector, a volume 200 μm × 50 μm × 50 μm is detected. This would produce the same intensity contribution from the bacterium as would a CCD, but with more than 100 times the background intensity.

Conventionally, a CCD image is made by opening a shutter, exposing the entire CCD array to an image, closing the shutter, and reading the device. After an exposure, a charge distribution exists across the CCD, with each pixel carrying an electronic charge proportional to the light having fallen on that pixel during the exposure. After the exposure, the charge is transferred, row by row, into a serial transport register. After each row transfer, the individual pixels are transferred, one at a time, through an on-chip output amplifier and digitized. The readout and digitization are generally performed as quickly as possible (in milliseconds), under existing noise constraints.

With the TDI technique, each row is shifted more slowly, to synchronize the pixel shift rate with the rate at which the image moves across the CCD. The CCD is not shuttered, but is read out continuously. Image smearing is avoided by moving the image across the CCD at the same rate that the CCD charge is being shifted (Fig. 3). For the TDI flow cytometer described here, the chip will be oriented so that the charge packets are shifted down, synchronously with the passage of bacteria through the detection region.

We assembled a CCD flow cytometer that demonstrated the practical and economic feasibility of our proposed method for real time detection of pathogenic microorganisms using an imaging CCD camera with a novel time delayed integration (TDI) technique (where the CCD imaging is synchronized with the flow cytometer stream velocity) to image and count individual microorganisms.

We initially chose not to test TDI/CCD flow cytometry with a conventional sheath/core flow cytometer. Instead, we based our initial proof-of-concept device on a flow cell consisting of 1-mm × 50 μm rectangular glass tubing. This eventually evolved into an improved, innovative, sheathless flow cytometer, which appears to be well suited to TDI/CCD flow cytometry. Without a sheath flow, the cytometer has been greatly simplified. In addition, with a ribbon flow geometry flow cytometer, the cross-sectional area, and therefore the sampling rate, can be easily increased by a factor of 10-100 over conventional flow cytometry. Side-illumination of the rectangular ribbon flow with a laser diode with a rectangular beam allows one to maximize the energy density of photons within the irradiated region of the flow. The dimensions of the ribbon flow are determined by the width of the CCD field of view and the depth of focus of the optics, which are in turn set to balance S/N and flow throughput.

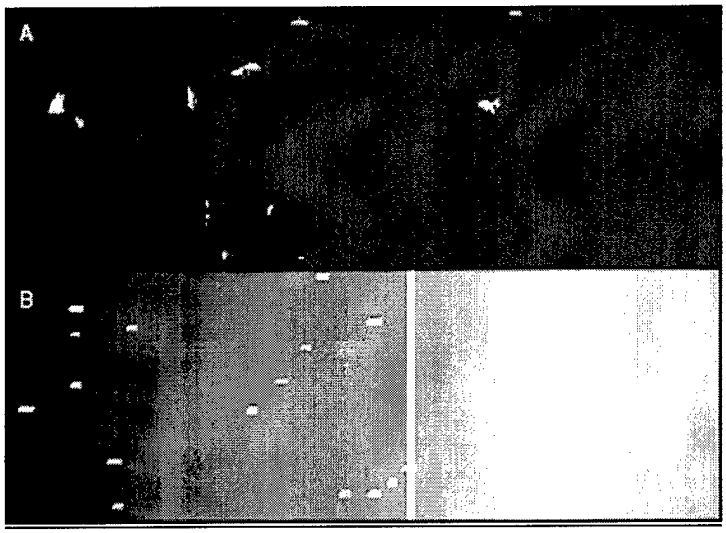

Figure 3. Initial tests with TDI were made with fluorescent 6.5-μm microspheres. These latex spheres were illuminated with a 2-mW HeNe laser and fluoresced at 671 nm. A. An image made through a 670-nm narrowband filter shows only the fluorescing microspheres. B. In unfiltered light, bubbles and other defects in the optical epoxy at the rectangular glass interface appear as streaks in TDI images.

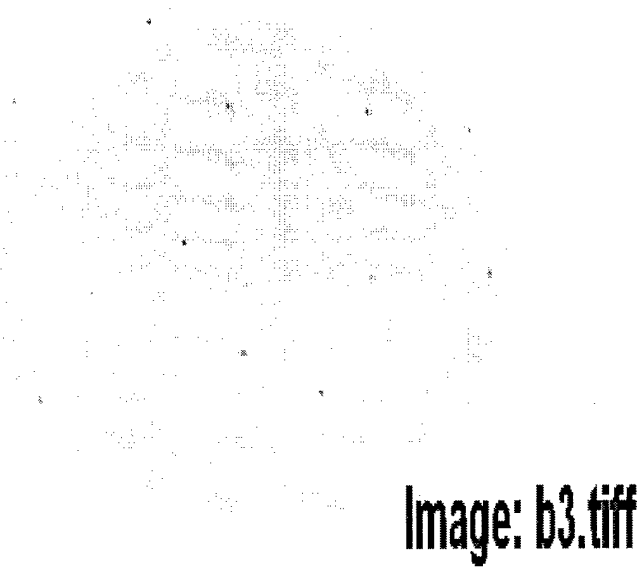

Figure 4. Fluorescing Nile red labeled polystyrene beads are seen under a Petroff-Hausser slide with an Olympus BH-2 epifluorescent microscope with 488 nm illumination. The negative fluorescence image is overlaid with a white light image of the Petroff-Hausser grid to facilitate concentration determination.

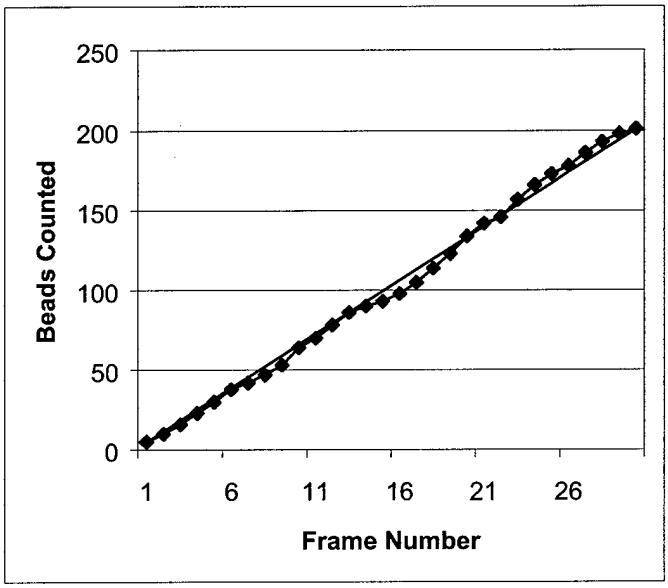

Figure 5. The cumulative number of beads per TDI image frame is shown for a 6.9 microliter sample counted by the TDI/CCD flow cytometer. This figure illustrates the consistency in counts from image to image.

We successfully performed the efficiency tests on our prototype flow cytometer configuration. Performance tests were made with 1-micron polystyrene beads labeled with Nile red dye. Known concentrations of calibration beads were prepared from a stock solution, then diluting this solution at a

number of lower concentrations. These concentrations were measured using a Petroff-Hausser slide with an epifluorescent microscope (Olympus BH-2). Petroff-Hausser measurements were made with an Electrim CCD camera. First a white-light image of the Petroff-Hausser slide was made. Then a fluorescent image was made of the bead dilution, illuminated at 488-nm. The white-light grid was digitally laid over the fluorescent image (Figure 4).

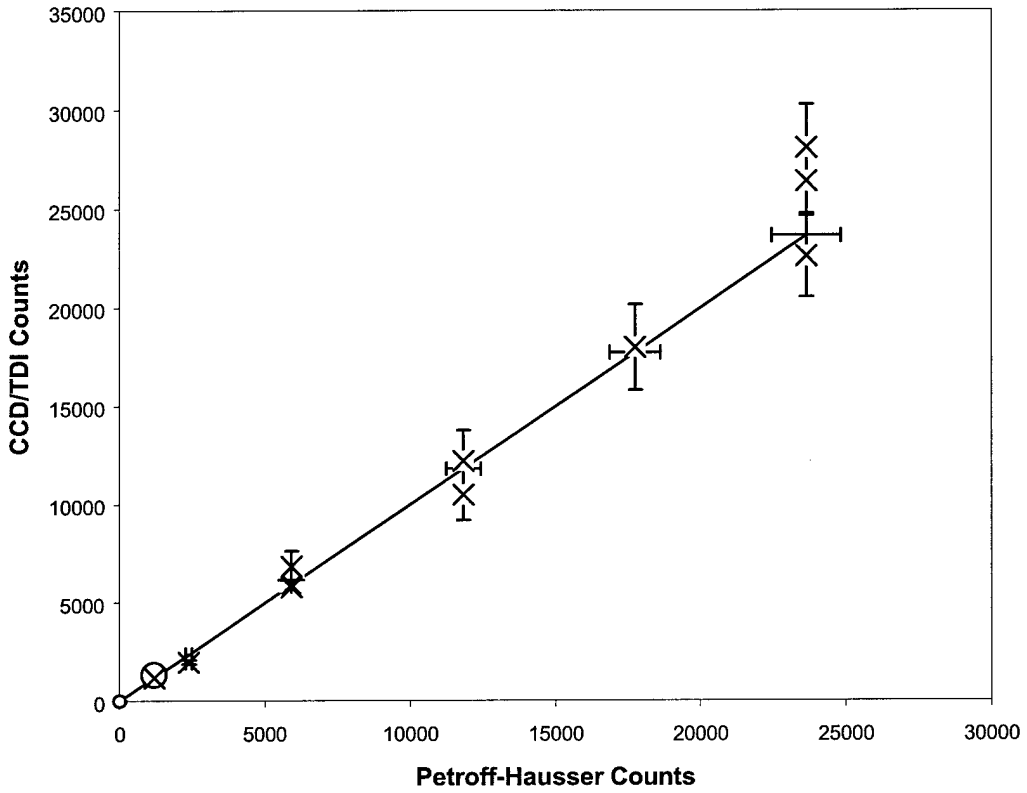

Figure 6. Comparison of CCD/TDI counts of Nile red labeled polystyrene bead dilutions with Petroff-Hausser counts (see Figure 5) on 6.9 microliter samples. Each of the clusters of measurements corresponds to a single dilution. Petroff-Hausser counts fall along the solid line. Horizontal error bars are the 1-σ error bars for the Petroff-Hausser counts. "X"s correspond to the CCD/TDI measurements. Vertical error bars represent the 1-σ error bars for the CCD/TDI counts. Each CCD/TDI measurement is the result of counting 30 frames, corresponding to 6,9 microliters of fluid. A sample of buffer solution with no beads was run as a null sample and yielded no counts. The result is a point plotted at the origin.

CONCLUSIONS

We counted the fluorescing beads in a CCD/TDI flow cytometer by TDI imaging the flow continuously as 1 ml of sample traversed the flow cell, then counting fluorescing cells from 30 of the TDI images by computer, corresponding to 6.9 microliters (230 nanoliters/frame). As each bead detection is based on imaging a single bacterium at high (>20) S/N ratio, we have shown that our technique is capable of single cell detection even at low (<10/ml) microbe concentrations.

ACKNOWLEDGMENTS

We acknowledge funding from the NSF STTR grant program under grant number DMI-9810567 (Phase I and II), NASA Space Grant NGT 40050, and NSF REU grant 9732039.

REFERENCES

[1] Barbe, *Solid State Imaging*, ed. P.G. Jespers, p. 659-671, 1975.
[2] J. F. Wright and C. D. Mackay, *Solid State Imagers for Astronomy*, J. C. Geary and D. W. Latham,Eds., *SPIE*, vol. 290, p. 160-164, 1981.

GAS CHROMATOGRAPHIC ANALYSIS OF THE STEREOISOMERS OF THE CHEMICAL WARFARE AGENT GF

Jan E. Kolakowski, Steven P. Harvey and Louis P. Reiff

U.S. Army Edgewood Chemical Biological Center
Aberdeen Proving Ground, MD 21010

ABSTRACT

Synthesis of the nerve agent cyclohexyl methylphosphonofluoridate (GF) yields a racemic mixture of two stereoisomers due to the presence of an asymmetric phosphorus atom. These two enantiomers, designated as P(+) and P(-), were separated in 8 minutes by chiral gas chromatography and quantified using flame photometric detection. Plots of peak area versus concentration of the individual enantiomers resulted in correlation coefficients greater than 0.99. The enantiomers were present in racemic GF in the ratio of 3:2 as P(-):P(+). The P(-) enantiomer was isolated using a method whereby the P(+) isomer was removed from the racemic mixture via preferential enzymatic catalyzed hydrolysis. The specific rotation of the P(-) enantiomer at 589 nm and 25 °C in methylene chloride was calculated to be –19.3°. The P(-) enantiomer also inhibited acetylcholinesterase more strongly than the racemic mixture, consistent with the findings for other optically active nerve agents.

INTRODUCTION

The chemical warfare agents GA, GB, GD, GF, and VX all have asymmetric phosphorus atoms resulting in pairs of P(+) and P(-) stereoisomers. GD also has an asymmetric carbon, which gives it four stereoisomers. Previously reported data on GA, GB, GD, and VX show that most of the toxicity of these compounds, as measured by inhibition rate of acetylcholinesterase (AchE), is due to the P(-) isomers.[1-5] No data have yet been published on the toxicities of the individual GF enantiomers. The enantiomers for all four of the G-agents have been separated by chiral gas chromatography (GC).[6] VX enantiomers were resolved using a chiral liquid chromatography method.[7] Separation of the GF enantiomers proved to be the most challenging, with retention times in excess of 80 minutes.[8] A chiral GC method was developed to perform rapid quantitative measurements of the enantiomers of GF. The work described here was part of an investigation into the stereospecificity of nerve agent degrading enzymes.[9,10]

EXPERIMENTAL

The gas chromatograph was a Hewlett-Packard model 6890 equipped with a flame photometric detector and an automatic sampler. The conditions were as follows:

Column: 25m X 250 um id X 0.12 um Chrompack Chirasil-Val-L.

Injection volume: 1 microliter, 100:1 split.

Inlet temperature: 200 °C.

Oven temperature: 90 °C (isothermal).

FPD temperature: 200 °C (phosphorus mode).

Carrier (helium) flow rate: 1 ml/min.

A chromatographically pure preparation of a single isomer of GF was made by degrading the isomer on which the enzyme had the greater activity. The enzymatic reaction was run at 15°C and pH 7.0 in order to minimize spontaneous hydrolysis. Just past the midpoint deflection, the reaction was extracted with methylene chloride and the extract was analyzed by GC using the above conditions. A single peak was observed representing a single GF isomer. When NaF was shaken with a solution of this isomer, subsequent GC analysis showed two peaks, consistent with NaF catalyzed racemization of GF. Since the racemization occurs in the absence of enzyme, the direct effect of NaF on GF appears to be at least one means by which GF is racemized.

The specific rotation of the single GF isomer was then calculated based on measurements of the observed rotation made at 589 nm (sodium line) and 25 °C using a Perkin Elmer 141 Electronic Polarimeter and a sample cell with a path length of 10 cm.

RESULTS AND DISCUSSION

The enantiomers of GF were consistently separated by 0.15 minutes at retention times near 8 minutes. A typical chromatogram is shown in figure 1a. Hydrolysis of the racemic mixture yielded the single isomer shown in figure 1b. Optical rotation measurements later revealed this to be the P(-) isomer, the specific rotation at 589 nm and 25 °C being calculated as -19.3°. The isomers were consistently present in the ratio P(-):P(+) of 3:2 based on peak area.

GA, GB, GD, and VX are known to stereospecifically bind acetylcholinesterase (AchE) resulting in a significant difference in toxicity between enantiomers.[1-5] Nerve agents and enzymes all exert their effects in a biological, chiral environment, so it should be expected that those effects would be stereoselective. For these agents, the P(-) isomers are all more toxic than the P(+) isomers. In the case of GA, the (-) isomer is 7 times more toxic than the (+) isomer.[3] Racemic GB is half as toxic as (-) GB, indicating that essentially all the toxicity is derived from the P(-) isomer.[1,5] Essentially all the toxicity of GD is derived from the two P(-) isomers.[2] The (-) isomer of VX is 13 times more toxic than the (+) isomer.[4] Figure 2 shows the results of an AChE inhibition assay in the presence of racemic and (-) GF as compared to spontaneous inhibition. The decrease in product yield is a result of the degree of binding of GF to AChE, or the increased inhibition of the enzyme. The rate of product formed is approximately halved in the

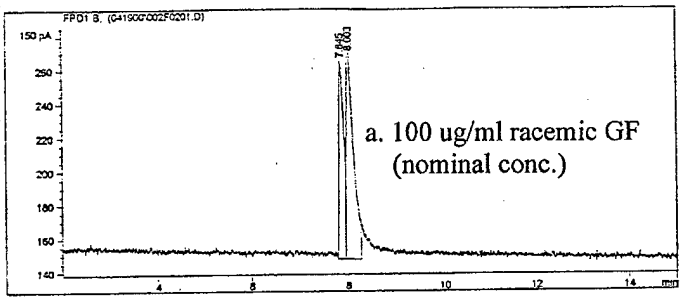

Peak #	RetTime [min]	Type	Width [min]	Area 150 pA*s	Height [150 pA]	Area %
1	7.845	VV	0.0851	746.98712	117.62490	37.40245
2	8.003	VV	0.1160	1250.17371	131.37010	62.59755

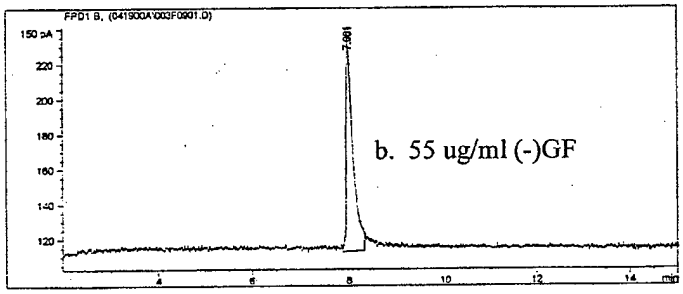

Peak #	RetTime [min]	Type	Width [min]	Area 150 pA*s	Height [150 pA]	Area %
1	7.981	VV	0.1160	1100.49902	122.31263	1.000e2

Figure 1. Gas Chromatograms of Racemic GF and (-)GF.

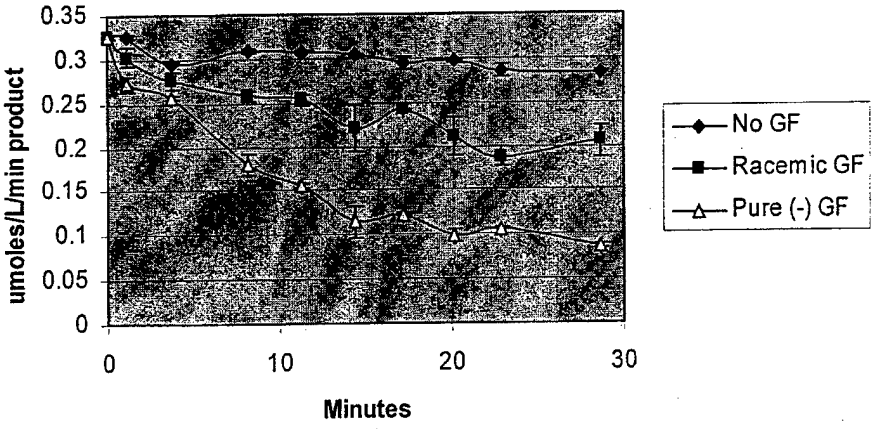

Figure 2. AChE Inhibition by GF.

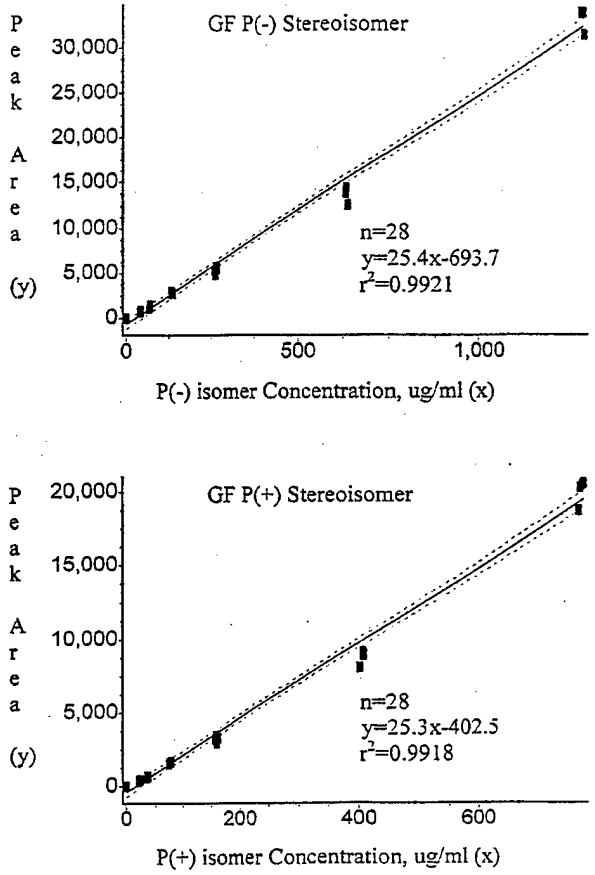

Figure 3. Standard Curves of GF Enantiomers.

presence of (-)GF when compared to racemic GF. This shows that pure (-)GF is more toxic than the racemic mixture.

Although baseline separation was not achieved, the separation between (-) and (+) GF was sufficient to quantitatively measure these isomers. Attempts to achieve baseline resolution of the enantiomers by modifying the GC conditions proved unsuccessful. Figure 3 shows sample plots of peak area versus concentration of the stereoisomers, as calculated from the ratio of peak area of the individual enantiomers to that of the racemic agent. Linear regression analyses of these data yielded correlation coefficients greater than 0.99.

CONCLUSIONS

A rapid and quantitative chiral GC method was developed to measure the individual stereoisomers of GF with retention times near 8 minutes. The P(-) enantiomer was successfully purified from the racemic agent and its specific rotation at 589 nm and 25 °C in methylene chloride was calculated to be $-19.3°$. The P(-) isomer of GF was shown to be more toxic than the racemic mixture and, consequently, much more toxic than the P(+) isomer. This is consistent with the findings for other nerve agents with optically active isomers.

REFERENCES

1. Boter, H.L. and Van Dijk, C, Biochem. Pharmacol. 18, 2403 (1969).

1. Benschop, H.P., et. al., Toxicol. Appl. Pharmacol. 72, 61 (1984).

2. Degenhardt, C.E.A.M., et. al., J. Am. Chem. Soc. 108, 8290 (1986).

3. Hall, C.R., et. al., J. Pharm. Pharmacol. 29, 574 (1977).

4. Van DeMeent, et. al., TNO, unpublished results (1987).

5. Smith, J.R. and Schlager, J.J., J. High Resol. Chromatogr. 19, 151 (1986).

6. Smith, J.R. and Shih, M.L., Analysis of the Stereoisomers of the Organophosphorus Chemical Warfare Agent VX Using Chiral LC and APCI Mass Spectrometry, Proceedings of the 47th ASMS Conference on Mass Spectrometry and Allied Topics, Dallas, Texas, June 1999.

7. Smith, J.R. and Schlager, J.J., Proceedings of the 1994 ERDEC Scientific Conference on Chemical and Biological Defense Research, ERDEC-SP-036, May 1996, p. 697.

8. Harvey, S.P., et. al., Catalytic Decontamination: Recent Developments, presented at the Army Research Office Decon Meeting, Jackson Hole, Wyoming, September 2000.

9. Harvey, S.P., et. al., Phosphotriesterase Mutants with Enhanced VX and G-agent Activity, presented at the 22nd Army Science Conference, Baltimore, Maryland, December 2000.

ACTIVITY OF PERA SAFE ™ AGAINST *BACILLUS ANTHRACIS* SPORES

Michael Bartoszcze, Krzysztof Chomiczewski, and Lidia Mizak
Military Institute of Hygiene and Epidemiology
Lubelska 2, 24-100 Pulawy, Poland
Tel/fax 48 818862822, e-mail obwwihe@man.pulawy.pl

ABSTRACT

Fast and effective decontamination of areas contaminated with *Bacillus anthracis* spores after a successful bio-terrorist attack proves to be a challenging task. There exist a variety of disinfectants that can inactivate *Bacillus anthracis* spores; however, most of them have negative side effects, such as equipment corrosion and environmental toxicity. The investigation described here shows that Pera Safe™ has high sporocidal activity on *Bacillus anthracis* spores within 20 minutes, while being safe for use with minimal impact on the environment.

INTRODUCTION

Bacillus anthracis is one of the main organisms that can be used in biological warfare or by bio-terrorists. This pathogen, in the form of spores, is characterized by considerable resistance to external factors, as is shown by its survival in the natural environment for years. *Bacillus anthracis* spores that are used as a biological weapon will result in environmental contamination that eventually must be decontaminated. Most of the disinfectants currently used to inactivate these spores are very corrosive, thus limiting the scope of their application. The purpose of this study was to estimate the sporicidal properties of a preparation of Pera Safe™ against *Bacillus anthracis* spores. A search of the literature showed no previous work with this material.

MATERIALS AND METHODS

For this study, a suspension of *Bacillus anthracis* spores, strain Sterne 34 F2, was used. The Pera Safe™ preparation (series 2194) was manufactured by Antec International and was supplied by Naturan LTD, Warsaw, Poland.

Spore suspension preparation: 200 ml of media, consisting of brain- heart agar with the addition of yeast extract and MnSo4 (0.1 g/l), was set in a level Roux bottle and was inoculated with 5 ml of a 24 hour broth bouillon culture of *Bacillus anthracis* (BA), strain Sterne 34 F2, and incubated for 72 hours at 37° C. The culture surface was then washed with Ringer's solution (dilution 1:4), filtered through sterile gauze, and centrifuged five times at 5-7,000 revolutions per minute. After each centrifugation, the precipitate was washed with sterile PBS. The washed spores were suspended in sterile, distilled water until a titer of $1.5x10^7$ spores/ ml was obtained. The number of spores was determined in a Thoma chamber using phase-contrast microscopy.

Preparation of the PeraSafe™ solution. A solution of a 1.62% concentration was prepared in 500 ml flasks with sterile, distilled water at a of temperature 35° C. After dissolving, the solutions were left for 1 hour at room temperature. Immediately before testing, 1% bovine albumin (Serva 11925) was added to one of the flasks. This is a standard load of organic substances used in investigations of preparations for the disinfection of instruments.

Determination of sporicidal activity. Suspensions of BA spores with concentrations between $1.5x10^7$ spores/ml and $1.7x10^4$ spores/ml were used for testing the PeraSafe™ preparation. The suspensions were centrifuged, and then 10 ml of the PeraSafe™ solution was added to each of the precipitates, respectively.

Concurrently, the same investigation was performed using the sporicidal preparation with a 1% bovine albumin supplement. The samples were mixed thoroughly and left at room temperature for 20, 40, 80, 160 and 240 minutes, respectively. After the measured time elapsed, the suspension was centrifuged, washed, and the sporicidal activity was established by incubation of 100 ul of each of the samples on blood agar.

RESULTS AND DISCUSSION

PeraSafe™ is a preparation in the form of powder containing sodium perborate, TAED, corrosion inhibitors, stabilizers, and dye. After dissolving the powder in water, supra-octane ions are liberated. This powder is used for general disinfection and shows bactericidal, fungicidal and virocidal properties.

The results are shown on Table 1. After 20 minutes, the solution of PeraSafe™ totally inactivates $5x10^4$ cfu/ml of *Bacillus anthracis* spores regardless of whether or not they are in the presence of bovine albumin. Higher concentrations of spores require a longer contact time, as is shown by the fact that a suspension of $1.5x10^6$ cfu/ml required 160 minutes for 100% inactivation. A concentration of $1.5x10^6$ spore/ml required at least 80 minutes of reaction time, irrespective of the presence of bovine albumin.

TABLE 1. Activity of Perasafe™ Against *Bacillus Anthracis* Spores.

PeraSafe™ contact time (min.)	**Spore Concentration (cfu/ml)**							
	1.5×10^7		**1.5×10^6**		**1.5×10^5**		**1.5×10^4**	
	Without albumin	**With albumin**	**Without albumin**	**With albumin**	**Without albumin**	**With albumin**	**Without albumin**	**With albumin**
20	$3{,}0 \times 10^2$	$5{,}4 \times 10^2$	$2{,}7 \times 10^1$	$4{,}0 \times 10^1$	0	$2{,}0 \times 10^1$	0	0
40	$1{,}1 \times 10^2$	$2{,}1 \times 10^2$	$1{,}2 \times 10^1$	$2{,}0 \times 10^1$	0	0	0	0
80	$2{,}7 \times 10^1$	$5{,}0 \times 10^1$	0	0	0	0	0	0
160	0	0	0	0	0	0	0	0
240	0	0	0	0	0	0	0	0

The results suggest that the PeraSafe™ preparation can be considered as one of the best products acting against BA spores. Currently, the following preparations are typically used for decontamination: formaldehyde, glutaraldehyde, hydrogen peroxide, peroxyacetic acid, chloramine, chlorine water(1,2,3,4,5). However, chlorine solutions corrode metals, oxidize rubber, and are rapidly neutralized by organic substances. Formaldehyde and glutaraldehyde solutions are harmful for the skin and respiratory tract. Likewise, one needs long exposure times for effective decontamination with these preparations (up to a few hours), considerably longer than PeraSafe™.

Pera Safe acts rapidly and effectively, even in cases of considerable contamination with BA spores. This preparation is not only safe to use but also is characterized by a pleasant odor.

CONCLUSIONS

PeraSafe™ inactivates *Bacillus anthracis* spores. The effectiveness of the sporicidal activity depends on the contact time and the concentration of spores. This preparation is safe for the environment.

REFERENCES

1.B aldry M.G.C.: The bactericidal, fungicidal and sporicidal properties of hydrogen peroxide and peracetic acid. J.Appl. Bacteriol. 1983,54,417-23.

2.D ietz P., Böhm R.: Results of an experimental study on testing disinfectants with spores of *Bacillus anthracis*. Hyg. und Med. 1980, 5, 103-7.

3.Fa ir G.M., Morris J.C.: The dynamics of chlorination. J. New. Eng. Water Works Ass. 1947, 61, 285-301.

4.Gorma n S.P., Scott E.M., Russell A.D.: A review – antimicrobial activity, uses and mechanisms of action of glutaraldehyde. J. Appl. Bacteriol. 1980, 48, 161-90.

5.H ussaini S.N., Ruby K.R.: Sporicidal activity of peracetic acid against *Bacillus anthracis* spores. Vet. Rec. 1976, 98, 257-9.

A BIOLOGICAL WARFARE DETECTION DEVICE (BIOWARD I)

Koen Gerritse[1], Bram van der Gaag[2], Edwin Stigter[2], Stefan van Hövell tot Westerflier[2]
Hans Harteveld[1] and Ruud Busker[1]

1. TNO-Prins Maurits Laboratory, Research Group Analysis of Toxic and Explosive Substances P. O. Box 45, 2280 AA Rijswijk, The Netherlands
2. TNO-Nutrition and Food Research Institute, Sensor Technology Department P.O. Box 360, 3700 AJ Zeist, The Netherlands

ABSTRACT

Using a bulk acoustic wave immunosensor device, Staphylococcus enterotoxin B and two simulant Biological warefare agents (bacteriophage MS-2 and bacteria *Erwinia herbicola*) could be detected in a direct fashion without the use of labelled antibodies. The detection device is incorporated into a ruggedized suit-case together with an aerosol sampler and sample handling system and can be used in the field for military monitoring purposes.

INTRODUCTION

Within the area of biological warfare there is a lack of modern biochemical sensors capable of real-time monitoring of pathogenic micro-organisms and toxins produced by them. General requirements for this type of sensors are: high sensitivity, short response times and high selectivity resulting in low false alarm rates. We here describe the development of an automated biosensor monitoring device for the detection of Staphylococcus Enterotoxin B (SEB), one of the protein toxins produced by the bacterium Staphylococcus aureus, MS-2 bacteriophage which is a simulant for a BW virus and *Erwinia herbicola* as a simulant for BW bacteria. These three agents are regarded as model agents covering a sufficiently broad spectrum.

The total system consists of an aerosol sampler, sample handling system, detection system and a PC and LCD screen for data acquisition. All subparts, which are thermostrated if necessary, are mounted in a box, which can be transported by a single person. For detection purposes three 20 MHz piezoelectric quartz crystal sensor devices are employed. Anti-BW "simulant" antibodies are coupled to the sensor surface using several interfaces. The assay is based on a direct immunological detection by anti-BW "simulant" antibodies as catching molecules.

RESULTS

By using the acoustic wave immunobiosensor system under laboratory circumstances, solutions of SEB or BW simulants could be detected in a direct fashion without the use of labelled compounds. The detection limit of the sensor for SEB was determined at 10 ng/ml. The detection limits for the simulant agents MS-2 and Erwinia herbicola were determined at 5 [x] 107 pfu and 107 cfu respectively. The sensor response is proportional to the concentration SEB or BW simulant in the samples.

After the sensor surface was cleaned by acid oxidation, an amino layer was deposited to the surface by plasma polymerisation. Antibodies directed to SEB or BW simulant were covalently bound to the amino functionilized surface [1]. Using the preconstructed interface the sensor response time for MS2 phages is approximately 10 min (Figure 1). SEB was injected as a control agent, which did not yield any response. The presented immunochemical detection principle is directly applicable to other BW agents.

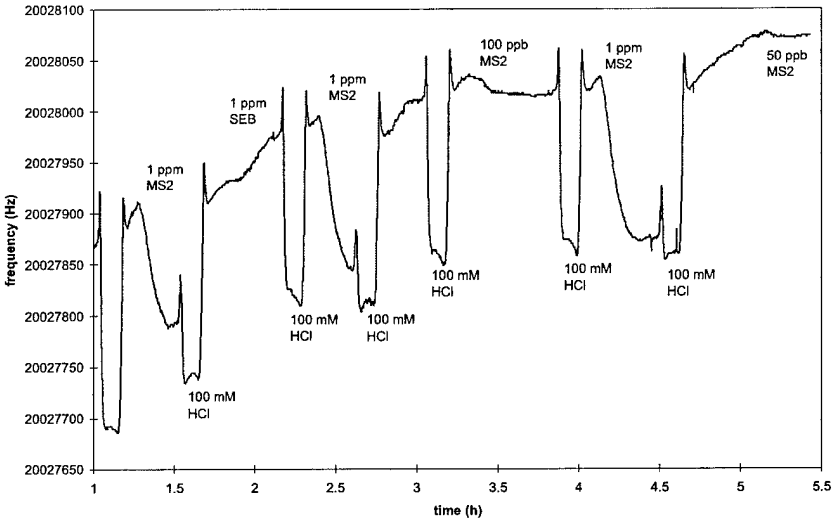

Figure 1. Sensor response of plasmapolymerised BAW crystals coated with anti-MS2 antibodies on injections of 1 μg/ml MS2 in HBS and 1 μg/ml SEB (control of specificity); 100 μl sample injection in carrier flow rate of 25 μl/min.

ACKNOWLEDGMENT

This work was performed in co-operation with GIAT Industries (France) and funded by the French and Dutch Ministries of Defence in the framework of Euclid RTP 13.7

REFERENCES

1. R. Nakamura, H. Muguruma, K. Ikebukuro, S. Sasaki, R. Nagata, I. Karube and H. Pedersen; A plasma polymerized film for surface plasmon resonance immunosensing; Anal. Chem. 69, 1997, 4649-4652.

THE INTERFERENCE OF STRESS ON PHYSOSTIGMINE PRETREATMENT AGAINST SOMAN INTOXICATION IN GUINEA PIGS

Ingrid H.C.H.M. Philippens , Marloes J.A. Joosen, Bas Groen, Raymond A.P. Vanwersch, Ruud W. Busker, Maarten S. Nieuwenhuzien

TNO Prins Maurits Laboratory, P.O.Box 45, 2280 AA Rijswijk ZH, The Netherlands

INTRODUCTION

During research efforts towards finding effective drugs are performed in a standard laboratory situation. However, in a more realistic situation other factors may interfere with the treatment regime. There is growing evidence that stress occurring during military operations can impair the efficacy and appearance of side effects of medical treatment. It is known that stress can change the kinetics of the pretreatment (1) and, therefore, affect the protective ratio and evoke the appearance of side effects. During operation Desert Storm soldiers were given pyridostigmine (PYR) tablets against intoxication with acetylcholinesterase (AChE) inhibitors. The employed dose of PYR was expected not to show undesirable cholinergic effects. Nevertheless, peripheral and central side effects were recorded (2). These effects could be the result of stress. First of all, stress itself could be an important factor. It induces prolonged corticosterone secretion that leads to a reduction of hippocampal corticosteroid receptors, which affects other transmitter systems, such as acetylcholine (3). Secondly, stress enhances the passage across the blood-brain barrier (1). In operation Desert Storm nine cases of PYR self-poisoning were encountered. These individuals only suffered from peripheral cholinergic symptoms, whereas no effects on the central nervous system were observed (4). This supports the idea that a combination of many factors including stress plays a role in the appearance of side effects.

In earlier studies pretreatment with physostigmine (PHY) has proved to be very effective against sarin or soman-intoxication (5). Furthermore, PHY was found to be more effective against soman intoxication than PYR in rats (6,7) and in guinea pigs (8). In the course of these studies it was realised that the protective efficacy and the side effects of the pretreatment should also be examined in stressful situations. Therefore, in tn this study the effects of stress on side effects of PHY (0.025 mg/kg/hr) pretreatment and its efficacy against soman intoxication was determined in guinea pigs. To prevent unwanted side effects due to AChE inhibition PHY the pretreatment was combined with the muscarinic receptor antagonist scopolamine (SCO) (0.018 mg/kg/hr) (9). Stress factors were chosen to represent military conditions: emotional stress, physical stress and psychological stress. Most effects can be expected to be centrally mediated effects that may induce changes in different types of behavior. For this reason behavioral read-out systems were used to elucidate the severity of PHY side effects and soman induced incapacitation.

MATERIALS AND METHODS

Animals: Male Dunkin-Hartley albino guinea pigs CrL:(HA)BR (Charles River) with an initial body weight of 400-450 g were used. The animals were kept singly in a cage (Makrolon type IV). The ambient temperature was 20-22°C. Relative humidity was kept over 50%. Food and water were always available. The experiments received prior approval by an independent ethical committee.

Drug solutions: Physostigmine (eserine) and scopolamine bromide were obtained from Sigma (St.Louis, U.S.A.). Atropine Sulphate was obtained from ACF (Amsterdam, The Netherlands). Soman (O-pinacolyl methylphosphonofluoridate) was synthesized at the TNO Prins Maurits Laboratory. The employed dose of PHY (0.025 mg/kg/hr) offers the recommended blood-AChE inhibition of about 35 % (8). SCO (0.018 mg/kg/hr for a period of ten days) leads to a SCO plasma concentration of 45 nM (8). This was comparable with the level found after a single SC injection of 0.1 mg/kg SCO (43 nM). This SCO plasma concentration did not lead to side effects on behavior, and could antagonise PHY induced side effects (9, 10). The vehicle consisted of 20% propylene glycol, 10% ethanol and 70% water (0.05 % v/v glacial acetic acid water). The drugs used were solved in the vehicle. Because the animals gain weight during the pretreatment period, the PHY and SCO concentrations were based on the estimated weight of the animals one week after implantation based on the normal growth curve for guinea pigs in our laboratory.

Implantation of osmotic mini-pump: Alzet® Osmotic Mini-pumps with a constant delivery rate of 0.55 µl/hr (Model 2002, Alza Corp., Palo Alto, USA) were used to deliver either the vehicle or drug solution. The pumps were implanted subcutaneously on the backs of the animals under ketamine/ventracil anaesthesia. The wounds were sutured with woundclips.

Study design: The study was performed in two different treatment groups of animals (n= 8 animals/group). Both groups were pretreated with PHY (0.025 mg/kg/hr) and SCO (0.018 mg/kg/hr) during 11 days, intoxicated with 2x LD50 soman at day 11, and after one minute followed by a post intoxication therapy with atropine sulphate (AS) (0.36 mg/kg im). The dose of soman (applied subcutaneously) used was 24.5 µg/kg (11) (1 LD50). The animals of the non-stress group were handled by the standard procedures and the animals of the stress group were exposed to intermittent variable, unpredictable and uncontrollable stress during 8 weeks, consisting of cold stress (30 min in a refrigerator), psychological stress (footshocks with an interval of 10 min), physical stress (swimming task and running wheel) and emotional stress (placing the animal in an unfamiliar territory for 30 min).

After the animals were trained in a conditioned learning task, the shuttlebox, the baseline values of the different read-out systems were collected. The body weight, plasma cortisol level, blood-AChE activity (for testing the efficacy of the osmotic pumps), shuttlebox, startle response, and exploration activity in the Open Field task were determined. Subsequently two matched subgroups of 8 animals each were formed that showed no significant differences in any of the behavioral tests. The animals from the stress group received the daily stress factors (with exception of the weekends). Once a week the shuttlebox performance, the startle response, and the body weight were determined. Every other week the animals were tested in the Open Field task and bloodsamples were collected for measuring the plasma cortisol level. After six weeks of stress induction, Alzet® osmotic mini-pumps, containing PHY and SCO, were implanted in all animals. This was called day 0. During the pretreatment period the animals from the stress group were still exposed to the daily stress occasions. At day eleven of the continuously administered pretreatment all animals were intoxicated with 2x LD50 soman as described above. Afterwards the osmotic pumps were not removed.

The efficacy of the PHY and SCO pretreatment with or without stress treatment in counteracting soman-induced post intoxication incapacitation was investigated by observing the post intoxication symptoms, such as hyper-salivation,

tremors and convulsions immediately after soman intoxication and by measuring behavioral parameters after the intoxication symptoms became less severe. These tests started 2 hours after soman intoxication (day 11) and were repeated at day 12, 13, 14 and 18. In a parallel experiment the brain AChE inhibition was measured after a single subcutaneous injection of PHY (0.3 mg/kg) or soman (16% and 40% of the LD50) in stressed and non-stressed guinea pigs. Stress was induced two days before injection and immediately before injection of the compound. Day one cold stress (30 min in a refrigerator), day two emotional stress (placing the animal in an unfamiliar territory for 30 min), and day three physical stress (swimming task) was induced. 30 minutes after injection the animals were decapitated for the brain AChE activity.

Behavioral tests: Four different behavioral tests werd employed during this study:

Shuttlebox test: In this test the active avoidance of an unpleasant event upon a conditioned stimulus is used to measure the retrieval of learned behavior. For this test an automated two-way shuttlebox, consisting of two equal compartments of 23x23x23 cm with rounded corners, connected by a photo-cell-guarded gate, is used. The animals have to learn how to avoid a stream of air (about 6 l/s, air tube diameter 1 cm) aimed at their fur within 10 s after presentation of a sound stimulus. During the daily training and test sessions the animals receive 20 trials at an intertrial interval of 20-30 s (random). Only animals that reaches the criterion of 80% or more correct avoidance reactions (CARs) after training, were used in the experiments (10). The number of CARs was used to express the active avoidance performance.

Open Field test: This technique is used to measure parameters of spontaneous behavior, like locomotor activity and exploration in a quantitative way (12). The test consists of a black field of 100 x 100 cm, with 25 cm high enclosing walls. A black grating covers the top of this box. The test room is homogeneously illuminated (100 lux) with a background noise of 52 dB. A videocamera is placed above the OF for registering the movement patterns of the white animal in the black area during a 10 min session. The moving patterns are downloaded into a computer. The following parameters were studied: 1) the distance run, 2) the time spent in the inner field, i.e. a 60x60 cm virtual area in the center of the field, 3) the number of crossings from outer to inner field, and 4) the number of times the rat changes corners. Corners are defined as virtual squares of 20x20 cm in each corner of the field. All parameters are expressed in a cumulative fashion.

Auditory startle response test: In this test the stretching movement of the hindpaws is used to reflect the reaction of the animal on a startle signal (13). For this test the animals are exposed to 20 auditory startle pulses (120 dB, 10 kHz, 20 ms) while standing with their hindpaws on a platform in a vertically mounted PVC-tube (diameter 7 cm, length 16.5 cm). The startle response of 200 ms duration is measured by a transducer connected with the platform, registering the force exerted by the animal upon presentation of the stimulus. An AD converter of an IBM-compatible PC digitised the responses. The area under the curve (AUC), amplitude and latency of the startle response are registered and used to express the motor reaction of the startle reflex.

Determination of cortisol plasma levels: Cortisol plasma levels were determined using a cortisol-kit of ICN. Blood (about 60 µl) obtained from the ear vein of the guinea pig were mixed with heparin and centrifuged for 8 min at 2000 g. The supernatants were stored at -20°C. Within 10 days the cortisol plasma level was determined in a radio immuno assay. Plasma (25µl) was applied in antibodies coated

tubes followed by 0.5 ml of a solution with ^{125} I-cortisol. Thereafter bound and unbound radioactivity was separated and bound radioactivity was counted after which the cortisol concentration could be calculated.

Determination of AChE-activity: Blood samples (5ìl) were obtained from the ear vein of the guinea pig, immediately mixed with 1% saponin (BDH, Poole, UK), frozen in liquid nitrogen and stored at -70 °C. After appropiate dilution, AChE-activity was assessed using a radiometric method. The ACh end-concentration used was 12 ìm; [3H]ACh iodide (NEN, Dreicich, Germany) was diluted to a specific activity of 602 MBq.mmol^{-1}. Ethopropazine (2.5 ìM, St. Louis, Mo, USA) was used as a specific inhibitor of butyrylcholinesterase. Electric eel AChE was used as a reference.
After decapitation the brain (cerebrum) was quickly isolated, weighed and homogenized (1:10, w/v) in 50 mM Tris/HCL (Ph 7.4), 1 M NaCl, 5 mm EDTA and 1% Triton X-100, using a Braun Melsungen Potter-Elvejhem type homogenizer (Melsungen, Germany). Homogenates were centrifuged for 10 min at 3000 g and the supernatants were kept in liquid N_2 until determination of AChE-activity was carried out as mentioned above.

Statistics: For statistical analysis of the behavioral tests an analysis of variance (two-way ANOVA) was used. For the symptomatology after soman intoxication a Fisher exact probability test or an unpaired t-test with Welch's correction was used. In all tests p values < 0.05 were considered significant.

RESULTS

In this study the effect of stress alone, on the appearance of side effects during PHY and SCO pretreatment, and on the efficacy of the pretreatment in preventing the toxic influences of 2x LD50 soman was tested.

Effect of the stress procedure alone:

Plasma cortisol levels were measured every two weeks. Blood samples were collected before stress induction, 15 min and 60 min after stress induction (see Fig. 1). The intermittent variable, unpredictable and uncontrollable stress used in this study, induced a strong increase of the plasma cortisol levels measured after 15 and 60 min after the stress induction (at both time-points $p < 0.05$). There was no difference found between 15 and 60 min after stress induction on the increase of plasma cortisol. During the first three weeks of intermittent variable, unpredictable and uncontrollable stress all animals from the stress group showed a significant higher number of intertrial response (ITR) in the shuttlebox (ITR non-stress group: 2.2 ± 0.3, ITR stress group: 7.6 ± 0.9; $p < 0.05$). However, after the first three weeks of stress induction the stressed animals reacted similar to the non-stress animals in the shuttle box. The activity in the Open Field test, on the other hand, was not affected (see also Fig 2). On the startle response a tendency towards an increase of the startle response (amplitude and AUC) was found (see also Fig 3). This effect was not found to be significant. Stress had no effect on the brain AChE inhibition after a single injection in a parallel group of animals (Fig. 4).

Effect of stress on side effects of PHY and SCO pretreatment:

During the 11 days of continuously applied pretreatment of PHY and SCO no effect was found in all test systems used under the standard conditions. Under the stressful conditions, on the other hand, an increase was found in the Open Field test:

the entries corners and inner field were significantly increased (Fig 2; p=0.028 and p=0.022 resp.).

Effect of stress on the efficacy of PHY and SCO pretreatment against 2x LD50 soman:

All animals of both groups (stress and non-stress) survived the 24 and 48 h criteria after intoxication with 2x LD50 soman. Four days after soman (day 15) one animal of the non-stress group died and one day later (day 16) one animal from the stress group died.

The post-intoxication symptoms observed following soman intoxication are summarised in Table 1. The appearance of symptoms is significantly different between stress versus non-stress (two-way ANOVA, p = 0.004)

TABLE 1. Post-intoxication symptomatology after 2x LD50 soman and AS in continuously PHY and SCO pretreated guinea pigs under standard conditions (non-stressed) or stress-full conditions (stressed) expressed as the % of the total scoring.

non-stress	animal number									
symptoms	5	9	10	12	13	14	20	21	total animal	severity: % of scorings
chewing	8.2	20.0	6.9	20.7	12.9	7.5	0	0	6/8	12.7 ± 2.6
hypersalivation	0	0	0	0	0	0	0	0	0/8	
mild tremors	25	54.3	72.4	10.3	54.8	38.5	23.1	54.5	8/8	41.6 ± 17.4
severe tremor	0	28.7	17.2	24.1	38.7	30.8	0	13.6	6/8	25.5 ± 3.8
convulsions	0	0	0	62.1	12.9	11.5	0	0	3/8	28.8 ± 16.6
dyspnoea	0	0	0	0	0	0	0	0	0/8	
total symptoms	2	3	3	4	4	4	1	2		2.9 ± 0.4

stress	animal number									
symptoms	3	6	8	15	16	17	19	22	total animal	Severity: % of scorings
chewing	12.2	57.9	69.7	53.6	31.4	51.9	28.6	63.6	8/8	16.3 ± 4.0
hypersalivation	0	0	0	0	14.3	0	17.9	0	2/8	16.1 ± 1.8
mild tremors	65.0	52.6	48.5	42.8	22.9	42.9	21.4	50.0	8/8	43.3 ± 5.2
severe tremor	40.8	34.4	18.2	35.7	31.4	29.5	17.9	31.8	8/8	30.0 ± 2.9
convulsions	30.6	0	0	13.9	37.1	11.1	35.7	0	5/8	25.7 ± 5.5
dyspnoea	4.1	0	0	0	40.0	0	3.6	0	3/8	15.9 ± 12.1
total symptoms	5	3	3	4	6	4	6	3		4.3 ± 0.5

Total animal: number of animals in which the symptom was observed.
Total symptoms: total number of different symptoms observed in the animal.
Severity of the symptom expressed as the % of total scoring hits of the animals in which the symptom was observed.

All animals of both groups were able to perform the task in the shuttlebox; they showed a normal ITR activity (compartment changes during the inter-trial interval) after soman intoxication. Their performance was significantly decreased from 96.9 ± 1.3 to 28.8 ± 8.8 in the stress group and from 93.8 ± 2.3 to 38.8 ± 8.9 in the non-stress group. No significant difference was found between the two test groups. 24 hours later this effect was slightly improved, but the effect was still present during one week after soman. The effects on the startle response observed after 2x LD50 soman intoxication are shown in Fig. 3. In both test groups an increase of the startle response was observed. This effect was more persistent in the stress group.

DISCUSSION

In this study the effects of exposure to variable, unpredictable and uncontrollable stress on PHY and SCO pretreatment in a therapeutically relevant dose (14), against 2xLD50 soman was tested. This was done by comparing two test groups: stress versus non-stress. All other factors were kept equal. Three aspects were studied: the effects of the stress procedure on the test systems used, the appearance of side effects during pretreatment, and the protection against post-intoxication incapacitation after intoxication by 2x LD50 soman.

The stress procedure did only affect the behavior in the shuttle box during the first three weeks (six weeks in total). The animals showed an increased inter-trial response (ITR: compartment changes during the inter-trial interval). This could be explained as a higher activity of the stressed animals. However, in the Open Field test no increase of the distance run (a measurement of activity) was observed. Presumably the increase of ITR was due of an increased alertness. In case the effect on learning was tested, these animals would learn faster then the non-stressed animals. This is in accordance with the results obtained by Douma et al. (15). They blocked the mineralocorticoid receptor which displays a high concentration and distinct distribution in the hippocampus, a brain region which is directly involved in the regulation of spatial orientation and learning. This blockade impairs cognitive behavior. However, in our experiment only the effects on learned behavior (memory) was tested. Both groups performed already on their maximum level. This alertness effect was also found on the startle response: a hardly significant increase of the startle reaction was found during the six weeks of stress induction which had disappeared after starting with the PHY and SCO pretreatment.

During the PHY and SCO pretreatment period of 11 days an effect was found in the Open Field test. The performances in the other test systems were not affected. In a previous study the side effects of PHY and SCO were already tested following the same procedures as in the non-stress group. No side effects were observed in the shuttle box, startle response and neurophysiological parameters (9). In former studies guinea pigs in the Open Field test. It was shown that the pretreatment with PHY and SCO also did not affect this task (Fig. 2). Remarkably, the Open Field test seems to be the only task in which side effects were found in the animals of the stress group. The type of effects (increase of "entries corners" and "inner field") corresponded with an increased activity. This activity which was also found (although not to be significant) in the "distance run" parameter is presumably due to stimulation of cholinergic receptors induced by the increase of ACh induced by AChE-inhibition after PHY and due to the increased release after stress (3).

The high protection which was found in this study is in accordance with our previous study. The addition of SCO to the pretreatment or addition of AS as post intoxication therapy enhances the protection synergistically against soman induced lethality (16). Only one animal of the non-stress group died after four days. This animal did not show the worst symptoms after soman (12.9 % convulsions observations of the total scoring hits; the mean value was 28.8 %). Presumably there were other factors that could play a role in the condition of that animal. It acted quite different in the behavior tasks before any treatment: there was a very high "time spent in inner field" in the OF task, a very small reaction on the startle reflex and a very gradually and late training curve in the shuttlebox performance. The animal died after a period of diarrhea. In the stress group also one animal died after a period of dyspnoea five days after soman. This animal exhibited the worst post-intoxication symptoms. If no AS post intoxication therapy or no SCO was added to the pretreatment the protection in a standard laboratory situation, was not 100% (16). In case only PHY was added to the pretreatment all animals died within 24 hours. Therefore, we have chosen for the complete treatment (PHY, SCO and AS). It could be that the scenario without SCO or AS would show a bigger difference on lethality between stress and non-stress.

That there is a difference between stress and non-stress animals can be concluded from the observations of the post-intoxication symptomatology. All stressed animals showed severe tremors and five of them convulsions instead of 3 in the non-stress group. Dyspnoea was only found in the stressed animals. In a former study effects like dyspnoea were only found in animals without a post-intoxication therapy

with AS (16). Therefore, these effects in a stressful situation could be the results of a combination of an increase of ACh release and AChE-inhibition or the system become more susceptible to ACh. Indeed after inescapable stress the ACh release was significant increased in the hippocampus and prefrontal cortex investigated with microdialysis technique (3), and the maximal number of muscarinic receptors (Bmax) in several brain areas such as the cortical layers, the CA1 field of the hippocampus and caudate-putamen was significantly increased (17). Furthermore, it could be that the blood-brain barrier permeability was increased through which PHY and soman could easier enter into the brain. It seems that already short-lasting immobilization stress shows this effect (18). Even when it is corrected for the decreased cerebral blood flow, a higher penetration into the CNS was found (19). However, no differences were found in brain AChE inhibition between stressed and non-stressed guinea pigs (Fig. 4).

The animals from the non-stress group showed the best protection against the soman induced intoxication incapacitation. After soman a high increase of the startle amplitude and AUC were found in both groups. In the stress group this effect is more persistent: an increase or a tendency towards an increase of the startle response was still found after one week.

In a previous study it was clarified that direct effects on nicotinergic receptors were involved in the effects on the startle amplitude instead of AChE inhibition (20). It is known that soman has besides its AChE-inhibiting effect, like PHY (21, 22), also direct effects on nicotinergic receptors (23). Furthermore, effects on the release of 5-HT after stress may play a role on the startle reflex (13). Serotonine also seems to play a role in the increased permeability of the blood-brain barrier under stress conditions (24).

From the present experiments it can be concluded that stress indeed affects the efficacy of the pretreatment. This can be due to the changes in the blood-brain barrier and other cholinergic effects, such as the increased release of ACh and up-regulation of muscarinic receptors. Although PHY already easily penetrate into the brain because of its structure, stress also influences the appearance of unwanted side effects of the pretreatment. This effect would be worse in case a drug is used that normally hardly enters the brain, especially when this drug is only tested in a standard laboratory situation.

In conclusion, in a more realistic situation stress seems to interfere with the pretreatment against soman intoxication. Stress evokes the appearance of side effects and decreases protection against soman intoxication. Therefore, other risk factors should be incorporated in the experimentation set-up and not be ruled out during research in the area of treatment by medication.

REFERENCES

1 Friedman, A et al. (1996) Nature Med. 2(12): 1382-1387
2 Keeler, J.R. et al (1991) JAMA 266(5): 693-698
3 Mark, G.P. et al. (1996) Neuroscience 74(3):767-74
4 Almog, S et al. (1991) Isr. J. Med. Sci. 27:659-722.
5 Leadbeater, L. et al. (1985) Fund. Appl. Toxicol. 5: S225-S231.
6 Harris, L.W. et al. (1984) Drug Chem. Toxicol. 7: 605-624.
7 Solana, R.P. et al. (1990) Fundam. Appl. Toxicol. 15: 814-819.
8 Philippens, I.H.C.H.M. et al. (1998) Pharmacol. Biochem. Behav. 59(4): 1061-1067.
9 Philippens, I.H.C.H.M. et al. (1996) Pharmacol. Biochem. Behav. 55(1): 99-105.
10 Philippens, I.H.C.H.M. et al. (1992) Pharmacol. Biochem. Behav. 42: 285-289.
11 Gordon, J.J.and Leadbeater, L. (1977) Toxicol. Appl. Pharmacol. 40:109-114.

12 Tanger, H.J. et al. (1978) Pharmacol Biochem Behav. 9(4):555-562.
13 Davis, M. et al. (1982) J. Neurosci. 2: 791-805.
14 Gall, D. (1981) Fundam. Appl. Toxicol. 1:214-216.
15 Douma, BR et al. (1998) Psychoneuroendocrinology 23(1):33-44.
16 Philippens, I.H.C.H.M. et al. (2000) Pharmacol Biochem Behav. 65(1):175-82.
17 Gonzalez, A.M. and Pazos, A. (1992) Eur J Pharmacol 223(1):25-31.
18 Skultetyova, I. et al. (1998) Brain Res Bull. 45(2):175-183.
19 Dvorska, I. et al. (1992) Endocr Regul. 26(2):77-82.
20 Philippens, I.H.C.H.M. et al. (1997) Pharmacol. Biochem. Behav. 58: 909-913.
21 Albuquerque, E.X. et al. (1984) Fundam. Appl. Toxicol. 4: 27-33.
22 Sherby, S. M. et al. (1984) Mol. Pharmacol. 27: 343-348.
23 Bakry, N. M. S. et al. (1988) J. Biochem. Toxicol. 3: 235-259.
24 Sharma, H.S. and Dey, P.K. (1981) Indian J Physiol Pharmacol.(2):111-22.

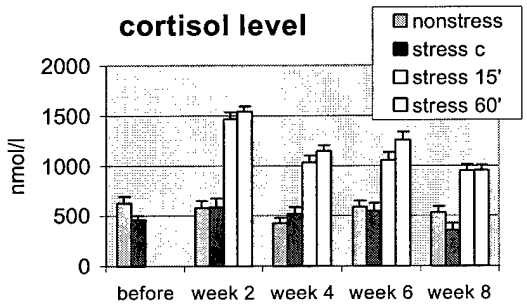

Figure 1. Plasma cortisol levels measured in stressed guinea pigs and in non-stressed guinea pigs after 2, 4, 6, and 8 weeks of stress induction. During week 7 and 8 all animals were also pretreated with PHY and SCO. The cortisol values of the stressed animals were measured before (stress c), 15 min, and 60 min after stress induction. All values after stress induction were significantly increased (ANOVA and Newman-Keuls post-hoc test, $p < 0.05$)..

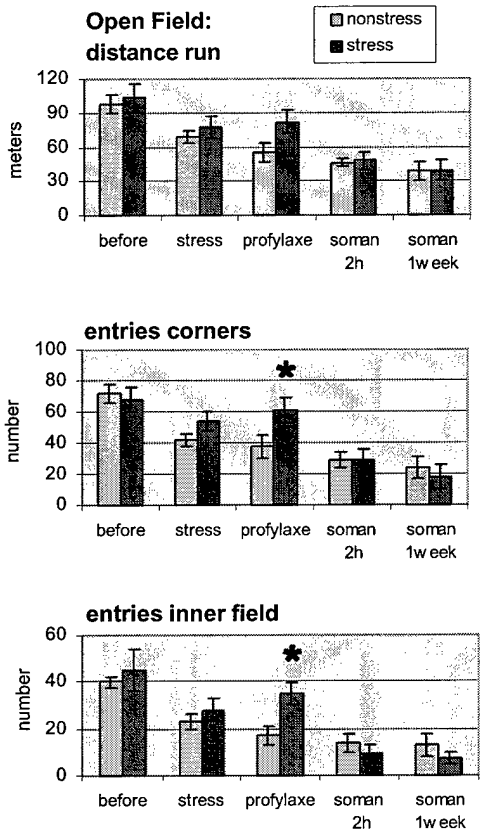

Figure 2. Performance in the OF measured in two different groups (n=8/group), non-stress or stress, before stress induction, after 6 weeks of stress induction (stress group), after 10 days of PHY and SCO pretreatment, two hours and 1 week after 2xLD50 soman. The distance run was expressed as the cumulative meters walked during the 10 min session (mean ± SEM). The entries corners or inner field were expressed as the cumulative number of entries in these virtual areas during the 10 min session (mean ± SEM). * Significantly different from non-stress.

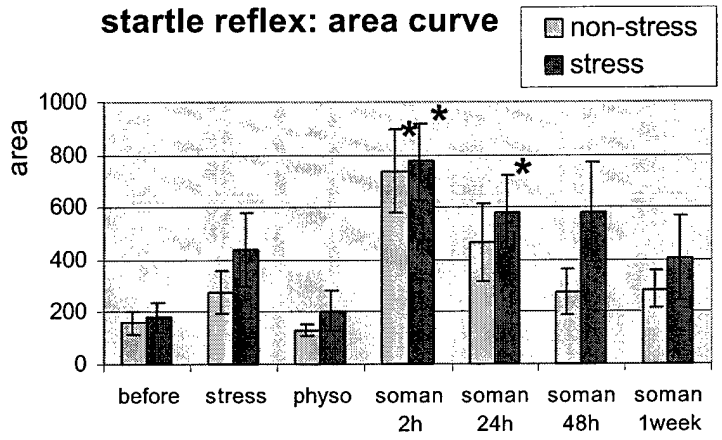

Figure 3. Area of the curve of the startle response of 200 ms duration (startle pulse: 20 ms, 120 dB, 10 kHz). Registration of the effects before, after 6 weeks of stress induction, after 10 days of PHY/SCO pretreatment and after soman intoxication (2, 24, 48 h and 1 week) in non stressed and stress aguinea pigs (n=8/group, mean ± SEM). * Significantly different from baseline value (before).

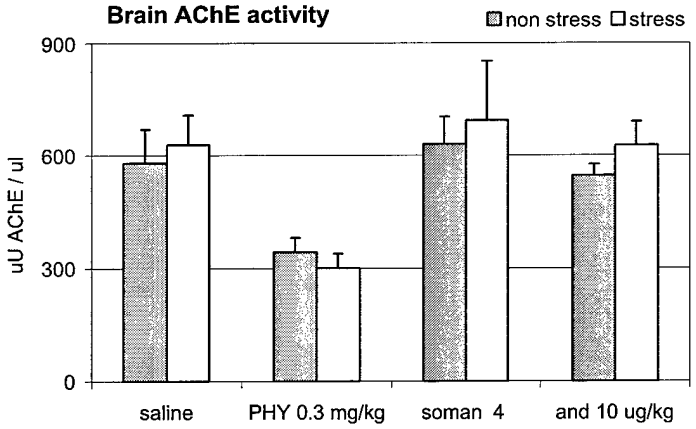

Figure 4. Brain AChE activity (in uU/l) measured in stressed guinea pigs and in non-stressed guinea pigs after 3 days of stress induction. The brain AChE activity was measured on day three, 30 minutes after a subcutaneous injection of saline (n=5) PHY (0.3 mg/kg, n=8), soman (4 ug/kg, n=5 or 10 ug/kg, n=4).

FACTORS INFLUENCING THE TRANSPORT OF BIOLOGICAL AEROSOL THROUGH THE ATMOSPHERE: AND THEIR INJECTION INTO IT

John Latham (1) & CH Wick (2)

(1) 601 East Street, Boulder, Colorado 80302-9771
(2) ECBC, Aberdeen Proving Ground, Maryland 21010-5423

ABSTRACT

The capacity to predict accurately the transport and deposition of biological aerosol introduced into the atmosphere is clearly an urgent military requirement.

Existing transport models do not adequately take account of some processes which can exercise a profound influence on aerosol transport. These include: dry deposition; wet deposition; cloud processing of aerosol; the effects of topography on aerosol deposition; and the (often profound) influence of naturally occurring electrostatic forces on the agglomeration and scavenging of aerosol particles.

Our objectives are to formulate reliable, quantitative descriptions of these processes which act to modify aerosol transport: so that these processes can then be adequately incorporated into models of the transport of biological aerosol through the atmosphere on all relevant scales.

The bursting of bubbles at the surface of the oceans, lakes and other stretches of water can cause the injection of massive quantities of biological aerosol into the atmosphere. The Earth's electric field can facilitate their redistribution and longevity in the atmosphere.

Our paper describes work conducted to date on these topics, together with future plans.

TRANSPORT OF BIOLOGICAL AEROSOL THROUGH THE ATMOSPHERE

It is crucially important, from a military standpoint, to identify, understand and be able to quantify the gamut of processes which act to modify the transport of biological aerosol through the atmosphere, over a wide range of spatial scales.

The dispersal and eventual deposition of aerosol introduced into or naturally resident in the atmosphere is a function of many parameters, such as the prevailing meteorological conditions, and the physical and chemical characteristics of the aerosol.

Existing transport models, designed to predict the movement of aerosol particles for a variety of meteorological scenarios, do not adequately take account of some other processes which can exercise a profound influence on aerosol transport. These include: dry deposition (deposition to ground in the absence of cloud); wet deposition (where the aerosol are scavenged by raindrops and thereby brought to ground); cloud processing of aerosol by cloud droplets (where the history of the droplets influences that of the aerosol particles they have captured); the effects of topography on aerosol deposition (where the shape of the terrain modifies crucial

parameters such as turbulence, cloudiness etc); and the effects of naturally occurring electrostatic forces (where the efficiency with which aerosol particles agglomerate or are scavenged by raindrops can be profoundly enhanced).

We believe that unless and until the above-mentioned processes are quantitatively and accurately incorporated into transport models, these models cannot be trusted to provide reliable estimates of aerosol transport, and may in some circumstances be catastrophically wrong. Our program of work is designed to help remedy these deficiencies.

Our objectives are to engage in a program of modelling and examination of exisiting data sets in order to formulate reliable, quantitative descriptions of processes (outlined in the preceding section) which act to modify aerosol transport: so that these processes can then be adequately incorporated into models of the transport of biological aerosol through the atmosphere on all relevant scales.

These processes are:-

(1) Wet deposition of aerosol.
(2) Dry deposition of aerosol.
(3) Cloud processing of aerosol by liquid hydrometeors.
(4) The effects of topography on aerosol deposition.
(5) Influence of electrostatic forces on aerosol agglomeration.
(6) Influence of electrostatic forces on scavenging of aerosol by raindrops.

Our work, together with studies by other investigators, has demonstrated that each of the above six processes can have a significant (sometimes predominant) influence on aerosol transport in natural conditions.

Data on aerosol of all sizes measured will be examined. This includes the size-range 10 to 250 nanometres, of particular military interest. Since we are concerned with physical processes which act to modify aerosol transport, data obtained from our field studies on non-biological aerosol (with concomitant computations) will be equally relevant to biological aerosol.

NATURAL INJECTION OF BIOLOGICAL AEROSOL INTO THE ATMOSPHERE

Violent disruption of a liquid surface - such as occurs when seawater droplets are created by the breaking of waves or the bursting of the thinning, roughly hemispherical bubble-films created when air bubbles rise to the ocean surface: or when air bubbles burst at the surface of lakes, ponds and other stretches of water - is accompanied by significant electric charging of the huge numbers of droplets so produced. This process is an extremely efficient mechanisim of injecting biological aerosol into the atmosphere. Preliminary laboratory experiments indicate that the characteristic charges (positive & negative) acquired by the typically hundreds of droplets in the size-range 0.1 to several micrometers created when a bubble bursts are sufficiently large that the electrostatic forces on them in the Earth's fine-weather field at the ocean surface will greatly exceed the gravitational force to which they are subjected (i.e. $qE>>mg$). Thus survival and

upward motion through the atmosphere of the negatively charged aerosol (roughly half the total) will be facilitated electrostatically. If such sign selectivity occurs over natural liquid surfaces to the degree suggested by our first crude laboratory studies the preferential ascent of negatively charged biological aerosol should create - in conditions of medium and strong wind-speed - readily measurable perturbations in the Earth's electric field, the magnitudes of which should allow estimates to be made of the upfluxes of the aerosol. We propose to conduct a series of laboratory experiments designed to examine this possibility in more detail.

This work reinforces earlier indications that electrostatic forces can be useful practically in protecting personnel and structures from biological aerosol.

PERFORMANCE OF THE ACWA PILOT SCALE IMMOBILIZED CELL BIOREACTOR IN DEGRADATION OF HD AND TETRYTOL PAYLOADS OF THE M60 CHEMICAL ROUND

Mark A. Guelta, Nancy A. Chester, Carl W. Kurnas, Mark V. Haley
U.S. Army Edgewood Chemical and Biological Center, APG MD 21010

F. Stephen Lupton, Mark Koch
Honeywell International, Des Plaines IL 60017

In 1996, public laws 104-208, 105-261, and 106-79 established and expanded the Assembled Chemical Weapons Assessment (ACWA) Program. To address public concerns over the safe destruction of the U.S. chemical weapon stockpile; the ACWA program was tasked to identify two or more viable alternative technologies to the "baseline" destruction method of incineration. Neutralization followed by biodegradation was one technology identified as having potential.

Guelta and DeFrank[1] conducted preliminary laboratory studies using 1-liter Immobilized Cell Bioreactors (ICB) to degrade hydrolyzed agents. These studies demonstrated the effectiveness of the ICB system to degrade hydrolyzed HD agent feed. In two follow-on studies, each conducted at Edgewood Chemical and Biological Command (ECBC), Edgewood MD, a scaled-up 1000-gallon pilot ICB system was operated for three and four months respectively. Over the course of these tests the ICB system degraded 61,274 lbs of 3.8% HD hydrolysis created from the HD stockpile stored at APG. Also degraded was approximately 2320 lbs of hydrolyzed tetrytol produced at the Pantex plant, Amarillo, TX. The neutralization/biodegradation process achieved a 99.9999% overall destruction removal efficiency (DRE) for HD agent, Tetrytol and schedule-2 compounds. This paper describes the ICB system and overall process employed for the ACWA Demonstration/Engineering Design Studies.

INTRODUCTION

Water Hydrolysis of Energetic and Agent Technology (WHEAT) is one alternative process to incineration proposed for complete destruction of warfare munitions containing energetics, propellants and mustard or nerve agents. The WHEAT technologies will be used to demonstrate destruction of materials representative of the M60, 105 mm projectile (HD/Tetrytol). The WHEAT technologies include water jet for cutting and boring operations to remove components from metal projectiles, a hydrolyzation step to detoxify and make biologically available projectile chemical components, and a high temperature steam process for 5X treatment of metal parts and other solid wastes. A more complete description of the entire study is available in the ACWA Demonstration Study Plan[2]. Viable alternatives to incineration must demonstrate a total solution to all aspects of the assembled chemical weapon destruction process.

The development of the ICB pilot scale design is based on a history of past benchtop/laboratory-scale studies with hydrolyzed HD. The use of Sequencing Batch Reactors (SBR) has demonstrated the ability to successfully degrade hydrolyzed HD[3] and was subsequently selected as the process-of-choice

for chemical destruction of HD in ton containers at the Edgewood Chemical Biological Center. Further research in the area of neutralization/biodegradation by Guelta and DeFrank[1] of ECBC, led to success in the degradation of HD hydrolysate and VX nerve agent by ICBs thereby laying the groundwork for expansion of the process to include the burster fills found in mustard agent projectiles. This report describes the demonstration run of a pilot-scale ICB system and its ability to degrade a feedstock of chemical agent (hydrolyzed HD as the sole carbon source for the microbial culture) mixed with energetic (Tetrytol) in proportions that simulate the contents of the M60 projectile.

METHODS AND MATERIALS

HD Hydrolysate is produced by adding HD to heated water and then agitating until the HD is degraded to thiodiglycol, plus a few breakdown products. This process is described by Harvey et al[3]. The primary product of the hydrolysis of HD is thiodiglycol (TDG). The NaOH required for the neutralization of the acids generated by the hydrolysis can be added either before or after the reaction. Studies have shown that a more complete conversion to TDG is achieved when the NaOH is added after the reaction has reached completion (Harvey et al.[3]). The reaction (without intermediates or by-products) is summarized below.

$$Cl\text{-}CH_2CH_2\text{-}S\text{-}CH_2CH_2\text{-}Cl + 2H_2O + 2NaOH \longrightarrow HO\text{-}CH_2CH_2\text{-}S\text{-}CH_2CH_2\text{-}OH + 2NaCl + 2H_2O$$

HD TDG

The HD hydrolysate used in these studies was prepared at an initial HD concentration of 3.8%.

In 1999 ACWA[4] funded demonstration testing of the ICB system as part of the larger ACWA program demonstration/validation study[4]. The ICB system was scaled-up to a 1000-gallon reactor housed in two 40-ft transportation containers. The HD/Tetrytol ICB system, located at ECBC, was operated by U.S. Army researchers for a 6-week validation period.

The ACWA demonstration program designated eight specific goals and objectives for the WHEAT HD biotreatment and associated systems. From the ACWA Program Study Plan, these objectives are listed below:

1. Validate the ability of the unit operation to eliminate schedule 2 compounds (TDG) present in the HD/Tetrytol hydrolysate feed.
2. Confirm the absence of HD agent in the unit operation's effluents.
3. Validate the ability of the agent hydrolysis process and the ICB, flocculation reactor, and clarifier unit operations to achieve a DRE of 99.9999% for HD.
4. Validate the ability of the energetic hydrolysis process and the ICB, flocculation reactor, and clarifier unit operations to achieve a destruction and removal efficiency (DRE) of 99.999% for Tetrytol.
5. Develop mass loading and kinetic data that can be used for scale-up of the ICB flocculation reactor, and clarifier unit operations.
6. Validate the ability of the catalytic oxidizer to eliminate chemical agents and schedule 2 compounds from the ICB process gas stream.
7. Determine the potential impact of operating conditions on the fouling and plugging of the catalytic reactor.
8. Characterize gas, liquid and solid process streams from the ICB, flocculation reactor, clarifier, and catalytic oxidizer unit operations for selected chemical constituents and physical parameters, and the presence/absence of hazardous, toxic agent and schedule 2 compounds.

The principle components of the HD/Tetrytol bioreactor system were housed in two 40- by 8-foot transportation containers (Figures 1 & 2). Major components include a 200-gallon feed tank for mixing HD and Tetrytol hydrolysates, a 200-gallon feed tank, a three-chambered 1000-gallon steel ICB tank, a 100-gallon flocculation reactor, a 300-gallon clarifier, and the water recycle system. The water recycle system consisted of activated carbon, microfiltration and reverse osmosis filter cartridges, and a 1000-gallon recycle water storage tank. A catalytic oxidation system and lime scrubber treated the air exhausted from the ICB. The pilot-scale ICB was designed to process 200 gallons of feedstock per day for a hydraulic retention time (HRT) of five days. Daily feedings of 200 gallons were to contain 40 gallons of 3.8% HD hydrolysate and 1.9 gallons of Tetrytol hydrolysate and the balance with recycled water. Sixty-five percent of the 200-gallon per day effluent was to be recycled into the system after sludge removal and desalination.

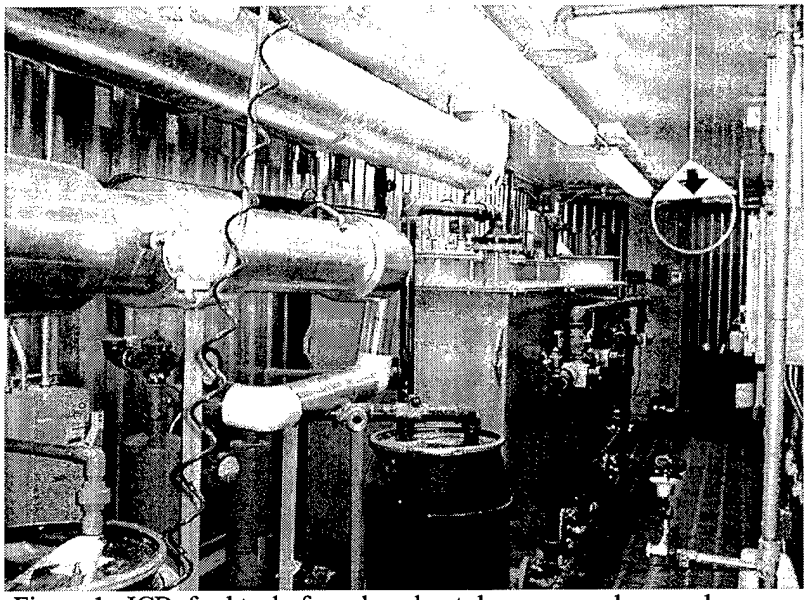

Figure 1. ICB, feed tank, foam knockout drum, sump drum and CATOX system in trailer one.

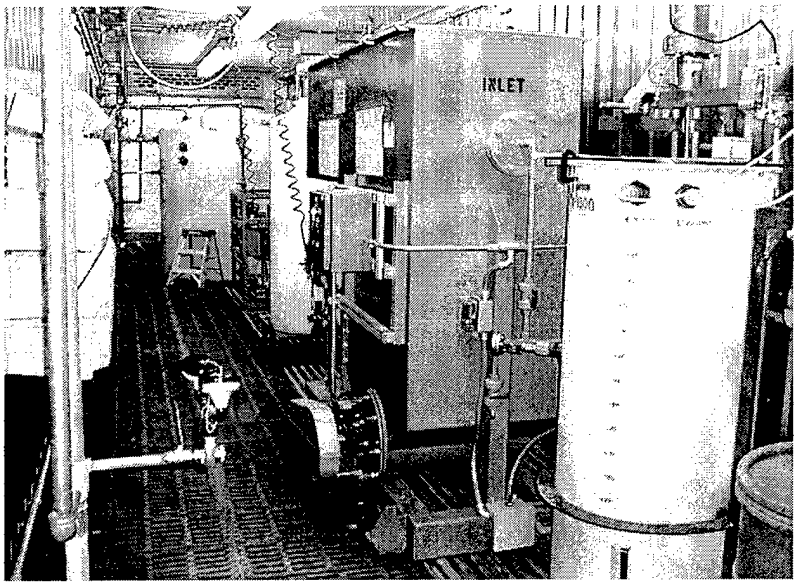

Figure 2. Fenton's reactor, clarifier, RO system, dirty water tank and recycle water storage tank in trailer two.

The ICB was initially filled with tap water for system checks and verification. Upon startup of the system[2] enough water was removed to allow addition of 55 gallons of a bacterial innoculum cultured by Honeywell[5]. During the run, additional sludge collected from Back River publicly owned treatment works (POTW) was added to the ICB. The system was initially started in a batch mode to allow bacterial growth and adaptation to the feed stream. The system was allowed a 32-day run-up period before starting the 40-day validation run at the required feed rate of 40 gal HD hydrolysate and 1.9 gal Tetrytol hydrolysate per day.

RESULTS

The ICB HD hydrolysate produced for the ICB feed was generated at the ECBC chemical transfer facility. The principle hydrolysis/breakdown product from this procedure is thiodiglycol, which is the sole carbon source for the ICB bacteria. Forty-seven drums of HD hydrolysate were used during the demonstration test. These drums were analyzed for HD and its breakdown products. These data are summarized in Table 1.

TABLE 1. Summary of data for 3.8% HD hydrolysate.

Analyte	Mean (mg/L)	STD-D
pH	8.25	4.2
Thiodiglycol	24060	1324.6
Thiodiglycol sulfoxide	99.19	66.2
1,4-dithane	113.5	46.3
1,2-bis(2-hydroxyethylthio) ethane	586.9	296.7
(2-hydroxylethylthio) ethane thiodiglycol	286.7	178.9
1,2-bis(2-hydroxyethylthio)ethyl ether	703.9	235.2
1,4-dithane-1-(2-chloroethane)	76.79	33.84
Total Organic Carbon	10823	172.9

***-pH** in standard units **(SU)**

The pilot ICB feed (S1), ICB chamber 1(S3), and ICB out-fall (S5) chemical oxygen demand (COD) was measured daily as a near real-time indicator of performance (Figure 3). A COD removal efficiency of 90% is considered a good indicator of complete utilization of the hydrolysate as food when measured during process monitoring. However, the true performance indicator is the measure of TDG removal. The feed rate of 40 gallons/day of 3.8% HD hydrolysate was stopped on day 40 after the reactor COD levels rose and TDG was detected in the ICB out-fall. The ICB was placed in batch mode until COD levels recovered. This set back was attributed to insufficient pH control and unseasonably cold weather in the Maryland area, and in the test bay that kept the ICB temperatures between 55 and 65°F during the start-up period.

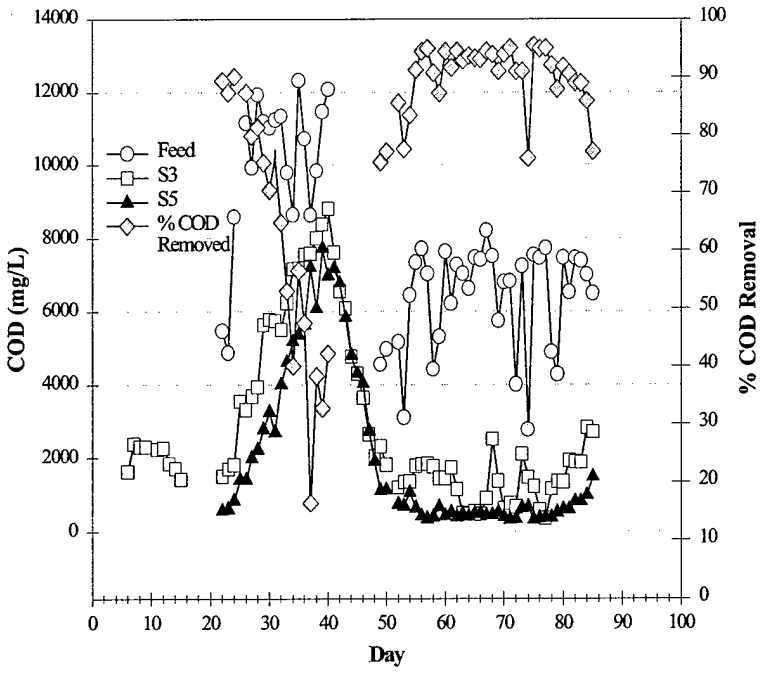

Figure 3. COD values for S1, S3, S5 and COD removal efficiency at location S5

The biodegradation of TDG produces an acidic by-product. PH for this system was controlled by a single caustic addition loop. The insufficient pH control capacity kept the pH in ICB chamber 1 between 5.0-6.5 for the first 40 days of operation. These two factors slowed biomass growth and contributed to poor initial performance. To remedy this, an additional 55 gallons of municipal sludge was added to the reactor, additional pH control capacity was added with a second pH control loop, sodium bicarbonate was added to the feed, and radiant heaters were placed in trailer 1 to keep the ICB temperature above 70°F.

To speed time to validation testing, the feeding regimen was lessened to 26.6 gal/day HD hydrolysate and 1 gal/day tetrytol hydrolysate. After recovery, the ICB was placed in continuous feed mode. Reduction in COD values at the ICB out-fall were 90% or greater for the rest of the study. PH and ICB temperatures were also in acceptable ranges for the remainder of the test.

After restart of testing to include lowered feed rate, HD and HD-breakdown products were measured in the feed (S1), chamber 1 (S3) and the ICB out-fall (S5). Those data are summarized in Table 2. At no time was HD ever detected in the hydrolysate, feed, or any effluents of the ICB.

TABLE 2. Schedule-2 and Breakdown Products by Week and Sample Location

Sample Date	Analyte	S1 (mg/L)	S3 (mg/L)	S5 (mg/L)
March 24	1,4-Dithane	15.6	0.7	0.4
	Thiodiglycol	3840	825	ND
	1,4-Thioxane	24.4	4.9	3.2
March 30	1,4-Dithane	17.98	5.22	0.52
	Thiodiglycol	3510	55.4	ND
	1,4-Thioxane	13.0	4.31	3.28
April 7	1,4-Dithane	14.05	2.88	ND
	Thiodiglycol	3310	ND	ND
	1,4-Thioxane	28.5	6.52	1.15
April 14	1,4-Dithane	11.1	1.85	ND
	Thiodiglycol	3257	ND	ND
	1,4-Thioxane	1	1	ND
April 21	1,4-Dithane	8.9	9.43	9.45
	Thiodiglycol	3241	186.3	ND
	1,4-Thioxane	173.7	6.21	6.27
April 28	1,4-Dithane	10.06	9.83	5.05
	Thiodiglycol	3836	12.4	ND
	1,4-Thioxane	<1	6.96	6.11

During validation testing, air exhausted from the ICB was treated with a catalytic oxidation (CATOX) system. Exhaust gases were sampled on the same dates as liquid effluents. No HD, Tetrytol or schedule 2 compounds were detected during the test period. Exhaust gas flow rates and temperature through the CATOX was monitored daily. No plugging of the CATOX or decreases in CATOX operating temperature were observed. Daily flow through the system was 55-60 CFM; CATOX operating temperature was 775-800°F.

It is anticipated that liquid effluents may require disposal as hazardous waste. The Toxicity Characteristic Leaching Procedure (TCLP) analysis was performed on liquid effluent samples. In Maryland, any waste originating from any chemical agent is considered hazardous and must therefore be disposed of in a hazardous waste disposal facility. Generally, effluents from biodegradation of hydrolyzed HD pass criterion established as non-hazardous waste, except for some special state codes like the Maryland code "MD-02" for waste originating from chemical agent.

The eventual site of any full-scale facility will come under scrutiny of that state's effluent discharge regulations and other requirements for an operating permit. In the event an operating permit may be required at a later date, samples of all effluents and exhaust streams were analyzed to attempt to completely characterize all outputs from the ICB system. These analyses included: Total Organic Carbon, Metals, Volatile Organic Chemicals, Semi-volatile Organic Chemicals, Cations, Dioxins, Furans, Mercury, Anions, Phosphate, Sulfate, Nitrates, Chloride, Energetics, Sulfides, Aldehydes, Ketones, Formaldehyde, Hydrogen sulfide, and Hydrogen cyanide. Waste collected in 275-gal waste tanks were analyzed using TCLP criteria. The results indicated waste generated was below Maryland state TCLP

regulatory limits. Due to the page limit of this paper, those results are not listed. These data are available from the coordinating contractor, Arthur D. Little, Inc.[6], with the permission of PM ACWA[4].

CONCLUSION

The basic ability of microorganisms cultured from activated sludge to degrade HD hydrolysate under laboratory and bench scale studies were again tested in the 1000-gallon pilot scale ICB system. While laboratory and bench scale studies of this system worked well, it can't be automatically assumed that if scaled up properly any pilot-scale biological system will work as efficiently as its laboratory predecessor. While this ability has been previously demonstrated in SBRs using HD hydrolysate as feedstock, the addition of energetic materials and the proposed utility of an ICB system necessitated a demonstration study of this type.

In addition to the challenge of scaling up a biological system, what would be the effect of the energetic hydrolysate? The primary goal of the WHEAT system is to provide a total alternative solution to incineration for destroying and detoxifying the combined waste from assembled chemical weapons systems. The hydrolysis step of the WHEAT process eliminated the primary components of the energetic materials, TNT and RDX. It was expected that the energetic wouldn't undergo any further measurable degradation and would simply pass through the system. For the most part that appears to have been the case. Most of the energetics and breakdown products were below detectable limits in the feed and all effluent samples.

Based on the ACWA program's eight designated specific goals and objectives for the WHEAT and biotreatment systems, we conclude the following:

1. The hydrolysis process eliminated HD and Tetrytol in the ICB feed stream to below detectable limits.
2. Data show no HD/Tetrytol was ever detected in the ICB feed, intermediate process or effluent streams.
3. Data show that the WHEAT system and ICB successfully achieved an Destruction Removal Efficiency of 99.999% for HD.
4. Data show that the WHEAT system and ICB successfully achieved an Destruction Removal Efficiency of 99.999% for Tetrytol.
5. Mass loading data were developed for scale-up. However[2] additional data are required and will be developed in a follow-on engineering design study (EDS).
6. Data show that the catalytic treater allowed no release of agent or schedule 2 compounds.
7. Data show no plugging or fouling of the catalytic treater from the ICB operation.
8. Although not completely reported here, all effluents and waste streams were characterized. No hazardous or toxic agents or schedule two compounds were detected.

While the ICB validation study was successful[2] improvements to the system should be made, particularly within the water recycle process. The RO system seems inappropriate for the amount of salt produced by the system. Plugging of the RO membrane and filters with unsettled particulate presented an intermittent problem. Perhaps an alternative method of effluent recycling may be employed. The feed schedule did not reach the desired contribution of 40 gal/day HD hydrolysate, perhaps partially due to some less than optimum bacterial growth conditions and time constraints placed on the study.

During the summer of 2000 ACWA[4] funded a follow-on Engineering Design Study (EDS). Changes were made to the ICB system to address problems encountered during the demonstration study. Three control loops were installed to improve pH control in the ICB, one for each ICB chamber. To improve effluent recycle ability the RO unit was replaced with an evaporator/condenser system serviced by a 25-

ton chiller. This system produced recycle water that may have improved the ICB culture health in comparison to the water from the RO system. The HD hydrolysate feed regimen of the EDS was also increased over the 4-month test to 50-gal/200-gallons of feed/day. Feed also included water collected from the continuous steam treater (CST) testing of metal parts and dunnage decontamination. During this successful test, no schedule-2 or HD breakdown products were detected in the ICB liquid effluent or exhaust gases. Water recycle efficiency was greatly improved with liquid waste generation dropping from 1:157 (lbs HD/lbs waste) to 1:27. Parsons/Honeywell[2] incorporated the data collected into a 35% design package by for their total solution for the Pueblo Chemical Depot full-scale facility.

LITERATURE CITED

1. Guelta, M.A., and DeFrank, J.J., Performance of Immobilized Cell Bioreactors For Treatment Of HD And VX Hydrolysates, ERDEC-TR-497, U.S. Army Edgewood Research Development and Engineering Center, Aberdeen Proving Ground, MD, May 1998, UNCLASSIFIED Report.

2. Parsons Infrastructure, Assembled Chemical Weapons Assessment Program, Demonstration Study Plan, Parsons Infrastructure & Technology Group, Inc., 1955 Jadwin Avenue, Richland Washington, 99352 1998.

3. Harvey, S. P., Szafraniec, L.L., Beaudry, W.T., Early, J. T., and Irvine, R.L., Neutralization and Biodegradation of Sulfur Mustard, ERDEC-TR-388, U.S. Army Edgewood Research, Development and Engineering Center, Aberdeen Proving Ground, MD, February 1997, UNCLASSIFIED Report (AD A322 638).

4. Program Manager Assembled Chemical Weapons Assessment, ATTN: AMSSB-PM-ACWA, 5183 Blackhawk Rd. Aberdeen Proving Ground, MD. 21010-5424

5. Honeywell International, Advanced Technologies Environmental Systems and Services. 50 East Algonquin RD Box 5016, Des Plaines Il. 60017-5016.

6. Arthur D. Little, Inc, Environmental Science and Technology, Acorn Park, Cambridge Mass. 02140-2390.

FURTHERING THE ENZYMATIC DESTRUCTION OF NERVE AGENTS

Ilya Elashvili and Joseph J. DeFrank

U.S. Army Edgewood Chemical Biological Center, Aberdeen Proving Ground, MD 21010-5424
Tel: 410-436-2580 Fax: 410-436-8026 E-mail: ilya.elashvili@sbccom.apgea.army.mil

ABSTRACT

This study was conducted to investigate the biodegradation potential of neutralized organophosphorus nerve agents: O-ethyl-S-(2-diisopropyl-aminoethyl) methylphosphonothioate (VX), Sarin (GB), Soman (GD), and O-cyclohexyl methylphosphonofluoridate (GF). Removing labile leaving groups from these compounds can be accomplished chemically (e.g. alkali) or enzymatically (by a variety of hydrolases) resulting in stable ionic methylphosphonate esters. Glyphosate utilizing *Burkholderia caryophilli* PG2982 was found to use for growth (as the sole phosphorus sources) low concentrations of ethyl-, isopropyl-, and pinacolyl methylphosphonates (EMPn, IMPn, and PMPn - alkali treatment products of VX, GB, and GD, respectively). Partially purified enzyme was obtained from crude extracts of the *B. caryophilli* PG2982 strain and tested for esterase activity against these phosphonate esters in addition to isobutyl- and cyclohexyl methylphosphonates (iBMPn and CMPn - alkali treatment products of Russian-VX and GF, respectively). Derivatized substrates and products were monitored by GC-FPD. Esterase activities were observed in the order: iBMPn>CMPn>EMPn>IMPn>PMPn. These results demonstrate the potential use of *B. caryophilli* derived enzyme(s) in furthering the destruction of these neurotoxic chemical compounds. This could be an important factor for the US and other nations in attempting to meet the requirements of the 1993 Chemical Weapons Convention agreement to destroy all chemical warfare agents within ten years of ratification (April 2007 for the US).

INTRODUCTION

Neurotoxic chemical warfare (CW) G-type agents: GB, GD, and GF and V-type agents: VX and O-isobutyl S-(2-diethyl-aminoethyl) methylphosphonothioate (Russian-VX or R-VX) are in the stockpiles of the U.S. and former Soviet Union (Chapalamadugu, 1992; Fedorov, 1994; Marrs, 1996; Somani, 1992). The U.S.A. signed the Chemical Weapons Convention agreement (UN, 1992) in 1993 and ratified it on 25 April 1997 that requires the destruction of all CW agents within ten years of ratification. Current chemical decontaminants contain corrosives (e.g. alkali) (Yang, 1992) and incineration has met with community opposition. The U.S. Army is pursuing alternative technologies, such as enzymatic decontamination, that are safe and environmentally friendly (DeFrank, 1993). Degradation of G- and V-type agents can be accomplished using phosphoric triester hydrolase enzymes (e.g. organophosphorus hydrolase [OPH] [Dumas, 1989, 1990] and organophosphorus acid anhydrolase [OPAA] [Cheng, 1993; DeFrank, 1991; Elashvili, 1999]), which - similar to alkali - remove labile leaving moieties resulting in stable ionic methylphosphonate ester products. This enzymatic degradation process for the five selected

Scheme 1. G- and V-agent hydrolysis by OPH or OPAA.

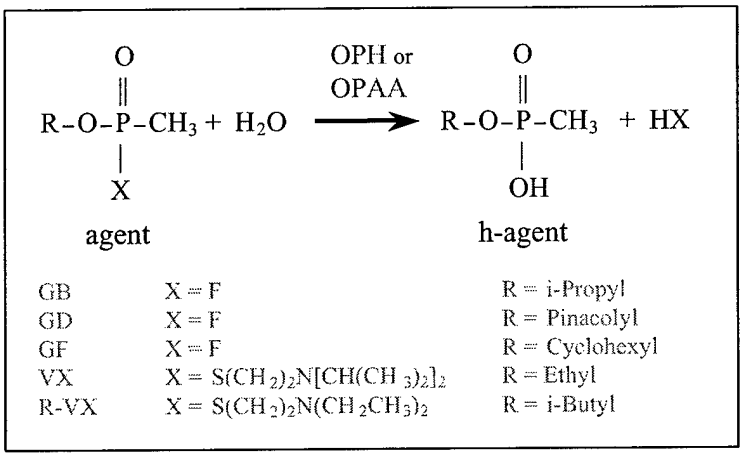

nerve agents GB, GD, GF, VX, and R-VX would result in h-GB (IMPn), h-GD (PMPn), h-GF (CMPn), h-VX (EMPn), and h-R-VX (iBMPn) products, respectively (Scheme 1).

In search of enzymes that could facilitate further degradation of these chemicals, we screened microorganisms for their ability to grow on methylphosphonate (MPn) and ethyl methylphosphonate (EMPn) as the sole sources of phosphorus. We hoped that these strains might contain enzymes that would degrade all or most phosphonate esters generated during the nerve agent hydrolysis via esterase cleavage resulting in MPn product for the five selected compounds (Scheme 2). We identified two bacterial strains *Burkholderia caryophilli* PG2982 (previously called *Pseudomonas caryophilli* PG2982) and *Pseudomonas testosteroni* that would utilize both MPn and EMPn as the sole sources of phosphorus. The *B. caryophilli* PG2982 strain, which has been known to be capable of utilizing the organophosphorus pesticide, glyphosate, reportedly contains phosphonate monoester hydrolase gene (Dotson, 1996; Moore, 1983; Shinabarger, 1984). It has been reported that the second strain of *P. testosteroni* would utilize alkylphosphonates as the sole sources of phosphorus (Cook, 1978a, 1978b). We investigated these two strains further.

Scheme 2. PEH degradation of hydrolyzed agents.

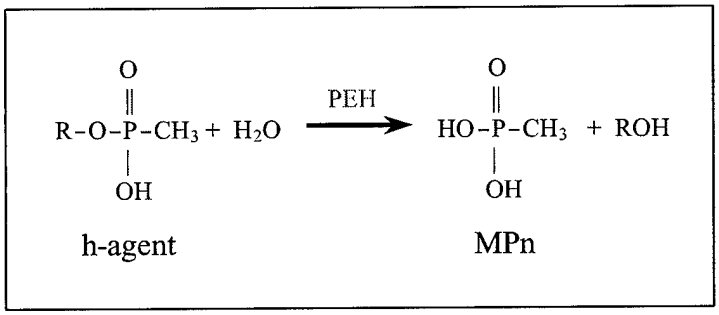

MATERIALS AND METHODS

Organism and Growth Conditions: The two bacterial strains used in this study were kindly provided by Dr. Braymer (*B. caryophilli* PG2982) and Dr. Alexander (*P. testosteroni*). Unless otherwise indicated, the cultures were routinely grown at 30°C for 40 hours in the new MOPS medium (NMM) adapted from the modified MOPS medium (Elashvili, 1997, 1998) supplemented with 0.3 mM h-GB as the sole phosphorus source. NMM contained (per liter) 8.372 g 3-(*N*-morpholino)propanesulfonic acid (MOPS), 0.717 g of *N*-Tris(hydroxymethyl)methyl glycine (Tricine), 2.92 g of NaCl, 0.51 g of NH_4Cl, 102 mg of $MgCl_2 \cdot 6H_2O$, 10 mg of thiamine, 6 mg of $MgSO_4 \cdot 7H_2O$, 3 mg of nitrilotriacetic acid, 48 mg of K_2SO_4, 1 mg of $MnSO_4 \cdot H_2O$, 2.8 mg of $FeSO_4 \cdot 7H_2O$, 0.1 mg of $CaCl_2 \cdot 2H_2O$, 0.1 mg of $CoCl_2 \cdot 6H_2O$, 0.1 mg of $ZnSO_4 \cdot 7H_2O$, 0.02 mg of H_3BO_3, 0.01 mg of $Na_2MoO_4 \cdot 2H_2O$, 0.01 mg of $CuSO_4$, and 1 g of

glucose, 1 g potassium D-gluconate, 1 g sodium citrate, and the pH was adjusted to 7.0 with KOH prior to sterilization through 0.2μ filter.

To ascertain PEH activities of different bacterial crude extracts, a one-liter Erlenmeyer flask with 300 ml media inoculated with *B. caryophilli* was routinely incubated at 30°C for 40 hours on a recirculatory shaker at 200 rpm. For the enzyme purification, *B. caryophilli* was cultured in four 6-liter flasks at 150 rpm in a total of 10 liters of the medium. The cells were collected by centrifugation at 7,000×g for 30 minutes at room temperature, gently resuspended in a minimum amount of 100 mM Tris buffer, pH 8.0, 100 mM KCl and spun again at 24,000×g for 20 minutes at 4°C. The supernatant was aspirated and the pellet was stored below -85°C. Unless otherwise indicated, subsequent procedures for the enzyme extraction and purification were conducted below 4°C and enzyme fractions were stored below -85°C.

Preparation of hydrolyzed agent substrates: GB, GD, GF, VX, and Russian-VX chemical agents (0.1-0.3 M, CASEARM grade) were hydrolyzed in 1 N NaOH for 2 days and subsequently titrated with HCl to neutral pH. We compared the resulting hydrolyzed agents – h-GB, h-GD, and h-VX – with the corresponding commercially obtained compounds – isopropyl methylphosphonate (IMPn), pinacolyl methylphosphonate (PMPn), and Ethyl methylphosphonate (EMPn) – of the highest available purity. The purity of our hydrolyzed agent preparations was compatible with commercially available corresponding compounds as judged by the analysis of their derivatives on GC-FPD.

Enzyme assays: Enzyme assays were conducted at 30°C with 10 mM substrate in 50 mM 1,3-bis-(tris-[hydroxymethyl]-methylamino)-propane (BTP) buffer, pH 8.5, 1 mM $MnCl_2$, and 2 il of enzyme sample in a total volume of 60 il. At appropriate time intervals of the reaction, aliquots were withdrawn and added to concentrated sodium hydroxide solution to stop the reaction to make the final NaOH concentration of 1N. Samples were dried, silylated with a mixture of BSTFA+1% TMCS (Pierce) (BSTFA = *N,O*-bis[trimethylsilyl]trifluoroacetamide and TMCS = trimethylchlorosilane) at ca. 110°C for 15 min, diluted with CH_2Cl_2, and analyzed on GC-FPD. The concentrations of the substrates (S_R) in aliquots of the reaction was determined by the formula shown on the right, where S_I is the initial substrate concentration of the reaction, whereas A_S and A_P denote the GC-FPD chromatograms' peak areas of the silylated derivatives of the substrate and product of the aliquot, respectively. The formula is based on the assumption that the ratio of the substrate and product chromatograms' peak area values represent the ratio of their concentrations in the reaction sample. Therefore, the substrate concentration (S_R) in the reaction sample is calculated as the fractional value of the substrate peak area over the combined peak areas of the substrate and the product that is subsequently normalized by the initial concentration of the substrate.

$$S_R = \frac{A_S \cdot S_I}{A_S + A_P}$$

To ascertain enzyme activities in chromatographic effluent samples, 2 mM chromogenic *p*-nitrophenyl phenylphosphonate substrate was used and the room temperature reaction was monitored on a spectrophotometer by measuring the absorbance of liberated *p*-nitrophenol at 405 nm.

Enzyme Extraction: All subsequent enzyme extractions and purifications were conducted at 4°C. Frozen pellets of collected cells were resuspended in 100 mM Tris buffer, pH 8.0, 100 mM KCl, 2mM DTT (3 ml per gram of wet weight). The cells were disrupted by passage through a pre-chilled French Pressure cell (SLM-Aminco) three times at 16,000 psi. Crude cell extracts were obtained after the removal of cellular debris by centrifugation at 37,000×g for 30 min at 4°C. In order to destroy heat labile enzymatic activities in a sample of supernatant, a small portion of the supernatant was boiled for five minutes and precipitates were removed by centrifugation at 13,000×g for 10 minutes.

Enzyme Purification on Ion-Exchange Column: To remove nucleic acids from the crude extract preparation, ten-percent suspension of a cationic polymer Biocryl BPA-1000 (Supelco, Bellefonte, PA) was added to make the final polymer concentration of one percent. After mixing, the extract was incubated on ice for 10 minutes and centrifuged at 37,000×g for 30 minutes. This treatment did not affect the enzyme activity, but it was very effective for nucleic acid removal as judged by the UV (between 200-300 nm) spectral comparisons of pre- and post-treatment samples (data not shown). The supernatant was diluted with 3-fold volume of 4°C chilled 2 mM DTT solution and the sample mix was chromatographed on a DEAE-Sepharose Fast Flow (Amersham/Pharmacia Biotech Inc., Piscataway, NJ) anion-exchange column (25×150 mm). Before the sample application, the column was washed with two column volumes of the 2 M KCl solution and equilibrated with five column volumes of the 20 mM Tris buffer, pH 8.0. After the sample loading, the column was washed with 3.5 column volumes of the 20 mM Tris buffer, pH 8.0, 2 mM DTT, followed by 7 column volumes of the 100 mM Tris buffer, pH 8.16, 100 mM KCl, 2mM DTT to elute loosely bound proteins. The enzyme was eluted with the 100 mM Tris buffer, pH 8.0, 270 mM KCl, 2mM DTT and collected in 20-ml aliquots (Fig. 2). Active fractions (60 ml) were pooled and precipitated with increasing concentrations of ammonium sulfate. Most of the PEH enzymatic activity was recovered in the ammonium sulfate cut between 50-80% (sat.). The resultant pellet was resuspended in the minimal amount of 100 mM Tris buffer, pH 8.0, 100 mM KCl, 2mM DTT and stored frozen below -85°C.

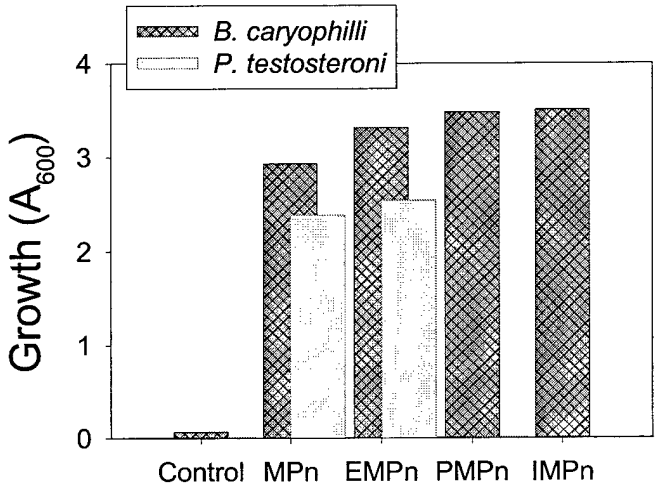

Figure 1. *B. caryophilli* PG2982 has broader phosphonate substrate utilization capability than *P. testosteroni*: Two bacterial strains, *B. caryophilli* PG2982 and *P. testosteroni*, were pregrown on MPn as the sole phosphorus source, washed three times with P-deficient NMM broth and used as inoculums at the seeding $A_{600} = 0.010$ in NMM broth with 0.3 mM phosphonates as the sole phosphorus source and 2% glucose as the carbon source. After 94 hours growth at 28°C total cell growth was determined turbidimetrically.

Protein Determination: For protein determination, a protein dye binding method (Bradford, 1976) was used, with bovine serum albumin as the standard.

RESULTS AND DISCUSSION

Selection of an organism for PEH enzyme purification: The *B. caryophilli* PG2982 strain has been known to be capable of utilizing the organophosphorus pesticide, glyphosate, as the sole phosphorus source and reportedly contains phosphonate monoester hydrolase gene (Dotson, 1996; Moore, 1983; Shinabarger, 1984). Similarly, our tests confirmed that, the *B. caryophilli* PG2982 strain was capable of utilizing the organophosphorus pesticide, glyphosate, as the sole phosphorus source (data not shown). The *P. testosteroni* strain has been reported to utilize alkylphosphonates as the sole phosphorus sources (Cook, 1978a, 1978b). We tested the growth of *B. caryophilli* PG2982 and *P. testosteroni* strains on 0.3

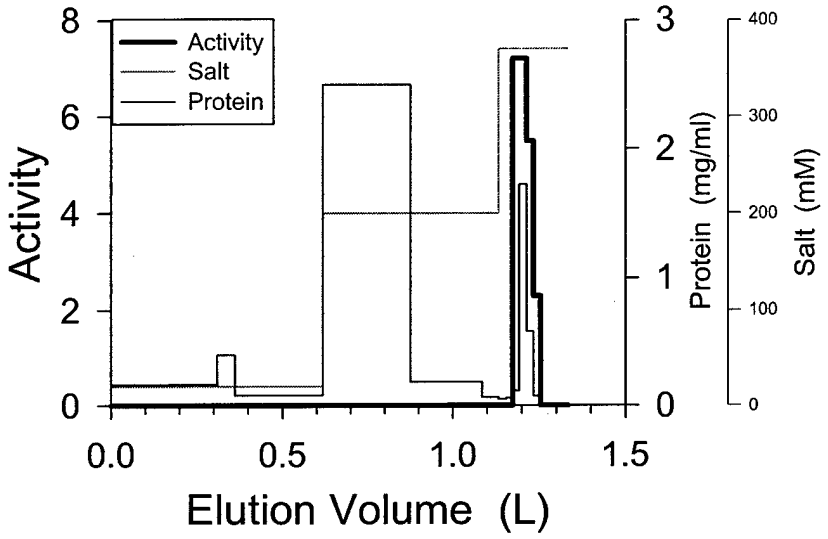

Figure 2. PEH purification on DEAE-Sepharose FF.

mM MPn, EMPn, PMPn, and IMPn as the sole sources of phosphorus (Fig. 1). The latter strain grew only on MPn and EMPn, whereas *B. caryophilli* PG2982 grew on all four phosphonates (Fig.1). No remaining phosphonate substrates were detected in the growth media of the successful growing cultures after the 40-hour incubation period. However, these media contained newly formed inorganic phosphate (data not shown). It should be noted that both the *B. caryophilli* PG2982 and the *P. testosteroni* strains grew on all four phosphonate substrates at 1 mM substrate concentrations as the sole sources of phosphorus, perhaps due to impurities contained in the substrates. However, *P. testosteroni* failed to grow on 0.3 mM concentrations of PMPn and IMPn, while showing robust growth when the phosphorus source was 0.3 mM inorganic phosphate. Since, *B. caryophilli* PG2982 was found to be capable of growth on all the phosphonate ester substrates tested the strain was selected for further investigation.

PEH enzyme purification and characterization: Both the cell-free native crude extract obtained from the *B. caryophilli* PG2982 strain and the denatured (boiled) sample derived from it were tested for the PEH enzymatic activity. The native extract was capable of transforming hydrolyzed nerve agents GB, GD, GF, VX and Russian VX to methylphosphonic acid as judged by the analysis of their silylated derivatives on GC-FPD, whereas the denatured extract had no activity (data not shown). This indicates that the activity was due to a heat-sensitive enzyme in the extract.

A larger scale *B. caryophilli* extract was obtained for purification. After removing nucleic acids and other negatively charged molecules with the cationic polymer, BPA-1000, the enzyme was purified on DEAE-Sepharose Fast Flow columns using KCl step elution. The activity was eluted between 60 ml and 120 ml after the start of 270 mM KCl step (Fig. 2). The active fractions were pooled and concentrated with 50-80% (sat) ammonium sulfate cut.

The partially purified PEH was used to test the enzyme specificity against the selected hydrolyzed agent substrates. The timeline chromatograms of the PEH degradation of two of the substrates, h-GF and h-GD, are shown on Fig 3. As can be seen on the chromatograms on the left panels, the peak denoting the h-GF substrate (the silylated derivative's R_f value ca. 8.24 minutes) decreases with the increase of the enzymatic reaction time, until it finally disappears (after 3 hours), while concomitantly the peak denoting the MPn product (the silylated derivative's R_f value ca. 4.39 minutes) increases (Fig. 3). Similarly, on the right panels, the h-GD substrate (the silylated derivative's R_f value ca. 6.25 minutes) degradation to MPn

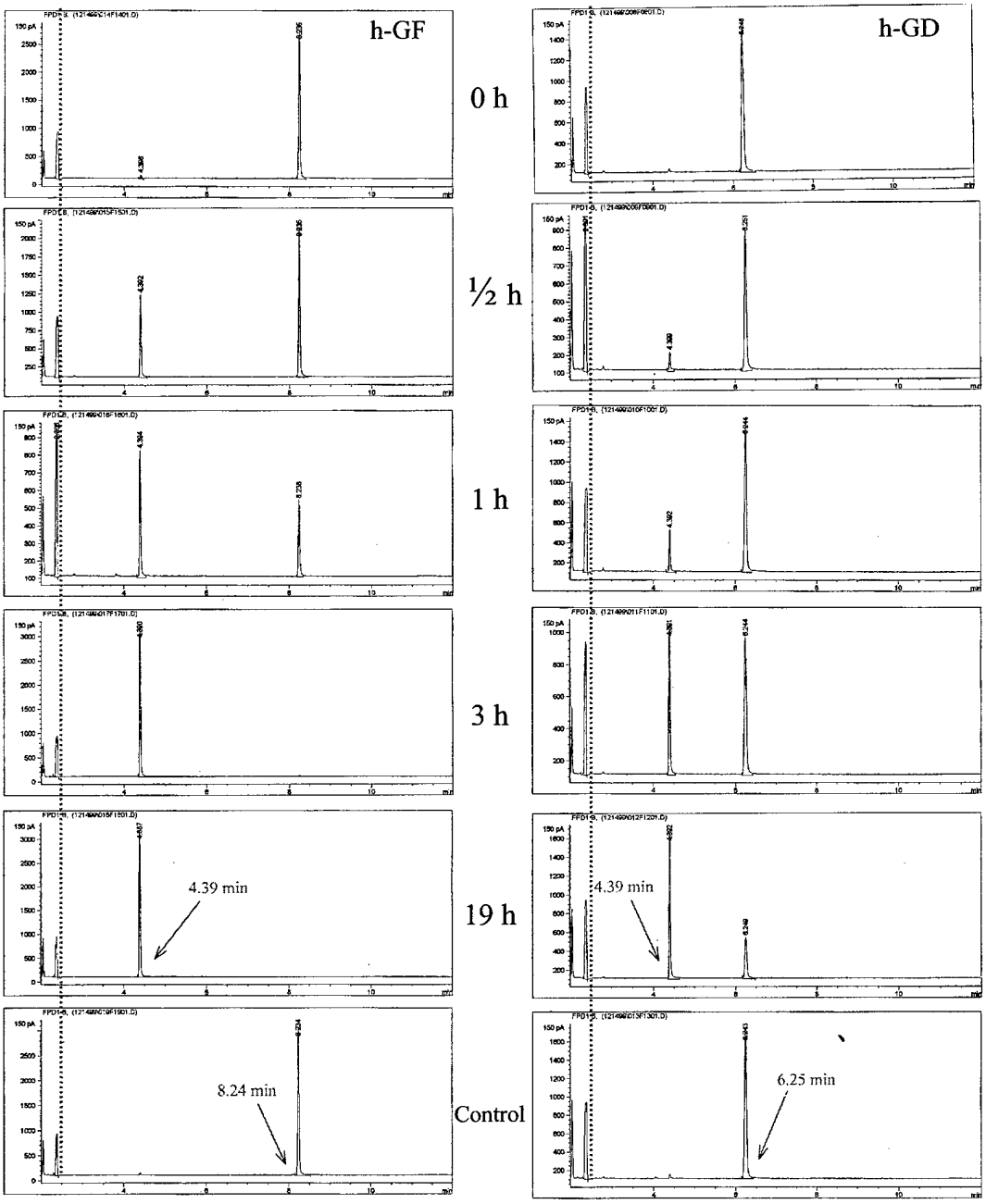

Figure 3. PEH degradation of h-GF and h-GD: The timeline of the GC-FPD chromatograms of the PEH reactions at 30°C with the two (h-GF and h-GD) out of the total of five substrates (ca. 10 mM) and their controls are shown. The 50-80% ammonium sulfate cut of the step gradient purified PEH enzyme constituted ~3.2 % of the total reaction mixture volume. The Control samples represent 19-hour reaction mixtures that contained the buffer used for the enzyme reconstitution instead of the PEH enzyme. The reaction samples were derivatized prior to GC-FPD chromatography. The R_f value of ca. 4.39 minutes of the derivatized enzymatic reaction products of all the five substrates was similar to that of the derivatized MPn standard. The R_f values for derivatized h-GD and h-GF were ca. 6.25 minutes and ca. 8.24 minutes, respectively. (The green dotted lines mark the end of the solvent peaks.)

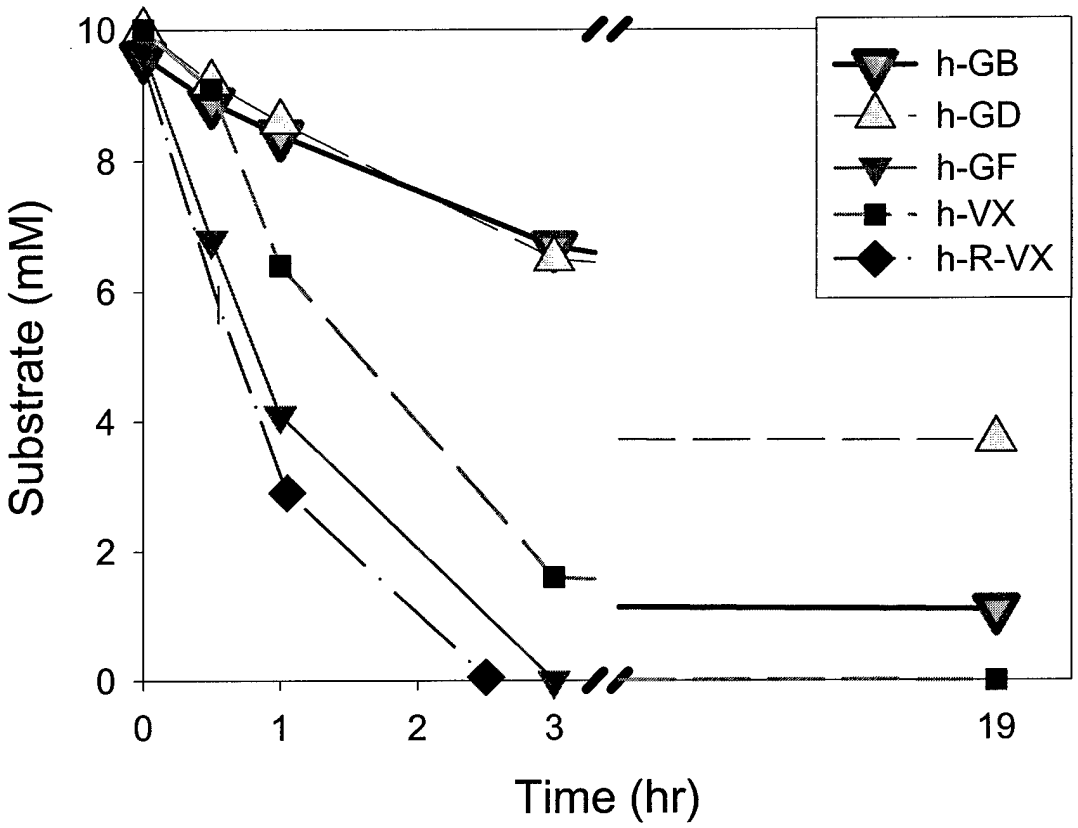

Figure 4. PEH degradation of hydrolyzed agents. The five substrates: h-GB, h-GD, h-GF, h-VX, and h-R-VX were incubated at 30°C with and without PEH enzyme as in Fig. 3. The remaining substrate concentrations were ascertained as outlined in MATERIALS AND METHODS No detectable degradation product was observed for any of the five substrates after 19 hours of incubation in controls without the PEH enzyme.

can be observed, although the enzymatic reaction here proceeds at a slower rate. In contrast, no observable degradation MPn product is visible on the Control chromatogram panels of either of the two substrates (Fig. 3).

The kinetics of the PEH enzymatic degradation of the five selected hydrolyzed nerve agents are shown on Fig.4. In this study the decline of the initial 10 mM h-GB, h-GD, h-GF, h-VX, and h-R-VX substrates are plotted as they are degraded by the PEH enzyme. It demonstrates that the enzyme is most effective against h-R-VX, closely followed by h-GF, both of which were completely degraded within the first three hours of the reaction. Only h-GD and h-GB were not completely degraded after 19 hours of the reaction, the former being the least reactive having 37 percent of the initial substrate still intact, while the latter had only 11 percent of the unaltered original substrate. No detectable degradation product was observed for any of the substrates after 19 hours of incubation in controls without the PEH enzyme.

These experiments demonstrate the effective degradation of the hydrolyzed nerve agents by the PEH enzyme. The order of the PEH activity at 10 mM substrate concentration and BTP bufffer, pH 8.5 was as follows h-R-VX>h-GF>h-VX>h-GB>h-GD (i.e., iBMPn>CMPn>EMPn>IMPn>PMPn).

REFERENCES

Bradford, M.M. (1976) A rapid and sensitive method for the quantitation of microgram quantities of protein utilizing the principle of protein dye binding. *Anal. Biochem.* **72**, 248-254.

Chapalamadugu, S. and Chaudhry, G.R. (1992) Microbiological and biotechnological aspects of metabolism of carbamates and organophosphates. *Crit. Rev. Biotechnol.* **12**, 357-89, 1992.

Cook, A.M.; Daughton, C.G. and Alexander, M. (1978a) Phosphorus-containing pesticide breakdown products: Quantitative utilization as phosphorus sources by bacteria. *Appl. Environ. Microbiol.* **36**, 668-672.

Cook, A.M.; Daughton, C.G. and Alexander, M. (1978b) Phosphonate utilization by bacteria. *J. Bacteriol.* **133**, 85-90.

Cheng, T.-c.; Harvey, S.P. and Stroup, A.N. (1993) Purification and properties of a highly active organophosphorus acid anhydrolase from *Alteromonas undina. Appl. Environ. Microbiol.* **59**, 3138-3140.

DeFrank, J.J. and Cheng, T.-c. (1991) Purification and properties of an organophosphorus acid anhydrase from a halophilic bacterial isolate. *J. Bacteriol.* **173**, 1938-1943.

DeFrank, J.J.; Beaudry, W.T.; Cheng, T.-c.; Harvey, S.P.; Stroup, A.N. and Szafraniec, L.L. (1993) Screening of halophilic bacteria and *Alteromonas* species for organophosphorus hydrolyzing enzyme activity. *Chem. Biol. Interact.* **87**, 141-148.

Dotson, S.B.; Smith, C.E.; Ling, C.S.; Barry, G.F. and Kishore, G.M. (1996) Identification, characterization, and cloning of a phosphate monoester hydrolase from *Burkholderia caryophilli* PG2982. *J. Biochem.* **271**, 25754-25761.

Dumas, D.P.; Caldwell, S.R.; Wild, J.R. and Raushel, F.M. (1989) Purification and properties of the phosphotriesterase from Pseudomonas diminuta. *J. Biol. Chem.* **264**, 19659-19665.

Dumas, D.P.; Durst, H.D.; Landis, W.G.; Raushel, F.M. and Wild, J.R. (1990) Inactivation of organophosphorus nerve agents by the phosphotriesterase from *Pseudomonas diminuta. Arch. Biochem. Biophys.* **277**, 155-159.

Elashvili, I., DeFrank, J.J., and Culotta, V.C. (1999) Purification and characterization of DFPase from *Alteromonas haloplanktis* ATCC 14393. Proceedings of the 1998 U.S. Army Edgewood Research, Development and Engineering Center Scientific Conference on Chemical and Biological Defense Research. ECBC-SP-004, pp 763-771.

Elashvili, I., DeFrank, J.J., and Culotta, V.C. (1998) *phnE* and *glpT* genes enhance utilization of organophosphates in *Escherichia coli* K-12. *Applied and Environmental Microbiology*, **64**:2601-2608.

Elashvili, I., DeFrank, J.J., and Culotta, V.C. (1997) Phosphonate transporter mutation enhances the utilization of diisopropylphosphate (DIPP) and diisopropyl fluorophosphate (DFP) in *E. coli* K-12. Proceedings of the 1996 U.S. Army Edgewood Research, Development and Engineering Center Scientific Conference on Chemical and Biological Defense Research, pp 189-195.

Fedorov, L. A. (1994) *Chemical Weapons in Russia: History, Ecology, Politics* [*Khimicheskoye Oruzhiye V Rossii: Istoriya, Ekologiya, Politika*]. Center of Ecological Policy of Russia, Moscow, Russia. http://www.fas.org/nuke/guide/russia/cbw/jptac008_l94001.htm.

Marrs, T.C.; Maynard, R.L. and Sidell, F.R.(Eds.) (1996) *Chemical Warfare Agents: Toxicology and Treatment*, John Wiley and Sons, New York.

Moore, J.K.; Braymer, H.D. and Larson, A.D. (1983) Isolation of a *Pseudomonas* sp. which utilizes the phosphate herbicide glyphosate. *Appl. Environ. Microbiol.* **46**, 316-320.

Shinabarger, D.L.; Schmitt, E.K.; Braymer, H.D. and Larson, A.D. (1984) Phosphonate utilization by the glyphosate-degrading *Pseudomonas* sp. strain PG2982. *Appl. Environ. Microbiol.* **48**, 1049-1050.

Somani, S.M.; Solana, R.P. and Dube S.N. (1992) Toxicodynamics of nerve agents. In *Chemical Warfare Agents* (Edited by Somani, S.M.) pp. 67-123. Academic Press, New York.

UN Document CD/1170 (1992) *Convention on the Prohibition of the Production, Stockpiling and Use of Chemical Weapons and on Their Destruction*. Geneva, Switzerland.

Yang, Y.-C.; Baker, J.A. and Ward, J.R. (1992) Decontamination of chemical warfare agents. *Chem. Rev.* **92**, 1729-1743.

MOLYBDATE/PEROXIDE OXIDATION OF MUSTARD IN MICROEMULSIONS

Lawrence R. Procell, George W. Wagner, Yu-Chu Yang

U.S. Army ECBC, ATTN: AMSSB-RRT-CA, 5183 Blackhawk Rd., APG, MD 21010-5424

and

Clifford A. Bunton

Department of Chemistry and Biochemistry, University of California, Santa Barbara, CA 93106-9510

Environmentally friendly and non-corrosive methods to decontaminate the blister agent mustard (HD), bis(2-chloroethyl) sulfide, are currently being developed. HD may be rendered non-vesicant by oxidation to the corresponding sulfoxide. Results will be presented for the use of the mildly-basic molybdate/peroxide oxidant system to achieve this transformation. Reactions are performed in microemulsions to enable the dissolution of oily, water-isoluble mustard.

INTRODUCTION

Environmentally friendly decontamination systems are needed to replace current, toxic and corrosive decontaminants such as hypochlorite and DS2.[1] Peroxides is a desirable reactant for decontamination owing to their non-toxic, non-corrosive nature. Indeed, hydrogen peroxide is widely used in so-called "Green" industrial processes,[2] replacing historical hypochlorite-based processes which are environmentally harmful.[3] Mustard (HD) may be oxidized to the non-vesicant sulfoxide (HDO),[4] but care must be taken to avoid further oxidation to the vesicant sulfone (HDO_2).[4] This reaction is shown in Scheme 1 where [O] represents an active oxidant.

SCHEME 1

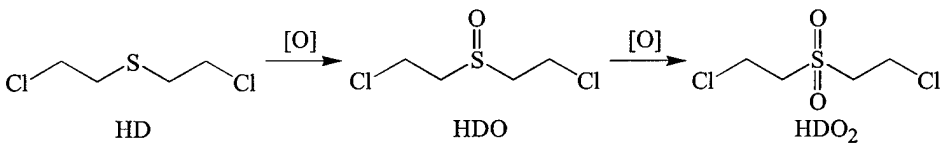

The recently developed peroxide-based "DECON GREEN"[5a] decontaminant accomplishes the selective oxidation of HD to HDO by using a hydrogen carbonate activator.[5b,c,6] However, the reaction of DECON GREEN with HD remains slow compared to the V and G agent reactions which are nearly

instantaneous and involve nucleophilic attack by the peroxy anion.[5a,b] Other potential peroxide activators are being explored to hasten the oxidation of HD.

Recently, Aubry and Bouttemy[7] demonstrated the rapid oxidation of a variety of organic compounds by using the peroxide/molybdate system in a water-in-oil (w/o) microemulsion. In this system, molybdate is believed to act as a peroxide activator by generating singlet oxygen ($^1O_2$) which diffuses out of the microemulsion and reacts with substrates in the bulk organic solvent, although the role of peroxo species was not excluded.[8] $^1O_2$ is reportedly generated from the triperoxomolybdate $MoO(OO)_3^{2-}$, and this species predominates at ratios of $[H_2O_2]/[MoO_4^{2-}]$ of four or less.[8] At higher ratios, the predominant formation of the more stable tetraperoxomolybdate $Mo(OO)_4^{2-}$ deceases $^1O_2$ production[8] and the associated peroxide decomposition. Besides the problem of peroxide decomposition, avoiding $^1O_2$ formation is further desirable as this species oxidizes sulfides non-selectively to both sulfoxides and sulfones.[7] Generation of HD-sulfone is to be avoided as it possesses substantial vesicant activity, similar to HD itself.[4] Thus $Mo(OO)_4^{2-}$ is a potentially stable and very effective reactant for the selective oxidation of HD to the non-vesicant sulfoxide. This reaction is shown in Scheme 2. In this paper the oxidation of HD in molybdate/peroxide microemulsions will be described with conditions such that the tetraperoxo species is dominant.

SCHEME 2

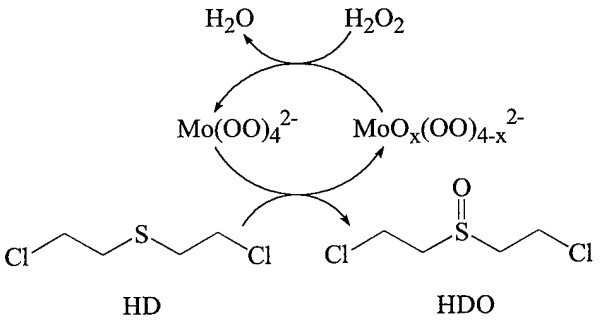

EXPERIMENTAL

K_2MoO_4, n-BuOH, CH_2Cl_2, sodium dodecyl sulfate (SDS, an anionic surfactant), Triton X-100 (a non-ionic surfactant), i-PrOH, hexane, and 50 % H_2O_2 were all obtained from Aldrich. Microemulsions were mixed by first adding the solid ingredients (e.g., SDS and/or K_2MoO_4), followed by cosurfactant (e.g., n-BuOH or i-PrOH), surfactant, organic solvent, and finally 50 % H_2O_2 to a 3 mL vial. The vial was capped and vortex mixed briefly. The microemulsions spontaneously formed and generation of $Mo(OO)_4^{2-}$ was immediately apparent from the amber color of the potassium salt of this species. Reactions were initiated by adding 9 μL neat liquid HD to 0.75 mL of the decon solution contained in a 5 mm NMR tube. The concentration of HD was 0.1 M. The tube was capped and shaken to assure complete dissolution of HD. Reactions were monitored by ^1H NMR by using a Varian Unityplus 300 NMR spectrometer to obtain kinetic data.

RESULTS AND DISCUSSION

Half-lives observed for the reaction of HD in various microemulsions (ME's) are shown in Table 1. The concentration of K_2MoO_4 in each ME was 0.01 M, which was low enough in most cases to allow

measurements of the half-lives. Higher concentrations would have rendered the reactions essentially instantaneous. It should be noted that 0.1 to 0.2 M hydrogen carbonate activator (or ten to twenty times the concentration of molybdate ion) would be required to achieve similar half-lives.[5] Thus as a peroxide activator for HD oxidation, molybdate ion is at least an order of magnitude more powerful than hydrogen carbonate ion.

TABLE 1. Half-Lives Observed for HD in Microemulsions.

ME	K_2MoO_4	Surfactant	Cosurfactant	Oil Phase	50 % H_2O_2	$t_{1/2}$
		SDS[a]	n-BuOH[a]	CH_2Cl_2[a]		
1	2.4 mg	99 mg	0.198 g	0.403 g	0.354 g	1.0 min
2	2.4 mg	96 mg	0.193 g	0.501 g	0.248 g	1.4 min
3	2.4 mg	86 mg	0.173 g	0.602 g	0.165 g	1.8 min
4	2.4 mg	76 mg	0.146 g	0.698 g	0.098 g	1.2 min
		Triton X-100	i-PrOH	Hexane		
5	2.5 mg	0.214 g	0.395 g	0.0786 g	0.300 g	< 30 sec
		Triton X-100	Solvent			
6	2.6 mg	0.224 g	0.695 g		0.307 g	< 30 sec[b]
7	2.4 mg	0.224 g	0.654 g		0.295 g	1.1 min
8	2.4 mg	0.224 g	0.713 g		0.236 g	53 sec
9	2.4 mg	0.224 g	0.773 g		0.177 g	1.3 min
10	2.4 mg	0.224 g	0.832 g		0.118 g	1.8 min

[a]Adapted from Aubry and Bouttemy.[7] [b]$t_{1/2}$ = 47 min for HDO → HDO_2.

Water-in-oil (w/o) ME's #1-4 were adapted from the work of Aubry and Bouttemy,[7] and these contain the constituents typical of such ME's: SDS (surfactant), n-BuOH (cosurfactant), CH_2Cl_2 (oil phase), and 50 % H_2O_2 (aqueous phase). Although HD dissolution and oxidation proceeded well in these ME's, they contain toxic CH_2Cl_2 and are thus environmentally unacceptable. Additional ME's were formulated using more environmentally friendly ingredients, which also yielded good HD dissolution/reaction. For example ME #5, composed of Triton X-100 (surfactant), i-PrOH (cosurfactant), hexane (oil phase) and 50 % H_2O_2 (aqueous phase), rapidly dissolved and oxidized HD with a half-life too fast to measure by NMR ($t_{1/2}$ < 30 sec). As a further step to meet "Green" criteria and to minimize the number of necessary components, an additional series of "ME's" were examined using only Triton X-100, 50 % H_2O_2, and a non-toxic industrial solvent currently being utilized in DECON GREEN formulations. The industrial solvent may be functioning merely as a cosolvent rather than a true cosurfactant. The resulting solutions are not true ME's as these streamlined mixtures lack a conventional cosurfactant and oil phase and can be regarded as modified micelles. However, HD is readily dissolved;
and thus briefly becomes the "oil phase" prior to reacting in these ME's. It is important to note that compared to the toxic series of ME's #1-4, no loss in HD reactivity is observed using the "Green" ingredients of ME's #6-10. For ME #6, the secondary oxidation of HDO to HDO_2 was monitored by ^1H and ^{13}C NMR, with a half-life of 47 min. Thus, fortunately, the undesired secondary oxidation of HDO is about two orders of magnitude slower than primary oxidation of HD.

CONCLUSIONS

As a peroxide activator molybdate ion affords at least an order of magnitude increase in the rate of HD oxidation compared to hydrogen carbonate ion, rendering the reaction nearly instantaneous. Secondary oxidation to the sulfone does occur, but this reaction is slower by about two orders of magnitude. The molybdate/peroxide reactive system functions in a variety of microemulsions, including those composed of non-toxic ingredients. These latter formulations in which tetraperoxomolybdate is the major peroxo species would be suitable for decontamination of HD and other toxic sulfides in the environment.

ACKNOWLEDGEMENT

An Army Research Office grant supporting work at UCSB is acknowledged.

REFERENCES

1. Yang, Y.-C.; Baker, J. A.; Ward, J. R. *Chem. Rev.* **1992**, *92*, 1729-1743.
2. (a) Dagani, R. *Chem. Eng. News* **1999**, *77*(27), 30-32. (b) McCoy, M. *Chem. Eng. News* **1999**, *77*(5), 18-19.
3. (a) McDonald, J. G.; Hites, R. A. *Anal. Chem.*, in press. (b) Zhang, Q.; Chuang, K. T. *Environ. Sci. Technol.* **1999**, *33*, 3641-3644. (c) Zheng, Y.; Allen, D. G. *Environ. Sci. Technol.* **1996**, *30*, 1890-1895.
4. (a) Marshall, E. K., Jr.; Williams, J. W. *J. Pharmacol. Exp. Therapeutics* **1921**, *16*, 259-272. (b) Lawson, W. E.; Reid, E. E. *J. Am. Chem. Soc.* **1925**, *47*, 2821-2836. (c) Anslow, W. P., Jr.; Karnofsky, D. A.; Val Jager, B.; Smith, H. W. *J. Pharmacol. Exp. Therapeutics* **1948**, *93*, 1-9.
5. (a) Wagner, G. W.; Yang, Y.-C., manuscript in preparation. (b) Wagner, G. W.; Yang, Y.-C. In the *Proceedings of the 1998 ERDEC Scientific Conference on Chemical and Biological Defense Research, ERDEC-SP-004*; U.S. Army Edgewood Research, Development and Engineering Center, 1999, pp. 285-291. (c) Drago, R. S.; Frank, K. M.; Wagner, G. W.; Yang, Y.-C. In the *Proceedings of the 1997 ERDEC Scientific Conference on Chemical and Biological Defense Research, ERDEC-SP-063*; U.S. Army Edgewood Research, Development and Engineering Center, 1998, pp. 341-342.
6. (a) Richardson, D. E.; Yao, H.; Xu, C.; Drago, R. S.; Frank, K. M.; Wagner, G. W.; Yang, Y.-C. In the *Proceedings of the 1998 ERDEC Scientific Conference on Chemical and Biological Defense Research, ERDEC-SP-004*; U.S. Army Edgewood Research, Development and Engineering Center, 1999, pp. 293-299. (b) Richardson, D. E.; Yao, H.; Frank, K. M.; Bennett, D. A. *J. Am. Chem. Soc.* **2000**, *122*, 1729-1739.
7. Aubry, J.-M.; Bouttemy, S. *J. Am. Chem. Soc.* **1997**, *119*, 5286-5294.
8. Nardello, V.; Marko, J.; Vermeersch, G.; Aubry, J. M. *Inorg. Chem.* **1995**, *34*, 4950-4957.

INTERACTION OF CANDIDATE CLEANING SOLUTIONS FOR SENSITIVE EQUIPMENT DECONTAMINATION WITH POLYMERIC MATERIALS

Brian S. Ince and Wendel J. Shuely
USA, SBCCOM, APG, MD 21010-5424

Chemical-polymer compatibility is an important criterion for the cleaning, decontamination, and extraction of hazardous chemicals from sensitive equipment (electronics, optics, and other advanced polymeric materials). Candidate cleaning fluids for sensitive equipment include fluorocarbons and supercritical fluids. The initial evaluation strategy involves the measurement of the sorption and desorption diffusion coefficients of the candidate cleaning fluid in a spectrum of polymer compositions. The objective was to characterize the complete desorption process by the continuous measurement of the entire diffusion process employing thermogravimetric instrumentation. These measurements and calculations provided an estimated 'time before reuse' after the cleaning process. The continuous measurement of desorption provided the high data density required to calculate a low concentration Fick's Law diffusion coefficient and equation for the extrapolations. The composition spectrum selected contains hydrogen bond donor, hydrogen bond acceptor, dipolar, and non-polar polymer structures; over 15 materials were studied.

INTRODUCTION

Chemical-material compatibility is a critical criterion in development of a decontamination system. The degradation of material properties and performance is especially important for sensitive equipment cleaning and decontamination. Sensitive equipment includes electronics, optics, and other high-value and unique equipment. The candidate cleaning fluids for sensitive equipment include supercritical carbon dioxide and fluorocarbons.

The overall material evaluation methodology for compatibility with decontaminants is under development (1-3). The selection of representative materials for compatibility testing is underway based on several parallel approaches. These include a top-down, materiel-to-material analysis that identifies surface materials in a spectrum of high-cost equipment; several material science based approaches were also applied to identify a spectrum of material physical states, molecular structures, and hydrogen bond and polarity classes (4).

The initial evaluation in any chemical-material evaluation test scheme usually involves measurement of sorption or solubility of the candidate cleaning fluid in a spectrum of relevant material compositions. The supercritical carbon dioxide processing conditions and material sorption experimentation is being reported separately. The experimentation reported herein concentrates on the desorption diffusion kinetic process for supercritical carbon dioxide from polymeric materials (5).

The purpose is to characterize the complete desorption diffusion process by continuous measurement of the entire diffusion curve, with the exception of a few minute time increment at the start of the experiment and a few percent of the final weight-loss. The next purpose was to use the continuous desorption curve to provide an accurate extrapolation of the zero-time sorption value immediately after supercritical carbon dioxide decompression. This extrapolation from the high concentration region of the desorption curve allowed calculation of a corrected sorption value for each material that provided an accurate ranking of material solubility relative to the uncorrected values. The characterization of the plateau to equilibrium desorption allowed the measurement of extractables and, therefore, the correction of the sorption value for this fraction extracted. Another purpose of diffusion coefficient measurements was to provide an estimate of the time required for each material to completely desorb all of the carbon dioxide cleaning fluid and return the material to the original unplasticized condition. These measurements and calculations provide an estimated 'time before reuse' after the decontamination process. The continuous measurement of desorption provided the high data density required to calculate a low concentration Fick's Law diffusion coefficient and equation for the extrapolation to initial material sample weight before exposure. The experimental strategy includes mechanical, optical, thermal, and electrical property characterization to measure the influence of the sorbed decontaminant; in this initial screening stage, indentation hardness measurements of surface mechanical properties were completed.

EXPERIMENTATION

Extraction Instrumentation. The extraction instruments and cells employed to expose the materials to supercritical carbon dioxide have been documented (5). In general, the diffusion specimens were relatively small; therefore, the smaller cell sizes cited in the reference were employed.

Desorption Instrumentation. The thermogravimetric instruments employed to measure the continuous desorption of sorbed supercritical carbon dioxide were a TA Model TGA 2950 and Model TGA 951 (New Castle, DE 19720). The final values reported were all measured with a combination of the Model TGA 2950 and control software Version 8.10B (2.3A). Custom specimen holders were required for the unique research measurements and were constructed to clamp the ca. 1-cm diameter disk shaped specimens, while allowing free surface diffusion on all sides. The 0.62-0.64 mm diameter nichrome wire was formed to a shape that matched the TGA Model 2950 hang down wire hook, cleared the furnace sides, and avoided buoyancy fluctuations. The supercritical carbon dioxide and polymeric materials used have been documented (5).

PROCEDURES

Supercritical Exposure Procedures. The supercritical exposure procedures and conditions employed were based on conditions that were found to successfully remove contaminants from non-sorptive surfaces in previous exploratory experiments (B. MacIver, D. Sorrick; SBCCOM). The supercritical conditions are documented in Table 1. The first column in Table 1 lists the supercritical pressure, temperature, and exposure-time conditions. The second column documents the units. The remaining columns define codes that document the set of experimental conditions in the table. These codes are used in experimental data sheets and computer data file documentation. The difference in RT#1 and RT#2 is only the Sorption Weighing Time; this weighing time at 20 minutes allows a direct comparison with literature (last column) that reported the first weighing at 20 minutes. The extraction time refers to a static exposure without flow through the cell. The decompression time is a rapid but controlled pressure drop to ambient at an approximately linear rate. The "Sorption Weighing" time defines the time lag required to disassemble the cell and manipulate the material specimen to obtain the initial weight. Carbon dioxide desorption under ambient conditions occurred during this lag and can be corrected by an extrapolation back to the end of the decompression period.

TABLE 1. Comparison of Experimental Conditions for Super Critical Carbon Dioxide Sorption in Polymeric Materials: Measurement Conditions versus Similar Literature (6-8) Conditions

Experimental Conditions	Units	RT#1	RT#2	Literature C3
Pressure	Psig.	1399	1399	2000
Temperature	Degrees, C	50	50	40
Time: Static Extraction @ PT	Minutes	15	15	60
Time: Decompression	Minutes	1	1	60
Time: 1st Sorption Weighing	Minutes	5	20	20

Kinetic Analysis Data Reduction Procedures. The basic data sets consisted of time, temperature, and weight measurements. These files were processed by various filtering techniques and data conversions to Fickian parameters. Interim results were processed with custom C++ code based on previous operational computational methods. A general description of the kinetic data analysis procedure has been provided (5). The final computations were performed using custom coded Excel functions.

RESULTS

Sorption Values Corrected for Fraction Extracted Employing Equilibrium Desorption Measurements. The sorption results in Table 2 are corrected for the fraction of mobile additives in the material that were extracted during the supercritical exposure. The value for the corrected sorption is followed by the uncorrected sorption value based on the fraction extracted. The relative error due to ignoring the extractables is calculated in the last column. Note that experimentation that ignores the extraction of the additives in the material causes considerable error that would change the relative ranking of materials for resistance to supercritical carbon dioxide sorption. The 'Not Applicable' entry refers to materials in which there was no measurable extraction. The methodology was capable of ranking the relative sorption levels for the spectrum of materials. The corrected sorption value was required to correctly rank the materials; the general trend in supercritical carbon dioxide was slightly influenced by fraction extracted, except for the combination of low sorption and high extractables. In these cases (for example, PEEK), the relative error was high but the ranking was only slightly in error.

Comparison of Sorption Values with Correction to Zero-time Mass Based on High Concentration Desorption Extrapolations. Most of the sorption values reported are based on an initial measurement that is often performed after considerable desorption has occurred. This measurement delay is due to the inherent lag between the end of the exposure or decompression time and the measurement time. Some modes of material damage may correlate with the maximum amount of decontaminant sorbed, therefore, accurate measurement of actual sorbed decontaminant is important. The reported measurements that ignore the desorption immediately after exposure give systematically low sorption values that underestimate the actual degree of interaction and solubility of fluids such as supercritical carbon dioxide in materials. In Table 3, the 'zero-time corrected sorption' values are calculated, followed by the error in ignoring the desorption immediately after the extractant exposure and decompression. Two delay periods are listed in the columns: the 7-12 minute delay inherent in the TGA experiment, reported herein, and the typical 20-minute measurement delay (U. Mass. Ref. 6-8). Large systematic relative errors of –15 to –86% were obtained by ignoring the extrapolation to zero-time. The methodology was capable of correcting for this measurement time lag after decompression and correctly ranking the materials. One can observe from the last two columns that there would be large ranking errors from not employing the methodology developed here.

TABLE 2. Supercritical Carbon Dioxide Sorption (%) into Polymeric Materials Based on Correction for Fraction Extracted: Conditions of 1400 psig and 50 degrees C after 15 minutes

No.	Polymer Codes	Sorption, Corrected, %	Sorption, Uncorrected, %	Extracted, %	Relative Error, %
1.	PDMS	0.44	0.44	-0.03	Not Applicable.
2.	PI	1.09	0.21	0.88	-80.7
3.	PEEK	1.49	1.20	0.28	-18.8
4.	PVC	1.65	1.65	-0.02	Not Applicable.
5.	PTFEP	2.39	2.24	0.15	-6.3
6.	PC	2.62	2.49	0.13	-5.0
7.	PBB	3.12	3.00	0.12	-3.8
8.	PEP	3.22	3.11	0.11	-3.4
9.	PPO	3.64	3.64	-0.24	Not Applicable.
10.	ABS	3.75	3.72	0.03	-0.8
11.	PIP	4.12	3.39	0.73	-17.7
12.	PSB	4.72	4.70	0.01	-0.2
13.	SMO	4.94	4.94	-0.20	Not Applicable.
14.	PMMA	6.24	6.24	-0.22	Not Applicable.
15.	PU	7.08	6.80	0.28	-4.0
16.	PSBR	7.32	6.58	0.74	-10.1
17.	PIB	7.88	7.88	-0.13	Not Applicable.

TABLE 3. Comparison of Sorption (%) Corrected for Extrapolation to Zero-time at the End of the Decompression Period Versus Uncorrected Sorption after 7-12 Minutes and 20 Minutes (6-8).

No.	Polymer Codes	Sorption, Zero-time Corrected	Sorption at 7-12 min, % (Relative Error, %)	Sorption at 20 min, % (Relative Error, %)
1.	PDMS	0.44	0.13 (-70.3)	0.06 (-86.8)
2.	PI	1.09	0.16 (-22.5)	0.04 (-80.0)
3.	PEEK	1.49	0.78 (-34.7)	0.60 (-50.3)
4.	PVC	1.65	1.37 (-17.2)	1.20 (-27.2)
5.	PTFEP	2.39	1.68 (-24.7)	1.31 (-41.3)
6.	PC	2.62	1.85 (-25.8)	1.48 (-40.5)
7.	PBB	3.12	1.41 (-52.8)	0.90 (-70.0)
8.	PEP	3.22	1.53 (-50.7)	0.93 (-70.0)
9.	PPO	3.64	2.57 (-29.5)	1.97 (-45.7)
10.	ABS	3.75	2.86 (-23.2)	2.37 (-36.3)
11.	PIP	4.12	1.08 (-68.2)	0.60 (-82.4)
12.	PSB	4.72	3.32 (-29.3)	2.76 (-41.4)
13.	SMO	4.94	3.92 (-20.8)	3.50 (-29.2)
14.	PMMA	6.24	5.26 (-15.7)	4.67 (-25.2)
15.	PU	7.08	5.07 (-25.5)	4.19 (-38.4)
16.	PSBR	7.32	3.67 (-44.3)	1.87 (-71.6)
17.	PIB	7.88	4.36 (-44.7)	2.72 (-65.5)

Time For Complete Desorption and Reuse of Sensitive Equipment After Exposure. The time required for complete desorption of all carbon dioxide from the material is important to establish the waiting time before equipment can be reused after decontamination and these values are provided in Table 4. The continuous measurement of desorption allowed the best possible estimate of the time to complete desorption since the high data densities provided robust extrapolations to the time required for the material specimen to regain its original weight. The approach to this final equilibrium can be extremely slow, however, and the continuous, high data densities combined with a Fick's Law diffusion coefficient allowed extrapolation to time axis zero-mass values. An example of a Fick's Law plot for Silicone Modified Organic (SMO) polymer is shown in the Figure. The mass has been normalized from 0 to 1 on the y-axis and the square root of time is employed on the x-axis. The Fick's Law equations for the linear portion of the initial and final desorption are shown adjacent to their respective section of the plot. The thinner line denotes the extrapolated section of the curve at both extremes of the plotted data. One can see the extrapolation to zero-time on the x-axis that defines the time-to-complete-desorption that can be used to specify the time-to-reuse for decontaminated items. The time for complete desorption is reported, followed by the Fickian diffusion equation and diffusion coefficient in the last two columns of Table 4. One can see that the methodology is capable of ranking the materials based on the time required to return to the unplasticized condition after super critical carbon dioxide exposure. For the materials studied, this period ranged from about 1 to 5 days.

TABLE 4. Time for the Complete Desorption of All Carbon Dioxide from Polymeric Materials Based on a Fick's Law Extrapolation of Low Concentration Desorption Diffusion.

No.	Polymer Codes	Time for Complete Desorption hrs (days)	Fickian Diffusion Equation: Relative Mass Fraction =	Diffusion Coefficient, cm-sq/second
1.	PEP	20.6 (0.9)	0.038 – 1.38E-4 time(1/2)	5.7250E-11
2.	PU	20.7 (0.9)	0.050 – 1.83E-4 time(1/2)	7.5549E-11
3.	PTFEP	22.4 (0.9)	0.083 – 2.92E-4 time(1/2)	1.5448E-10
4.	PBB	23.5 (1.0)	0.056 – 1.91E-4 time(1/2)	7.9684E-11
5.	PSB	24.2 (1.0)	0.042 – 1.44E-4 time(1/2)	1.4751E-10
6.	PIP	24.4 (1.0)	0.070 – 2.38E-4 time(1/2)	1.2030E-10
7.	SMO	30.3 (1.3)	0.209 – 6.33E-4 time(1/2)	2.8522E-09
8.	PIB	31.5 (1.3)	0.041 – 1.21E-4 time(1/2)	3.0844E-11
9.	PEEK	38.7 (1.6)	0.163 – 4.38E-4 time(1/2)	9.4139E-11
10.	PSBR	40.5 (1.7)	0.081 – 2.11E-4 time(1/2)	9.3694E-11
11.	ABS	42.8 (1.8)	0.124 – 3.15E-4 time(1/2)	4.8703E-10
12.	PI	46.4 (1.9)	0.363 – 8.88E-4 time(1/2)	1.1647E-10
13.	PC	57.9 (2.4)	0.119 – 2.60E-4 time(1/2)	1.1518E-10
14.	PVC	60.0 (2.5)	0.175 – 3.77E-4 time(1/2)	3.2042E-10
15.	PDMS	83.0 (3.5)	0.110 – 2.02E-4 time(1/2)	1.1404E-10
16.	PPO	111.3 (4.6)	0.124 – 1.96E-4 time(1/2)	5.9724E-11
17.	PMMA	130.1 (5.4)	0.199 – 2.90E-4 time(1/2)	1.6240E-10

Indentation Hardness. Chemical exposure often influences the surface properties of materials that are critical to there performance. Indentation hardness is one of the most important of these surface properties and the values before versus after exposure were measured and are documented in Table 5. About a third of the materials exposed to supercritical carbon dioxide showed surface hardening of about 1 to 3 %.

Another one-third experienced surface softening of over ca 1%. Note that the measurement shows the relatively low level of surface change after the plasticizing supercritical fluid had completely desorbed. The methodology was capable of ranking the materials based on these longer term indentation effects.

TABLE 5. Indentation Hardness Changes to Polymeric Materials After Exposure to Supercritical Carbon Dioxide, Followed by Complete Desorption: Exposed to 1400 psig at 50 degrees C for 15 Minutes

No.	Polymer Codes	Scale	Initial	Final	Change, %
1.	PSB	Shore D	63.6	45.8	-28.0
2.	PVC	Shore D	73.4	71.5	-2.6
3.	PMMA	Shore D	82.0	81.0	-1.2
4.	PC	Shore D	76.9	76.1	-1.0
5.	PTFEP	Shore A	91.7	91.2	-0.5
6.	PI	Shore D	82.5	82.2	-0.4
7.	PU	Shore A	96.9	97.0	0.1
8.	PEP	Shore A	93.6	93.9	0.3
9.	PPO	Shore D	76.2	76.6	0.5
10.	SMO	Shore A	58.6	58.9	0.5
11.	PEEK	Shore D	76.4	77.0	0.8
12.	ABS	Shore D	72.6	73.4	1.1
13.	PSBR	Shore A	85.8	87.1	1.5
14.	PDMS	Shore A	63.9	64.9	1.6
15.	PIB	Shore A	66.2	67.7	2.3
16.	PIP	Shore A	66.9	68.7	2.7
17.	PBB	Shore A	65.9	67.8	2.9

CONCLUSIONS

A methodology was developed and applied for evaluation of desorption diffusion of decontamination extractants such as supercritical fluids and fluorocarbons. The instrumentation and methods were capable of ranking polymeric materials based on interaction with supercritical carbon dioxide for several types of measurements. These measurements included: sorption, corrected for fraction of polymer additives extracted; sorption, corrected for extrapolation to the end of decompression; time for complete desorption to the initial weight; low-concentration diffusion coefficient; and change in surface indentation hardness.

ACKNOWLEDGEMENTS

The authors gratefully acknowledge programmatic and technical support from Mr. Brian MacIver, Mr. David Sorrick, and Dr. John Weimaster, SBCCOM.

REFERENCES

1. Shuely, Wendel J., and Ince, Brian S., Computerized TGA Method for Determination of Diffusion Coefficients for Liquids in Polymeric Materials, Presented at the 18th Annual North American Thermal Analysis Society (NATAS) Conference, CA, September 1989.
2. Shuely, Wendel J., and Ince B. S., "Thermogravimetric Method for Measurements of Equilibrium and Transport Properties Relevant to Chemical-Polymer Compatibility Evaluation" in the Proceedings of the 22nd Conference of NATAS, p 354-259, September 1993.
3. Shuely, Wendel J., "Standard Test Methodology for Measurement of Polymer Solubility, Equilibrium Sorption and Desorption Diffusion Coefficients for Hazardous Liquids," Proceedings of the Symposium on Performance of Protective Clothing: Improvement Through Innovations," J. Johnson and Z. Mansdorf, Ed., American Society for Testing and Materials, January 1994, Philadelphia, 19103.
4. Shuely, Wendel J., "Computerized Polymer Solubility Phase Diagrams and Prediction of Polymer-Liquid Interaction," in American Chemical Society Papers, COMP 95, April 1995.
5. Shuely, Wendel and Ince, Brian. Supercritical Carbon Dioxide Interaction with Polymeric Materials: Desorption Diffusion Coefficient Measurements. ECBC-TR. 2001. Unlimited Distribution Report.
6. Sawan, Samuel P., Shieh, Yeong-Tarng, Su, Jan-Hon. Evaluation of the. Interaction of Supercritical Carbon Dioxide with Polymeric Materials. Los Alamos National Laboratory Report LA-UR-94-2341. 1994.
7. Yeong-Tarng Shieh, Jan-Hou Su, Gurusamy Manivannan, Paul H. C. Lee, Samuel P. Sawan, and W. Dale Spall. Interaction of Supercritical Carbon Dioxide with Polymers. I. Crystalline Polymers. Journal of Applied Polymer Science, Vol. 59, 695-705 (1996).
8. Yeong-Tarng Shieh, Jan-Hou Su, Gurusamy Manivannan, Paul H. C. Lee, Samuel P. Sawan, and W. Dale Spall. Interaction of Supercritical Carbon Dioxide with Polymers. I. Amorphous Polymers. Journal of Applied Polymer Science, Vol. 59, 707-717 (1996).

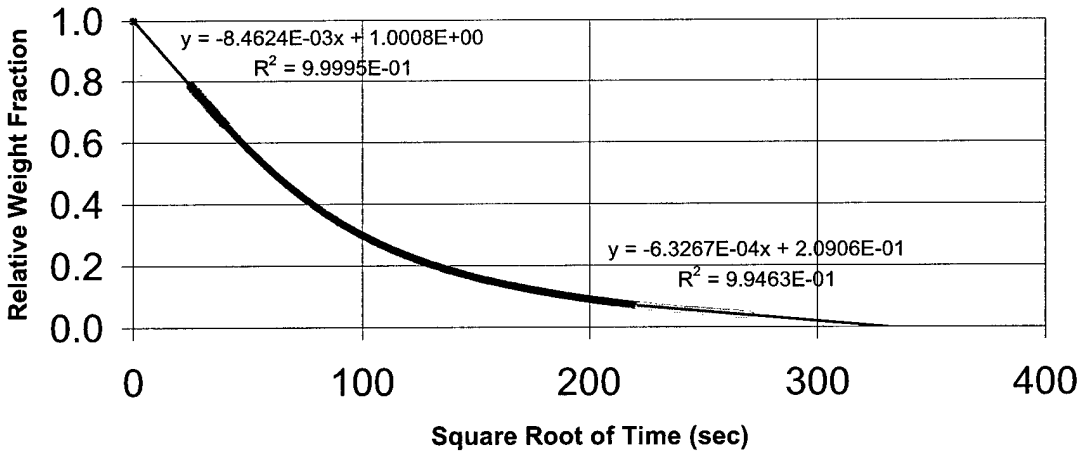

Figure. Desorption Plot for Determination of Low Concentration Diffusion Coefficient for a Fick's Law Calculation of Time-to-Complete-Desorption (Polymeric Material: SMO).

ASSESSMENT OF ENVIRONMENTALLY BENIGN DECONTAMINANT TOWARDS ANTHRAX SPORES

Vipin K. Rastogi,
GEO-Centers, Inc., Gunpowder Branch, PO Box 68, APG, MD 21010, USA

Tu-chen Cheng and Abe Turetsky*
US Army, AMSSB-RTL, ECBC, APG, MD 21010, USA

Phillip Bartram and George Wagner
US Army, AMSSB-RRT-CE, ECBC, APG, MD 21010, USA

In recent years, production and storage of CBW agents in large quantities by a number of rogue nations and extremist groups have raised the probability of their use in armed conflicts and against civilian populations around the world. While the CW agents include nerve agents, G-type and V-type, and blistering agents such as mustard gas; the BW agents include pathogenic viruses, bacterial cells, dormant spores, and protein-based toxins. The current decontaminant used by first responders and the US armed forces is not environmentally friendly. Consequently, development of alternative decontaminants is urgently needed. Three environmentally benign decontaminant formulations, two based on hydrogen peroxide and a third based on hypochlorite, have recently been developed for CW agents. We were interested in evaluating these formulations against BW agents in a quest to develop environmentally benign CBW decontaminants. In this study, these formulations were evaluated against *Bacillus anthracis* (NNRΔ1 strain) spores. While, both peroxide-based formulations resulted in a 7-log reduction in spore viability, the hypochlorite-based formulation was much less effective. These results provide support for continued efforts in a quest for the development of an environmentally benign universal CBW decontaminant.

Currently, decontaminants such as the U.S. Army's DS2, the German C8 emulsion, the British and Canadian CASCAD, the commercial Italian BX-24, the German GD-5, Sandia National Laboratory's SNLF and other NATO decontamination and experimental solutions are designed for use primarily against chemical agents. These decontaminants have also been

assessed for biological decontaminant efficacy[1] and although CASCAD and SNLF have demonstrated a significant reduction of *B. anthracis* spores and several vegetative bacterial forms, none were sufficiently efficacious to warrant further laboratory study. Although these decontaminants presented activity toward the chemical agents, none were active against all chemical agents assessed. The goal of this study is to initiate research which would contribute to development of a single effective non-corrosive environmentally benign dual use chemical and biological agent decontamination formulation, initially against all common chemical warfare agents and realistic simulants for *B. anthracis, Yersinia pestis,* and ricin bio-toxin . Strong oxidants such as halogen and oxygen donors are known to degrade both chemical and biological agents. With this property in mind, three typical formulations were prepared. The investigation was initiated by examining the decontamination properties of one calcium hypochlorite and two hydrogen peroxide based decontaminants. Hydrogen peroxide is inherently environmentally benign since its reaction product is water. Initial results are promising. In particular the hydrogen peroxide formulations demonstrated activity toward all chemical agents assessed as well as significant activity toward the three biological agents included in the study to date.

MATERIALS AND METHODS

1. PREPARATION OF SPORES:

Bacillus anthracis cells of a non-virulent strain (NNRΔ1; plasmid-free) were grown in sporulation media (Turnbull, 1999; personal communication) containing peptone, yeast extract, sodium chloride, and dextrose. The cells were seeded on the plates containing the media solidified with 1.5% Difco Bacto agar, and grown for 2-3 weeks at 28°C, until the surface was 99-100% phase bright. The spores were suspended in sterile water using a sterile spreader, and collected in sterile tubes. The spore suspension was heated at 62.5°C for 15 min, and then washed five times with sterile distilled water. Aliquots of spores (10^8-10^9/ml) were kept at 4°C.

2. "DECON GREEN" FORMULATIONS:

Three "DECON GREEN" formulations, DG1, DG2, and DG3, were prepared after Bartram (personal communication). The DG1 was prepared by first mixing sulfolane and methyl sulfolane (45% and 55%, respectively). The final formulation contained 8 parts saturated HTH, 42 parts water and 50 parts sulfolane mixture. The second formulation, DG2 contained (volume basis) 73 parts propylene carbonate plus 2 parts Triton X-100 plus 25 parts hydrogen peroxide (the stock hydrogen peroxide used was at 50% concentration) and just before mixing it was made 0.2M with respect to both potassium carbonate and potassium bicarbonate. The third formulation was prepared by first preparing the solvent mixture, 33.33 parts 2-ethyl hexanol plus 6.66 parts Triton X-100 plus 6.66 parts dodecyl pyrrolidinone plus 53.33 parts methyl pyrrolidinone. 75 parts of this solvent mixture was then mixed with 25 parts hydrogen peroxide. The hydrogen peroxide used was at 50% concentration and just before mixing, it was made 0.2M with respect to both potassium carbonate and potassium bicarbonate.

3. SPORE VIABILITY ASSAYS:

In initial experiments, freshly-prepared "DECON GREEN" formulations were spread on to nutrient agar plates, and let dry. 100 µl of spore suspension ($5x10^8$/ml) was spread evenly over

the control and test plates. Appropriately diluted spore suspension was spread to observe accurate cfu (colony-forming units). The plates were incubated at 30C for 18-36 hrs, and cfu were accurately counted.

4. TOXIN SIMULANT ASSAY:

Two protein simulants, the ricin A chain purified from native Ricin D (Inland Lab. Inc., Austin, TX) and BSA (bovine serum albumin), were used as toxin simulants. In initial experiments, the effect of hydrogen peroxide on BSA was analyzed using a spectrophotometric assay (absorbance @ 260 nm). Due to overlapping extinction bands of BSA and peroxide at 260 nm, this procedure was rejected for further use. An SDS-PAGE (sodium dodecyl sulfate-polyacrylamide gel electrophoresis) assay was used to analyze the effect of the "DECON GREEN" active ingredient on protein toxin. The gel was stained with Coomassie Brilliant Blue R-250 (0.025% R 250 prepared in 40% methanol,7% acetic acid), and destained using destaining solution (40% methanol and 7% acetic acid).

RESULTS

1. ANTHRAX SPORES:

Figure 1 shows anthrax spores as prepared by the method described in the Materials and Methods section. Over 99% of the structures in the viewing area are spores. These spores were used in the present study.

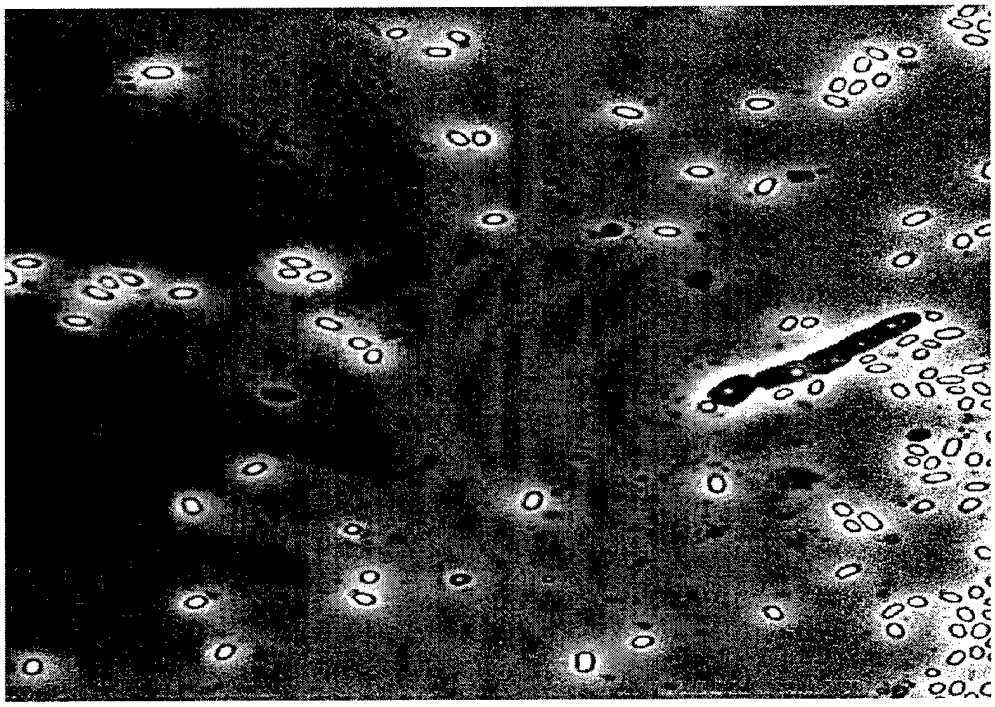

Figure 1. Anthrax Spores seen as Refractile Structures.

2. EFFICACY OF THE THREE "DECON GREEN" FORMULATIONS:

The three formulations, DG1, DG2, and DG3, were prepared as described in the Materials and Methods section. The number of cfu was determined after counting the colonies on the plates 24 hours after plating and incubation. As seen in Table 1, the DG1 formulation was ineffective as a decontaminant against anthrax spores. However, the other two formulations, DG2 and DG3, were highly effective as spore decontaminants. There were no survivors out of $2x10^7$ spores plated. These findings demonstrate that both these formulations result in a 7-log reduction of spores.

TABLE 1. Number of Anthrax Spore Survivors in the Presence of Three "DECON GREEN" Formulations.

Dilution	**Control Cells/mL**	**DG1 Cells/mL**	**DG2 Cells/mL**	**DG3 Cells/mL**
10^{-1}			0	0
10^{-3}			0	0
10^{-5}			0	0
10^{-5}	$6x10^8$	$1.1x10^8$		
10^{-6}	$2x10^8$	$1.2x10^8$		
10^{-7}	$2x10^8$			

The two formulations, DG2 and DG3 were highly effective as spore decontaminants, however, since the formulations were spread on the plates, spores were in constant contact with these chemicals. The effect of the decontaminant on viability or survival could be due to its activity on the vegetative cell resulting from germination of the spore. To resolve this question, the spores were first mixed with each the two formulations, and after overnight treatment, the spores were washed 3x with sterile saline solution. An aliquot was plated on the agar plate and the number of colonies was counted the next day. The results are summarized in Table 2. As seen in Table 2, both formulations were effective in decontaminating anthrax spores within 15 min of treatment. Since, no decontaminants were spread on the plate, the observed lack of any survivor must have resulted from the effect of these chemicals on the spore itself.

TABLE 2. Number of Anthrax Spore Survivors in the Presence of Three "DECON GREEN" Formulations.

	10^0	10^{-1}	10^{-2}	10^{-3}	10^{-4}	10^{-5}
Control	**	**	**	390, 440	43, 40	4, 3
DG2	0*	0	0	0	0	
DG3	0*	1,0	0	0	0	

* 10 million spores treated and approximately 400,000 spores plated on each plate
** TNTC, too numerous to count

3. EFFECT OF HYDROGEN PEROXIDE ON SPORE SURVIVAL:

The active component of the DG1 formulation is HTH (chlorine donor), and hydrogen peroxide is the active component in the other two formulations, DG2 and DG3. It was of interest to quantitatively determine if the active component by itself was an effective decontaminant. The active component was spread on a nutrient agar plate before plating the spores. The colonies were counted after overnight incubation. The results are summarized in Table 3. In the presence of 0.8% HTH, an approximately 10% reduction in number of cfu was observed. In contrast, presence of 12.5% peroxide resulted in complete loss of spore/vegetative cell viability.

TABLE 3. Number of Anthrax Spore Survivors in the Presence of Active Components.

	10^{-1}	10^{-2}	10^{-3}	10^{-4}	10^{-5}	10^{-6}
Background	*	*	*	*	$5.4x10^7$	$4x10^7$
HTH Test	*	*	*	$3.2x10^6$	$3x10^6$	
H_2O_2 Test	0	0	0			

* = too numerous to count accurately

An experiment was designed to observe the effect of a brief -time exposure to hydrogen peroxide on spore viability. A spore suspension ($2x10^8$/0.5ml) was mixed with hydrogen peroxide (final concentration = 6.25%), and after 25 min incubation, the spores were washed 3x with sterile water before plating. The same number ($2x10^8$/0.5 ml) of cfu was recovered in the control sample, however in the test sample, $1\text{-}2x10^4$ (a 4-log reduction) was observed in spore viability. These results are consistent with the conclusion that a brief exposure of anthrax spores to 6.25% hydrogen peroxide results in a significant reduction in spore survival.

4. EFFECT OF HYDROGEN PEROXIDE ON TOXIN SIMULANTS:

A large number of toxins, such as botulinum and ricin, are binary (require two chains for activity) and proteinaceous in nature. Ovalbumin and BSA are among the common simulants used in lieu of active toxins. In this study, we used the A chain of ricin derived from ricin D and BSA as toxin simulants. Results are displayed as an electropherogram of the proteins, comparing hydrogen peroxide treatment to that of controls.

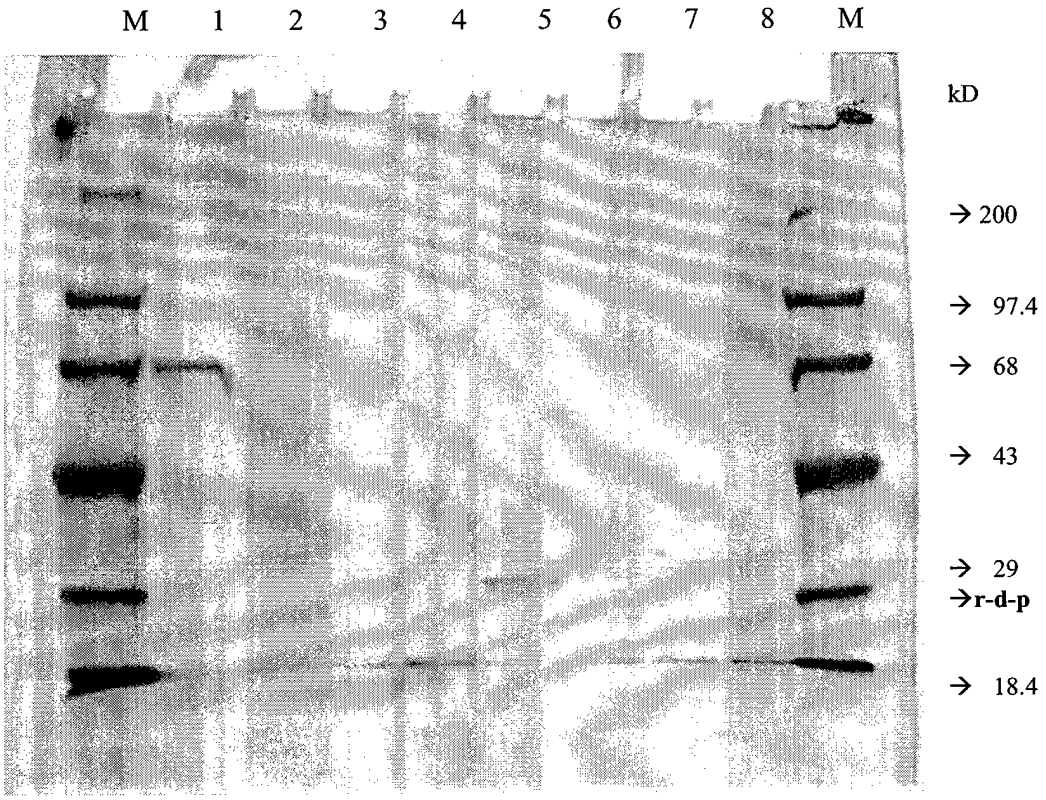

Lanea 1-4 = BSA and 5-8 = Ricin. Lanes 1,5 = control; 2,6 = 7.5% peroxide; 3,7 = 15% peroxide; 4,8 = 22.5% peroxide. Six µl sample was mixed with an equal volume of loading buffer containing SDS and heated for 10 min at 95C. The arrow (r-d-p) in the electropherogram shows the position of degradation products of the A chain of ricin D.

Figure 2. Effect of Varying Concentration of Hydrogen Peroxide on Protein Toxin Surrogate BSA and the A chain of ricin D.

CONCLUSIONS

In conclusion, the present study demonstrates:

1. Of the three DECON GREEN formulations, the two formulations based on hydrogen peroxide are very effective decontaminants;
2. The active component, hydrogen peroxide, itself brought about a 4-log reduction in spore number;
3. Hydrogen peroxide, was effective against the protein toxin simulants BSA and the ricin A chain.

REFERENCES

1. Lee, Fred K. and Turetsky, Abe L. Internal report, The Evaluation of Eight Candidate Decontamination Formulations for the Joint Services Fixed Site Decontamination System on Simulants of Potential Biological Warfare Agents. December, 2000.

Microarray Bactericidal Testing of Natural Products Against *Yersinia intermedia* and *Bacillus anthracis*

I.J. Fry[1], F.K. Lee[2], A. Turetsky[2] and J.J. DeFrank[2]

[1]GEO-CENTERS, Inc.
[2]U.S. Army Chemical and Biological Center
Gunpowder, Maryland

ABSTRACT

To address the Defense Department's need for safe, effective protection against biological warfare agents (BWA's), natural products with a historical record of bactericidal efficacy such as bacteriocins, biosurfactants, lytic enzymes and essential oils or their active components were tested against non-pathogenic *Bacillus anthracis* and the plague pathogen surrogate *Yersinia intermedia.* Unlike the traditional well diffusion or spot lawn tests, the microplate/microarray test method used in these studies greatly simplified screening and interpretations of dose-response testing of the natural compounds as it relates to decontamination applications. Growth of treated cultures was measured turbidometrically with a microplate reader. Dose-reponse plots were made from the resulting turbidometric data to assess bactericidal efficacy of the test compounds. Several natural compounds were found effective against *Yersinia* and *B. anthracis* cells and spores using this method. These results show the promise of natural compounds in the development of environmentally responsible BWA decontamination preparations.

INTRODUCTION

The US Department of Defense recognizes the threat of biological warfare agents (BWA's) as a weapon of mass destruction from foreign military powers and terrorists. Although the chemical warfare agent (CWA) decontamination solution 2 (DS2) is also an effective bactericide, it is corrosive and it's use produces hazardous waste. As the DoD is concerned with the environmental impact of decontaminants for fixed site and large area applications, decontamination solutions with an adverse effect on the environment are less desirable so alternatives were sought.

Microbial chemical agent decontaminating enzymes such as Organophosphorus Acid Anhydrolase (OPAA) and Organophosphorus Hydrolase (OPH) are good alternatives to DS2 for nerve agent decontamination, but they lack bactericidal activity. Inclusion of a bactericide to these enzymes for an anti-CWA/BWA preparation would require chemicals with little effect on enzyme activity or the environment.

Several natural products are effective bactericides and have low environmental impact, making them good candidates as biological decontaminants. Among these are the bacteriocins, essential oils and biosurfactants.

Bacteriocins are anti-microbial polypeptides that are bactericidal to non-host bacteria. Some bacteriocins have chacteristics that make them desirable biological decontaminants, such as resistance to proteolytic degradation, heat stability and a wide target range. Commercially available Nisin, from *Lactococcus lactis*, has these characteristics and in addition is a FDA GRAS food additive.

Plant essential oils (e.g. oil of cloves, eucalyptus, etc) are attractive as BWA bactericides because of their historical use in the preservation of food, embalming and medicine. These oils and their active components (AC's) are also commercially available. As the bacteriocins from the lactic acid bacteria were more noted for their effectiveness with gram positive bacteria than gram negative bacteria, we also included the active components of plant essential oils in our decontamination studies for the Yersinia in addition to *Bacillus anthracis.*

Biosurfactants are detergent compounds produced from biological sources. Microbial surfactants are harvested as secondary metabolites from bacteria such as *Pseudomonas, Acinetobacter, Arthrobacter*. Although the role of these compounds is usually associated with mobilization of hydrophobic nutritional sources, some of them are bactericidal to non-producer bacteria. Because the rhamnolipid microbial surfactant from *Pseudomonas aeruginosa* is a bactericide for *Bacillus subtilis* with low human toxicity, we also included it in our screening procedures.

Catalytic biodegradation agents such as the enzymes lysozyme and lysostaphin effect the structural integrity of many bacterial cells. Because of this property, these potential bactericides were also included in our studies.

Although procedures to quantitate the effects of bactericides were in place (e.g. spot lawn, well diffusion, sensidisks, tube and plate culture etc.), these methods were cumbersome for our BWA decontamination studies. We needed to know what concentration of bactericide (e.g. wt/vol or M) in aqueous media was needed to kill a given population of BWA at a designated growth stage. We also had to compare our results with natural product bactericides against results obtained with the harsh chemical agent decontaminants slated for replacement with more innocuous materials. A microarray/microplate testing method was devised to test the susceptibility of non-pathogenic *Bacillus anthracis* cells and spores and the plague pathogen surrogate, *Yersinia intermedia* to Natural products.

MATERIALS AND METHODS

Strains and Culturing Methods: Bacterial test strains are listed in Table 1. Isolation medium for the Lactococcus and Lactobacilli derived from cheese and buttermilk was TYM at either pH 5.5 or 7 incubated at either 37°C or 30°C. Growth medium for bacteriocin isolation was Lactobacillus MRS Broth. Nutrient broth was used as the test medium at 37° for *B. anthracis* and 30°C for *Y. intermedia* unless otherwise indicated (Brain Heart Infusion Broth and Turnbull' sporulation medium). Overnight cultures of *B. anthracis* were grown for 20 h prior to inoculation in the microplates. The ON or spore inoculua were used routinely as they provided the most rigorous antimicrobial test matrices. Vegetative cultures of of *B. anthracis* or *Y. intermedia* were obtained from an early-log culture (A600= 0.2). *B. anthracis* spores originated from frozen spore stocks, and diluted to 10^7spores/ml in the test wells with growth medium.

TABLE 1
Test Strains of *Bacillus anthracis, Yersinia intermedia*
and Lactic Acid Bacterial Food Isolates

Strain	Strain
Yersinia intermedia ATCC 33647	*Bacillus anthracis* NNR1-Δ 1
Bacillus anthracis ΔAmes	*Bacillus anthracis* VNR1-Δ 1
Bacillus anthracis ΔSterne	LJ (LAB cheese isolate)
Bacillus anthracis ΔNH-1	UB (LAB cheese isolate)

Isolation of the LJ and UB LAB isolate Bacteriocins: Bacteriocins were obtained from a one liter culture of each organism using the cell elution method of Yang, et al.[1].

Microarray testing: All microplates were read with a Bio-Tek 340i microplate reader. All assays were performed in duplicate with replicate negative and positive controls. All the outside wells on the plates were filled with uninoculated medium to provide an evaporation barrier for the test wells. Plant essential oils active components (AC's) were diluted with ethanol from a 0.1 M stock to make final concentrations of

10 mM to 10 µM in the wells. The ethanol was evaporated from the plates in a Biosafety cabinet before medium or inoculum addition. Biosurfactants were either diluted in water and filter sterilized before use, or diluted in isopropanol and dispensed. The isopropanol was evaporated from the plates in a biosafety cabinet overnight before inoculation. AC's tested and their sources are shown in Table 2.

Table 2
Active Components of Essential Oils Tested against
B. anthracis and *Y. intermedia* in Microarray Format

AC	Plant Source	AC	Plant Source
Cineole	*Eucalyptus globulus*	Carvacrol	Oregano (*Origanum vulgaris*)
Estragole	Tarragon(*Artemisia Dranunculus)*	Thymol	Thyme (*Thymus vulgaris*)
Linalool	Lavender(*Lavendula officianalus)*	Eugenol	Cloves (*Eugenia carophyllata*)
Linalyl acetate	Lavender(*Lavendula officianalus*)	Terpenin-4-ol	Tea Tree (*Melaleuca alternifolia)*

Stock solutions of Lysozyme and Lysostaphin (Sigma Chemical) were filter sterilized and prior to dilution (1 mg/ml to 0.5 µg/ml final) with culture medium in the microplate wells. Nisin (Sigma Chemical), 1 mg/ml (Nisin), was sterile filtered and diluted in growth medium to a final concentration (in the well) ranging from from 1 mg/ml to 1 pg/ml. Bacterial inoculua were added last to initiate the test (zero time). Untreated wells were also included on all microplates, and the turbidity in these wells (after the blank correction) used to calculate % growth treated/untreated data that is presented in the dose-response plots. Turbidity readings were taken at 630 nm periodically (15 min to hour intervals) and after overnight incubation. For compounds producing aqueous emulsions (e.g. biosurfactants), a set of uninoculated controls was run concurrently and these turbidity values subtracted from the inoculated+test compound turbidity readings. Real time data for single microplates used microplate lids treated with sterile diluted and dried antifog to prevent fogging. The incubation temperature was 37°C. The reader was programmed to shake at low speed for 10 seconds prior to each read for real time monitoring.

Micrographs: The effects of Nisin at varying concentrations on the Bacilli after ON incubation was captured with an Olympus BX-50 Phase Contrast Microscope at 1000X on Kodak 400 ASA Gold Film. Photos were scanned and exported to MS Power Point.

RESULTS

Testing candidate BWA decontaminants in microarrays proved a convenient and rapid method to gather viability data on treated bacteria. Because the wells hold less liquid than the culture tubes (0.2 ml vs. 5 ml), the amounts of biological waste and treatment candidates were greatly reduced. Several hundred assays could be run simultaneously using this method. However, many technical refinements were needed to obtain consistent results.

Technical issues:

Lid fogging: Solved with sterile antifog to plate lids or incubating plates in a plate incubator, then heating the lids prior to reading. Other solutions are a plate reader that heats evenly or a warm room for all operations.

The one plate/reader limit: Incubate plates in a plate incubator; remove plates periodically to read them.

Uniform culture distribution: Critical for non-motile *B. anthracis*-solved with a rotating platform in the plate incubator during the incubation period. *Y. intermedia* was not as problematic, as it is motile.
Evaporation: Solved by adding uninoculated and untreated media to "barrier wells" in all the outside wells.
AC vapor migration: Minimized with barrier wells between rows of different AC's.
Addition of Matrix components: Solved with 12 well reservoirs.
Insoluble (turbid) anti-BWA components: Not suited to turbidometric analysis in microplates or tubes: plate counts are more reliable. Reasonable compensation for the emulsion's contribution to the total optical density can be obtained by running a set of treated, but uninoculated wells concurrently with the treated and inoculated wells. The data obtained from the unioculated set is subtracted from the total optical density reading to obtain turbidity produced by the growing cells.
Data reduction: Export data to a communications program (e.g. MS hyperterminal) then to Spreadsheet program (Excel, Quattro Pro, etc.). Better solution: acquire the appropriate reader software.

Findings

Several natural compounds gave excellent bactericidal activity against the test BWA's. The Minimum Inhibitory Concentrations (MIC) was the concentration of treatment agent in aqueous medium that prevents culture growth. Nisin and preparations of LJ and UB lactic acid bacterial isolates all showed good activity against *B. anthracis* at low concentrations (Figure 1, Table 3). Only the AC's thymol, eugenol and carvacrol were effective against both *B. anthracis* and *Y. intermedia* (Figures 2, 3, 7, Table 4). None of the biosurfactants tested were effective against *Y. intermedia*, but the Petrogen, Battelle and Janeil biosurfactants were effective against *B. anthracis* (Table 5). The highly purified Janeil biosurfactant (99% rhamnolipid) was the most effective (Figure 9), and also formed transparent solutions (no emulsion) at all but the highest concentration tested. Lack of an emulsion greatly simplified data reduction and results interpretation. The enzymes lysozyme and lysostaphin were not effective against *B. anthracis* or *Y. intermedia* cells at any concentration.

Table 3
Minimum Inhibitory Concentration of Bacteriocin Needed
for the Several *Bacillus anthracis* Strains

Strain	MIC, µg/ml, for ON zero growth
ΔAmes	600*
ΔSterne	1000*
ΔNH-1	850*, 50**, 850***
NNR1-Δ 1	950*
VNR1-Δ 1	1000*

*Nisin, using overnight cultures as the inoculum.
**LJ preparation (ref. 1), using spores as inoculum.
***UB preparation (ref. 1), using spores as inoculum.

Table 4

Minimum Inhibitory Concentration of the Active Component of Essential Oils needed for an Overnight Inocula of *B. anthracis* VNR1-Δ1 and *Y. intermedia*

Active component	MIC (mM) B.A.	MIC (mM) Y.I.
Carvacrol	1.2	1.0
Thymol	0.3	3.5
Eugenol	2.5	4.5

Table 5

Bactericidal Testing of Biosurfactants with *Bacillus anthracis* ΔNH-1

Biosurfactant*	MIC, µg/ml, for ON zero growth
Janeil (*P. aeruginosa*)	100 (spores)
Petrogen (*P. aeruginosa*)	100 (spores), 10 (cells)
Battelle (unknown)	500 (cells)
ML2 or ML3 (*P. aureofasciens*)	Not effective (600 to 0.6 µg/ml)

* The rhamnolipid purity of the Janeil biosurfactant was 99%. The surfactant content for the Petrogen or Battelle surfactants was not provided.

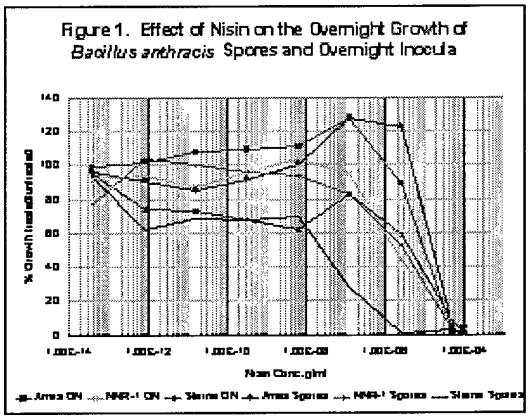

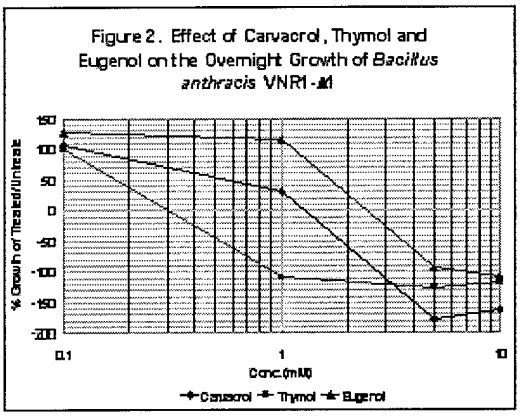

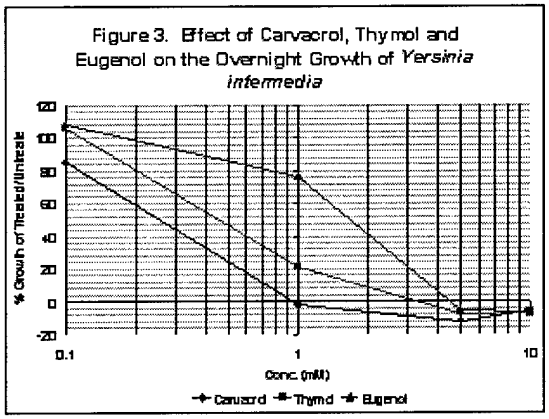

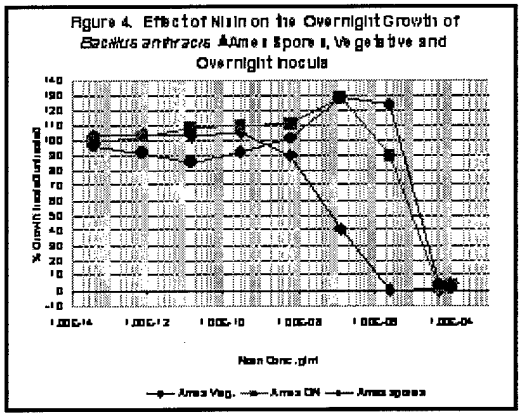

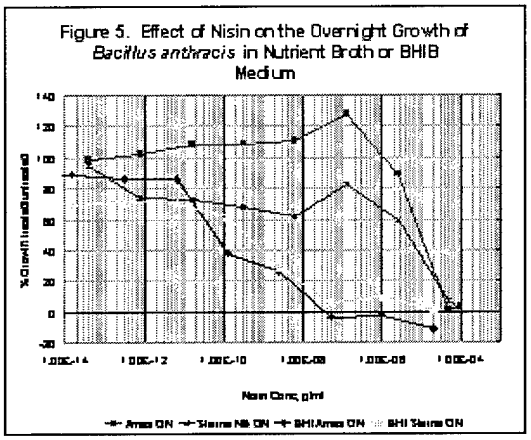

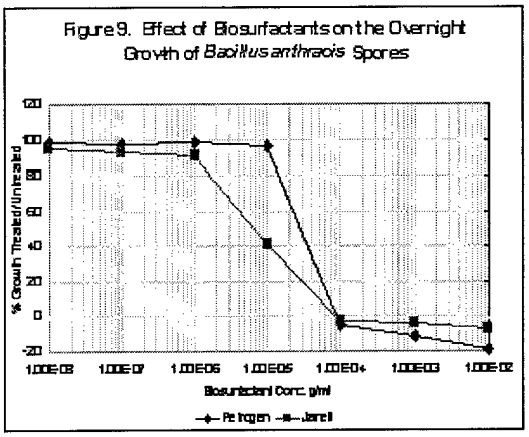

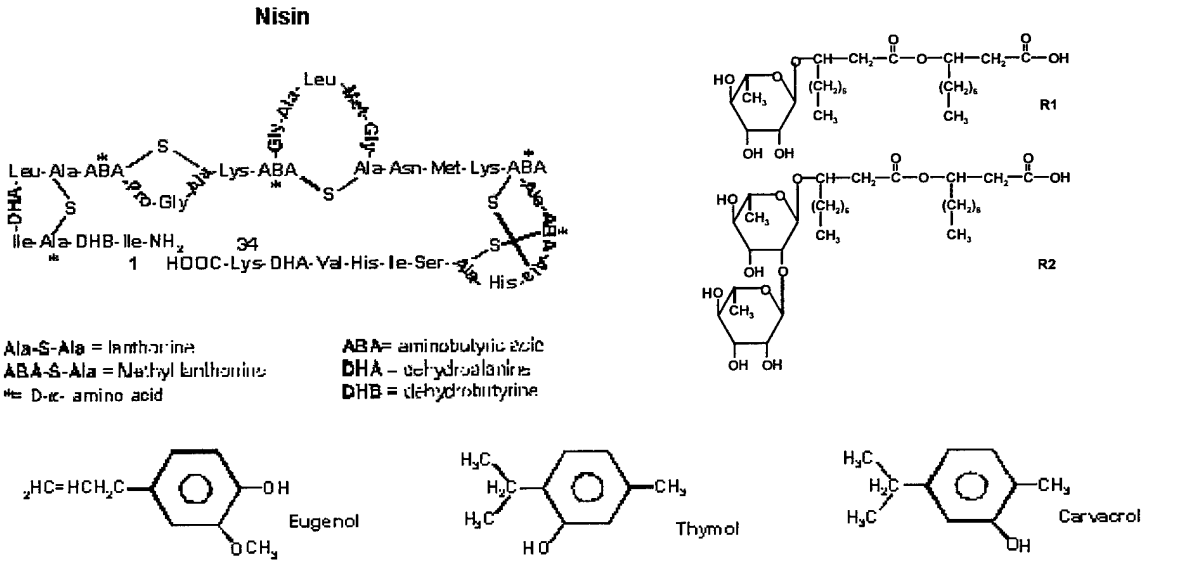

Figure 7. Natural Product Biological Decontaminants. R1 & R2 are the *Pseudomonas aeruginosa* biosurfactants. Nisin is the bacteriocin from *Lactococcus lactis*[3]. Eugenol, Thymol and Carvacrol are essential oils active components (ACs).

Comparative testing between different growth stages of *Bacillus anthracis* showed that exponentially growing cells are the most vulnerable to Nisin, followed by either overnight cultures or spores (Figure 4). Many investigators use BHI as a growth medium for anti-microbial testing of the Bacilli. We learned from our early studies that sporulation of *B. anthracis* is inhibited by BHI, and therefore more susceptible to growth inhibition and lysis by Nisin than those tested on Nutrient Broth (Figure 5). The best results were obtained with Turnbull's sporulation medium, which gave excellent growth and also supported good sporulation.

There was considerable strain to strain variation in the susceptibility of the Bacilli to Nisin over the concentration range tested, but the growth of all strains (including the spores) was prevented at 1 mg/ml Nisin (Figure 1). It was also observed that cell lysis of the inoculum occurred at these higher concentrations (negative zero% treated/untreated values). Microscopic observations also

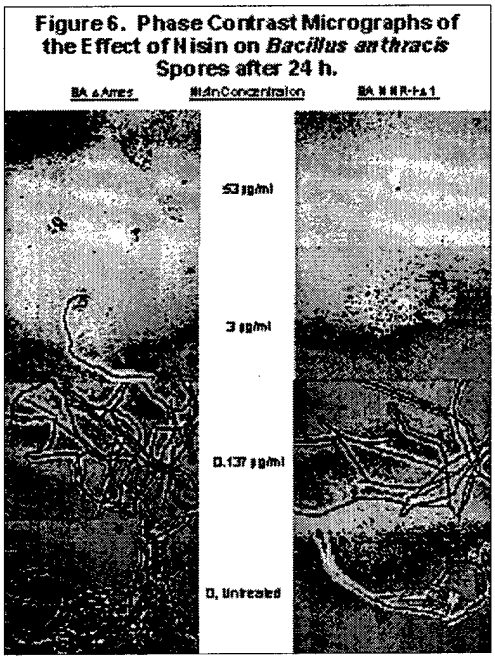

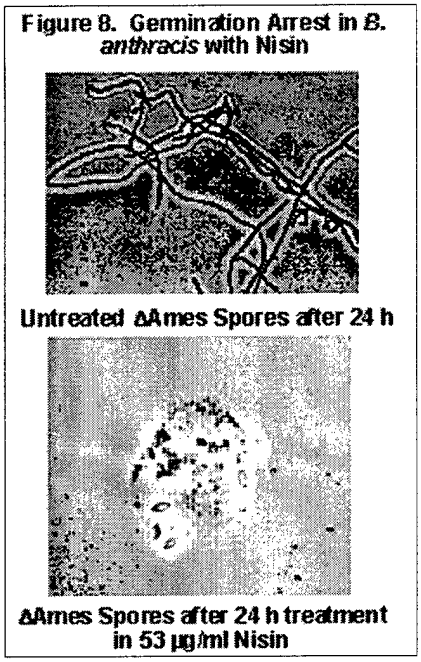

confirmed cellular lysis and indicated that the spores met the same end (Figure 6). At lower Nisin concentrations, the spores were "arrested" during germination (refractile football shapes in the Figure 8 micrographs). Some of the dose/response plots show an increased level of growth at lower Nisin concentrations for spores or ON cultures (Fig. 1, 4). We speculate that lower Nisin concentrations may in fact speed the spore germination process, as pretreatment of the spores with hot water is done by some investigators to get the same effect.

CONCLUSIONS

Microarray viability testing is an expedient method of testing a large number of samples with careful handling. Data obtained from these studies was comparable to that obtained with the spot lawn assay.

1. Data obtained from these testing methods indicates that the bacteriocins from some Lactic Acid bacteria are lethal to spores, vegetative and sporulating *B. anthracis* at low concentrations (1 mg/ml or less). These bacterocins were not effective against *Y. intermedia*, *Y. ruckeri* or *Y. rhodei* (spot lawn).

2. The active components of some essential oils (Thymol, Eugenol and Carvacrol) were also very good bactericides on both *B. anthracis* (MIC=0.3-2.5 mM) and *Y. intermedia* (1-4.5 mM). The observed MIC for carvacrol and *B. anthracis* (1.5 mM) is very close to that determined for *B. cereus*[2] (3 mM).

3. Commercial preparations of the Microbial surfactants of *Pseudomonas aeruginosa* were effective sporicides (MIC 100 μg/ml) and bactericides (MIC 10 μg/ml) for *B. anthracis*, but ineffective against *Y. intermedia* at the concentrations tested (10 mg/ml to 10 μg/ml).

4. This method has was used to test the anti-BWA activity of current chemical agent decontamination solutions by the DoD. MIC values for these chemicals ranged from 62 μg/ml to 125 mg/ml [4].

REFERENCES

1. R. Yang, M.C. Johnson and B. Ray. 1992. Novel Method to Extract Large Amounts of Bacteriocins from Lactic Acid Bacteria. Appl. Environ. Microbiol. 58: 3355-3359.
2. A. Ultee, L.G. Gorris and E.J. Smid. 1998. Bactericidal Activity of Carvacrol towards the Food-borne Pathogen *Bacillus cereus*. J. Appl. Microbiol. 85: 211-218.
3. T. J. Montville and K. Winkowski. 1997. Biologically Based Preservation Systems and Probiotic Bacteria. In Food Microbiology: Fundamentals and Frontiers. M. P. Doyle, L.R. Beuchat and T.J. Montville, Eds. ASM Press, Washington D.C.
4. F.K. Lee and A.L. Turetsky. October, 2000. The Evaluation of Eight Candidate Decontamination Formulations for the Joint Services Fixed Site Decontaminaion System on Simulants of Potential Biological Warfare Agents. ECBC report.

METHYLPHOSPHONOFLUORIDIC ACID
A THERMAL DEGRADATION PRODUCT OF SOME NERVE AGENTS

Michael D. Crenshaw
Battelle Memorial Institute
Columbus, Ohio

ABSTRACT

The nerve agent sarin (isopropyl methylphosphonofluoridate) thermally breaks down to form methylphosphonofluoridic acid and propylene. The thermal breakdown of soman (pinacolyl methylphosphonofluoridate) probably forms methylphosphonofluoridic acid as well. Continued high temperature treatment such as that of an incinerator would continue the breakdown process. In order to prove that no methylphosphonofluoridic acid is produced, an analytical standard is required. Methylphosphonofluoridic acid was produced by disproportionation of methylphosphonic difluoride with methylphosphonic acid. However, to obtain methylphosphonofluoridic acid in high purity, modifications to its preparation were required. First, a suitable laboratory preparation of methylphosphonic difluoride containing as little methylphosphonic dichloride or methylphosphonic chloride fluoride as possible was required. Several modifications to the reaction of methylphosphonic dichloride with sodium fluoride to yield methylphosphonic difluoride were pursued with good results. Ultimately, the reaction of methylphosphonic dichloride with sodium hexafluorosilicate proved to be the most convenient. Using the methylphosphonic difluoride produced in this way, its reaction with methylphosphonic acid required prolonged heating in a sealed tube to produce methylphosphonofluoridic acid.

INTRODUCTION

The US stockpile of chemical weapons includes the nerve agents sarin (isopropyl methylphosphonofluoridate, GB), *S*-(2-(diisopropylamino)ethyl) ethyl methylphosphonothioate (VX) and mustard gas (HD). The US Army must destroy its stockpile of chemical weapons to be in compliance with the Chemical Weapons Convention. Currently, incineration is being used to destroy the chemical weapons at Johnston Atoll and Tooele, UT. Liquid agent is treated first at 1400 °C, and the gases generated are then treated at 1200 °C in an afterburner.[1]

Sarin is known to thermally decompose to yield methylphosphonofluoridic acid and propylene at temperatures greater than 160 °C (Equation 1).[2-4] Continued high temperature incineration will further decompose the methylphosphonofluoridic acid. Complete combustion would yield carbon dioxide, phosphate (P_2O_5), water, and hydrogen fluoride. In order to support analysis of the incineration process, a chemical standard of methylphosphonofluoridic acid is required. Methylphosphonofluoridic acid has been prepared by the controlled thermal degradation of sarin or the disproportionation reaction between methylphosphonic difluoride and methylphosphonic acid (see Equation 2).[2,5] The disproportionation reaction was selected as the method for preparing methylphosphonofluoridic acid. In order to have methylphosphonofluoridic acid of suitable quality as an analytical standard, it was thought that high

quality precursors would be required. The purity of the commercial grade methylphosphonic acid was thought to be sufficient; however, methylphosphonic difluoride would require synthesis and purification. Also discussed here is the author's experience over the past decade with the solvent-less laboratory-scale (5-15 g) preparation of methylphosphonic difluoride and methylphosphonofluoridic acid.

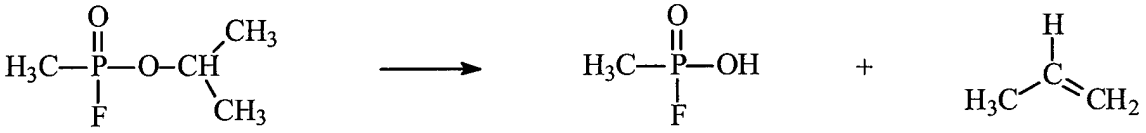

Equation 1. Thermal decomposition of sarin to yield methylphosphonofluoridic acid and propylene.

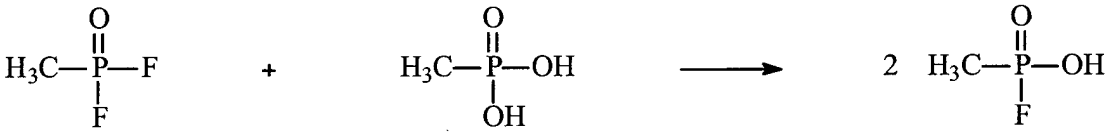

Equation 2. Disproportionation reaction of methylphosphonic difluoride with methylphosphonic acid to yield methylphosphonofluoridic acid.

RESULTS AND DISCUSSION

Previous syntheses of methylphosphonic difluoride from methylphosphonic dichloride and sodium fluoride without solvent were met with varying degrees of success. Methylphosphonic dichloride and methylphosphonic chloride fluoride were the usual impurities and sometimes were the major products. The published method calls for further treatment of the unreacted methylphosphonic dichloride and intermediate methylphosphonic chloride fluoride with sodium fluoride.[6] The presence of methylphosphonic dichloride in the methylphosphonic difluoride can lead to methylphosphonic chloride fluoride.[7] At the time this work was performed, it seemed that older sodium fluoride worked better than more recently purchased sodium fluoride. Though insufficient work was done to verify this explanation, it is possible that the older NaF powder contained enough moisture to hydrolyze a very small portion of the methylphosphonic dichloride to produce HCl which in turn produced HF and that this HF catalyzed the reaction. It is known that HF will convert methylphosphonic dichloride to methylphosphonic difluoride.[8] Variations of the reaction with sodium fluoride were also pursued. The addition of zinc(II) fluoride, cobalt(III) fluoride, or mercury(II) fluoride to the sodium fluoride in the method described above at a rate of 15-35% (wt/wt) did improve the yield of methylphosphonic difluoride. However, the addition of these heavy metal fluorides, especially mercury, can compound the waste disposal problem. When ZnF_2 was added to the sodium fluoride at 5% (wt/wt), no difference was observed compared to those reactions with no ZnF_2. An alternative was sought. Zinc(II) fluoride, antimony(III) fluoride, and arsenic(III) fluoride have each been used to convert phosphorus dichlorides to phosphorus difluorides.[9-12] A potential problem with the use of SbF_3 is the contamination of the product with $SbCl_3$.

In 1961, the use of sodium hexafluorosilicate to prepare phenylphosphonic difluoride from phenylphosphonic dichloride was published.[13] The by-products of the reaction with sodium hexafluorosilicate are sodium chloride and gaseous silicon tetrafluoride. Because of the extreme volatility or non-volatility of these by-products, this method seemed promising. Using this reagent, a yield of 88% and a purity of >98% were obtained. Since this work began, Farooq has published the use of sodium hexafluorosilicate, sodium tetrafluoroborate, and sodium hexafluorophosphate to prepare a variety of

phosphorus fluorides from the corresponding chlorides.[14-16] The disproportionation reaction of methylphosphonic difluoride with methylphosphonic acid was performed as described.[5] However, it was found that a much longer duration was required. During distillation, some decomposition occurred. One reference states the boiling point of methylphosphonofluoridic acid to be 69-72 °C at 2 mm. A significantly higher boiling point was observed in this work (90 °C/2.0 mm and 60 °C/0.2 mm).

EXPERIMENTAL

Reaction of methylphosphonic dichloride with sodium fluoride and zinc, cobalt, or mercury fluoride. Fifteen grams of methylphosphonic dichloride was added in portions to a mixture of 3 to 3.5 molar equivalents of sodium fluoride containing 15-35 wt/wt percent of ZnF_2, CoF_3, or HgF_2 at room temperature under an inert atmosphere. Some fumes were generated during the addition. The mixture was heated slowly, requiring about 2 hours to reach 110 °C. The reaction was maintained at 110 °C for an additional hour and then the temperature was raised to 120 °C and the distillate of methylphosphonic difluoride collected. Yields ranged from 86 to 91%.

Reaction of methylphosphonic dichloride with sodium hexafluorosilicate. Ten grams of methylphosphonic dichloride was mixed with 1.3 molar equivalents of sodium hexafluorosilicate. The reaction mixture was slowly heated to 110 °C under an inert atmosphere over 3 hours. A gas began forming when the reaction temperature was 85 °C. Distillation gave 6.62 grams (88%) of methylphosphonic difluoride (bp 98 °C)[lit.[6] bp 97-100 °C]. ^{1}H-NMR (300 MHz, $CDCl_3$) 1.90 ppm (dt, $J_{H\text{-}P}$ = 19.2 Hz, $J_{H\text{-}F}$ = 5.80 Hz) (see Figure 1).

Preparation of methylphosphonofluoridic acid. Methylphosphonic difluoride (3.5 grams) and methylphosphonic acid (3.3 grams) were heated to 120 °C in a sealed tube for 64 hours. Distillation gave 3.9 grams (58% yield) of methylphosphonofluoridic acid (bp 60 °C/0.2 mm)[lit.[5] bp 48 °C/0.15 mm]. ^{1}H-NMR (300 MHz, $CDCl_3$) 12.975 ppm (s, 1H), 1.670 ppm (dd, 3H, $J_{H\text{-}P}$ = 18.9 Hz, $J_{H\text{-}F}$ = 6.10 Hz) (see Figure 2). When the reaction time was 48 hours, the yield was 49%.

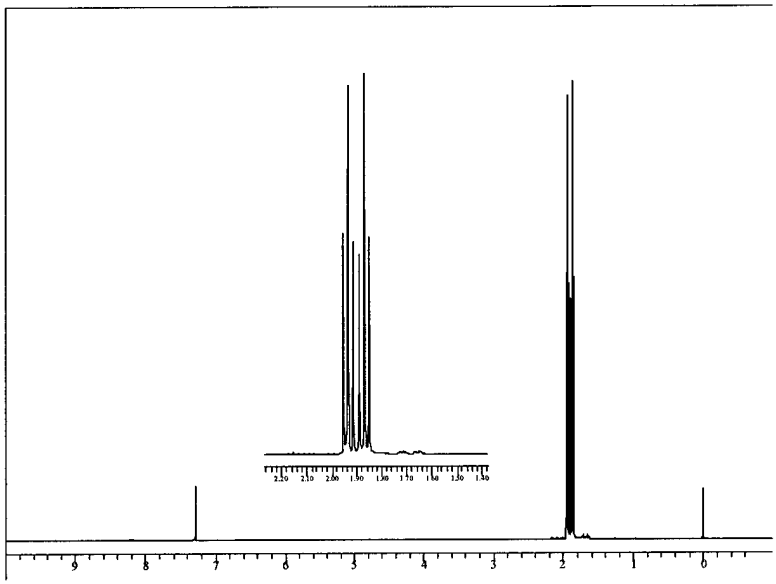

Figure 1. ^{1}H-NMR Spectrum of Methylphosphonic Difluoride.

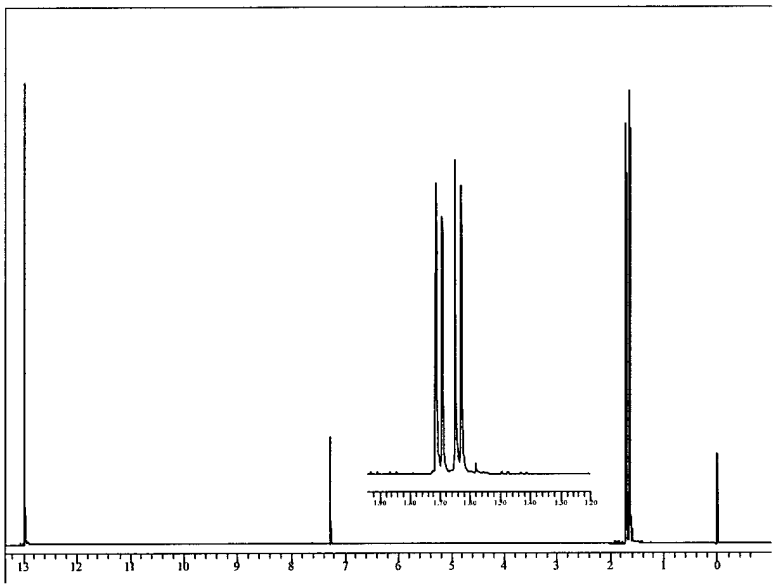

Figure 2. ^{1}H-NMR Spectrum of Methylphosphonofluoridic Acid.

CONCLUSIONS

A convenient synthesis of methylphosphonofluoridic acid was performed without using a toxic chemical warfare agent as the starting material. Methylphosphonofluoridic acid was prepared by the prolonged reaction of methylphosphonic difluoride with methylphosphonic acid. Distillation of the methylphosphonofluoridic acid provided a material suitable for use as an analytical standard. Variations of the reaction of methylphosphonic dichloride with sodium fluoride improved the yield and purity of methylphosphonic difluoride but sodium hexafluorosilicate was found to be the more convenient reagent for this conversion. None of these reactions required a solvent which could complicate the purification of these chemicals and possibly contaminate the product.

REFERENCES

1. F. C. Gouldin and E. M. Fisher, "Incineration and Thermal Treatment of Chemical Agents and Chemical Weapons," Emerging Technologies in Hazardous Waste Management 7 [Proc. I&EC Div. ACS Sympos.] 1996 (Pub. 1997), 33-47.
2. F. W. Hoffman and A. M. Reeves, "Organic Phosphorus Compounds. VII. The Preparation of Methylphosphonic Chlorofluoride," J. Org. Chem. 1961, 26, 3040-3041.
3. R. W. Baier and S. W. Weller, "Catalytic and Thermal Decomposition of Isopropyl Methyl Fluorophosphonate," I&EC, Proc. Des. Develop. 1967, 6, 380-385.
4. G. D. Sides, R. B. Spafford, and M. D. Howard, "Literature Review of Thermal Decomposition Studies of the Agents GB, VX, and HD," Proc. of the US Army CRDEC 1984 Sci. Conf. on Chemical Defense Research.
5. R. Bender, C. Demay, J.-C. Elkaim, and J. G. Riess, "Synthesis of Fluorophosphonic Acids by Redistribution of Fluorine Atoms and Hydroxy Groups on Phosphonic Moieties," Phosphorus 1974, 4, 183-186.

6. C. Monard and Jean Quinchon, "Preparation et Caracteristiques Physiques du Methylfluorophosphonate d'Isopropyle. I. Preparation et Caracteristiques Physiques de deux Echantillons de Produit pur Etalon," Bull. Soc. Chim. Fr. 1961, 1084-1086.
7. J. G. Riess and R. Bender, "Les Reactions de Redistribution dans les Composes Fluorophosphores. I. Redistribution du Substituant Fluor avec les Substituants Chlore, Brome, Thiocyanate, Methoxy et Dimethylamino dans les Derives Phosphoryles," Bull. Soc. Chim. France 1972, 3700-3708.
8. P. J. R. Bryant, A. H. Ford-Moore, B. J. Perry, A. W. H. Wardrop, and T. F. Watkins, "The Preparation and Physical Properties of Isopropyl Methylphosphonofluoridate Sarin)," J. Chem. Soc. 1960, 1553-1555.
9. L. M. Yagupol'skii and Zh. M. Ivanova, "p-Trifluoromethylphenyltetrafluorophosphorus and its Derivatives," Zh. Obshchei Khim. 1960, 30, 4026-30 (Chem. Abstr. 55: 22196c).
10. R. Schmutzler, "Phosphorus-Fluorine Chemistry. Part VIII. Some Comments on the "Group Shift Theory," as Applied to the ^{31}P Nuclear Magnetic Resonance Spectra of Certain Phosphorus Fluorides," J. Chem. Soc. 4551 (1964).
11. E. Fluck and N. Seng, "Anisotropic-Effekt in Acetylenyl-Phosphor-Verbindungen Darstellung von Acetylenylphosphonsaure-difluoriden," Z. Anorg. Allg. Chem. 1972, 393, 126-130.
12. M. Fild and H.-P. Rieck, "Reaktion von (Dichlorophosphinyl)methansulfonyl chlorid," Chem. Ber. 113, 142 (1980).
13. V. Gutmann, P. Heilmayer, and K. Utvary, "Phenylphosphoroxydifluorid," Monatsh. Chem. 1961, 92, 196-198.
14. O. Farooq, "Fluorination of Organodichlorophosphorus Compounds with Sodium Hexafluorosilicate, Part 1," J. Chem. Soc. Perkin Trans. 1, 1998, 839-840.
15. O. Farooq, "Fluorination of Organochlorophosphorus Compounds with Alkali Metal Salts of Perfluorinated Complex Anions. Part 2," New J. Chem. 2000, 24, 81-84.
16. O. Farooq, "Fluorination of Organo-dichlorophosphorus Compounds with Alkali Metal Salts of Perfluorinated Complex Anions – Part 3," Inorganica Chimica Acta 2000, 303, 124-127.

SYNTHESIS AND CHARACTERIZATION OF A NEW GENRE OF CS-COMPOUNDS

S. Munavalli[1], D. K. Rohrbaugh[2], G. W. Wagner[2], F. R. Longo[1], B. Black[1] and H. D. Durst[2]

[1]Geo-Centers, Inc., P. O. Box 68, Gunpowder Branch, APG, MD 21010 and [2]U. S. Army Edgewood Chemical Biological Center, APG, MD 21010

ABSTRACT

Three groups of organic compounds are currently being used as riot control and crowd management agents. Included in these three groups are: ω–chloroacetophenones (CN), benzylidene malononitriles (CS) and dibenzo-oxazepines (OR) (Fig. 1). o-Chlorobenzylidene malononitrile (1) is the most popularly used non-lethal agent in riot control situations and military exercises. Since this compound contains chlorine, it is not environmentally safe. With a view to improve its properties and enhance its effectiveness, a new group of CS compounds containing fluorine have been synthesized using micro-wave exposure and new inorganic catalysts in neat reactions. The synthesis and characterization of a novel group of CS compounds are described herein.

INTRODUCTION

Since World War I, three groups of organic compounds namely (**CN**, **CS** and **OR**) have been used to cause temporary incapacitation and have found application in crowd control and management situations, though prior to this they were employed as CW agents. The latter activity has been banned [1]. Of the three groups, two groups namely the CN and OR, seem to have fallen out of grace and the CS compounds have almost completely replaced the CN. The CS compounds are primarily used as riot control and anti-personnel agents and in military training exercises and testing of the protective masks. The most commonly used crowd control agent is o-chlorobenzylidene malanonitrile (**1**) [2]. Recently, compound **1** was used in copious amounts by law enforcement authorities in Seattle (WA) during the meeting of the World Trade Organization to control and manage disruptive activities of the unruly crowds. The CS are internationally used as tear gas agents. Sweden employs compound **1** (**Fig. 1**), under the trade name **K 62**, in military exercises and testing of the protective masks. In low concentration, the CS compounds primarily act as irritants and temporary incapacitants by eliciting and inducing various physiological effects including skin irritation, copious flow of tears, running nose, coughing, dizziness, etc [3]. In high concentrations, they cause nausea and vomiting. The median concentration for respiratory effects is said to be 12~20 mg/m^3, while for eye effects it is 1~5 mg/m^3. The onset time for maximum effects is 20~60 seconds and the duration of time is 5~10 minutes after the cessation of exposure [4]. The parent compound (**1**) exhibits LD_{50} in rats 28 mg/kg, i.v. rats 48 mg/kg and i.p. LC_{50} in rats 88,480 mg/min/m^3 [5a]. Comparative toxicological studies of CS and CN have been described [5a]. Also, the toxicological profile of CS has been published [5b]. At room temperatures, these compounds are colorless stable solids and possess low vapor pressure. The CS compounds have a half-life of 15 minutes and are readily removed by water at pH 7. **Table 1** shows the threshhold concentrations [$TC_{(50)}$] and incapacitating concentrations [$IC_{(50)}$] values in mg/m^3. [4].

With a view to make the CS compounds environmentally more benign and safe and biologically more effective and potent, the synthesis of a new groups of CS compounds containing fluorine and fluorine containing moieties instead of chlorine has been accomplished under the influence of microwave exposure using new catalysts in the solid state. It is proposed to eventually synthesize a dozen or so new CS compounds containing

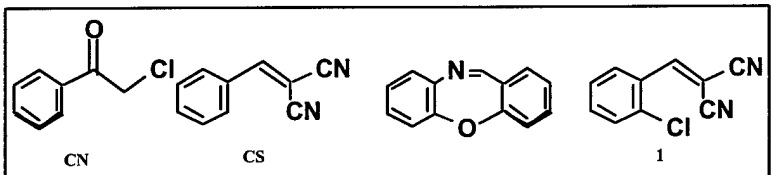

Figure 1: Common Crowd Management Agents

fluorine and to develop structure activity and property relationship profile to generate a computerized database for use in the unambiguous detection of their use. This paper describes the preparation and mass spectral characterization of the five such compounds.

Table 1: Threshhold and Concentrantions of Non-lethal Incapacitants

	CN	CS	CR
$[TC_{(50)}]$ (eyes)	0.3	0.004	0.004
$[TC_{(50)}]$ (respiration	0.4	0.023	0.002
$[IC_{(50)}]$ values	20.5	3.6	0.7

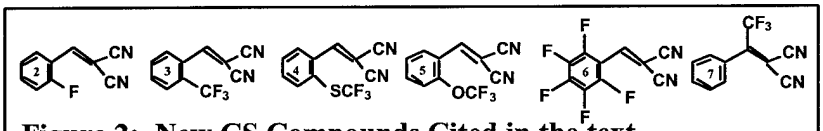

Figure 2: New CS Compounds Cited in the text

RESULTS AND DISCUSSION

Benzylidene malononitriles have attracted considerable attention recently for use as non-lethal chemical agents. Alkylidenation of the carbonyl compounds via the classical Knoevengel condensation of carbonyl substrates with compounds containing reactive methylene moieties is of general and wide application for creating carbon-carbon double bond. In general, this reaction is catalyzed by amines or ammonium salts [6]. Recently a variety of catalysts such as $TiCl_4$ [7a-b], CdI_2 [7c] alumina [7d-e], xeolites [7f-g], $TeCl_4$ [7h], silica [7i-j]; silica functionalized amines

Table 2: Product Distribution with Different Catalysts

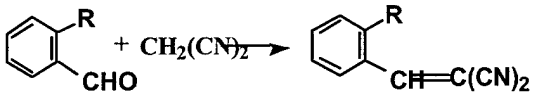

2: R=F; 3: R=CF_3
4: R=SCF3; 5: R=OCF3

3: R=CF_3	$CH_2(CN)_2$	R CHO	R CO_2H	R $CHCl_2$	R $=C(CN)_2$	$=C(CN)_2$
Dry freshly powdered alumina beads	11.4%	27.8%	1.5%	0.3%*	49.0%	-
Europium (lll) fluoride	2.2%	3.7%	2.9%	0.7%	90.0%	-
Hexafluoroammonium aluminate **	5.9%	19.5%	19.5%	-	62.0%	-
Piperidine		37.0%	4.0%		56.6%	0.4%
No catalyst					<8.0%	

* impurity present in the starting material, o-(trifluoromethyl)benzaldehye
** Two additional compounds were characterized from this reaction product, namely o-(trifluoromethyl)phenol (0.6%) and o-(trifluoromethyl) ω–dicyanaomethylketone (10.8%)

[7k] and $AlPO_4$-Al_2O_3 complex [7l] have found application in the Knoevenagel reaction. Solvent free microwave reactions have also been employed for the synthesis of these compounds [8]. Instead of the carbonyl precursors the imines have been used and found to give similar results [9a]. Even amino acids have been stated to catalyze this condensation [9b]. The Knoevenagel condensation has been carried out diastereoselectively [10a-b] and enatioselectively [10c-d]. dilithio N-methanesulfinyl-p-toluidine [10e], tosylmethylisocyanide [10f], α-methoxyvinyllithium [10g], lithiated allylic carbamate [10h] and lithium bis(ethylene-dioxyboryl)methide [10l] have been employed as catalysts in the modified version of the Knoevenagel reaction. Recently, antimony based *in situ* generated catalysts have been employed to successfully alkylidenate steroidal ketones [11]. From the above narrative it seems that the Knoevenagel reaction can be brought about by any reagent! Two mechanisms have been advanced to explain and rationalize the formation of the reaction products [6a]. Over a century ago, Knoevenagel himself proposed that the Schiff base type intermediates are initially formed from the carbonyl compounds, which then go on to react with the reactive methylene moiety and yield the alkylidene derivative. Based on the observation that organic bases catalyze the reaction, Hann and Lapworth suggested that the organic bases generate carbanions from the reactive methylene group, which subsequently react with the carbonyl compounds to furnish β–hydroxyl compounds [6a, pp.213 - 15]. The latter compounds undergo dehydration to yield the end products of the reaction. The survey of the published literature indicates that both the mechanisms are operative. Our own results indicate that these mechanisms may be operating independently of each other.

With a view to developing synthetic methodology, microwave assisted synthesis of benzylidene malononitriles in the neat phase has been explored using new catalysts such as europium (lll) fluoride, ammonium hexafluoroaluminate and dried freshly powdered alumina beads. **Table 2** summarizes the results of the reaction of o-(trifluoromethyl)benaldehyde with malononitrile. Six

Table 3: Mass Spectral Fragmentation of Fluorobenzylidene Malononitriles

(1) o-Fluorobenzylidene malononitrile (2): M^+=172 (99%); 152 (M - HF); 145 (M - HCN, 100%); 121 (145 - CC); 118 (145 - HCN); 94 (121 - HCN); 75 (C_6H_3) and 51 (C_4H_3).

(2) o-(Trifluoromethyl)benzylidene malononitrile (3): M^+=222 (100%); 202 (M - HF); 195 (M - HCN); 176 (195 - F); 153 (M - CF_3); 107 (126 - F); 99 [176 - {$C_2H(CN)_2$}].

(3) o-(Trifluoromethylthio)benzylidene malononitrile (4):M^+=254; 235 (M - F); 215 (235 - HF); 208 (235 - HCN); 185 (M - CF_3, 100%); 158 (185 - HCN); 153 (M - SCF_3); 114 [$C_4H_2C(CN)_2$]; 75 (C_6H_3); 69 (CF_3); 63 (CSF) and 51 (C_4H_3).

(4) o-(Trifluoromethoxy)benzylidene malononitrile (5):M^+=238 (100%); 219 (M - F); 211 (M - HCN); 187 (211 - CC); 172 (M - OCF2); 169 (M - CF3); 153 (172 -F); 143 (M - OCF3); 114 [$C_4H_2C(CN)_2$]; 75 (C_6H_3) and 51 (C_4H_3).

(5) Pentafluorobenzylidene α-(methyl)malononitrile (6):M^+=258 (100%); 143 (M - CH_3); 238 (M - HF); 231 (M - HCN); 212 (231 - F); 193 (212 - F); 181 ($C_6F_5CH_2$); 168 (C_6H_5H); 161 (181 - HF); 148 (167 - F); 143 ($C_6F_3N_2$); 117 (148 - F)and 93 (C_3F_3).

(6) Benzylidene α-(trifluoromethyl)malononitrile (7):M^+=222 (100%); 203 (M - F); 195 (M - HCN); 176 (195 - F); 172 (M - CF_2); 153 (M - CF_3); 145 [$CF_3C_2(CN)_2$]; 176 (153 - HCN)107 (149 -2F); 75 (C_6H_3); 69 (CF_3) and 51 (C_4H_3).

new benzyliedene derivatives containing fluorine and fluorine containing functional groups have been synthesized (**Fig. 2**) and characterized by their NMR and Mass Spectral data. The mass spectral fragmentation of the said six compounds is given in **Table 3**. What is unique about the present work is the characterization of two ω–dicyanoacetophenones, namely o-(trifluoromethyl)- and o-(trifluoromethylthio)-ω–dicyanoacetophenone. This suggests that the β–hydroxyl intermediates can also get oxidized by the catalysts to furnish the ω–dicyanoacetophenones. To the best of our information, this has not been observed in the Knoevenagel reaction before. Another interesting observation is that both o-fluoro- and o-(trifluoromethyl)benzaldehydes themselves are extremely powerful irritants and as such are readily amenable for use as CS compounds. Their effect is temporary and they can be conveniently washed off with copious amounts of water and soap. Secondly the melting points of o-(chloromethyl)- and o-(fluoromethyl)benzyledene malononitriles (**1** and **2**) are 95 – 96° and 118 – 19° respectively. This was somewhat unexpected. It was thought that the m.p. of compound **2** would be lower than that of compound 1. However, the melting points of

o-(chloromethyl)- and o-(trifluoromethyl)benzyledene malononitriles (**1** and **3**) are 95 – 96° and 48 - 49° respectively. This means that the vapor pressure of compound **3** is considerably lower than the popularly used CS agent. The microwave-technique described herein possesses a distinct advantage; in that the reactions can be carried without the use of any solvent and thus decreasing the generation and accumulation of hazardous laboratory waste. In addition, the reaction times can be dramatically reduced and the formation of side products minimized.

EXPERIMENTAL

Stoichiometric amounts of the respective reagents were mixed in glass vials or 5 ml ground joint round bottom flasks and stoppered, vigorously shaken on a vibro-mixer and heated in the microwave oven for a specified period. The reaction mixture was allowed to come to ambient temperature, the cooled product was filtered over cotton-wool, first analyzed by gas chromatography and then was subjected to GC-MS analysis. Mass spectra were obtained using a Finnigan TSQ-7000 GC/MS/MS equipped with a 30 m x 0.25 mm. i.d. DB-5 capillary column (J and W Scientific, Folsom, CA) or a Finnigan 5100 GC/MS equipped with a 15 m x 0.25 mm. i.d.Rtx-5 capillary column (Restek, Bellefonte, PA). The conditions on 5100 were: oven temperature 60-270° C at 10° C/min, injection temperature was 210°, interface temperature 230° C, electron energy 70 eV, emission current 500 μA and scan time 1 sec. The conditions on the TSQ-7000 were: oven temperature 60-270° C at 15° C/min, injection temperature 220°, interface temperature 250° C, source temperature 150°, electron energy 70 eV (EI) or 200 eV (CI) and emission current 400 μA (EI) or 300 μA (CI) and scan time 0.7 sec. Data was obtained in both the electron ionization mode (range 45-450 da) and chemical ionization mode (mass range 60-450 da). Ultrahigh purity methane was used as the CI agent gas with a source pressure of 0.5 Torr (5100) or 4 Torr (TSQ-7100). Routine GC analyses were accomplished with a Hewlett-Packard 5890A gas chromatograph equipped with a J and W Scientific 30 m x 0.53 mm i.d. DB-5 column (J and W Scientific, Folsom, CA). The NMR spectra (^{1}H and ^{13}C) were recorded in $CDCl_3$ with TMS as the internal standard on a Varian VXR-400S spectrometer at 100 MHz and 376 MHz respectively.

Alumina Catalyzed Synthesis of o-trifluoromethylbenzylidene malononitrile: A mixture of stoichiometric amounts of o-trifluoromethylbenzaldehyde (43 mg) and malanonitrile (23 mg) and catalytic amount alumina oxide catalyst (20 mg) in small vial was exposed to microwave radiation for 1.5 minutes. The reaction was cooled to room temperature, treated with a small amount of chloroform, filtered to remove the catalyst and analyzed by GC and then by GC-MS.

The above reaction was repeated using different catalysts such as europium (lll) fluoride, ammonium hexafluoroaluminate, piperidine and silica. The results are summarized in **Table 2**. A similar reaction was carried out under identical conditions except that no catalyst was used in the condensation. Less than 8% of expected product was obtained. o-Fluoro-, o-(trifluoromethylthio)-, o-(trifluoromethoxy)- and pentafluorobenzylidene malononitriles (**2**, **4**, **5** and **6**, **Fig. 2**) were similarly prepared

REFERENCES

(1). Renunciation of Certain Uses in War of Chemical Herbicides and Riot Control Agents, Executive Order, 11850 (1975).
(2). B. B. Carson and R. W. Stoughton, J. Am. Chem. Soc. **50**, 2825, 1928.
(3). (a) Military Chemistry and Chemical Compounds, U. S. Army Field Manual 3-9/U. S. Air Forces Field Manual 355-7, U. S. Governemnt Printing Office, Washington, D. C.; (b) R. N. Sterlin, V. I. Yemel'yanov and V. I. Zimin, "Chemical Weapons and Defense Against Them", Khim. Oruzhiye I Zashchita ot Nego (1975).
(4). U. Ivarsson, H. Nilsson and J. Santesson (eds), A FOA Briefing Book on Chemical Weapons – Threat, Effects and Protection", No. 16, Forsvarets Forskningsanstalt (FOA), Orebro (Sweden) (1992).
(5). B. Ballantyne and D. W. Swanston, Arch. Toxicol. **40**, 75, 1978; (b) J. R. Gaskins and coworkers, Arch. Environ. Health. **24**, 449, 1972.
(6). (a) G. Jones, Organic Reactions, Volume 15, A. Cope (ed) Wiley and Sons, New York (1967) pp. 204; (b) L. T. Tietze and U. Beifuss in Comprehensive Organic Synthesis, vol. 2, B. M. Trost and I. Fleming (eds), Pergamon Press (Oxford), (1991) pp. 341.
7. (a) W. Lehnert, Synthesis 667, 1974], $ZnCl_2$ [b] (b) P. S. Rao and R. V. Venkataratnam, Tetrahedron Lett. **32**, 5821, 1991; (c) D. Parajatapati and J. S. Sandhu, J. Chem. Soc. Perkin Trans. **1**, 739 1993; (d) F. Texier-Boulett and A. Foucod, Tetrahedron Lett. **23**, 4927, 1982; (e) G. Cooke and O. Shultz, Synth. Comm. **26**, 2549, 1996; (f) T. I. Reddy and R. S. Varema, Tetrahedron Lett. **38**, 1721, 1997; (g) Q. L. Wang, M. Yudao and B. Zua, Synth. Comm. **27**, 4107, 1997; (h) Y. U. Subba Rao and B. M. Choudary, Synth. Comm. **21**, 1163, 1991; (i) S. Y. Kim, P. S. Kwon and T. W. Kwon, Synth. Comm. **27**, 533, 1997; (j) R. H. Khan, R. K. Mathur and A. C. Ghosh, Synth. Comm. 26, 683, 1996; (k) I. Angeletti, C. Canepa, C. Martinetti and P. Venturella, Tetrahedron Lett. **29**, 2261, 1988; (l) J. A. Cabella, J. M. Campelo, A. Garcia, D. Luna and J. M. Marinas, J. Org. Chem. **49**, 5195, 1984.
(8). (a) A. S. Abdallah-El, F. Texier-Boulett and J. Hamelin, Synthesis 258, 1994; (b) S. Balalaie and N. Nemati, Synth. Comm. **30**, 869, 2000.
(9). (a) Nair and Jahnke, Synthesis 424, 1984; (b) Y. Yamada, K. Iguchi, K. Hosaka and K. Hagisawa, Synthesis 669, 1974.
(10). (a) A. G. M. Bennett, C. Rokyr and C. D. Spilling, J. Org. Chem. **54**, 1233, 1989; (b) S. G. Pyne and C. B. Boeche, J. Org. Chem. **55**, 2663, 1989; (c) A. Togni and S. D. Pasyor, J. Org. Chem. **55**, 1649, 1990; (d) H. Sakuraka and S. Ushiki, Tetrahedron Lett. **31,** 5349, 1990; (e) S. Niwa and N. Soai, J. Chem. Soc. Perkin Trans. **1**, 937, 1990; (f) S. B. Bowlus and J. A. Katzenellebogen, Synth. Comm. **4**, 137,1974; (g) U. Schollkopf, Pure Appl. Chem., **51**, 1347, 1979; (h) K. Tanaka, T. Nakai and N. Ishikawa, Tetrahedron Lett. 4809, 1978; (i) D. Hoppe, Angew. Chem. int. Ed. **23**, 932, 1984; (j) X. Huang and H.-Z. Zhang, Synthesis 42, 1989.
(11). A. P. Davis and K. M. Battarai, Tetrahedron **51**, 8033, 1995.

BATCH AND HIGH CELL DENSITY FED-BATCH CULTURE PRODUCTIONS OF AN ORGANOPHOSPHORUS HYDROLASE

Michael H. Kim, Vipin K. Rastogi
Geo-Centers, Inc., Gunpowder Branch, P. O. Box 68, APG, MD 21010

Tu-chen Cheng, and Joseph J. DeFrank
U. S. Army Edgewood Chemical Biological Center, APG, MD 21010

ABSTRACT

Organophosphorus hydrolases (OPH) are of great interest to the U. S. Army for their potential use in the non-toxic, non-corrosive decontamination against VX. OPH genes had been cloned and over expressed in *Escherichia coli* by other researchers. However, a common problem has been that of a low expression level. In this study, batch cultures in both complex (e.g., Lauria Broth) and minimal (succinate) media as well as high cell density cultures in the succinate medium were performed to obtain a yield information for a cobolt-requiring OPH.

High cell density fed-batch cultures of *E. coli* carrying a cloned OPH gene were achieved by a pH control with an acidic 200 g/L succinate (pH = 4 to 4.3) medium. The uptake of carbon source, succinic acid instead of succinate, by the cell cultures raised the pH of broth culture which triggered an addition of the acidic succinate medium. This also provided an additional amount of carbon source for high cell density cultures. Up to 300 mg OPH/L of fermentation broth was achieved using the high cell density fed batch cultures.

INTRODUCTION

Current decontamination of areas and equipment potentially exposed to the various chemical agents requires the use of a caustic solution DS2. However, the use of DS2 in field uses is limited due to its toxic and corrosive properties, in addition to being environmentally hazardous. Alternative technology to DS2 decontamination, organophosphate (OP) degrading enzymes could be potentially used in detoxification of chemical agents. To this end, a number of such enzymes responsible for degradation of nerve agents have been identified[1]. Particularly, organophosphorus hydrolase (OPH), which degrades VX, has been cloned into *E. coli*, produced, and purified. However, two common problems for cloned OPHs have been their low activities[2] toward VX and low levels of expressed protein in the host *E. coli*[3].

Effective enzyme decontamination technology requires research on three areas of development: manipulating the OPH gene for a higher activity toward VX, optimizing fermentation for higher cell mass and expressed protein level, and establishing a purification protocal that maximizes purity of the enzyme while minimizing loss of yield that also requires a minimum number of downstream process steps.

MATERIALS AND METHODS

ORGANISM

The strain employed for this study was *E. coli* XL1 that carries a plasmid pVSEOP7. The plasmid contain the ampicillin resistance marker and the gene for *Flavobacterium* organophosphorus hydrolase. In the pVSEOP7 plasmid, the gene is under regulation of the *trc* promotor, which is inducible by IPTG.

FERMENTATION

Batch cultures fermentations were carried in a Bio-Flow 3000 (New Brunswick) unit fitted with 5 L working volume vessel. Both complex Lauria Broth (LB: 10 g/L Tryptone, 5 g/L yeast extract, 10 g/L NaCl, pH adjusted to 7.0 with NaOH) and succinate-minimal medium consisting (per L) of 9.2 g KH_2PO_4, 1.2 g $(NH_4)_2SO_4$, 10 ml of modified Wolin salts and 25 g succinic acid were used. In both media, 100 mg/L each of ampcillin and thiamine was added to maintain plasmid stability and for thiamine auxotroph of the host strain *E. coli* XL1. The modified Wolin salts contained the following ingredient (per L): 3.0 g nitrilotriacetic acid, 6.0 $MgSO_4 \cdot 7H_2O$, 1.0 g NaCl, 1.0 g $MnSO_4 \cdot H_2O$, 0.5 g $FeSO_4 \cdot 7H_20$, 0.1 $CaCl_2 \cdot 2H_2O$, 0.1 $CoCl_2 \cdot 6H_2O$, 0.1 g $ZnSO_4 \cdot 7H_2O$, 0.02 g H_3BO_3, 0.01 g $NaMoO_4 \cdot 2H_2O$, and 0.01 g $CuSO_4$.

Fed-Batch Fermentations were carried out in the same Bio-Flow 3000 unit fitted with 10 L working volume vessel. The bioreactor was initially filled to 5 L with 50 g KH_2PO_4, 50 g $(NH_4)_2SO_4$, 50 g succinic acid, 50 mL of modified Wolin salt, and 500 mg each of ampcillin and thiamine, and the pH was adjusted to 6.5 with NaOH. As growth will increase pH of the bioreactor, an acidic succinate-minimal medium (pH adjusted to 4 to 4.3 by adding NaOH) containing (per L) 200 g succinic acid, 40 mL modified Wolin salts, 40 mL NH_4OH, and 100 mg each of ampcillin and thiamine was used to control the pH at 6.5. Induction was started by adding 3 mL of 200 mM IPTG per L into both the bioreactor and the acidic succinate-minimal pH control medium.

A colony from either LB or succinate-minimal (10 g/L) medium plate was transferred to 5 mL (10 x 18 mm) tube of either LB or succinate-minimal (10 g/L) suspension medium and incubated in a rotary shaker (New Brunswick) overnight at 25°C and 200 rpm, after which 4 ml was transferred to 100 ml of LB or succinate-minimal (10 g/L) medium in a 250-mL Erlenmeyer flask and incubated in a rotary shaker at 25°C and 200 rpm. The overnight-grown cultures were used to inoculate a New Brunswick 5- or 10-liter bioreactor with pH control and dissolved oxygen (DO) monitoring. A strip chart (LKG) was used to record DO with a range of 0 to 100 saturation, and pH of the bioreactor was controlled at 7.0 for batch fermentations with 6 N HCl and 6.5 for fed-batch fermentations. Temperature was maintained at 25°C (otherwise noted), agitation at 700 rpm, air pressure at 50 psi. Periodic samples were taken for monitoring optical density and OPH activities at different times of growth. Protein expression was induced with 0.6 mM IPTG at optical density of 0.5 to 1 for an early induction and at optical density of 3 to 8 for a late induction. For fed-batch fermentations, 0.6 mM IPTG was separately added to both the

bioreactor and the acidic succinate-minimal (e.g., 200 g/L) medium used for pH control.

Cells were harvested by centrifugation (10,000 rpm for 15 minutes) at 4°C, resuspended in 4 mL of 10 mM BTP buffer (pH = 7.2) containing 1 mM $CoCl_2$ to wet gram cell pastes, and broken with a French press at 1000 psi. The resulting crude lysate mixture was centrifuged (17500 rpm for 20 minutes) at 4 °C, decanted, and the supernatant stored at -40 °C.

ANALYTICAL

Optical Density (OD) at 600 nm was measured with a Spectronic 20D spectrometer. Chemical oxygen demand (COD) of culture media without cells was colorimetrically measured using HACH COD kit. Protein determination was carried out using the Pierce protein assay kit. OPH enzyme activity was quantitatively assayed via colorimetric assay using a chromogenic substrate, paraoxon, at a concentration of 100 iM, in 1 mL of 50 mM CHES buffer (pH = 9.1).

RESULTS

BATCH FERMENTATION

The clone pVSEOP7 expressed the enzyme at a relatively similar level in crude lysates for both LB and succinate-minimal (25 g/L) batch fermentations (Table 1). However, the amount of cells harvested was much higher from the succinate-minimal batch than the LB fermentation, resulting a higher volumetric yield (approximately 50.3 mg OPH/L), as compared to only 18.1 mg OPH/L. Specific growth rate of the host *E. coli* XL1 was higher in LB than the succinate-minimal medium (Figure 1), but it appears that not all the soluble substrates in the LB medium was used for cell growth, resulting in a less amount of cells. The final ODs achieved in the succinate-minimal media, i.e., the host *E. coli* XL1 without pVSEOP7, XL1 with pVSEOP7-induced and uninduced control were similar to 4.5 to 5.0.

FED-BATCH FERMENTATION

Typical time-dependent data from a high cell density fed batch fermentation are shown in Figures 2-a, 2-b, 2-c. Cell growth was exponential until the DO became a limiting factor around the culture time of 50 hrs (Figure 2-c). The decreases in OD values could also be attributed to the increases in the total fed-batch culture volume due to pH control and the high succinate concentration. The COD concentration eventually reached 15000 mg/L (Figure 2-a), and, by noting the low extracellular protein concentration of 250 mg/L (Figure 2-a), the high COD is mostly consisted of succinate added for pH control. In fact, high cell density fed batch cultures with 200 g/L succinate resulted in a higher COD of 30000 mg/L. The volume activity exponentially increased upon the IPTG induction (Figure 2-b).

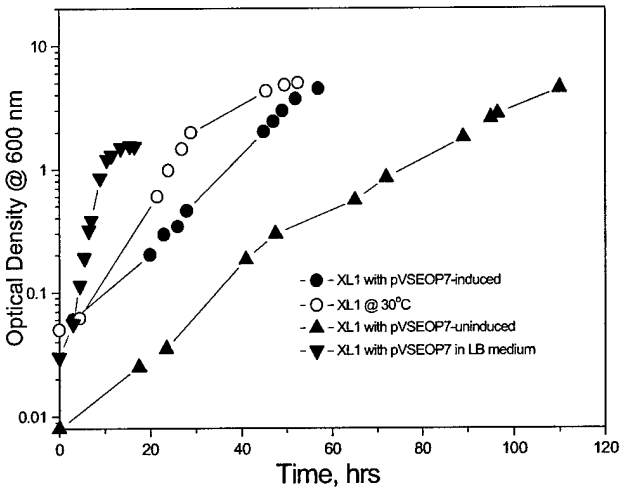

Figure 1. Batch culture growth data .

TABLE 1*. Comparison of Batch OPH Yields in Different Media

Medium	Cell conc., Wet g/L	Volume of crude lysate, mL	OPH activity, U**/mL	Volume activity, U/L	Eq. OPH, mg OPH/L
LB	7.1	120	3767	90370	18.1
Succinate (25 g/l)	21.6	385	3333	256640	51.3

* These values are based on an average of two batch fermentations in each medium.
** The OPH enzyme unit activity (U) is defined as ìmole p -NP produced/min

The high cell density fed-batch fermentation produced a much higher amount of cells per liter as well as higher unit activities in the crude lysates (Table 2), resulting in as much 300 mg OPH/L of fermentation broth. The increased amount of OPH production is largely due to a higher cell mass (up to 63.5 wet g cells/L) obtained through high cell density fed-batch technique.

However, a higher unit activity in the crude lysates (up to 6500 U/mL) was also contributing factor to the overall increases in the OPH yield. The final volumes achieved in these fed batch fermentations varied greatly and could be an important factor for optimization of OPH production.

CONCLUSIONS

High cell density fed batch cultures were successfully used to achieve up 300 mg OPH/L of fermentation broth. The high concentration of recombinant enzyme allows multi-gram quantitie of enzyme to be produced on the bench scale (10-liter). The overall OPH yield can be further improved by optimizing the fermentation and/or carrying out the fermentation in a larger pilot scale (100-liter).

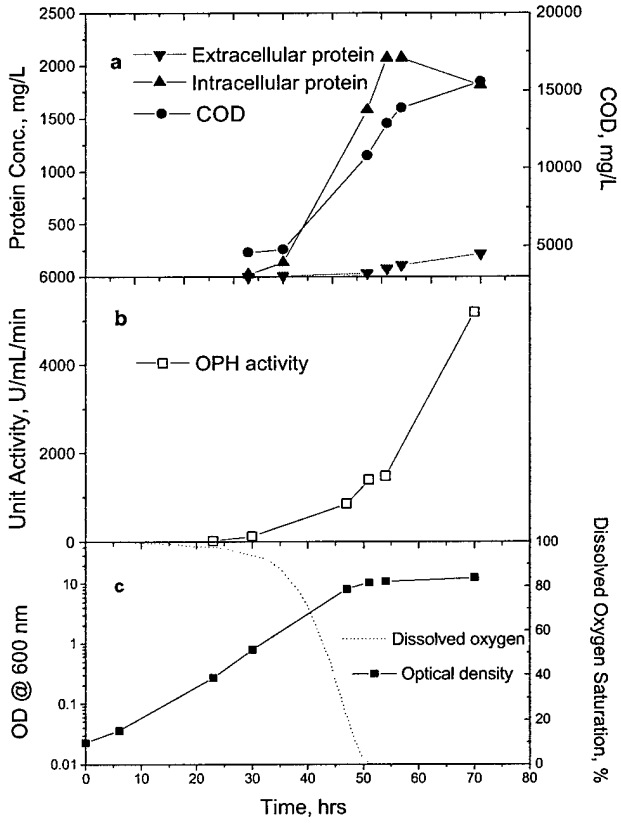

Figure 2. Time-dependent data from fed-batch cultures.

TABLE 2. Data from High Cell Density Fed Batch Cultures.

Final volume, L	Cell conc., wet g/L	Volume of crude lysates, mL	OPH activity, U/mL	Volume activity, U/L	Eq, OPH, mg OPH/L	Succinate conc., g/L
6.0	44.6	1050	4738	829100	166	200
8.5	44.7	1534	5786	1044151	209	200
11.0	50.8	2036	6516	1206052	241	150
10.5	61.3	2728	6000	1558857	312	150
10.2	63.5	2500	5301	1262143	252	200
9.4	60.0	2139	5028	1024275	205	200

REFERENCES

1. Grimsley, J. K., Rastogi, V. K. and Wild, J. R. (1998) ABiological Detoxification of Organophosphorus Neurotoxins..@ in S. K. Sikdar and R. L. Irvine (eds), Bioremediation: Principle and Practice, Vol. II: Biodegradation Technology Developments, Technomic Publishing Inc., 577-613.

2. Sriram, G., Rastogi, V. K., Ashman, W., and Mulbry, W. (2000) AMutagenesis of Organophosphorus Hydrolase to Enhance Hydrolysis of the Nerve Agent VX.@ *Biochem. Biophys. Res. Commun.* **279**(2), 516-519.

3. Lai, K., Dave, K. I., and Wild, J. R. (1994) ABimetallic Binding Motifs in Organophosphorus Hydrolase are Important for Catalysis and Structural Organization.@ *J. Biol. Chem.*, **269**, 16579-16584.

MICROWAVE INDUCED REACTION OF H-DIMETHYLPHOSPHONATE WITH STYRENE OXIDE

S. Munavalli[1], D. K. Rohrbaugh[2], G. W. Wagner[2], F. R. Longo[1] and H. D. Durst[2]

[1]Geo-Centers, Inc., P. O. Box 68, Gunpowder Branch, APG, MD 21010 and [2]U. S. Army Edgewood Chemical Biological Center, APG, MD 21010
*Phone # 410-436-2819, Fax # 410-436-3764; e-mail address: Munavalli Shekar, @SBCCOM.apgea.army.mil

ABSTRACT

The reaction of a neat mixture of styrene oxide and H-dimethyl-phosphonate under microwave catalysis and without any solvent for six minutes furnished a complex mixture containing dimethyl methylphosphonate, trimethylphosphate, phenylacetaldehyde, 1-methoxy-2-phenylethanol, 1-phenylethleneglycol, cis- and trans-1, 3-diphenylcyclobutanes, hydrogen 1-(2-phenylethyl)methylphosphinate, (1-phenylethyl)dimethylphosphonate and (1-phenylethyl)-dimethylphosphonate via free radical processes. The mechanism of formation of the said compounds and their GC-MS characterization are described herein.

INTRODUCTION

Oxiranes comprise an extremely versatile group of intermediates and as such have attracted considerable attention [1]. Because of their ready availability and exceptional reactivity, the epoxides have found varied applications as a versatile functional group in synthetic organic chemistry. The oxirane ring can be opened under almost all conditions: electrophilic, nucleophilic, neutral, gas-phase, thermal and free radical conditions (Fig. 1) [1a]. An excellent review on the preparation and synthetic applications of the oxiranes has appeared [1f]. Recently we investigated the free radical cleavage of styrene oxide with trifluoromethylthiocopper and reported the formation of products arising from the C – C and C – O bond fission [2]. However, their reaction with phosphorus compounds has found only a limited application including their routine use in the Michaelis-Becker reaction to prepare phosphinates [3, 4]. Tri-coordinated pentavalent phosphorus compounds or *in situ* generated intermediates have been found to react with oxiranes [3, 4]. Thus, phosphorus azide reacted with propylene oxide to furnish cyclic oxazaphoranes as well as acyclic compounds [5]. Also, the *in situ* formed highly reactive metaphosphates have been described to open the oxirane ring to yield isomeric 1, 3, 2-dioxaphospholane-2-oxide derivatives [6].

The *in situ* generated electrical energy from microwaves has been used to thermally catalyze chemical reactions. This type of energy transformation depends on the molecular properties of the reacting chemicals [7]. Since the advent of commercially available microwave cookers, the microwave thermal process is finding increasing and interesting applications in synthetic organic chemistry [8]. The popularity of the microwave-induced chemistry appears to rest primarily on

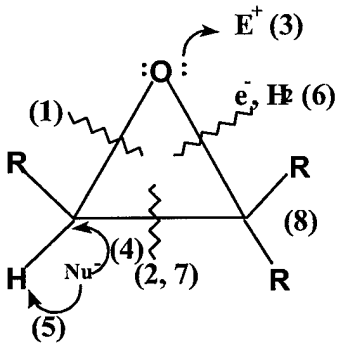

Figure 1. Types of Oxirane Cleavages and Reactions.

(1, 2) Homolytic cleavages (free radica,, photlytic, thermal)
(3) Electrophilic attack on the ring oxygen
(4) Nucleophilic attack on the ring carbon
(5) Nucleophilic attack on the ring hydrogen
(6) Reactions with electrons and surface reactions
(7) Cycloadditions
(8) Reactions of the substituent

its dramatic reduction of the reaction time and the possibility of carrying out neat reactions in "dry media" (solid phase). In fact, the latter appears to have significantly contributed to its enhanced usage [9]. The use of dielectric solvents seems to facilitate the transfer of the *in situ* generated thermal energy to chemical reactants [9b]. We became interested in adopting microwave chemistry for two reasons, namely the possibility of micro-scale chemistry and elimination of the hazardous waste thus generated during the normal work-up and its consequent disposal problems. In continuation of our interest in the chemistry of the oxirane cleavage reactions [10], the microwave catalyzed oxirane ring opening in the presence of hydrogen dimethylphosphonate has been examined and observed to lead to the formation of unusual products. This paper describes the probable mechanism of the formation of the novel compounds formed during the said reaction and their GC-MS characterization.

RESULTS AND DISCUSSION

Recently, H-phosphonates have attracted considerable attention and have found useful applications in phosphorylation reactions [11]. Microwave induced reaction of styrene oxide (**1**) with hydrogen dimethylphosphonate (**2**) has been found to furnish ten compounds excluding the starting materials (**Fig. 2**). Hydrogen dimethylphosphonate (**2**) itself gives two compounds, namely trimethylphosphonate (**3**) and trimethylphosphate (**4**). There is nothing unusual about this, for these compounds are usually formed during the oxidation and/ or free radical reaction of hydrogen dimethylphosphonate (**2**). The presence of the readily removable hydrogen at the phosphorus center of the H-phosphonates appears to be the genesis of its reactivity [12]. Among other things, H-phosphonates are known to be involved in the addition to: (i) multiple bonds [13a] and (ii) carbonyl group [13b] and (iii) in trans-esterifications [13c]. Dealkylations [13b]. as well as P – O and C – O bond cleavages [13d] have been observed. Methyl radicals have been stated to react with trimethylphosphite, albeit sluggishly, to give trimethylphosphonate [14].

What is unusual about the reaction described here is the non-specific radical formation from H-dimethylphosphonate.

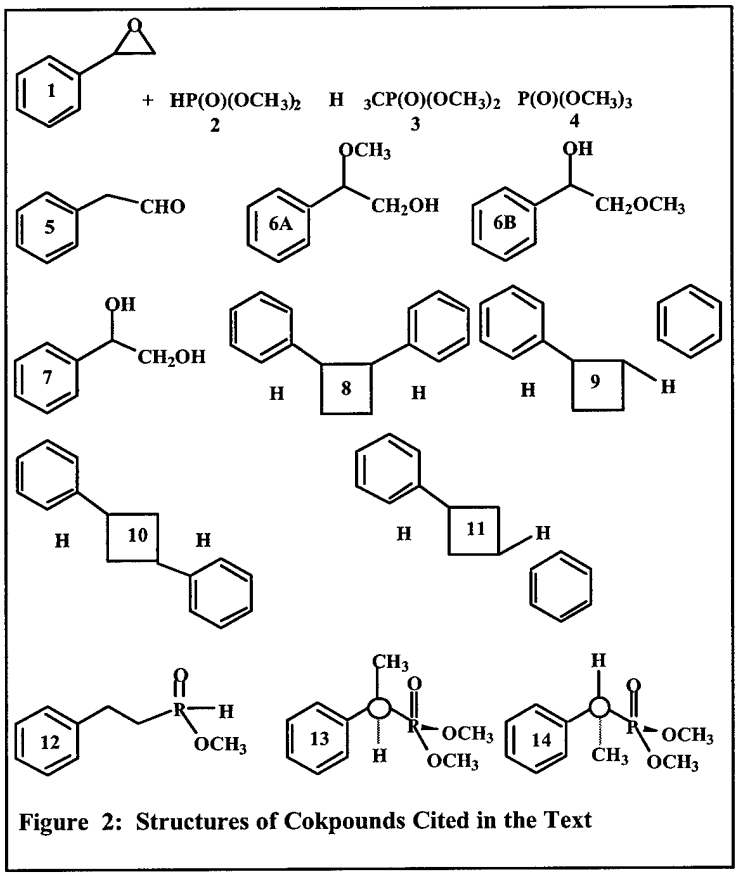

Figure 2: Structures of Cokpounds Cited in the Text

Deoxygenation of organic peroxides with phosphites has been described [15]. However, epoxides have also been said to remain unaffected in the presence of phosphites [16]. It has also been stated that phosphites [17a] and phosphines [17b] deoxygenate epoxides to furnish alkenes. Thus, there seems to be some contradiction as regards the reaction of epoxides with phosphorus compounds. Phosphorus stabilized carbanions are said to give various products on reacting with oxiranes. Thus, the formation of alkenes, cyclopropanes and ketones has been rationalized [18a]. Significant formation of the ketones was observed via hydrogen migration [18b]. However, the treatment of styrene oxide with benzylidene trimethylphosphorane yielded (2-phenylethyl)ketone as the minor product and cis trans 1,3-diphenylpropene as the major product [18b]. With methylenetriphenylphosphorane, styrene oxide has been reported to give a ketone and triphenylphosphine. With strongly basic ylides, cyclic ethers have been reported [18c]. The reaction of styrene oxide with ethoxycarbonyl triphenylphosphorane has been reported to give cyclopropanoids [18d-e].

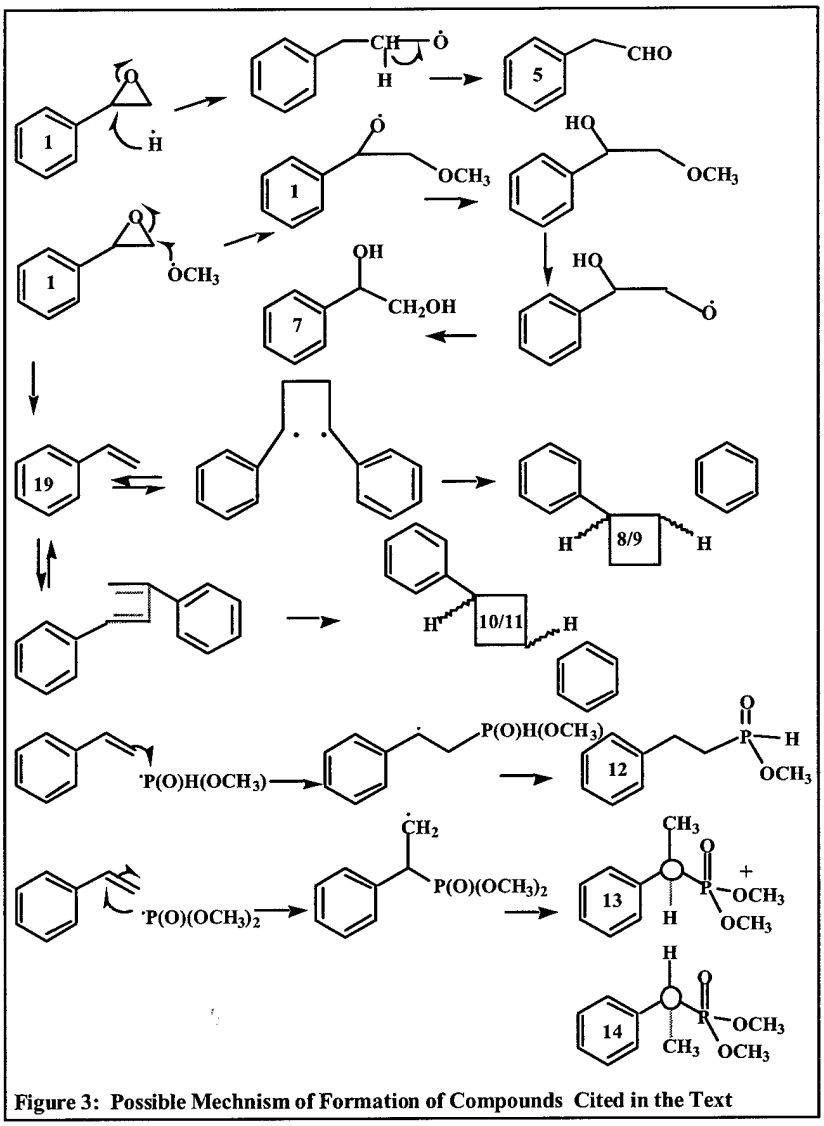

Figure 3: Possible Mechnism of Formation of Compounds Cited in the Text

The microwave catalyzed reaction of styrene oxide (**1**) with H-dimethylphosphonate (**2**) yields ten compounds. Of these, two are derived from the oxidation H-dimethylphosphonate (**2**) and the remaining have their origin in styrene oxide (**1**). It appears that the compounds identified herein are formed via the free radical processes. **Fig. 3** attempts to describe the probable mechanism of the formation of the compounds described in the narrative.

EXPERIMENTAL

Stoichiometric amounts of the respective reagents were mixed in glass vials or 5 ml ground joint round bottom flasks and stoppered, vigorously shaken on a vibro-mixer and heated in the microwave oven for a specified period. The reaction mixture was allowed to come to ambient temperature, the cooled product was first analyzed by gas chromatography and then subjected to GC-MS analysis.

Mass Spectral Fragmentation of Compounds Cited in the Text

1. Styrene oxide (**1**): M^+=120 (r.t.=4.83 min, 57.8%); 105 (M - CH_3); 93 (M - C_2H_3); 91 (C_7H_7, 100%); 89 (C_7H_5); 77 (C_6H_5); 65 (C_5H_5); and 51 (C_4H_3).

2. Hydrogen dimethylphosphonate (**2**): M^+=110 (r.t.=2.47 min. 31.9%); 109 (M - H); 95 (M - CH_3); 93 (M - OH); 80 (95 - CH_3, 100%); 79 (M - OCH_3); 65 (80 - CH_3); 63 (PO_2); 49 (PH_2O) and 47 (PO).

3. Trimethylphosphonate (**3**): M^+=124 (r.t.=2.98 min. 0.2%); 109 (M - H); 109 (M - CH_3); 94 (109 - CH_3, 100%); 79 (94 - CH_3); 79 (M - OCH_3); 65 (PH_2O_2); 63 (PO_2); 49 (PH_2O) and 47 (PO).

4. Trimethylphosphate (**4**): M^+=140 (r.t.=3.4 min, 0.6%); 110 (M -O CH_2, 100%); 109 (M - OCH_3); 95 (110 - CH_3 100%); 79 [P(O)H (OCH_3)]; 79 (M - OCH_3); 65 (PH_2O_2) and 47 (PO).

5. Phenylacetaldehyde (**5**): M^+=120 (r.t.=4.58 min, 3.4%); 91 (C_7H_7, 100%); 65 (C_5H_5); and 51 (C_4H_3).

6. 1-Methoxy-2-phenyl-2-ethanol (**6B**) M^+=152 (r.t.=6.29 min, 1.6%); 105 (C_6H_5CO); 103 (121 - H_2O); 93 (121 - C_2H_4); 91 (C_7H_7); 78 (C_6H_6); 77 (C_6H_5); 65 (C_5H_5); and 51 (C_4H_3).

7. 1-Phenylethylene glycol (**7**) M^+=138 (r.t.=7. 25 min. 0.9%); 107 (M - CH_2OH, 100%); 105 (C_6H_5CO); 91 (C_7H_7); 79 (C_6H_7); 77 (C_6H_6); 65 (C_5H_5); and 51 (C_4H_3).

8. 1, 2-(cis/trans)-diphenycyclobutane (**8**) and 1, 2-(91 (C_7H_7);)-diphenycyclobutane (**9**): M^+=208 (not seen in both cases); (r.t.=8.34 min, 0.3%/ r.t.=8.48 min, 0.7%); 104 (C_8H_8, 100%); 91 (C_7H_7); 77 (C_6H_6) and 51 (C_4H_3).

9. 1, 3-(cis/trans)-diphenycyclobutane (**10**) and 1, 3-diphenycyclobutane (**11**): M^+=208 (not seen in both cases); (r.t.=8.34 min, 0.3%/ r.t.=8.48 min, 0.7%); 104 (C_8H_8, 100%); 91 (C_7H_7); 77 (C_6H_6) and 51 (C_4H_3).

10. Hydrogen (2-phenylethyl)methylphosphonate (**12**): M^+=184 (r.t.=10.32 min, 2.2%); 169 (M - CH_3); 153 (M - OCH_3); 136 (M - PHO); 134 ($C_8H_7OCH_3$); 121 (136 - CH_3, 100%); 105 ($C_6H_5C_2H_4$); 91 (C_7H_7); 79 [PH(O)(OCH_3)]; 77 (C_6H_6); 65 (C_5H_5) and 51 (C_4H_3).

11. Hydrogen (1-phenyl)ethyl-1-dimethylphosphinate (**13**): M^+=214 (r.t.=10.83 min, 7.8%); 199 (M - CH_3);169 [199 - (OCH_2)]; 153 (M - OCH_3 - OCH_2); 136 [C_6H_5(OH) (OCH3)CH2]; 121 (136 - CH_3); 119 (C_8H_7O); 105 [M - P (O) (OCH_3)$_2$]; 102 (C_8H_6, 100%); 95 [P(O)(OH)-(OCH_3)]; 91 (C_7H_7); 79 [PH(O)(OCH_3)]; 77 (C_6H_6); 65 (C_5H_5) and 51 (C_4H_3).

12. Hydrogen (1-phenyl)ethyl dimethylphosphinate (**14**): M^+=214 (r.t.=11.0 min, 0.2%); 199 (M - CH_3);169 [199 - (OCH_2)]; 153 (M - OCH_3 - OCH_2); 136 [$C_2H_3P(O)(OCH_3)_2$]; 121 (136 - CH_3); 119 ($C_6H_5COCH_2$); 105 [M - P (O) (OCH_3)$_2$]; 102 (C_8H_6, 100%); 95 [P(O)(OH)-(OCH_3)]; 91 (C_7H_7); 79 [PH(O)(OCH_3)]; 77 (C_6H_6); 65 (C_5H_5) and 51 (C_4H_3).

Mass spectra were obtained using a Finnigan TSQ-7000 GC/MS/MS equipped with a 30 m x 0.25 mm. i.d. DB-5 capillary column (J and W Scientific, Folsom, CA) or a Finnigan 5100 GC/MS equipped with a 15 m x 0.25 mm. i.d.Rtx-5 capillary column (Restek, Bellefonte, PA). The conditions on 5100 were: oven temperature 60-270° C at 10° C/min, injection temperature was 210°, interface temperature 230° C, electron energy 70 eV, emission current 500 μA and

scan time 1 sec. The conditions on the TSQ-7000 were: oven temperature 60-270° C at 15° C/min, injection temperature 220°, interface temperature 250° C, source temperature 150°, electron energy 70 eV (EI) or 200 eV (CI) and emission current 400 μA (EI) or 300 μA (CI) and scan time 0.7 sec. Data was obtained in both the electron ionization mode (range 45-450 da) and chemical ionization mode (mass range 60-450 da). Ultrahigh purity methane was used as the CI agent gas with a source pressure of 0.5 Torr (5100) or 4 Torr (TSQ-7100). Routine GC analyses were accomplished with a Hewlett-Packard 5890A gas chromatograph equipped with a J and W Scientific 30 m x 0.53 mm i.d. DB-5 column (J and W Scientific, Folsom, CA). The NMR spectra (^{1}H and ^{13}C) were recorded in $CDCl_3$ with TMS as the internal standard on a Varian VXR-400S spectrometer at 100 MHz and 376 MHz respectively.

Microwave Catalyzed Reaction of Styrene oxide (1) with H-Dimethylphosphonate (2): Stoichimetric amounts of styrene oxide (**1**, 0.22 g., 2 mmol) and H-dimethylphosphonate (**2**, 0.22 g., 2 mmol)were mixed in a glass vial or glass joint round bottom flask (5 ml), the mixture was shaken for a few minutes using the vibro-mixer and then heated in a table top microwave oven for two minutes. The reaction mixture after cooling to ambient temperature was analyzed by gas chromatography. Then, it was heated again for two minutes and reanalyzed. This process was repeated one more time to a total of six minutes of microwave heating. When no additional peaks appeared in the g. c. chromatogram, it was then subjected to GC-MS analysis. Thus, the following compounds were characterized based on their mass spectral fragmentation behavior: (1) dimethyl methylphosphonate (**3**), (2) trimethylphosphate (4), (3) phenylacetaldehyde (**5**), (4) 1-methoxy-2-phenylethanol (**6B**), (5) 1-phenylethleneglycol (**7**), (6) cis- and trans-1,3-diphenylcyclobutanes (**10-11**), (7) hydrogen 1-(2-phenylethyl)methylphosphinate (**12**), (8) (1-phenylethyl)dimethylphosphonate (**11**) and (1-phenylethyl)dimethylphosphonate (**12**). Their retention times, percentages of the yields of the compounds and mass spectral fragmentation are described in **Table 1**.

REFERENCES

1. (a) L. G. Lewis in "Comprehensive Heterocyclic Chemistry", vol.7. , A. R. Katritzsky, C. W. Rees, W. Lawoski (eds.), Pergamon Press, New York, 1984, p.100; (b) J. G. Buchanon, H. Z. Sable in "Selective Organic Transformations", vol. 2, B. S. Thyagarajan (ed), Wiley, New York, 1972, p. 1; (c) M. Bartok and K. C. Long in "The Chemistry of Ethers, Crown Ethers, Hydroxy Groups and their Sulfur Analogs", Part 1, Suppl., S. Patai (ed), Wiley, New York, 1980, p.609; (d) **G. Smith, 629, 1984;** (e) C. Bonini, R. DiFabio, G. Sotgiu, and S. Cavgnero, Tetrahedron **1989**, *45*, 2895; (f) A. S. Rao, S. K. Paknikar and J. G. Kirtane, Tetrahedron **1983**,*39* , 2323; (g) K. Maruko, M. Hasegawa, H. Yamamoto, K. Suzuki and G. Tsuchihashi, J. Am. Chem. Soc. **1986**, *108*, 3827; (h) K. Maruko, S. Nagahara, T. Ooi, and H. Yamamoto, Tetrahedron Lett. **1989**, *30*, 5607,; (i) C. Bonini and G. Righi, Synthesis **1994**, 225.

2. S. Munavalli, D. K. Rohrbaugh, D. I. Rossman, L. R. McMahon and H. D. Durst, J. Organometal. Chem. **587**, 160, 1999;

3. A. G. Rowley in "Organophosphorus Reagetns in Organic Synthesis', J. I. G. Cadogan, Academic Press, NewYork (1979), p.306.

4. A Guide to Organophsophorus Chemistry, L. D. Quin, Wiley-Interscience, New York (2000).

5. G. Bertrand, J.-P. Majoral and A. Baceiredo, Tetrahedron Lett. **1980**, *21*, 5015.

6. R. Bodalski and L. D. Quin, J. Org. Chem. , **1991**, *56*, 2666.

7. D. M. P. Mingos and D. R. Baghurst, J. Chem. Soc., Chem. Soc. Rev. **1991**, *20*, 1,.

8. (a) R. J. Gedye, F. Smith, K. Westaway, H. Ali, L. Baldisera, L. Laberge and J. Rousell, Tetrahedron Lett. **1986**, *27,* 279; (b) R. J. Giguere, T. L. Bray, S. M. Duncan and G. Majetich, Tetrahedron Lett. **1986**, *27*, 4945; (c) A. Abramovitch, Org. Prep. Proc. Int. **1991**,*23* , 685; (d) S. Caddick, Tetrahedron **1995**, *51*, 10403; (e) P. de la Cruz, E. Diez-Barra, A. Loupy and F. Langa, Tetrahedron Lett. **1996**,*37*, 1113; (f) A. Dandia, H. Teneja, R. Gupta and S. Paul, Synth. Comm. **1999**, 29, 2323; (g) B. K. Banik, M. S. Manhas, S. N. Newaz and A. K. Bose, Bioorg. Med. Chem. Lett. **1993**, *31*, 2363.

9. (a) P. Kumar and K. C. Gupta, Chem. Lett. **1996**, 635; (b) S. Jolivet, S. A.-E. Ayoubi, D. Mathe, F. T. Boullet and J. Hamelin, J. Chem. Res(s), **1996**. 300.

10. (a) S. Munavalli, D. I. Rossman, D. K. Rohrbaugh and H. D. Durst, National Meeting, American Chemical Society, Anheim (CA) 1995; (b) S. Munavalli, D. I. Rossman, D. K. Rohrbaugh and H. D. Durst (under preparation); (c) S. Munavalli, D. K. Rohrbaugh, F. R. Longo, F. J. Berg and H. D. Durst, 213th National Meeting, American Chemical Society, San Diego (CA). 2001.

11. T. Wada, A. Mochizuki, Y. Sato and M. Sekine, Tetrahedron Lett. **1998**,*39*, 7123,; (b) Y. Hayakawa in "Comprehensive Organic Synthesis", Vol. 5, B. M. Trost and I. Flemming (eds), Pergamon Press, New york (1991), p. 601; (c) J. Stawinski in "Handbook of Organophosphorus Chemistry", R. Engel (ed), Dekker Publishers, New York (1992), p.377; (c) L. D. Quin, "A Guide to Organophosphorus Chemistry", Wiley-Interscience, New York (2000).

12. (a) P. J. Garegg, I. Smith, T. Redberg, J. Strowinski and R. Stromberg, Tetrahedron Lett. **1986**, *27*, 4051; (b) P. Westerduin, G. H. Veeneman, G. A. van der Marcel and J. H. van Boom, Tetrahedron Lett. 1986, *27*, 6271.

13. (a) Methoden der Oragnischen Chemie, E. Muler (ed), Houben-Weyl, Georg Theime, Struttgart (1964) p.463; (b) M. S. Kharasch, R. A. Mosher and I. S. Bengelsdorf, J. Org. Chem. **1960**, *25*, 1000; (c) K. Troev and G. Borris, Phosphorus Sulfur, **1987**, *29*, 129; (d) W. Gerrard, W. J. Green and R. A. Nutkins, J. Chem. Soc. **1952**, 4067.

14. (a) D. A. Bafus, E. J. Gallegos and R. W. Kiser, J. Phys. Chem. **1966**, *70*, 2614; (b) J.-J. L. Fu and W. G. Bentrude, J. Am. Chem. Soc. **1972**., *94*, 7710

15. (a) J. Krusic, W. Mahler and J. K. Kochi, J. Am. Chem. Soc. **1972**., *94*, 6033; (b) A. G. Davies, D. Griller and B. P. Roberts, J. Chem. Soc., Perkin Trans,. *II*, **1972**, 993; (c) K. J. Humphris and G. Scott, J. Chem. Soc., Perkin Trans,. *II*, **1973**, 831,.

16. (a) G. O. Pierson and O. A. Runquist, J. Org. Chem. **1969**, *34*, 3654; (b) Y. Ito, M. Oda and Y. K. Kitahara, Tetrahedron Lett. **1975**, 239; (c) C. H. Foster and G. A. Betchtold, J. Org. Chem. **1975**, *40*, 3743.

17. (a) C. B. Scott, J. Org. Chem. **1957**, *22*, 1118; (b) M. J. Borkin and D. B. Denney, Chem. and Ind. (London), **1959**, 330.

18.(a) S. Trippett, J. Chem. Soc., Quart. Rev. **1963**, *17*, 406; (b) W. E. McEwen, A. Blade′-Font and C. A. Vanderwerf, J. Am. Chem. Soc. **1962**, *84*, 677; (c) R. Huisgen and J. Wulff, Ber. **1969**, *102*, 1841; (d) W. J. Wadsworth, J. and W. D. Emmons, J. Am. Chem. Soc. **1961**, *83*, 6330; (e) R. M. Gerkin and B. Rickborn, J. Am. Chem. Soc. **1967**, *89*, 5850 and refs. cited therein.

DEHALOGENASE: THE FOLLOW-UP ENZYME AFTER MUSTARD OXIDATION

Ilya Elashvili and Joseph J. DeFrank

U.S. Army Edgewood Chemical Biological Center, Aberdeen Proving Ground, MD 21010-5424
Tel: 410-436-2580 Fax: 410-436-8026 E-mail: ilya.elashvili@sbccom.apgea.army.mil

ABSTRACT

Sulfur mustard (HD) has been used as a chemical warfare agent since 1917. Currently fielded M258A1 and M280 decontamination kits and prospective oxidative decontaminants convert HD to HD sulfoxide (HDSO). Although, the latter is not considered a vesicant, it is highly recalcitrant and its systemic toxicity, reportedly, is comparable to the agent. We found that live cells of a known hexachlorocyclohexane (lindane) metabolizing *Sphingomonas paucimobilis* bacterium could degrade HDSO. Cell free crude extract was obtained and found capable of HDSO enzymatic dehalogenation. Dehalogenase activity was monitored by determining chloride release using the Iwasaki colorimetric method. The reaction was also monitored by using GC-FPD and GC-ECD on derivatized samples. These results demonstrate the potential use of *S. paucimobilis* derived enzyme(s) in furthering the destruction of HD agent, thus providing significant contribution to the "Green" solution of the decontamination problem. This could be an important factor for the US and other nations in attempting to meet the requirements of 1993 Chemical Weapons Convention to destroy all chemical warfare agents within ten years of ratification (April 2007 for the US).

INTRODUCTION

The emphasis is to develop CW decontamination approaches that are more environmentally friendly than currently employed decontamination solutions, such as DS2. Bicarbonate/peroxide system (BAP) is one of the formulations proposed for this purpose (Wagner, 1999; Richardson, 1999). It has been shown that mustard sulfoxide (HDSO) is the sole product of sulfur mustard (HD) decontamination with BAP (Wagner, 1999; Drago, 1998). It has been reported that the use of other oxidative decontaminant systems with HD, including M258A1 and M280 kits for skin and individual equipment decontamination, also produces HDSO (Yang, 1992). Although the latter has been shown not to be a vesicant, its subcutaneous toxicity has been reported to be comparable to that of HD (Marshall, 1921; Groesbeck, 1923). In addition, HDSO is highly recalcitrant, reportedly resistant to hydrolysis even at 100°C (Helfrich, 1920).

We are interested in finding enzymes that are capable of hydrolytic removal of chlorine from HDSO. In this effort, we screened the microorganisms that have been reported to possess dehalogenase

enzymes. A bacterial strain, *Sphingomonas paucimobilis* UT26 (formerly known as *Pseudomonas paucimobilis* UT26), was found to grow on hexachlorocyclohexane (HCH, or lindane) as a sole source of carbon (Senoo, 1989; Imai, 1989). Subsequently, the enzymes involved in HCH degradation had been purified (Nagata, 1993a, 1997) and the relevant genes in the metabolic pathway were cloned and sequenced (Imai, 1991; Nagata, 1993b, 1994; Miyauchi, 1998).

We obtained the *S. paucimobilis* UT26 strain and tested the live bacterial cells for HDSO dehalogenation activity. After ascertaining that the live cells were capable of removing chloride from HDSO, the organism was studied for the HDSO halidohydrolase (HDH) enzymatic activity (Scheme 1).

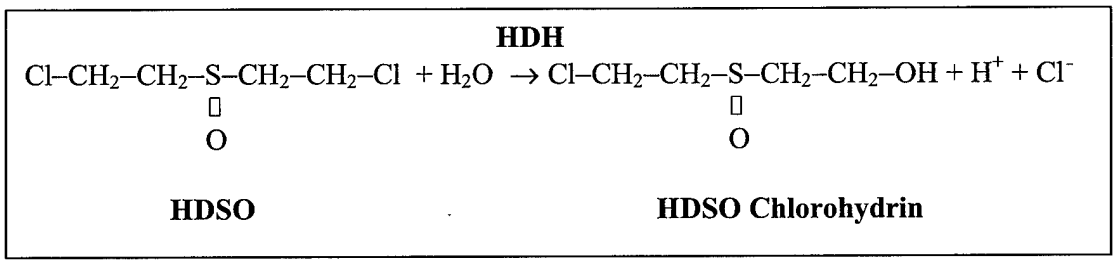

SCHEME 1. HDSO dehalogenation reaction by halidohydrolase (HDH).

MATERIALS AND METHODS

Organism and Growth Conditions: *S. paucimobilis* UT26 strain was kindly provided by Dr. Nagata. Unless otherwise indicated, the cultures were grown in a Luria broth (Nagata, 1999) supplemented with nalidixic acid containing (per liter): 3.3 g Bacto tryptone, 1.7 g yeast extract, 5 g sodium chloride, 25 mg nalidixic acid. To ascertain HDH activities of different bacterial crude extracts, one-liter Erlenmeyer flasks with 300 ml media inoculated with *S. paucimobilis* UT26 were routinely incubated at 30 °C for 40-70 hours on a recirculatory shaker at 200 rpm. For the enzyme purification, *S. paucimobilis* UT26 was cultured in a six 4-liter flasks at 150 rpm in a total of 10 liters of the medium. The cells were collected by centrifugation at 7,000×g for 30 minutes at room temperature, gently resuspended in a minimum amount of 20 mM N-2-hydroxyethylpiperazine-N'-2-ethanesulfonic acid (HEPES) buffer, pH 7.7 and spun again at 24,000×g for 20 minutes at 4°C. The supernatant was aspirated and the pellet was stored below -85°C. Unless otherwise indicated, subsequent procedures for the enzyme extraction and purification were conducted below 4°C. Also, all subsequent centrifugations were conducted at 24,000×g and enzyme fractions were stored below -85°C.

Enzyme Extraction: Frozen pellets of collected cells were resuspended in 20 mM HEPES buffer, pH 7.8 (3 ml per gram of wet weight). The cells were disrupted by passage through pre-chilled French Pressure cell (SLM-Aminco) at 16,000 psi three times. Crude cell extracts were obtained after the removal of cellular debris by centrifugation at 37,000×g for 30 min at 4 °C. In order to destroy heat labile enzymatic activities in a sample of supernatant, a small portion of the supernatant was boiled for five minutes and precipitates were removed by centrifugation at 13,000×g for 10 minutes.

Enzyme Purification on Ion-Exchange Column: Crude extracts were chromatographed on a DEAE-Sepharose Fast Flow (Amersham/Pharmacia Biotech Inc., Piscataway, NJ) anion-exchange column (25×150 mm). Before the sample application, the column was charged with two column volumes of the 2 M sodium acetate solution, and equilibrated with five column volumes of the 20 mM HEPES buffer, pH 7.8. After sample loading, the column was washed with four column volumes of the 20 mM HEPES buffer, pH 7.8, followed by the same amount of the 20 mM HEPES, 0.1 M sodium acetate,

buffer, pH 7.8 to elute loosely bound proteins. The enzyme was eluted with the 20 mM HEPES, 0.3 M sodium acetate, buffer, pH 7.8. Active fractions (60 ml) were pooled and frozen. The pool of the active fractions was defrosted and was diluted with 440 ml of the 20 mM HEPES buffer, pH 7.8, to be applied on the linear gradient anion-exchange column. The same DEAE-Sepharose Fast Flow anion-exchange column employed for the step gradient chromatography was used for the linear gradient chromatography. The column treatment, sample loading and pre-elution washes were conducted as above. Loosely bound proteins were again eluted with four column volumes of 20 mM HEPES, 0.1 M sodium acetate, buffer, pH 7.8. The enzyme was eluted by 2000 ml of a 0.1 to 0.27 M sodium acetate linear gradient in 20 mM HEPES buffer, pH 7.8. Active fractions (50 ml) were analyzed and stored frozen below -85 °C.

Molecular Weight Determination on Gel-filtration Column: The enzyme solution (0.2 ml) was applied on an HPLC (high-performance liquid chromatography)-GTi system (LKB) using GF-250 column (0.94 by 25 cm; DuPont) and eluted with the 20 mM HEPES, 0.1 M sodium acetate buffer, pH 7.8 at a flow rate of 1.0 ml/min.

Enzyme Assays: HDH enzymatic activity were routinely assayed in 20 mM HEPES buffer, pH 7.7 at 30°C or 37°C. Bis-Tris propane buffer (50mM) was substituted instead of HEPES buffer to study the pH optimum of HDH activity. Stock solution (50 mM) of mustard sulfoxide (HDSO) was added to the reaction medium to achieve the final concentration of 10 mM. At the appropriate times, the aliquots were withdrawn from the reaction medium for chloride concentration determination or were dried and derivatized for GC-FPD and GC-ECD analysis. One unit of HDH enzyme is defined as the catalyzing activity that released one µmole of chloride in one minute.

Chloride Determination: To determine chloride concentrations in the reaction medium we used the method of Iwasaki (Iwasaki, 1952) as follows: the reaction was stopped and the orange color was developed with the addition of 10% (v/v) 0.25 M $FeNH_4(SO_4)_2$ in 9 M HNO_3 and 10% (v/v) of 0.9 M $Hg(SCN)_2$ in ETOH. Precipitates were removed by centrifugation at 12,000×g for 2 min and the absorbance of the supernatant was read at 460 nm. It should be noted that the standard curve of the chloride although reproducible was not linear (Fig.1). Sigmastat application's polynomial regression analysis was used to find the coefficients of the polynomial expression that give the best fitting curve for the experimental data points of the standard curve. The derived polynomial function was used to ascertain the chloride concentrations from the absorbance of the sample.

Protein Determination: For protein determination, a protein dye binding method (Bradford, 1976) was used, with bovine serum albumin as the standard.

RESULTS AND DISCUSSION

HDH activity in crude extract: We obtained the cell free crude extracts of the *S. paucimobilis* UT26 strain by homogenizing the cells with French Pressure cell and subsequent centrifugation of the homogenate. In order to find out whether the extract had HDH enzymatic activity, the native supernatant and the supernatant denatured by boiling was separately incubated in the reaction medium that contained HDSO (10 mM). A steady increase of chloride release from HDSO was observed in the incubation medium containing the supernatant, but not in the medium containing the boiled supernatant (Fig. 2). This indicates that the supernatant possessed HDSO dehalogenase enzyme that is denatured by boiling. The HDH catalytic activity of the extract was found to be 5.6 units per gram protein at 30.5 °C, at 10.6 millimolar HDSO concentration and pH of 7.7. HDSO degradation by crude extract was also confirmed by GC-FPD and GC-ECD analysis of derivatized samples (data not shown).

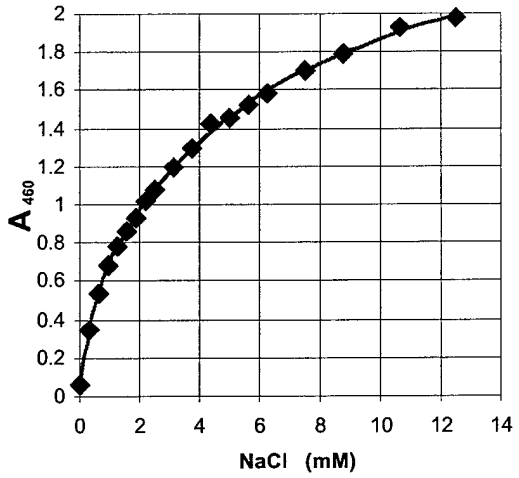

Figure 1. Chloride standard curve.

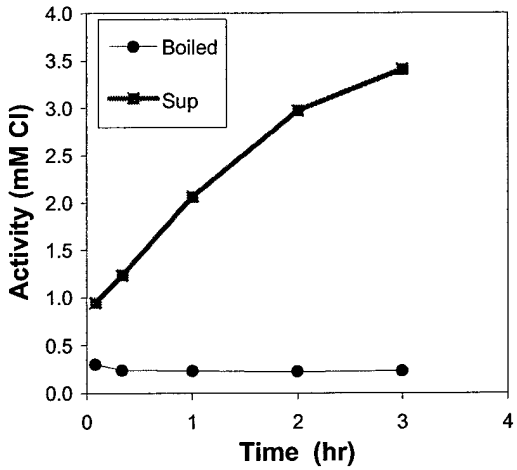

Figure 2. Boiling abolishes HDH activity.

Determining temperature and pH optimum: In order to find the temperature optimum of the HDH enzymatic activity, the experiments were conducted at temperatures varying from 25 °C to 30 °C at pH 7.7 (Fig. 3a). The maximum enzymatic activity was observed at 37 °C. The enzymatic activity at 30 °C was about 65 percent of the maximum and 45 percent at 25 °C. The enzymatic activity was nearly abolished at 49 °C (about 7.5 percent of the maximum). The initial experiments at 37 °C showed that the optimum enzymatic activity was above pH 7.5 (data not shown). Therefore, further studies were conducted in buffers with varying pH from 7.35 to 9.95 (Fig. 3b). We found that the HDH enzymatic activities increased with the increasing pH in the entire pH range that was tested. However, while HDSO was very stable at near neutral pH, the compound became unstable above pH 8.5 demonstrating increasingly higher spontaneous hydrolysis rate with increasing pH (Fig. 3b). Therefore, pH range of 8.0 to 8.5 was selected as the most suitable pH range for the analysis of HDH enzymatic activity.

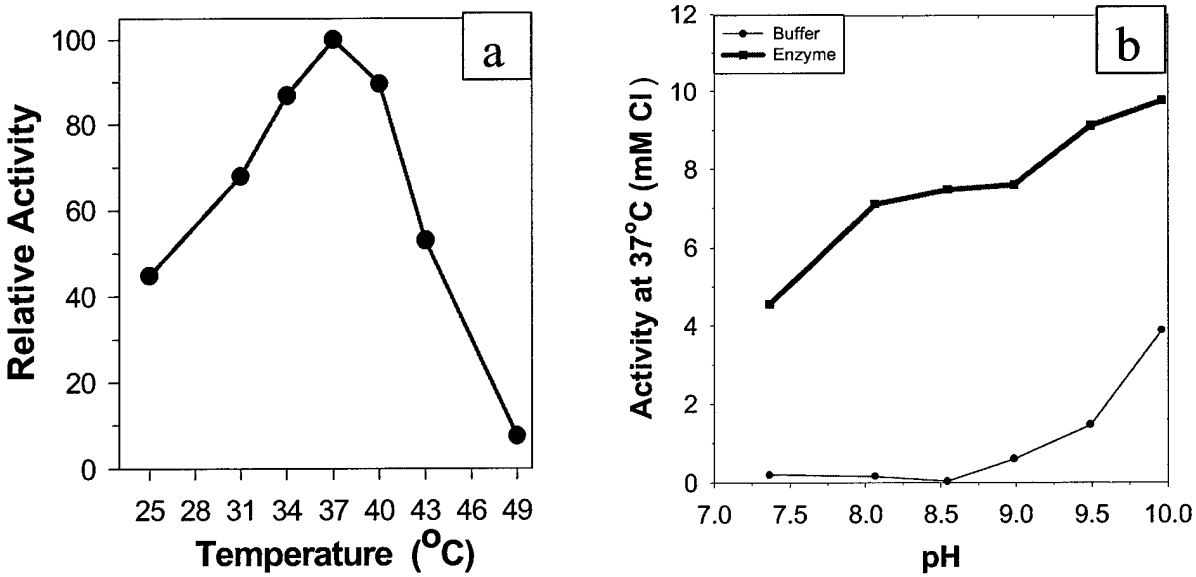

Figure 3. HDH activity versus (a) temperature and (b) pH.

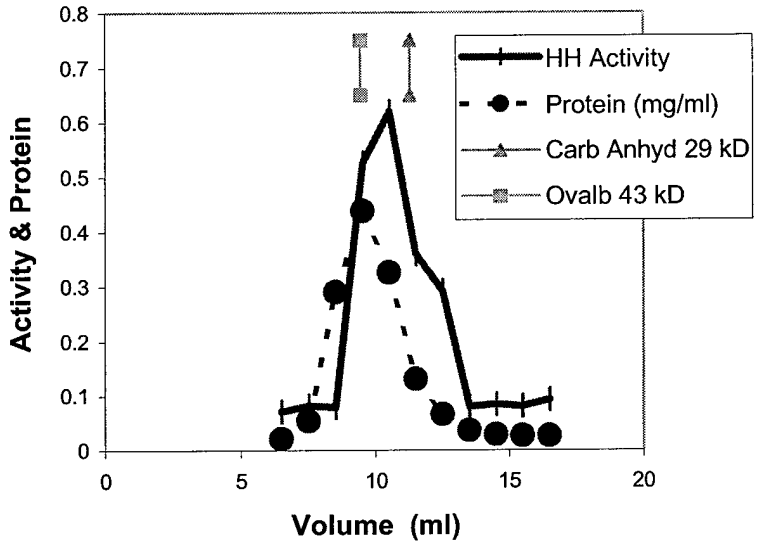

Figure 4. HDH gel-filtration on GF-250 column.

Chromatography: The gel-filtration HPLC chromatography was used to estimate the approximate size of HDH enzyme (Fig. 4). The maximum HDH enzymatic activity was eluted between the peaks of protein molecular weight standards of carbonic anhydrase (29 kD) and ovalbumin (43 kD). This result is consistent with earlier finding for LinB protein's gel-filtration elution profile and its deduced molecular weight of 33.1 kD (Nagata, 1993b, 1997). The HDH enzyme was partially purified on DEAE-Sepharose using the sodium acetate step gradient (Fig. 5), followed by the linear gradient of sodium acetate (data not shown). Further purification of the enzyme is in progress.

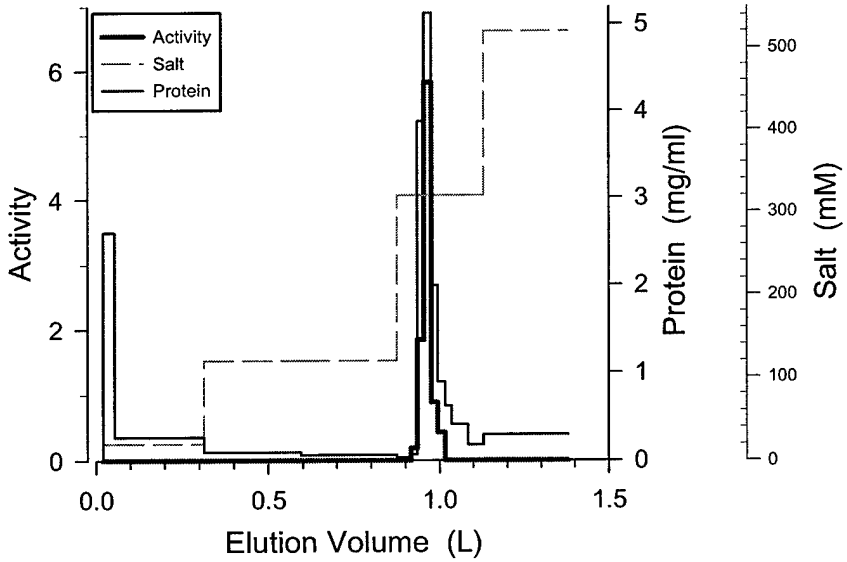

Figure 5. HDH purification on DEAE-Sepharose FF.

REFERENCES

Bradford, M.M. (1976) A rapid and sensitive method for the quantitation of microgram quantities of protein utilizing the principle of protein dye binding. *Anal. Biochem.* **72**, 248-254.

Drago, R.S.; Frank, K.M.; Wagner, W.G. and Yang, Y.-C. (1998) Catalytic activation of hydrogen peroxide – a green oxidant system. Proceedings of the 1997 U.S. Army Edgewood Research, Development and Engineering Center Scientific Conference on Chemical and Biological Defense Research. ERDEC-SP-063, pp 341-342.

Groesbeck, W.M. (1923) The toxicity for white mice, by injection, of certain compounds chemically related to mustard gas. EAMRD-16, pp.7-8. War Department, Chemical Warfare Service, Edgewood Arsenal, MD.

Helfrich, O.B. and Reid, E.E. (1920) Reactions and derivatives of ❂,❂'-dichloro-ethyl sulfide. *J. Am. Chem. Soc.* **42**, 1208-1232.

Imai, R.; Nagata Y.; Senoo, K; Wada, H.; Fukuda, M.; Takagi, M. and Yano, K. (1989) Dehydrochlorination of ❋-hexachlorocyclohexane (❋-BHC) by ❋-BHC assimilating *Pseudomonas paucimobilis. Agric. Biol. Chem.* **53**, 2015-2017.

Imai, R.; Nagata Y.; Fukuda, M.; Takagi, M. and Yano, K. (1991) Molecular cloning of a *Pseudomonas paucimobilis* gene encoding a 17-kilodalton polypeptide that eliminates HCI molecules from ❋-hexachlorocyclohexane. *J. Bacteriol.* **173**, 6811-6819.

Iwasaki, I.; Utsumi, S. and Ozawa, T. (1952) New colorimetric determination of chloride using mercuric thiocyanate and ferric ion. *Bull. Chem. Soc. Japan* **25**, 226.

Marshall, E.K. Jr. and Williams, J.W. (1921) The toxicity and skin irritant effect of certain derivatives of dichloroethyl sulfide. *J. Pharmacol. Exp. Ther.* **16**,259-272.

Miyauchi, K.; Suh, S.-K.; Nagata, Y. and Takagi, M. (1998) Cloning and sequencing of a 2,5-dichlorohydroquinone reductive dehalogenase gene whose product is involved in degradation of ❋-hexachlorocyclohexane by *Sphingomonas paucimobilis. J. Bacteriol.* **180**, 1354-1359.

Nagata, Y.; Hatta, T.; Imai, R.; Kimbara, K.; Fukuda, M; Yano, K. and Takagi, M. (1993a) Purification and characterization of ❋-hexachlorocyclohexane (❋-HCH) dehydrochlorinase (LinA) from *Pseudomonas paucimobilis. Biosci. Biotechnol. Biochem.* **57**, 1582-1583.

Nagata, Y.; Nariya, T.; Ohtomo, R; Fukuda, M; Yano, K. and Takagi, M. (1993b) Cloning and sequencing of a dehalogenase gene encoding an enzyme with hydrolase activity involved in the degradation of ❋-hexachlorocyclohexane in *Pseudomonas paucimobilis. J. Bacteriol.* **175**, 6403-6410.

Nagata, Y.; Ohtomo, R.; Miyauchi, K.; Fukuda, M; Yano, K. and Takagi, M. (1994) Cloning and sequencing of a 2,5-dichloro-2,5-cyclohexadiene-l,4-dial dehydrogenase gene involved in the degradation of ❋-hexachlorocyclohexane in *Pseudomonas paucimobilis. J. Bacteriol.* **176**, 3117-3125.

Nagata, Y.; Miyauchi, K.; Damborsky, J.; Manova, K.; Ansorgova, A. and Takagi M. (1997) Purification and characterization of haloalkane dehalogenase of a new substrate class from a ❋-hexachlorocyclohexane-degrading bacterium, *Sphingomonas paucimobilis* UT26. *Appl. Environ. Microbiol.* **63**, 3707-3710.

Nagata, Y.; Futamura, A.; Miyauchi, K. and Takagi, M. (1999) Two different types of dehalogenases, LinA and LinB involved in ❋-hexachlorocyclohexane degradation in *Sphingomonas paucimobilis* UT26 are localized in the periplasmic space without molecular processing.. *J. Bacteriol.* **181**, 5409-5413

Richardson, D.E.; Yao, H.; Xu, C.; Drago, R.S.; Frank, K.M.; Wagner, W.G. and Yang, Y.-C. (1999) Kinetics and equilibrium formation of a weakly basic oxidant system for decontamination. Proceedings of the 1998 U.S. Army Edgewood Research, Development and Engineering Center Scientific Conference on Chemical and Biological Defense Research. ECBC-SP-004, pp 293-299.

Senoo, K. and Wada, H. (1989) Isolation and identification of an aerobic ❋-HCH decomposing bacterium from soil. *Soil Sci. Plant Nutr.* **35**, 79-87.

Wagner, W.G. and Yang, Y.-C. (1999) Baking soda, hydrogen peroxide, alcohol: the refreshing, universal decon for VX, GB and HD. Proceedings of the 1998 U.S. Army Edgewood Research, Development and Engineering Center Scientific Conference on Chemical and Biological Defense Research. ECBC-SP-004, pp 285-291.

Yang, Y.-C.; Baker, J.A. and Ward, J.R. (1992) Decontamination of chemical warfare agents. *Chem. Rev.* **92**, 1729-1743.

ROOM TEMPERATURE MINERALIZATION OF CHEMICAL WARFARE AGENTS USING HYDROGEN PEROXIDE – Pd/C

George W. Wagner, Lawrence R. Procell and Yu-Chu Yang

U.S. Army ECBC, ATTN: AMSSB-RRT-CA, 5183 Blackhawk Rd., APG, MD 21010-5424

The deep oxidation of toxic organics and chemical warfare (CW) agent simulants using Pd/C and dioxygen or hydrogen peroxide at 80–90°C was recently demonstrated by Sen et al.[1] This process offers a chemical means of destroying CW materials in a manner traditionally achievable only by incineration. Our investigations of the common simulant dimethyl methylphosponate (DMMP) have shown mineralization to inorganic phosphate using H_2O_2–Pd/C at 90°C. Oxidative cleavage of DMMP to methylphosphonic acid is most effective at room temperature, apparently due to reduced H_2O_2 decomposition. Similarly, GD and VX also showed oxidative cleavage at room temperature, and formation of inorganic phosphate. For HD and its simulant thiodiglycol, mineralization is also evident at room temperature.

INTRODUCTION

Historically, the demilitarization of chemical warfare agents has been accomplished by incineration, thus rendering the elements comprising the agents to their oxidized, mineral salts, i.e. CO_3^{2-}, PO_4^{3-}, SO_4^{2-}, NO_3^-, etc. However, concerns about the safety of incineration at storage sites, especially near populous areas, has prompted the adoption of chemical neutralization strategies.[2] Such methods require post-treatment of the non-toxic, neutralized products, e.g. by incineration or biodegradation, to yield mineral salts; the preferred state for ultimate disposal.[2]

Sen and coworkers[1] recently demonstrated the mineralization of organophosphorus and organosulfur compounds using Pd/C, O_2 and CO or H_2 at 80–90°C. The proposed mechanism, shown in Scheme 1 for VX, involves the following steps: 1) initially, H_2 (or H_2 formed in the water gas shift reaction* from CO) generates a metal-hydride; 2) the metal-hydride reacts with O_2 to yield a metal-hydroperoxide; and 3) the metal-hydroperoxide forms the active oxidant, a metal-oxo species. It is this latter species that is thought to carry out the observed deep oxidations of heteroatom organics. Thus in an aqueous setting, VX would yield nitric, sulfuric, phosphoric and carbonic acid (the latter evolving CO_2 under acidic conditions) as shown in Scheme 1. Alternatively, the metal-hydroperoxide, and subsequently the metal-oxo, may be generated directly from H_2O_2, and Sen et al.[1] proved that replacing the gases with aqueous H_2O_2 did yield similar deep oxidation behavior for phenol. As attractive as working with heated, pressurized O_2 and H_2 or CO may be, aqueous H_2O_2 is perhaps more acceptable for the demilitarization of CW agents. This is especially true if the reactions could be performed at room temperature. Indeed hydrogen peroxide-based decontaminants[3] are gaining popularity amoung military

and civil defense planners. The intent of the current study is to explore the mineralization of VX, GD and HD using the H_2O_2–Pd/C system.

SCHEME 1

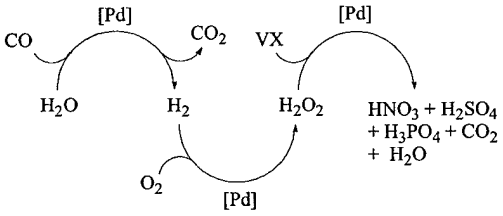

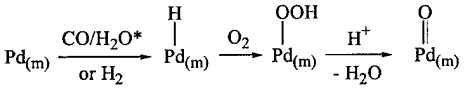

$^*CO + H_2O \longrightarrow CO_2 + H_2$

EXPERIMENTAL

50% H_2O_2 and 5% Pd/C (Degussa type E101) were obtained from Aldrich. Reactions were carried out in a stirred glass vessel by adding Pd/C, substrate, 50% H_2O_2 and, in some cases, water and conc. HCl. The H_2O_2 was either added all at once or metered in slowly with a syringe pump. Caution: the reaction of 50% H_2O_2 with 5% Pd/C is highly exothermic and results in substantial H_2O_2 decomposition! At selected intervals, ca. 1mL aliquots were taken for NMR analysis. ^1H, ^{13}C and ^{31}P NMR spectra were obtained using a Varian Unityplus 300 NMR spectrometer. Chemical shifts were referenced to external TMS (^1H, 0 ppm), $CDCl_3$ (^{13}C, 77.0 ppm) and 85% H_3PO_4 (^{31}P, 0 ppm). A sample of the HD reaction was also analyzed by capillary electrophoresis (CE) using a Hewlett Packard ^{3D}CE system employing indirect UV detection to confirm SO_4^{2-} formation, i.e. mineralization.

RESULTS AND DISCUSSION

Data obtained for various simulants and agents are given in Table 1. Initial studies were carried out with DMMP with the intention of detecting inorganic phosphate (PO_4^{3-}) by ^{31}P NMR, thus proving oxidative cleavage of the P-C bond and mineralization of the phosphorus. However, this conclusive proof was hampered by two phosphorus-containing stabilizers present in the 50% H_2O_2; one of which was PO_4^{3-} itself. For the DMMP reactions reported in Table 1, no substantial PO_4^{3-} formation was evident, and the conversions reported in Table 1 merely reflect the amount of DMMP remaining compared to detected products. These products varied with temperature. At 90°C, both methyl methylphosphonic acid (MMPA) and methylphosphonic acid (MPA) formed, but at room temperature, decomposition occurred directly to MPA. A possible explanation for this difference is that the reaction pathway DMMP → MMPA → MPA is expected for simple hydrolysis, which would be competitive with oxidative cleavage at elevated temperatures. At room temperature, the lone MPA product is consistent with exclusive oxidative cleavage. The overall conversions at 90, 50°C and room temperature were 94.2, 35 and 100%, with the latter conversion achieved using only 5.63 mL H_2O_2 (compared to 10 mL for the other reactions). At 50°C no MMPA hydrolysis product was observed, and oxidative cleavage was the major mechanism. The low conversion is attributed to heightened H_2O_2 decomposition at elevated temperatures. The high conversion at 90°C is largely attributed to hydrolytic cleavage. Thus oxidative cleavage appears most effective at room temperature, where undesired H_2O_2 decomposition is minimized. For the reactions

shown in Table 1 no substantial PO_4^{3-} formation beyond that of the H_2O_2 background was observed; a testament to the resiliency of the P-C bond. Yet, as anticipated, in extended reactions done with DMMP at 90°C, and for GD and VX at *room temperature* (see below), significant additional PO_4^{3-} was detected after several days.

TABLE 1.

Substrate	Temp	Pd/C[a]	H_2O	HCl[b]	H_2O_2[c]	Time	Conversion[d]
25 µL DMMP[e]	90°C	250 mg	5.63 ml	1.87 ml	10 ml	20 h	94.2%
25 µL DMMP	50	250	5.63	1.87	10	22	35.0
25 µL DMMP	22	250	none	1.87	5.63	24	100
23 µL TG[f]	22	250	none	none	5	72	>91[g]
38 µL HD	22	250	none	none	10	24	100[h]
81 µL VX	22	250	none	none	10	24	96.3
55 µL GD	22	250	none	none	10	24	79.6
					10[i]	24	100

[a]5 wt% Pd. [b]Conc. HCl. [c]50% H_2O_2. [d][1 - (moles substrate/moles product)] × 100. [e]Dimethyl methylphosphonate. [f]Thiodiglycol. [g]Lower limit estimate; product interfered with TG detection. [h]HD completely hydrolyzes to TG in water. [i]Second H_2O_2 addition allowed to react for an additional 24 h.

For TG and HD reactions at *room temperature*, ^{1}H NMR showed definite loss of C-H bond intensity relative to a TG control sample (Figure 1). Furthermore, the all important sign of mineralization, SO_4^{2-}, was observed by capillary electrophoresis. However, HCO_3^- was not observed,

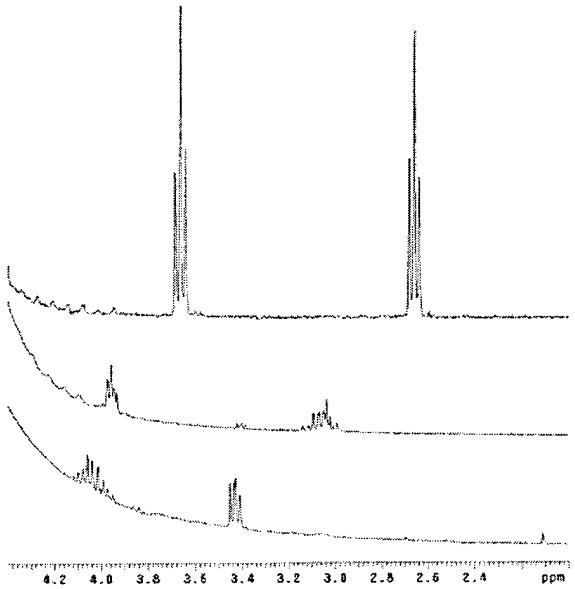

Figure 1. ^{1}H NMR spectra obtained for TG control (top) and TG (middle) and HD (bottom) reaction mixtures (see Discussion).

consistent with the evolution of CO_2 as shown in Scheme 2. ^{1}H NMR showed that TG reacted to the sulfoxide (TGO) and sulfone (TGO_2), but no further products were observed. As detected by ^{1}H NMR and confirmed by ^{13}C NMR, the initial HD product was the sulfoxide (HDO, ^{13}C: 53.7, 37.3 ppm), which proceeded directly to TGO_2 (^{13}C: 55.0, 54.4 ppm) (Scheme 2). No other products were observed. Thus intermediates involved in the passage of TGO_2 into mineral oblivion must be short lived. For HD, the non-detection of HD-sulfone (HDO_2) or TGO is consistent with the facile hydrolysis of HDO_2 to TGO_2 and the extreme hydrolytic stability of HDO.[4]

SCHEME 2

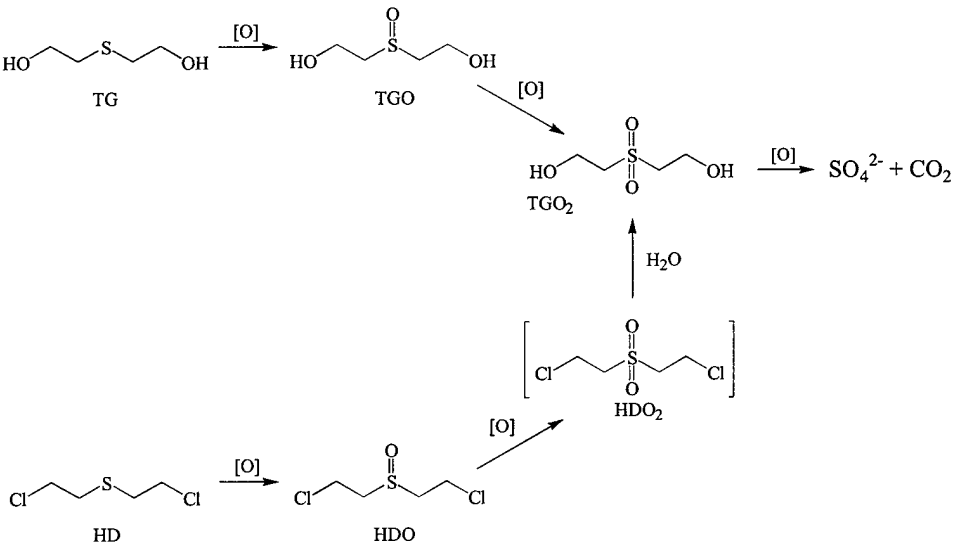

Similar to DMMP, the detected products for GD (MPA) and VX (EMPA) indicate *room temperature* oxidative cleavage of their pinacolyl and 2-(diisopropylamino)ethanethiol groups, respectively (Scheme 3). As shown by the conversions in Table 1, these reactions require a day or two to complete, with the VX reaction occurring somewhat faster. Over the course of several days, substantial increases in the amounts of PO_4^{3-} are observed in these reactions. For GD, this increase corresponded to the decrease in the amount of MPA (Scheme 3). The reaction was more complex for VX, where the initially formed EMPA degraded to MPA, PO_4^{3-} and an unknown phosphonate postulated as acetyl methylphosphonic acid. This tentative assignment is made based on a similar product, phosphonoacetic acid, observed by Sen et al.[1] in the oxidation of triethylphosphine oxide.

SCHEME 3

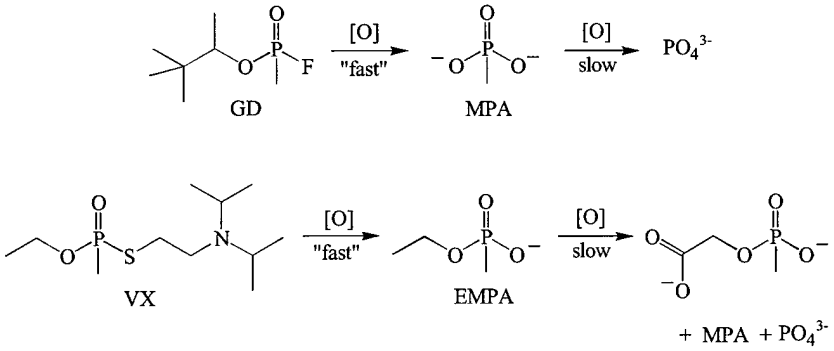

CONCLUSIONS

GD, VX and HD are mineralized at room temperature using the Pd/C-catalyzed peroxide system. Mineralization of HD and the oxidative cleavage of the pinacolyl and 2-(diisopropylamino)ethanethiol groups of GD and VX are facile compared to the slow oxidative cleavage of the P-C bond of MPA.

ACKNOWLEDGEMENTS

We thank Mr. Richard L. Cheicante, EAI Corp., for CE analysis of the HD sample.

REFERENCES

1. Pifer, A.; Hogan, T.; Snedeker, B.; Simpson, R.; Lin, M.; Shen, C.; Sen, A. *J. Am. Chem. Soc.* **1999**, *121*, 7485–7492.
2. Yang, Y.-C. *Chem. Ind.* **1995**, 334-337, and references therein.
3. (a) Wagner, G. W.; Yang, Y.-C. In the Proc. 2001 Sci. Conf. Chem. Biol. Def. Res., in press. (b) Wagner, G. W.; Yang, Y.-C. In the Proc. 1998 ERDEC Sci. Conf. Chem. Biol. Def. Res., ERDEC-SP-004; U.S. Army Edgewood Research, Development and Engineering Center, 1999, pp. 285-291. (c) Ember, L. *Chem. Eng. News* **1999**, *77* (Mar. 8), 10.
4. Lawson, W. E.; Reid, E. E. *J. Am. Chem. Soc.* **1925**, *47*, 2821-2836.

DECON GREEN

George W. Wagner, Philip W. Bartram, Lawrence R. Procell, Vikki D. Henderson and Yu-Chu Yang

U.S. Army ECBC, ATTN: AMSSB-RRT-CA, 5183 Blackhawk Rd., APG, MD 21010-5424

Simple solutions of hydrogen peroxide, carbonate/bicarbonate, and co-solvents afford the rapid, broad-spectrum decontamination of chemical warfare agents. Such formulations, termed "DECON GREEN", are non-toxic, non-corrosive and environmentally friendly. Reactivity arises from in situ generated peroxy anion OOH^- and peroxocarbonate HCO_4^-, which, respectively, afford the rapid perhydrolysis of VX and GD to their non-toxic phosphonic acids, and the oxidation of HD to its non-vesicant sulfoxide. DECON GREEN performs well at decontaminating CARC painted panels.

INTRODUCTION

The U.S. Army is developing environmentally friendly decontamination systems to replace current, problematic decontaminants such as hypochlorite.[1] Desirable characteristics for the replacement include maintaining a broad-spectrum reactivity towards all agents, even in cold weather operations, while achieving a significant reduction in the toxic, corrosive and environmentally harmful nature of the decontaminant. Decontaminants such as hypochlorite are corrosive and produce undesirable reaction products for HD which retain irritant and/or vesicant properties.[1]

In industrial applications, environmental concerns have been driving the replacement of chlorine based bleaching processes with peroxide based systems.[2] These "green" peroxide systems avoid the formation of toxic, carcinogenic chlorinated organic compounds such as those produced in paper production.[3] Peroxide based systems may also be employed in *military* applications, replacing historical chlorine based "bleach" decontaminants. Such systems afford the necessary rapid reactions and, as in the case of industrial bleaching, avoid undesirable products. We call this fledgling, but promising decontamination system "DECON GREEN." In this paper, the reaction chemistry and kinetics of agents in DECON GREEN formulations will be discussed, and results for the performance of DECON GREEN at decontaminating painted panels will be presented.

EXPERIMENTAL

Aqueous 30 and 50 wt % hydrogen peroxide (H_2O_2), urea hydrogen peroxide addition compound ($NH_2C(O)NH_2 \cdot H_2O_2$, 98 % pure, 36 wt % H_2O_2), polypropylene glycol (PPG-425, avg. MW 425) and other solvents were obtained from Aldrich. Decon solutions were mixed by first dissolving bicarbonate

and/or carbonate in the aqueous H_2O_2 prior to adding the co-solvents. Urea hydrogen peroxide and $NaHCO_3$ were simultaneously dissolved in water before adding the co-solvent. Reactions of GB, GD, VX and HD with decon solutions were monitored by ^{31}P and ^{1}H NMR using a Varian Unityplus 300 NMR spectrometer. Spectra were referenced to external 85% H_3PO_4 (^{31}P, 0 ppm) and TMS (^{1}H, 0 ppm). Reactions were initiated by adding neat GB, GD, VX and HD to the decon solution contained in a 5 mm NMR tube. The tubes were capped, wrapped with parafilm and shaken to thoroughly mix the contents. **Caution**: These experiments should only be performed by trained personnel using applicable safety procedures. Final concentrations of 0.01M GB, GD and VX, and 0.1M HD were used.

Chemical Agent Resistant Coating (CARC) painted coupons were contaminated with several 2 µL drops of VX, TGD, or HD to obtain a challenge of 1 mg/cm^2 (10 g/m^2). The panels were allowed to stand for 1 h, at which point sufficient decon solution was applied to just cover the panel. The decon solution was allowed to act for 30 min before being removed with a water rinse. The panel was then allowed to briefly dry in air before being immersed in chloroform for 1 h to extract residual agent. The agent extracts were assayed by a Hewlett-Packard 5890 GC.

RESULTS AND DISCUSSION

Basic peroxide has been known to rapidly decontaminate GB (Sarin) for decades,[4] via generation of the powerful nucleophile peroxy anion OOH^-. This reaction is shown in Scheme 1. We have observed the long-suspected[4] peroxyphosphonate intermediate using ^{31}P NMR for both GB and GD, which yield peaks at 42.2 and 41.6, 41.0 ppm (two diasteriomers), respectively. Representative reactions for GB and GD are shown in Table 1. GB in neutral peroxide exhibits an initial half-life of 67 h, apparently reacting with background OOH^-. But the reaction quickly slows prior to completion as the pH and [OOH^-] drop. However, with even small amounts of bicarbonate the reactions for both GB and GD become too fast to measure by NMR ($t_{1/2}$ << 1 min) and go to completion. Although perhydrolysis is indeed fast, G agents are also easily decontaminated by dilute alkali,[1] so peroxide offers limited advantage for these agents.

SCHEME 1

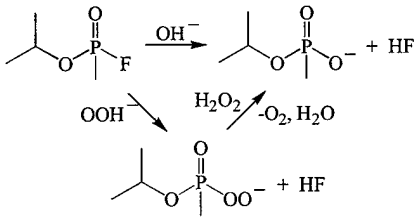

Quite recently, however, it was found that VX also undergoes rapid perhydrolysis to selectively yield ethyl methyphosphonic acid (EMPA) as shown in Scheme 2.[5] The *N*-oxide of VX (VX-NO) also forms; similarly undergoing perhydrolysis, but at a slower rate. No peroxy-EMPA intermediate is observed, perhaps owing to immediate reaction with liberated thiolate.[5] Unlike the G agents, perhydrolysis is a much more effective decontamination reaction for VX as toxic EA-2192 is avoided.[5] Basic hydrolysis yields about 22% EA-2192.[6] Representative reactions for VX are shown in Table 1. In neutral peroxide, some autocatalytic behavior is evident owing to protonation of the VX amine group with concomitant generation of OOH^-. However, formation of acidic products lowers the pH such that the reaction stops prior to completion and no further perhydrolysis or hydrolysis occurs over the course of

several hours. But with the addition of bicarbonate, the additional buffering capacity drives the reaction to completion.

TABLE 1. Half-Lives Observed for VX, GB and HD.

No.	Activators	Peroxide	Co-Solvents	$t_{1/2}$ VX	GB	HD	HDO
1	None	1.3 ml 30% H_2O_2[a]	1.9 ml t-BuOH	>>16 h[b,c]	29 days	42 min	
2	0.037 M $NaHCO_3$	1.3 ml 30% H_2O_2[a]	1.9 ml t-BuOH	120 min[c]	<1 min[d]	20 min[e]	
3	0.1 M $NaHCO_3$	1.3 ml 50% H_2O_2[f]	1.9 ml t-BuOH	11 min[c]	<1 min[d]	2.1 min	
4	"	"	1.9 ml EtOH		-	-	1.8 min
5	"	"	1.9 ml i-PrOH		-	-	1.8 min
6	"	"	1.9 ml PPG-425		-	-	1.9 min
7	0.33 M $NaHCO_3$	1.0 ml 50% H_2O_2[g]	1.0 ml t-BuOH	56 sec[c]	-	-	
8	0.75 M $NaHCO_3$	0.743g urea·H_2O_2[h] in 1 ml H_2O	1.0 ml t-BuOH	7.5 min[c]	<1 min[d]	1.6 min	
9	0.2 M $KHCO_3$	0.5 ml 50% H_2O_2[i]	0.2 ml i-PrOH + 0.3 ml Triton X-100	2.6 min[c]	-	2.1 min	245 h
10	0.1M $KHCO_3$ + 0.1M K_2CO_3	"	"	< 1 min[c,d]	-	2.4 min	40 h

[a]Final solution contains 15 wt% H_2O_2. [b]About 50% VX/VX-NO reacted within 1 h, but no further reaction occurred after 16 h. [c]Includes decay of slower-reacting VX-NO. [d]Reaction too fast to measure. [e]From reference 13a. [f]22 to 26 wt% H_2O_2, depending on the density of the alcohol. [g]30 wt% H_2O_2. [h]11 wt% H_2O_2. [i]28 wt% H_2O_2.

SCHEME 2

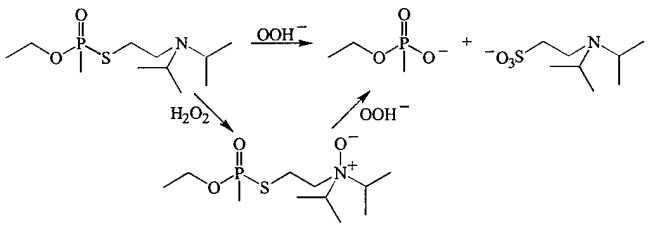

Although HD may be decontaminated by hydrolysis to non-toxic thiodiglycol,[1] its nucleophilic substitution is quite slow, proceeding exclusively via S_n1.[7] On the other hand, the oxidation of HD to the sulfoxide and sulfone can be extremely rapid.[1,8] As to the suitability of the sulfoxide and sulfone as decontamination products, relevant properties[9-11] are shown in Table 2. The sulfoxide is non-vesicant[9,10] and quite stable towards hydrolysis.[9] However, it should be noted that the sulfoxide does retain a subcutaneous toxicity identical to HD.[9] The sulfone retains both appreciable vesicant activity[9,10] and subcutaneous/intravenous toxicity,[9,11] but does undergo slow hydrolysis.[9] Thus HD may be rendered non-vesicant via selective oxidation to the sulfoxide. And, if formed, the sulfone is water-soluble and thus more amenable to hydrolysis than HD itself. Although powerful oxidants such as hypochlorite and peroxyacids (i.e. *m*-chloroperoxybenzoic acid) effect rapid oxidation of HD, they are rather non-selective, simultaneously producing both sulfoxide and sulfone. The milder oxidant hydrogen peroxide selectively yields the sulfoxide, but the reaction is too slow for the purpose of immediate decontamination. As shown in Table 1, HD is oxidized fairly slowly in only peroxide and co-solvent. Yet, ironically, this reaction is much faster than those observed for comparable amounts of VX and GD under the same conditions. Recently it has been shown that the activator bicarbonate[12,13] is able to effect the rapid oxidation of sulfides and HD catalytically. In peroxide, bicarbonate forms peroxocarbonate HCO_4^- which selectively oxidizes sulfides and HD to their corresponding sulfoxides.[12,13] This reaction is shown for HD in Scheme 3. $[HCO_4^-]$ is maximized near pH 7 and goes to zero near pH 11.[14] However, in the pH vicinity required for effective GB and VX hydrolysis (pH 8 to 9, see above), sufficient HCO_4^- remains to quickly oxidize HD with a half-life of less than 2 min. The last two entries in Table 1 show that HD sulfoxide (HDO) is subject to further oxidation to the sulfone (HDO_2), but the rate of this undesirable reaction is orders of magnitude slower than the oxidation of HD itself.

TABLE 2. Toxic Properties of HD, HDO and HDO_2.

	Toxicity (mouse, mg/kg)	Vesicant Action	Relative Hydrolysis Rate
HD	125[a]; 8.6[b]	most irritating[c]; severe[d]	Fast (50% in 10 min, 20°C)[c]
HDO	125[a]	scarcely irritating[c]; none[d]	Not hydrolyzed, even at 100°C[c]
HDO_2	105[a]; 50[b]	slightly less than HD[c]; severe[d]	Slow (55.9% in 150 min, 22°C)[c]

[a]Subcutaneous, reference 10. [b]Intravenous, reference 12. [c]Reference 10. [d]Reference 11.

SCHEME 3

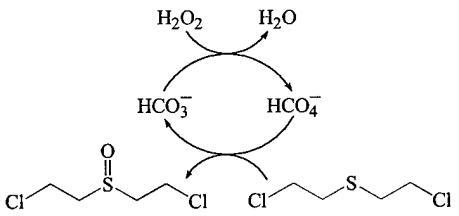

Thus a simple solution of hydrogen peroxide, bicarbonate, and a suitable co-solvent for water-insoluble HD achieves the desired broad-spectrum, rapid decontamination of all three types of agents.[12b] It

is interesting to note that with the use of edible co-solvents such as EtOH or PPG-425 (a food additive) the decontamination of GB, VX, and HD can be accomplished using *only* food-grade materials! The environmental advantages of such formulations are self-evident. Further note that solid urea peroxide addition compound (urea·H_2O_2) may be substituted for aqueous peroxide as this material yields solutions of the correct pH. Other common solid peroxides yield pH's that are either too high (e.g. sodium percarbonate, pH 10.5[15]) or too low (potassium peroxomonosulfate. pH 2-3[15]). Additionally, urea peroxide possesses the highest active oxygen content of the solid peroxides, though still less than that of aqueous 50% H_2O_2.

Although the above solutions are quite adept at decontaminating VX, GB, GD, and HD in agitated, homogenous solution, decontamination of agents and thickened agents on surfaces is more challenging. Results for the decontamination of VX, thickened GD (TGD), and HD on Chemical Agent Resistant Coating (CARC) painted panels using select DECON GREEN formulations are shown in Table 3.

TABLE 3. Decontamination of CARC Panels.

			% Agent Decontaminated[a]		
No.	Solvents/Peroxide (Vol%)	Activators	VX	TGD	HD
1	Diacetone Alcohol (52.5) Sulfolane (22.5) 50% H_2O_2 (23) Triton X-100 (2)	0.1M $KHCO_3$ 0.1M K_2CO_3	95.91%	99.66%	-
2	Propylene Carbonate (75) 50% H_2O_2 (23) Triton X-100 (2)	Same	96.66%	99.95%	-
3	Diacetone Alcohol (44) Sulfolane (19) 50% H_2O_2 (36) Triton X-100 (1)	Same	-	-	87.55%
4	Propylene Carbonate (62.5) 50% H_2O_2 (36.5) Triton X-100 (1)	Same	-	-	97.20%

[a]Initial contamination level 1000 μg-cm^{-2}. [b]Average of three runs.

The various DECON GREEN formulations signify a promising decontamination efficacy. However, to achieve this feat inedible, but non-toxic industrial co-solvents are required; primarily to dissolve TGD. In the case of VX and HD, significant amounts of agent remain, and this is attributed to sorption or swelling of these agents into the paint itself during the hour-long residence time. In this regard, thickened agents are actually *easier* to decontaminate since they do not sorb readily into surfaces. Work is continuing to examine the decontamination of agent sorbed within paint.

CONCLUSIONS

The fast, effective decontamination of GB, VX, TGD, and HD using activated hydrogen peroxide and suitable co-solvents has been demonstrated. For non-thickened agents, decontamination may be realized using only innocuous food-grade materials. Inedible, but non-toxic solvents allow the decontamination of thickened agents from surfaces. These latter formulations of DECON GREEN perform well in the decontamination of CARC painted panels.

ACKNOWLEDGEMENTS

We thank the late Prof. Russell S. Drago, Prof. David E. Richardson, and Prof. Clifford A. Bunton for many helpful discussions, and Messrs. Brian MacIver and David Sorrick for assistance with the agent operations.

REFERENCES

1. Yang, Y.-C.; Baker, J. A.; Ward, J. R. *Chem. Rev.* **1992**, *92*, 1729-1743.
2. (a) Dagani, R. *Chem. Eng. News* **1999**, *77*(27), 30-32. (b) McCoy, M. *Chem. Eng. News* **1999**, *77*(5), 18-19.
3. (a) McDonald, J. G.; Hites, R. A. *Anal. Chem.*, in press. (b) Zhang, Q.; Chuang, K. T. *Environ. Sci. Technol.* **1999**, *33*, 3641-3644. (c) Zheng, Y.; Allen, D. G. *Environ. Sci. Technol.* **1996**, *30*, 1890-1895.
4. (a) Epstein, J.; Demek, M. M.; Rosenblatt, D. H. *J. Org. Chem.* **1956**, *21*, 796-797. (b) L. Larsson, Acta Chem. Scand., 12 (1958) 723-730.
5. (a) Yang, Y.-C.; Szafraniec, L. L.; Beaudry, W. T.; Bunton, C .A. *J. Org. Chem.* **1993**, *58*, 6964-6965. (b) Yang, Y.-C.; Berg, F. J.; Szafraniec, L. L.; Beaudry, W. T.; Bunton, C. A.; Kumar, A. *J. Chem. Soc., Perkin Trans. 2* **1997**, 607-613.
6. Yang, Y.-C.; Szafraniec, L. L.; Beaudry, W. T.; Rohrbaugh, D. K. *J. Am. Chem. Soc.* **1990**, *112*, 6621-6627.
7. Yang, Y.-C.; Szafraniec, L. L.; Beaudry, W. T.; Ward, J. R. *J. Org. Chem.* **1988**, *53*, 3293-3297.
8. Yang, Y.-C.; Szafraniec, L. L.; Beaudry, W. T.; Davis, F. A.; *J. Org. Chem.* **1990**, *55*, 3664-3666.
9. Marshall, E. K., Jr.; Williams, J. W. *J. Pharmacol. Exp. Therapeutics* **1921**, *16*, 259-272.
10. Lawson, W. E.; Reid, E. E. *J. Am. Chem. Soc.* **1925**, *47*, 2821-2836.
11. Anslow, W. P., Jr.; Karnofsky, D. A.; Val Jager, B.; Smith, H. W. *J. Pharmacol. Exp. Therapeutics* **1948**, *93*, 1-9.
12. (a) Drago, R. S.; Frank, K. M.; Wagner, G. W.; Yang, Y.-C. In the *Proc. 1997 ERDEC Sci. Conf. Chem. Biol. Def. Res., ERDEC-SP-063*; U.S. Army Edgewood Research, Development and Engineering Center, 1998, pp. 341-342. (b) Wagner, G. W.; Yang, Y.-C. In the *Proc. 1998 ERDEC Sci. Conf. Chem. Biol. Def. Res., ERDEC-SP-004*; U.S. Army Edgewood Research, Development and Engineering Center, 1999, pp. 285-291.
13. (a) Richardson, D. E.; Yao, H.; Xu, C.; Drago, R. S.; Frank, K. M.; Wagner, G. W.; Yang, Y.-C. In the *Proc. 1998 ERDEC Sci. Conf. Chem. Biol. Def. Res., ERDEC-SP-004*; U.S. Army Edgewood Research, Development and Engineering Center, 1999, pp. 293-299. (b) Richardson, D. E.; Yao, H.; Frank, K. M.; Bennett, D. A. *J. Am. Chem. Soc.* **2000**, *122*, 1729-1739.
14. Flanagan, J; Jones, D. P.; Griffith, W. P.; Skapski, A. C.; West, A. P. *J. Chem. Soc., Chem. Commun.* **1986**, 20-21.
15. Degussa Corporation, company literature.

AB INITIO STUDIES ON HEXAVALENT PHOSPHORUS COMPOUNDS

Ashley L. Wilson*
Aberdeen High School
Aberdeen, Maryland 21001

William E. White
Research & Technology Directorate
Edgewood Chemical Biological Center
Aberdeen Proving Ground, Maryland 21010

ABSTRACT

The reaction of some organophosphorus compounds with cholinesterase is thought to proceed by nucleophilic substitution through a pentacoordinate trigonal bypyramidal structure. Recently, Robert Holmes suggested that a hexacoordinate species might be involved instead. Hartree-Fock calculations were performed on a series of hexavalent phos-phorus compounds in which a nitrogen atom provided both electrons for the sixth bond — thereby forming an octahedral complex. In general, electron-withdrawing groups on the phosphorus atom increased the strength of the coordinate covalent bond between the nitrogen and phosphorus atoms. When the hexavalent phosphorus species was constructed by addition of ammonia and hydroxide to a phosphonate, the P-N distance was over 4 Å. This weak interaction is inconsistent with the hypothesis that nitrogen ligands accelerate the rate of hydrolysis by forming a hexavalent transition.

INTRODUCTION

When a neural impulse, traveling down the axon from the nerve body, reaches the nerve terminal, acetylcholine is released, which diffuses across the synapse between the two neurons. The acetylcholine molecule binds to the cholinergic receptor on the postsynaptic neuron and stimulates a new neural response.[1] Acetylcholine dissociates from the receptor and is hydrolyzed into acetate and choline by a reaction catalyzed by acetylcholinesterase. Because

*2000 DoD High School Science and Engineering Apprentice

neither product is capable of stimulating the cholinergic receptor subsequent stimulation does not occur. Nerve agents inhibit the acetylcholinesterase, irreversibly. Inhibition occurs by the formation of a covalent bond with serine in the active site of protein, thereby blocking the active site and preventing the binding of the acetylcholine molecule.[2,3] Inhibition of the enzyme leads to uncontrolled accumulation of acetylcholine at the synapse and continued stimulation until the neurons become depolarized.

The reaction leading to inhibition occurs by nucleophilic attack of the serine on the organophosphorus ester. For several years, the consensus has been that the reaction proceeded through a pentavalent transition structure. Recently, Robert Holmes postulated that some enzyme reactions, specifically, the hydrolysis of cyclic AMP by phosphodiesterases, might progress through a hexavalent transition or intermediate.[4,5] This hexavalent species is formed from the five traditional ligands and a coordination complex, with neighboring amino groups in the active site of the enzyme. This coordination complex is formed by the donation of two electrons from a Lewis base to the phosphorus atom.

Most of the research on phosphorus compounds has been on trivalent and pentavalent species.[6] Although there has been some interest in hexavalent phosphorus, most of the activity has been empirical with relatively little theoretical work on the nature of molecular bonding. The first step in testing the hexavalent transition hypothesis of Holmes is a quantum chemistry study of various hexavalent phosphorus compounds and ions to determine the effects of the sixth ligand on the geometry of the molecule and electronic structure of the central phosphorus atom.

METHODS

All calculations were performed with Gaussian 94 using the Berny optimization routine and the default parameters. Input matrix was created with Gaussview 2.0. Quantum calculations were run at the restricted Hartree Fock level of theory with the following basis sets: 3-21G, 6-31G, 6-31G*, and 6-31+G*. Frequency calculations were performed on all optimized structures to confirm that the stationary points were minima. Calculations were performed on isolated molecules (gas phase) without any solvation models. Output was visualized with Gaussview.

RESULTS

Table #1 delineates the bond lengths of small fluorophosphorus compounds. PF_3 had a trigonal symmetry with the lone pair at the apex. The F–P–F bond angles were 96° for the 3-21G basis set, 96° for the 6-31G basis set, 97° for the 6-31G* basis set, and 97° for the 6-31+G* basis set. These angles compare with the experimental value of 98°.

The PF_4^+ molecule was tetrahedral (F–P–F bond angle=109.5°) with all basis sets. In contrast, the PF_4^- anion must accommodate a lone pair of electrons and therefore cannot have tetrahedral symmetry. The C_2V structure is a pseudo trigonal bipyrimid having a lone pair of electrons in one of the equatorial positions rather than a fifth ligand. The results from x-ray

crystallography for $N(CH_3)_4PF_4$ were not conclusive.[7] The $N(CH_3)_4^+$ cations were well ordered; however there was considerable disorder in the PF_4^- anions. The authors used a disorder model to resolve the discrepancies and with the assistance of density functional theory obtained the most probable bond lengths indicated in Table 1.

The PF_5 molecule had trigonal bypyramidal geometry, where the axial bond lengths were longer then the equatorial bond lengths. The difference between the axial and equatorial bond lengths increase as the basis set increases.

The bond lengths in the PF_6^- anion depend to some extent upon the cation. Two are listed in Table 1. All have an octahedral geometry with the obligate 90° bond angles. In the clathrate of hexafluorophosphoric acid, the PF_6^- anion occupies two distinct sites within the cavity.[8] Resolution of the diffraction pattern gave P—F bond lengths of 1.601 & 1.568 Å. These compare with 1.609Å with the 6-31+G* basis set. In this study, calculated bond lengths decreased as the size of the basis set increased.

TABLE 1. Bond Lengths of Phosphorus Fluorides (in Å).

Basis Set	PF_3	PF4-	PF_4^+	PF_5	PF_6^-
	Pyramidal	Pseudo Trigonal Bipyramidal	Tetrahedral	Trigonal Bypyramidal	Octahedral
3-21G	1.609	Axial 1.724 Equitorial 1.642	1.548	Axial- 1.604 Equatorial- 1.581	1.625
6-31G	1.663	Axial 1.798 Equitorial 1.695	1.598	Axial-1.655 Equatorial- 1.633	1.680
6-31G*	1.564	Axial 1.719 Equitorial 1.610	1.479	Axial- 1.568 Equatorial- 1.535	1.606
6-31+G*	1.569	Axial 1.746 Equitorial 1.609	1.479	Axial- 1.572 Equatorial- 1.535	1.609
Empirical	1.570	Axial 1.74[7] Equitorial 1.60	N/A	Axial- 1.577 [9] Equatorial- 1.534	1.56[10] 1.601 &1.568[8]

Based on the results produced with the 4 basis sets for the PF_3 and PF_5 molecules, it appears that the largest basis set (6-31+G*) generates values closest to the empirical. In addition to providing a double zeta number of basis functions, this set contains d orbitals on the non hydrogen atoms. The diffuse functions are important for the negatively charged species in which greater electron density may be present in areas more distant from the nucleus. Results with the smallest basis set (3-21G) are included for comparison.

The bond lengths of the PF_4NH_2 molecule calculated with the 3-21G and the 6-31+G* basis sets are indicated in Table 2. The amine moiety occupies one of the equatorial positions in the trigonal bipyrimid. The axial fluorines have a bond length of 1.599 Å ,which is slightly longer than those in the PF_5 molecule described in Table 1. The equatorial P—F bonds (1.590 Å) are also shorter that in PF_5. The P—N bond length determined with the larger basis set (6-31G*) is 1.614 Å. In contrast, the small 3-21G basis set gave a longer bond length of 1.642 Å.

TABLE 2. Calculated Bond lengths (Angstroms) for PH_4NH_2.

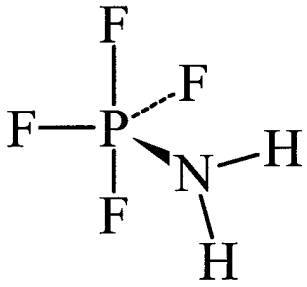

(Bond lengths in Å)

Basis Set	P–F	P–N	N–H
3-21G	Equatorial 1.590 Axial 1.624	1.642	0.996
6-31+G*	Equitorial 1.546 Axial 1.599	1.614	0.995

Addition of another fluoride ion produces the $PF_5NH_2^-$ anion. The geometry of this ion is indicated in Table 3. The bond lengths in this octahedral structure are considerably longer than the PF_4NH_2 molecule described in Table 2. The P—N bond at 1.735Å (6-31+G*) is about 1.2 Å longer than the corresponding bond.

TABLE 3. Calculated Bond lengths of $PF_5NH_2^-$.

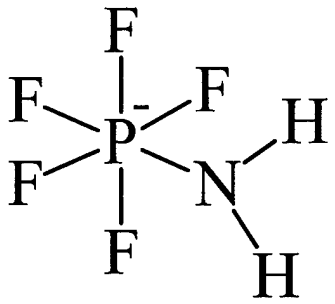

(Bond lengths in Å)

Basis Set	P–F	P–N	N–H
3-21G	Adjacent 1.640 Trans 1.647	1.722	0.994
6-31+G*	Adjacent 1.627 Trans 1.644	1.735	1.000

Addition of a proton to the amine produces an uncharged species also having octahedral geometry (Table 4). This molecule can be considered a coordination complex with the NH_3 molecule serving as a Lewis base and the PF_5 molecule as a Lewis acid. It is not surprising that the P—N bond length is longer (1.919 Å for the 6-31+G*) than in the anion. As would be expected, the P—F bonds shorten to 1.594 Å for the 4 fluorines adjacent to the nitrogen. In the neutral molecule, the trans P—F bond is shorter than the adjacent; whereas the opposite occurs in the PF_5NH_2 anion.

The inhibition of acetylcholine by organophosphorus nerve agents occurs as a result of nucleophilic substitution of the fluorine by the serine moiety in the active site of the enzyme. As indicated in the introduction, it is generally believed that this reaction proceeds through a pentavalent trigonal bipyramid intermediate or transition structure.

Table 5 contains bond lengths of a similar intermediate resulting from the nucleophilic attack of OH^- upon $CH_3P(O)FOCH_3$. The optimized geometries were slightly different for the two basis sets. With the smaller 3-21G, the hydroxyl occupied one of the equatorial positions and the phosphonyl oxygen was axial. The larger 6-31+G*, which contains diffuse functions produced a more reasonable geometry in which the nucleophile (OH) and the leaving group (F) occupied the two axial positions. As would be expected, the single bond P—OH was considerably longer than the polar phosphonyl bond, which is frequently written as P==O. The axial P—F bond is also longer than analogous bonds indicated in Tables 1 and 2.

TABLE 4. Calculated Bond Lengths of PH_5NH_3 Molecule.

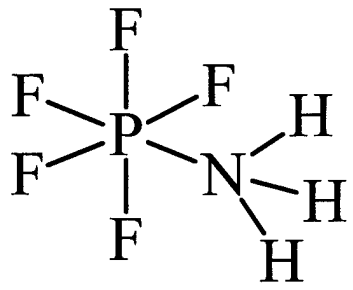

(Bond lengths in Å)

Basis Set	P–F	P–N	N–H
3-21G	Adjacent 1.616 Trans 1.593	1.946	1.012
6-31+G*	Adjacent 1.594 Trans 1.558	1.919	1.006

TABLE 5. Calculated Bond Lengths of $PO(CH_3)F(OH)OCH_3^-$.

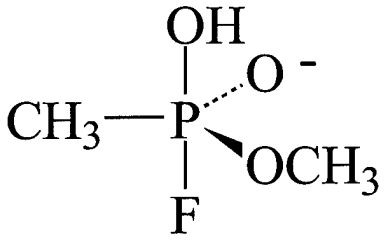

(Bond lengths in Å)

Basis Set	P–F	P–C(H)	P–O(C)	P–O(H)	P–O
3-21G	1.762	1.838	1.644	1.645	1.530
6-31+G*	1.743	1.847	1.697	1.731	1.558

Reducing the electron density in the intermediate by adding a Lewis Base (BH_3) to the phosphonyl oxygen shortens the bond lengths for all the other atoms (Table 6). Addition of the BH_3 group, lengthens the P=O bond from 1.558 Å to 1.824Å. Electrons are shifted from the P=O bond to form the O—B bond — thereby weakening and lengthening the P=O bond. The P—F bond shortens from 1.74Å to 1.58 Å — about the same as that in the uncharged PF_5 molecule

TABLE 6. Calculated Bond lengths for the Pentavalent/BH_3 complex.

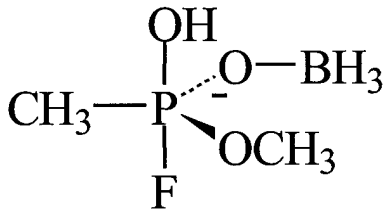

(Bond lengths in Å)

Basis Set	P–F	P–C(H)	P–O(C)	P–O(H)	P–O(B)
3-21G	1.634	1.726	1.667	1.657	1.843
6-31+G*	1.580	1.745	1.621	1.607	1.824

Addition of NH_3 to the pentavalent structures indicated in Table 5 and 6 produce analogous hexavalent ions whose bond lengths are listed in Tables 7 and 8. As indicated in Table 7, the P—N bond distance is over 4 Å. At this distance, essentially no electron interaction occurs between the nitrogen and the phosphorus. Addition of the BH_3 to the phosphonyl oxygen shortened the P—C, P—OH, and P—C bonds (P—F bond lengthened) but had little effect on the phosphorus-nitrogen bond distance.

TABLE 7. Bond Lengths of Octahedral Complex.

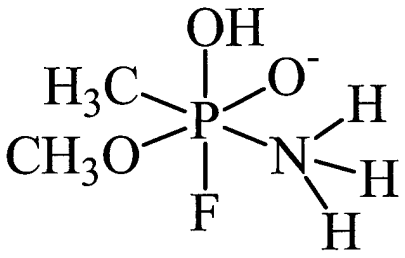

(Bond lengths in Å)

Basis Set	P–F	P–O(C)	P–O(H)	P–O	P–C(H)	P–N(H)
3-21G	1.701	1.665	1.730	1.492	1.846	3.252
6-31+G*	1.717	1.633	1.752	1.498	1.834	4.101

TABLE 8. Bond Lengths of Octahedral Complex with BH_3.

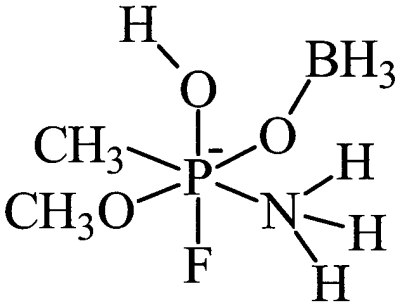

(Bond lengths in Å)

Basis Set	P–F	P–O(C)	P–O(H)	P–O(B)	P–C(H)	P–N(H)	O–B
3-21G	1.756	1.663	1.693	1.600	1.834	3.594	1.220
6-31+G*	1.742	1.619	1.665	1.534	1.826	4.284	1.224

The Mulliken partial charges on the individual atoms for the penta and hexavalent phosphorus compounds and ions are indicated in Table 9. For PF_6^-, the partial charge on phosphorus is 4.43 with negative charges evenly distributed among the six fluorines. Replacement of one of the fluorines with nitrogen adds electron density to the system and reduces the phosphorus charge to 3.92. Addition of H^+ to the $PF_5NH_2^-$ anion creating a neutral molecule has little effect on the electron density of any individual atom because the electrons needed to form the new N—H bond are averaged over the entire molecule.

The pentavalent anion formed by addition of OH^- to methyl methylphosphonofluoridate has a positive charge of 2.48 on the phosphorus. Addition of the Lewis acid BH_3 causes a slight reduction in the negative charge on the phosphonyl oxygen (electrons originally on the oxygen form the O—B bond) and creates additional positive charge on the phosphorus (i.e., 2.48 $\rightarrow$2.87).

Addition of NH_3 to the pentavalent phosphonate anion has only a small effect on partial charges. The changes may be the result of a different geometry around the phosphorus rather than electronic contributions by the ammonia molecule. Addition of BH_3 to the phosphonyl oxygen in the hexavalent system induced the same effects qualitatively as in the pentavalent; however, the magnitude of the changes in electron density was considerably less. The partial negative charge on the nitrogen in all P—NH_3 systems with hexavalent phosphorus was in the range of -1.3 ± 0.1. The various substituents on the phosphorus had little effect. As a corollary, the NH_3 moiety exerted little influence on the partial charge on the phosphorus and the other substituents.

CONCLUSIONS

Hexavalent phosphorus compounds formed by the addition of ammonia to PF_5 are stable species having P—N bonds about 1.9 Å in length. These bonds are longer than traditional P—N bonds in tetravalent and pentavalent phosphorus compounds. The hexavalent phosphorus nitrogen compounds are sufficiently stable to be synthesized and crystallized. In contrast, quantum calculations at the Hartree-Fock level of theory using double zeta quality basis sets containing both polarization and diffuse functions provide no evidence of a complex between an anionic phosphonic intermediate and ammonia. Upon optimization, the nitrogen separated from the phosphorus. Attempts to stabilize the complex by adding a Lewis base (BH_3) to the phosphonyl complex did not increase the interaction between the phosphorus and nitrogen. These calculations are inconsistent with the premise that nucleophilic substitution of phosphorus fluoridates by serine proceeds through a hexavalent transient in which the sixth bond results from a coordination complex between the phosphonate and an amino acid such as lysine or histidine.

TABLE 9. Mulliken Partial Charges.

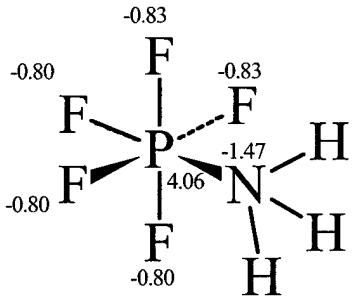

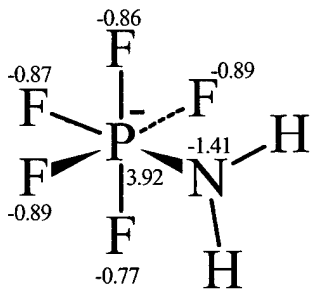

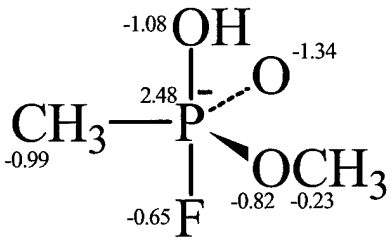

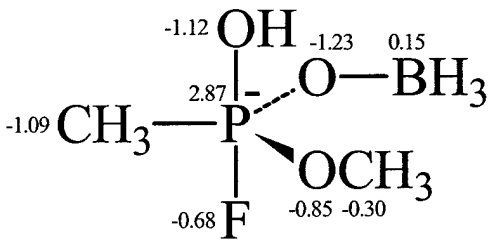

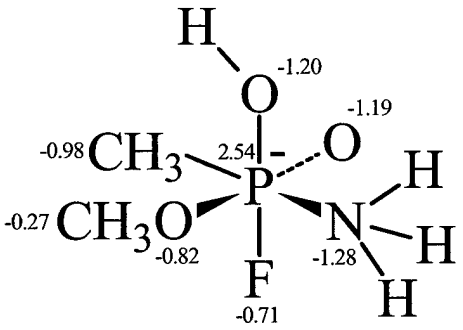

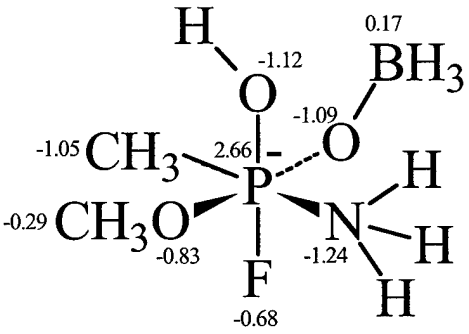

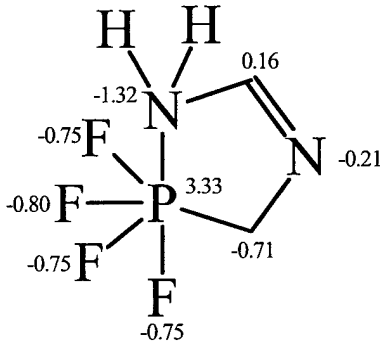

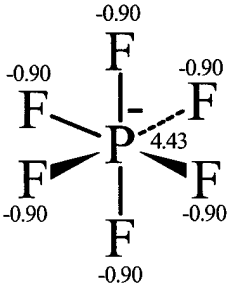

REFERENCES

1. Taylor, P.; Brown, J. H. In *Basic Neurochemistry. Molecular, Cellular, and Medical Aspects*; 5th ed.; Siegel, G. J., Agranoff, B. W., Albers, R. W., Molinoff, P. B., Eds.; Raven Press: New York, 1994; pp 231-260.

2. Eto, M., *Organophosphorus Pesticides: Organic and Biological Chemistry*; CRC Press: Boca Raton, FL, 1979.

3. Black, R. M.; Harrison, J. M. In *The Chemistry of Organophosphorus Compounds,*; Hartley, F. R., Ed.; John Wiley and Sons, 1996; Vol. 4; pp 781-840.

4. Holmes, R. R.; "Hexacoordinate Phosphorus via Donor Interaction. Implications Regarding Enzymatic Reaction Intermediates;"*Accounts of Chemical Research* **1998**, *31*, 535-542.

5. Holmes, R. R.; "Donor Interactions at Phosphorus. Implications Regarding Enzymatic Reaction Intermediates;"*Phosphorus, Sulfur, Silicon and Related Elements* **1999**, *144-146*, 1-4.

6. Quin, L. D., *A Guide to Organophosphorus Chemistry*; Wiley Interscience: New York, 2000.

7. Christe, K. O.; Dixon, D. A.; Mercier, H. P. A.; Sanders, J. C. P.; Schrobilgen, G. J.; Wilson, W. W.; "Tetrafluorophosphite PF4-, Anion;" *Journal American Chemical Society* **1994**, *116*, 2850-2858.

8. Mootz, D.; Oellers, E.-J.; Wiebcke, M.; "First Examples of the Type 1 Clathrate Hydrates of Strong Acids: Polyhydrates of Hexafluorophosphoric, Tetrafluoroboric, and Perchloric Acid;"*Journal of the American Chemical Society* **1987**, *109*, 1200-1202.

9. Holmes, R. R., *Pentacoordinated Phosphorus Vol 1 Structure and Spectroscopy*; American Chemical Society: Washington, D.C., 1980.

10. Corbridge, D. E. C.; *Phosphorus, An Outline of its Chemistry, Biochemistry, and Uses* 5th ed.; Elsevier: Amsterdam, 1995; pp 151.

NEXT-GENERATION RECOMBINANT ANTIBODIES AND ANTIGENS FOR THE DETECTION OF BIOLOGICAL THREAT AGENTS AND SIMULANTS

Kevin P. O'Connell*, Roy G. Thompson, Akbar S. Khan, and James J. Valdes

*Presenting author. Edgewood Chemical Biological Center, U. S. Army Soldier and Biological Chemical Command, AMSSB-RRT-BM, 5183 Blackhawk Road, Aberdeen Proving Ground, Maryland 21010 USA

ABSTRACT

Antibodies are currently the essential component in immunological sensors that detect BW (biological warfare) agents, giving them both sensitivity and selectivity. There is considerable lot-to-lot variability in the production of antibodies. The process of developing antibodies in animals or in mammalian cell culture is also time-consuming, which limits the capacity for "just-in-time" or surge production. Powerful recombinant DNA technologies are allowing the development and eventual replacement of these traditional affinity assay reagents with novel reagents that have improved performance and ease of production. This paper describes our efforts in two such technologies, recombinant antibodies and affinity-isolated peptide aptamers.

INTRODUCTION

Advances in the ability to clone very large peptide and protein libraries and display these structures on the surfaces of bacteria and bacteriophages have led directly to their use in isolating peptides and proteins that can bind and detect BW agents and their simulants. These recombinant products can be expressed and produced in large-scale bacterial fermentations, simplifying their production over the current method of mammalian cell culture (hybridoma production of monoclonal antibodies). These recombinant methods also offer investigators the option of modifying and further improving the product through molecular evolution methods.

Advances in genetic technologies have enabled scientists to clone gene fragments encoding for antibody specificity into host expression vectors, such as bacteriophage[1,2,3] and rapidly screen the library of random gene combinations to identify those fragments of the whole antibody molecule that mediate an antibody's specific recognition of a given antigen[4,5].

RECOMBINANT ANTIBODIES

A recent advance in antibody production technology is the cloning of antibody genes and their expression in bacterial fermentations. This technology has been proven capable of producing antibodies for BW agent detection that are of higher quality and uniformity from lot to lot. Recombinant antibodies are also faster and potentially less expensive to produce and acquire in quantity; therefore, establishing a process for their production would improve the maintainability and supportability of fielded biodetection systems. We describe here the cloning

and initial characterization of antibodies that bind the biothreat simulants bacteriophage MS2 (a non-pathogenic virus of the bacterium *Escherichia coli*, which is used to simulate viruses) and ovalbumin (a benign protein which is used to simulate protein toxins, such as ricin). To meet the need for high-quality, inexpensive antibody reagents, we have used phage display to isolate antibody genes from immunized mice. The resulting antibody molecules are called Fabs, indicating that they are comprised of heavy and light chain antibody sequences that form the antigen-binding variable region, but do not contain the IgG constant region.

Immunization, antibody gene amplification, and cloning. Antibody genes for immunoglobulin library construction were obtained from the spleens of BALB/c mice immunized with MS2 and ovalbumin. cDNA was synthesized from total spleen RNA, and amplified by PCR to isolate individual sets of immunoglobulin genes. PCR-amplified heavy chain genes are shown in Fig. 1. Heavy and light chain gene PCR fragments were assembled by ligation (MS2) or by PCR assembly (ovalbumin) and digested with restriction enzymes *Not*I and *Spe*I for cloning into the phage display vector. The primary antibody library was transformed into *E.coli* and expressed on filamentous phage particles by infection of the *E. coli* host cells with the helper phage VCSM13 (Stratagene, La Jolla, CA).

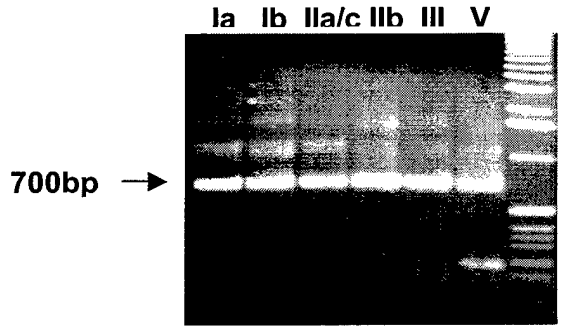

Figure 1. Amplification of heavy chain genes. Each family of mouse immunoglobulin heavy and light chain was amplified separately using PCR primers specific to that family. Shown are amplified gene fragments of six heavy chain families (Roman numerals). The desired gene fragments are 700 bp long. Other bands represent PCR artifacts. Right lane, DNA size marker.

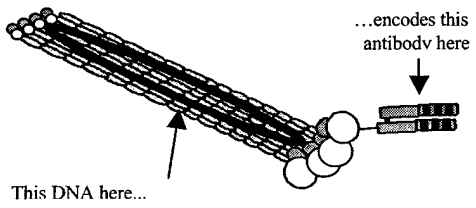

Figure 2. Schematic of antibody-displaying particle. A phage particle in the display library contains DNA encoding an antibody, and displays that same antibody on its surface. The entire repertoire of antibodies cloned from the mouse is converted to a form that can be screened by applying the population to a surface coated in the antigen of interest.

Affinity enrichment ("biopanning") of antibody clones. A purified recombinant form of the MS2 coat protein was used to screen the antibody library for clones that bind MS2. Ovalbumin for both immunization and biopanning is was obtained commercially (Pierce Co, Rockford, IL) in highly purified form. The display of the recombinant antibodies on the surface of the phage allowed for the enrichment of antigen specific clones through biopanning against

recombinant MS2 coat protein immobilized in the wells of microtiter plates. Phage particles displaying anti-MS2 or anti-ovalbumin antibodies (and containing the corresponding cloned antibody genes) were obtained by a form of affinity purification called "biopanning".

Subcloning and expression of the antibody genes. Following the last round of biopanning, individual phage clones containing the desired antibodies were identified by culturing individual clones and screening for binding of the appropriate antigen by ELISA. Verified positive clones were sequenced fully and from the sequence, the IgG subclass of each clone was determined. Genes for each Fab antibody were then removed from the phage display vectors and cloned into expression vectors that incorporate a 6x histidine tag on each heavy chain for subsequent expression and purification in fermentations of *E. coli*.

Expression and purification of recombinant anti-MS2 antibody. The introduction of antibody genes into the expression vector pHis1.1 fused the heavy chain genes with a 6xHis tag. The pHis1.1 expression vector (carrying the anti-MS2 antibody genes) was introduced into an *E. coli* strain constructed to optimize protein expression (TOPP I, Stratagene). Cells were grown in a 20-liter fermentor and the compound IPTG was added to induce expression of the antibody genes. After fermentation, cells were disrupted with a sonicator to release a crude lysate containing the recombinant anti-MS2 antibodies. The crude cell lysate was applied to a column packed with Talon metal affinity resin according to the manufacturer's instructions, and eluted with imidazole buffer. Eluted anti-MS2 antibody was further purified by passage over Sephadex gel filtration columns to greater than 90% purity. Fractions were analyzed by sodium dodecyl sulfate-polyacrylamide gel electrophoresis (SDS-PAGE) and HPLC for purity and protein content. Proteins were detected by staining with Coomassie Brilliant blue and by immunoblotting (Figure 4). Similar results were obtained when purifiying anti-ovalbumin antibodies (data not shown).

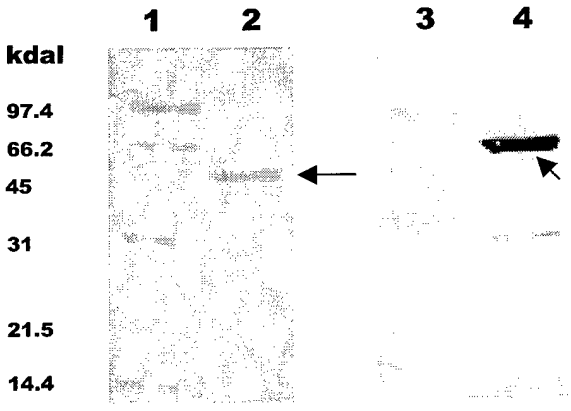

Figure 4. Purified recombinant anti-MS2 antibody. After purification as described in section 2.7, anti-MS2 antibody (lanes 2 and 4, **arrows**) was >90% pure as determined by SDS-PAGE and staining with Coomassie Brilliant blue (left image). Lane 1, molecular weight standard; lane 2, purified anti-MS2 antibody. Right image, experiment identical to lanes 1 and 2, but demonstrating the identity of the protein as mouse antibody by immunological detection. Lane 3, molecular weight marker; lane 4, purified anti-MS2 antibody. The anti-MS2 antibody was transferred to a nitrocellulose membrane after SDS-PAGE and detected with goat anti-mouse antibody conjugated to alkaline phosphatase, using NBT/BCIP as substrate.

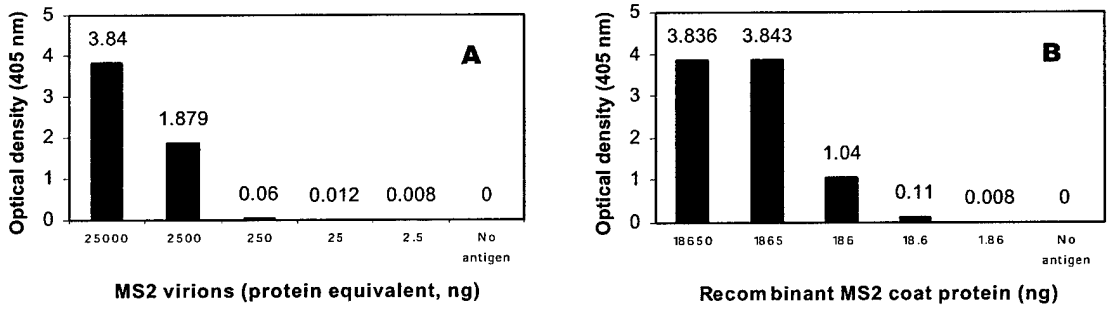

Figure 5. ELISA detection of (A) MS2 virions and (B) recombinant MS2 coat protein using purified anti-MS2 Fab antibody. Values represent the mean of 2, normalized to a no-antigen control experiment.

Detection of MS2 and ovalbumin with recombinant antibodies. Recombinant anti-MS2 and anti-ovalbumin antibodies were used in enzyme-linked immunosorbent assays (ELISAs) to detect their corresponding antigens. Density-gradient-purified bacteriophage MS2 and ovalbumin (Sigma) were serially diluted and bound by adsorption to wells of microtiter plates. Purified MS2 was detectable down to a level of 250 ng (protein equivalent) in this experiment (Figure 5). The recombinant coat protein used for biopanning and screening, however, was detected to a level of approximately 20 ng. This apparent greater sensitivity for the recombinant coat protein over the intact virus may reflect the isolation of the antibody using the recombinant protein as the biopanning target. Use of intact virions as the target, as well as performing the affinity capture of anti-body-displaying phage in solution will allow the isolation of Fabs with even greater affinity for intact MS2. Anti-MS2 did not bind phage M13, BSA, or ovalbumin (data not shown). Using partially purified recombinant antibodies OVA-3 and OVA-4, ovalbumin was detectable down to a level of 1 microgram (data not shown).

PEPTIDE-BASED BIODETECTION

Further reductionism in defining the molecular determinants of antibody specificity for antigen has been pursued by using combinatorial random peptide displays to map the specific amino acid sequences of the hypervariable region of the antibody that actually binds to the antigen epitope. It has been shown that the essential binding domains of an antibody may be as small as 5-15 amino acids[6,7,8,9]. Random peptide display libraries can be applied to two significant issues in the requirements for biodetection: 1) the design of molecular recognition elements that are smaller than whole antibodies and antibody fragments, and 2) the design of peptide sequences that can mimic the epitope binding sites on antigens and thus be used as positive controls for the antigen in assay validation. We have employed a random dodecapeptide library to screen for peptide sequences that may mimic the binding of antibody to the ricin and

staphylococcal enterotoxin B (SEB) toxins and to monoclonal antibodies generated against ricin and SEB.

Random Peptide Library. The FliTrx random peptide library was obtained commercially from Invitrogen. The library is composed of 1.77 X 10^8 primary clones of *E. coli* with the dodecamer peptide sequence inserted within the Thioredoxin (TrxA) active site loop. The TrxA peptide fusion is cloned into the nonessential domain of the major bacterial flagellin protein (FliC) under control of a P_L promoter from bacteriophage ë. When induced, the peptide sequence is expressed on the surface of the *E. coli* flagella with the N- and C-terminal ends constrained by a disulfide bond (Fig. 6).

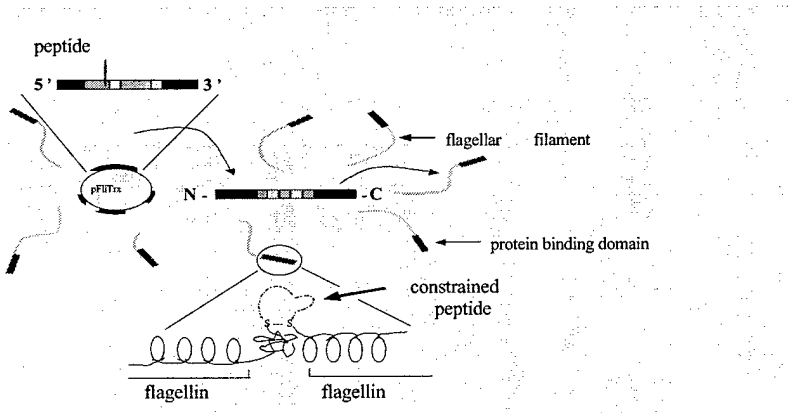

Figure 6. Schematic of peptide library construction and display.

Peptide library expression and panning. A stock culture of the cell-displayed peptide library was grown according to the manufacturer's instructions, and expression of the peptides were induced by addition of tryptophan. The library was panned against two toxins (ricin and SEB, obtained from Sigma). Antigens were diluted and adsorbed onto tissue culture plates, rinsed and blocked. After decanting the blocking solution, the induced cell culture was added to the culture plates. Cells bound to the plate were eluted into 10 mls fresh culture media by placing the plate on a vortex to shear the flagella and release the cells to the media. The cells were then cultured overnight and the complete procedure repeated for five rounds of panning. After the fifth round of panning, culture and peptide induction, cultures expressing peptides that bound the targets were identified by competitive ELISA; antigen or antibody ligands were added to compete with the binding of the peptide clones. Individual clones that tested positive in the ELISA were selected and the peptide-encoding DNA was isolated and sequenced.

Peptides that bind SEB or ricin. Figure 8 shows the ELISA screening results obtained from peptide binding to the SEB toxin. Four of the ten clones show significant interactions with the SEB toxin, as measured by the inhibition of peptide binding in the presence of a monoclonal antibody to SEB. Four of the ten peptide clones isolated after panning against ricin show

significant activity in inhibiting the binding between ricin and a monoclonal antibody. The peptide sequences of the clones isolated did not display a consensus sequence (data not shown).

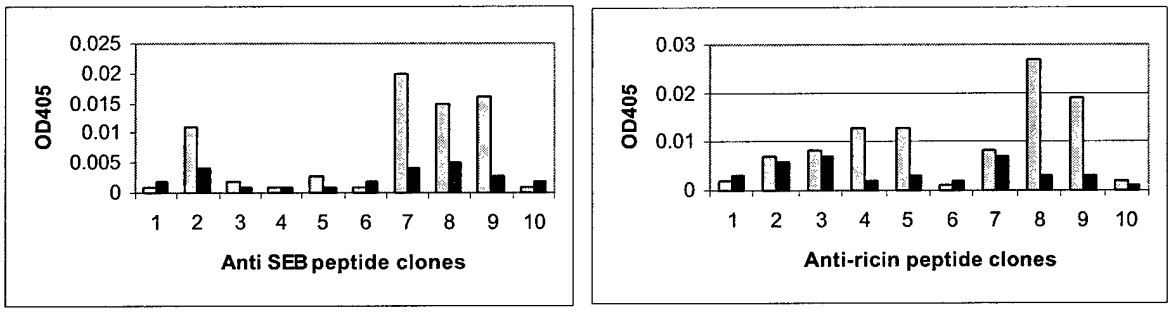

Figure 7. ELISA screening of peptide clones against SEB toxin (left) and ricin (right). Noncompetitive ELISAs are indicated by the shaded bars. Solid bars represent the inhibition of peptide-toxin interactions in the presence of anti-SEB or anti-ricin monoclonal antibody, respectively.

DISCUSSION AND CONCLUSIONS

A recombinant products approach to biodefense reagent development has several technical, logistical, and animal use advantages over traditional methods of isolating and producing antibodies. The technical advantages include the potential to produce antibody diversity greater than that obtainable by the immune systems of mammals. The biopanning procedure by its nature allows the library to self-select by allowing particles displaying a desirable antibody or peptide to bind to an immobilized target. Logistically, producing peptides and antibodies in bacterial fermentation offers several advantages. Bacteria are relatively easy to grow, and scale up in production. Their rapid growth provides the capacity for surge production. Lastly, recombinant reagent production in bacteria minimizes animal use by using only those animals initially immunized in the process. All subsequent manipulation and manufacture takes place in bacterial cells, reducing the numbers of animals used from hundreds to fewer than ten per antibody cloned.

REFERENCES

1. Winter, G. and C. Milstein. 1991. Nature, 349: 293-299.
2. Smith, G.P. 1985. Science, 228:1315-1317.
3. Parmley, S.F. and G.P. Smith. 1988. Gene, 73: 305-308
4. Krebber, C. *et al.* 1995. FEBS Letters, 377: 227-231.
5. Davies, J. and L. Riechmann. 1995. FEBS Letters, 339: 285-290.
6. Devlin, J.J., *et al.* 1990. Science, 249:404-406.
7. Davies, J. and L. Riechmann. 1995. Bio/Technology, 13: 475-479.
8. Horwell, D.C. 1995. TIBTech, 13:
9. Luzzago, A., *et al.* 1993. Gene, 128: 51-57.

SELF-DISINFECTION AND DECONTAMINATING INTERIOR SURFACES BASED ON PHOTOCATALYTIC TITANIA/EASY-RELEASE COATINGS

Robert E. Baier
Biomaterials Graduate Program, University at Buffalo, Buffalo, NY 14214
Christopher M. Izzo
Harmac Industries, Buffalo, NY 14215
Paul J. Nicotera
Rensselaer Polytechnic Institute, Troy, NY 12180

ABSTRACT

We have demonstrated that easy-release qualities imparted by thin methyl-terminated silane coatings, when combined with catalytic disinfection by titanium dioxide particles embedded in or superficially attached to duct-liner fiberglass surfaces and coated fiberglass-based architectural fabrics, can improve the sanitary performance of HVAC air-handling systems. This project evaluated the application of such coatings/particles to duct-wall fiberglass surfaces and coated fibrous glass compositions. The surface-modified materials were placed in a HEPA-filtered laboratory air-duct system, infused with calibrated bioaerosols and sampled with surface science methods sufficiently sensitive to determine the additives' efficacies with regard to discouraging bacterial colonization and habitation. Photocatalytic disinfecting and self-cleaning activity, induced by exposure to "black light" (UV-A) illumination, was followed by spectrometry of methylene blue solution bleaching, as well as by infrared and bacterial culture techniques.

INTRODUCTION

It has previously been demonstrated and confirmed[1,2] that air can be disinfected by photocatalytic techniques similar to those proved to be successful in killing microorganisms in water[3,4,5]. The specific scientific details, most relating to the reaction chemistry of titanium oxides, are published in a 1997 review[6].

Regarding the goal of sanitizing and keeping potentially infected contact surfaces of interior building surfaces clean, one of the main differences from underwater systems for reliable and repeatable disinfection is that dead or destroyed microbes are not as easily washed off the ducts' or building envelopes' antimicrobial surfaces. Thus, an additional probable improvement in building and duct-liner properties would be to make the liners less retentive of particulate debris. This has been accomplished earlier with underwater easy-release coatings[7] and now the same concept is newly extended to serve as the surrounding easy-release matrix for photocatalytic titanium dioxide particles.

Many indoor air quality problems have been associated with bioaerosols of more than 60 different types. These include mainly bacteria, viruses, and fungi that can cause tuberculosis, Legionnaires' disease, flu outbreaks, mumps, measles, pneumonia, and meningitis, as well as increasing incidences of asthma, upper respiratory distress syndromes, and the common cold[8,9,10]. It has been a difficult problem to study the influences of various possible infection control techniques in HVAC systems and other building structural spaces because of the presence of complex backgrounds of occupant- and furnishings-generated aerosols in most interior work environments and because of the absence of controlled, safe sources of representative bioaerosols.

We recently have produced and calibrated a reliable bioaerosol generating technique[11] and utilized the so-generated aerosols to test bioaerosol-collection equipment at the end of a HEPA-filtered air-duct system that is more versatile than "clean room" test environments previously described[12].

Thus, we have now completed several series of tests of combinations of titanium dioxide photocatalysts and fouling-release coatings in air-ducts lined with fibrous glass blankets, rigid fibrous glass duct board, and other potential building envelope interior linings.

Most prior uses of titanium oxide photocatalysts have required illumination of the oxide particles with ultraviolet [UV] light, to produce the highly reactive free radical species that not only can disinfect an air stream but also break down volatile organic compounds for odor control[13,14]. We have used UV sources, and also explored the use of miniscule amounts of coating additives/amendments and other special treatments that might allow these processes to take place in the dark or under only modest, visible-light illumination. The experimental program monitored (1) the proportions of standardized bioaerosol colony-forming-units [CFU] that were collected and inactivated by the various coating surfaces, (2) the levels of surface-cleanliness maintained over long operating times in continuously operated air-duct systems, and (3) the collectibility and viability of microorganisms advected through ducts and/or admixed with TiO_2 powder at various atmospheric conditions [dry v. humid; "sunlight" illuminated v. dark]. We believe the results can lead to suitable manufacturing applications as pre-coated systems for building interiors that can be cut and fabricated according to current procedures, with current tools.

The experimental techniques employed so far included internal reflection infrared spectroscopy, UV and visible light spectrometry, critical surface tension analysis, scanning electron microscopy and energy dispersive x-ray analysis, as well as air-impaction/collection techniques and standard plate-counting microbial methods for active CFU. A follow-up study now in progress is addressing the basic scientific issues about the mechanisms of reaction. One prospect to be considered is that the titanium dioxide free radical is uniquely produced[15], rather than the ubiquitously generated hydroxy and superoxide-anion free radicals thought to degrade pesticides[16] and phenolic pollutants (especially in the presence of silica)[17], formaldehyde, and trichloroethylene[18]. Of special interest to ongoing research is further exploration of the finding that some titanium dioxide coatings are both self-cleaning and anti-fogging, as ultraviolet radiation converts them from initially hydrophobic to "amphiphilic" surfaces[19]. It is generally agreed that titanium dioxide coatings can be a suitable approach for mass building envelope use, since they are nontoxic, extremely stable, function at normal room temperatures, and inexpensive to manufacture[20,21]. Indeed, there is growing use of titanium (oxide) foil in the food processing industry[22].

MATERIALS AND METHODS

A supply of titanium dioxide (P25) powder was obtained from Degussa Corporation, and commercially pure titanium foil as prepared for food processing equipment from IBR Corporation[22]. New, custom-fitted ductwork was constructed (Capital Heat, Inc., Depew, NY) and installed adjacent to the

laboratory Class 100 Clean Room. The duct received HEPA-filtered, constant- temperature, constant-humidity air exiting from the Clean Room. The air flowed at controlled velocities of 1-2 meters per second [2-5 miles per hour], at static positive pressure of about 3mm [one-eighth of an inch] of water, through removable test duct sections at a volume flow rate of about 240 cubic feet per minute [about 9 cubic meters per minute]. The emerging flow, after having received calibrated aerosol injections and exposures to control techniques, passed into various analytical devices prior to exiting through a continuously operating chemical fume hood. There was great versatility to this test system, which is currently being further instrumented to allow video microscopy of events internal to and at the walls of the modified ducts [Figure 1].

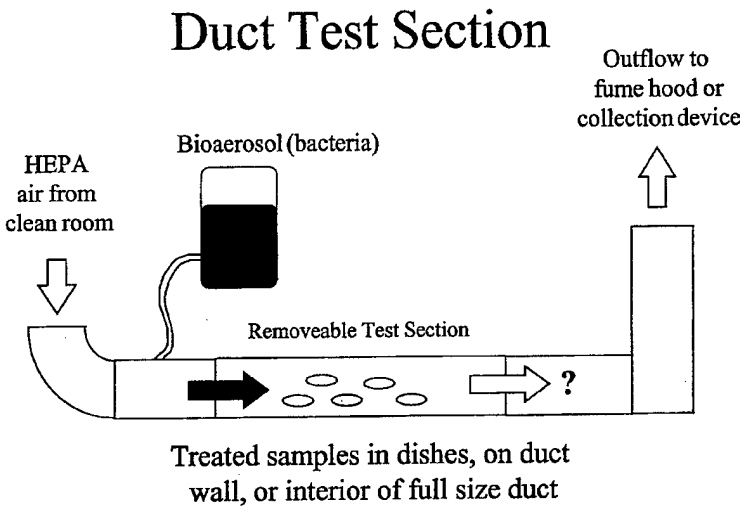

Figure 1. Schematic diagram of the laboratory test apparatus.

Numerous ultraviolet and visible illumination sources were used as required to photoactivate the titanium dioxide powder and, based on significant prior work in the development of fouling-release coatings[23], supplies of coating reagents were obtained from Petrarch Division of United Chemical Technologies, Inc. Specialized equipment for glow-discharge-activation and disinfection of the various test surfaces[24] was used for test specimen pre-cleaning and sterilization, and for conversion of TiO_2 coatings to "visible-light-activatable" status. Custom-built equipment for source assessment of atmospheric aerosols was used routinely[25]. CertainTeed Corporation (Blue Bell, PA) supplied fibrous glass insulation blanket and duct board materials to initiate work, and architectural membranes were supplied by BIRDAIR, Inc. (Amherst, NY).

The analytical methods used are described below:

Internal Reflection Infrared Spectroscopy was applied to confirm the chemical composition of test surfaces (e.g. insulation tissues, coating materials) and to confirm that coatings were, indeed, present on the interior building materials. Infrared spectroscopy detects covalently-bound moieties (e.g. hydroxyl, hydrocarbon, amide, silica, silicone, phosphate) present in a sample. Use of the multiple-attenuated internal reflection mode of IR spectroscopy enables analysis of the outermost 1000 Angstroms,

approximately, of the sample surface, eliminating interfering signals from the sample bulk. Test samples are spread on or clamped against internal reflection test plates (germanium or salt blends that allow for transmission of IR energy), which serve as "lightpipes" for IR energy. While the maximum thickness sampled by this ambient-environment technique is 1000 Angstroms, the minimum detection limit is one monolayer (approximately 15 Angstroms). Other surface spectroscopies (e.g. Xray photoelectron spectroscopy [XPS or "ESCA"] or secondary ion mass spectrometry) are more surface-specific (evaluating only the outermost 15-50 Angstroms of a material) than internal reflection IR spectroscopy, but work only under ultra-high vacuum environments. The efficacy of UHV spectroscopies also tends to be hampered by irregular surface textures, such as the fine fibrous geometries presented by insulation materials. UHV spectroscopic techniques were available to this project, however, and used as necessary to evaluate model films of coating materials.

Critical Surface Tension Analysis, or "comprehensive contact angle analysis" was the most surface-specific physical/chemical technique utilized, probing the outermost 5-10 Angstroms of test materials. Surface descriptors determined from measurements of contact angles of each of up to 15 diagnostic fluids included (a) critical surface tension - indicated overall material "wettability" and dominant chemical functionality at the solid surface, and predicted the relative bioadhesive strength of macromolecules and cells that might attach to the material surface) and (b) surface free energy and its various components – measured the total "potential" for a material to interact with its environment (e.g. extremely clean glass is a high-energy material; "Teflon" is a very-low-energy material); surface energy components included the dispersion force and polar force; polar forces were defined and calculated according to several different theories.

Scanning Electron Microscopy and Energy-Dispersive Xray Analysis were used to confirm surface morphology (SEM) and general elemental composition (EDXray), as well as to visualize the presence of microorganisms and other particulates that collected on the treated and control interior surfaces.

Air Impaction Techniques included the use of customized air-sampling units that deposit particulates from the sampled air onto either germanium internal reflection plates (for subsequent IR spectroscopic and SEM/EDXray analyses) or culture plates (for detection/enumeration of microorganisms in the airstream).

Microbial Culture Techniques were used to detect microorganisms present in the airstream (as described above), and to detect/enumerate cells present on the treated and control insulation surfaces; both agar- and broth-based culture methods were evaluated. Lacking reliable means to quantitatively remove cells from the test surfaces (e.g. washing and/or sonication failed in this regard), the numbers of viable organisms present after different exposure periods were determined by direct placement of the test specimens on nutrient agar surfaces and followed for several days of incubation.

RESULTS

Numerous experiments were executed in accord with the typical experimental plan diagrammed in Figure 2. A parallel series of experiments was done with replicate specimens immersed in methylene blue solutions (rather than being exposed to bacterial "seeding"), and the UVA-induced bleaching of the solutions was followed quantitatively by UV/visible spectroscopy. The spectroscopic results correlated well with the bacterial growth observations.

Due to the visual and somewhat subjective nature of the bacterial growth observations, photo-documentation was employed to record the results of placing samples on agar culture plates. These photos were printed and archived as color slides.

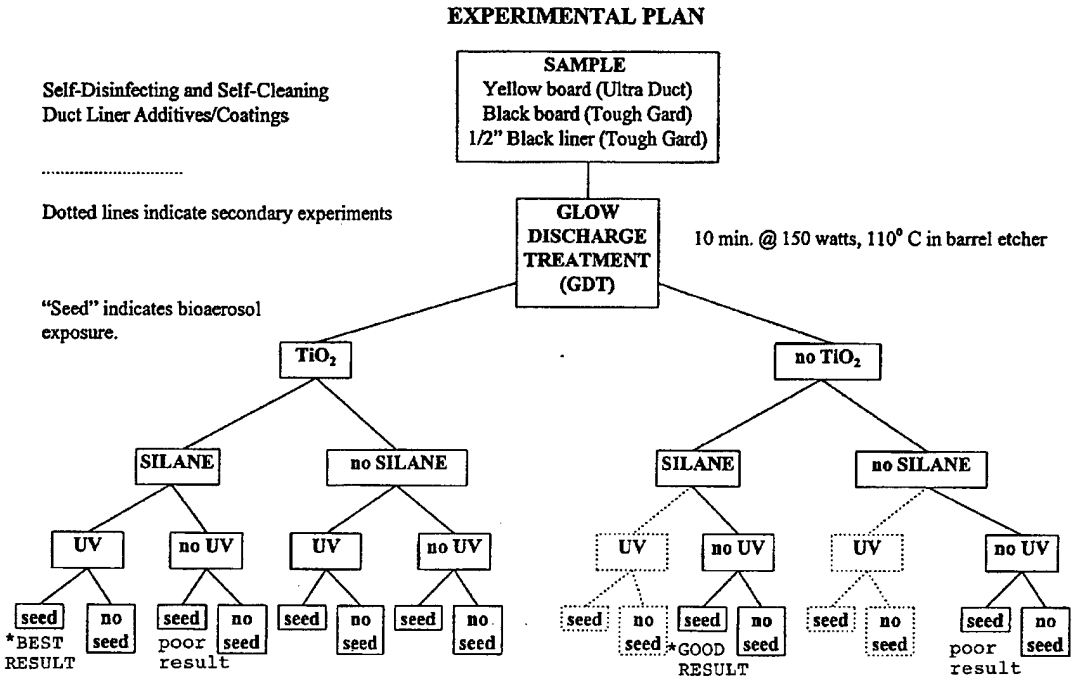

Figure 2. A typical experimental plan, leading to final results noted by asterisk [*] on diagram above. Experimental variations included substituting standard steam autoclaving for the glow discharge treatment [GDT] sterilizing step. The best-performing easy-release coating was octadecyl silane.

Baseline analysis showed clear morphological and chemical differences among interior surface and insulation types and confirmed the ability of glow-discharge treatment to change the surface chemistry sufficiently to make the fiberglass accepting of further modification by easy-release coatings. Particle-amended insulation surfaces without UV-A illumination showed little evidence of antibacterial action and, in fact, showed a greater rate and extent of bacterial growth than unmodified insulation types. Differences in propensity for bacterial growth were observed among insulation and fabric types, as well as between as-received and glow-discharge-treated [GDT] samples, with the GDT specimens usually being sterile.

Titanium dioxide suspension coating at low concentrations gave observable and measurable coating of fibers, as evidenced by SEM and x-ray analysis, and good photocatalytic action was displayed by these materials when illuminated by standard "blacklights" (UV-A). Silane coatings were readily concurrently imparted to insulation samples and further changed the surface chemistry, providing an easy-release, as well as a strong hydrophobic character to samples.

The presence or absence of biology on test samples was viewed most readily by culturing out on agar plates, followed by photo-documentation and visual analysis. Titanium dioxide-containing samples, exposed to UV-A light, sometimes showed a delayed action in the attenuating of bacterial growth on agar plates. That is, despite an initial outgrowth of biology that was just as robust as that of untreated samples, there was a visible reduction in vigor and rate of that growth in the days following the initial seeding experiment.

Work in Progress: A setup for parallel flow IR analysis is being implemented for more sensitive examination of the mechanisms involved in disinfection at the interior surfaces. This involves passing the air flow over germanium and silicon plates in place in a spectrophotometer so that real-time measurements can be made during introduction of bacteria, illumination by UV light, and with the passage of time. Parallel flow will be achieved by constructing an alternative air passage that fits within the physical confines of a dedicated infrared spectrophotometer and horizontal testplate holder. Appropriately coated germanium plates duplicate the surfaces of modified and unmodified fiberglass insulation and architectural membranes, and will facilitate a closer look at the surface chemistry involved in the disinfection processes. In addition to providing a better understanding of the work being performed, this method of examination provides the basis for student thesis work (C. Izzo, M.S. candidate).

CONCLUSIONS

Photocatalytic titanium dioxide (TiO_2) fine particles and easy-release, low-critical-surface-tension (CST) coatings have been shown to be independently capable, respectively, of diminishing viability and minimizing bioburdens on interior surfaces. Unique combinations of TiO_2 and methyl-terminated [CST = 22 mN/m] monolayer coatings on germanium, silicon, fiberglass, and coated fiberglass substrata have been tested in controlled flows of a "zero" air-duct system emerging from a Class 100 clean room, seeded midway to a final exit hood from a controlled bioaerosol generator, and monitored by a new Computer Optimized Aerosol Sampling Technique (COAST II)[26]. Data from cultures for generated versus final colony-forming units, supported by internal reflection infrared spectra, scanning electron micrographs, and energy-dispersive x-ray spectra, show that both active bacterial bioburdens and total retained biomass can be significantly reduced by these surface modifications. Interior surface coatings of TiO_2/easy-release adducts, particularly on fiberglass and coated fiberglass substrata, can substantially aid in maintaining and improving air quality in biologically challenged closed spaces.

ACKNOWLEDGMENTS

Graduate thesis work of C. Izzo partially supported by CertainTeed Corporation (Blue Bell, PA). P. Nicotera supported by University at Buffalo's Industry/University Center for Biosurfaces.

REFERENCES

1. Goswandi DY, Trivedi, DN, Block, SS (1997) J Solar Energy Eng, 119:92-96
2. Jacoby WA, Maness PC, Blake DM, Fennell JA (1998) Environ Sci Technol, 32:2650-2653
3. Wei C, Lin WY, Zainal Z, Williams NE, Zhu K, Kruzic AP, Smith RL, Rajeswar K (1994) Environ Sci Technol, 28:934-938
4. Matsunaga T, Tomoada R, Nakajima T, Nakamura N, Komine T (1988) Appl Environ Microbiol, 54:1668-1670
5. Sunada K, Kikuchi Y, Hasimoto K, Fujishima A (1998) Environ Sci Technol, 32:726-728
6. Mills A and LeHunte S (1997) J Photochem Photobiol A:Chem, 108:1-35
7. Meyer A, Baier R, Kohl IL, Griffith J, Haslbeck E, Montemarano J, Ross A, Schultz M, Swain G (1997) *Duplex Foul-Release Coatings, Environmental Security Technology Certification Program:*

Advanced Nontoxic Antifouling Coatings Technology Demonstration, Report Number NSWCCD-TR-64-96/15, US Naval Research Laboratory, Washington, DC
8. Burge HA (1995) Bioaerosols, Lewis Publishers, Boca Raton, FL
9. Morey PR, Freely JC, Otten JA (eds) (1990) Biological Contaminants in Indoor Environments, ASTM Publication Code Number 04-010710-17, ASTM, Philadelphia, PA
10. Pope A.M, Patterson R, Burge H (eds) (1993) Indoor Allergens--Assessing and Controlling Adverse Health Effects, National Academy Press, Washington, DC
11. Baier RE, Gollus SM, Meyer AE (1997) *Calibration and Testing with a Portable Bioaerosol Generator,* Project Report, Industry/University Center for Biosurfaces, SUNY Buffalo
12. Buttner MP and Stetzenbach LD (1996) in Characterizing Sources of Indoor Air Pollution and Related Sink Effects, ASTM STP 1287 (B.A. Tichenor, Ed.) Amer. Soc. for Testing Materials, Philadelphia, PA, pp 75-86
13. Jacoby WA, Blake DM, Fennell JA, Vargo LM, Dollberg SK, George MC, Boulter J (1996) J Air Waste Manage Assoc, 46:891-898
14. Obee TN and Brown RT (1995) Environ Sci Technol, 29:1223-1231
15. Tengvall P (1989) Titanium-Hydrogen Peroxide Interaction with Reference to Biomaterial Applications, Linkoping Studies in Science and Technology; Dissertation No. 218, Linkoping, Sweden
16. Zhao J (1995) Photocatalytic Degradation of Organophosphorus Pesticides using TiO_2 Supported on Fiberglass, Abstract 131, 210th Amer. Chem. Soc. Mtg., Div. Colloid and Surface Chemistry
17. Tsai SJ and Chemg S (1995) Photocatalytic Degradation of Phenolic Pollutants over TiO_2 Semiconductor with Various Structures, Abstract 161, 210th Amer. Chem. Soc. Mtg., Div. Colloid and Surface Chemistry
18. Fu X, Zeltner WA, Anderson MA (1995) A Comparison of the Catalytic and Photocatalytic Properties of Microporous TiO_2 Materials, Abstract 163, 210th Amer. Chem. Soc. Mtg, Div. Colloid and Surface Chemistry
19. Hashimoto K and Fujishima A (1998) New Developments in Self-Cleaning and Anti-Fogging TiO_2-coated Surfaces, Abstract 050, 216th Amer. Chem. Soc. Mtg., Div. Colloid and Surface Chemistry
20. Wilson E (January 15, 1996) Titanium dioxide catalysts break down pollutants, Chemical and Engineering News, pp23-24
21. Concannon M (1998) World Business and Technical Outlook for Titanium and Titanium Alloys, Gorham Advanced Materials, Inc., international conference
22. Nippon Steel Corporation, Titanium in Food Processing Equipment, April 1988, courtesy of CJ Rhee, President, Harbortown Division, IBR Corporation, Barrington, IL, October, 1990
23. Wells AW, Meyer AE, Matousek JA, Baier RE, Neuhauser EF (1997) in Waterpower '97, Proceedings of the International Conference on Hydropower, Volume 1, American Society of Civil Engineers, NY, pp 451-460
24. Baier RE, Carter JM, Sorensen SE, Meyer AE, McGowan BD, Kasprzak SA (1992) J Oral Implantol, 18:236-242
25. Baier RE, Mack EJ, Rogers CW, Pilie RJ, DePalma VA (1981) Optical Engineering, 20:866-872
26. Baier R, Cloutier T, Forsberg R, Wrazen B, Barnes J, Fisher E (2001) Proceedings of the 24th Annual Meeting of the Adhesion Society, February 25-28, 2001, Williamsburg, VA , pp 450-451

DISTRIBUTED SOFTWARE DECISION SUPPORT SYSTEMS FOR HETEROGENEOUS COORDINATION IN CHEMICAL AND BIOLOGICAL RESPONSE

K. Suzanne Barber, Matthew T. MacMahon, and Cheryl E. Martin
The Laboratory for Intelligent Processes and Systems
The University of Texas at Austin
Phone: (512) 471-6152
barber@mail.utexas.edu

ABSTRACT

During detection and response to a Chem-Bio incident, heterogeneous groups, who may not ordinarily interact, must form a team. A Sensible Agent is a type of *software agent* (a Distributed Artificial Intelligence component that uses sensing, reasoning, and acting capabilities to achieve a set of goals) with additional coordination capabilities. For the Chem-Bio terrorism domain, Sensible Agents can offer the following decision-support capabilities: (1) belief revision based on models, certainty and the trustworthiness of incoming information sources, (2) situation-based recommendations on the composition of decision-making groups, the relative strength of members of the group and over whom the group has authority, and (3) planning and resource allocation. This paper describes possible benefits of applying a Sensible Agent system to provide Chem-Bio detectors and responders with *in situ* decision support for task and resource management.

1 INTRODUCTION

Acts of biological and chemical terrorism may be hard to predict, to detect, and to remedy. Both detection and response involve highly dynamic, uncertain, and complex scenarios. Especially in Chem-Bio response, many groups are involved with diverse and sometimes conflicting goals. The use of intelligent software agents as decision support tools can mitigate some of these problems. An intelligent agent is a type of distributed artificial intelligence that plans, models its environment, and has some degree of autonomy to achieve a set of goals. A Sensible Agent is an agent that can reason about the decision-making frameworks it uses to achieve its goals; which affect its level of autonomy over decisions about action selection.

This paper envisions the application of Sensible Agents to the domain of detection and response to a chemical or biological terrorism incident, allocating a Sensible Agent to each decision-maker who must assess incoming information, determine appropriate actions and take action. Sensible Agents are designed so that an agent can integrate distributed information sources and create plans of action based on acquired information and derived situation assessment. A Sensible Agent uses awareness of the situation -- other agents, the status of communication, and other environmental conditions -- to find the best decision-making framework for each goal. A decision-making framework (DMF) describes the interactions, if any, of a group of agents as the group works to determine how to achieve a goal. A DMF specifies (1) the amount of decision-making control each agent has over how each goal should be achieved and (2) which agents are bound to follow the decisions. Prior research has shown that agents

using Adaptive Decision-Making Frameworks (ADMF) can achieve better system performance in uncertain, dynamic worlds [1].

During the detection of a biological terrorism event, a Sensible Agent could assimilate multiple, heterogeneous information sources and develop beliefs about the certainty and trust-worthiness of such information. Even a small Chem-Bio response brings together many independent groups, such as fire departments, local, state, and federal law enforcement agencies, local and state health departments, public and private hospitals, and city office of emergency management in a situation where none may be fully capable to respond and manage the incident alone. Each of these groups has skills, equipment, manpower, training, and contacts they can apply towards handling the situation. However, the groups may also have conflicting subordinate goals under the common goal of mitigating the effects of the incident. Additionally, these groups may work together infrequently and only in training or situations with little in common with a particular incident. Even when groups share the same goals, they may conflict with each other in the execution of those goals. Coordination among these groups is difficult, but clearly necessary for a successful response to a Chem-Bio incident.

Other researchers in the field have published some related research. Leake et al. discuss the application of case-based reasoning to generate simple disaster response plans from short textual descriptions of events [2]. Simonovic discusses the design and deployment plan of an automated decision support system for sustainable flood management in Winnipeg, Canada [3]. Grathwohl et al. discuss the application of description logics in the domain of forming disaster management response plans [4]. The ENCOMPASS system, a DARPA project, focused on consequence management for first responders in Chem-Bio terrorism, routine fire, and hazardous materials incident response [5]. Schreckenghost et al. have applied a design philosophy known as Adjustable Autonomy, which is similar in some ways to the Adaptive Decision Making Frameworks (AMDF) described herein, to monitoring and controlling life support systems for NASA [6]. However, Adjustable Autonomy lacks some of the flexibility and power of AMDF. While Adjustable Autonomy allows the developer or the user to adjust the distribution of decision-making control between a human user and automated system, ADMF gives any human or autonomous decision-making agent some control over the distribution of decision-making control among a system of human and automated decision makers.

To illustrate the utility of ADMF and the potential application of Sensible Agents to Chem-Bio terrorism detection and response, the remainder of the paper is organized as follows. Section 2 gives a brief overview of the organization and operation of the Sensible Agents Architecture. Section 3 presents an application of Sensible Agents during the detection phase of a Chem-Bio incident, and Section 4 continues the example scenario by showing how Sensible Agents could be applied during the response phase. Section 5 concludes.

2 SENSIBLE AGENT ARCHITECTURE

Sensible Agents have been designed and implemented to operate in dynamic, uncertain worlds. The reader should consider the possible application of a Sensible Agent tied to each decision maker conducting bio-surveillance and coordinating Chem-Bio incident response The Sensible Agent logical architecture, shown in Figure 1, is composed of four modules, each of which provides a distinct set of functionality for the agent. All information from the environment is filtered through a set of formally defined sensors. Sensible Agents are capable of responding deliberately and reactively to fulfill their goals in the context of sensed environmental changes. Each Sensible Agent sends all actions (e.g. communication, movement, etc.) to a set of actuators that passes information to the environment. The sensor and actuator suites provide a layer of abstraction and a well-defined interface between Sensible Agents and their environment.

The ***Perspective Modeler*** (PM) contains the agent's explicit model of its local, subjective viewpoint of the world. The model includes behavioral, declarative, and intentional models of the agent itself, other agents, and the environment [7]. The behavioral model specifies the current state and possible transitions to other states, which are represented using an Extended State Chart (ESC) [8]. The declarative model holds a set of facts represented as name-value pairs. The agent intentional model includes the Intended Goal Structure (IGS), which represents the goals an agent intends to achieve [9]. The PM interprets

internal events and information obtained through sensors and communication, allowing the agent to sense environmental change, store relevant information in the declarative model, and update the behavioral model accordingly.

The ***Action Planner*** (AP) interprets domain-specific goals, plans to achieve these goals, and executes the generated plans [10]. The AP uses a suite of actuators to act on the environment, which in most domains includes a communication actuator for sending messages to other agents in its system.

The ***Autonomy Reasoner*** (AR) determines the appropriate decision-making framework (DMF) for each of the self-agent's goals. An agent's collaborative decision-making behavior is constrained by how it participates in a given framework. Figure 2 shows the different interaction styles an agent can employ within a decision-making framework: (1) ***Command-driven***— the agent does not make decisions and must obey orders given by a master agent, (2) ***Consensus***— the agent works as a team member, sharing decision-making equally with other agents, and (3) ***Locally Autonomous/Master***— the agent makes decisions alone and may or may not give orders to other agents. These DMFs constrain the collaborative problem solving of the AP. Sensible Agents use a form of dynamic reorganization called Adaptive Decision-Making Frameworks (ADMF), which allows agents to form, dissolve, and modify decision-making interactions with other agents. The effectiveness of decision-making frameworks can vary across situations. ADMF allows agents to employ the most effective decision-making framework in any given situation [11].

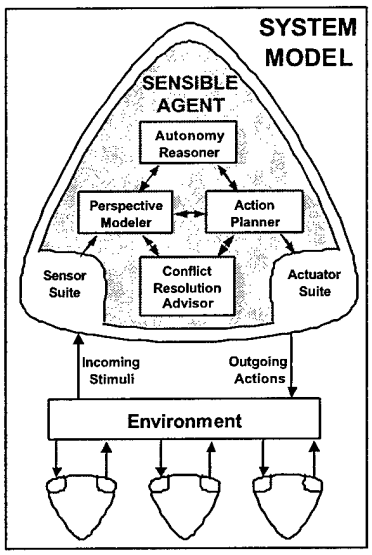

Figure 1: The Sensible Agent architecture.

The ***Conflict Resolution Advisor*** (CRA) identifies, classifies, and generates possible solution strategies for conflicts between agents. The CRA monitors the AP and PM to identify conflicts. Once a conflict has been detected, it classifies this conflict and suggests a resolution strategy (voting, negotiation, arbitration, self-modification) to the AP. The appropriateness of each strategy varies based on the situation [12].

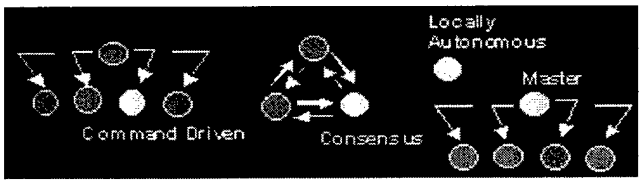

Figure 2: Interaction styles individual Agents use within Decision-Making Frameworks.

The AP, AR, and PM all use of inter-agent communication in their operation. The AP and AR use communication for inter-agent coordination, while the PM communicates to share knowledge. Communication, like all other interactions with the agents' environment, is carried out via actuators and sensors. Sensible Agents use KQML as the basis for their inter-agent communication language [13].

Sensible Agents not only react and plan to influence the state of the world, but also explicitly reason about the beliefs of other agents and search for an optimal decision-making framework as the world changes dynamically. These capabilities make Sensible Agents particularly appropriate for domains where agents' actions greatly affect one another and the cost/benefit tradeoffs of DMFs may change.

3 SENSIBLE AGENT APPLICATION TO BIOLOGICAL TERRORISM DETECTION

This section presents a bio-surveillance scenario and illustrates how a Sensible Agent-based system could be used for decision support throughout the scenario. During bio-surveillance, Sensible Agents could assist in information collection, analysis and propagation. A Sensible Agents approach can provide

high-level sensor fusion and situation-aware assessment to supplement the traditional techniques of information analysis automation.

The Center for Disease Control is facilitating and funding the formation of state health alert networks to bring together information from traditionally under-utilized or unavailable health indicators, such as school attendance, pharmacy sales, and EMS dispatch calls [14]. Currently, some health information is mailed to state departments of health (DOH). Under the new system, epidemiologists will have access to a much larger amount of information much more quickly. The increased volume of information flowing into the DOH will necessitate more automated filtering, and the Texas DOH is currently evaluating several methods for this automation.

This example scenario follows the pattern used in many biological terrorism tabletop exercises [15]. A contagious respiratory disease is released on Day 0 at a large public event. The attack is unannounced and undetected. The disease incubates during Day 1 without any visible indicators. On Day 2, many students are absent from school, EMS dispatches for respiratory problem are abnormally high, and pharmacies sell a lot of decongestants. Additionally, hundreds of people present themselves to medical facilities, are assessed as having a flu-like illness and are released. The information from Day 2 is comes into the DOH during the late afternoon and evening hours of Day 2 and the early morning hours of Day 3.

What role could a Sensible Agent based system play at this point? A Sensible Agent could assist each decision maker in a network of automated systems and human epidemiologists analyzing the health information for a bio-surveillance effort. Sensible Agents could provide decision support by building models of the indicative trust-worthiness of information sources, combining disparate sources of possibly conflicting, incomplete, and uncertain information to form a coherent picture, notifying off-duty DOH staff members after initial analysis and planning allocation of computational and other resources. The following sections focus on the application to a bio-surveillance task of three Sensible Agents modules, the Perspective Modeler (PM), Autonomy Reasoner (AR), and the Action Planner (AP).

3.1 PERSPECTIVE MODELER (PM)

Sensible Agents employ the Perspective Modeler (PM) to assess the state of itself, other agents, and the environment based on incoming information from multiple types of sources, e.g. other agents, humans, databases, and other automated systems. A valid analysis should attend to important relationships within the information. For example, different sources of information may confirm or refute one another. Pure statistical techniques often assume independence of data; however, it is exactly the dependencies among information that can allow disambiguation. The PM uses semantic networks to model the relationships among information. As information comes into the system, the conclusions drawn from previous information may become more or less likely, or even impossible. For instance, a lab test may conclusively rule out a disease, even if all other factors strongly indicated it.

When two sets of information are directly contradictory, one must disregard one or the other to use either. The question is, which one to trust? The PM assigns a reputation to each source of information, giving a higher reputation to sources that have proven accurate or trustworthy and

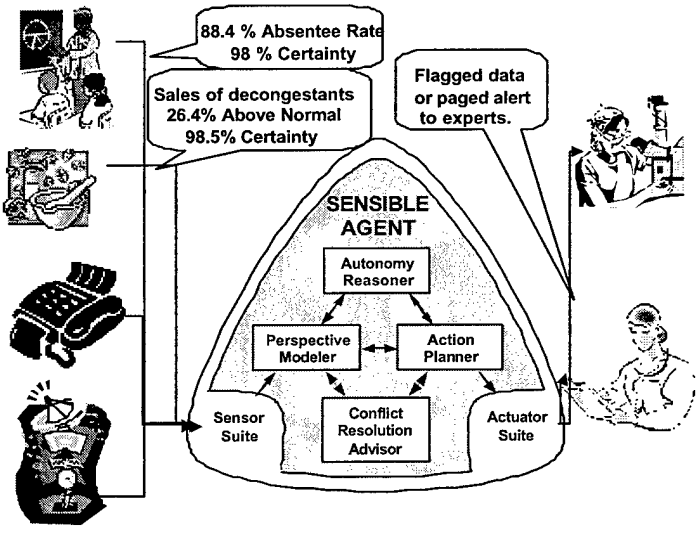

Figure 3: Sensible Agent supports decision makers by combining information sources and alerting staff.

decreasing its trust in faulty, dishonest, or imprecise sources. Thus, when new information arrives from a source, the PM uses Bayesian techniques to model the certainty of information based on its reported certainty and the PM's modeled reliability of the reporting information source [16].

Additionally, the PM could initiate queries for more information when it deems necessary. For example, the PM of Agent1 could notice that it does not have enough information to make a certain classification of an incident, but that another agent, say Agent2, has additional relevant information. The PM would then send a message through the AP to Agent2, requesting that Agent2 send more information to Agent1. Agent1 may then have enough information to make a justifiably assured classification of the state of the world. Because the PM models it own and others' current states and the viable transitions between states, the PM can provide reactive plans specifying a set of actions which transition the agent from its current state to a desired future state.

3.2 AUTONOMY REASONER (AR)

For each goal a Sensible Agent is pursuing, the Autonomy Reasoner assigns a decision-making framework (DMF) specifying which agents can make a decision about that goal and which agents fall under their authority for that decision. For Chem-Bio terrorism, one important application of decision-making frameworks concerns the goal: "Classify each set of information as a potential biological incident, natural epidemic, or inconsequential information anomaly." A Sensible Agent monitoring this process must decide when the automated system can classify the information on its own and when the system should flag it for further review by a human epidemiologist. Each time the agent has the goal of classifying a set of information, the agent must assign a DMF to the goal: **Locally Autonomous** if the agent can assess the information on its own, or **Consensus** or **Master/Command-Driven** if the agent defers some or all of the decision to another agent, such as a human expert. Using a learning technique such as case-based reasoning, a Sensible Agent could learn from experience when to defer decisions to a human or when to assume full responsibility for the decision.

3.3 ACTION PLANNER (AP)

The Action Planner (AP) generates and executes a course of action; for example, the AP could determine whether the agent should page an off-duty epidemiologist or merely flag the information for review in the morning. The AP selects an action based on the PM's assessment of the current state and the AP's assessment of how to best achieve a desired future state. The AP creates, picks, and executes a plan of action based on the decision-making framework chosen by the AR. During bio-surveillance, the AP could also allocate computational resources to analyzing different sets of information based on the PM's situation assessment of the information.

4 SENSIBLE AGENT APPLICATION TO CHEM-BIO TERRORISM RESPONSE

Continuing the scenario, how could Sensible Agents help during the response phase of a Chem-Bio incident? During response, heterogeneous groups possibly including local, state, and federal civilian and military organizations, which may not ordinarily interact, must form a team. Each group provides a set of skills, equipment, and facilities that must be coordinated in the response. Sensible Agents can assist with response, especially with the coordination of a heterogeneous team. A Sensible Agent-based system could perform belief revision, team building combined with facilitating unified command, resource allocation, and conflict detection and resolution.

Many regions already use the Incident Command System (ICS) to coordinate during Hazardous Materials incidents, large fires, and other multi-jurisdictional events [17] [18]. ICS is a set of guidelines, terminology, and forms for organizing the command of such incidents that scales with the size of the event. For instance, for small events, one person may handle all financial concerns. As the response grows, some of the responsibilities of that person are delegated to a hierarchical staff built up as demand necessitates. When the event begins to wind down, the command structure shrinks with it, progressively concentrating tasks into fewer people. In addition to the original ICS designed primarily by fire departments, specialized versions have been created for law enforcement (LEICS) and health care (HEICS), although all types of organizations can collaborate within the classic ICS framework [19]. Using the capability of Adaptive Decision-Making Frameworks, a Sensible Agent-based system could be used to both simulate and recommend dynamic changes in coordination for Chem-Bio incidents.

4.1 PERSPECTIVE MODELER (PM)

The Perspective Modeler plays much the same role in response as in detection. As the situation dynamically unfolds, especially with inadequate communications and rapidly changing conditions, the ability to derive a centralized global assessment is greatly diminished, if not impossible. Each decision maker must be capable of good local situation assessment – creating a sufficient coherent view from what information is available, even if it is inconsistent. The lack of such good intelligence summaries and intra-agency communication conduits was one of the driving forces behind ICS [18]. The PM could integrate information sources from across an event to form a status report based on declarative and behavioral models of events and to point out inconsistencies in reports. Trust metrics can play a greater role, as there might be more unknown and untrusted agents, such as untrained volunteers.

4.2 AUTONOMY REASONER (AR)

The Autonomy Reasoner could help coordinate the disparate groups in a Chem-Bio response. Not only does the structure of organizations change along with the organization, but the people filling those roles may also change. The AR could propose decision-making frameworks apportioning authority in a way appropriate to the current situation. The AR can propose decision-making frameworks based on timing and deadlines, information-based situation assessment, mandated rules (for instance, mandates specifying that certain organizations must have primary decision-making control in some situations), and a database of easily retrieval experiences specifying what command structures worked best in similar past experiences. Additionally, the AR may facilitate the establishment of agreements between agencies to share authority over scarce resources through various types of decision-making frameworks.

4.3 ACTION PLANNER (AP) AND CONFLICT RESOLUTION ADVISOR (CRA)

Inadequate joint planning and resource management were also relevant problems. The AP and CRA modules can assist with generating efficient, conflict-free action plans and resources allocations. The AP could serve as a decision support tool for Command, Operations, Planning, and Logistics staff. Alternatively, it could act directly, for instance ordering supplies on the internet for the Support Branch of the Logistics Section. The CRA serves within a Sensible Agent as an integrated plan checker. The CRA can watch for conflicts between the planned actions of agents intending to work together within a DMF. For detected conflicts, the CRA can suggest resolution strategies.

5 CONCLUSIONS

The detection of and response to a Chem-Bio incident involves efficient management of complexity, dynamism and uncertainty. As the situation changes in Chem-Bio events involving many decision-makers assessing large amounts of variously reliable data, decision-makers must have the ability to change decision-making frameworks (e.g. change who is involved in a decision, their relative strength in the decision-making process, and to whom the group can dictate orders) based on the capabilities and objectives of each decision-maker. Sensible Agents can be applied to engineer a decision support system providing (1) Belief revision based on synthesis of information from multiple information sources using evaluation of trust-worthiness based on information certainty and the reputation of the source providing the information, (2) Dynamic, situation-based assessment of the best decision-making group formations (e.g. who should be making decisions, who should be taking orders), and (3) Distributed, coordinated planning and execution (e.g. resource allocation). In the face of unexpected situations, deadlines, changing priorities, unreliable communication, and scarce resources, Sensible Agents are flexible in the way they make decisions, integrate information, and plan. With these capabilities, the application of Sensible Agents to assist in the detection of and response to a Chem-Bio incident is promising.

6 ACKNOWLEDGEMENTS

This research was supported in part by the Texas Higher Education Coordinating Board, the U.S. Army Research Laboratory (ARL) under contract DAAA21-93-C-0101, and The Defense Advanced

Research Projects Agency (DARPA). Special thanks to Michael Mastrangelo from the Texas Department of Health for assistance with domain familiarization.

7 REFERENCES

1. Barber, K.S. and C.E. Martin, *Dynamic Reorganization of Decision-Making Groups*, in *Autonomous Agents 2001*. 2001: Montreal, Canada.

2. Leake, D.B., A. Kinley, and D. Wilson. Learning to integrate multiple knowledge sources for case-based reasoning. in Fourteenth International Joint Conference on Artificial Intelligence. 1997. Nagoya, Japan: Morgan Kaufmann.

3. Simonovic, S.P., *Decision Support System For Flood Management In The Red River Basin*. 1998, International Joint Commission Red River Basin Task Force: Winnipeg, Canada.

4. Grathwohl, M., F. de Bertrand de Beuvron, and F. Rousselot. A New Application for Description Logics: Disaster Management. in International Workshop on Description Logics '99. 1999. Linkoping, Sweden.

5. Barber, K.S., et al., *Requirements Evolution and Reuse Using the Systems Engineering Process Activities (SEPA)*. Australian Journal of Information Systems, 2000. 7(1): p. 75-97.

6. Schreckenghost, D., et al. Intelligent Control of Life Support Systems for Space Habitats. in Tenth Conference on Innovative Applications of Artificial Intelligence. 1998. Madison, WI.

7. Barber, K.S. and J. Kim. Constructing and Dynamically Maintaining Perspective-based Agent Models in a Multi-Agent Environment. in Third International Conference on Autonomous Agents (Agents-99). 1999. Seattle, WA: Association for Computing Machinery, Inc. (ACM).

8. Suraj, A., S. Ramaswamy, and K.S. Barber, *Extended State Charts for the Modeling and Specification of Manufacturing Control Software.* International Journal of Computer Integrated Manufacturing, Special Issue on Design and Implementation of Computer-Integrated Manufacturing Systems: Integration and Adaptability Issues, 1997. **10**(1-4): p. 160-171.

9. Martin, C.E., Representing Autonomy in Sensible Agent-based Systems, in Electrical and Computer Engineering. 1997, University of Texas at Austin: Austin, TX.

10. Barber, K.S., T.H. Liu, and D.C. Han, Agent-Oriented Design, in Multi-Agent System Engineering: Proceedings of the 9th European Workshop on Modelling Autonomous Agents in a Multi-Agent World, MAAMAW'99, Valencia, Spain, June 30 - July 2, 1999, F.J. Garijo and M. Boman, Editors. 1999, Springer: Berlin. p. 28-40.

11. Barber, K.S., A. Goel, and C.E. Martin, The Motivation for Dynamic Adaptive Autonomy in Agent-based Systems, in Intelligent Agent Technology: Systems, Methodologies, and Tools. Proceedings of the 1st Asia-Pacific Conference on IAT, Hong Kong, December 14-17, 1999, J. Liu and N. Zhong, Editors. 1999, World Scientific: Singapore. p. 131-140.

12. Liu, T.H., C.J. Chuter, and K.S. Barber. Virtual Environment Simulation for Visualizing Conflict Resolution Strategies in Multiple Robot Systems. in 5th IASTED International Conference, Robotics and Manufacturing. 1997. Cancun, Mexico: IASTED Press.

13. Labrou, Y., T. Finin, and Y. Peng, *Agent Communication Languages: The Current Landscape.* IEEE Intelligent Systems, 1999. **14**(2): p. 45-52.

14. CDC, *Health Alert Network*. 2000, Center for Disease Control.

15. Program, B.W.I.R., *Response Decision Tree Workshop*. 1999, U.S. Army Soldier and Biological Chemical Command: Edgewood Area APG, MD.

16. Barber, K.S. and J. Kim, Belief Revision Process based on Trust: Agents Evaluating Reputation of Information Sources, in Fraud, Deception, and Trust in Agent Societies, R. Flacone, M. Singh, and Y.-H. Tan, Editors. 2001, Springer.

17. SMCEMS, *The Hospital Emergency Incident Command System.* 1998, San Mateo County Emergency Medical Services.

18. Auf der Heide, E., Disaster Response: Principles of Preparation and Coordination. 1989, Atlanta, GA.

19. Institute, E.M., *Basic Incident Command System.* 2000, Federal Emergency Management Agency.

AN EFFECTIVE CB MATERIAL FROM COMBINED COMPONENTS OF TRIOSYN® RESIN AND SURFACE ENHANCED CARBON

Lucy Di Ionno
Jean-Pierre St-Louis
Stéphane Bourget
Pierre Jean Messier
Triosyn Corp.
1233 Shelburne Road, Suite 200
South Burlington, Vermont, 05403-7752
Tel: (802) 865-5084 / Fax: (802) 658-2681

ABSTRACT

The tremendous concern over the threat of biological and chemical warfare agents has necessitated the research and development of greatly improved methods for the absorption and catalytic destruction of these toxic contaminants. With the use of proven biocidal efficiency of the Triosyn® iodine resin and carbon based new materials, the research objective is to produce a barrier possessing the dual properties of decontaminating both chemical warfare and biological agents. Vapor testing performed allowed for the down selection of prototypes; POX3/1/0/A, OX5H/C, and OX5H/D which displayed excellent absorption capacity, microbiological reduction rates greater than 99.9% against MS2 phage, and displayed non-toxic threshold limit values.

INTRODUCTION

Triosyn® resins have been proven to kill on contact the most difficult bacterial spores, viruses, protozoa, parasites and fungi. Acute toxicology studies have shown no harmful or lethal dosage associated with exposure to the Triosyn® polymer. Triosyn® harnesses the power of iodine through the nontoxic application of demand release polymer technologies. The resin incorporates I^{-3} iodine, releases molecular I_2 upon contact with a microorganism through ionic transfer devitalizing the microorganisms surface proteins.

Prototype generation: In order to achieve an adequate balance of the properties of CB materials, the carbon's adsorption capacity must be increased by enhancing carbon's chemisorption of compounds, which contain oxygen, chlorine, sulfur and phosphorus[1]. The presence of surface bound oxygen and hydrogen on carbon exercise a profound influence on the surface characteristics such as absorption of polar and non-polar gases and vapors. Surface bound molecular oxygen is formed on activated carbon when they are treated with different oxidizing agents using various synthetic techniques. As a result, carbon's capacity for toxic vapor removal does not simply depend on the surface area of the activated carbon but on the number of oxygen

atoms in and on the carbon surface[2]. For a spherical activated carbon such as the NATO standard carbon (Ambersorb 572), the adsorbate molecule (methyl salicylate) must pass through the macro and transitional pores to the absorption site in the micropores. The absorption of MeS in the large cavities of the macropores is more readily susceptible to desorption of MeS and the subsequent transfer out through the material, than if the vapor molecule were to be absorbed by the micropores. By oxidizing the interstices and surface sites of carbon, one is essentially tailoring the size of the macropores by introducing chemisorbed oxygen groups within and on the carbon surface, thus reducing the pore size. Fixation of the acidic groups on the surface of the activated carbon not only affects the surface area and pore texture but it also produces a more hydrophilic surface[3456]. As a result, the surface-bound oxygen groups can also enhance the absorption capacity of MeS, which contains an electronegative methyl-ester and hydroxyl functional groups, through inter-molecular hydrogen bonding between the surface oxide groups of carbon and the hydroxyl functionality of the vaporized simulant. Conventional metal oxides such as alumina, possess reactivity toward chemical warfare simulants, subsequently, absorption is enhanced by the addition by impregnation of the nanosized inorganic oxide particles, which also served to increase the basicity of the carbon surface. The increase in absorption is most probably due to the larger surface area of the smaller oxide particles[789]. A merger of the above synthetic methodologies has resulted in a new class of prototypes represented under the heading of combined technologies.

EXPERIMENTAL METHODS

Vapor testing: Among the tests conducted on canisters and textiles, is the service-life or gas-life which is a measure of the capacity for the removal of toxic contaminants. Our research assessed the service-life of the carbon/Triosyn® materials' capacity for absorbing methyl salicylate (MeS). MeS was selected as a surrogate since it exhibits similar physical properties to the mustard chemical warfare agent (HD)[10] i.e. it exhibits similar vapor pressure and water solubility, as well as low toxicity and the ability to be easily detected by analytical methods. It is the approved simulant used in CRDC-SP-84010 and EATM 311-3 testing. MeS (99+% purity) was purchased from Aldrich (product# 24,082-6, CAS# 119-36-8) and was used as received.
The vapor testing apparatus contains the following three major sections: (1) a challenge gas mixture generator to provide a constant challenge gas flow rate and concentration, (2) a sample chamber to house the test prototypes, and (3) a detection system to continuously measure and record the concentration of the challenge vapor in the effluent stream.

A polydispersed aerosol vapor of MeS solution is generated using a 6-jet collision nebulizer (model MRE CN-24) purchased from BGI Inc. The compressed air system is allowed to operate at 26.0 □ 3.0 °C and 23% relative humidity. The challenge stream generator provides an air stream at 5 L/min (83.5 cm^3/s) containing 800 ppm (8 x 10^5 mg/m^3) of MeS. A cylinder of compressed air, that has been passed through an air filter, equipped with a two-stage regulator, is set to provide a feed pressure of 65 psi to the flow system. The compressed air flow is split and regulated by precision metering valves so that 3 L/min passes through the nebulizer containing MeS solution and 5 L/min by-passes the nebulizer and enters into the mixing chamber where vaporized MeS and by-pass streams are combined to generate the desired challenge gas mixture flow rate and MeS concentration under specified conditions. The influent air stream passes through the test material for a period of 30 minutes whereby the effluent air stream is directed to a trapping medium and subsequently, a UV-Vis absorption spectroscopy is used to determine the amount of MeS that has permeated through the prototype. The effluent samples were analyzed using the Ocean Optics UV-Spectrophotometer, model SD-2000 (acquisition enhanced UV resolution), and the lamp type utilized is the DT-1000 (Deuterium Tungsten-Halogen light source). A charged coupled device (2048 element linear CCD array detector) is used to detect the

signals. A quartz fibre optic dip probe (T300-RT-UV/VIS) is used to measure the concentration of MeS in the samples. This specific reflective probe has a total pathlength of 1 cm. Working at ambient temperatures, the detector is sensitive in the range of 200-800 nm. This is within the range of MeS detection. MeS has strong absorption peaks that occur at wavenumbers 236 nm and 302 nm. The absorption used for analysis is the peak at 302 nm. Effluent concentrations are extrapolated from calibration curves.

The breakpoint concentration, which determines service-life of the prototype, occurs when MeS concentration down-stream reaches 40 ppm (4×10^4 mg/m^3, 5% of challenge concentration). The service-life measurements, in this research phase, will represent the physisorption capacity of the activated carbon.

The protocol for aerosol/vapor testing was extrapolated from TOP 8-2-501 entitled "Permeation and Penetration Testing of Air-Permeable, Semi-Permeable and Impermeable Materials with Chemical Agents or Simulants". The vapor testing station was specifically designed based on previous testing modules outlined in the DREO document #89-13 entitled "Apparatus and Methodology for Cyanogen Chloride Gas-Life Measurement of Gas-Mask Canisters" from National Defense Canada through the Defense Research Establishment Ottawa. This protocol describes the most recent apparatus and experimental procedure used to determine the absorption capacity of carbon/Triosyn-based hybrid materials as required by military specifications for the modified activated carbon. Adaptations of these protocols were essential in order to test according to set government standards and military specifications[11][12][13].

Microbiological efficacy: A tridimensional impregnation of the Triosyn® biocidal interactive polymer in a low pressure drop membrane and a separate impregnation of the new carbon based material provided a fraction of the pressure drop as compared to already marketed membranes. This produced a chemical and biological (C/B) prototype derived from a complex membrane whereby the first step provides the effective biocidal properties and the second step provides the enhanced absorption capabilities while allowing air stream velocity to be unhindered. Pressure drops were measured using U-tube manometer.

MS2 coliphage (ATCC 15597-B1), a bacterial virus known for its survival capacities in the environment, was used as a biological agent to challenge the different prototypes.

Different prototypes were tested in Aeromicrobiology Testing in order to assess the effectiveness of the treated filters in reducing a viral aerosol. Refer to system set-up in Figure I. The MS2 phage was diluted in DH_2O and the solution placed in a 6 jet modified collision nebulizer. An air tank was used to pressurize the nebulizer and subsequently aerosolize the microbial suspension into the chamber. Different pre-vaporization times (0, 5, 15, and 30 minutes) were essayed at a rate of 10 LPM. Dilution air was added to the solution entering the chamber at a rate of 15 LPM. The airflow was distributed in the chamber with a built-in low speed fan and a vacuum pump ensured that it was passing through each filter unit with a velocity of 5 LPM. All experimental samples (carbon and PP3 Triosyn®) were embedded in a non-woven low quality/low pressure drop 95% of 0.3-micron retention material. The filter prototypes comprised three successive layers: non-woven with the chemical prototype, non-woven low quality / low pressure drop membrane (LPDM) and non-woven material impregnated with Triosyn® PP3. The filter prototypes were placed into BGI filter holders. Blanks were used for positive controls. These filter units were placed between the chamber and the sampling units (gelatine membrane filters placed into BGI filter holders). Filtration occurred for 15 minutes at 10 LPM and room temperature (approximately 20°C). Temperature and relative humidity (RH) were monitored at the beginning and at the end of each filtration run. Gelatin membranes were loaded in BGI filter holders. These collector units were placed after the test filter units. After filtration, gelatin membranes were placed in a 9 ml tube of neutralizing dilution solution buffer (NDS) kept in a 35°C water bath until complete dissolution of the membranes. Dilutions of MS2 assays were made in sterile PBS. Serial dilutions of the collection buffer (1ml) were plated in MS2 media and incubated at 35°C for 16-18 hours for subsequent enumeration of the number of PFU/ml.

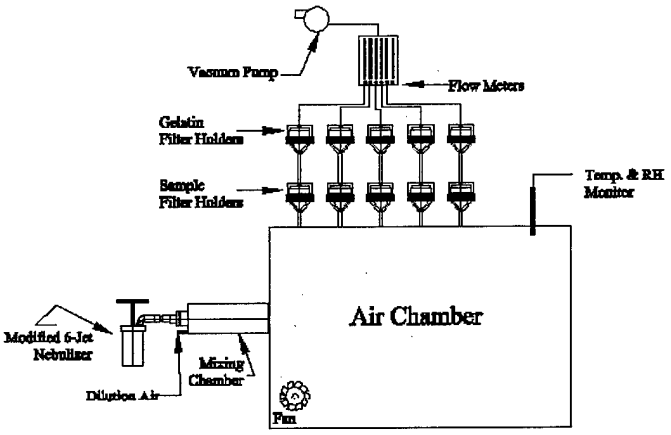

Figure 1. Aeromicrobiology testing chamber.

Toxicology: Experimental samples were tested to detect leaching of iodine content in the effluent air stream. An airflow passes through the air filter membrane samples allowing free particles to be transported into an AGI (all glass impinger) containing 100 ml of osmotic water. The duration of the test is 30 minutes at 30 L/min for a circular surface diameter of 4.5 cm. An aliquot of water from the glass impingers is sampled. Iodine testing must occur within 5 minutes of sampling. Total iodine content is measured with a spectrophotometer at a wavelength of 592 λ for absorbance values.

The flow meter manufacturer provides correlation charts for positive pressures only. Consequently, the flow meters used in this experiment were calibrated for a vacuum environment, which differs from standard atmospheric conditions. Absorbance values measured with the spectrophotometer are converted first to ppm and then in mg/100ml. For a representative value of the effective surface of a human facemask, the values have to be converted in mg of iodine/100 cm^2 of tissue/m^3 of air.

Iodine method: Mercuric chloride (Fisher Scientific) added to an aqueous elemental iodine solution results in complete hydrolysis of iodine and the stoichiometric production of hypoiodous acid. The compound 4,4,4 methylidynetris (N,N-dimethylaniline) (Leuco crystal violet, Aldrich #21,921-5) reacts with the hypoiodous acid to form crystal violet dye. The maximum absorbance the crystal violet dye solution produces in the pH range of 3.5-4.0 is measured at a wavelength of 592 nm. The absorbance follows Beer-Lambert's law over a wide range of iodine concentrations. Iodine can be measured in the presence of a maximum of 50 ppm iodide ions without interference.

Total Iodine Method: Iodide is selectively oxidized to iodine by the addition of potassium peroxymonosulfate (Oxone, Aldrich #22,803-6). The iodine produced reacts instantaneously with the indicator reagent Leuco crystal violet over the same conditions described previously for

iodine methods. Total iodine plus iodide is formed from this reaction and the iodide content is calculated from a subtraction of iodine concentration. Readings of absorbance have to be performed on a spectrophotometer with a pathlength of 1.0 cm set at a wavelength of 592 nm.

Prototypes tested: The investigations reported in this paper were conducted on two different types of activated carbon samples. Carbon in the form of Ambersorb 572 was used in the sphere, and particulate form and Nuchar (10-50 μm), for comparison to Ambersorb 572 in particulate form.

The quantity of spheres tested was set to form a monolayer of spherical carbon beads, similar to thin film coatings seen in textiles applications and testing. It is important to note that since we the samples were examined on a weight basis, for the quantities present of the prototypes, which contain a greater amount of oxygen molecules and impregnated material, the volume of prototype is generally less than that of the standard NATO carbon, Ambersorb 572.

RESULTS AND DISCUSSION

The focus of phase I of CB-Materials research was to develop a new class of materials that have the capacity of adsorbing Chemical Warfare Agents in the vapor phase and retain the biocidal efficiency of the iodinated resin. The research in this phase was devoted to the synthesis of these new materials, and subsequent vapor testing with the mustard gas simulant MeS, the evaluation of microbiological activity of the selected prototypes and the toxicological assessment. The prototype materials underwent vapor testing against chemical warfare simulant MeS after the test materials were left at ambient temperature and 23% humidity for three days.

The UV-Vis absorption data presented in Table 1 is of effluent concentrations of MeS that has permeated through the prototype material from the vapor tests. MeS is collected in gas sampling impingers and detected by UV-Vis absorption spectroscopy. The testing station which is set-up to run a control, the standard carbon (in the form of Ambersorb 572 or Nuchar) and the prototype, allowed us to make an accurate comparison of prototype absorption efficiency of HD simulant MeS. The vapor testing protocol utilizes a high influent concentration, low air speeds and as a result, has allowed us to process a great number of prototypes for down-selection before decreasing the influent concentration of MeS and increasing air flows. The prototype OX5H/572 (carbon modified by surface oxidation) showed a significant improvement in vapor absorption with a 48% increase over Ambersorb 572. Another prototype, POX2/1/A572, which was synthesized using another surface oxidation technique, also resulted in an improved absorption of 26% over carbon spheres.

Combined technology: To further enhance the absorption capabilities of the carbon hybrid materials, a new class of prototypes was synthesized using a combination of synthetic methodologies from the polyoxometallate impregnation, nanoparticulate adsorbents and/or the oxidation of the carbon macrostructure. This novel synthetic methodology produced new materials, which result in a 10-20% increase in MeS vapor absorption over prototypes from previous carbon modifications. The carbon hybrid prototypes OX5H/D, OX5H/C, POX3/1/0/B and POX3/1/0/A result in MeS vapor absorption capacities of 67%, 59%, 54%, and 63% improvement over Ambersorb 572. The prototypes POX3/1/0/A, OX5H/C, and OX5H/D were down-selected for further studies.

TABLE 1. Vapor testing results for spherical beads.

	MES concentration (ppm)						Absorption
Sample ID	Avg. Control	Avg. A572	Avg. Prototype	Std. Control	Std. A572	Std. Prototype	Avg. %
POX2/1/A572	7.21	1.49	1.09	0.23	0.17	0.09	26%
OX5H/A572	6.07	1.94	0.99	1.10	0.45	0.51	48%
OX5H/D	6.92	1.84	0.61	0.93	0.43	0.20	67%
OX5H/C	6.79	1.71	0.73	1.85	0.71	0.22	59%
POX3/1/0/B	6.75	1.75	0.84	0.88	0.68	0.46	54%
POX3/1/0/A	7.24	1.60	0.61	1.44	0.90	0.36	63%

In order to further increase the absorption capacity of carbon, we examined particulate forms of carbon that originated from micronized Ambersorb 572 beads and Nuchar granules. This finely divided material imparts an increase in the surface area of the material. It was chemically modified as the spherical carbon beads. For the vapor tests, approximately 30 milligrams of the material was impregnated uniformly within a low-pressure drop membrane (LPDM). For the particulate samples, the above prototypes resulted in similar absorption capacities to the spherical carbon hybrids, with % MeS absorption of 57%, 58%, and 64%, for prototypes POX3/1/0/A, POX3/1/0/B and OX5H/D, respectively. The prototype OX5H/C showed a remarkable increase in MeS vapor absorption of 84% over micronized Ambersorb 572.

Of the prototypes selected, we undertook a study using Nuchar particulates functionalized similarly to Ambersorb 572. Vapor testing of the Nuchar-based prototypes POX3/1/0/A, POX3/1/0/B, OX5H/C and OX5H/D resulted in MeS absorption that ranged between 49%-60% better than Nuchar. Refer to Table 2.

TABLE 2. Comparative vapor testing results for particulates vs. Nuchar.

	MES concentration (ppm)						Absorption
Sample ID	Avg. Control	Avg. A572	Avg. Prototype	Std. Control	Std. A572	Std. Prototype	Avg. %
OX5H/C particulates	6.76	2.46	0.38	1.69	1.24	0.28	84%
OX5H/D particulates	6.23	3.17	1.14	1.52	1.23	1.13	64%
POX3/1/0/A particulates	5.62	2.29	1.12	1.05	0.98	1.09	57%
POX3/1/0/B particulates	5.29	2.15	0.91	1.03	1.05	0.61	58%
OX5H/C nuchar	5.66	1.76	0.79	0.47	0.39	0.18	55%
POX3/1/0/A nuchar	6.25	3.30	1.73	1.04	1.12	1.12	49%
POX3/1/0/B nuchar	8.02	4.48	1.82	0.77	1.47	1.12	60%
OX5H/D nuchar	5.44	1.72	0.78	0.75	0.95	0.78	55%

In order to investigate the absorption efficiency of beads versus particulate samples, we carried out a series of tests that examined the selected prototype being vapor tested simultaneously with both forms of carbon materials. The results presented in Table 3 suggest that the beads are about 42% better at absorbing MeS vapors. What is important to note, is that the quantity of beads present is *4 times greater* than the particulates, resulting in *only* a 1.5-fold increase in vapor absorption. This suggests that by doubling the quantity of particulates (60 milligrams), which is half the amount present for the beads (120 milligrams), the MeS vapor absorption would theoretically be similar. Further increases in the amount of particulates to 120 milligrams would subsequently result in drastic improvements over the modified beads. This study is still in its first phase, however, these preliminary results clearly suggest that the particulates have greater surface area than the beads and that far less material is required to perform better than the beads in MeS vapor absorption.

TABLE 3. Comparative vapor testing results for spherical beads vs. particulates.

	MES concentration (ppm)						Absorption
Sample ID	Avg. Control	Avg. Beads	Avg. Particulates	Std. Control	Std. Beads	Std. Particulates	Avg. %
OX5H/C	6.26	1.16	1.99	0.94	0.20	1.07	42%
OX5H/D	6.36	0.99	2.40	0.09	0.03	1.09	59%
POX3/1/0/A	7.68	1.21	2.73	0.90	0.34	1.12	56%
POX3/1/0/B	5.87	0.93	1.06	0.28	0.12	0.38	12%

Aeromicrobiology testing was conducted following the established protocol described above. CB prototype membranes produced reduction rates greater than 99,9% against MS2 phage at a concentration of 10^9 PFU/ml for all configurations involving prototypes from OXH and POX families Refer to Table 4.

TABLE 4. Filtration performances of C/B prototypes against MS2 phage.

First Run	PFU/ml	Reduction %
OX5H/D + Triosyn® PP3	1.05E+03	99.98
OX5H/D + Triosyn® PP3	8.60E+02	99.984
OX5H/C + Triosyn® PP3	4.70E+02	99.9913
OX5H/C+ Triosyn® PP3	1.64E+03	99.969
C+	5.40E+06	0

Initial Temperature & Relative Humidity 21.8°C & 18%
Final Temperature & Relative Humidity 23.3°C & 48%

Second Run	PFU/ml	Reduction %
POX 3/1/0 B + Triosyn® PP3	5.00E+02	99.99390
POX 3/1/0 B + Triosyn® PP3	4.30E+02	99.99476
POX 3/1/0 A + Triosyn® PP3	4.60E+02	99.9944
POX 3/1/0 A + Triosyn® PP3	1.70E+02	99.9979
C+	8.20E+06	0

Initial Temperature & Relative Humidity 21.8°C & 20%
Final Temperature & Relative Humidity 22.9°C & 52%

LPDM: Low pressure drop membrane
Parameters: challenge microorganism: MS2 phage; aerosol generated by: 6 jets modified collision nebulizer; air flow velocity: 5 LPM; nebulizer airflow: 10 LPM; dilution airflow: 10 LPM; orifice diameter: 4 cm; time: 15 min; pre-vaporization: 30 min; collection fluid: NDS; collection device: BGI holding a gelatine membrane; sampling on MS2 media by single layer soft agar.

TABLE 5. Efficacy of commercially available standard dust filter and Triosynated dust filter against MS2 phage @ 6 LPM.

Membrane	Äp (mm H_2O)	PFU upstream	PFU downstream	% reduction
00315-3BM	38	2.70E+07	1.30E+04	99.952
Standard dust filter	1	3.40E+07	5.24E+06	84.590
Triosynated dust filter	1.5	3.40E+07	7.30E+01	99.999

Pressure drop readings showed commercially available filter papers having a pressure drop 25 times greater than Triosynated filter with less efficient percent reduction values. This provides a more efficient protective layer with a low pressure drop, thus minimizing the thermal load increase.

A toxicology evaluation was performed to ensure that the iodine gaseous/ particulate content leaching in the effluent air stream does not represent a health issue with regards to the use intended (face mask for individual protection). The total iodine content in ppm was determined following the established protocol described above. The values were then mathematically converted in Threshold Limit Values (TLV) to establish the toxicity level on a comparison basis using the following equation: $mg/100cm^2/m^3$= (mg/L) iodine x 0,1L x $100cm^2$/surf (cm^2) x ($1000(L/m^3)$/(flow (L/min) x time min))).

As seen in Table 6, the TLVs established for selected prototypes were significantly below the acceptable standard of 1,0 mg/m^3 [ACGIH], 0,07 mg/m^3 being the highest value recorded.

TABLE 6. Toxicological evaluation.

CB Prototype	Total Iodine Absorbance (Average)	Free Iodine Absorbance (Average)	Total Iodine Concentration (ppm)	Free Iodine Concentration (ppm)	TLV (mg/m^3)
OX5H/C + Triosyn® PP3	0.0035	0.0005	0.014	0.002	0.02
OX5H/D + Triosyn® PP3	0.005	0.001	0.048	0.004	0.05
POX3/1/0/A + Triosyn® PP3	0.0205	0.001	0.062	0.004	0.07
POX3/1/0/B + Triosyn® PP3	0.005	0.001	0.002	0.004	0.00

Parameters: material surface: 10.18 cm^2; Air Flow: 30 liters/minute; Time: 30 minutes; Collector: AGI (all glass impinger); Spectrophotometer at 592ë
LPDM: low pressure drop membrane

Calculation: TLV ($mg/100cm^2/m^3$) = [iodine] (mg/L) * 0.1 L* 100 (cm^2) / surface (cm^2) * 1000(L/m^3) / flow (L/min) * time (min)

Where 100 cm^2 is the human facemask surface

The Threshold Limit Value is an exposition standard estimated for workers. Consequently, 40 hrs/week, 50 weeks/year and the average expected life span of an individual are the presupposed conditions of exposition. The utilization of a facemask for individual protection would imply a much smaller exposition factor.

CONCLUSIONS

The prototypes resulting from nanoparticulate impregnation and surface oxidation and a combination of the various synthetic methodologies have resulted in improved efficiency in MeS vapor absorption. These technologies have produced new materials with enhanced capabilities at absorption of toxic vapors over the standard NATO carbon. Vapor testing using Nuchar-based carbon demonstrate similar results in MeS vapor absorption over Ambersorb 572-based materials. A comparative study of the vapor absorption of beads versus particulates suggests that the particulates present have a greater surface area of absorption than the beads. The C/B protective barrier was therefore lighter in weight and had a low pressure drop without toxic iodine gaseous/particulate content in the effluent air stream. The prototypes down-selected from the MeS vapor tests in the bead form are: POX3/1/0/A, OX5H/C, and OX5H/D and those prototypes selected from the particulates are: OX5H/C and OX5H/D.

In aeromicrobiology, excellent results were obtained with selected prototypes from OXH and POX families. Reduction rates greater than 99,9% against MS2 phage at a concentration of 10^9 PFU/ml were observed for all configurations.

The Threshold Limit Values established in the toxicology study for selected prototypes (OX5H/C, OX5H/D, POX3/1/0/A and POX3/1/0/B) were below the standard of 1,0 mg/m^3, with the highest recorded value of 0.7 mg/m^3. Therefore, the amount of iodine is significantly below the permissible levels that workers may be exposed to day after day without adverse effect.

FUTURE WORK

In this research phase, our vapor testing conditions focused on utilizing high influent concentrations of the simulant compound and low air speeds similarly seen in vapor testing of textile materials. A direct examination of these new materials using lower challenge agent influent concentrations and higher air speeds is essential in order to examine the rate of simulant absorption in the vapor phase as well as gain an understanding of the diffusional effects of the material. Reproducibility of the down selected prototypes will undergo testing to assess any loss of efficacy over time. We are also continuing work on improving the detection limits of the UV-Vis spectrophotometer and this will allow us to increase the detection limits to low ppb and subsequently allow testing to occur using lower influent concentrations and higher air speeds This research study has focused on the absorption properties using HD simulant MeS. Our lab designed and synthesized these new carbon-based materials with the potential to catalytically destroy chemical agents and simulants. Key issues to be addressed are the breakdown products

formed and the materials' capacity to absorb these contaminants. These new materials may impart beneficial characteristics in terms of catalyst activity and selectivity as well as contribute advances in tailor-made CW reactive absorbents and biocidal products.

REFERENCES

[1] **Bandosz, T.J.** 1999. *Effect of pore structure and surface chemistry of virgin activated carbons on removal of hydrogen sulfide.* Carbon, 37, 483-491.

[2] **Figueiredo, J.L., Pereira, M.F.R., Freitas, M.M.A., Orfao, J.J.M.** 1999. *Modification of the surface chemistry of activated carbons.* Carbon, 37, 1379-1389.

[3] **Xie, F., Phillips, J., Silva, I.F., Palma, M.C., Menendez, J.A.** 2000. *Microcalorimetric study of acid-sites on ammonia- and acid-pretreated activated carbon.* Carbon, 38, 691-700.

[4] **Mochida, I., Korai, Y., Shirahama, M., Kawano, S., Hada, T., Seo, Y., Yoshikawa, M., Yasutake, A.** 2000. *Removal of SO_x and NO_x over activated carbon fibers.* Carbon, 38, 227-239.

[5] **Raymundo-Pinero, E., Cazorla-Amoros, D., Salinas-Martinez de Lecea, C., Linares-Solano, A.** 2000. *Factors controlling the SO_2 removal by porous carbons: relevance of SO_2 oxidation step.* Carbon, 38, 335-344.

[6] **Stark, J.V., Park, D.G., Lagadic, I., Klabunde, K.J.** 1996. *Nanoscale metal oxide particles/clusters as chemical reagents. Unique surface chemistry on magnesium oxide as shown by enhanced adsorption of acid gases (sulfur dioxide and carbon dioxide) and pressure dependence.* Chem. Mater., 8, 1904-1912.

[7] **Wagner, G.W., Bartram, P.W.** 1995. *^{31}P MAS NMR study of the hydrolysis of O,S-diethylphenylphosphonothioate on reactive sorbents.* Journal of Molecular Catalysis A: Chemical, 99, 175-181.

[8] **Wagner, G.W., Bartram, P.W.** 1995. *^{31}P MAS NMR study of the hydrolysis of O,S-diethylphenylphosphonothioate on reactive sorbents.* Journal of Molecular Catalysis A: Chemical, 99, 175-181.

[9] **Wagner, G.W., Bartram, P.W., Koper, O., Klabunde, J.,** 1999. *Reactions of VX, GD, and HD with Nanosize MgO.* Journal of Physical Chemistry, 103, 3225-3228.

[10] **Yang, Y.C., Baker, J.A., Ward, J.R.** 1992. *Decontamination of Chemical Warfare Agents.* Chem. Rev., 92, 1729-1743.

[11] **Liang, S.H.C., Poirier, R.T., Harrison, B.H.** 1989. Technical Note 89-13 *Defence Research Establishment Ottawa. Apparatus and methodology for cyanogen chloride gas-life measurement of gas-mask canisters*

[12] **Campbell, L.E., Pappas, A.G**. 1999. ERDEC-TR. *Domestic preparedness: Sarin vapor challenge and corn oil protection factor (PF) testing of powdered air purifying respirator (PAPR) systems and cartridges.*

[13] **Commander U.S. Army Dugway Proving Ground**. 1997. TOP 8-2-501. Permeation and penetration testing of air-permeable, semi-permeable and impermeable materials with chemical agents or simulants (swatch testing).

BROAD BANDWIDTH LIDAR FOR STANDOFF BIOAEROSOL SIZE DISTRIBUTION

James B. Gillespie, David L. Ligon , Paul M. Pellegrino, and Nicholas F. Fell, Jr.
U.S. Army Research Laboratory, 2800 Powder Mill Road, Adelphi, MD 20783-1197
jgillesp@arl.mil

ABSTRACT

We are examining the possibility of using a broad bandwidth lidar system to estimate size distributions of aerosol clouds that may possess respirable biological particles. An optical parametric oscillator has been specially designed and fabricated for broad bandwidth operation in the 1.4 to 1.8 micrometer spectral region. We have determined the spectral bandwidth, output, and pumping power characteristics of this device as a potential lidar source. We have developed a Monte Carlo technique to analyze backscattering data that would result from our hyperspectral lidar. Lidar simulation results show good estimates of size distributions for respirable size aerosols.

1. INTRODUCTION

Current methods of stand off detection of bioaerosols involve either point sensors in remote locations, or use of planned lidar systems. Two types of lidar considered are (a) ultraviolet (UV) laser induced fluorescence systems that can detect the presence of biological particles and (b) elastic backscattering lidar systems that can detect the presence and perhaps the shape of an aerosol plume. The UV lidar systems lack specificity in that they can only detect a spectrally broad spectrum—usually the emission of triptophan, an amino acid found in biological cells. UV systems are also generally do not operate in an eye safe mode of operation. The UV system has limited range at night and will not operate satisfactorily in the daytime because of the presence of background light. The elastic backscattering lidar systems have longer range, will operate in the daytime, and are eye safe. From a practical standpoint however, there will be aerosol plumes present almost everywhere in the environment; so there is a complete lack of any specificity. We have been developing a third type of lidar technology for standoff detection of biological aerosol plumes—a hyperspectral, broad bandwidth lidar. This type of lidar would emit a pulse of "laser" light that is several hundred nanometers in spectral bandwidth and centered at 1.55 micrometers so it can be eye safe. The backscattered return from an aerosol plume would be collected and dispersed spectrally on a detector array so that backscattering versus wavelength could be analyzed for particle size information (and perhaps refractive index information). This type of system combines two new technologies: (1) inverse Monte Carlo (IMC) signal analysis of the backscattered light and (2) a new broad bandwidth optical parametric oscillator (OPO) laser source for the 1.5 micrometer spectral region. This type of lidar could be hyperspectral, if required, by simply collecting the return light at high resolution. For the application at hand, the high resolution is not essential, but the spectral width is important. This system will have daytime operation capability and will be eye safe. It also will have some specificity in that the aerosol size distribution can be estimated. The determination of the size of the aerosol particles is important because biological endospores are typically one to a few micrometers in size while most background aerosols are submicrometer in size with the exception of fog type water droplets which are one to ten micrometers, or greater than 40 micrometers in size. Soil-derived aerosol particles are typically much greater than ten micrometers in diameter. Detection of an aerosol plume that has a significant concentration of particles in the 1 to 10 micrometer size range would be cause for concern and act as an alert to probe the aerosol with a more specific point sensor. We have demonstrated feasibility of

the our notional hyperspectral lidar system though a computer simulation based on a Monte Carlo method to solve the inverse scattering problem. We have obtained and characterized an OPO device which can be used for the source of the system.

2. THEORY

This work originated from an effort to remotely size atmospheric aerosols using multi-wavelength, multi-angle light scattering data. Since a lidar only receives backscattering. We investigated the applicability of the method to one angle with many wavelengths. This section summarizes the results of a Monte Carlo method to invert lidar scattering data.

2.1 INVERSE MONTE CARLO METHOD

For a system of particles in the single scattering regime, we can write the volume extinction coefficient as a Fredholm integral of the first kind:

$$c(\lambda) = N_0 \int_0^\infty K_{ext}(r,\lambda) g(r) dr ,$$

where N_0 is a scaling parameter (in our case it is the total particle density), K_{ext} is the Mie Kernal function, r is the particle radius, and g(r) is is probability distribution function for the aerosol (corresponding to the normalized size distribution). The spectral backscatter coefficient can be written in the same form, and for computer computations it can be approximated by a sum over a discreet set of M radii

$$b(\lambda) = N_0 \sum_{i=1}^{M} K_{back}(r,\lambda) f(r)$$

where K_{back} is the Mie backscatter kernel and f(r) is the size distribution. The standard problem is to solve for the backscatter coefficient knowing the size distribution, number density, and the Mie kernel. The inverse problem is to experimentally collect backscattering data and then determine the size distribution. The above expression is for a number distribution. By adding a weighting term

$$w(r) = 4/3\pi r^2 ,$$

we can determine a volume size distribution. The use of the weighting function makes this method more stable for inversion. The resulting volume distribution can then be converted to a number distribution for plotting purposes.

Standard inversion methods require much data and are computationally intensive (sometimes several hours of computer time). They are also very sensitive to propagation of errors because of the matrix methods involved. There are usually problems of uniqueness because of incomplete data sets and noise in the data. For scattering, the kernel can be multivalued causing additional uniqueness problems.

The Monte Carlo approach to solving the inverse scattering is a mathematical brute force, random-walk, curve fitting approach using physics through the application of Mie theory. It also uses practical assumptions and constraints. Briefly, walkers representing the particle sizes are distributed on a grid. A walker is moved on the grid and scattering computations are made and compared to the experimental data set. If there is improvement (through comparison to a chi-squared error analysis), the walker stays in the new position and another walker is moved. If there is no improvement the walker is returned to its position and another walker is moved. The process is repeated until a predetermined error constraint is

obtained. When a fit to within 5% of the input data is obtained, the process ends and the resulting size distribution is considered to be the estimate of the actual size distribution. This method is described by Ligon, et al.[1]. A flow chart of the IMC process is shown in the figure below.

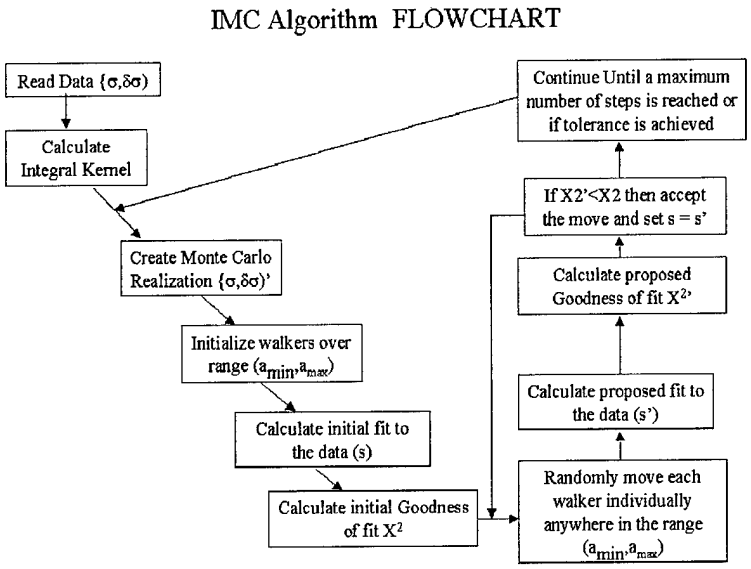

Figure 1. The flow chart for the Inverse Monte Carlo method.

INVERSION FOR LIDAR

The use of multi-wavelength lidar measurements allows for the characterization of aerosol properties from retrieved backscatter coefficients[23]. The retrieval of aerosol properties from multi-wavelength lidar is a two-step process. The first step involves retrieval of the spectral backscatter coefficient, aerosol extinction coefficient, or both from the lidar signal. The second step is to retrieve from these values the aerosol properties such as refractive index, and size distribution. In previous work, we developed a novel inverse Monte Carlo algorithm that was shown to be effective in retrieving the aerosol properties from spectral backscatter and extinction measurements[4]. The exact nature of the inversion methodology for our broadband lidar is still in progress, however some salient features can be discussed.

One standard for for the lidar equation for the return power, P(r), is given by

$$P(z) = P_0 \frac{c\tau}{2} \frac{A}{z^2} \eta\, \beta(z) \exp\left[-2\int_0^z \alpha(z)dz\right]$$

where: $\eta(z,\lambda)$ is the receiving efficiency (overlap) of the lidar, A is the receivers aperture area, $\beta(z,\lambda)$ is the backscatter coefficient at range z and wavelength λ (principally due to aerosols), and the two-way transmission is

$$T(z,\lambda) = \exp\left[-2\int_0^r \alpha(z,\lambda)dz'\right]$$

is the atmospheric transmission to the range z for the atmospheric volume extinction coefficient α which has contributions from both atmospheric aerosols and molecular absorption by atmospheric gases. The inversion is complicated by the fact that we are interested in determining properties of aerosol clouds that may be composed of more than one type of aerosol at different ranges. One possible choice of inversion procedures incorporates a modified form of the constrained slope method on the quantity

$$\ln[S(z,\lambda)] = \ln\left[\frac{P(z)z^2}{A}\right] = \ln[\eta(z,\lambda)\beta(z,\lambda)dr] - 2\int_0^r \alpha(z,\lambda)dz$$

in which the value $\ln[\eta(z,\lambda)\beta(z,\lambda)dz]$ is determined from a metropolis optimization algorithm given a constraint on the allowable range for the extinction coefficient α and an estimate of the molecular contribution to the extinction.

3. EXPERIMENTAL

There are two aspects to the experimental work, a computer simulation to demonstrate that backscattering from an aerosol can be successfully inverted to yield a good estimate of the aerosol size distribution and an experimental characterization of the broad bandwidth laser source.

3.1 AEROSOL BACKSCATTER INVERSE MONTE CARLO SIMULATION

We examined the Monte Carlo inversion method using synthetically generated scattering data. This section is a brief summary of a more complete analysis recently published in reference 4. Using Mie scattering theory we calculated the extinction and backscatter coefficients for 3 different log-normal distributions of water droplets for the wavelength range 0.4 to 0.8 micrometers at 41 evenly-separated wavelengths in the interval. The distributions chosen correspond to three regions: Region I, a distribution with modal radius smaller than the minimum wavelength in the data set; Region II, a distribution with modal radius within the wavelength region of the data set and Region III, a distribution with modal radius greater than the maximum wavelength in the data set. The particular modal widths chosen for these distributions were selected in order to keep the same standard deviation for each distribution. W assumed an error of 1% in the generated data and used a boot strap method for 50 different realizations of the data for error analysis.

Figure 2 shows the results of an inversion for a broadly distributed, bi-modal aerosol. This is for the 1.5-micrometer spectral region. For this case the log normal distribution parameters for the first mode are: modal radius = 1.5-micrometers and the modal width is 0.2. For the second mode the parameters are: modal radius = 2.5-micrometers, and the modal width is 0.25. Five percent noise was used on the data. The calculated fit is in good agreement with the simulated data. Simulations worked well even for noise levels of 33%. In general, if the size distribution was completely contained within the broad output then the size distribution was very accurately obtained. If the size distribution was for particles that were all larger than the wavelengths, then we could only determine where the distribution was located. We could determine the index of refraction by iterating the entire process over a range of refractive indices and observing the minimum chi-squared value.

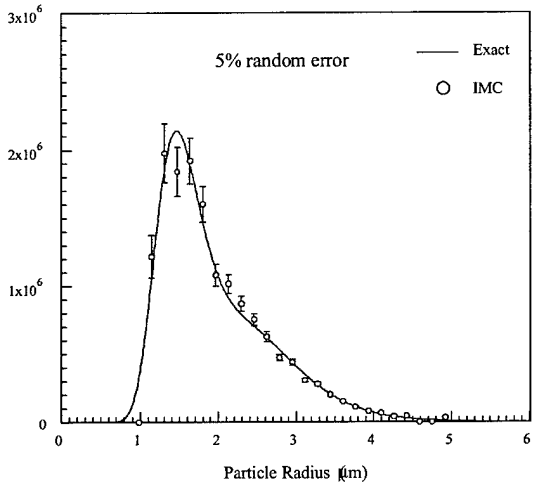

Figure 2. Bi-modal broad distribution.

3.2 BROAD BANDWIDTH SOURCE

The source for the proposed hyperspectral lidar system is a BBO optical parametric oscillator (OPO) that was specially designed for broad bandwidth operation by scientists at DERA in the United Kingdom[5]. This device is based on a visible broad bandwidth device patented for a white light laser[6]. It is pumped with a 532-nm Nd:YAG laser.

The OPO cavity is 2.54 cm long and is designed to resonate the OPO signal (700 to 950-nm). The crystal was extensively modeled to design the BBO crystal and the cavity. Both high and low signal to pump angle phase matching configurations were investigated. It was found that the high angle solution produced an unwanted blue component in the light; so the low angle solution was used. The pump angle was about 23.8 degrees and the signal angle was about 21.4 degrees. The Cavity consists of a high reflector (99%) at one end and an output coupler (95%) at the other. The idler beam (in the 1.4 to 1.8 micrometer spectral region) will be the source for the laser. The beam divergence of the idler was recollimated using a grating, and the beam divergence was 0.2-mr in the horizontal and 7.9-mr in the vertical. Figure 3 shows the wavelength structure of the signal beam in the 720 to 920-nm region. Because there was no suitable detector for the idler, the idler spectrum was theoretically calculated from the signal spectrum. The resulting calculations indicate that the idler is greater than 220-nm broad. The entire 1.4 to 1.8 region can be obtained by tuning the OPO.

The slope efficiency and power output levels were characterized for the OPO system. The OPO was pumped with three Nd:YAG lasers. First the system was tested at DERA with an injection seeded laser the idler had a 14.3% energy efficiency and the signal was 4.5%. The pump threshold was 44.8-mj per pulse. When installed at the Army Research Laboratory, two unseeded Nd:YAG lasers were tried, one in a Schwartz ElectroOptic (SEO) Ti:sapphire laser and a Big Sky laser. The results are shown in figure 4.

The SEO had a threshold of about 60-mj per pulse with 23% energy efficiency and the Big Sky was about 90-mj with 11% energy efficiency.

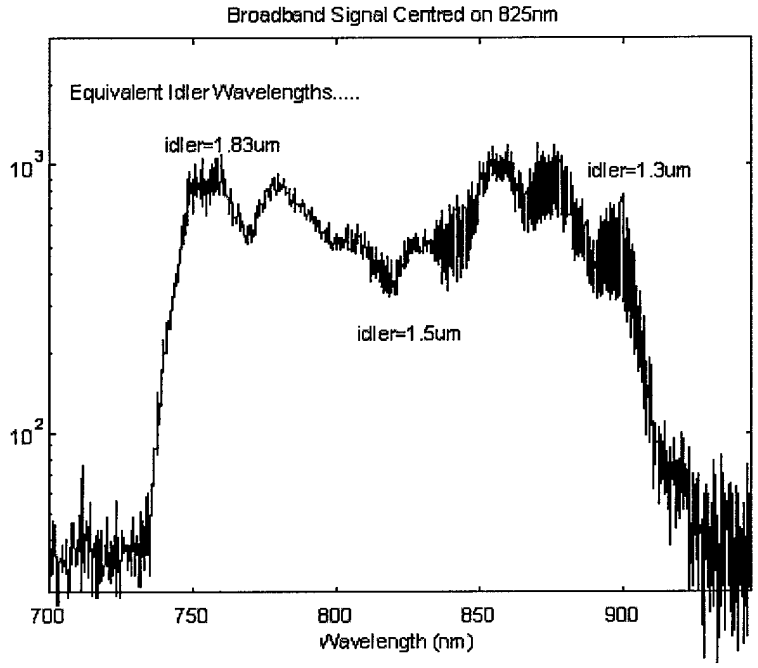

Figure 3. The wavelength spectrum of the OPO signal.

The OPO cavity oscillated and produced broad output in the 1.5 micrometer region as predicted by the modeling work. A collimator was necessary to correct for the beam dispersion. The current power output is about 7-mj per pulse for the system as configured.

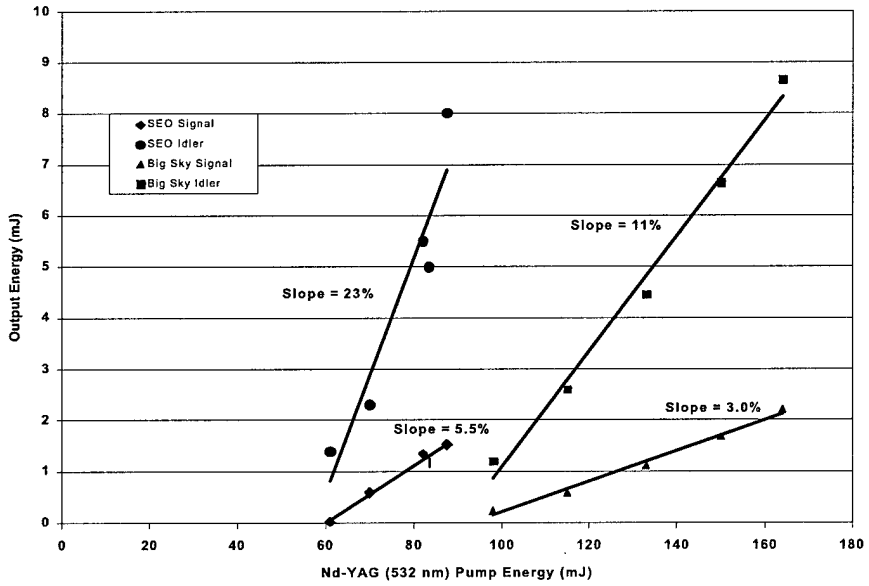

Figure 4. The slope efficiency plot for the SEO laser and the Big Sky laser.

4. CONCLUSIONS

We have designed a notional hyperspectral lidar system for standoff determination of aerosol size distributions. The lidar system is based on two new technologies: a broad bandwidth "laser" OPO source that operates in the 1.5-micrometer spectral region and an inverse Monte Carlo algorithm for analyzing the data. The hardware aspect of the system is currently a laboratory breadboard system, and aerosol experiments will commence shortly. The broad bandwidth laser has been characterized and will emit pulses of broad bandwidth light that are greater than 220-nm broad with 7-mj of power. The IMC analysis method has been rigorously tested and simulations on backscatter from aerosols have shown great promise. The inverse Monte Carlo method is very fast—typically two minutes on a desktop workstation for the entire analysis. One must assume a refractive index; however there are techniques to estimate this from the data using an iterative method. The simulation results in Section 3 demonstrate that the IMC is a stable method for inversion of scattering data. This stability comes from application of a boot strap error method. Noise levels of up to 33% can be handled successfully. The method works best when the size distributions are narrow, or wholly contained with the source spectral region; however even when the size distribution is outside the excitation region, meaningful information on the particle size is obtained. The second part of the software development is an actual lidar simulation in which the atmospheric transmission and the backscatter coefficients are analyzed. This second part is well underway and simulations have been performed. The lidar aspect may involve a calibration reflector in the near field of the lidar to provide enough information for all the required information.

5. ACKNOWLEDEGMENTS

We would like to acknowledge Dr. Nicholas Wood and his colleagues of DERA, Portsdown West for their work on the BBO optical parametric oscillator.

REFERENCES

[1] Ligon, David, T.W. Chen, and James B. Gillespie, "Determination of aerosol parameters from light-scattering data using an inverse Monte Carlo technique", Appl. Opt. 35, 4297-4304, (1996).

[2] Gonzalez, R., Y. Yee, J. Thompson, R. Rosen, "*Two-wavelength lidar inversion technique*," in SPIE *Proceedings on Atmospheric Propagation and Remote Sensing*, vol. 1688, 266-271 (1992).

[3] Feingold, G., and C.J.Grund, "*On the feasibility of using multi-wavelength lidar measurements to measure cloud condensation nuclei*," J. Atmos. Ocean. Tech., **11**, 1543-1558 (1994).

[4] Ligon, D., Gillespie, J. and P. Pellegrino, "*Aerosol properties from spectral extinction and backscatter estimated by an inverse Monte Carlo method*," Appl. Opt., **39**, 4402-4410 (2000)

[5] Wood, Nicholas, "Design specification for a pulsed neri-infrared broadband optical parametric oscillator, DERA/WSS/WS6/TR990309/1.0, June 1999.

[6] Laser Device, Patent GB 2315360, DERA

COOPERATIVE RELATIONAL DATABASE INITIATIVE FOR THREAT REDUCTION

Michelle Sheahan and Luther E. Lindler
Department of Bacterial Diseases
WRAIR
Silver Spring, MD 20910

ABSTRACT

In order to create a resource for basic and clinical research in biological threat reduction, we have developed an annotated relational database. This database is comprised of gene sequences from public databases and researchers' laboratory results, the Bioterrorism Defense Database runs on a Microsoft SQL platform and is accessible on a password-protected Internet site. The Biodefense database project is a collaborative effort between the Walter Reed Army Institute of Research, the US Army Medical Research Institute of Infectious Diseases, the Los Alamos National Laboratory, and the University of Alabama at Birmingham.

INTRODUCTION

We have developed a relational database of genes relevant to the studies aimed towards biological threat reduction. The database is comprised of individual gene sequences with their amino acid translations that have been annotated with information about toxicity, available probes, antibiotic resistance, source organism, strain, and literature references. Gene sequences of toxins, virulence factors and antibiotic resistance are taken both from GenBank searches and from researchers' own unpublished sequence data. The database is accessible on a password-protected web site, and is searchable by various criteria including organism, gene name and accession number. The immediate goal of the Bioterrorism Defense Database creation effort has been to present microbial pathogen data to researchers in a format that is useful, clear and comprehensive. The unique feature of this database is the one gene-one sequence design and the way in which the information is compiled and annotated. Over the next year, we plan to include more extensive annotations for each gene sequence, prepared by expert curators. Our database is one facet of a large-scale biological threat portal that is a collaborative effort between researchers at USAMRIID (Kevin Anderson), WRAIR, DOE-CBNP (Gerald Myers and Electra Sutton) and the University of Alabama at Birmingham (Elliot Lefkowitz). Our vision is that the final portal include database information that is crucial to researchers performing studies in the area of biodefense.

METHODS

The Bioterrorism Defense Database is a gene-based relational database. Many of the entries are selected from publicly released gene sequences submitted to GenBank while others are unpublished laboratory sequences. The gene entries are identified by gene name, GenBank accession number, and the unique DNA sequence of the gene's specific coding region. Additional information on antibiotic resistance, toxins, virulence factors, and probes is added into each record, as well as links to references and the protein translation (Figure 1.) This enables the

researcher to search for homologies based on gene sequence, and to view an annotated record that can be further analyzed with compatible DNA or protein sequence analysis software.

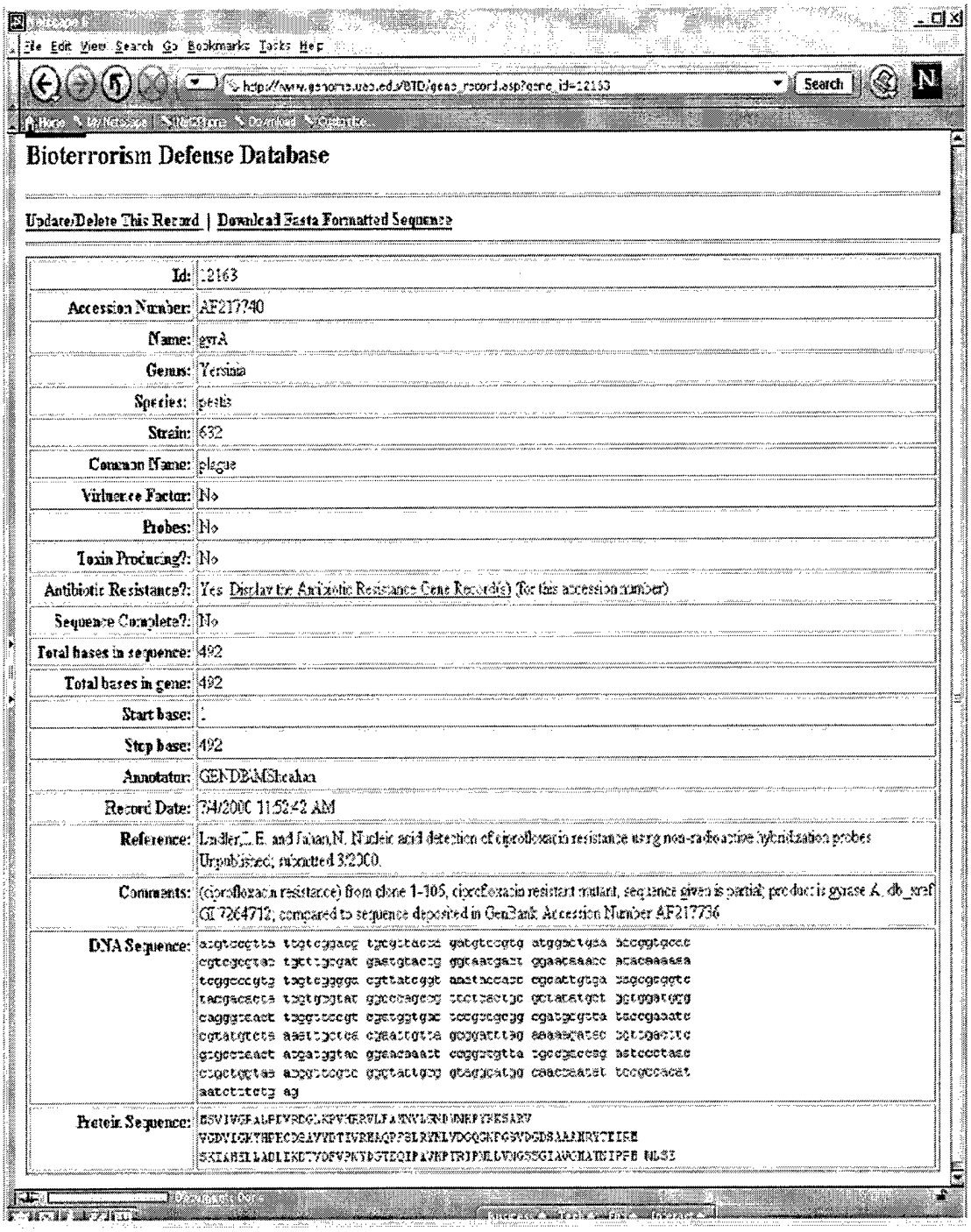

Bioterrorism Defense Database

Update/Delete This Record | Download Fasta Formatted Sequence

Id:	2163
Accession Number:	AF217740
Name:	gyrA
Genus:	Yersinia
Species:	pestis
Strain:	632
Common Name:	plague
Virulence Factor:	No
Probes:	No
Toxin Producing?:	No
Antibiotic Resistance?:	Yes Display the Antibiotic Resistance Gene Record(s) for this accession number)
Sequence Complete?:	No
Total bases in sequence:	492
Total bases in gene:	492
Start base:	1
Stop base:	492
Annotator:	GENDB\AMSheahan
Record Date:	7/4/2000 11:52:42 AM
Reference:	Lindler,L. E. and Tajan,N. Nucleic acid detection of ciprofloxacin resistance using non-radioactive hybridization probes Unpublished; submitted 3/2000.
Comments:	(ciprofloxacin resistance) from clone 1-105, ciprofloxacin resistant mutant, sequence given is partial; product is gyrase A. db_xref GI:7264712; compared to sequence deposited in GenBank Accession Number AF217736
DNA Sequence:	atgtccgtta tgtcggacg tgcgttacca gatgtccgtg atggactgaa tccggtgcca cgtcgccgtac tgttgcgat gaatgtacag ggcaatgact ggaacaaatc acacaaaaaa tcggccctg tagtcgggga cgttatcggt aaatccatc cgcattgtga tagcgcggtc tacgacatta tagtggtat ggccgagcg ttcttactgc gctatatgct ggtggatgcg caggatcaat tagctccgt cgatggtgac tccgtacgcg cgatgcgtta tacgcaaatc cgtatgttta aaattgctca cgaattgtta gcggatttag aaaacgatcc tgttgacttc gtgccatcaa tcgatggtac ggcacaaatt cagggcgtta tgcgtacgta tccgtacgcg aatcgcgtta tgcgcatccg aatccctacc ctgctgctac acggttcgtc ggctattgcg gtagtgcatg caacgaatct tccgccacat aatcttctcg ag
Protein Sequence:	SSVIVSFALPFVRDGLKPVHRRVLFAMNVLGNDWNKPYKKSARV VGDVIGKYHPHGDSAVYDTIVRMAQPFSLRYMLVDGQGNFGSVDGDSAAAMRYTEIKM SKIAHELLADLEKETVDFVPNYDGTEQIPAVMPTRIPNLLVNGSSGIAVGMATNIPPH NLSE

We have included genes and organisms that are relevant to the study of biological defense, including bacterial and viral threat agents. The organisms and diseases used in our current search criteria are shown in Table 1.

TABLE 1. Organisms/diseases/genes of interest.

Anthracis	Junin
Anthrax	Lassa
apamin	Machupo
Batrachotoxin	Marburg
Beta-bungarotoxin	Notexin
Botulism	pilin
Brucella	Ricin
Chloramphenicol resistance	Rift Valley
Clostridium perfringens toxin	Sabia
Conotoxin	Salmonella toxin
Coxiella	Salmonella virulence
Crimean-Congo	Salmonella pathogenicity
curare	Saxitoxin
Dengue	SEB
Diamphotoxin	Shiga toxin
Diptheria toxin	Shigella
Ebola	Strep Resistance
EEEV	T2 toxin
Escherichia coli toxin	Taipoxin
Escherichia coli pathogenicity	Tet Resistance
Escherichia coli virulence	Tetanus Toxin
fimbrillin	Tetrodotoxin
Francisella	Topoisomerase
Guanarito	Vaccinia
Hantavirus II	Variola
HantavirusI	VEENCGR
Heat-Labile	Vibrio cholerae
Heat-stabile	WEEV
	Yersinia pestis
	Yersinia enterocolitica

Data is entered into the Bioterrorism Defense Database either manually, by cutting and pasting from researchers' gene sequence results, or automatically, by reading web-accessible data with a parse application. This parse application was developed in collaboration with the Los Alamos National Laboratory and makes downloading web-accessible gene databanks more efficient and accurate. Once the fields of the gene entry page are populated, the annotator reviews the entries, makes any changes or corrections, and adds information from further analyses. Antibiotic resistance, toxin, and probe data is entered as separate tables within the database. Our plans include organizing the gene entries into clusters and adding the functionality of protein and gene analysis tools linked directly to the gene entry pages. The annotator will thus be able to complete additional analyses and predictions for each set of clustered gene products, enhancing the information available to the community of researchers using the Bioterrorism Defense Database.

Users can search the database with a BLAST routine using protein or nucleotide sequences, and view annotated search results. All-against-all search capability will be added in the near future. In addition, the Bioterrorism Defense Database is part of a larger effort to organize and present relevant data to the research community through a portal website. This Tri Agency Chemical and Biological National Security Program Portal is the result of a bioinformatics collaboration between Lawrence Livermore National Laboratory, Los Alamos National Laboratory, and USAMRIID/WRAIR. The CBNP portal will include the capability of simultaneously searching several participating biological threat databases, including the Bioterrorism Defense Database presented here, so that the researcher has access to the most comprehensive, up-to-date annotated analyses from experts in the field of biological terrorism defense.

CONCLUSIONS

Over the past year, we have worked to streamline the data entry process so that the most basic information about relevant genes can be accurately and efficiently added to the database. The next step is making the Bioterrorism Defense Database more valuable and informative to the researcher, by both expanding the breadth of information on our sequences of interest, and on improving its graphical presentation. With our collaborators at USAMRIID, DOE-CBNP, and the University of Alabama at Birmingham, we envision that the database will be a valuable source of data on the following:

- genes, transcripts, and gene products
- genomes and plasmids
- homologies: orthologies, paralogies, xenologies
- regulatory elements and repeats
- pathogenicity islands
- primers and probes
- molecular signatures; fingerprints
- recombinant constructs
- mechanisms of pathogenicity
- antibiotics and resistance
- growth properties; phenotypic data
- variability; alignments and cluster analyses
- protein structures; immunological properties
- geographical distribution and backgrounds
- clinical and host data
- prophylaxis and treatment
- literature

CHEMICAL CHARACTERIZATION OF THE PYROTECHNICALLY DISSEMINATED XM30 MAIN GUN SIGNATURE SIMULATOR

J.Steven Anthony, Mark V. Haley, and Sandra A. Thomson Ph.D,
Edgewood Chemical Biological Center (ECBC)
Bldg. E3150, Aberdeen Proving Ground, MD. 21010-5423
Phone: 410-436-4622 Fax: 410-436-7977
email: jsanthon@sbccom.apgea.army.mil

Charles L. Crouse
Geo-Centers, Inc.
Aberdeen Proving Ground , MD. 21010-5423

ABSTRACT

Development of the Multiple Integrated Laser Engagement System (MILES) 2000 device has been selected as the replacement to the currently used Hoffman systems. On the M1 or M60 tanks, a laser is activated to simulate firing of the main gun, which triggers a signal to the Main Gun Signature Simulator (MGSS) to activate the XM30 simulator. The XM30 simulator was designed to produce a flash and bang so the tank crew will receive a visual as well as an audible confirmation of the firing.

The purpose of this study was to pyrotechnically disseminate the XM30 simulators in a controlled chamber environment and to maintain a specified concentration range for chemical characterization of the combustion products. Data was needed prior to material release and for incorporation into the item's Life Cycle Environmental Assessment (LCEA). Characterization was to principally include compounds of toxicological significance such as benzene, formaldehyde and carbon monoxide, but detection of other volatile organic compounds, inorganic metals, and particle size analysis were also performed. The inorganic gases NO_x and SO_x were not analyzed for because previous data had already shown their concentrations to be far below their TLV-TWA's. A detailed mass balance was also well outside the scope of this study.

For it's current use in combat training exercises, this study provides evidence that the combustion products produced by firing of the XM30 simulator are of a safe and non-toxic nature.

1. INTRODUCTION

Development of the Multiple Integrated Laser Engagement System (MILES) 2000 device has been selected as the replacement to the currently used Hoffman systems. These devices are used in battlefield training exercises to simulate the flash / bang firing of a battle tank. On the M1 or M60 tanks, a laser is activated to simulate firing of the main gun, which triggers a signal to the Main Gun Signature Simulator (MGSS) to activate the XM30 simulator. The XM30 simulator was designed to produce a flash and bang so the tank crew will receive a visual as well as an audible confirmation of the firing.[1]

Prior to fielding, a detailed Health Hazard Assessment (HHA) and Life Cycle Environmental Assessment (LCEA) were prepared for review.[2,3,4] Although these documents have been completed, additional information on the chemical characterization of the combustion byproducts was needed. This information is vital to assure that soldiers conducting combat training exercises with the simulators are not being exposed to potentially harmful byproducts.

The purpose of this study was to pyrotechnically disseminate the XM30 simulators in a controlled environment and to maintain a specified concentration range for chemical characterization of the combustion products. The inorganic gases NO_x and SO_x were not sampled during the characterization for two reasons. First, the Health Hazard Assessments had stated that previous detection of them did not exceed standards for exposure inside the M1 hatch.[2,3] Second, previous studies containing similar starting materials at higher quantities had also shown levels of NO_x and SO_x not to exceed their TLV-TWA's.[5] Initial characterization was to principally include compounds of toxicological significance, such as benzene, formaldehyde, and carbon monoxide, that have been shown to exist in combustion analyses from other smoke studies. Detection of other volatile organic compounds (VOC's), inorganic metals, and particle size analysis were also performed. A detailed mass balance was not within the scope of work defined by this study.

2. MATERIALS AND METHODS

2.1 MATERIALS - XM30 SIMULATORS

The XM30 is an electric match initiated device consisting of a thermoplastic elastomere cap, polypropylene case, flash/smoke charge, and nickel plated brass contact pins. Figure 1 shows an exterior view of the simulator and figure 2 shows a more detailed interior view. A listing of the chemicals and their respective percentages found in the flash/smoke charge is shown in Table 1. Each of the simulators initially contains about 6 grams of pyrotechnic / energetic material. All of the simulators (Lot # CPA99A004-003) were manufactured by Comet GmbH in Germany and transported from Picatinny Arsenal to the Edgewood Chemical and Biological Center's (ECBC) Engineering Directorate. On the days of testing, a simulator was received and delivered to the pyrotechnic chamber at Bldg. E3266. All test items were weighed before and after dissemination to assure complete combustion of the smoke charge

2.2 CHAMBER EXPOSURE SYSTEM

The simulator was clamped loosely on a metal table in the middle of the 20,000 liter pyrotechnic chamber (figure 3). While wearing a grounding strap, two alligator clips were connected to the contact pins, and run to an electric discharge device (Black Magic, Pyromate Inc.) about 4-5 meters from the outside of the chamber. The door to the chamber was secured and latched, the electric discharge device was activated, and the simulator was fired. As recorded in the interim hazard classification, the sound output of the simulator is 135 decibels at a distance of 20 meters.[1] Audio confirmation of firing from a distance of 4-5 meters was therefore easily detected. Following dissemination, the fan was activated in the chamber to provide uniform dispersion and the smoke was diverted through a 4 inch diameter duct to a smaller 500 liter chamber (figure 4). Chamber environmental parameters monitored during all of the tests were temperature, relative humidity, and airflow.

TABLE 1. Chemical components of the XM30 flash / smoke charge.

Chemical
*Potassium nitrate (CAS # 7757-79-1)
Magnesium (CAS # 7439-95-4)
Black powder
Silica, amorph (CAS # 112945-52-5)

* preprocessed with 3% of boiled linseed oil

2.3 CHAMBER CONCENTRATION

To monitor chamber concentration, 25 mm A/E glass fiber filter pads (Gelman Scientific) were used to collect particulate samples for total aerosol concentration at 5, 15 and 25 minute intervals during a 30-minute test. Forty liters of air (10 l/min x 4 min) from the 500 liter chamber were drawn onto the pads using a vacuum pump (Sierra Instruments). Gravimetric analysis was performed on the resulting pads using a Cahn microbalance to determine chamber concentration.

2.4 PARTICLE SIZE ANALYSIS

The Thermal Systems Incorporated (TSI) Aerodynamic Particle Sizer (APS) system with model 3302 diluter was used to determine the particle size and distribution from the 500 liter chamber. The diluter was necessary to avoid overloading the APS system.[6] Several backgrounds were run of the 500-liter chamber prior to collecting data at the five, fifteen and twenty-five minute time intervals to assure the absence of any particles. All instrument specifications are provided in Appendix A.

2.5 CHEMICAL CHARACTERIZATION

2.5.1 VOLATILE ORGANIC COMBUSTION PRODUCTS (VOC'S)

At 5, 15, and 25 minutes into the run, VOC's of the combusted smoke were collected from the 500 liter chamber onto tenax tubes for subsequent analysis by thermal desorption gas chromatography/mass spectrometry (Appendix B for instrument conditions). Samples were drawn from two ports of the 500-liter chamber at 200 ml/min for five minutes. Background checks prior to grenade dissemination were performed to rule out potential contaminants and to allow background subtraction by Gas Chromatography/Mass Spectrometry (GC/ MS).

2.5.2 FORMALDEHYDE ANALYSIS

Previous characterization studies of other disseminated smoke materials had shown the presence of formaldehyde (CAS # 50-00-0) after combustion.[5] LpDNPH air monitoring cartridges (Supelco, Inc.) were used to trap formaldehyde on a high purity silica absorbent coated with 2,4-dinitrophenylhydrazine (CAS # 119-26-6). Over 30 minutes, the maximum flow rate through the tube (2 l / min) was initially used to determine the presence or absence of formaldehyde. Following collection, the samples were eluted with high purity acetonitrile (CAS # 75-05-8), and analyzed using gas chromatography / flame ionization detection (Appendix C for instrument conditions). Standards of 0.91, 2.74, 5.49, 12.80, and

18.29 ug/ml were prepared in acetonitrile from formaldehyde 2,4 -dinitrophenylhydrazone (CAS # 1081-15-8). Under this method, the detection limit for formaldehyde was determined to be 2 ug/ml.

2.5.3 INORGANIC ANALYSIS (SOLID)

Previous environmental assessments had determined that a majority of the solid material collected after dissemination of the XM30 simulators were potassium or magnesium carbonates and hydroxides.[4] Atomic Absorption (AA) spectroscopy was used to look at elemental potassium (CAS # 7440-09-7) and magnesium (CAS # 7439-95-4) and to quantitatively determine the percentages of all solid combustion products containing either of these elements. Due to the inherent nontoxic nature of these compounds, it was not within the stated objectives to separate the percent magnesium and potassium compounds into their individual carbonate and hydroxide percentages. Past work on other smoke devices with similar materials and higher quantities than those listed in Table 1 have also shown levels of SO_x and NO_x to be far below their respective Threshold limit value – Time Weighted Averages (TLV-TWA's).[5] Solid material from the 500 liter chamber was collected onto the 25 mm A/E glass fiber filter pads and solvent desorbed. Pads could not be analyzed for potassium and magnesium simultaneously because the method used to dissolve magnesium would reduce the observable response for potassium.[7]

2.5.3.a POTASSIUM ANALYSIS

Since potassium is water soluble[7], the filter pad was placed in a glass beaker, rinsed with 10 ml of deionized water, and sonicated for approximately 5 minutes. Solid material from the pad was completely desorbed into solution. Sample aliquots dependent on the amount of initial pad material were transferred and diluted into 100 ml of water. Standards of 0.5, 1.0, 5.0 and 10.0 ug/ml were prepared from a 1000 ppm atomic absorption standard (EM Science).

2.5.3.b MAGNESIUM ANALYSIS

Magnesium compounds are relatively insoluble in water, and therefore needed to be dissolved in acid prior to analysis by AA.[7] Ten ml of concentrated hydrochloric acid was added, heated for a few minutes, transferred, and diluted into 100 ml. Standards of 0.5, 1.0, 5.0 and 10.0 ug/ml were prepared from a 1000 ppm atomic absorption standard (EM Science).

2.5.4 INORGANIC ANALYSIS (GAS)

The AIM electrochemical Logic Series 500/501 gas detector was used in a diffusion mode to monitor carbon monoxide that may have appeared from combustion. Sampling was performed by placing the detector inside the small 500-liter chamber and recording any response seen at the sampling intervals.

3. RESULTS

All statistical analysis were performed using the Jandel computer software package Sigma Stat 2.03 for Windows.

3.1 CHAMBER EXPOSURE SYSTEM

Daily adjustments were made to chamber flow rates due to ambient conditions (humidity, temperature, and pressure differential at the exhaust vent due to outside wind velocity) in an attempt to maintain a predetermined chamber concentration. However, these fluctuations in chamber concentrations become more evident as the target chamber concentration dropped. With a small amount of material

initially contained in the XM30 simulator, these fluctuations were inevitable in the described dynamic system. Therefore, it was assumed that there would be differences between sample days that could not be avoided and that the chemical characterization would be reported over a concentration range.

3.2 CHAMBER CONCENTRATION BETWEEN SAMPLING DAYS

A Two Way ANOVA / Tukey Test was performed to compare the differences between sampling days while eliminating any variance between sampling intervals. As expected, results confirmed that there were chamber concentration differences between sampling days (figure 5). Table 2 also lists the days that were significantly different at $p \leq 0.05$.

3.3 MEAN CHAMBER CONCENTRATION

A Two Way Analysis of Variance (ANOVA) / multiple comparison test (Tukey Test) was also performed to determine if there were differences between sampling intervals (5-9 min, 15-19 min and 25-29 min) while accounting for the variability between sampling days. Results confirmed that there were significant differences between all three sampling intervals at $p \leq 0.05$ (figure 6). The mean chamber concentrations were 182.5 ± 4.9, 144.7 ± 4.9, and 115.5 ± 4.9 mg/m^3. In a dynamic system, it would be expected that chamber concentrations would fall with time, but the study was designed to obtain the smallest concentration range over which chemical characterization was performed.

3.4 PARTICLE SIZE ANALYSIS

The mass median aerodynamic diameters (MMAD's) of the particles were 1.27 , $\sigma_g = 1.1$, 1.25, $\sigma_g = 1.1$ and 1.21, $\sigma_g = 1.1$ um at the sampling intervals (figure 7). Although the size of the particles is in the respirable range, chemical characterization results will show them to be non-hazardous.

3.5 CHEMICAL CHARACTERIZATION

3.5.1 VOLATILE ORGANIC COMBUSTION PRODUCTS

A small amount of material present in the XM30 simulator caused characterization to be performed on a low mean concentration range of generated smoke in the 500-liter chamber. With a total sample volume of one liter drawn onto a Dynatherm tube, collected combustion products were expected to be small and not deviate much from the inherent background of the chamber. Therefore it was important to collect background tubes each day prior to dissemination (figure 8) and to subtract them from the collected samples. There are some small peaks seen in the background but this is a result of the high sensitivity of the analytical technique (thermal desorption GC/MS). To illustrate this, figure 9 compares the large response of a 0.262 ug spiked benzene standard with the background and equation 1 shows the corresponding concentration.

Equation 1: $$\text{ppm} = \frac{[(\text{benzene collected (ug)} / \text{total volume drawn (l)})](24.46 \text{ l/mole})}{\text{MW benzene (g/mol)}} = .0821\text{ppm}$$
(ug/g)

Some of the background-subtracted chromatograms typically seen for the XM30 simulator are shown in figures 10-12. Within the specified concentration range, responses seen on the tenax tubes were either slight deviations above the chamber background or extremely low concentrations of VOC's produced from dissemination. Chromatograms and peak responses will differ slightly between sampling days and at differing sampling times due to the statistical results presented earlier. Slight differences in abundance were also observed between the two ports, but only because responses were recorded near or

at the instrument's detection limit. All detectable VOC's seen and presented in Table 3 were of low response, and those of toxicological significance were far below their TLV-TWA's.[8] For example, after making a response factor comparison with the 0.262 ug benzene (CAS # 71-43-2) standard, the benzene response seen in figure 10 (retention time 3.58 min) corresponds to an approximate quantity of 1.05×10^{-2} ug. Insertion into equation 1 yields .003 ppm (or 3 ppb), which is approximately 150 times below benzene's TLV-TWA. By observation, quantitation of the other peaks was therefore not necessary due to their similar small responses. There were no peaks that were significantly different from the benzene response to allow them to approach their TLV. The largest three peaks on the chromatograms at retention times 11.13, 15.48, and 21.62 were results of column bleed due to a low column flow rate and slow temperature ramp approaching elevated temperatures. These experimental conditions were necessary for peak resolution and complete detection of all possible VOC's.

3.5.2 FORMALDEHYDE ANALYSIS

Quantitation of formaldehyde (HCHO) concentration was calculated according to equation 2. At a detection limit of 2 ug/ml, minimal elution volume of 2 ml, and maximum air sample of 60 liters, the concentration of formaldehyde was calculated to be 0.054 ppm (approximately 5 times lower than the established TLV-STEL of 0.3 ppm). Since there was no formaldehyde detected at this concentration, any formaldehyde that may be present in the combustion products must be at a level below this detection limit concentration.

Equation 2: $$ppm = \frac{[(\text{HCHO (ug/ml)})(\text{elution volume (ml)}) / \text{total volume drawn (l)})](24.46\text{l/mole})}{\text{(ug/g)} \qquad \text{MW formaldehyde (g/mol)}}$$

3.5.3 INORGANIC ANALYSIS (SOLID)

Magnesium and potassium analysis was calculated as a percentage of the total residue collected on the filter pads and recorded as elemental magnesium and potassium compounds (figure 13). Since the results were determined as a percentage of total residue collected, it was not necessary to account for daily variability. A One Way ANOVA was performed to determine the differences between sampling intervals. There were no significant differences between magnesium concentrations or potassium concentrations at the sampling intervals. The mean magnesium compound concentrations were 33.9 ± 3.0, 32.9 ± 3.7 and 32.1 ± 3.3 % and the mean potassium compound concentrations were 16.3 ± 3.4, 17.2 ± 1.2 and 17.8 ± 2.3 %.

3.5.4 INORGANIC ANALYSIS (GAS)

The AIM electrochemical Logic Series 500/501 gas detector did not sense the presence of carbon monoxide down to 1 ppm at the 5, 15 and 25-minute sampling intervals. The TLV-TWA for carbon monoxide as established by the ACGIH is 25 ppm.

4. DISCUSSION

Prior to material release of the XM30 simulator, work was required to chemically characterize the combustion products. Additional data was needed for incorporation into the item's Life Cycle Environmental Assessment (LCEA). Characterization was to principally include compounds of toxicological significance such as benzene, formaldehyde and carbon monoxide, but detection of other volatile organic compounds, inorganic metals, and particle size analysis were also performed. The inorganic gases NO_x and SO_x were not analyzed for because previous data had already shown their concentrations to be far below their TLV-TWA's[5].

With only 6 grams of starting material contained in the pyrotechnic charge, an initial concern was whether the simulator would generate enough smoke for combustion product analysis to be performed. The main issue to overcome was that the simulators had to be disseminated from the large pyrotechnic chamber for safety reasons, but sampling was easier to perform from the smaller chamber. The smoke was therefore diverted from the large chamber and dynamically run for 30 minutes through the small chamber. The mean chamber concentration range at which characterization took place was from 182.5-115.5 mg/m^3. This corresponds to a low chamber concentration (approximately 150 mg/m^3) at which other documented reports have successfully performed characterizations of alternate smoke materials.[9] Statistical analysis did reveal chamber concentration differences between sampling days and between sampling intervals (5,15, 25 minutes), but all characterization was performed within the mean chamber concentration range.

Benzene, formaldehyde, and carbon monoxide were at concentration levels far below their respective TLV-TWA's. These results were somewhat expected due to the initially small amount of starting material present in the simulators. Other trace VOC's detected by thermal desorption GC/MS included several different carbonyl derivatives. Aldehydes (but-, hex-, non-, dec-, and benzaldehyde), ketones (acetone and hexanone) and amides (2-propanamide) were all seen. The non-carbonyl compound hexanol was also seen at trace levels.

Following combustion, inorganic analysis showed that nearly 50% of the solid material were compounds containing either magnesium or potassium. Most likely, they would be present as hydroxides or carbonates. At the 5, 15, and 25 minute time intervals, the mean magnesium compound concentrations were 33.9 ± 3.0, 32.9 ± 3.7 and 32.1 ± 3.3 % and the mean potassium compound concentrations were 16.3 ± 3.4, 17.2 ± 1.2 and 17.8 ± 2.3 %. Release of these metal compounds into the environment should not cause any environmental impact; however, there have been no studies that examined what long-term effects the salt concentrations might have on aquatic salt-sensitive organisms.

Particle size analysis showed MMAD's of the particles to be 1.27 , $\sigma_g = 1.1$, 1.25, $\sigma_g = 1.1$ and 1.21, $\sigma_g = 1.1$ um at the sampling intervals. These particles are considered small and in the respirable range, but quick diffusion of the smoke cloud and it's inherent nontoxic nature have already been shown.

5. CONCLUSIONS

Chemical characterization of pyrotechnically disseminated smoke released from the XM30 main gun signature simulator did not produce toxicologically important compounds at concentration levels above their respective TLV-TWA's. Benzene, formaldehyde, and carbon monoxide were far below their threshold values. Other VOC's detected in trace amounts included various short chain carbonyl compounds and an alcohol compound. Inorganic analysis of the solid residue showed a high percentage of magnesium / potassium compounds, and particle size analysis showed the production of small diameter particles.

For it's current use in combat training exercises, this study provides evidence that the combustion products produced by firing of the XM30 simulator should not place the soldier in hazardous conditions. Data will be used for input into the item's Life Cycle Environmental Assessment (LCEA).

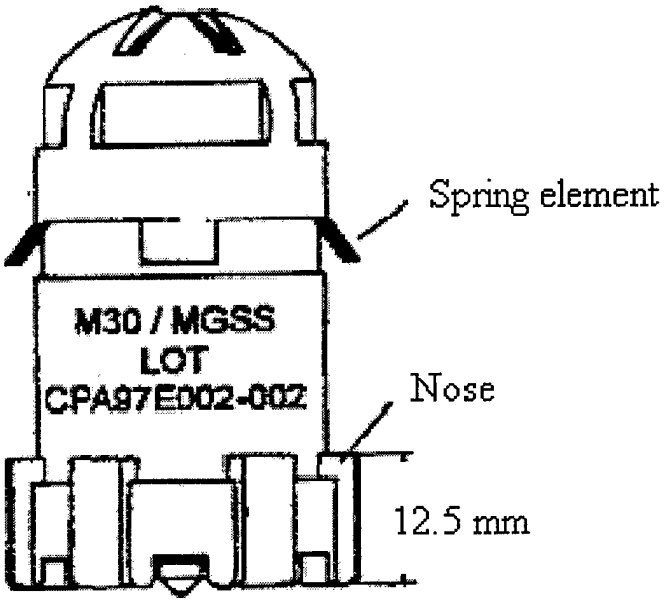

Figure 1. Exterior side view of XM30 simulator.

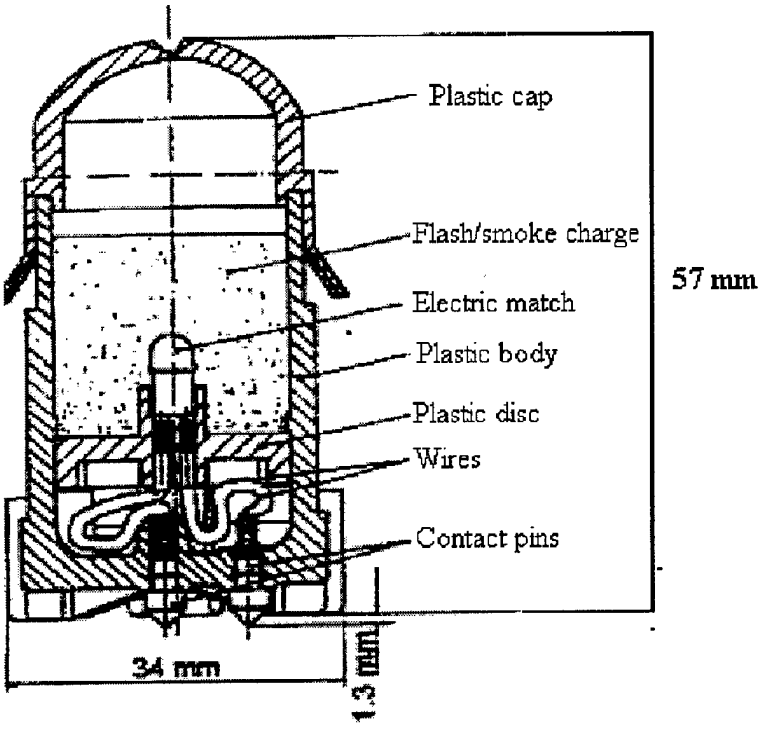

Figure 2. Interior view of XM30 simulator.

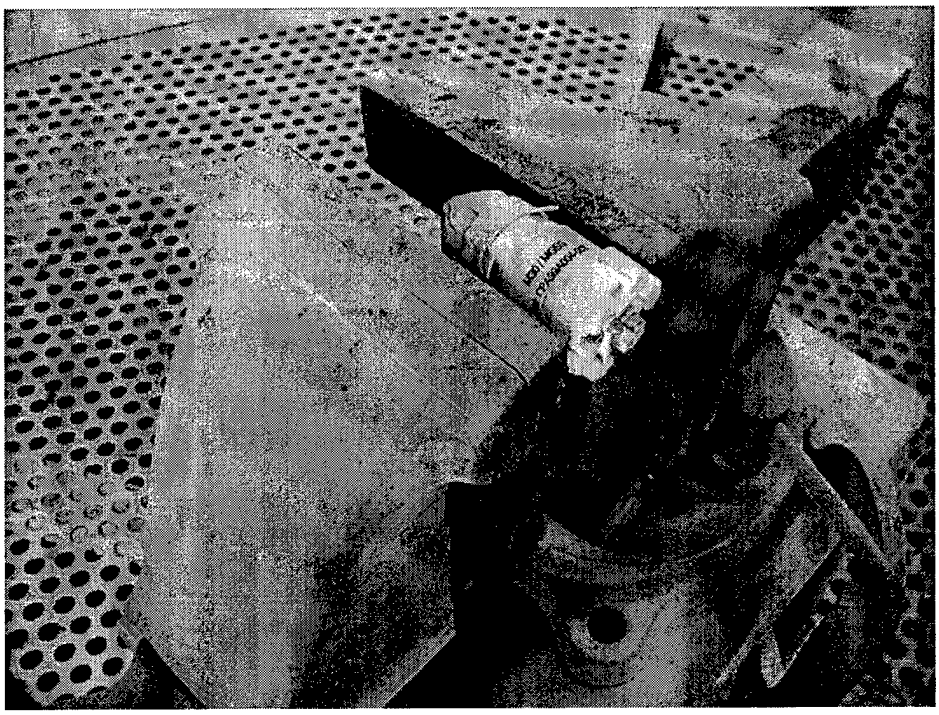

Figure 3. XM30 simulator clamped in 20,000 liter chamber.

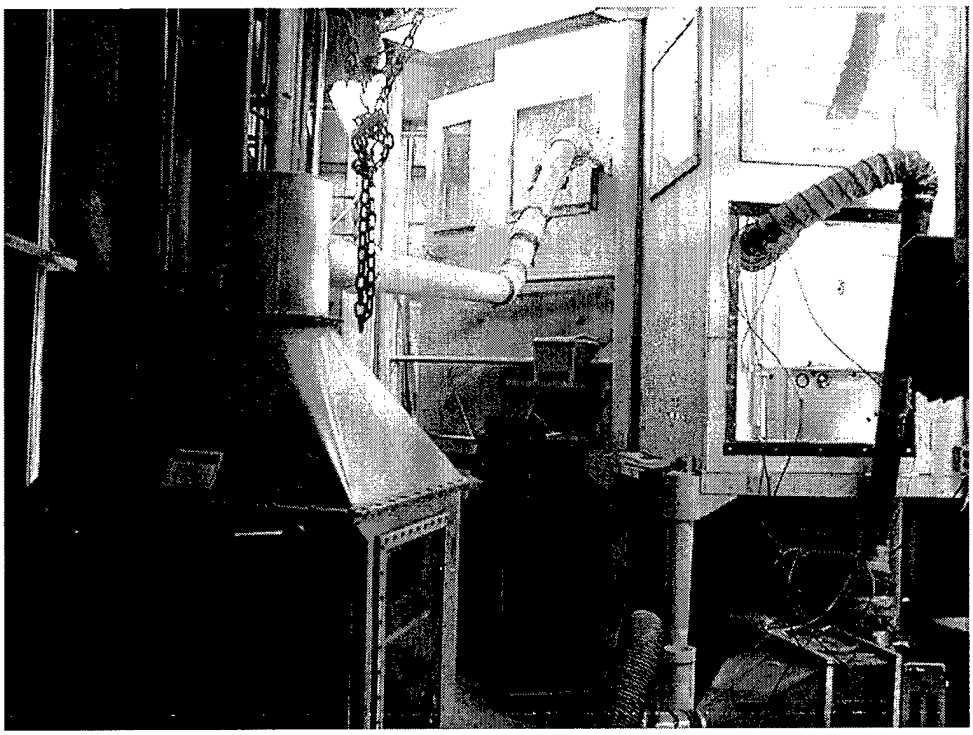

Figure 4. 20,000 pyrotechnic chamber diverted to 500 liter sampling chamber.

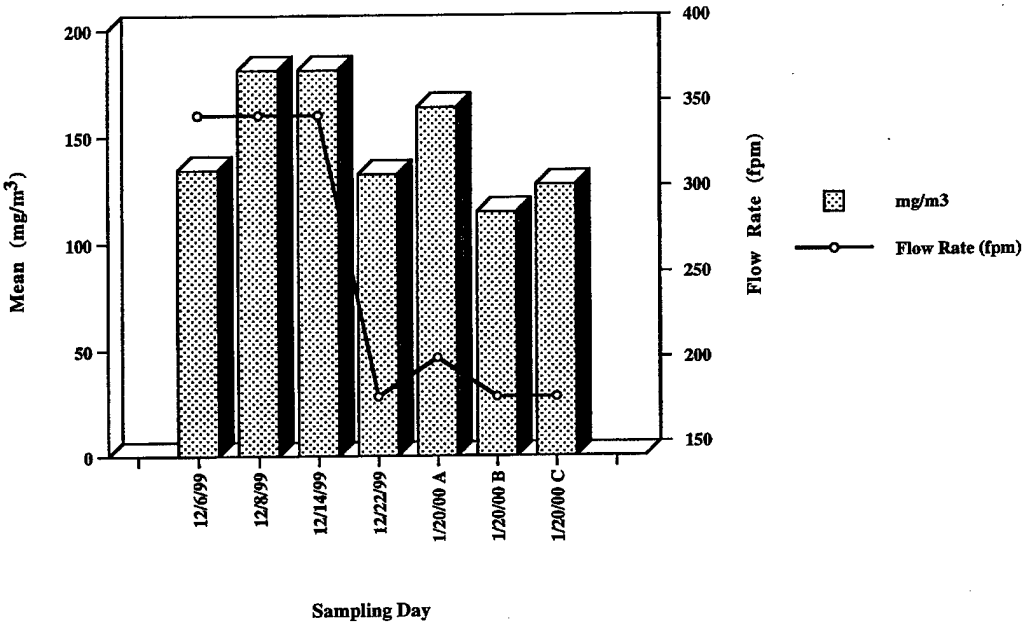

Figure 5. Chamber concentration differences between sampling days.

TABLE 2. Multiple Comparison for Chamber Concentration.

Run Dates	12/6/99	12/8/99	12/14/99	12/22/99	1/20/00 A	1/20/00 B	1/20/00 C
12/6/99							
12/8/99	yes						
12/14/99	yes	no					
12/22/99	no	yes	yes				
1/20/00 A	no	no	no	no			
1/20/00 B	no	yes	yes	no	yes		
1/20/00 C	no	yes	yes	no	no	no	

The multiple comparison test used was the Tukey Test.
$P \leq 0.05$, Power of performed test was 1.0.

Yes - significant difference between sampling days.
No - no significant difference between sampling days.

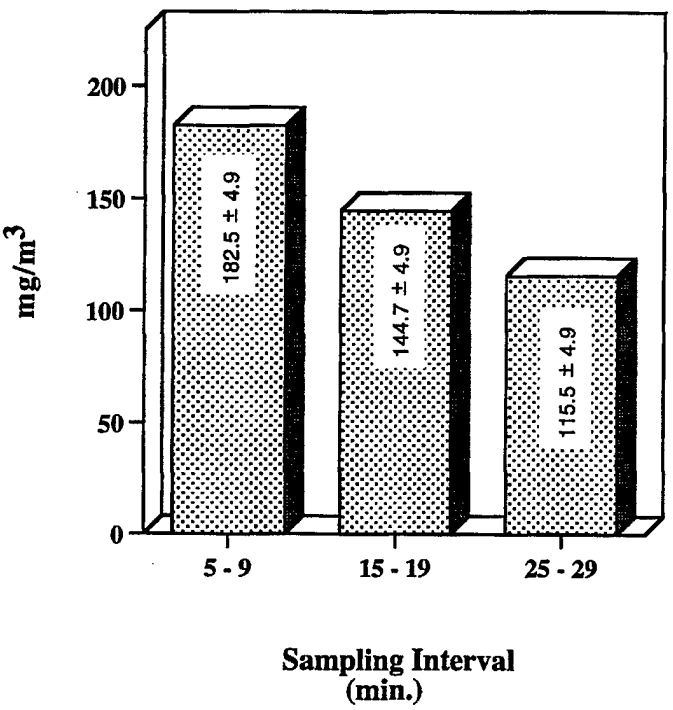

Figure 6. Mean chamber concentrations at sampling intervals.

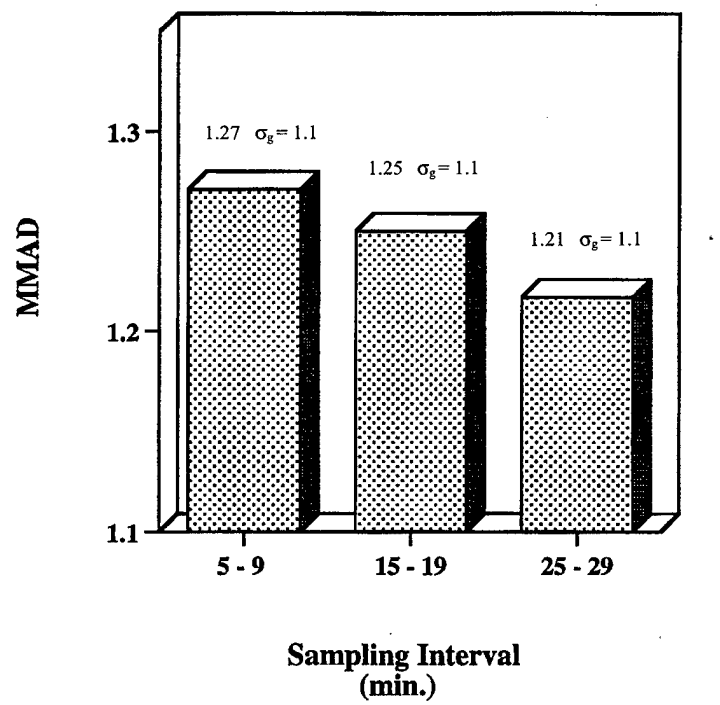

Figure 7. Mean particle size at sample intervals.

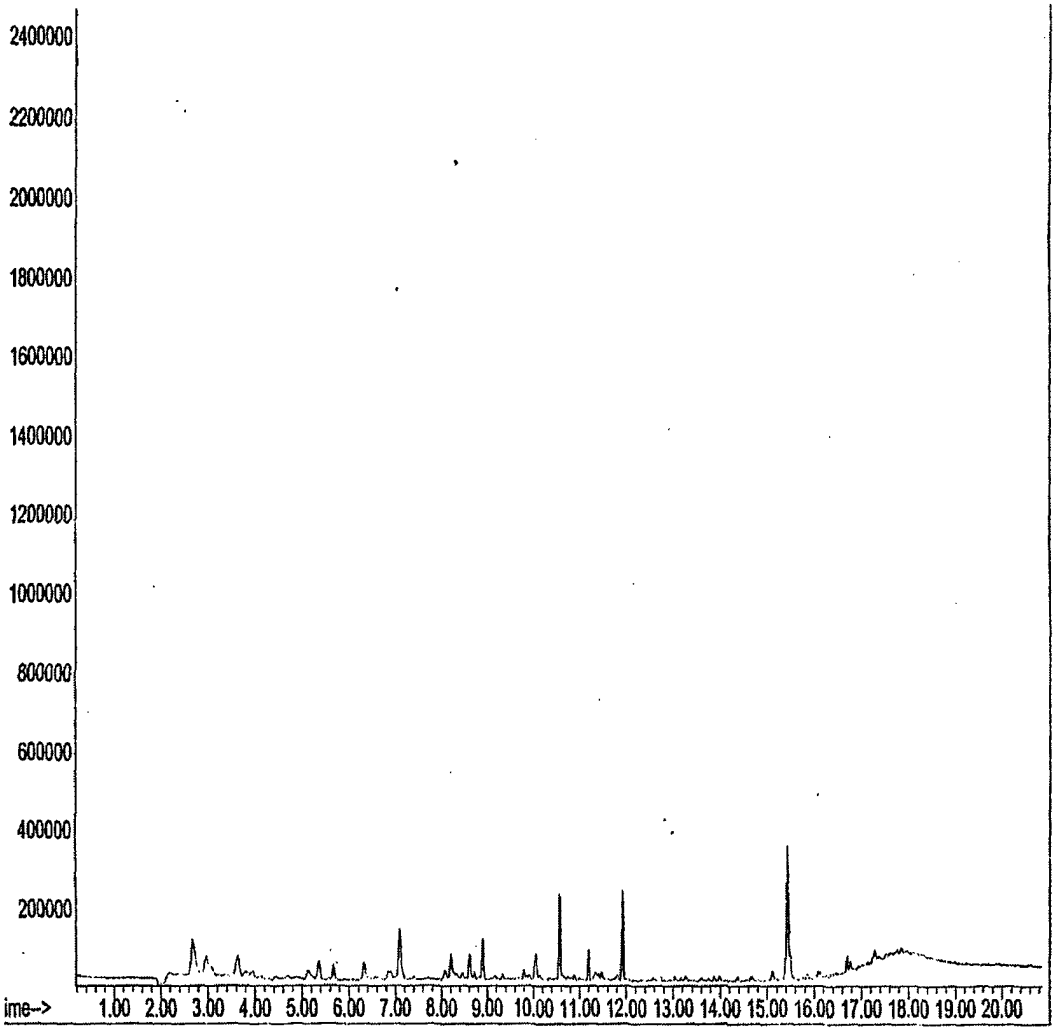

Figure 8. Sample background chromatogram from 500 liter chamber.

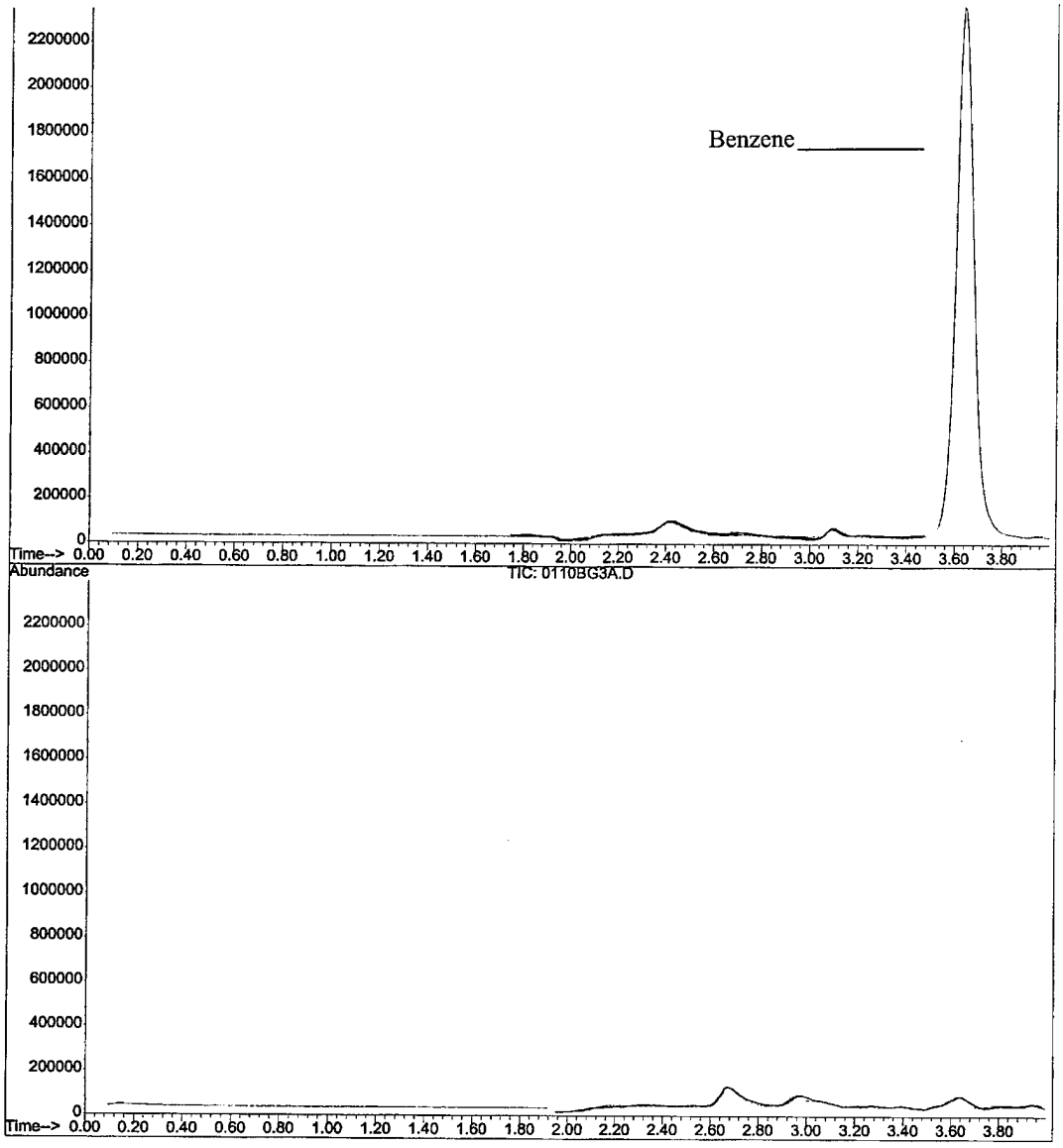

Figure 9. Comparison of 0.262 ug spiked benzene peak against chamber background (0.0821 ppm).

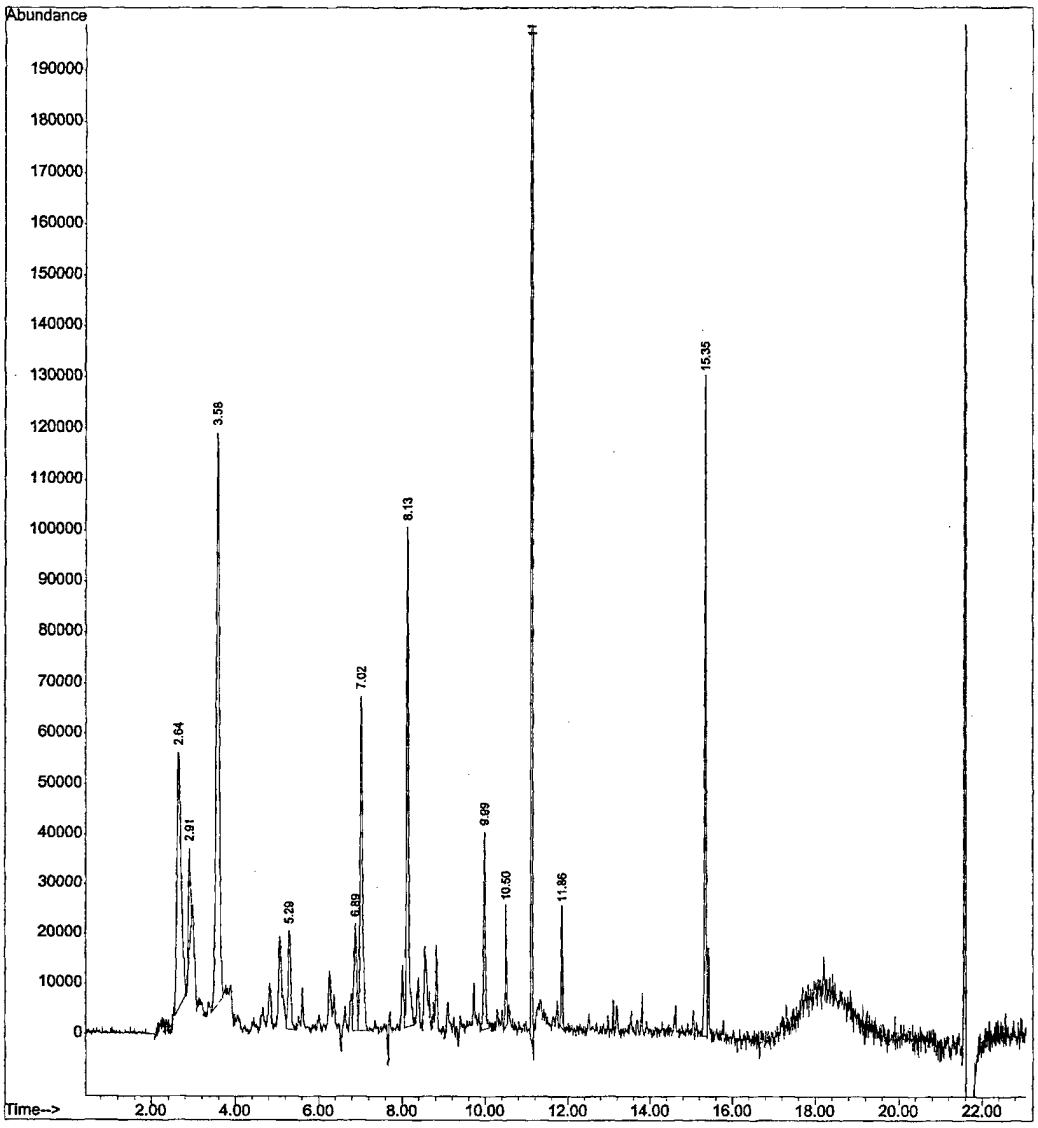

Figure 10. Background subtracted GC/MS chromatogram taken at 5 minute interval.

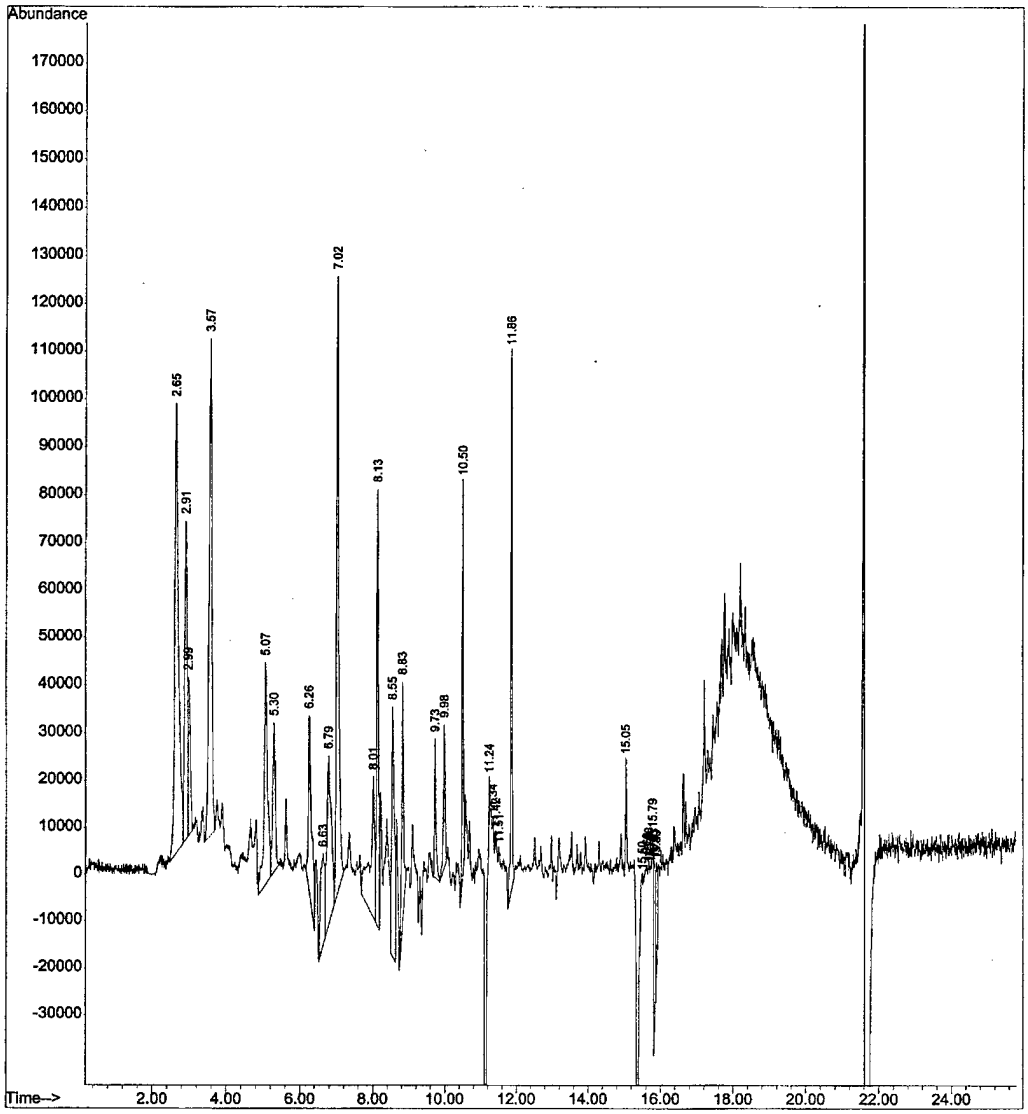

Figure 11. Background subtracted GC/MS chromatogram taken at 15 minute interval.

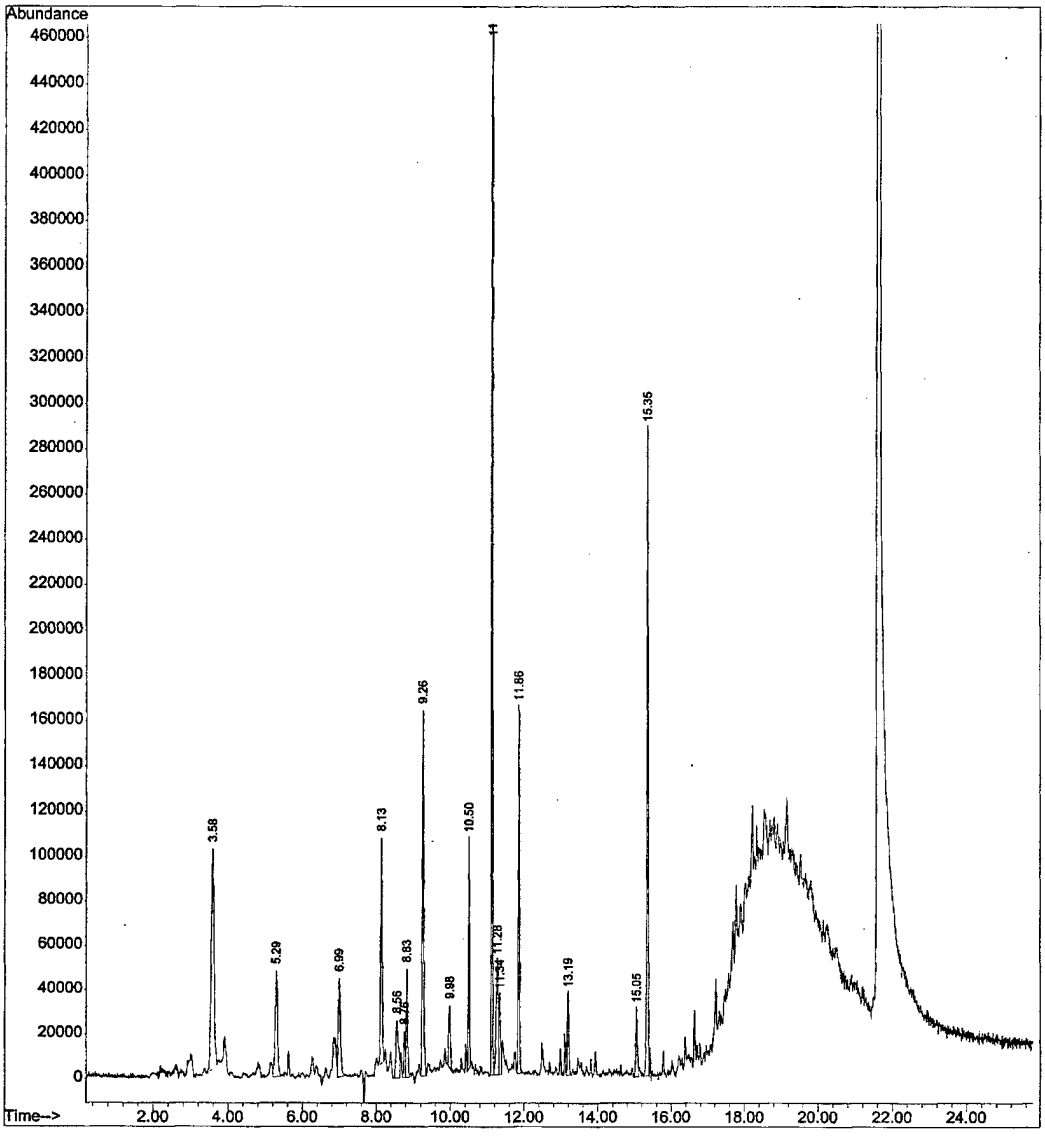

Figure 12. Background subtracted GC/MS chromatogram taken at 25 minute interval.

TABLE 3. VOC's detected by thermal desorption GC/MS.

Retention time (min)[a]	Compound[b] (TLV-TWA in ppm)
2.67	acetone (500 ppm)(CAS # 67-64-1)
2.96	butanal (CAS # 123-72-8)
3.63	benzene (0.5 ppm) (CAS # 1076-43-3)
5.36	hexanal (CAS # 66-25-1)
6.31	hexanone (5 ppm)(CAS #589-38-8)
7.08	acrylamide (CAS # 79-06-1)
8.20	benzaldehyde(CAS # 100-52-7)
9.26	hexanol(CAS # 111-27-3)
10.50	nonanal(CAS # 124-19-6)
11.86	decanal(CAS # 112-31-2)

[a]Retention times are not meant to be exact. Slight differences do occur between samples.
[b]Compounds with trace abundances much less than presented compounds are not listed. Compounds resulting from column bleed are also not listed. TLV-TWA's are shown for those compounds listed by the American Conference of Governmental Industrial Hygienists (ACGIH).[8]

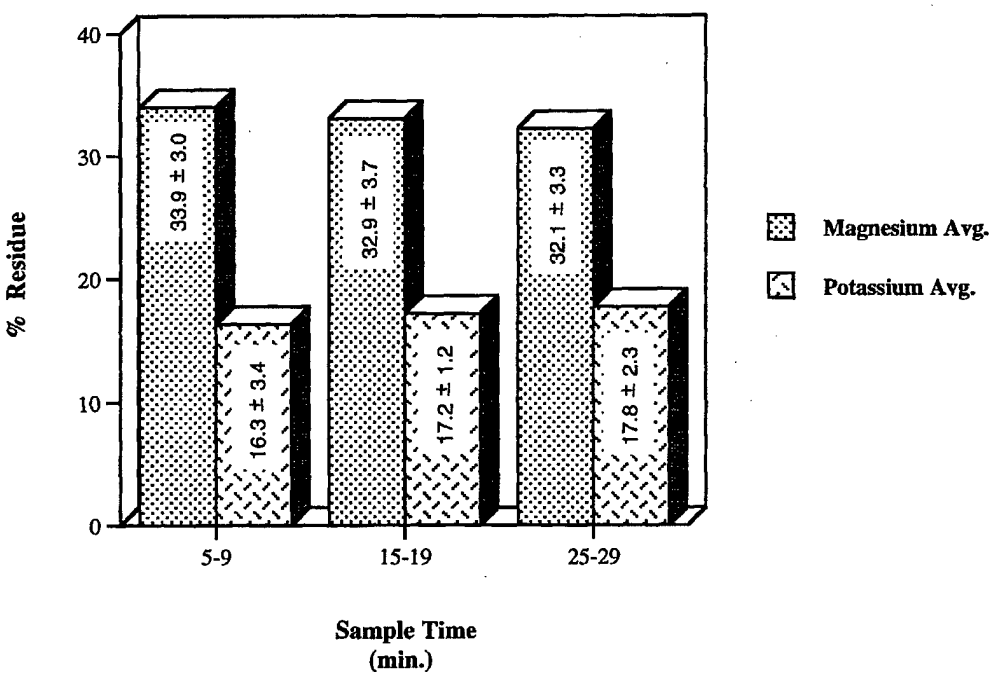

Figure 13. Mean percentages of elemental magnesium and potassium compounds in solid residue (principally carbonates and hydroxides).

ACKNOWLEDGEMENTS

The authors would like to thank Joe Domanico and Gene Tracy, Engineering Directorate, for their help in receipt and storage of the simulators. Thanks are also in order to Robyn Lee, Robyn B. Lee and Associates, for her helping with the statistical analysis.

LITERATURE CITED

1. Interim Hazard Classification for the Main Gun Signature Simulator and Audio Visual Cue Pyrotechnic simulator, January 1999.

2. Initial Health Hazard Assessment Report For Multiple Integrated Laser Engagement System (MILES 2000), Project No. 69-37-4584-96, U.S. Army Center for Health Promotion and Preventative Medicine, August 1996.

3. Initial Health Hazard Assessment Report For Multiple Integrated Laser Engagement System (MILES 2000), Project No. 69-37-4584-98, U.S. Army Center for Health Promotion and Preventative Medicine, February 1998.

4. Life Cycle Environmental Assessment for the Audio/Visual Cue Pyrotechnic Simulator (AVCPS) Main Gun Signature Simulator (MGSS) Simulator (M30).

5. Muse, W.T. , Anthony, J.S. , Bergmann, J.D. , Burnett, D.C. , Crouse, C.L. , Gaviola, B.P. , Thomson, S.A. , Acute and Repeated Dose Inhalation Toxicity Effects of Pyrotechnically Dissemiated Terephthalic Acid Smoke (XM83 Grenade), ERDEC-TR-256, US. Army Edgewood, Research, Development and Engineering Center, Aberdeen Proving Ground, MD, September 1995, UNCLASSIFIED Report.

6. TSI Incorporated, Model APS33B System Aerodynamic Particle Sizer – Operating and Service Manual, TSI Incorporated, February 1988.

7. Varma, Asha, Handbook of Atomic Absorption Analysis Volume 1, CRC Press, 1984, p.177.

8. TLV'S and BEI's – Threshold Limit Values for Chemical Substances and Physical Agents – Biological Exposure Indices, American Conference of Governmental Industrial Hygienists, 1999.

9. Hilaski, R.J. , Bergmann, J.D. , Carpin, J.C. , Muse, W.T. , Thomson, S.A. , Acute Inhalation Toxicity Effects of Explosively disseminated – XM82 – Titanium Dioxide, CRDEC-TR-363, U.S. Army Chemical, Research, Development, and Engineering Center, Aberdeen Proving Ground, MD, June 1992, UNCLASSIFIED Report.

APPENDIX –INSTRUMENT CONDITIONS

A. Particle size analysis

TSI Inc. Aerodynamic Particle Sizer	
Model No.:	3310
Photomultiplier tube background:	0.262
Nozzle(Δ P):	3.041
Sheath Flowmeter:	3.401
Total Flowmeter:	3.910

Diluter	
Model No:	3302
Flowrate:	0.05 SLPM
Aerosol path(ΔP):	0.34"
Total path(Δ P):	0.60"

B. Thermal Desorption Gas Chromatograph/ Mass Spectrometer analysis

Thermal desorption conditions

Instrument: Dynatherm ACEM900 Thermal Desorption Unit

Valve temp:	150 C	Dry time:	1 min
Tube temp:	250 C	Tube heat:	3 min
Transfer line temp:	200 C	Tube cool:	1 min
Trap temp:	250 C	Trap heat:	3 min

GC conditions

Instrument:	HP 6890 Gas Chromatograph
Column:	HP-5MS 30m x 0.25mm x 0.25 um
Column Flow(He):	1.0 ml/min (velocity 36 ml/min)(head pres 7.06 psi)

Temperature program

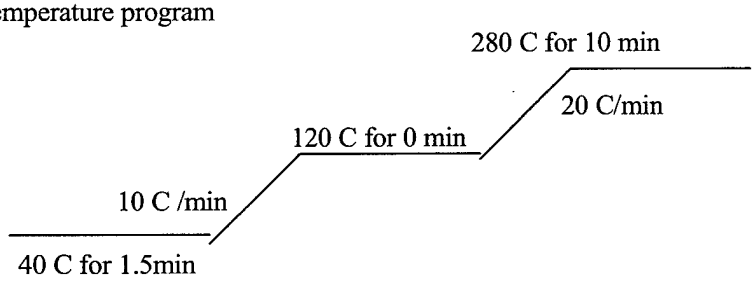

Detector conditions

Detector:	HP5973 mass selective detector
MS quad temp:	150 C
MS source temp:	230 C
Scan parameters:	30-550 amu ; threshold 150

C. GC-FID analysis

Instrument:	HP 5890 Gas Chromatograph
Column:	J+W Scientific DB-5 30m x 0.53mm x 1.5um
Liner:	Single Taper (HP part number 5181-3316)
Injection volume:	2 ul splitless
Column flow(He):	1.0 ml/min (velocity 36 ml/min)(head press = 8.5 psi)
Inlet purge:	Off time: 0 min; On time: 0.5min
Injector temp:	220 C

Temperature program

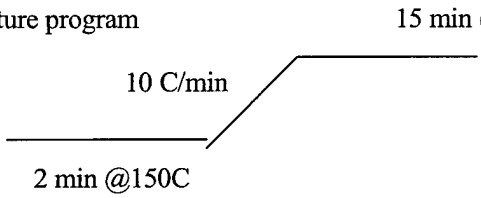

Detector conditions

Detector	Flame ionization detector
Detector temp	300 C
Detector flow	400 ml/min (air); 30 ml/min (hydrogen)

D. Atomic Absorption analysis

Instrument:	Perkin Elmer 2380 Atomic Absorption Spectrophotometer
Air Flow:	40 psi
Acetylene flow:	20 psi

Potassium analysis	Magnesium analysis
λ = 766.5	λ = 284.2
slit width = 0.7	slit width = 0.7
lamp operating current = 30	lamp operating current = 20

GENERATION, SAMPLING AND ANALYSIS OF GB (SARIN) VAPOR FOR INHALATION TOXICOLOGY STUDIES

William T. Muse, Steven J. Anthony, Leonard C. Buettner, Charles L. Crouse, Lee C. Crouse, Robert J. Mioduszewski, and Sandra A. Thomson

USA Soldier Biological Chemical Command
Edgewood Chemical Biological Center
ATTN: AMSSB-RRT-TT
5183 Blackhawk Road
Aberdeen Proving Ground, MD 21010-5424 USA

ABSTRACT

This study tested and optimized various methodologies to generate, sample and characterize GB test atmospheres in an inhalation chamber. A syringe drive spray atomization system was used for GB vapor generation. Stable GB test atmospheres (0.5 – 50 mg/m^3) were generated over different duration's (60, 240, 360 min) and sampled with solvent bubblers as well as an automated solid sorbent sampling system. Concentrations derived from each sampling method were compared against each other and statistically evaluated. A paired t-test showed no statistical difference between the two methods at the 95% confidence interval. Future applications include the ability to generate and monitor GB levels approaching the TLV-TWA of 0.0001 mg/m^3.

1. INTRODUCTION

Sampling for organic vapors in air has traditionally been performed using solvent bubblers. In this methodology, organic vapors are typically drawn through a glass collection tube or "bubbler" containing an appropriate solvent.[1] The dissolution of the organic vapor with the solvent traps the vapor within the bubbler. Once sampling is completed, the solvent containing the absorbed organic is diluted to a known volume and quantitated, typically through gas chromatographic analysis. Problems with bubbler usage include handling, dilution of analyte, time consumption, and sample flow rate correction particularly as a result of solvent evaporation.

The development of a solid sorbent tube sampler followed by thermal desorption, has become a more recently accepted methodology for the analysis of organic vapors in air. This technology has provided near real time monitoring for occupational exposure to chemical warfare agents since 1992.[2] A solid absorbent, such as Tenax TA is packed into a small glass sampling tube. As the test atmosphere is sampled through the tube, organic vapors are adsorbed onto the resin. At the completion of sampling, the trapped organics are thermally desorbed directly onto a gas chromatograph for quantitation. Advantages

of this method over bubblers include, higher sampling flow, ease of use, automation, no solvent dilution, and increased sensitivity.

Previous inhalation studies (Cullumbine et al,[3] Barrett,[4] and Callaway and Blackburn[5]) have traditionally used bubblers to quantitate for GB vapor to establish lethality (LCt_{50}) on different animal species. A recent study by Mioduszewski et al.,[6] has repeated some of these previous GB vapor concentrations but varied exposure time to determine whether Haber's Rule (Concentration x Time = Constant) applies in predicting GB lethality. To compare previous GB toxicity studies with the Mioduszewksi study, bubbler samples were drawn to determine the chamber concentration. At the same time, an automated solid-sorbent tube system sampled the chamber concurrently with the bubblers. A statistical comparison of the data from the two sampling methods was conducted. A favorable comparison between the two sampling techniques would place increased confidence on the solid-sorbent tube methodology, particularly when conducting future GB vapor toxicity studies below the practical limits for bubbler sampling.

This study also tested the performance of a syringe drive coupled with a modified spray-atomizer to determine it's effective range and capability to generate long term stable GB vapor concentrations in an inhalation chamber.

2. MATERIALS AND METHODS

2.1 CHEMICALS

Chemical agent standard analytical reagent material (CASARM)-grade Sarin (GB) (lot # GB-U-6814-CTF-N (GB2035) was verified as 97.2 $\pm$ 0.2 wt % (as determined by quantitative NMR ^{31}P) in samples obtained from USAECBC and stored in sealed ampules containing nitrogen. Ampules were opened as needed to prepare external standards or to be used as neat agent for vapor dissemination. All external standards for GB vapor quantitation were prepared on a daily basis. Triethylphosphate (99.9% purity), obtained from Aldrich Chemicals, Milwaukee, WI, was used as the internal standard for the GB purity assay.

The majority of impurities in the CASARM GB consisted of 0.2% o,o'-diisopropyl methylphosphonate (DIMP), 0.2 % methylphosphonic difluoride (DF), 0.3% methylphosphonofluoridic acid (Fluor Acid), and 0.3% excess HF/F ion. Impurity percentages were based on mole ratios from acid-base titration.

2.2 GB TEST ATMOSPHERE, OVERVIEW

GB test atmospheres were generated by dispensing liquid GB into a vapor generation system, which in turn was connected to the inlet of a dynamic flow inhalation chamber. The GB vapor was monitored in the chamber with a variety of sampling techniques, including bubbler, sorbent tube and a continuous phosphorus analyzer (Fig 1). Concentrations derived from the bubbler and sorbent tube were compared against each other and statistically evaluated. The phosphorus analyzer was used primarily to monitor the chamber vapor profile, that is the rise, equilibration and fall of the GB vapor concentration during a chamber run. Testing and evaluation ranged from 2 - 7 mg/m^3 GB to compare the bubbler vs. sorbent tube. Concentrations from 0.5 - 50 mg/m^3 were run to test the performance of the syringe drive/spray atomizer.

2.3 GENERATION SYSTEM

The generation system consisted of a syringe drive and spray atomization system located on top of the inhalation chamber (chamber inlet). The system was confined within a stainless steel generator box (23"l x 14"w x 18"h) which was maintained under negative pressure (0.25" H_2O). A Plexiglas door at the front of the box allowed for syringe loading and syringe drive adjustments during set-up operations.

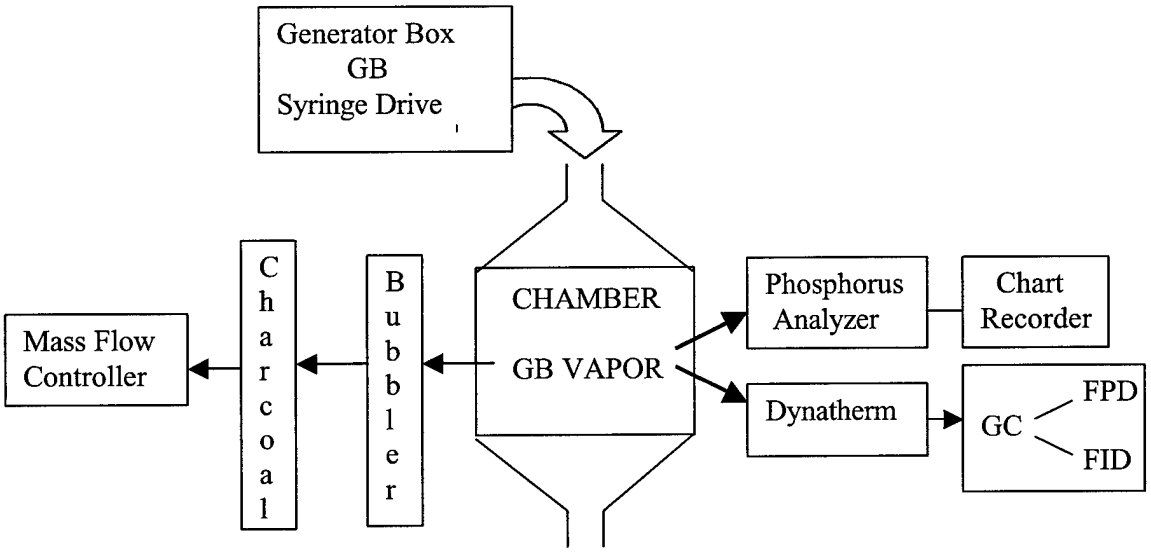

Figure 1. Schematic for GB inhalation chamber and monitoring systems.

2.3.1 SYRINGE DRIVE/SPRAY ATOMIZATION SYSTEM

Prior to chamber operation, the liquid GB was drawn into a gas-tight syringe (Hamilton, Reno, NV), transported to the generator box, then mounted onto a variable rate syringe drive (Model 22, Harvard Apparatus Inc., South Natick, MA). Once activated, the syringe drive delivered a constant flowrate of GB (ul/min) through a flexible plastic line (~ 8") into a spray atomization system (Spray Atomization Nozzle 1/4 J SS, Spraying Systems Co., Wheaton Ill) (Fig 2). The atomizer was modified by inserting a syringe needle (SS 25 gauge 3") into the top of the sprayer to decrease the orifice size. As liquid GB entered through the top of the atomizer, compressed air (30-40 psi) entered through the side to atomize the liquid into fine droplets. Due to the volatility of GB, these droplets quickly evaporated into GB vapor, which were then drawn down through the chamber.

2.4 INHALATION CHAMBER.

GB vapor was monitored in a 750-liter dynamic airflow inhalation chamber located within a 20,000-liter containment chamber. The Rochester style chamber was constructed of stainless steel with Plexiglas windows on each of the six sides. The chamber's negative pressure (~0.25" H_2O) was monitored with a calibrated magnehelix (Dwyer, Michigan City, Ind). Chamber airflow (500 - 650 L/min) was measured at the chamber outlet with a thermo-anemometer (Model 8565, Alnor, Skokie, IL). Monitored environmental parameters included temperature and relative humidity.

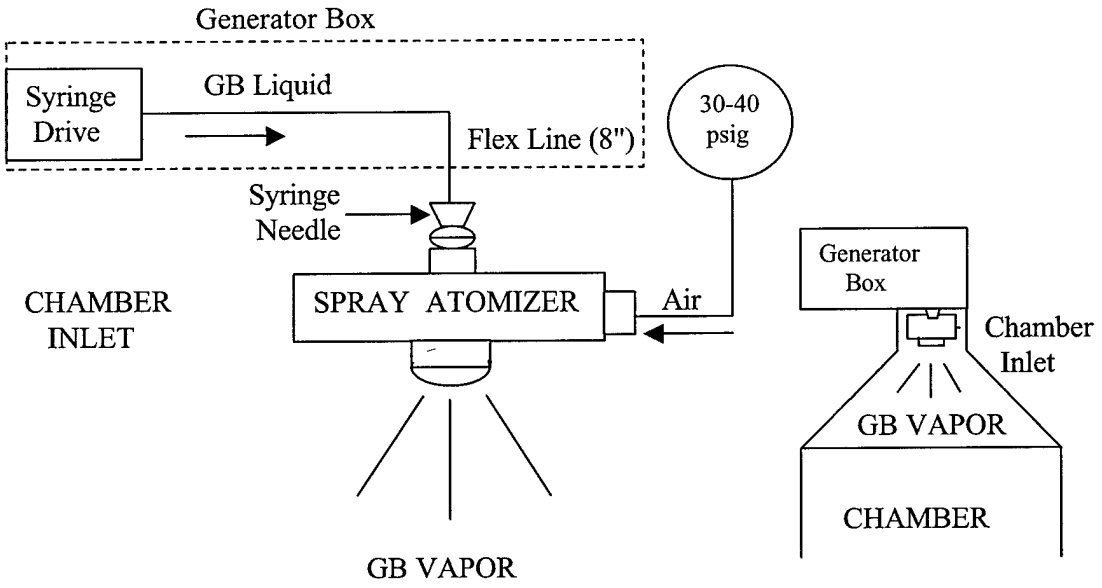

Figure 2. Schematic of spray atomization system.

2.5 SAMPLING SYSTEM

A variety of sampling systems were used to monitor GB vapor in the chamber. The bubbler and sorbent tube systems were quantitative measures of GB while the phosphorus analyzer was used primarily to follow the chamber profile.

All sample flowrates for the bubbler and sorbent tube systems were controlled with calibrated mass flow controllers (Matheson Gas Products, Montgomeryville, PA). Typical flow rates were 0.9 - 1.0 L/min for the bubblers and 100 sccm for the sorbent tubes. Due to solvent (hexane) evaporation during sampling, an in-line charcoal filter was installed between the bubbler and mass flow controller to prevent the cooling effect of the solvent from affecting the mass flow sensor. Flow rates from both systems were verified before and after sampling by temporarily connecting a calibrated flowmeter ("DryCal", Bios Int'l, Pompton Plains, NJ) in-line to the sample stream.

2.5.1 BUBBLER SAMPLING

The concentration of GB in the chamber was determined by collecting chamber air samples into "Edgewood" bubblers containing hexane.[7] During sampling, chamber air was drawn through glass sample lines (.25" o.d.) into paired bubblers (front & rear) at the rate of 0.9 - 1.0 L/min. The collected solvent was diluted to a known volume and injected into a gas chromatograph with flame photometric detection, (GC-FPD) phosphorus mode. External standards (GB/hexane) were injected into the GC-FPD to generate a calibration curve. A linear regression fit ($R^2 = 0.999$) of the standard data was used to compute for GB concentration in the chamber. Instrument parameters for GB analysis by the GC-FPD are listed in Appendix A.

2.5.2 SORBENT TUBE SYSTEM

The automated sorbent tube sampling system (Fig 3) was comprised of four parts: (1) a heated sample transfer line, (2) heated external switching valve, (3) thermal desorption unit and (4) gas

chromatograph. A stainless steel sample line (1/16 in o.d. x .004 in i.d. x 6 ft l) extended from the middle of the chamber to an external sample valve. The sample line was commercially treated with a silica coating (Silicosteel® Restek, Bellefonte, PA) and covered with a heated (60°C) sample transfer line (CMS, Birmingham, Alabama). The combination line coating and heating was to minimize GB adsorption onto sample surfaces. From the transfer line, the sample entered a heated (125°C) 6-port gas switching valve (UWP, Valco Instruments, Houston, Texas). In the by-pass mode, chamber air was continuously drawn through the sample line onto a charcoal vent filter. In the sample mode, the gas sample valve would redirect the chamber air to a 10 mm Tenax TA sorbent tube located in the thermal desorption unit (ACEM-900, Dynatherm Analytical Instruments, Kelton, Pa). Temperature and flow programming within the Dynatherm desorbed GB from the sorbent tube and injected the vapor directly onto the gas chromatograph (GC) for quantitation. Either flame ionization (FID) or flame photometric (FPD) detection could be used depending upon the level of sensitivity required. Instrument parameters for both the GC and the Dynatherm are listed in Appendix A.

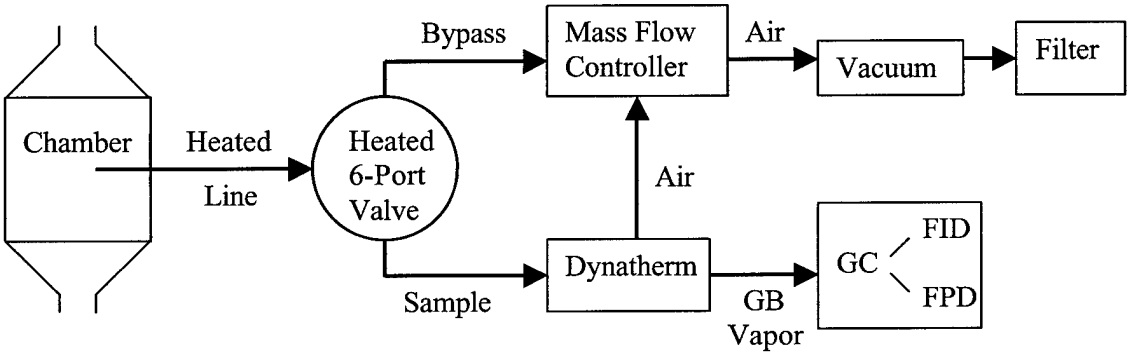

Figure 3. Automated sorbent sampling of GB vapor from the chamber.

Calibration of the sampling and analysis system was conducted by starting the Dynatherm program and injecting external standards (GB/hexane) directly into the inlet of the heated sample line. In this way, injected GB standards were put through the same sampling and analysis stream as were the chamber samples. Standards injected through the sample line as well as directly onto the sorbent tube showed comparable data and demonstrated the integrity of the sample line system. A linear regression fit ($R^2 = 0.999$) of the standard data was used to compute for GB concentration from the chamber samples.

2.5.3 PHOSPHORUS MONITOR (HYFED)

GB levels in the chamber were continuously monitored with a phosphorus analyzer (HYFED, Model PH262, Columbia Scientific, Austin, Texas). The analyzer output was recorded on a strip chart recorder, which showed the rise, equilibrium, and decay of the chamber vapor concentration during each experimental run. In addition, it gave a close approximation of the amount of GB (mg/m^3) in the chamber based on data (bubbler and sorbent tube quantitation with HYFED response) from previous chamber runs.

2.6 CHAMBER RUNS FOR BUBBLER AND SORBENT TUBE COMPARSION

Ten separate chamber runs were conducted to make the bubbler and sorbent tube comparison. Samples were drawn at different chamber concentration's ranging from 2 - 7 mg/m^3 GB. All samples were drawn from the middle of the chamber. Bubbler and sorbent tube samples were drawn after the

chamber attained equilibration (t_{99}) while the HYFED monitored the entire run. Two separate sets of bubblers ran concurrently during each sample collection period while each sorbent tube represented a single measurement. Frequency of sampling for the bubblers was approximately every 20 min for each 60 min run, every 60 min for each 240 min run and every 90 min for each 360 min run. Each bubbler sampling collection period lasted from 8-12 min. Sorbent tube samples were drawn from the chamber approximately every 10 - 15 min with each sample draw lasting 2-3 min.

3. RESULTS

3.1 GB VAPORIZARION SYSTEM

The syringe drive/spray atomization system delivered a constant and stable vapor concentration throughout all testing periods. The system was easy to manipulate and tested effectively at a range of 0.5 to 50 mg/m^3 GB. Chamber profiles from the HYFED phosphorus response showed the stability of the generator over six hour periods. Appendix B illustrates GB vapor (6.0 mg/m^3) stability during a 1 hr chamber run with concurrent sampling via bubblers and sorbent tubes.

3.2 BUBBLER AND SORBENT TUBE COMPARSION

A total of 75 bubbler samples and 145 sorbent tube samples were collected throughout the 10 chamber runs. The mean GB vapor concentration from each sampling method was determined for each run (Table 1). The mean values from each set of runs (60 min, 240 min, and 360 min) were computed and compared against each other using a paired t-test (Table 2). Results showed that the difference of the means between the two sampling techniques were well within the computed 95% confidence interval. Thus, there were no significant differences between the means for the two sampling methods.

TABLE 1. Mean and Variance of GB Vapor Concentrations (mg/m^3) from Bubbler and Sorbent Tubes Obtained during Chamber Runs.

60 Min Chamber Runs	(N)	Bubbler	Sorbent Tube	(N)
1	(4)	5.91 ± 0.23	6.00 ± 0.12	(5)
2	(4)	6.95 ± 0.29	6.98 ± 0.23	(5)
3	(4)	6.55 ± 0.34	6.37 ± 0.16	(5)
240 Min Chamber Runs	**(N)**	**Bubbler**	**Sorbent Tube**	**(N)**
4	(8)	2.12 ± 0.08	2.04 ± 0.04	(12)
5	(8)	3.28 ± 0.09	3.26 ± 0.05	(16)
6	(8)	4.79 ± 0.13	4.87 ± 0.08	(15)
7	(7)	2.64 ± 0.08	2.81 ± 0.10	(15)
360 Min Chamber Runs	**(N)**	**Bubbler**	**Sorbent Tube**	**(N)**
8	(8)	2.99 ± 0.10	2.99 ± 0.09	(25)
9	(8)	2.76 ± 0.19	2.66 ± 0.08	(24)
10	(8)	2.78 ± 0.10	2.77 ± 0.09	(23)

N = Number of Samples

TABLE 3. Paired T-test* of Mean GB Concentrations (mg/m^3) Obtained from each set of Chamber Runs (Bubbler versus Sorbent Tube Samples).

Chamber Run Time	(N)	Bubbler	Sorbent Tube	Difference of Means	95% Confidence Interval
60 Min	3	6.47 ± 0.50	6.45 ± 0.53	-0.02	(-0.37 - 0.33)
240 Min	4	3.21 ± 1.16	3.25 ± 1.20	-0.04	(-0.14 - 0.21)
360 Min	3	2.84 ± 0.13	2.81 ± 0.17	0.03	(-0.37 - 0.33)

*All data was normally distributed with no statistically significant difference between the two sampling methods. Ho = 0.

N = Number of chamber runs per chamber run time (60, 240 & 360 min).

4. DISCUSSION

4.1 VAPORIZATION SYSTEM

The spray nebulization system tested effectively from 0.5 - 50 mg/m^3 GB. A typical chamber run required a syringe drive flow (liquid GB) of 1 - 10 ul/min with a chamber flow of 550 -650 L/min. Adjustments in the syringe drive and chamber flow parameters could probably achieve a lower limit of approximately 0.1 mg/m^3 GB. Testing for subtle clinical effects (i.e. miosis), or at the recommended "TLV-TWA level" of 0.0001 mg/m^3 GB[8] would require the use of a different generator.

4.2 SAMPLING SYSTEMS

Traditionally, discrete sampling for GB vapor has been accomplished through the use of bubblers. Herd *et al.*, (1983), and Bartram *et al.*, (1988), have evaluated the sampling efficiency of bubblers and impingers to monitor GB vapors.[7,9] Although labor intensive, bubblers have provided a reliable method for the quantitation of GB vapor. Unfortunately, as the GB vapor concentration decreases, the length of sampling time significantly increases. Drawbacks to extended sampling times include increased risk of analyte loss due to evaporation, hydrolysis and breakthrough. In addition, the numbers of samples drawn during an exposure are significantly reduced. An automated solid sorbent system was introduced to offset these drawbacks, especially for use at lower (< 2.0 ug/L) GB concentrations. A comparison of GB concentrations between the bubblers and the sorbent tubes confirmed the performance of the automated approach. A table summary of the advantages and disadvantage of each of the two sampling systems is listed in Appendix C.

Although bubblers can be drawn almost indefinitely, the lower practical limit for bubblers sampling GB in the chamber would probably fall within the range of 0.5 to 2.0 ug/L. Below that range, problems associated with extended sampling times (hydrolysis, breakthrough, sample throughput, solvent evaporation and flow rate adjustments) would occur which may increase error.

Although solid sample tube collection is not a new technology, difficulties may arise when (1) attempting to provide a continuous and deactivated sampling system and (2) quantitation of sample from an automated system. Samples such as GB have a tendency to adsorb onto active metal surfaces. For example, Trumit *et al.*, (1953) reported on the adsorption of GB on the chamber walls.[10] For this reason, a combination of sample line deactivation (silicosteel®) and uniform heating (heated transfer line) were essential to ensure the recovery of the vapor. In addition, the transference of vapor from a chamber

atmosphere to an analytical instrument must follow the ideal gas law (PV = nrt). In other words, for gas sample loop operation, the effects of pressure and temperature that the vapor undergoes during transference must be considered for proper quantitation. In this technique, the flow of GB vapor through the continuous flow sample line was simply diverted to the sorbent tube. Thus, integration of a switching valve with the controlled mass flow meter provided an accurate sample volume.

Future work to detect "low level" GB (< 0.1 - 0.0001 mg/m^3) would include sampling at significantly higher flow rates (2 L/min) and sampling times to increase loading on the Tenax TA. In addition, connection to a GC-FPD detector would increase sensitivity by 2 - 3 orders of magnitude compared to the FID.

4.3 BUBBLER AND SORBENT TUBE COMPARSION

The paired t-test was used to compare the two sampling methods conducted on one sample (GB vapor). In this case, the paired t-test compared the difference between the means of each of the two sampling methods for chamber runs conducted at 60, 240 and 360 min. The null hypothesis (H_o) was that the difference between the two methods equaled zero. Results of the paired t-test failed to reject Ho and concluded that there was no significant difference between the two methods, $p>0.05$.

5. CONCLUSION

A syringe drive coupled to a spray atomizer was effective for the generation of GB vapor in an inhalation chamber at a range of 0.5 to 50 mg/m^3 GB. Investigation into different generation systems will be required for studies below 0.5 mg/m^3 GB.

The automated sorbent tube approach provided a rapid, sensitive methodology for the sampling and quantitation of GB vapor. The system demonstrated an inert sample pathway for continuous sampling from the chamber. A statistical comparison of the bubbler and sorbent tube methods showed that there was no significant difference between the two methods. This study verifies the performance of the Dynatherm-GC sampling and analysis system for future "low-level" GB studies.

REFERENCES

1. Levaggi, D.A., Sampling and Storage of Gases and Vapors in "Methods of Air Sampling and Analysis", Ed. Lodge, J.P., 3rd Edition, Lewis Publishers, Inc. Chelsea, MI., 1989.

2. Abrams, W.C., and Albro, T.G., "Chemical Warfare Agents – Breakdown Products and Precursor Analysis", Presented at the 1993 Scientific Conference on Chemical and Biological Defense Research, Aberdeen Proving Ground, MD.

3. Cullumbine, H., Callaway, S., Ainsworth, M., and R. Lynch. Porton Technical Paper No. 495. The Inhalation Toxicity of GB to Rats, Sheep, Monkeys and Guinea Pigs. 1955. UNCLASSIFIED Report.

4. Barrett, H.M., Porton Technical Paper No. 2756. Studies on the LCt50 of Nerve Gas Vapour in the Rat and the Mouse. 1951 UNCLASSIFIED Report.

5. Callaway, S., and J.W. Blackburn. Porton Technical Paper No. 404. A Comparative Assessment of the Vapour Toxicities of GB, GD, GF, T.2132, T.2137 and T.2146 to Male and Female Rats. Feb 1954. UNCLASSIFIED Report.

6. Mioduszewski, R.J., Manthei, J., Way, R., Burnett, D, Gaviola, B., Muse, W., Anthony, J., Durst, H., Thomson, S., Crouse, C., Crouse, L., Sommerville, D., and R. Crosier. "Estimating Probability of Sarin (GB) Vapor Toxicity in Rats as a Function of Exposure Concentration and Duration", Presented at the 2000 International Chemical Weapons Demilitarisation Conference, May 22-24, The Hague, Netherlands.

7. Bartram, P.W. and Meyers, M.B.,. The Efficiency of Scrubbing CW Agent Vapors in Impingers. CRDEC-TR-88162. August 1988.

8. McNamara, B.P. and F Leitnaker. Toxicological Basis for Controlling Emission of GB into the Environment. Special Publication F.A-SP-100-98, AD 914271L. Medical Research Laboratory, Edgewood Arsenal, Aberdeen Proving Ground, MD. 1971.

9. Herd, R.E., Bouck, J., Kolakowski, J. E., Miskelly, P.P., and Norris, G. Evaluation of the Sampling Efficiency of Beaded Glass Bubblers for Monitoring GB Emissions in Air. ARCSL-TR-82027. May 1983.

10. Trurnit, H.J., Bales, P.D., Esposito, E.J., and Horowitz, P., Comparative Study of GB Inhalation Toxicity on Mice, Rats, Guinea Pigs, Cats, Dogs and Monkeys with Exposure Times Between One Second and Several Minutes. Chemical Corps Medical Laboratories Research Report No. 205. August 1953.

APPENDIX A

GC Parameters for GB Analysis

GC/FPD Operation for Bubblers

Gas chromatograph	Hewlett Packard 6890
Capillary column	DB-5, 30m x 0.53mm i.d., x 1.5 mm film thickness
Injection volume	2 µl
Column flow (He)	13.1 ml/min (velocity 84 cm/sec) (head pres = 9.0 psi)
Septum purge (He)	15 ml/min (9.0 psi)
Detector flow (FPD)	110 ml/min (air); 150 ml/min (hydrogen)
Detector temp (FPD)	250°C
Injector temp	200°C
Injection mode	Splitless, Single taper liner (HP part no 5181-3316)
Inlet Purge	Off Time: 0.00 min; On Time: 0.50 min
Col temperature program	60°C (hold 1 min) to 100°C @ 25°/min (run time: 4 min)

GC/FID Operation for Dynatherm

Same Chromatographic Parameters as above except:

Detector flow (FID)	400 ml/min (air); 30 ml/min (hydrogen)
Detector temp (FID)	250°C

Instrumental Parameters for Thermal Desorption

Model: Dynatherm (ACEM 900)

Temperature/Flow Program:

Tube Desorb	275°C	Tube Heat	3 min
Transfer Line	150°C	Trap Heat	1 min
Trap Desorb	300°C	Tube Dry	1 min
		Tube Cool	1 min
Purge Flow	5 ml/min (He)		
Solid Sorbent	Tenax TA (11.5 cm x 6 mm o.d.)		

Sample Time:

External Sample	External Standard Calibration through sample line	5-7 min
	External Standard Calibration directly on sorbent tube	0 min
	Chamber Sample	2-3 min

APPENDIX B

GB Vapor Stability During One Hour Chamber Run

Dynatherm Samples (1 – 5)

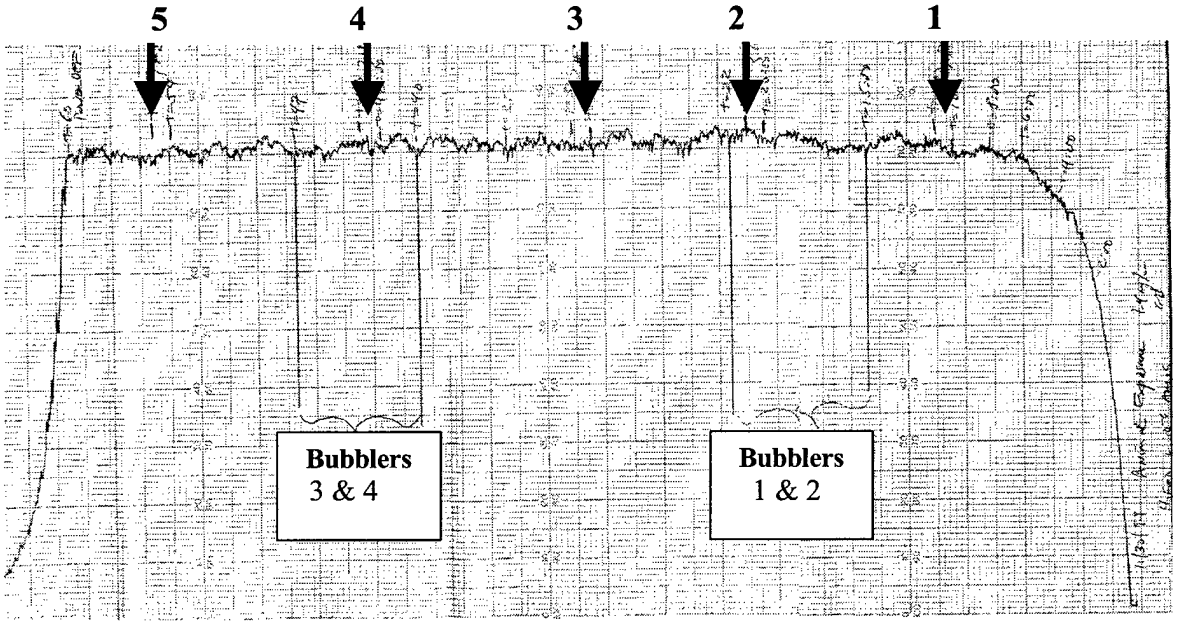

60 min **45 min** **30 min** **15 min** **0 min**

APPENDIX C

Advantages and Disadvantages of Bubbler vs. Sorbent Tube Sampling

BUBBLERS

Advantages	Disadvantages
1. Reliable method	1. Labor intensive (set-up, sample manipulation connections and leak check).
2. Many previous studies have used bubblers, therefore, provides a basis for comparison studies.	2. Requires front and back bubblers to prevent significant analyte (GB) breakthrough.
	3. Extended sampling draws water into the bubbler solution, which may affect the analyte over time.
	4. Cannot automate
	5. Lower GB concentrations require extended sampling times (iced) which limits the number of samples taken during a run.

SORBENT SAMPLING

Advantages	Disadvantages
1. Continuous sample line from the chamber to the GC. Less chance for leaks or errors.	1. Dust particles in sample line may act as absorption sites. May require sample line deactivation (inject dilute GB) prior to calibration.
2. Not labor intensive (same sorbent tube can be reused, no reconnections or sample manipulations).	
3. System can be easily automated.	
4. Samples can be drawn frequently.	
5. Water vapor does not collect in the sorbent tube.	
6. Larger dynamic range and more sensitive.	
7. Amount of Tenax TA in one tube prevents GB breakthrough.	

TOXICITY AND TREATMENT OF RUSSIAN V-AGENT (VR) INTOXICATION IN GUINEA PIGS[1]

Irwin Koplovitz, Michael Shutz, Susan Schulz and Roy Railer
Drug Assessment Division
U.S. Army Medical Research Institute of Chemical Defense
Aberdeen Proving Ground, MD 21010-5400

ABSTRACT

VR (O-isobutyl-S-[2-(diethylamino)ethyl]methyl phosphonothioate) is a structural isomer of VX and is thought to be the principal V-agent found in Russian chemical weapons. We evaluated the toxicity (24 hr LD_{50}) of VR and determined the effectiveness of oxime and atropine (ATR) treatment and pyridostigmine (PB) pretreatment in guinea pigs. Lethality dose-response curves for VR were generated in untreated animals and in animals treated with atropine (ATR) and oxime with or without PB pretreatment. PB was injected i.m. 30 min prior to s.c. VR challenge. One min after VR the animals were treated i.m. with ATR (16 mg/kg) plus an equimolar dose of either 2-PAM (25 mg/kg) or HI-6 (55 mg/kg). Mortality was assessed at 24 hours. The LD_{50} of VR was 11.3 ìg/kg. Treatment with ATR plus 2-PAM or HI-6 resulted in protective ratios (PR) of 6.5 and 43.9, respectively. In PB-pretreated animals, the PRs were 7.1 and 28.7, respectively. The results indicate that 1) VR is a highly toxic organophosphorus agent, 2) it can be effectively treated with oximes and atropine, 3) HI-6 is significantly more effective than 2-PAM, and 4) PB pretreatment affords no further enhancement to the efficacy of atropine and oximes. When compared with previous findings in guinea pigs, ATR + 2-PAM is significantly less effective against VR than against VX. This observation may necessitate a careful examination of the best oxime to use as an antidote against V-agents, particularly for personnel involved in international chemical weapons disposal where exposure to VR is possible.

INTRODUCTION

Although both the United States and Russia possess chemical weapons identified as V-agents in their respective chemical munitions stockpiles (Ember,1990; Maynard and Beswick,1992; Federov and Svetlakova, 1995), it has been suggested that the U.S. and Russian V-agents are not identical. Recently this suggestion was confirmed with the identification of O-isobutyl S-[2-(diethylamino)ethyl] methyl - phosphonothioate (VR) as the standard Russian V-agent (Fig 1), a structural isomer of VX, the standard U.S. V-agent (Szafraniec *et al.*, 1995).

---

1. The opinions or assertions contained herein are the private views of the author(s) and are not to be construed as official or as reflecting the views of the Department of the Army or the Department of Defense.

"The Research was conducted in compliance with the Animal Welfare Act and other Federal statutes and regulations relating to animals and experiments involving animals and adheres to principles stated in the *Guide for the Care and Use of Laboratory Animals,* National Research Council, 1996. The facility where this research was conducted is fully accredited by the Association for Assessment and Accreditation of Laboratory Animal Care International."

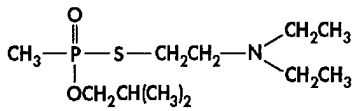

VR

Figure 1. Structure of VR.

The purpose of this investigation was to characterize the toxicity of VR, and determine the effectiveness of pretreatment and treatment countermeasures in an intact animal. Experiments included pretreatment with pyridostigmine bromide (PB) and/or postchallenge treatment with atropine plus an oxime. The oximes used were 2-pyridine aldoxime methyl chloride (2-PAM), the currently fielded U.S. antidote for nerve agent intoxication, and 1-(((4-(aminocarbonyl)pyridino)methoxy)methyl)-2-((hydroxyimino)methyl pyridinium dichloride (HI-6), a bispyridinium oxime that has been widely studied and reported to be more effective than standard oximes (toxogonin and 2-PAM) against nerve agent intoxication, especially soman (Lallement *et al.*, 1997). The guinea pig was used as the animal species since it has been generally regarded as the best nonprimate model for assessing the efficacy of pretreatment and treatment countermeasures against organophosphorus (OP) poisoning (Lundy, 1992).

METHODS

Animals: Male Hartley albino guinea pigs (Charles River Laboratories) weighing 300-450 gms were used. Animals were quarantined and observed for a minimum of five days for evidence of disease under an AAALAC accredited animal care and use program prior to being put on study. Guinea pig ration and tap water were provided *ad libitum*. The guinea pig holding rooms were maintained at 21 $\pm$ 2°C with 50% $\pm$ 10% relative humidity using at 12-15 complete air changes per hour of 100% conditioned fresh air. The animals were maintained on a 12-hour light/dark, full-spectrum lighting cycle with no twilight.

Chemicals: VR (O-isobutyl S-[2-(diethylamino)ethyl]methylphosphonothioate) was synthesized by the U.S. Army Edgewood Chemical Biological Center (ECBC), Aberdeen Proving Ground, Maryland. A stock solution was prepared gravimetrically at a concentration of 1 mg/ml in deuterium oxide (D_2O). The VR concentration was verified by gas chromatography with flame ionization detection. Stock solutions were stored in 1 or 5 ml aliquots at -70°C until needed. Dilutions were prepared from thawed stock and maintained on ice. Atropine (ATR) sulfate (Lot# BL09195), 2-PAM (Lot# BK96362), HI-6 (Lot# BM08862), and pyridostigmine bromide (PB) (Lot # BM03894) were obtained through the Walter Reed Army Institute of Research (WRAIR), Washington, D.C. PB, ATR and oximes were prepared in sterile water daily. ATR was admixed with the oxime to provide a single solution for injection.

Agent Toxicity Studies: VR was injected s.c. in the nape of the neck using a dose volume of 1 ml/kg. A lethality dose-response curve was generated in sequential stages using the stage-wise adaptive approach described by Feder *et al.* (1991a, 1991b, 1991c). In each stage 1-2 animals were allocated to each of 4-5 agent challenge levels selected to span the predicted range of lethality from 0-100%. Mortality was assessed 24 hours after exposure. Results of each stage were evaluated and combined to aid in selecting agent doses for the next stage. The stage-wise approach enabled agent dose allocation in later stages to be optimized to better estimate the dose-lethality relations. A total of three experimental stages were conducted. In each stage, animals were randomly assigned to the challenge levels.

Efficacy Studies: The efficacy of the pretreatment and treatment countermeasures was determined using a similar stage approach design described in the previous section. Lethality dose-response curves for VR were generated in saline-treated animals and in animals treated with atropine (ATR) and oxime with or without PB pretreatment. PB (0.026 mg/kg) or saline was injected i.m. 30 min prior to s.c. VR challenge. The dose of PB was selected to give approximately 40% inhibition of erythrocyte AChE 30 min after injection (Lennox *et al.*, 1985). One min after VR challenge the animals were treated i.m. with saline or ATR (16 mg/kg) plus an equimolar dose of either 2-PAM (25 mg/kg) or HI-6 (55 mg/kg). Mortality was assessed at 24 hours. In each stage pretreatment, agent doses, and treatments were allocated to the animals randomly.

Data Analysis: Probit models were fitted to the dose-lethality data using the method of maximum likelihood. The models were fitted using the general purpose nonlinear regression procedure, PROC NLIN, in the SAS statistical computing system and specialized programs written by Battelle Memorial Institute (Columbus, Ohio) for the sequential stage approach (Feder *et al.*, 1991c). The estimated regression coefficients were used to compute LD_{50} values, protective ratios (PR), predicted survival estimates, and their associated 95% confidence limits. The PR was defined as the ratio of the OP LD_{50} in treated animals divided by the OP LD_{50} in untreated animals.

RESULTS

VR Toxicity: Table 1 summarizes the toxicity of VR in guinea pigs. The 24-hour LD_{50} was 11.3 ug/kg with a 95% confidence interval of 10.5 to 12.1 ug/kg. The slope of the dose-lethality curve was 19.5. The sample size of 56 was obtained by pooling the data from the acute toxicity study and the saline control group in the efficacy study. The two studies were not different statistically.

TABLE 1. Lethality of VR in Guinea Pigs.

N[1]	Slope (ig/kg, s.c.)	24hr LD_{50}	95% C.I.
56	19.5	11.3	10.5 - 12.1

1. Combined data from 2 studies- see Results

Countermeasure efficacy: Tables 2, 3, and 4 summarize the effectiveness of atropine and oxime treatment with or without PB pretreatment against lethal intoxication by VR. Table 2 presents the data as protective ratios (PR), while Table 3 and 4 present the data as predicted survival against varying exposure levels of the OPs.

The PR for 2-PAM + atropine treatment of VR intoxication without PB pretreatment was 6.5, while the PR for HI-6 + atropine was 43.9. The PR for HI-6 was significantly greater ($p<0.05$) than the PR for 2-PAM (Table 2).

TABLE 2. Effectiveness of Medical Countermeasures Against VR Intoxication in Guinea Pigs.

Treatment	Protective Ratio (95% C.I.) - PB	+PB
Atr + 2-PAM	6.5 (5.4-7.7)	7.1 (5.8-8.6)
Atr + HI-6	43.9* (35.2-54.8)	28.7 (18.5-44.5)

* $p<0.05$ compared with Atr + 2-PAM

The disparity in the efficacy between 2-PAM and HI-6 against VR can be further seen from the predicted survival data in Table 3. Survival in 2-PAM-treated animals was 100% at 2 LD_{50}s, 81% at 5 LD_{50}s but only 7% at 10 LD_{50}s, while in the HI-6-treated guinea pigs 100% survival was maintained over the entire range of VR doses from 2-10 LD_{50}s.

TABLE 3. Predicted Survival Against VR Intoxication Following Treatment with Atropine and Oximes.

No. VR LD_{50}s	(LCL - *% Survival* - UCL)[1] Atr + 2-PAM	Atr + HI-6
2	100 - *100* - 100	100 - *100* - 100
3	96 - *100* - 100	100 - *100* - 100
4	79 - *95* - 100	100 - *100* - 100
5	55 - *81* - 100	100 - *100* - 100
6	36 - *61* - 85	100 - *100* - 100
7	18 - *40* - 62	100 - *100* - 100
8	0 - *24* - 48	100 - *100* - 100
9	0 - *14* - 35	100 - *100* - 100
10	0 - *7* - 25	100 - *100* - 100

1. LCL = Lower 95% Confidence Level; UCL= Upper 95% Confidence Level

PB pretreatment did not enhance the efficacy of ATR and oxime therapy against VR intoxication. The PR in PB-pretreated animals treated with ATR+ 2-PAM was 7.1 compared with 6.5 in nonpretreated animals, and the PR in PB-pretreated animals treated with HI-6 + ATR was 28 compared with 43.9 in animals not pretreated; this difference was not significant (Table 2). The predicted survival data in Table 4 demonstrates further that PB provided no enhancement of Atr + oxime efficacy. There was little change in expected survival over a VR exposure range of 2 to 10 LD_{50}s in PB (Table 4) vs non-PB-pretreated (Table 3) animals. In the HI-6-treated animals, there was a trend for survival in the PB-pretreated animals (Table 4) to be reduced over the challenge range compared with nonpretreated animals if the worse case scenario (i.e., survival at the lower 95% CI) is considered (Table 4).

TABLE 4. Predicted Survival Against VR Intoxication Following Pretreatment with PB and Treatment with Atropine and Oximes.

No. of VR LD_{50}s	(LCL - *% Survival* - UCL)[1] Atr + 2-PAM	Atr + HI-6
2	100 -*100*- 100	100 - *100* - 100
3	98 -*100*- 100	98 - *100* - 100
4	86 - *97*- 100	95 - *100* - 100
5	63 - *87* - 100	91 - *99* - 100
6	42 - 70 - 99	87 - *97* - 100
7	25 - *51* - 77	82 - *96* - 100
8	10 - *34* - 57	78 - *95* - 100
9	0 - *21* - 43	73 - 93 - 100
10	0 - 13 - 31	68 - *91* - 100

1. LCL = Lower 95% Confidence Level; UCL= Upper 95% Confidence Level

DISCUSSION

Our studies indicate that VR was a highly toxic organophosphorus agent in the guinea pig with a LD_{50} similar to VX (9.0 ug/kg.s.c.) (Koplovitz *et al.*, 1992). VR was also more toxic than soman, sarin, cyclosarin (GF) and tabun (Koplovitz, 2000). The slope of the VR dose-lethality curve was very steep indicative of a very specific mechanism of toxicity. In this regard, Maxwell et al. (1997) found that VR was a potent inhibitor of AChE with a bimolecular rate constant 3-fold greater than the inhibition rate constant for VX.

Our results indicate that VR was very treatable with atropine and oximes, with HI-6 being 7-fold more effective than 2-PAM. The greater efficacy of HI-6 over 2-PAM was likely due to differences in reactivating ability. This is supported by studies showing that HI-6 was a 5-fold better (faster) reactivator of VR-inhibited AChE than was 2-PAM *in vitro* (Maxwell *et al.,* 1997). The PR of 6.5 that we found with atropine +2-PAM treatment is significantly less than what this treatment regime has been reported to achieve against VX. Maxwell *et al.* (1997) reported a PR against VX of 36.9 using the same doses of atropine and 2-PAM and the same treatment time as used in the present study. Inns and Leadbeater (1983) reported a PR of 25 using an atropine dose of 17.4 mg/kg and a P2S dose of 30 mg/kg. In the latter study, 1/2 of the P2S dose was given 10 min prior to VX challenge, and the rest was administered 1 min after challenge together with the atropine. Koplovitz *et al.* (1992) reported a PR of 59 using atropine 32 mg/kg and 2-PAM 25 mg/kg administered 1 min after challenge. The greater efficacy of 2-PAM against VX compared with VR, however, cannot be explained as convincingly based on differences in enzyme reactivation. Maxwell *et al.* (1997) reported that 2-PAM was only 1.6-fold better in reactivating VX-inhibited AChE than VR-inhibited enzyme *in vitro*. However, *in vivo* 2-PAM appears to be approximately 6-fold more effective against VX than it is against VR . It may be that other factors such as differences in the distribution between the VX and VR could account for the difference in the efficacy of 2-PAM (Maxwell *et al.*, 1997). Ligtenstein *et al.* (1991) have observed that oximes are more effective against OP compounds whose distribution is predominately peripheral in comparison to OP compounds that distribute in the central nervous system. Maxwell *et al.* (1997) also found that VR has a lower pK_a than VX, which may allow more VR to distribute into the central nervous system, making it less susceptible to oxime treatment.

The failure of PB pretreatment to enhance the efficacy of atropine and oxime treatment of VR intoxication was similar to previously reported results against VX and sarin (Koplovitz *et al.*,1992). In the latter study, the authors hypothesized that the inability of PB to enhance the efficacy of atropine and 2-PAM treatment of VX and sarin intoxication might be due to several factors. First, these OPs are easily reactivated by 2-PAM, and second 2-PAM is a more effective reactivator of phosphonylated than of carbamylated AChE . Therefore, when the rate of oxime-induced reactivation is absolutely critical to the demonstration of efficacy (*e.g.*, when lethal doses of OPs are used), there would be more phosphonylated enzyme available for reactivation in the absence of PB pretreatment than in the presence of PB. The results of the present study lend further support to the contention that OPs, which are easily reactivated with oximes show no benefit from PB pretreatment. Also, it would appear that the more effective the oxime is in reactivating the phosphonylated enzyme the greater the likelihood of a negative interaction in the presence of PB. In our studies, PB had a more dramatic effect on the efficacy of atropine and HI-6 than on the efficacy of atropine and 2-PAM.

The PR, historically, has been the standard method of representing the efficacy of medical countermeasures against nerve agent intoxication; however, PRs can be misleading if not completely understood. The tendency (for those who are not experts in the field) is to interpret a PR as the challenge level against which complete protection (100%) can be provided, while in fact, by definition the survival at any given PR is only 50%, since it is the ratio of agent LD_{50} doses (treated/untreated). Also, the PR does not give any information on survival (mortality) at higher or lower challenge levels, nor does it provide information on the slope of the dose-response. Predicted survival, on the other hand, provides information on survival (mortality) over a range of challenge doses of interest and also gives an indication of the slope of the response. We feel it is a more practical and useful method of presenting this type of data. For example, although the PR for atropine and 2-PAM is 6.5 (Table 2), the data in Table 3 show that survival is reduced to 81% at 5 LD_{50}s and could be as low as 55% based on the lower limit of the 95% confidence interval. Similarly, at 4 LD_{50}s, survival could be as low as 79%. The PR does not give the same amount of information as predicted survival over a range of exposure levels.

CONCLUSIONS

1. VR is as toxic as VX.
2. VR is significantly less treatable with atropine and 2-PAM.
3. HI-6 is significantly more effective than 2-PAM in treating VR intoxication.
4. PB pretreatment does not enhance the efficacy of atropine and oxime treatment of VR intoxication.
5. Depending on the level of exposure, the choice of oxime for treatment of VR intoxication needs to be carefully considered.

REFERENCES

1. Ember LR. (1990) Chemical weapons disposal: daunting challenges still ahead. *Chem Eng News* 68(33): 9-19.

2. Feder PI, Hobson DW, Olson CT, Joiner RL, and Matthews MC. (1991a) Stagewise, adaptive dose allocation for quantal response dose-response studies. *Neurosci. & Biobehav. Rev.* 15: 109-114.

3. Feder PI, Olson CT, Hobson DW, Matthews MC, and Joiner RL. (1991b) Stagewise, group sequential experimental designs for quantal responses. One-sample and two sample comparisons. *Neurosci & Biobehav Rev* 15: 129-133.

4. Feder PI, Olson CT, Hobson DW, Matthews MC, and Joiner RL. (1991c) Statistical analysis of dose-response experiments by maximum likelihood analysis and iteratively reweighted nonlinear least squares regression techniques. *Drug Information Journal* 25: 323-334.

5. Fedorov LA and Svetlakova MS. (1995) Russian V-gas and its legacy. *ASA Newsletter* 95(6): 1-13.

6. Inns RH and Leadbeater L. (1983) The efficacy of bispyridinium derivatives in the treatment of organophosphonate poisoning in the guinea pig. *J Pharm Pharmacol* 35: 427-433.

7. Koplovitz I, Harris LW, Anderson DR, Lennox WJ, and Stewart JR. (1992) Reduction by pyridostigmine pretreatment of the efficacy of atropine and 2-PAM treatment of sarin and VX poisoning in rodents. *Fundam Appl Toxicol* 18: 102-6.

8. Koplovitz I. (2000) (Unpublished data).

9. Lallement G, Clarencon D, Brochier G, Baubichon D, Galonnier M, Blanchet G, and Mestries J-C. (1997) Efficacy of atropine/pralidoxime/diazepam or atropine/HI-6/prodiazepam in primates intoxicated with soman. *Pharm Biochem Behav* 56(2): 325-332.

10. Lennox WJ, Harris LW, Talbot BG, and Anderson DR. (1985) Relationship between reversible acetylcholinesterase inhibition and efficacy against soman lethality. *Life Sci.* 37: 793-798,

11. Ligtenstein DA and Moes GWH. (1991) The synergism of atropine and the cholinesterase reactivator HI-6 in counteracting lethality by organophosphate intoxication in the rat. Toxicol Appl Pharmacol 107:47-53.

12. Lundy PM, Hansen AS, Hand BT, and Boulet CA. (1992) Comparison of several oximes against poisoning by soman, tabun, and GF. *Toxicology* 72:99-105.

13. Maxwell DM, Brecht KM, and Koplovitz I. (1997) Characterization and treatment of the toxicity of O-isobutyl S-[2-(diethylamino)ethyl]methylphosphonothioate, a structural isomer of VX, in guinea pigs. *J Amer Coll Toxicol* 15 (Suppl. 2) s78-s88.

14. Maynard RL and Beswick FW. (1992) Organophosphorus compounds as chemical warfare agents. In: Ballantyne B, Marrs TC eds. *Clinical and Experimental Toxicology of Organophosphates and Carbamates*. Oxford: Butterworth-Heinemann, 375-85.

15. Szafraniec LL, Beaudry WT, and Szafraniec LJ. (1995) Decontamination chemistry of Russian VX. *Proceedings of the Scientific Conference on Chemical and Biological Defense Research*, Aberdeen Proving Ground, Maryland: Nov. 14-17.

THE POTENTIAL NEUROTOXIC EFFECTS OF LOW-DOSE SARIN EXPOSURE IN A GUINEA PIG MODEL

Melinda R. Roberson, PhD, Michelle B. Schmidt, SSG Mary D. Gonzales and
John H. McDonough, Jr., PhD
Pharmacology Division, U.S. Army Medical Research Institute of Chemical Defense,
Aberdeen Proving Ground, MD 21010 USA

ABSTRACT

This study is assessing the effects in guinea pigs of repeated low-dose exposure to the nerve agent sarin. Preliminary results suggest no effects of either repeated 0.2 or 0.4 X LD50 sarin exposure (compared with saline) on body weight or temperature, general physical signs, flinch threshold or activity level, or on EEG activity. In contrast, RBC cholinesterase levels dropped to 20% of baseline following the tenth exposure in the 0.4 group. Since this study is ongoing, data from receptor binding and brain cholinesterase assays and histopathology are still being collected and analyzed, and may be influenced by the dramatic changes in cholinesterse activity.

INTRODUCTION

A great deal of research has been conducted to study the single acute effects of chemical warfare nerve agents (CWNA) and how to protect against the acute toxic effects. Consequently, the sequence of events following a single, seizure-eliciting exposure to organophosphorus (OP) CWNA has been relatively well characterized. However, much less is known about the effects of repeated low dose exposure to OP nerve agents, and there has been concern that such exposure may have contributed to the adverse health effects reported by Gulf War veterans. Due to the uncertainty of the effects of prolonged low dose chemical exposure, there is a need to better understand the potential adverse health consequences of such exposure and to determine what level of exposure may produce adverse effects.

The experiments detailed here are intended to furnish initial data that should address a number of these issues and form the basis for further research. These ongoing studies concurrently examine electrophysiological, behavioral, biochemical, neurochemical, and histopathological parameters in an animal model that utilizes repeated exposure to low levels of the nerve agent sarin.

There have been numerous studies of the neurobehavioral effects of repeated low-level exposure to a variety of OP agents such as DFP or paraoxon (see Russell and Overstreet, [15] 1987 for a review), and some limited studies with nerve agents. Previous studies of repeated administration of the nerve agent soman shows that such treatment produces transient, but reversible, changes in regional brain cholin-

esterase (ChE) activity and regional brain muscarinic receptor (mAChR) numbers.[3,9] During the time of repeated exposure the animals can display altered behavior and may develop a tolerance to the agent as the exposures continue.[12,14] In addition, it has been reported that repeated low level exposures to sarin may produce permanent alterations in brain electroencephalographic (EEG) spectrum that far outlast the period of exposure.[2] Because of this persistent change in EEG, there have been continuing concerns that exposure to low doses of nerve agents can also produce neural lesions in brain such as those seen after exposure to high doses of nerve agent that produce prolonged seizures.[7,8]

In the present study, guinea pigs, previously instrumented to record EEG activity, were exposed daily (5 days/wk for two weeks) to two doses (0.2 X LD50 and 0.4 X LD50) of sarin. Measures of red blood cell (RBC) ChE, EEG activity, body weight, body temperature, flinch thresholds (nociception), and general activity levels were determined during the exposure phase as well as 2 hrs, 3, 10, 30, or 100 days following exposure in different groups.

The two-week period of nerve agent exposure was selected because this period of exposure provides sufficient time for ChE to be driven to a low, stable level. The nerve agent, sarin, and the doses (0.2 and 0.4 X LD50) were selected to allow replication and expansion on a database of low-dose work begun at USAMRICD.[1] These doses, particularly the higher 0.4 dose, also produce no notable adverse physiological effects such as weight loss or lethality. The current LD50 has its basis in protection studies historically conducted in guinea pigs at USAMRICD.

MATERIALS AND METHODS

General Methods: Guinea pigs (Final N = 180) are anesthetized with isoflurane and stereotaxically implanted with stainless steel cortical screw electrodes.[10,11] Following a one-week recovery period and initial handling days (M, Tu), baseline EEG (30 min/day), baseline blood ChE, and behavioral data is being gathered on two pre-exposure days (W, Th). Animals are then injected daily, s.c., 5 days/wk for 2 wks with saline or sarin (0.2, or 0.4 x LD50; LD50 = 42 ìg/kg). On each day of exposure, body temperature (pre- and post-exposure) and body weight are measured, and the animals are monitored for EEG activity (power spectral analysis, broken into five EEG bands) for 15 minutes to establish a daily pre-exposure baseline. After each injection the animals are monitored for EEG activity for 1 hour and are assessed for general signs of sarin exposure, including eyelid closure, facial tremor, fasciculation, writhing, vocalization, circling, biting, the ease of handling, lacrimation and salivation. Following EEG recording, animals are assessed for change on measures of nociception (flinch threshold/foot shock) and general activity. Blood is drawn on selected days for analysis of RBC ChE activity. After the termination of the exposure phase, separate groups of animals are evaluated for EEG and behavioral changes at 3, 10, 30 and 100 days. In addition, at each of these times (plus at 2 hrs post exposure), groups of animals are euthanized (75 mg/kg, i.p., pentobarbital) and transcardially perfused. The brain and heart are removed, and regional brain ChE activity, regional brain receptor B_{max} and K_d, and brain neuropathology are being determined. [^{3}H]-Pirenzepine is being used for mAChR binding to M_1 receptors,[5] and [^{3}H]-CGP-39653 is being used for glutamatergic NMDA (N-methyl D-aspartate) receptor binding.[16] Separate brain and heart evaluations for histopathological assessment are carried out with a number of staining techniques, including hematoxylin and eosin (H & E) and glial fibrillary acidic protein (GFAP).[6] Apo-tag will be used to identify potentially apoptotic neurons.[13]

Nociceptive (flinch) thresholds are determined by the up-and-down procedure.[4] The animal is placed in a test chamber (16 cm L; 11 cm W; 13 cm H) with a stainless steel grid floor through which varying intensities of electric shock can be delivered. After a 1-min habituation period, single shock pulses (0.5 sec) are delivered at 15-sec intervals. Shock intensities are available from 0.05 to 4.0 mA in 20 steps arranged logarithmically. Flinch is being defined as any visual withdrawal reaction in response

to shock presentation, and shock intensity will be varied according to each response. An adaptation of the "up-down" method for small samples is used for determining the order of presentation of shock intensities during each series. The midpoint of pre-exposure baseline measurements serves as the starting point from which the shock intensities will be varied for each animal.

General activity is measured for 30 minutes in a 40 cm X 40 cm X 30 cm clear plexiglas chamber utilizing a grid of photo beams. Horizontal and vertical activity (number of beam breaks) is measured in 10-min segments along with total activity for the 30-min session. Habituation is being defined as the decline in activity as a function of time during the session [14] (results not shown).

Animal Care and Handling: Research was conducted in compliance with the Animal Welfare Act and other Federal statutes and regulations relating to animals and experiments involving animals and adheres to principles stated in the Guide for the Care and Use of Laboratory Animals, National Research Council, 1996. The facility where this research was conducted is fully accredited by the Association for Assessment and Accreditation of Laboratory Animal Care International.

TABLE 1. General Experimental Scheme.

Implant Electrode	Baseline	Chronic Exposure	Post-Exposure					
All Ss	2 days	2 weeks/M-F	2 hrs	3	10	30	100 days	
	(EEG, Behavior)	(EEG, Behavior)	(EEG, Behavior, Neurochem, Histology)					Animal # Subtotal
		Saline	6, 6	6, 6	6, 6	6, 6	6, 6	60
		Sarin: 0.2 LD50	6, 6	6, 6	6, 6	6, 6	6, 6	60
		Sarin: 0.4 LD50	6, 6	6, 6	6, 6	6, 6	6, 6	60 180 Total

Two groups of 6 animals at each time point: six are being tested for flinch threshold and six for activity level. Animals from both behavioral groups are being used for ChE and receptor assays, and neuropathological evaluation.

RESULTS

The present report represents interim results of this ongoing study. Since within a dose condition, all animals are treated the same during the exposure phase, there are sufficient animals to determine any obvious trends that may have developed during this phase of the study (See figure legends for Ns).

During the daily post-exposure EEG recording period (1 hr), there were no observable signs of sarin exposure on behavioral and sensory indices: eyelid closure, writhing, vocalization, circling, biting, and the ease of handling, lacrimation and salivation. For further discussion of the results, see Figures 1-7:

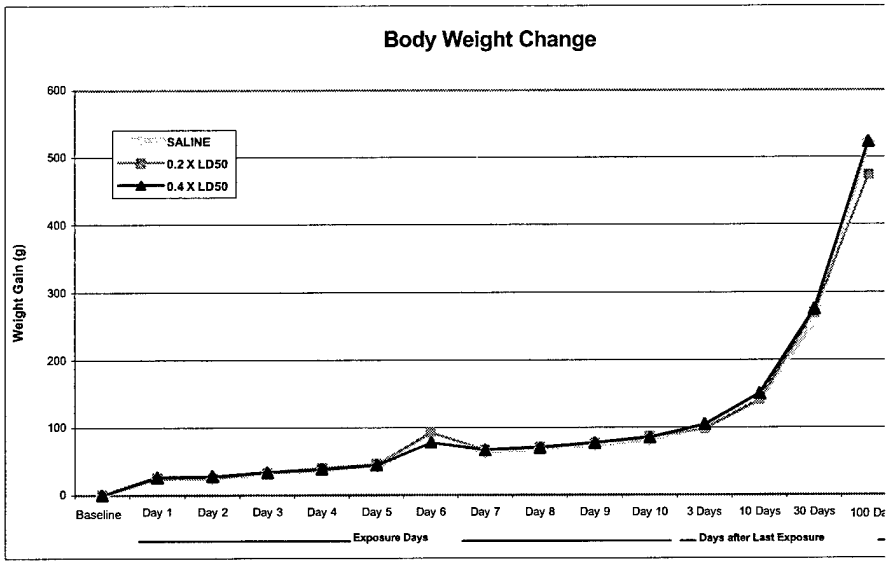

Figure 1. Body Weight Change: There was no difference in body weight gain (g) between saline and either 0.2 or 0.4 X LD50 sarin animals over the 2-week exposure period or up to 100 days post-exposure. (Ns = 20-23 animals for all three groups from initial the baseline day throughout the exposure period, however, at 3 days after the last exposure, Ns = 16-19; at 10 days, Ns = 11-14; at 30 days, Ns = 9; and at 100 days, Ns = 2-3.)

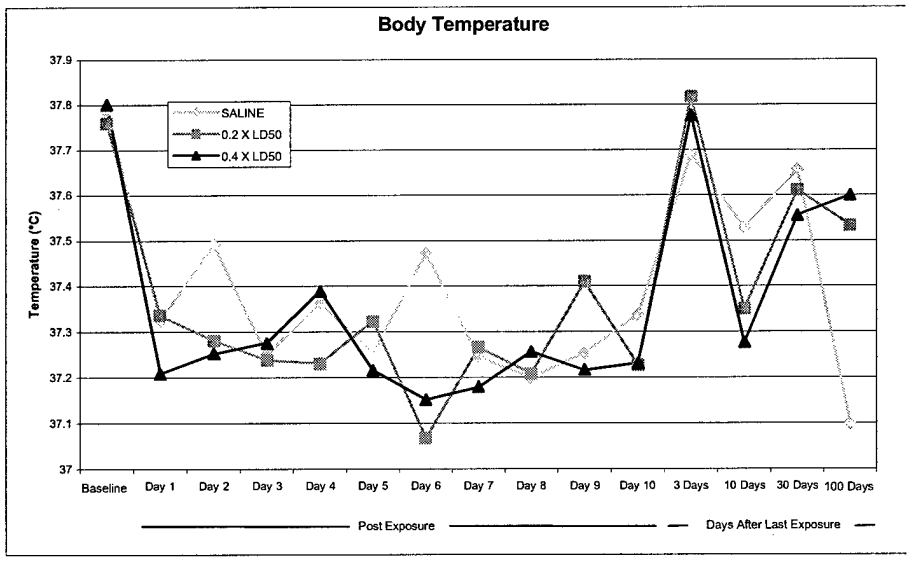

Figure 2. Body Temperature: There was no significant difference in body temperature (°C) between saline and either 0.2 or 0.4 X LD50 sarin animals. Temperature shown on exposure days 1-10 was taken 1 hour post-injection. All temperature measures in this portion of the study were taken using a rectal probe (YSI Thermometer). (Ns = same as for Body Weight, see Figure 1.)

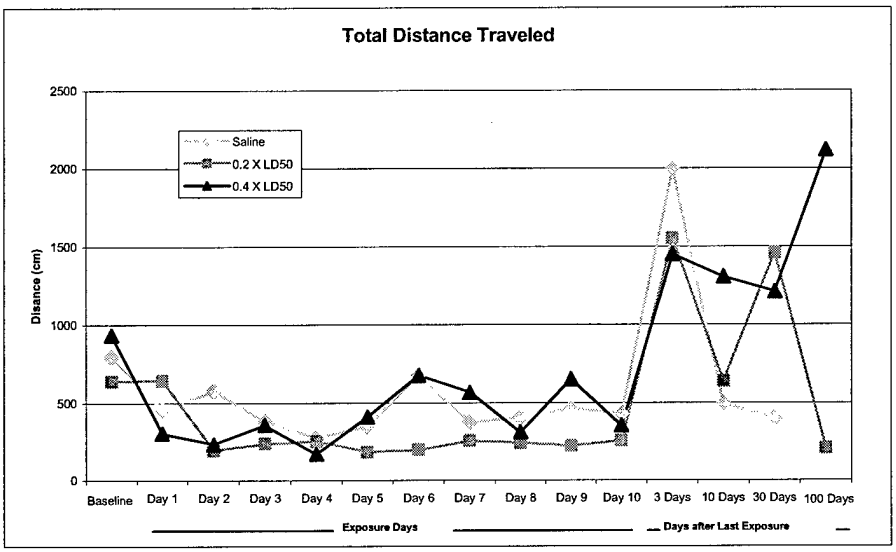

Figure 3. Total Distance Traveled (Activity Level): There was no effect of dose on activity level, stated as a function of distance traveled (cm). The large jump in activity level observed in all three groups at 3 days after the last exposure is likely due to the weekend break and the absence of the injection handling. Additionally, animals are present in the EEG chamber (prior to activity testing) for only 15 minutes, compared to 1 hr, 15 min on injection days. (Ns = same as for Flinch Threshold (see Figure 5), except for the 100-day time point in which (at this point in the study) Ns = 1 for the saline and 0.4 LD50 groups, and N = 0 for the 0.2 LD50 group.)

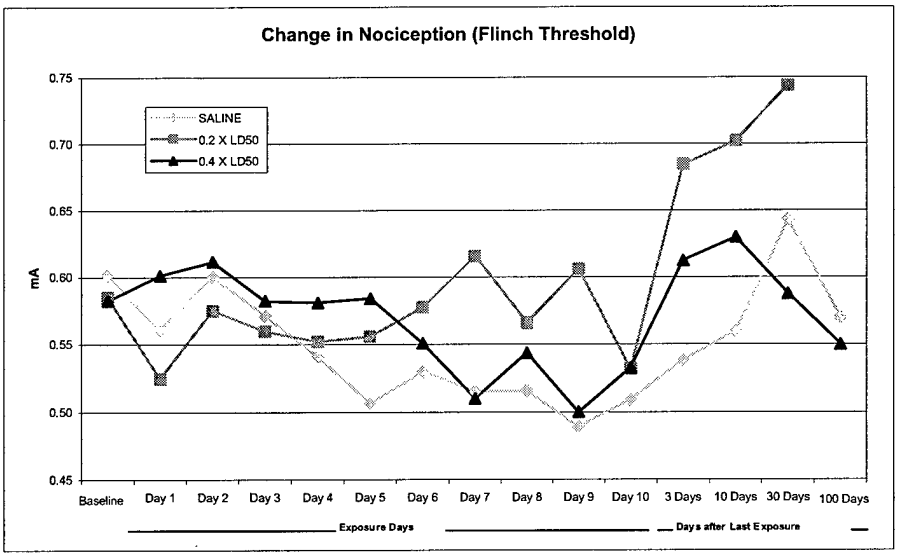

Figure 4. Change in Nociception (Flinch Threshold): There was no meaningful effect of sarin dose on a measure of nociception (flinch threshold). Shown are raw flinch thresholds (mA) for pre-exposure period baseline, exposure days 1-10 (measured 1 hr post-injection), and selected days after the exposure period. (Ns = 9-16 for all three groups for baseline through exposure day 10; however, at 3 days after the last exposure, Ns = 6-11; at 10 days, Ns = 6-9; at 30 days, Ns = 3-6; and at 100 days, Ns = 1-2.)

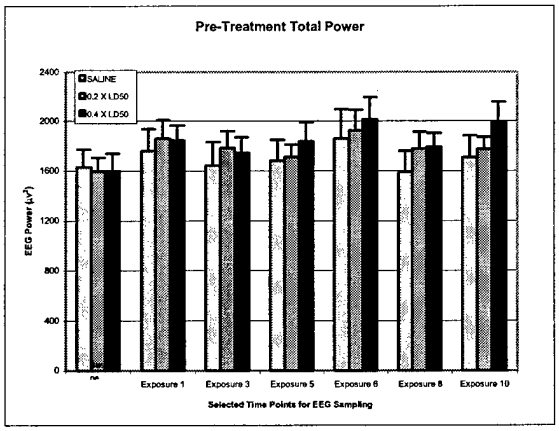

Figure 5. Pre-Treatment Total EEG Power: There was no significant effect of either the 0.2 or 0.4 LD50 sarin dose on total EEG power (iv^2), when pre-exposure period baseline EEG was compared with the 10-day exposure period pre-injection EEG recordings ($F_{12,6} = 0.60$, $P > 0.83$). (For Figures 3 and 4, N = 11 (saline); N = 12 (0.2 LD50), N = 13 (0.4 LD50.)

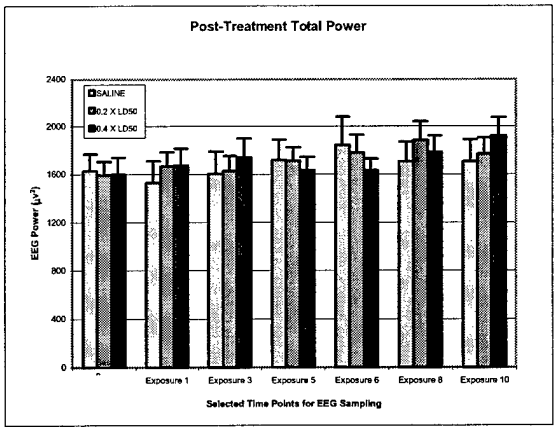

Figure 6. Post-Treatment Total EEG Power: There was no significant effect of either the 0.2 or 0.4 LD50 sarin dose on total EEG power (iv^2), when the pre-exposure period baseline EEG measures were compared with exposure period daily post-injection EEG recordings ($F_{12,6} = 1.035$, $P > 0.43$). (On both pre- and post-treatment EEG, analysis of the five individual bands (spectral analysis: ä, è, á, $â_1$, $â_2$) also resulted in no significant effect of sarin dose on individual band power.)

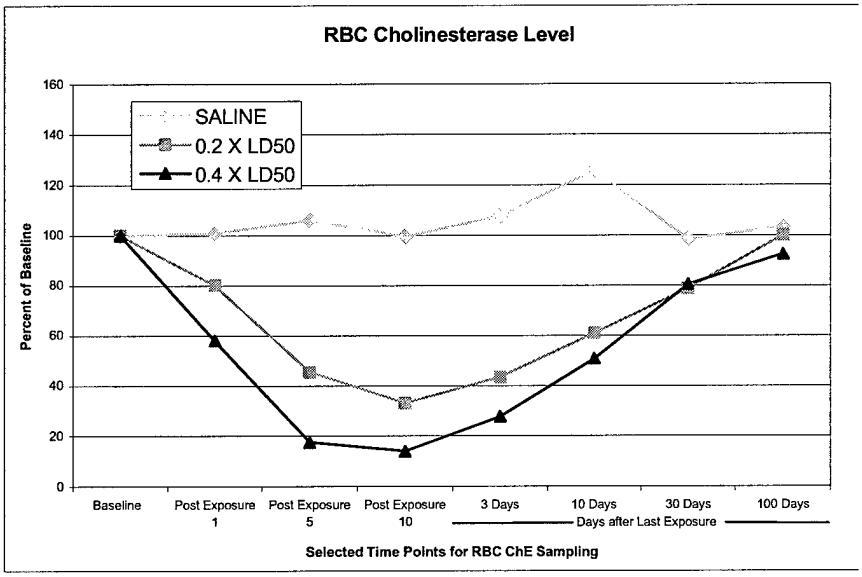

Figure 7. RBC Cholinesterase Level: In contrast to the absence of behavioral or EEG signs, RBC ChE activity dropped to less than 20% of baseline following the tenth exposure in the 0.4 LD50 sarin animals, and to less than 40% of baseline in the 0.2 LD50 animals. Both agent groups showed a steady increase in ChE activity following the exposure period, with 0.2 animals returning to baseline and 0.4 animals remaining just below baseline at 100 days after the last exposure.

CONCLUSIONS

It is important to reiterate that these results are preliminary, since the study is ongoing. While it is informative to gain an idea of the direction the results may be taking, drawing definitive conclusions at this point would be premature. Further, the receptor binding and brain ChE activity assays and the histopathological analyses are currently being carried out; consequently those data sets are insufficiently complete to be presented here.

However, during the pre-exposure period baseline and exposure day pre- and post-injection measures, the N's are sufficiently large (~20) on a number of parameters to allow speculation. So far, we have observed no behavioral indication of an effect of low-dose sarin exposure, at least at the doses and schedule used here. However, the drop of RBC ChE activity to below 20% of baseline in the 0.4 LD50 sarin group, and to below 40% of baseline in the 0.2 LD50 group, represents a dramatic contrast. How this change in ChE activity will affect receptor binding, brain ChE activity and neuropathology is not known. Nevertheless, the drop to 40% and 20% of baseline ChE activity is sufficient to suggest that alterations in intracellular parameters--either biochemical or histopathological--will be observed in the sarin-exposed animals, at least transiently (at the earlier time points) and perhaps persistently (at 30 and 100 days post-exposure). When the study is complete, it may be possible to connect these suggested neurochemical and/or neuropathological alterations with some of the adverse health effects reported by Gulf War veterans.

REFERENCES

1. Atchison, C.R., Holmes, C., Akers, S., Duniho, S., Briscoe, C., Armstrong, K., Clark, C. and Shih, T.-M. (2000) US Army Medical Defense Bioscience Review.
2. Burchfiel, J. L., Duffy, F. H. and Sim, V. M. (1976). Toxicol. Appl. Pharmacol. **35**, 365-379.
3. Churchill, L., Pazdernik, T.L., Jackson, J.L., Nelson, S.R., Samson, F.E. and McDonough, J.H. (1984. J. Neurosci., **4,** 2069-2079.
4. Crocker, A. D. and Russell, R. W. (1984). Pharmacol. Biochem. Behav. **21**, 133-136.
5. Hammer, R., Berrie, P., Birdsall, N., Burgen, A. S. and Hilme, E. C. (1980). Nature **183**, 90-92.
6. Heimer, L. and Robards, M. J., Eds., (1981) Neuroanatomical Tract-Tracing Methods. Plenum Press, New York and London.
7. Hymowitz, N. Ploshnick, A., Laemle, L. and Brezenoff, H. (1990). Neurotoxicol. Teratol. **12**(1), 47-56.
8. Kadar, T., Cohen, G., Sahar, R., Alkalai, D. and Shipira, S. (1992). Hum. Exp. Toxicol. **11**, 517-523.
9. McDonough, J. H. Jr., Hackley, B. E. Jr., Cross, R., Samson, F. and Nelson, S. (1983). Neurotox. **4**(2), 203-210.
10. McDonough, J. H., McMonagle, J., Copeland, T., Zoeffel, D. and Shih, T.-M. (1999). Arch. Toxicol. **73**, 473-478.
11. McDonough, J. H. Jr., Zoeffel, L. D., McMonagle, J., Copeland, T. L., Smith, C. D. and Shih, T.-M. (2000). Epilepsy Res. **38**(1), 1-14.
12. Modrow, H. E. and McDonough, J. H. (1986). Pharmacol. Biochem. Behav. **24** (4), 845-848.
13. Roux, P. P., Colicos, M. A., Barker, P. A. and Kennedy, T. E. (1999). J. Neurosci. **19**, 6887-6896.
14. Russell, R. W., Booth, R. A., Lauretz, S. D., Smith, C. A. and Jenden, D. J. (1986). Neurobehav. Tox. Terat. **8**, 675-685.
15. Russell, R. W. and Overstreet, D. H. (1987). Prog. Neurobiol. **28**, 97-129.
16. Sills, M. A., Fagg, G., Pozza, M., Angst, C., Brundish, D. E., Hurt, S. D., Wilusz, E. J. and Williams, M. (1991) Euro. J. Pharmacol. **192**, 19-24.

Author Index

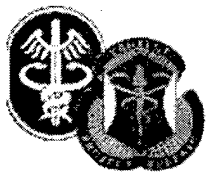

Home | Introduction | Table of Contents | Download | Author Index

Sorted alphabetically by authors last name.

| A | B | C | D | E | F | G | H | I | J | K | L | M |
| N | O | P | Q | R | S | T | U | V | W | X | Y | Z |

- A -

Anthony, J. Steven – Jakubowski - platform, Anthony, Muse
Arca, Victor J. – Fedele
Asprey, William – Johnson

- B -

Babin, Michael C. – Smith
Baier, Robert – Baier
Ballough, Gerald P. H. – Newmark, Filbert
Barber, K. Suzanne – Barber
Bartman, Philip W. – Wagner
Bartoszcze, Michal – Bartoszcze
Bartram, Phillip – Rastogi
Ben-David, Avishai – Jensen
Black, B. – Munavalli 1
Boezer, Gordon – Kornguth
Bourget, Stéphane – Di Ionno

- C -

Caretti, David M. – Caretti
Casillas, Robert P. – Smith
Cheng, Tu-chen – Schreuder-Gibson, Rastogi, Kim
Chester, Nancy A. – Guelta
Chomiczewski, Krzysztof – Bartoszcze
Clarkson, Edward D. – Gordon - platform
Coon, Philip A. – Gray
Crenshaw, Michael D. – Crenshaw

- M -

Macalalag, Rudy C. – Gordon - platform
Mackay, Dr. Raymond A. – Mackay
MacMahon, Matthew – Barber
Mahle, John J. – Mahle
Manthei, James A. – Mioduszewski, Jakubowski - platform
Marijnissen, Jan C. M. – van Baar
Marinelli, William – Jensen
Marshall, Stephen M. – Fedele
Martin, Cheryl – Barber
Martin, Chuck – Partch
Matta, Richard – Jensen
Maxwell, Donald M. – Gordon - platform
McDonough, Jr., John H. – McDonough, Shih, Roberson
McKay, Ryan – Barber
Mershon, Millard M. – Mershon
Messier, Pierre Jean – Di Ionno
Mioduszewski, Robert J. – Mioduszewski, Jakubowski - platform, Muse
Mizak, Lidia – Bartoszcze
Munavalli, Shekar – Munavalli 1, Munavalli 2
Muse, William – Mioduszewski, Jakubowski - platform, Muse

- N -

Newmark, COL Jonathan – Newmark
Nicotera, Paul – Baier
Nieuwenhuizen, Maarten S. – Nieuwenhuizen

- O -

Cronin, Tracy – Gordon - poster
Crosier, Ronald B. – Mioduszewski
Crouse, Charles – Jakubowski – platform, Anthony, Muse
Crouse, Lee – Muse
Curnas, Carl W. – Guelta

- D -

DeFrank, Joseph J. – DeFrank, Elashvili 1, Fry, Kim, Elashvili 2
Di Ionno, Lucy – Di Ionno
Dingus, Michael L. – Hall
Doctor, Bhupendra P. – Gordon - platform, Gordon - poster
Duniho, S. – Shih
Durst, H.D. – Jakubowski – platform, Jakubowski - poster, Munavalli 1, Munavalli 2

- E -

Elashvili, Ilya – Elashvili 1, Elashvili 2
Ercanbrack, Wesley – Ercanbrack

- F -

Feaster, Shawn R. – Gordon - platform, Gordon - poster
Fedele, Paul D. – Fedele
Fell, Jr., Nicholas F. – Pellegrino, Fell, Gillespie
Filbert, Margaret G. – Newmark, Filbert
Freudenberger, Steve – Ercanbrack
Fry, Ilona J. – Fry

- G -

Gaviola, Bernardita P. – Mioduszewski, Jakubowski – platform
Gerritse, K. – Busker
Gillespie, James – Pellegrino, Fell, Gillespie
Gittens, Christopher – Jensen
Gonzales, SSG Mary D. – Roberson
Gordon, Richard K. – Gordon - platform, Gordon - poster
Gray, David L. – Gray
Grim, Dustin – Jensen
Groen, Bas – Nieuwenhuizen
Gruber, Thomas – Jensen
Guelta, Mark A. – DeFrank, Guelta
Gunduz, Alper T. – Gordon - platform, Gordon - poster

- H -

Hall, Michael L. – Hall
Hamilton, Jr., Robert M. – Hamilton
Hanson, Jeffrey – Hanson
Hardy, Jr., Robert L. – Hardy
Hayes, Jeffrey – Hayes
Hayes, Thomas L. – Hayes
Hendricks, Jeffrey – Hendricks
Hendricks, Jeffrey O. – Hendricks
Hoffman, Jeffrey – Hoffman
Hoffman, Jeffrey D. – Hoffman
Hoffman, Jeffrey S. – Hoffman
Hoffman, Jeffrey T. – Hoffman
Hoffman, Jeffrey W. – Hoffman
Hoffman, Jeffrey Y. – Hoffman
Hoffman, Jeffrey Z. – Hoffman
Hoffman, Jeffrey [illegible] – Hoffman
Hoffman, Jeffrey [illegible] – Hoffman
Hoffman, Jeffrey [illegible]

Smirniotis Panagiotis G. - Smirniotis
Smith, William J. – Smith
Smoll, Jennifer – Reed
Sommerville, Douglas R. – Mioduszewski
Stigter, E. – Busker
St-Louis, Jean-Pierre – Di Ionno
Stopa, Peter J. – Gray
Stowers, Michael A. – van Baar
Swanson, Jerome – Johnson

- H -

Haley, Mark V. – DeFrank, Guelta, Anthony
Hall, Peyton W. – Hall
Harteveld, H. – Busker
Harvey, Steven P. - Kolakowski
Henderson, Vikki D. – Wagner
Heykamp, L. S. – Jakubowski - platform, Jakubowski - poster
Hill, Craig – Schreuder-Gibson
Hoskin, Francis – Schreuder-Gibson
Huang, Xiaozhe – Lindler

- I -

Ifarraguerri, Agustin I. – Jensen
Ince, Brian S. – Ince
Izzo, Christopher – Baier

- J -

Jakubowski, E. Michael – Jakubowski - platform, Jakubowski - poster
Jenkins, Aaron – Ercanbrack
Jensen, James O. – Jensen
Johnson, Paul E. – Johnson
Joosen, Marloes J. A. – Nieuwenhuizen

- K -

Kellog, Julie – Johnson
Khan, Akbar S. – O'Connell
Kientz, Charles E. – van Baar
Kim, Michael H. – Kim
Kiser, Robyn C. – Smith
Koch, Mark – Guelta
Kolakowski, Jan E. - Kolakowski
Koplovitz, Irwin – Koplovitz
Kornguth, Steven – Kornguth
Krauss, Morris – Krauss

- T -

Thompson, Roy G. – O'Connell
Thomson, Sandra A. – Mioduszewski, Jakubowski - platform, Jakubowski - poster, Anthony, Muse
Tomkins, Bruce A. – Tomkins
Trudil, David – Gray, Trudil
Turetsky, Abraham L. – Rastogi, Fry

- U -

- V -

Valdes, James J. – Kornguth, O'Connell
van Baar, Ben L. M. – van Baar
van der Gaag, B. – Busker
van Hövell tot Westerflier, S. – Busker
van Wuijckhuijse, Arjan L. – van Baar
Vanwersch, Raymond A. P. – Nieuwenhuizen
Votaw, Amanda – Johnson

- W -

Wagner, George W. – Procell 1, Rastogi, Munavalli 1, Munavalli 2, Procell 2, Wagner
Walker, John – Schreuder-Gibson
Way, Ruth A. – Mioduszewski, Jakubowski - platform
White, William – Wilson
Wick, C. H. – Latham
Wilson, Ashley L. – Wilson

- L -

Lake, William L. – Fedele
Latham, John – Latham
Lee, Fred K. – Fry
Lenz, David – Lenz, Gordon - platform
Ligon, David L. – Gillespie
Linden, Dr. Carol – Linden
Lindler, Luther E. – Lindler, Sheahan
Loerop, William R. – Jensen
Longo, F. R. – Munavalli 1, Munavalli 2
Lund, Michael – Johnson
Lupton, F. Stephen – DeFrank, Guelta

- X -

- Y -

Yang, James W. – Jensen
Yang, Yu-Chu – Procell 1, Procell 2, Wagner
Yeomans, Walter – Schreuder-Gibson
Yin, Ray – Schreuder-Gibson

- Z -

Zaiee, Saeed – Mahle
Zeller, Frank T. – Hall
Zhao, Dehua – Johnson
Zielinski, Walter – Kornguth